

# Proceedings of the 11<sup>th</sup> International Conference on Conveying and Handling of Particulate Solids

---

*Edinburgh, UK*

*September 2<sup>nd</sup> - 4<sup>th</sup>, 2024*



## *Editors*

*Jin Y. Ooi*

School of Engineering,  
University of Edinburgh,  
Edinburgh, UK.

*J.P. Morrissey*

School of Engineering,  
University of Edinburgh,  
Edinburgh, UK.

*Kevin Hanley*

School of Engineering,  
University of Edinburgh,  
Edinburgh, UK.

*Stefanos-Aldo*

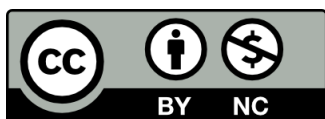
*Papanicolopoulos*  
School of Engineering,  
University of Edinburgh,  
Edinburgh, UK.

ISBN: 978-1-0369-0364-0

Proceedings of the 11<sup>th</sup> International Conference on Conveying and Handling of Particulate Solids © 2024 by the *School of Engineering*, University of Edinburgh is licensed under Creative Commons

Attribution-NonCommercial 4.0 International (CC BY-NC 4.0). To view a copy of this license, visit

<https://creativecommons.org/licenses/by-nc/4.0/>



The use of general descriptive names, registered names, trademarks, service marks, etc. in this publication does not imply, even in the absence of a specific statement, that such names are exempt from the relevant protective laws and regulations and therefore free for general use.

The publishers, the authors and the editors are safe to assume that the advice and information in this publication are believed to be true and accurate at the date of publication. Neither the publishers nor the authors or the editors give a warranty, express or implied, with respect to the material contained herein or for any errors or omissions that may have been made. The publishers remains neutral with regard to jurisdictional claims in published maps and institutional affiliations.

*Cover Design:* J. P. Morrissey

*Cover Image:* J. P. Morrissey



## PREFACE

This volume contains the extended abstracts of the **11th International Conference on Conveying and Handling of Particulate Solids (CHoPS)** which was held in Edinburgh UK on 2<sup>nd</sup> – 4<sup>th</sup> September 2024.

CHoPS 2024 builds upon the successes of the previous conferences in bringing together academic and industrial colleagues working in the multidisciplinary fields of handling and processing of particulate solids and particle technology.

The Conference presents an excellent forum for the exchange of technical expertise and scientific findings with a strong participation from both academia and industry. The conference programme featured more than 190 technical presentations including five plenary and ten keynote lectures.

The CHoPS 2024 conference is organised around **method-specific** and **application-specific** themes. We strive to achieve a balance between applications and scientific methods as well as integrating industrial case studies alongside fundamental research within each theme. The fully subscribed technical programme delivers a wide range of high-quality papers comprehensively covering the conference themes. These include the classical themes as well as new and emerging fields of research addressing the challenges in energy and sustainability.

The conference also hosted the final TUSAIL Symposium which was integrated within the conference programme to allow key findings to be disseminated to the relevant communities. **TUSAIL** (Training in Upscaling particle Systems: Advancing Industry across Length-scales) is a doctoral training consortium funded under the EU *Marie Skłodowska-Curie* Actions (Grant agreement No. 955661). The Early-Stage Researchers are in the final year of their PhD programme and the Symposium provides a great opportunity for them to disseminate the key findings of their work to the community.

On behalf of the Organising Committee and the CHoPS International Scientific Committee, we thank all the authors for their contributions to an excellent technical programme as can be seen in this conference proceedings, and all the conference participants, many of whom have travelled far from around the world to be at this event in the beautiful city of Edinburgh and Scotland.

*CHoPS 2024 Conference Chair*

**Prof. Jin Y. Ooi**

*Institute for Infrastructure and Environment, School of Engineering,  
The University of Edinburgh, Edinburgh, Scotland, U.K.*



## ORGANISING COMMITTEE

**Jin Ooi**, *University of Edinburgh, UK*  
**J.P. Morrissey**, *University of Edinburgh, UK*  
**Kevin Hanley**, *University of Edinburgh, UK*  
**Stefanos Papanicolopoulos**, *University of Edinburgh, UK*  
**Deborah Stitt**, *University of Edinburgh, UK*  
**Vivek Garg**, *University of Greenwich, UK*  
**Prashant Gupta**, *Procter & Gamble, UK*  
**Colin Hare**, *Newcastle University, UK*  
**Ali Hassanpour**, *University of Leeds, UK*  
**Jerry Heng**, *Imperial College London, UK*  
**Carlos Labra**, *Altair, UK*  
**Eddie McGee**, *Ajax Equipment Ltd., UK*  
**Don McGlinchey**, *Glasgow Caledonian University, UK*  
**Raffaella Ocone**, *Heriot-Watt University, UK*  
**Amalia Thomas**, *Freeman Technology, UK*  
**Kit Windows-Yule**, *University of Birmingham, UK*  
**Chuan-Yu (Charley) Wu**, *University of Surrey, UK*

## INTERNATIONAL SCIENTIFIC COMMITTEE

<b>Michael Bradley</b> , <i>University of Greenwich, UK</i>	<b>Stefan Luding</b> , <i>University of Twente, Netherlands</i>
<b>Vijay K. Agarwal</b> , <i>Indian Institute of Technology Delhi, India</i>	<b>Don McGlinchey</b> , <i>Glasgow Caledonian University, UK</i>
<b>Diego Barletta</b> , <i>University of Salerno, Italy</i>	<b>Vadim Mizonov</b> , <i>Ivanovo University, Russia</i>
<b>Tim Bell</b> , <i>Consultant, retired from DuPont, USA</i>	<b>Koichiro Ogata</b> , <i>National Institute of Technology, Japan</i>
<b>Giuseppe Bonifazi</b> , <i>Sapienza Università di Roma, Italy</i>	<b>Tomasz Olejnik</b> , <i>Lodz University of Technology, Poland</i>
<b>Thierry Destoop</b> , <i>Neu Process, France</i>	<b>Massimo Poletto</b> , <i>University of Salerno, Italy</i>
<b>Hermann Feise</b> , <i>BASF, Germany</i>	<b>Alvaro Ramirez</b> , <i>Universidad Politécnica de Madrid, Spain</i>
<b>Janos Gyenis</b> , <i>University of Pannonia, Hungary</i>	<b>Agba Salman</b> , <i>University of Sheffield, UK</i>
<b>David Hastie</b> , <i>University of Wollongong, Australia</i>	<b>Hans Schneider</b> , <i>Zeppelin GmbH, Germany</i>
<b>Mark Jones</b> , <i>University of Newcastle, Australia</i>	<b>Amos Ullmann</b> , <i>Tel Aviv University, Israel</i>
<b>Haim Kalman</b> , <i>Ben Gurion University, Israel</i>	<b>Pavel Vlasak</b> , <i>The Czech Academy of Sciences, Czech Republic</i>
<b>George Klinzing</b> , <i>University of Pittsburg, USA</i>	<b>Jin Ooi</b> , <i>University of Edinburgh, UK</i>
<b>Avi Levy</b> , <i>Ben Gurion University, Israel</i>	



# Contents

<b>Preface</b>	<b>ii</b>
<b>Organising Committee</b>	<b>iii</b>
<b>International Scientific Committee</b>	<b>iii</b>
<b>1 Plenary Lectures</b>	<b>1</b>
Particle technology as a key enabler for sustainable high performance batteries and their recycling . . .	2
The high cost of performance and structural failures of silos and their transfer systems . . . . .	4
Linking particle scale interactions to bulk behaviour: a geomechanics perspective . . . . .	6
Industrial Solids Processing from Discovery Through the Valley of Death to Consistent Production. . . . Why is This so Hard? . . . . .	8
Predicting the performance of particulate products: linking process and performance models . . . . .	9
<b>2 Keynote Lectures</b>	<b>10</b>
Strategies for Particulate Systems Design in Formulated Products . . . . .	11
GrainDB: Making experimental measurements FAIR . . . . .	13
Temporal and spatial scaling of granular flow by NN-based DEM surrogate model and coarse-graining DEM model . . . . .	14
Expediting Fluidized Bed Scale-Up for Sustainability Challenges . . . . .	15
Numerical investigation of multidimensional particle fractionation in microchannels . . . . .	16
Measurement of Flowability and Layer Spreadability of Polymeric Powders for Powder Bed Fusion Processes at Ambient and Process Conditions . . . . .	17
Granular and photoelastic avalanches . . . . .	18
Present and Future of Computer Modelling in Particle Technology: From Academia to Industry . . . . .	19
Upscaling granular solids and flows . . . . .	19
Maritime bulk material safety in remote operations: Practicalities in delivering Science to Ship loading Operations . . . . .	19
<b>3 Extended Abstracts</b>	<b>20</b>
Beyond the Beverloo Equation: Prediction of Solids Discharge Rates from Hoppers . . . . .	21
The Value of Experience . . . . .	23
Industrial Needs in Solids Flow - A 25 Year Retrospective . . . . .	25
Evaluation of Segregation of Pharmaceutical Formulations in Direct Compression Process . . . . .	27
Effects of Electrostatic Charge on Particle Adhesion and its Influences on Powder Flow Properties . . . . .	29
Model predictive control simulation of pneumatic conveying of plastic pellets using nonlinear dynamics analysis and sparse identification of nonlinear dynamics with control . . . . .	31
On the effect of Powder Cohesion on the location of Geldart Group A to Group C Fluidisation boundaries	33
Application of Machine Learning to Granular Systems and Processes . . . . .	35
Exploring predictive laws for the flowability of powder mixtures: the case of UO <sub>2</sub> powder . . . . .	37
Machine Learning for the Calibration of Discrete Element Method Simulations . . . . .	39
Insights from DEM Simulations for Shear Cell Experiments with Wooden Spheres . . . . .	41
Study of the infiltration of non-spherical slurry particles in a sand stratum during slurry shield tunnelling by CFD-DEM simulations . . . . .	43
Terminal Velocity and Drag Coefficient of Falling Particles in Newtonian Fluids . . . . .	45
Acceleration and Acceleration Length of Falling Particles in Newtonian Fluids . . . . .	47
Applying DEM-CFD coarse graining strategies to fluidized particle systems with geometrical constrictions	49



Drying Dynamics of Acoustically Levitated Wet Porous Agglomerates: Incorporating Nonisothermal Absorption Effects . . . . .	51
Study on Density Segregation under Vertical Vibration-Mechanism of Inverse and Sandwich Segregations- . . . . .	53
Quantifying cohesive, frictional and interlocking effects for universal powder flow characterisation . .	55
A robust indicator for the dense to dilute phase transition under horizontal moving bed flow during Fluidized Dense phase Conveying (FDC) of Geldart A powders by Eulerian modelling . . . . .	57
Intra-Particle Stresses: Insights into SAG Mill Mechanics . . . . .	59
3D Reconstruction and Morphological Characterization of Falling Non-Spherical Particles . . . . .	61
Deep learning-based measurements of segregation of iron ore pellets, sinter and coke . . . . .	63
Comparing Aspherix against open-source DEM frameworks for simulations of common bulk processes .	65
A DEM-FEM coupling approach to model wheel loader bucket loading . . . . .	67
An investigation into pneumatic conveying characteristics of carbon granules in low velocity slug flow .	69
Simulating particle-structure interaction with MercuryDPM . . . . .	71
On the Difference in Pneumatic Conveying Properties of the Same Product from Different Manufacturers; a Case Study Based on Quicklime . . . . .	73
Influence of non-isothermal sorption processes on evaporation of acoustically levitated slurry droplet .	75
Evaluating the sustainability of competing granulation technologies . . . . .	77
Food Phantom Packaging: Prolonging Product Shelf life via Microstructure Engineering of Tableted Granular and Powdered Consumer Foods . . . . .	79
Laboratory evaluation of wear properties for targeted application of wear-resistant liners through first principles calculations and DEM simulations . . . . .	81
An Experimental Investigation into Sifting and Fluidisation Segregation Characteristics for Coal Fly Ash	83
A robotic solution for autonomous weighing of powder materials . . . . .	85
Simulation of UO <sub>2</sub> particles behavior in a powder rheometer . . . . .	88
Predictive Analysis for Ingredient Weighing Cycle Time in Manufacturing Industries . . . . .	90
3D graphical representation technique for complex-shape particles and DEM modelling . . . . .	92
A simulation model development for moisture migration in glass beads under oscillations . . . . .	95
Investigating the influence of ultrasonic waves on the wall friction of bulk solids . . . . .	97
Heat transfers in a flowing granular material: towards and efficient cooling for agrofood applications .	99
Evolution of Pore Geometry and Flow Properties of Polyhedral Particles Discharged From a Model Silo	101
Analysis and optimization of failures during transport and processing of Solid Alternative Fuels (SAFs) for combustion in a heating plant . . . . .	103
Liquid-gas flow around resolved densely-packed objects in CFDEMcoupling . . . . .	105
Design principles for composite wear liners with inserts . . . . .	107
RFID-based Early Failure Detection for Composite Idler Rollers for Belt Conveyors . . . . .	109
Design and simulation of a powder feeding system for LP-DED process under zero gravity . . . . .	111
the effect of heat transfer on small particle moving pattern in static bulk liquid . . . . .	113
Simulation and validation of a highly cohesive paste inside a storage bin . . . . .	115
Alternative Measures in DEM Calibration of Cohesive Materials via Angle of Repose Test . . . . .	117
Investigating the Impact of Bubble Explosion on Particle Size Variation in Single Droplet Drying Processes	119
Hydrodynamic and Heat Transfer Investigation of A Fluidised Bed Solar Receiver . . . . .	121
Electrostatic removal of CaCO <sub>3</sub> particles using dielectric barrier discharge . . . . .	123
The future - CO <sub>2</sub> Absorption (Carbonation) and Bulk Materials Handling . . . . .	125
Heat transfer augmentation in horizontal dilute-phase pneumatic conveying . . . . .	127
Application of Principal Component Analysis (PCA) and Regression with Lagged Variables to Identify the Effect of Blower Speed and Feed Rate in Pneumatic Conveying . . . . .	129



Quantifying Variability in Wall Friction Measurements – An EFCE Supported International Study . . . .	131
Verification of the Contact Mechanics Calculation of Superquadrics in the Discrete-Element-Method . .	133
Integration of Spectroscopic Techniques and Machine Learning for Predictive Characterisation of Coal Tailings . . . . .	135
Predicting Powder Flow from Containers with Flexible Walls . . . . .	137
Investigating the effect of agitator dynamics on the twin-screw feeder performance for pharmaceutical powders . . . . .	139
Ultrafine Air-Classification of Plant based Proteins: A Step Towards Reducing Carbon Footprints . . . .	141
Particle levitation by ultrasound for on-orbit powder-based additive manufacturing . . . . .	143
Investigating Pellet Durability in Storage and Pneumatic Conveying Systems . . . . .	145
Compression behaviour of elastic-plastic microparticles sedimented in a centrifugal field: Experiments and CFD-DEM simulations . . . . .	147
Microdynamic Flowability to Characterize Die-filling Processes . . . . .	149
DEM simulation comparative study of train wheel abrasive wear . . . . .	151
Experimental investigation of the fracture characteristics of bicomponent agglomerates using in-situ X-ray tomography . . . . .	153
Modelling of metallurgical coke breakage to examine the influence of the pore structure using X-ray computed tomography and discrete element method (DEM) . . . . .	155
CFD-DEM Simulation Validation of Metal Powder Conveying in Thin Pipes . . . . .	157
On the Convergent Flow Property Behaviour of Different Fine Dry Powders Across Wide Size Ranges, and the Concept of Critical Particle Size . . . . .	159
Modelling and optimization of scrap flows for on-demand metal recycling . . . . .	161
Development of DEM Particle Trajectory Surrogate Model for Mixing Predictions Using Machine Learning	163
<b>4 TUSAIL Symposium</b>	<b>165</b>
Strategies for CFD–DEM modelling of plug flow pneumatic conveying using meso-scale particles . . . .	166
A hybrid discrete-continuum method for simulating particle laden flows . . . . .	168
Coupled CFD-DEM and PBM framework for Wet Stirred Media Milling . . . . .	170
Influence of particle shape on macroscopic rotational properties during shearing . . . . .	172
Upscaling mixing in rotating drum simulations . . . . .	174
Mixed discrete-continuum modelling of dense granular flow . . . . .	176
Coarse-grained DEM simulations of wet granulation in a rotating drum . . . . .	178
A Multi-Regime Continuum Model with Application to Powder Dosing . . . . .	180
Effect of coarse-graining on simulated powder flow properties . . . . .	182
CFD-DEM-PBM based parametric study on an opposed jet mill . . . . .	184
Flowability assessment of weakly consolidated fine powders . . . . .	186
An experimental and modelling investigation of solid state sintering using X-ray tomography and DEM- based elasto-plastic adhesive model . . . . .	188
<b>5 Abstracts</b>	<b>189</b>
A review of triboelectrification and electrostatic charge measurement techniques - promises and chal- lenges . . . . .	190
Hard Modeling of Raman spectra for coating endpoint detection in a titanium dioxide-free pharma- ceutical coating process . . . . .	191
Effect of Relative Humidity and Temperature on Particle Adhesion Using MSET . . . . .	192
Particulate emission control in port operations . . . . .	193



Dynamic granular flow in a continuous blender: GPU-based DEM simulation and Positron Emission Particle Tracking (PEPT) experimental validation . . . . .	194
Flowability and processability of reactive particles . . . . .	195
Ensuring reliable feed of shredded biomass to a pyrolysis system . . . . .	196
Computationally efficient boundary representation for the particle-scale simulation of filtration . . . . .	197
The role of machine learning for intelligent digital twins of fluidized beds . . . . .	198
The Behaviour of Rotating Intruders in Dense Granular Beds . . . . .	199
Scaling of battery slurry mixing processes using CFD . . . . .	200
Thermo-mechanical characterization of polymer powders via powder-pocket DMA and shear cell measurements . . . . .	201
Comparing open-source DEM frameworks for simulations of common bulk processes . . . . .	202
Development of a Hybrid Model for battery electrode production with a physics-inspired data-driven approach . . . . .	203
Contact Electrification of Rough Particles in Particle-Laden Flows . . . . .	204
DEM analysis of compression process of cohesive elastoplastic powder . . . . .	205
Leveraging a DEM Solids Database for Material Bulk Calibration: Analysis of the Database . . . . .	206
Enhancing Recycling Efficiency of Residual Refractory Materials: Experimental Methods and Fine Particle Classification Techniques . . . . .	207
Modeling of Agglomeration Processes in Multi-Component Suspensions: Challenges and Data-Driven Solutions . . . . .	208
Industrial-Scale Bin Blending: Insights from DEM Simulations of Realistic Pharmaceutical Powders . . . . .	209
DEM Modeling of direct shear test using periodic boundary: Sample size, boundary conditions, and computation efficiency . . . . .	210
The second decade of DEM at BASF . . . . .	211
Calibrating the Bonded-Particle Model for coated tablets in order to investigate the occurrence of chipping defects during coating processes . . . . .	212
Optimisation of Overland Conveyor Systems using Large Diameter Idler Rolls . . . . .	213
Characterizing sulfur/porous-carbon composite particles prepared from the hot-melt kneading process for all-solid state batteries . . . . .	214
Influence of surface modifications on bulk solids properties of powders for concrete 3D-printing . . . . .	215
Introduction to the ON-DEM COST Action . . . . .	216
Development of a model for die filling under suction for different scales and setups of rotary tablet presses . . . . .	217
Dry What? Dry Water: Bulk Properties and Mechanical Stability . . . . .	218
Decoding Attractive Interactions in Granular Materials through Vibration-Induced Densification . . . . .	219
Dead zones aren't dead: state of the art and a model concept for eccentric discharge . . . . .	220
Pneumatic conveying of irregular solids: experimental study and CFD-DEM simulation at pilot scale . . . . .	221
A novel experimental setup to study powder spreading with a wide range of process conditions . . . . .	222
DEM modelling of the effect of particle shapes on packing behaviours and their resistances to plate penetrations . . . . .	223
Estimate of solids rate in air-impeded silo discharge with a novel calculation procedure . . . . .	224
Characterizing the mixing quality of nanoscale hetero-aggregates by TEM-EDX image analysis . . . . .	225
Numerical and Experimental Investigation of Sodium Borohydride as Circular Fuel for Marine Vessels . . . . .	226
Taking One-Way Coupled CFD-DEM to the Next Level . . . . .	227
Make measurable that which is not: How to deal with terrible samples in powder flow measurements . . . . .	228
Production and powder properties of nanoparticle coated metal particles for additive manufacturing . . . . .	229

Investigating the effect of temperature on powder spreading behaviour in powder bed fusion additive manufacturing process by Discrete Element Method . . . . .	230
Modelling of Parameters of Resonant Acoustic Mixer . . . . .	231
From solid to powder- Multilevel approach of coffee bean and powder characterization . . . . .	232
Development of a Process Control Strategy for Continuous Aqueous Two-Phase Flotation (ATPF) . . . .	233
Influence of viscous liquid bridges on wet particle dynamics in DEM simulations . . . . .	234
Particle interactions in the submicrometer range - A combined colloidal probe AFM and capillary rise approach . . . . .	235
Dynamics of model cohesive granular materials in a rotating drum . . . . .	236
Cohesion of ice powders at very low temperatures . . . . .	237
Relation between the powder layer quality and the GranuDrum Dynamic Cohesive Index for polymeric powders at SLS process temperatures . . . . .	238
DEM Simulation of the Fundamental Response of Multi-disperse Granular Materials to Applied Vibration	239
Understanding the effect of permeability on tablet manufacturing . . . . .	240
Effect of particle properties on stable/unstable flow on powder discharge and pneumatic conveying using fluidization . . . . .	241
Influence of the implementation method of liquid bridge force model on DEM simulation results of wet powder behavior . . . . .	242
Extreme electrostatic charge peaks in powder processing . . . . .	243
Optimizing Continuous Pharmaceutical Blending through Advanced AI / ML Techniques. . . . .	244
Computational analysis of the tribocharging and electrostatic behaviour of polarisable particles in fluidised beds . . . . .	245
Simulation of the moisture and temperature dynamics in electromagnetic field assisted drying of particles in fluidised beds . . . . .	246
Toward a Best Practice for DEM Calibration: Learnings from 5 years working with industrial DEM users	247
Reaching below the Surface: Breaking the Boundaries of Granular Locomotion . . . . .	248
Enhancing Concentrated Solar Power Plant Efficiency: A Comparative Study of Flowability and Heat Transfer Properties of Non-Spherical and Spherical Bauxite Particles . . . . .	249
Surrogate and transformer models for particulate process modelling . . . . .	250
Characterization of the Heat Sealing Process Based on the Heat-Seal Strength of Pharmaceutical Blister Packages . . . . .	251
Microdosing: Small-scale powder handling to create 3D property gradients . . . . .	252
Effect of particle size, shape and density differences on binary mixture segregation during blast furnace charging . . . . .	253
A world of pure imagination? Understanding the dynamics of Vertical Stirred Mills within chocolate processing . . . . .	254
Transient particulate flow statistics: between static and dynamic . . . . .	255
The Effect of High Process Temperature on the Flow Behaviour of Zeolite Powders . . . . .	256
Modelling the Breakage Behaviour of Irregular Particles with Varied Contact Curvature and Area . . .	257
Parallel Discrete Element Method Software for Heterogeneous Shared- and Distributed-Memory Architectures . . . . .	258
The effect of particle size distribution on the behaviour of assemblies of spheres under generalised stress condition - A comparison of results between two different open-source DEM codes. . . . .	259
On the role of numerical calibration in setting up real-time recurrence CFD (rCFD) simulations of single- and multiphase flows . . . . .	260
Modelling hydrodynamic lubrication using DEM . . . . .	261



Revolutionizing the generation and reconstruction of particle models using advanced AI-driven computational techniques . . . . .	262
Overcoming Crushing Challenges: DEM-MBD Simulation for Jaw Crusher Optimization . . . . .	263
Powder characterisation and analysing flow behaviour of metal powders during the dosing process in a 3D printing system . . . . .	264
One dimensionless number to rule the dimensionless performance characteristics of a cyclone . . . . .	265
Utilizing Machine Learning for Efficient Parameter Inference of Granular Material Simulations . . . . .	266
Journey to the CFD-DEM model of a cold plasma-assisted fluidized bed powder coating process . . . . .	267
Optimising the rheology of dense granular suspensions using DEM modelling and machine learning . . . . .	268
Timestep in DEM Modelling: Critical Component or Minor Detail? . . . . .	269
Effect of aspect ratio of ellipsoidal particles on mixing in vibrated packed bed using discrete element method . . . . .	270
A DEM bonding contact model for curved, heterogeneous fibers with bending and torsion . . . . .	271
DEM simulation of the compaction behaviour of compressible powders with a new elastic-plastic contact model . . . . .	272
Towards an Understanding of Tablet Bonding Fundamentals . . . . .	273
Characterisation of the breakage behaviour of multi-component systems . . . . .	274
Process design in planetary roller melt granulation . . . . .	275
A multi-scale study of the dissolution process of wet soybean meal based on the three-phase Euler model	276
Assessing dry powder coating in a pilot-scale ribbon mixer . . . . .	277
Exploration of segregation in large size ratio two-sized vibrated systems using DEM . . . . .	278
Quasistatic response in DEM versus size, boundary conditions, and other numerical parameters. . . . .	279
Micromechanical Differences Between Spherical and Ellipsoidal Representations of Sand Particles in Direct Shear Testing . . . . .	280
Simulating the Abrasion of Arbitrarily Shaped Particles in DEM . . . . .	281

<b>Author Index</b>	<b>283</b>
---------------------	------------

# 1 PLENARY LECTURES

# Particle technology as a key enabler for sustainable high performance batteries and their recycling

Arno Kwade<sup>1,2</sup>, Tim Grenda<sup>1,2</sup>, Alexander Diener<sup>1,2</sup>, Marcella Horst<sup>1,2</sup>, Franziska Beverborg<sup>1,2</sup>, Caroline Willuhn<sup>1,2</sup>, Marco Ahuis<sup>1,2</sup>, Finn Frankenberg<sup>1,2</sup> and Peter Michalowski<sup>1,2</sup>

<sup>1</sup> Institute for Particle Technology, TU Braunschweig, Germany

<sup>2</sup> Battery LabFactory Braunschweig, TU Braunschweig, Germany

**Abstract**—Along the circular battery process chain, from recycling of end-of-life batteries over (re-)synthesis of the cathode and anode materials to the production of the electrodes and cells, particle technology plays an important role. Within the recycling of lithium-ion batteries, comminution, classification and separation processes are decisive to recover almost 100% of the so-called black powder mass out of cathode and anode materials before the hydrometallurgical treatment. Based on the gained secondary as well as primary materials, particulate active materials have to be synthesized and functionalized or, in case of graphite, tailored. For the production of lithium-ion battery electrodes, the active material particles like graphite (for anode) and lithium metal oxides (for cathode) have to be mixed dry and today subsequently usually wet in an appropriate solvent together with a conductive agent (e.g. carbon black) and a binder to produce a homogenous and well dispersed slurry. The electrode slurry is coated on a thin metal foil, is dried to a porous film and is densified (calendered) between two rollers to produce the electrodes, from which in further process steps the battery cells are built. The cell performance is determined by the material itself and very strongly by the electrode structure, which depends very much on the processing of the different particles (material-process-structure-performance relations). Today, the ecological footprint of cell production is supposed to be enhanced by dry mixing, particle structuring and coating to avoid wet coating and, thus, expensive drying. The dry processing is even more valuable for the production of so-called solid state batteries with particulate electrolytes.

**Keywords:** lithium-ion-batteries, battery recycling, electrode production, electrode structure dry film coating

## 1. Introduction

A major task achieving a sustainable electro mobility is the energy efficient production and recycling of batteries as well as the circular usage of the materials [1]. Today lithium-ion batteries (LIB) with liquid electrolyte are very dominant, but in the future other battery types as solid state batteries (SSB) can get superior. For the LIB the active material particles (graphite on anode side and lithium metal oxides on cathode side) have to be mixed with conductive additives (carbon black, CNT) and a binder to achieve a stable electrode film. For LIB, by applying a high intensity dry mixing process in advance of wet dispersing the material mixture, the carbon black can be well structured and a short wet dispersing process can be achieved [2]. However, more and more a fully dry production of electrodes comes into focus.

In the future particle technology will also gain much importance for the design and production of all solid state batteries, especially based on sulfides. An effective way to produce the sulfide solid electrolytes is a mechanochemical synthesis in high energy mills. Moreover, the sulfide solid electrolytes have to be structured with cathode material particles and conductivity

additives like carbon black in a way, that maximum ionic and electronic conductivities are achieved at a maximum cathode material content.

## 2. Wet electrode production

For the wet electrode production, the mixing and dispersing of the particulate electrode components and the densification by calendaring is very decisive for the electrode structure and by that for the later cell performance. The importance of Particle Technology will be displayed by two examples. At first, the dispersing of the conductive additives as carbon black is important, which dispersing state can be described either by the additives particle size distribution, e.g. by the so-called dispersing index which describes the surface of the aggregates related to the one of the agglomerates, or by the internal porosity of the carbon black. By applying the appropriate stress intensity in the high intensity mixing step an optimum specific capacity at high C-rates can be achieved. However, the dispersing process also determines the compaction properties of the coatings. All the different processes can be described by using DEM-based simulations.

## 3. Dry electrode production

Today, the wet coating process of electrodes is intended to be changed to a fully dry process. For this process the dry mixing and dry film formation, e.g. between rolls, is very decisive for the later cell performance. It will be shown, that the mixing strategy is determining not only the later cell performance, but also the ability to form a homogeneous film between the rollers. For mixing and pre-granulation beside high intensity mixers also extruders can be applied. The thickness of the dry film is determined as known for dry roller granulation by the friction properties, but can nicely be adjusted by the roller speed difference. Additional Considerations

## 4. Battery recycling

The recycling of the production scrap as well as of end-of-life battery cells requires as a rule mechanical processes as comminution, classification and sorting [3]. In order to gain above 95% of the cathode materials, after shredding the cells the cathode materials have to be de-coated from the metal foils and afterwards separated from the other material components. Thereby, it is very difficult to get more than 95% back without thermal treatment. Measures to achieve a good recycling yield are discussed.

## 5. Outlook - solid state batteries

Even higher energy densities are predicted for so-called solid state batteries. Beside homogeneous polymers or polymer based composites as solid electrolyte sulphide and oxide particles can be used. Especially, sulphides gain high attentions due to their superior ionic conductivities. For a good performance the particles sizes of the different components (active material, solid electrolyte, conductive additive) must be optimized. Moreover, the particles must be mixed very homogeneous what is relatively



difficult due to high cohesiveness of the different powders. It will be shown how high intensity mixing or milling can provide sufficient ionic conductivities of the solid state cathodes and that the stress intensity of the mixing or comminution process is decisive for the later performance. Moreover, the recycling of SSB battery cells requires new, more sophisticated recycling processes [4].

## 6. Conclusion

Within the oral presentation some examples will be presented which show the importance of particle technology for the battery technology. Especially, deep knowledge on material-process-structure-performance relationships are basis for high performance battery cells. This will become even more obvious and important for solid state batteries with dry particulate electrolytes. Moreover, the recycling of battery production scrap as well as of end-of-life batteries relies very much on mechanical processes before metallurgical treatment of the materials. Therefore, particle technology can be an enabler for future high performance batteries.

## Acknowledgement

The financial support by the German federal ministry of education and research is strongly acknowledged.

## References

- [1] A. Kwade, W. Haselrieder, R. Leithoff, A. Modlinger, F. Dietrich, K. Droeder (2018) Current status and challenges for automotive battery production technologies, *Nature Energy* 3 (4), pp. 290
- [2] H. Bockholt, W. Haselrieder, A. Kwade (2016) Intensive powder mixing for dry dispersing of carbon black and its relevance for lithium-ion battery cathodes. *Powder Technology* 297, pp. 266-274
- [3] C. Sangrós Giménez, B. Finke, C. Nowak, C. Schilde, A. Kwade (2018) Structural and mechanical characterization of lithium-ion battery electrodes via DEM simulations, *Advanced Powder Technology* 29 (10), pp. 2312-2321. DOI: 10.1016/j.appt.2018.05.014
- [4] S. Doose, J. Mayer, P. Michalowski, A. Kwade (2021) Challenges in Ecofriendly Battery Recycling and Closed Material Cycles: A Perspective on Future Lithium Battery Generations. *Metals* 11, 291; 10.3390/met11020291
- [5] L. Froböse, J. F. van der Sichel, T. Loellhoeffel, L. Helmers, A. Kwade (2019) Effect of microstructure on the ionic conductivity of an all solid-state battery electrode, *Journal of Electrochemical Society*, Volume 166, Issue 2, pp. A318-A328. DOI: [10.1149/2.0601902jes](https://doi.org/10.1149/2.0601902jes)
- [6] M. Ahuis, S. Doose, D. Vogt, P. Michalowski, S. Zellmer, A. Kwade (2024) Recycling of solid-state batteries, *Nature Energy* 9(4), pp. 373–385. DOI: [10.1038/s41560-024-01463-4](https://doi.org/10.1038/s41560-024-01463-4)

# The high cost of performance and structural failures of silos and their transfer systems

John Carson Ph.D.

Jenike & Johanson, Inc., Tyngsboro, MA, USA

**Abstract—** Performance and structural failures of bulk solids handling systems such as silos and transfer systems are far too common. As Merrow pointed out some 40 years ago, the problem is the result of the field of bulk solids handling not being well understood. Three examples illustrate the high cost of such failures. What needs to be done to correct this situation is described.

**Keywords:** silos, transfer systems, structural failures, performance failures

## 1. Introduction

Some years ago, a survey found that nearly 80% of the products sold by one of the world's largest chemical companies was sold in particulate form or had particulate additives. [1] As a result, reliable handling of bulk solids is a critical process step in that industry as it is with most other industries around the world.

Merrow [2] showed that, since the field of bulk solids handling is not well understood, startup of new plants handling raw bulk solids is, on average, three to four times longer than plants that use liquid or gas as the feedstock. Furthermore, even well after startup, the operating capacity as a percentage of design for plants handling bulk solids is often 10 to 20% lower than plants that use only gas or liquids.

When a process or structural failure occurs at an industrial facility, the cost is often very high: lost sales and profit, production delays, extra labor, wasted capital, serious injury including death, lost market share, litigation and more.

## 2. Examples of process and structural failures

Following are three examples of process and structural failures of plants handling bulk solids. Many more examples can be found in the literature [3].

### 2.1 Ravensthorpe Nickel Operation

The technology employed in this plant in Western Australia was the first of its kind: combined pressurized acid leach and atmospheric leach. The study phase lasted seven years and included standard pre-feasibility and feasibility stages. Salient features/achievements included:

- USD 85 million Front End Loading study,
- 200,000 engineering-hours,
- Eight months continuous pilot plant operation,
- Evaluation of ore blends covering Life of Mine (20y),
- Five independent technical reviews, and
- Detailed mine planning.

The approved capital cost was USD 1.04 billion with a planned production capacity of 50,000 tonnes/yr.

Startup occurred 18 months after it was scheduled. After several years of working to make the plant operational, the cost had ballooned to USD 2.1 billion, a 110% overrun, but production was only 20% of design. At that point the owner decided to abandon the project resulting in the loss of 1,800 jobs and a book loss of USD 3.165 billion. The plant was eventually sold for USD 340 million. After 18 months of modifications, the new owner operated it profitably for about 10 years before closing it due to poor market conditions.

The cutting-edge transformational step performed exceptionally well, but the system was starved of feed due to front-end bulk solids handling problems. All the studies, engineering hours, pilot operations, ore evaluation, and reviews focused mainly on the new processes, not the fundamental solids flow.

### 2.2 Unique silo design

A supplier of steel silos developed a unique support system for large silos having a conical hopper and single, centered outlet. In order to better distribute loads on the silo foundation, the designer incorporated two sets of ring beams and support legs – one at the cylinder/hopper transition and another about halfway down the cone.

The new design consisting of a 14.55 m diameter cylinder with a 45° hopper was installed at two industrial facilities. The first installation consisted of two silos, each with a 17 m tall cylinder and a capacity to store 5,500 tonnes of sand. The second consisted of 15 silos, each with a 23 m tall cylinder and a capacity to store 3,500 tonnes of grain.

As one of the two silos at the first installation was being filled, an operator noticed bulging in the hopper just above the inner ring beam. He notified the silo supplier who stated that this was natural, so it was ok to continue filling. Within a few seconds after the silo was full and the discharge gate opened, the silo collapsed killing two workers who were under the silo. There was extensive property damage which delayed starting up the plant for many months. Eventually the owner decided to remove the undamaged silo and replace both silos with flat storage.

When the owner of the second facility learned of the silo collapse, he asked the silo supplier if the same thing could happen to his silos. The owner was assured that the design was sound. However, upon filling the first silo, operators again noticed bulging of the hopper just above the inner ring beam. Again, the answer was the same – ok to continue filling.

Soon after the silo was full and the gate opened, the silo collapsed. Fortunately, no one was under it so there were no injuries, but there was extensive property damage and major

disruption to plant operation. The owner decided to remove the undamaged silos and replace all 15 using a conventional design.

Clearly, the design of this silo was flawed. Upon investigation it was found that the designer used only a crude spreadsheet to analyze the structure's ability to resist material-induced loads. Such a complex structure should have been designed using Finite Element Analysis followed by independent review by a silo design expert.

### 2.3 ESKOM/Majuba

The state-owned power utility in South Africa, ESKOM, commissioned the first units in their six-unit coal-fired Majuba plant in 1996. The silos were designed in 1980s. One of several large silos collapsed in 2014 resulting in reduction in generating capacity from 4,100 MW to 600. This necessitated load shedding throughout country for weeks.

Upon investigation it was found that the silos were designed in accordance with an out-of-date, inadequate silo design code. Problems were compounded by continuous eccentric discharge that caused horizontal and vertical bending moments for which the silo was not designed. Non-symmetrical and excessive coal buildup also contributed to the problem.

## 3. Why do these problems continue to occur?

In 1955, two American psychologists, Joseph Luft and Harry Ingram, created a concept they called the "Johari Window Model" [4]. It illustrates the interaction between what is known by an individual compared to what is known by others. See Figure 1. Consider first the "Open Area". Here the information about the person, his attitudes, behaviour, emotions, feelings, skills and views, is known by the person as well as by others. This is mainly the area where good communications occur. Contrast this with the "Blind Spot" where information about an individual is known by others but the person is unaware of it.

This psychological concept can be applied to other areas of endeavor such as the design of industrial plants. Consider the science of hydrodynamics, which is well understood by most mechanical engineers. As a result, design of plants involving liquids can be described as an "Open Area".

A "Blind Spot" explains why problems such as those described above occur. Knowledge of how to avoid such problems is known but only by a relatively small group of individuals and institutions. Most designers, operators and managers of solids handling plants have little understanding of the technology and the problems that can occur if that technology is not used properly.

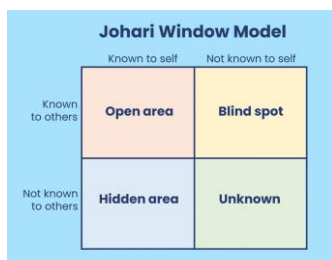


Fig. 1 Johari Window

Merrow concluded that performance problems in solids processing plants were caused by mechanical and physical

difficulties – not process chemistry. Such problems did not fit well into the way that oil and chemical industries evolved their R&D programs. As a result, industry tended to neglect this area, and government funding reflected this. He urged industries that use solids processing to change R&D priorities.

Forty years later the situation remains mostly unchanged. The reasons are many:

- Pressure to accelerate the study phase for a new plant. Remember, "haste makes waste".
- Failure to consider in the Basis of Design the materials through the life of the operation, not just their early life.
- Failure to recognize that bulk solids science is complex and not usually included in undergraduate engineering courses.
- Failure to recognize that, while they can quickly and effectively *destroy* value, bulk solids handling elements can *add* value by ensuring continuous, reliable, robust solids feed.

## 4. What needs to be done

It is essential that flow properties of site-specific bulk materials to be handled be measured over the full range of process conditions. These properties then need to inform the Basis of Design, which is the single source of truth for all ensuing design activities. One must avoid use of "library values" in an attempt to minimize effort and cost of testing. Caution must be exercised when pilot-scale work is conducted on material blends that cannot be practically replicated in the production environment.

Downstream blends as well as side and dosing streams must be included in the materials characterization program together with their upstream constituents. Finally, one must consider "dry" front ends in predominately "wet" processes.

## 5. Conclusion

Those of us who have knowledge in the field of bulk solids handling have an obligation to society to use every means at our disposal to stress the importance of bulk solids science. We must make decision makers aware of the risks that this blind spot poses as well as the best way to obtain the expertise required. We must insist that this science be respected and applied to all new projects and retrofits.

This field is future proof with little competition. There is no shortage of opportunities to advance the science and make a real difference in the world.

## References

- [1] R.D. Nelson, R. Davies, and K. Jacob, *Teach 'em particle technology*, Chemical Engineering Technology, p. 12-16, Winter 1995.
- [2] E.W. Merrow, (1986). *A quantitative assessment of R&D requirements for solids processing technology*, R-3216, RAND Corp., Santa Monica, CA, 1986.
- [3] J. W. Carson, *Silo failures: Case histories and lessons learned*, Handbook of Conveying and Handling of Particulate Solids, vol. 10, pp. 153-166, 2002.
- [4] J. Luft and H. Ingham, *The Johari window, a graphic model of interpersonal awareness*, Proceedings of the Western Training Laboratory in Group Development. Los Angeles, University of California, Los Angeles, 1955.



# Linking particle scale interactions to bulk behaviour: a geomechanics perspective

Catherine O'Sullivan<sup>1</sup>

<sup>1</sup> Imperial College London, London, UK

**Abstract—** Almost 50 years since the seminal publication outlining the discrete element method (DEM) by Cundall and Strack [1] in a geotechnical journal (*Géotechnique*), clear evidence is available to demonstrate the value of DEM simulations in advancing understanding of soil behaviour. Following an introductory overview of current research in geotechnical engineering, this presentation will focus on state, stiffness, and seepage. It will introduce key concepts, frameworks and correlations that are well-established in geotechnical engineering. At the same time, the presentation will show how DEM simulations can be applied to interrogate these accepted ideas to either provide a basis for their ongoing application in engineering practice, or highlight inherent limitations. The insight gained by analysis of DEM-generated data can be used to develop new approaches to test materials or to support the development of new technologies in the field (polymer support fluids).

**Keywords:** soil; sand; clay; DEM, CFD

## 1. Introduction

Geotechnical engineering is concerned with the interaction between new and existing structures and infrastructure and the surrounding ground, the design of geostructures, including dams and embankments, the mitigation of natural disasters including earthquakes and landslides. The complex behaviour of geomaterials including clay, silt, sand and rock, which are natural particulate materials, poses many challenges in geotechnical engineering. Research into soil properties and behaviour was consequently the most popular topic in geotechnical engineering research between 1998 and 2022 [2]. Conventional laboratory experiments in soil mechanics and geotechnical engineering provide significant insight, but the advent of DEM has transformed understanding of soil behaviour. This presentation will focus on three very fundamental concepts in geotechnical engineering. For each concept, the conventional (mostly empirical) understanding will be presented, and then the ability of DEM or high-resolution computational fluid dynamics (CFD) simulations to critically analyse this understanding will be demonstrated.

## 2. State

Within the frameworks of material behaviour accepted in soil mechanics, the initial state of the material a key determinant of the stress-strain or load-deformation behaviour of soil. The packing density is most often characterized in terms of the void ratio. The idea that soil attains a critical state upon shearing to large strain levels is a central concept. For a given sand, the critical state void ratio depends on the mean effective stress. Been and Jefferies [3] proposed linking the sand's current void ratio to the critical state void ratio to predict behaviour. However, the critical state framework, and other empirical frameworks to predict stand behaviour start to break down when the polydispersity of the material is large, particularly in the case of bi-modal mixtures of large and small particles. Recent DEM simulations have looked in detail at the way in which stress is transmitted in soil packings at rest to explain why empirical

frameworks based on void ratio as a measure of state cannot always be applied [4,5].

## 3. Stiffness

Soil, like any granular or particulate material, exhibits a highly non-linear load-deformation response and the material's elastic stiffness is only directly relevant for very small levels of deformation (e.g. [6]). However, the elastic stiffness plays a key role in site response during earthquakes and it is a reference point in calibrating constitutive models for continuum numerical analyses. Current practice in geotechnical engineering is to link this stiffness to void ratio via well-established empirical correlations (detailed in Mitchell and Soga [7]). However, it is clear these correlations are inherently limited (e.g. [8]), particularly in the case of mixtures of large and small particles. By advancing understanding importance of coordination number, and the nature of stress wave propagation in granular materials, DEM simulations can inform new approaches to identify the extent to which the finer particle are mechanically active in mixtures [9,10].

While the vast majority of DEM simulations in geomechanics have focussed on sand, DEM or coarse-grained molecular dynamics (CGMD) can also be applied to clay (e.g. [11]) with particle sizes of less than 10 micron. Assuming clay (kaolinite) particles behaviour can be approximated by DLVO theory with reasonably accuracy, CGMD simulations can be applied to look at the way in which surface charge anisotropy on individual clay platelets impacts upon the stiffness of the material response in compression [12,13]. Perhaps of more significance, CGMD simulations can also be used to advance understanding of the very large difference between the stiffness of normally consolidated clay (loaded for the first time) and over consolidated clay (that has previously experienced a larger stress) [14].

## 4. Seepage

Predicting and controlling the flow of water through soil is important in many applications. While coarse-grained coupled DEM-computational fluid dynamics simulations (CFD) simulations are now well established in the granular mechanics community their application in fundamental research may be hindered by the limited range of accuracy of the empirical drag coefficients. Experiments using Particle Image Velocimetry (PIV) have shown that fully resolved CFD simulations of flow in the pore space of real granular materials or in packings generated using DEM can provide an accurate picture of the real system [15]. These CFD simulations can then be used to interrogate less computationally expensive options for coupled DEM-fluid modelling. Pore network models (PNMs) present a viable alternative but their applicability to materials with low packing fractions that are encountered outside geomechanics may be limited [16,17]. Within geomechanics fully resolved CFD simulations coupled with PNM analyses and applied to DEM generated data can establish how permeability varies

during shear deformation; this information cannot be obtained in conventional laboratory experiments (Salomon et al. 2024).

Fully resolved CFD simulations of flow in the pore space can play an important role in understanding the penetration of polymer fluids in sand. Polymer fluids have the potential to significantly reduce the cost and the environmental impact of excavation support in underground urban construction. The mechanics of unsaturated soils, in which there is a mixture of air and water in the pore space, remains poorly understood and the presentation will conclude by demonstrating the potential of multi-phase high resolution CFD to study hysteresis in the response of sand to wetting and drying cycles.

## 5. Conclusion

Through focussing on state, stiffness and seepage, the presentation will introduce some of the ways in which geotechnical engineers predict and interpret the behaviour of soil. For each topic, both the general geotechnical perspective and details of recent research using DEM or CFD will be presented. The presentation will hopefully open a dialogue with CHoPS participants that will may lead to increased collaboration between the CHoPS community and geotechnical engineers.

## Acknowledgement

Funding for this research was provided by the MATHEGRAM Marie Curie ITN, EPSRC, and NERC.

## References

- [1] Cundall, P. A., and Strack, O. D. L. 1979. A discrete numerical model for granular assemblies, *Géotechnique*, Vol. 29, pp. 47–65.
- [2] Patino-Ramirez, F. and O'Sullivan, C (2024) Growth, trends and prevalent topics in geotechnical engineering (1998–2022) using topic modelling *Géotechnique Letters* 14 (1), 18-24 <https://doi.org/10.1680/jgele.23.00097>
- [3] Been, K. and Jefferies, M. G. 1985. A state parameter for sands, *Géotechnique*, Vol. 35, No. 2, pp. 99–112, <https://doi.org/10.1680/geot.1985.35.2.99>
- [4] Liu, D., O'Sullivan, C., Carraro, JAH (2021) The Influence of particle size distribution on the proportion of stress-transmitting particles and implications for measures of soil state *Journal of Geotechnical and Geoenvironmental Engineering* 147 (3), 04020182. [https://doi.org/10.1061/\(ASCE\)GT.1943-5606.0002466](https://doi.org/10.1061/(ASCE)GT.1943-5606.0002466)
- [5] Liu, D., O'Sullivan, C., Carraro, JAH (2023) The influence of particle size distribution on the stress distribution in granular materials *Géotechnique* 73 (3), 250-264 <https://doi.org/10.1680/jgeot.21.00127>
- [6] Jardine (1992) Some observations on the kinematic nature of soil stiffness *Soils and Foundations* 32 (2), 111-124 [https://doi.org/10.3208/sandf1972.32.2\\_111](https://doi.org/10.3208/sandf1972.32.2_111)
- [7] Mitchell, J.K. and Soga, K. (2005) *Fundamentals of Soil Behavior*, Third Edition. John Wiley & Sons, Hoboken, NJ, 577 0.
- [8] Liu, D., Morimoto, T., O'Sullivan, C., Carraro, JAH (2022a) A semi-empirical re-evaluation of the influence of state on elastic stiffness in granular materials *Granular Matter* 24 (2), 56 <https://doi.org/10.1007/s10035-022-01215-9>
- [9] Liu, D., Morimoto, T., O'Sullivan, C., Carraro, JAH (2022b) Use of combined static and dynamic testing to quantify the participation of particles in stress transmission *Journal of Geotechnical and Geoenvironmental Engineering* 148 (11), 04022100 [https://doi.org/10.1061/\(ASCE\)GT.1943-5606.0002902](https://doi.org/10.1061/(ASCE)GT.1943-5606.0002902)
- [10] Otsubo, M., Kuwano, R., O'Sullivan, C., Shire, T. (2022) Using geophysical data to quantify stress transmission in gap-graded granular materials *Géotechnique* 72 (7), 565-582 <https://doi.org/10.1680/jgeot.19.P.334>
- [11] Bandera, S., O'Sullivan, C., Tangney, P., and Angioletti-Uberti, S. (2021) Coarse-grained molecular dynamics simulations of clay compression *Computers and Geotechnics* 138, 104333 <https://doi.org/10.1016/j.compgeo.2021.104333>
- [12] Bandera, S., O'Sullivan, C., Tangney, P., Angioletti-Uberti, S. (2024) Composite ellipsoidal particles to simulate charge anisotropy in particle-scale simulations of kaolinite. *Géotechnique Letters* 14 (1), 1-8 <https://doi.org/10.1680/jgele.23.00085>
- [13] Nakamichi, Y., O'Sullivan, C., Tangney, P., Angioletti-Uberti, S. (2024) Modelling anisotropic surface charge of kaolinite particles depending on

- pore water pH *Computers and Geotechnics* 173, 106505 <https://doi.org/10.1016/j.compgeo.2024.106505>
- [14] Nakamichi, Y., O'Sullivan, C., Tangney, P., Angioletti-Uberti, S., Bandera, S. (2023) Isotropic compression simulation of kaolinite using coarse-grained molecular dynamics, *Proc. IS Porto, E3S Web of Conferences* 544, 07006
  - [15] Sanvitale, N., Zhao, BD, Bowman, ET, C O'Sullivan (2023) Particle-scale observation of seepage flow in granular soils using PIV and CFD *Géotechnique* 73 (1), 71-88 <https://doi.org/10.1680/jgeot.20.P.432>
  - [16] Morimoto, T. , Zhao, B., Taborda, DMG, O'Sullivan C. (2022) Critical appraisal of pore network models to simulate fluid flow through assemblies of spherical particles *Computers and Geotechnics* 150, 104900 9 <https://doi.org/10.1016/j.compgeo.2022.104900>
  - [17] Sufian, A., Knight, C., O'Sullivan, C, van Wachem, B., Dini, D. (2019) Ability of a pore network model to predict fluid flow and drag in saturated granular materials *Computers and Geotechnics* 110, 344-366 <https://doi.org/10.1016/j.compgeo.2019.02.007>
  - [18] Salomon, J., Morimoto, T., Patino-Ramirez, F., O'Sullivan, C. (2024) Quantifying Shear-Induced Permeability Changes in Medium-Loose Sands *Journal of Geotechnical and Geoenvironmental Engineering* 150 (2), 04023133 <https://doi.org/10.1061/JGGEFK.GTENG-11874>

## **Industrial Solids Processing from Discovery Through the Valley of Death to Consistent Production. . . Why is This so Hard?**

**Willie Hendrickson**

*AVEKA Group, Woodbury, USA*

### **Abstract**

As attendees at this conference, we are all aware that solids handling and processing can be challenging. Consistent outcomes can appear to be transient from day to day or from one piece of equipment to another. Great strides in understanding the fundamentals of particle processing have been made over the past 50 years, but all of us, academic and industrial practitioners, will have moments when we struggle. While getting consistent, publishable results in the lab can be a challenge, the problems of consistency, scale-up, and reproducibility in large scale processing with variations in ambient conditions (e.g. humidity), raw materials, and seemingly small process changes are vexing and require constant control and analysis.

This talk will present how industry approaches solids handling, uses engineering solutions to help with consistency, and what are some of the gaps in our understanding of the fundamentals of particle processing that would be helpful in full scale industrial processing. Examples and opportunities in blending, size separation, drying, and particle formation using polymer, food, and ceramic materials will be provided to illustrate these challenges. A discussion of Technology Readiness Levels (TRL) as it relates to the difficulty of transitioning lab discoveries into products will be made along with the criticality of knowing how to overcome the barriers to full-scale, consistent production. Finally, time will be spent during this presentation on the needs of industry in education and research and how academia and industry can best interact to both parties' advantage.

## Predicting the performance of particulate products: linking process and performance models

Rachel Smith

*The University of Sheffield, Sheffield, United Kingdom*

### Abstract

A primary aim of process model development is to understand the relationships between process parameters, material properties, and the properties of the products. For particulate manufacturing, products typically have essential required performance characteristics. For example, pharmaceutical products such as tablets and granules need to meet the desired dissolution and disintegration performance, strength and attrition resistance, and good stability. In the case of batteries, electrodes need to have the specified electro-chemical performance for the expected environmental conditions, along with other important characteristics such as cycling ability. Great progress on process model development has been made in recent years however to truly use models to design products with desired performance, we need to generate models which relate the *performance* of the products to *properties* of these products.

In this talk, two cases of product performance model development will be presented. In the first case, a new mathematical model which describes the swelling mechanism of disintegrating pharmaceutical granules is described. This mechanistic model considers important physical rate processes from liquid uptake to liquid absorption by the disintegrant particles and finally, swelling of the granule. Through these mechanisms, the model can predict changing granule size along with the porosity, saturation and size of the primary particles. The model is further parameterised and validated through individual granule experiments with formulations consisting of sodium starch glycolate as the superdisintegrant, microcrystalline cellulose as the filler and polyethylene glycol/water as the binder. To experimentally track the individual size of a granule, a bespoke flow cell was coupled with an optical microscope to capture the behaviour of a swelling granule quantified through an in-house image-based algorithm.

In the second case, current work within the Faraday Institution funded research project Nextrode is presented. Discrete Element Method (DEM) with a bonded particle model is used to investigate the evolution of electrode microstructure under varying calendaring conditions. DEM simulations of electrode calendaring are validated using X-ray tomographic data, and structural properties including porosity distribution and tortuosity factors are studied and compared with corresponding tomography scans. Additionally, the relationship between battery performance and microstructure is explored. By combining DEM simulation and electrochemical analysis, this work provides a promising method to quantitatively predict lithium-ion battery electrode performance, and presents a potential tool for electrode micro-structural design.



## 2 KEYNOTE LECTURES

# Strategies for Particulate Systems Design in Formulated Products

Martin de Juan, L.

Oral Product Development, Pharmaceutical Technology & Development, AstraZeneca, Gothenburg, Sweden

**Abstract**— Keynote lecture will provide some industrial perspective on the design and development of formulated particulate products such as pharmaceutical oral dose formulation or powder detergent formulations. Examples of current approaches, use of digital tools and challenges will be included in the discussion.

**Keywords:** particle; structure; design; process

## 1. Introduction

Particulate systems are fundamental to numerous industries, including pharmaceuticals, chemicals, biotechnology, metallurgy, ceramics, household goods, and food production. The design and optimization of these systems are crucial for ensuring product performance and cost-efficiency.

Industries dealing with particulate systems focus on three main areas:

**Product Design:** Engineering particle systems that meet specific performance criteria for various applications.

**Process Design:** Developing efficient processes to create particle systems with desired structures.

**Transport and Storage:** Ensuring the integrity, stability and dosing of the products from production to end user application.

The performance of particulate systems hinges on several core attributes:

**Dosing:** The flow properties and homogeneity of the product, essential for consistent application.

**Mass Transfer:** The dynamics of the product in its final application, including dissolution rates, controlled release, and reaction kinetics.

**Appearance:** Characteristics such as colour, shape, size distribution, and bulk density, which influence handling and user perception.

**Structural Integrity:** The ability to maintain the initial structure during handling and usage.

## 2. Particulate system structure at different scales

To manage particulate system attributes described previously, particulate product structure is defined at four scales [1]:

1. **Supramolecular:** The arrangement of molecules within a domain [2].
2. **Particle:** The organization of domains within a single particle.
3. **Mesoscale:** The spatial distribution of particles within a given volume.

4. **Macroscale:** The arrangement of particle volumes within unit operations.

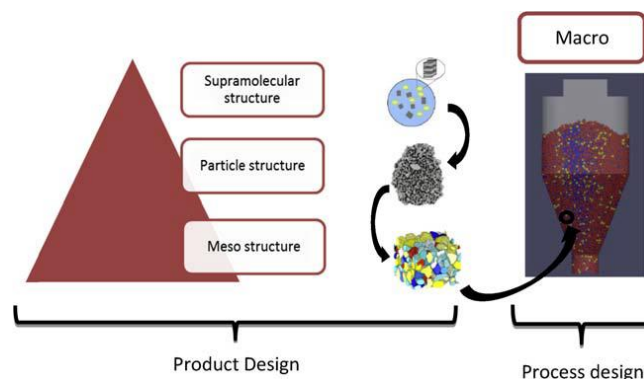


Figure 1. Particulate product structure [1].

## 3. Examples of particulate product design.

Examples of industry applications will be provided to demonstrate the manipulation of particle structures at these scales:

**Supramolecular Scale:** defining approaches to achieve desired functionality such as processability, stability and porosity via manipulation of supramolecular structure [3] [4].

**Particle Scale:** Use of process design and operating conditions to define particle properties: i) Decision trees in pharmaceutical industry [5]. ii) Application of coatings for controlled release [6] and enhanced stability, iii) Influence of particle structure on attrition [7], dosage [8] or dissolution [9]

• **Meso Scale:** Utilizing process aids to influence flowability [10], segregation, and compressibility [11] during processing and handling.

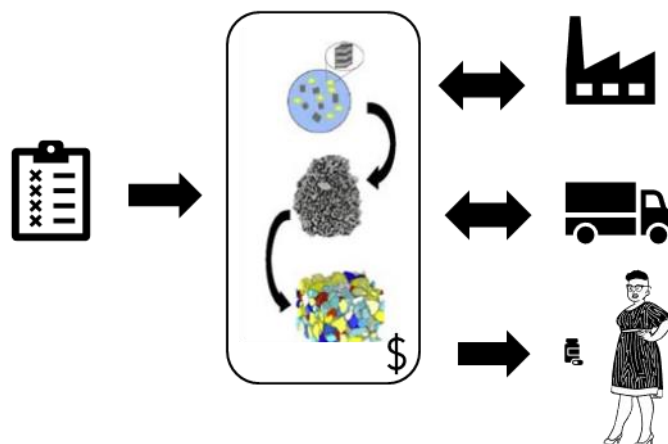


Figure 2. Interactions between particulate structure, manufacturing process, transport and storage and final application. Successful product structure needs to be “processable” and preserve critical quality attributes at the time of use. All of this subjected to financial boundaries.

Use of digital tools for designing and evaluating particulate structures, including end-to-end model networks will be

included highlighting current challenges and opportunities such as:

Detailed characterization of particulate structure at various scales.

Development of multiscale models to link properties across different structural levels.

Establishing process functions that relate operating conditions to particle structure.

Defining property functions for critical performance factors.

Creating optimization frameworks that incorporate process and property functions [12].

#### 4. Final remarks

Addressing these challenges requires interdisciplinary collaboration, involving expertise from chemical engineering, chemistry, physics, mechanical engineering, and more. A coordinated effort across industry and academia is essential to develop effective models and optimization procedures for particulate systems.

#### Acknowledgement

I would like to dedicate this work to the memory of Professor David W. York from the University of Leeds, who recently passed away. Dave was not only my mentor and the person who introduced me to this exciting world of particle technology but also a good friend.

#### References

- [1] Amador C., Martin de Juan L., 2019. Chapter 19 - Strategies for Structured Particulate Systems Design, *Computer Aided Chemical Engineering*, 39, 2016, 509-579.
- [2] Palzer, S., 2011. Agglomeration of pharmaceutical, detergent, chemical and food powders similarities and differences of materials and processes. *Powder Technology* 206, 2-17.
- [3] Moore H. A., Marucci M., Härdelin L., Hjærtstam J., Stading M., von Corswant C., Larsson A., 2018. New insights on the influence of manufacturing conditions and molecular weight on phase-separated films intended for controlled release, *International Journal of Pharmaceutics* 536, Issue 1, 261-271.
- [4] Ordoubadi M., Gregson F.K.A., Wang H., Nicholas M., Gracin S., Lechuga-Ballesteros D., Reid J.P., Finlay W.H., Vehring R., 2021. On the particle formation of leucine in spray drying of inhalable microparticles. *Int J Pharm.* 592, 120102.
- [5] Leane M., Pitt K., Reynolds G. R., Dawson N., Ziegler I., Szepes A., Crean A.M., Dall Agnol R. & The Manufacturing Classification System (MCS) Working Group, 2018. Manufacturing classification system in the real world: factors influencing manufacturing process choices for filed commercial oral solid dosage formulations, case studies from industry and considerations for continuous processing, *Pharmaceutical Development and Technology*, 23:10, 964-977
- [6] Marucci M, Ragnarsson G, von Corswant C, Welinder A, Jarke A, Iselau F, Axelsson A., 2011. Polymer leaching from film coating: effects on the coating transport properties. *Int J Pharm.* 411, 1-2, 43-8.
- [7] Bonakdar, T., Ghadiri, M., Ahmadian, H., Martin de Juan, L., Xu, D., Tantawy, H., Smith, D., 2016. Impact of attrition of spray dried burkeite particles. *Powder Technology* 304, 2-7.
- [8] Nguyen D., Rummelgas J., Niklasson Björn I., van Wachem B., Thalberg K., 2018. Towards quantitative prediction of the performance of dry powder inhalers by multi-scale simulations and experiments, *International Journal of Pharmaceutics*, Volume 547, Issues 1–2, 31-43.
- [9] Stepanek, F., Ansari, M.A., 2005. Computer simulation of granule microstructure formation. *Chemical Engineering Science* 60, 4019-4029.
- [10] Megarrry A.J., Swainson S.M.E., Roberts R.J., Reynolds G.K., 2019. A big data approach to pharmaceutical flow properties. *Int J Pharm.* 30. 555. 337-345
- [11] Reynolds G.K., Campbell J.I., Roberts R.J. 2017. A compressibility-based model for predicting the tensile strength of directly compressed pharmaceutical powder mixtures. *Int J Pharm.* 531, 1, 215-224

- [12] Ansari, M.A., Stepanek, F., 2006. Design of granule structure: computational methods and experimental realization. *AIChE Journal* 52, 11, 3762-3774.

## GrainDB: Making experimental measurements FAIR

John P. Morrissey

*University of Edinburgh, Edinburgh, United Kingdom*

### Abstract

FAIR Data Management is becoming an ever more important aspect within research. Generated datasets need to be findable and reusable so that they can help generate long-term impact and data repositories such as Edinburgh DataShare or Edinburgh DataStore are crucial in achieving these criteria by providing secure long term access and a permanent DOI. However, these services are also quite limited in the amount of metadata they store, particularly with regards to finding details about a specific granular material (particles sizes, shapes, etc). This makes it quite difficult for researcher and industrialist alike to find useful datasets across the many different online repositories.

To achieve the goal of making datasets more findable we propose that a method of incorporating richer, domain specific metadata be developed to help better define the contents of an experimental dataset. This will in effect become a searchable database of all available data, enabling the user to find detailed experimental datasets that match their needs.



# Temporal and spatial scaling of granular flow by NN-based DEM surrogate model and coarse-graining DEM model

Hideya Nakamura

*Osaka Metropolitan University, Sakai, Japan*

## Abstract

Numerical simulations using a discrete element method (DEM) have been widely used to simulate powder mixing processes. However, one of the current limitations of the DEM simulation is its high computational cost. A large scale DEM simulation with a large number of particles and long-time evolution inevitably requires an extremely long computing time. Thus, new method which can extend the spatial and temporal scales have been required. To address this issue, we recently developed DEM surrogated model utilizing neural-network (NN) [1] and coarse-grained DEM model [2-4] for simulating powder mixing. In this presentation, I would like to share these works.

For extending temporal scale, we developed a machine learning NN-based DEM surrogate model, namely, a recurrent NN (RNN) with stochastically calculated random motion (RNNSR). The RNNSR is designed to learn individual particle dynamics from short-term DEM simulation results and predict powder mixing for a longer period. The RNNSR combines an RNN and a stochastic model to predict both convective and diffusive mixing. The simulation results obtained using the RNNSR were quite similar to those obtained using the DEM in terms of the degree of powder mixing, particle velocity, and granular temperature. It was also demonstrated that the RNNSR has the capability of ultrafast computing in powder-mixing simulations [1].

For extending spatial scale, a coarse-grained discrete element method for granular shear flow, namely CGSF, was also developed [3, 4]. The CGSF was developed for a dense granular shear flow. The CGSF was built to match four types of energies between the coarse-grained and original particles under a granular shear flow. A scaling law for the sliding friction coefficient was derived considering the sliding friction damping between the original particles in the intra-coarse-grained region as well as those in the inter-coarse-grained regions. The CGSF was applied to the coarse-grained DEM simulation of a rotating drum mixer and high-shear mixer. The CGSF exhibited a result quite similar to the original case in terms of the particle velocity, kinetic energy, and degree of particle mixing [3, 4].

## References

- [1] N. Kishida, H. Nakamura, S. Ohsaki, and S. Watano. Chem. Eng. J. 475 (2023) 146166.
- [2] M. Saruwatari and H. Nakamura. Chem. Eng. J. 428 (2022) 130969.
- [3] N. Kishida, H. Nakamura, H. Takimoto, S. Ohsaki, and S. Watano. Powder Technol. 390 (2021) 1-10.
- [4] H. Nakamura, H. Takimoto, N. Kishida, S. Ohsaki, and S. Watano. Chem. Eng. J. Adv. 4 (2020) 100050.

## Expediting Fluidized Bed Scale-Up for Sustainability Challenges

Jia Wei Chew<sup>1</sup>, Ray Cocco<sup>2</sup>

<sup>1</sup>*Chalmers University of Technology, Gothenburg, Sweden,* <sup>2</sup>*Particles In Motion, Chicago, USA*

### Abstract

The scaling up of fluidized beds has been purposefully pursued for more than 100 years. Yet, over that time, scale-up tools have not significantly changed. Data analysis is typically a standard analysis of variances (ANOVA) statistical exercise, perhaps reinforced with a design of experiment procedure. Flow sheeting and equipment design are based on institutional knowledge, albeit graphical user interface (GUI)-based process flow models make that job more manageable. Advanced models such as computational fluid dynamics (CFD) are used but often as a supplement and not a primary driver. As a result, the scale-up process for a fluidized bed can take more than ten years.

Fluidized beds remain at the forefront of the present time-critical sustainability challenges, e.g., carbon capture by particulate sorbents, methane-to-hydrogen, plastic-to-chemicals, etc. In view of the exigency towards net-zero, today's scale-up efforts need to be accelerated, leveraging the advanced new tools that have become readily available. The problem is that such tools are often neglected, inadequately implemented, ineffectively resourced and/or poorly understood. This motivated the current effort, which is targeted at reviewing how scale-up tools have evolved over the years and the promising new tools, addressing some of the barriers of these tools in the design and scale-up of fluidized beds, as well as what can be done to circumvent these barriers.

# Numerical investigation of multidimensional particle fractionation in microchannels

Harald Kruggel-Emden

*Technische Universität Berlin, Berlin, Germany*

## Abstract

Significant progress has been made in the field of microfluidic separation processes in recent years. Various studies have presented systems that are able to separate particle fractions at relatively high throughputs. The focus was often on fractionation by size. The influence of other particle properties such as density, shape or deformability on particle behavior has been less frequently investigated so far. Even rarer are studies that analyze the combined influence of different particle properties. To address this lack of knowledge, the dynamics of particles of different size, density and shape at different Reynolds numbers in passive microfluidic systems were investigated. In particular, trajectories (and in some parts rotation systematics) in deterministic lateral displacement (DLD) and square wave serpentine channels were investigated.

The investigations were carried out numerically and the results were validated using experimental data. The Lattice Boltzmann Method (LBM) and the Discrete Element Method (DEM) were used. These were coupled and applied to determine the fluid dynamics and the fluid forces acting on the particles (LBM) as well as particle positions, velocities and collisions (DEM).

When investigating the DLD systems, the focus was on the development of the critical diameters. These represent the threshold between the two main transport modes and thus are the essential variable for fractionation. After validating the system, the (previously rarely investigated) combined influence of particle density and Reynolds number on the critical diameters was investigated in different channel geometries. The results show potential for multidimensional fractionation and were summarized in a correlation.

When investigating the square wave serpentine systems, the focus was on the development of equilibrium trajectories. These were initially used to validate the numerically obtained results against experimental data. Then, their positions and local widths in the channel were investigated for different combinations of particle sizes, shapes and densities as well as Reynolds numbers in order to explore the possibilities for fractionation. The results show possibilities for (individual and combined) size and density fractionation. The influence of particle shape on the equilibrium trajectories turned out to be much less pronounced. However, the particles partially showed periodic rotation behavior, which in some places could be directly attributed to the respective flow conditions.

# Measurement of Flowability and Layer Spreadability of Polymeric Powders for Powder Bed Fusion Processes at Ambient and Process Conditions

Massimo Poletto<sup>1</sup>, Sina Zinatlou<sup>1</sup>, Marco Lupo<sup>2</sup>, Diego Barletta<sup>1</sup>

<sup>1</sup>University of Salerno, Salerno, Italy, <sup>2</sup>Granutools, Awans, Belgium

## Abstract

Powder Bed Fusion processes, such as Selective Laser Sintering (SLS), are additive manufacturing techniques that involve spreading powders in thin layers during the process. Using fine powders can enhance the final artefact's quality by improving the definition of details. However, the cohesion of fine powders poses challenges for the spreading process. To address this, spreading is often performed at high temperatures to minimize defects caused by temperature peaks during the selective sintering/melting phases, which alternate with powder spreading.

In this study, we conducted an extensive experimental campaign on the flowability and spreadability of commercial SLS polymeric powders at both ambient and high temperatures. We measured powder flowability using an Anton Paar Shear Cell at varying temperatures. Spreading tests were performed with an experimental setup that simulated the powder spreading process at different temperatures. We analyzed the quality of the powder spread using image analysis techniques on macroscopic and microscopic images of the spread powder layer. Macroscopic images provided indications of layer defects and uncovered areas, while wavelet analysis offered spectral power densities related to characteristic wavelengths of surface roughness, serving as a valuable tool for characterizing and validating DEM simulations of the powder spreading process.

The results indicate that powder flowability and spreadability are only partially related. Notably, the effects of temperature on powder flowability become evident in the spreading process under conditions where powder flowability is only marginally affected.

Keywords: Powder Bed Fusion; Selective Laser Sintering; Powder flowability; Powder spreadability.

## Granular and photoelastic avalanches

Nathalie Vriend

*University of Colorado Boulder, Colorado, USA*

### Abstract

Flowing granular materials arise everywhere around us, in industry from pharmaceutical processes to bulk good transport lines, and in nature from snow avalanches to captivating dune fields.

In landslides, we have an interesting interplay between microscale (grain-grain contacts) and macroscale processes (continuum behavior). In order to understand critical macroscale processes such as stability of a slope, creep and failure, we need to be able to visualize and characterize the microscale interactions.

In this talk, I will introduce a laboratory technique called photoelasticity to visualize grain-grain contacts in time and space. Collisions between grains create a fascinating network of so-called force chains, which are responsible for the inhomogeneous distribution of stresses in a granular medium. We discover stress distributions in 2D granular avalanches, visualized with bespoke, superior-quality birefringent photoelastic particles. This technique gives us for the first time access to the full velocity, density and stress fields inside of a dynamic avalanche, and allows us to experimentally validate granular rheological models.



## **Present and Future of Computer Modelling in Particle Technology: From Academia to Industry**

**Carlos Labra**

*Altair EDEM, Barcelona, Spain*

## **Upscaling granular solids and flows**

**Vanessa Magnanimo**

*University of Twente, Enschede, Netherlands*

## **Maritime bulk material safety in remote operations: Practicalities in delivering Science to Ship loading Operations**

**Kenneth Williams**

*The University of Newcastle, Callaghan, Australia*

### **3 EXTENDED ABSTRACTS**

# Beyond Beverloo: Prediction of Solids Discharge Rates from Hoppers

Greg Mehos, Ph.D., P.E.<sup>1</sup>

<sup>1</sup> University of Rhode Island, Kingston, Rhode Island USA

**Abstract**—The Johanson equation, which predicts the discharge rate of coarse solids from hoppers, was modified to account for the adverse pressure gradient that can develop when fine powders are handled. The modified equation agrees with published data.

**Keywords:** discharge rate, powder, hopper.

Andrew Jenike's pioneering work on bulk solids handling fundamentals [1,2] allows designers of hoppers to specify minimum outlet dimensions that prevent obstructions to flow. However, the calculations do not reveal if a hopper outlet will provide the desired solids discharge rate.

The most common formula for calculating discharge rates from hoppers is the Beverloo equation [3]:

$$\dot{m}_s = C \rho_b g^{\frac{1}{2}} (B - k d_p)^{\frac{5}{2}} \quad (1)$$

where  $d_p$  is the particle diameter,  $\rho_b$  is the bulk density (at the hopper outlet),  $g$  is acceleration due to gravity, and  $C$  and  $k$  are empirical parameters. An empirical equation is philosophically unsatisfying, especially since a similar formula based on engineering fundamentals can be derived.

When deriving his formula for calculating solids discharge rates from hoppers, Jerry Johanson [4] began with a force balance:

$$-\frac{a}{g} = 1 - \frac{(m+1)f_c}{\rho_b g B} \quad (2)$$

where  $a$  is the acceleration of the solids,  $m = 0$  or  $1$  for an elongated or round outlet, respectively,  $B$  is the width or diameter of the hopper outlet, and  $f_c$  is the unconfined yield strength. It can be shown that [4]

$$a = -\frac{2(m+1)v_o^2 \tan \theta'}{B} \quad (3)$$

where  $\theta'$  is the hopper angle referenced from vertical and  $v_o$  is the solids velocity at the outlet. Equation 2 can then be rewritten as

$$\frac{2(m+1) \tan \theta'}{Bg} v_o^2 = 1 - \frac{(m+1)f_c}{\rho_b g B} \quad (4)$$

Johanson elegantly recast Equation 4 as

$$\frac{2(m+1) \tan \theta'}{B} v_o^2 = g \left( 1 - \frac{ff}{ff_a} \right) \quad (5)$$

where  $ff$  is the flow factor (the ratio of the major principal stress ( $\sigma_1$ ) to the stress on the abutments of an arch) and  $ff_a$  is the actual flow function defined by

$$ff_a = \frac{\sigma_{1o}}{f_c} \quad (6)$$

where the solids stress of the outlet  $\sigma_{1o}$  was calculated from

$$\sigma_{1o} = ff \frac{\rho_b g B}{m+1} \quad (7)$$

Figure 1 plots the flow factor as a function of the effective angle of friction  $\delta$ , which is valid for wall friction angles ( $\phi$ ) greater than about 12° and hopper angles in the neighbourhood of the mass flow boundary [5].

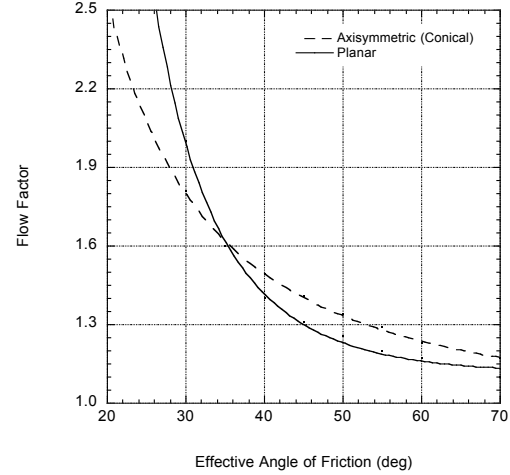


Figure 1. Johanson's flow factor [5].

Solving Equation 5 for  $v_o$  gives

$$v_o = \sqrt{\frac{Bg}{2(m+1) \tan \theta'} \left( 1 - \frac{ff}{ff_a} \right)} \quad (9)$$

The mass discharge rate  $\dot{m}_s$  is the product of the solids velocity and the cross-sectional area of the hopper outlet  $A_o$ :

$$\dot{m}_s = \rho_b A_o \sqrt{\frac{Bg}{2(m+1) \tan \theta'} \left( 1 - \frac{ff}{ff_a} \right)} \quad (10)$$

Equation 10 is called the Johanson equation. The Johanson equation can be used to determine the size of a hopper outlet required to provide the desired discharge rate of a coarse, cohesive bulk solid. It is similar to the Beverloo equation, but it was derived from first principles. Comparison of Equations 1 and 10 suggests that the term  $C$  is related to the hopper geometry and  $k d_p$  is related to the powder's cohesive strength.

Johanson assumed that the angle of the slope of the failing arch was equal to 45°. Jenike [1] noted that its angle is equal to  $\beta + \theta'$ , where

$$\beta = \frac{1}{2} \left[ \phi' + \sin^{-1} \left( \frac{\sin \phi'}{\sin \delta} \right) \right] \quad (11)$$

Hence,

$$\frac{ff}{ff_a} = \frac{2(m+1) \cos \theta' \sin(\beta + \theta') f_c}{\rho_b g B} \quad (12)$$

In addition, Jenike [1] modified Equation 7 to account for the non-uniformity of the arch:

$$\sigma_{1o} = ff \frac{\rho_b g B}{H(\theta')} \quad (13)$$

where  $H(\theta')$  is a function defined by Jenike [1,2] approximately equal to 1 for a planar hopper with a slotted outlet and 2 for a conical hopper.

For fine powders, gas-phase effects cannot be neglected as vacuum develops inside the hopper, and therefore a pressure gradient term should be included in the force balance:

$$\frac{2(m+1)\tan\theta'}{Bg}v_o^2 = 1 - \frac{ff}{ff_a} + \frac{1}{\rho_{bo}g} \frac{dP}{dz} \Big|_o \quad (14)$$

where  $dP/dz$  is the interstitial gas pressure gradient.

Darcy's Law describes flow of gas through a bed of material:

$$u = -\frac{K}{\rho_b g} \frac{dP}{dz} \quad (15)$$

where  $u$  is the gas slip velocity and  $K$  is the permeability. From continuity of the gas and solids, Gu [6] derived the following relationship between the solids velocity and the gas slip velocity:

$$u = v_o \rho_{bo} \left( \frac{1}{\rho_{bmp}} - \frac{1}{\rho_{bo}} \right) \quad (16)$$

where the subscript  $mp$  denotes the location where the interstitial gas pressure is at a minimum and the pressure gradient is zero. The pressure gradient is therefore related to the solids velocity by:

$$\frac{dP}{dz} = \frac{v_o \rho_{bo}^2 g}{K_o} \left( \frac{1}{\rho_{bmp}} - \frac{1}{\rho_{bo}} \right) \quad (17)$$

Substitution of Equation 17 into Equation 14 yields the following quadratic formula:

$$\left[ \frac{2(m+1)\tan\theta'}{Bg} \right] v_o^2 + \left[ \frac{1}{K_o} \left( 1 - \frac{\rho_{bo}}{\rho_{bmp}} \right) \right] v_o + \frac{ff}{ff_a} - 1 = 0 \quad (18)$$

from which the solids discharge rate can be calculated from

$$\dot{m}_s = \rho_{bo} A_o v_o \quad (19)$$

The solids stress where the gas pressure is at a minimum is rather cumbersome to calculate. Kerry Johanson [7] noted that it is approximately equal to the maximum solids stress  $\sigma_1$  in the cylinder section, which can be calculated from the Janssen equation:

$$\sigma_1 = \frac{\bar{\rho}_b g R_H}{k \tan\phi'} \left[ 1 - \exp\left( \frac{-k \tan\phi'}{R_H} z \right) \right] \quad (20)$$

where  $\bar{\rho}_b$  is the average bulk density,  $R_H$  is the hydraulic radius,  $k$  is the ratio of the horizontal and vertical solids stresses in the cylinder (approx. equal to 0.4), and  $z$  is the depth of solids in the cylinder. If the level of solids in the cylinder section is low, the maximum solids stress can be estimated from

$$\sigma_1 = \frac{\rho_b g D}{(m+1)\tan\theta'} \quad (21)$$

where  $D$  is the diameter or diagonal of the cylinder. The solids stress at the outlet is determined from

$$\sigma_{1o} = ff \frac{\left( \rho_{bo} g + \frac{dP}{dz} \Big|_o \right) B}{H(\theta')} \quad (22)$$

The solids velocity is calculated by first estimating the solids stress at the outlet and then using that value to calculate

the bulk density, permeability, and unconfined yield strength at the outlet. The outlet solids velocity  $v_o$  can then be calculated by solving Equation 18. Knowing the velocity allows the pressure gradient to be calculated from Equation 17. An updated value of the solids stress at the outlet can then be calculated from Equation 22. The calculations are repeated until the correct value of  $\sigma_{1o}$  is found. The solids mass discharge rate is the product of the velocity, cross-sectional area, and bulk density at the solids stress at the outlet.

Figure 2 compares solids discharge rates measured by Gu [8] with those predicted from Equations 18, 21, and 22. The author provided the relationships between the fundamental flow properties (cohesive strength, internal friction, wall friction, compressibility, and permeability) and solids stress for ten powders and measured solids discharge rates from conical hoppers filled to various depths. The hopper consisted of a 15° (from vertical) cone with a 44.5- or 20-mm diameter outlet and a 145-mm diameter cylinder. The wall material of the hopper was polished galvanized steel.

The agreement is acceptable for design purposes, although a safety factor of, say, 25 per cent should be employed if specifying the size of a hopper outlet that will provide the desired maximum steady solids discharge rate is critical.

By measuring a bulk material's fundamental flow properties, *i.e.*, its unconfined yield strength, internal friction, compressibility, wall friction, and permeability, the size of the outlet of a hopper required to allow the desired discharge rate can be specified. While the solids discharge rate data were obtained from experiments on a small-scale hopper, the model, which is based on fundamental principles, can be expected to provide a reasonable estimate for larger hoppers, bin, and silos.

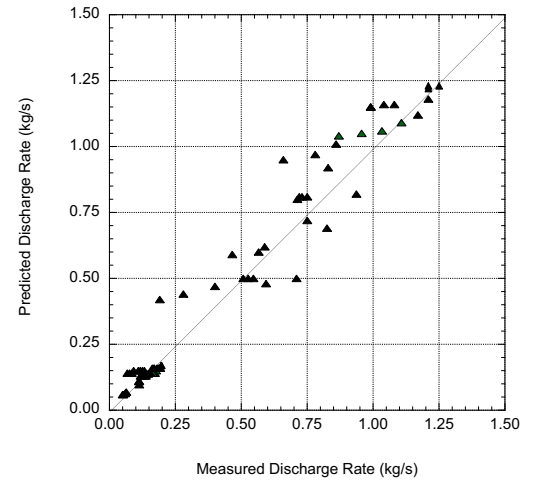


Figure 2. Comparison of observed and predicted solids discharge rates – Gu data [8].

### References

- [1] Jenike, A.W., *Gravity Flow of Bulk Solids*, Bulletin 108, University of Utah Engineering Station, 1961.
- [2] Jenike, A.W., *Storage and Flow of Solids*, Bulletin 123, University of Utah Engineering Station, 1964 (revised, 1976).
- [3] Beverloo, W.A., H.A. Leniger, and J. Van de Velde, "The Flow of Granular Solids Through Orifices", *Chem. Eng. Sci.*, 15, 260 (1961).
- [4] Johanson, J.R., "Method of Calculating Rate of Discharge from Hoppers and Bins", *Transactions of the Society of Mining Engineers*, 232, 69 (1965).
- [5] Kulwiec, *Materials Handling Handbook*, John Wiley and Sons, Hoboken, NJ, 1985.
- [6] Gu, Z.H., P.C. Arnold, and A.G. McLean, Modeling of Air Pressure Distributions in Mass Flow Bins", *Powder Techn.* 72, 121 (1992).
- [7] Johanson, K., "Powder Flow Properties", Chapter 13, *Encapsulated and Powdered Foods*, Onwulata, C., ed., CRC Press, Boca Raton, FL, 2005.
- [8] Gu, Z.H., "Gravity Flowrate of Bulk Solids from Mass Flow Bins", Ph.D. Thesis, University of Wollongong Department of Mechanical Engineering, 1991.

# The Value of Experience

Harald Wilms<sup>1</sup>

<sup>1</sup> Wilms-ITC, Bremen, Germany

**Abstract**—University education in engineering is suitable for teaching fundamentals in solids handling. Experience is another vital element in the making of valuable engineers. This, however, can only be gained in companies from experienced engineers having gained practical expertise from successfully executed projects. The expertise in solids handling operations also results from failures or troubleshooting. Examples of learning from experience and a format to pass on the experience gained are presented.

**Keywords:** Solids handling, trouble-shooting, experience, training, knowledge management

## 1. Introduction

Universities and colleges are great for learning basics and for teaching fundamentals in on bulk solids handling – from basics in powder mechanics to design calculations for pneumatic conveying systems or statistics for blender evaluation and analysis method and finally to newer developments in nanoparticle technology and DEM-simulation. However, when it comes to commissioning or trouble-shooting, young engineers depend on the knowledge and guidance of experienced colleagues. Especially failures generate a vast source of learning potential. It is known that the initial start-up of systems and plants involving bulk solids processes takes longer and the effective capacity reached after one year still lacks behind the nameplate capacity [1].

## 2. Silo Lessons

With very few exceptions, silos and gravity flow blenders [2] need to be designed for mass flow [3] for reliable operation and structural integrity. However, with standardization and ease of manufacturing in mind, frequently a ‘standard’ 60°-hopper is being used. This may have significant implications, especially with blender performance [4], as the ultimate proof by demonstrating the difference of mass flow and funnel flow by physical modelling in a transparent half-model shows.

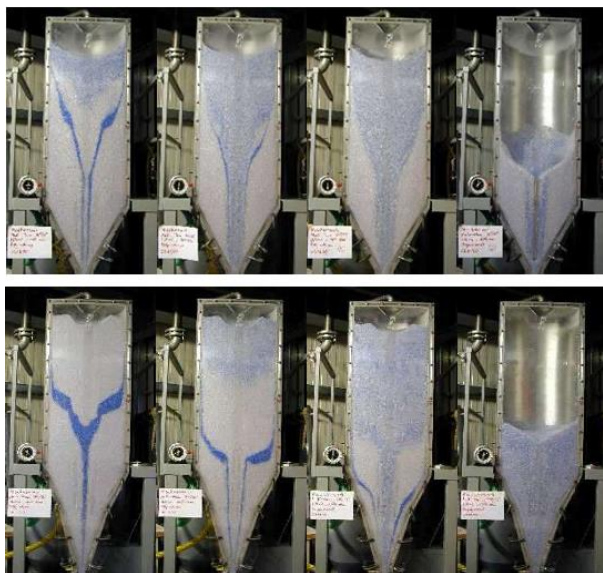


Figure 1. Demonstrating the influence of hopper geometry on blender performance

By not testing flow properties and using this knowledge may result in operation difficulties. The installation of a few aeration nozzles in a silo for a fibrous powder resulted in piping for the solids flow and channelling above the aeration nozzles for the injected gas flow. A bin activator sized in accordance with the flow properties was the expensive lesson to be learnt.



Figure 2. Discharge problems initiated by ignoring of flow properties

Also, structural problems may result from ignoring bulk solids flow properties, because eccentric flow may result in buckling and collapse of arches may result in vacuum damages.

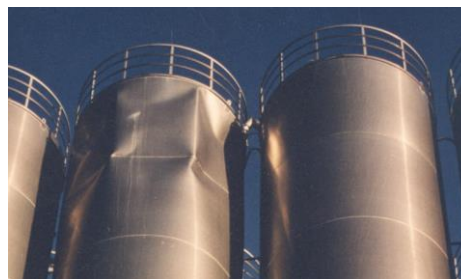


Figure 3. Vacuum damage caused by collapsing arch

Collecting examples from silo failures and classifying their cause into categories has resulted in the establishment of an evaluation scheme for silo damages [5]. A special lesson is to be learnt from structural silo failures resulting from non-uniform support or settlement of the foundation.

## 3. Pneumatic Conveying Lessons

Design of a pneumatic conveying system can be based on multi-phase rules with parameters to be determined in tests. Complying with clients' boundary conditions sometimes may be a challenge.

In one example a conveying system was to be designed for a maximum operating pressure of 800 mbar, because – according to the client – this special product would block the line at higher a pressure. An inspection of the existing system with this limitation was arranged – and the system did fail at 800 mbar conveying pressure. A walk along the conveying line revealed the problem: The safety valve of the blower was erroneously set at 800 instead of 1000 mbar, resulting in a collapse of the gas flow and subsequent line blockage at this pressure.



Putting a closed-loop conveying system into service may offer additional challenges. During start-up, the air initially contained in the system including the silo is compressed, resulting in a vacuum upstream of the compressor. If only an insufficient air flow to compensate the vacuum is supplied, e.g. by an inadequately designed balancing system, then the vacuum will result in an non-permissible vacuum in the silo – resulting in vacuum buckling.



Figure 4. Vacuum damage of a silo during start-up of a closed loop conveying system

#### 4. Conceptual Design Lessons

Frequently plant concepts are specified in detail in an inquiry package, based on licensor's requirements, clients' preference or previous experience. In many cases these specifications do not include the experience of suppliers and respective equipment limitations. This could lead eventually to systems with inadequate performance or reduced economics.

In one example for a polymer plant [6], dense-phase conveying technology without pellet cleaning was specified. Due to the anticipated layout of the plant, this would have resulted in a too high final fines content and inefficient as well non-economic design of the pneumatic conveying system. This could only be changed into a more efficient concept through the involvement of the final customer. The solution was a combination of high-pressure dilute-phase conveying, pellet cleaning and dense-phase conveying.

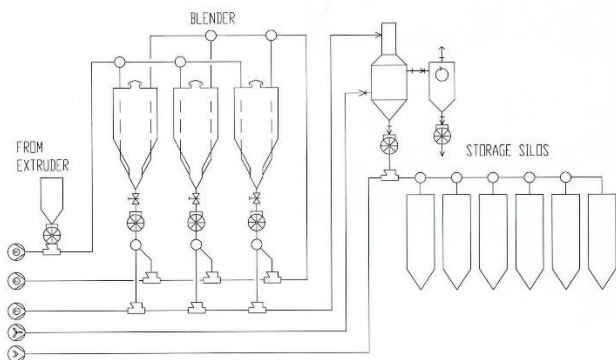


Figure 5. Optimized conveying concept for a polymer plant

A much smarter approach to derive at an optimum plant concept is for clients and engineering contractors to issue only a 'functionality spec' describing capacities, product quality and distances and then leaving the concept development and technical solutions to suppliers, eventually in an early project phase of FEED or FEL. A respective project management

approach was chosen for a different plant yielding the most efficient logistic plant [7].

#### 5. Conclusions and Recommendations

Utilizing existing experience, involving process technologies, applying bulk solids handling fundamental, questioning previous performance, and allowing alternatives to be evaluated are the best tools for improving solids handling performance in plant engineering.

The examples described are only a selection of experiences gained during more than 30 years in plant engineering for solids handling plants. Another resource of experience and lessons learnt can be told by start-up engineers, because they frequently must suffer from mistakes being made due to lack of experience of the project, process or design engineers.

Therefore, in-house education seminars and industry-wide training courses held by senior engineers form a good platform for knowledge and experience transfer to younger colleagues. The investment made with respect to manpower, time and cost for such training pays well off with the improvement of professionalism in plant engineering – surely contributing to shortened start-up periods and improved on-time plant capacities.

#### Acknowledgement

To all clients and colleagues from Zeppelin Systems that have provided the learning base.

#### References

- [1] T. Bell, *Challenges in the scale-up of particulate processes—an industrial perspective*. Powder Technology 150 (2005), 60-71
- [2] H. Wilms, *Blending Silos – an Overview*, Powder Handling & Processing, 4 (1992), 3, 293-299
- [3] A.W. Jenike, *Storage and Flow of Bulk Solids*, Bull. #123, Univ. Utah, 1964
- [4] H. Wilms and H. Schneider, *The Role of Solids Handling Expertise in Plant Engineering*. CHoPS 2012
- [5] H. Wilms and H. Schneider, *Proposal to structure Silo Failure Analysis*. CHoPS 2022
- [6] H. Wilms, *Optimized Solids Handling Concept for a Polymer Plant*. Proc. ECCS-3, 2001
- [7] P. Lakeman, F. Bunge and H. Wilms, *Dow's Polymer Logistic Operations at the Schkopau Plant*, Proc. 4<sup>th</sup> Annual Polymers Producers Conf., AIChE, New York, 2000.

# Industrial Needs in Solids Flow - A 25 Year Retrospective

Timothy A. Bell<sup>1</sup>

<sup>1</sup> DuPont Engineering, Wilmington, Delaware USA (retired)

**Abstract**— In 1999 the author wrote a short article that described frequently occurring problems in the application of solids handling technology to industrial problems. The topics included the prediction of critical rathole diameters, the effective application of flow promotion devices, tedious measurements using Jenike shear cells, the handling of elastic materials such as biomass, pneumatic conveying system design and the prediction of bulk behavior from individual particle attributes. Additional topics of interest at the time (and now) include the prediction of segregation, dynamic flow behavior, mechanical mixing performance and flow patterns and stresses within silos. In the 25 years since the publication of the article, significant scientific progress has only been made on some of these problems. Implementation of the available technology in industry has come at an even slower pace. This paper illustrates the practical problems in these fields encountered by engineers in the chemical, plastics, and food fields, and highlight both the progress and delays in the development of practical solutions.

**Keywords:** Industrial solids handling; silo flow; flow promotion; rathole; pneumatic conveying; mixing; segregation; education

## 1. Introduction

The author has worked in industry since 1976, specializing in solids handling since 1985. In 1999 he wrote a short article on industrial needs in the field [1]. The current article reviews progress and remaining challenges for industrial bulk solids handling. There is a significant gap between the state of academic research and the needs and application of the technology to industry.

## 2. Calculation of Critical Rathole Diameters and Selection of Flow Promotion Devices

### 2.1. Jenike's Rathole Calculation Procedure

In his Bulletin 123 (1980 version and later) Jenike [2] offers a method to calculate the hopper outlet diameter necessary to overcome ratholing. This method is known to produce a conservative upper bound on the parameter. For very cohesive powders the method will frequently calculate a nonsensical outlet diameter that is larger than the actual silo diameter. Improvements to the calculation method have been suggested both by Roberts and Ittershagen [3,4] but Robert's work was aimed at stockpile drawdown and Ittershagen utilized data from a specialized tester that is not commercially available. Consequently, critical rathole diameters for cohesive materials are more often used as indicators than as design parameters.

### 2.2. The Selection of Flow Promotion Devices

The recommended placement of flow promotion devices such as vibrators, air cannons, or other air injection devices on hoppers is based on the difference between the actual outlet diameter and that recommended by Jenike methods. For example, a 0.5 meters diameter outlet may exist, but the data suggests that 1.0 meters is necessary. In this case we would want to promote flow in the region along the hopper wall between the two diameters. The problem is that we do not have

an analytical method to select what type of flow promotion device to use, or how much energy it must deliver. The performance of vibratory devices will be affected by the stiffness of the structure, as well as the mechanical properties of the bulk solid, while the effect of air will be influenced by both the permeability and mechanical properties of the bulk solid and how the air is applied. New flow promotion devices are purchased every day, but there are very few scholarly articles on this subject. The recommendations of the equipment supplier are typically vague, and the field is dominated by trial-and-error approaches.

## 3. Measurement of Powder Flow Properties

### 3.1. Developments in Shear Cell Technology

Shear testing has been an area of great progress in the field of solids handling in the past 25 years. Since the 1990's, computer controlled rotational shear testers have become widely available from Schulze, Brookfield, and Freeman. None of these devices are cheap, and most have some limitations, but overall, there has been a step change in the commercially available technology. The laboratory time required for "instantaneous" measurements of cohesive strength has been reduced by more than 50%, and the formerly manual processing of the resultant data to produce yield loci and flow functions has been automated. Unfortunately, as will be discussed later, the people receiving the data may be no more skilled in its interpretation than they were in the past.

### 3.2. Dynamic Measurements at Low Consolidation Stresses

For many years, people working with small amounts of powder that is not confined to a bin have complained that shear cell results do not correlate well to the problems they are trying to solve. This is partly because the shear rates (and voidage) are much higher in their process than what happens in shear testing and partly because the amount of stress/strength that is developed is much less than can be measured with shear cells. Computerized devices that quantify the behaviour of a sample that is tumbled in a drum (Granutools, Mercury Scientific) or stirred with an impeller (Freeman Technology) have become popular in the past 25 years and now are commonly used to correlate a measured test result to a practical outcome in a manufacturing process. Numerical conversion of test results, in engineering units, has been limited to aspects of the Freeman tester in a research environment.

### 3.3. Interpretation of Test Results

DuPont [5] estimated that 78% of its products involved bulk solids as ingredients, intermediates, or final products. Despite the prevalence of solids in the workplace, nearly all chemical and mechanical engineers in the US and many other countries receive no academic training in particle technology or specifically bulk solids handling. The need for this coursework has been raised repeatedly by particle technology specialists working in industry, but there has been little lasting effect on undergraduate education in the field since the 1990's. As a result, working engineers that are confronted with a problem, especially regarding silo flow, may lack the training necessary to diagnose the problem and/or properly interpret laboratory test results.

## 4. Pneumatic Conveying

### 4.1. Conveying Design Parameters

The two most critical parameters for the design of a dilute phase pneumatic conveying system are the minimum pick-up velocity for a given solids feed rate and the total system pressure drop for a specific system configuration and solids flow rate. A conservative design will increase capital and operating cost and may increase particle attrition. There is a direct interaction between velocity and pressure drop, and system design calculations must be iterative. Commercial-grade software is now available to explore the parameter space. Equations to predict pick-up velocity have been very slow to evolve, probably due to a serious lack of researchers and the scale of apparatus needed to validate experiments. The most useful recent correlation is by Kalman [6] in 2005. It is noteworthy that Kalman's sophisticated correlation uses six system or particle parameters but still does not explicitly account for some aspects of particle behaviour. We have found it necessary to conduct large scale (75mm or 100 mm pipe) experiments for any critical applications. This is a problem for new processes or whenever supplies of a material are limited.

### 4.1. Particle Attrition in Conveying

Damage to particles in conveying can reduce their commercial value and increase dust explosion risks. Empirical evidence suggests that in many cases the rate of attrition scales to the particle velocity raised to an exponent (such as the 2.5 power). However, without conducting a conveying test at relatively large size we cannot begin to estimate the attrition. Testers that fire single particles from air guns or fling the particles against targets using centrifugal force exist at a few universities, but their application has not been broadly extended to industry.

## 5. Segregation and Mixing

### 5.1. Segregation

The quantitative prediction of segregation at the production scale is not possible with physical experiments in the lab. (Modelling is discussed later in this paper). While segregation is often visible in the lab or a full-scale process, we cannot always predict whether the segregation will have an adverse effect on the process or if a subsequent handling step might reverse the segregation. Consequently, we might feel obligated to take very conservative design strategy or receive unpleasant surprises at the start-up of a process.

### 5.2 Mixing

A closely related problem is predicting the behaviour of mixers. If a new mixing operation is needed, the standard practice is to guess at the required mixer type and mixer process conditions (such as RPM or residence time) and conduct a pilot or full-scale test. A diligent engineer will take multiple samples from inside the blender or a series of samples as the blender is discharged. These samples usually require a costly chemical analysis to see if the desired level of uniformity has been achieved. For one process we found that a proper analysis was going to cost \$30,000 USD per pilot scale mixer batch. It was no surprise that the scope duration of the pilot studies was cut to the minimum necessary to make a minimally acceptable product, and no further optimization was ever attempted.

## 6. Modelling of Powder Flow

### 6.1. DEM, FEM and CFD

Given industry's inability to reliably calculate important parameters needed for process design requirements, there has

been strong interest in the modelling of solids handling processes via Discrete Element, Finite Element and Computational Fluid Dynamics methods. As evidenced at the 2024 CHoPS conference, there is significantly more current academic interest in modelling than in research based on physical experiments at meaningful scale. This is understandable considering the difficulties in conducting such experiments and the frequent inadequacies of the results when applied to situations beyond the original experiments. While CFD has been in industrial use for decades, the use of the other two methods (or combinations of all three) for solids handling problems has grown greatly since the 1990's.

However, to build a model, we need to know the fundamental physics and have a way to utilize that knowledge to mathematically describe situations of meaningful size and complexity. Both considerations are especially difficult with particles smaller than about 50 microns since the number of particles involved in a model could be billions or more, and a wide variety of complex interparticle forces are relevant at the micron scale. Because of this limitation, the majority of successful industrial applications have been in processes where the particles are millimetre size or larger, and the particles number in the millions (or less), not billions. Reducing these limitations is a major focus of academic research. In the meantime, the usefulness for routine problems involving the flow of fine powders is limited.

### 6.2. Skill Sets Required to Use Models

As previously noted, the typical chemical or mechanical engineer will have little to no formal training in solids handling. Effective use of the available modelling techniques requires both a high level of computer skills and strong knowledge of solids handling/particle technology. This is a rare combination and is seldom found in industry. There is risk that modelling problems will be handed off to "modellers" who lack the practical insights necessary to detect faults in the model, or the judgement to know if the potential return on the effort to build the model is worth it. While significant advances have been made in the past 25 years, the utilization of DEM modelling for industrial solids handling problems by "rank and file" engineers is currently at a stage of development that may be 10 years or more behind CFD.

## 7. Conclusion

There has been little industrial progress in many important areas of solids handling. In some cases, productive academic research has not yet been routinely applied in industry, but in others there does not seem to have been much progress. One bright spot is powder flowability measurement equipment, and we hope that the pace of development in modelling will increase.

## References

- [1] T.A. Bell, *Industrial Needs in Solids Flow for the 21st Century*; Powder Handling and Processing, Vol. 11 No. 1 pp. 9-12, 1999.
- [2] A. Jenike, "Storage and Flow of Solids, Bulletin 123," Utah Engineering Experiment Station, University of Utah, Salt Lake City, 1964, 14th Printing, Revised 1980.
- [3] A.W. Roberts, in "Characterisation of Bulk Solids", D. McGlinchey, Ed., Oxford, Blackwell Publishing Ltd., pp. 85-131. 2005
- [4] T. Ittershagen, et al., "Anisotropic behaviour of bulk solids and its effect on silo design," *Powder Technology*, vol. 247, pp. 260-264, 2013.
- [5] R.D. Nelson, R. Davies, K. Jacobs, Teach 'Em Particle Technology; Chemical Engineering Education, pp.12-16, 1995.
- [6] H. Kalman, et al., Pickup (critical) velocity of particles, *Powder Technology* 160 pp. 103 – 113, 2005

# Evaluation of Segregation of Pharmaceutical Formulations in Direct Compression Process

Vivek Garg<sup>1\*</sup>, Tong Deng<sup>1</sup>, Lucas Massaro Sousa<sup>2</sup>, and Michael SA Bradley<sup>1</sup>

<sup>1</sup> Wolfson Centre for Bulk Solids Handling Technology, Faculty of Engineering & Science, University of Greenwich, Central Avenue, Chatham ME4 4TB, UK

<sup>2</sup> IFP Energies nouvelles, Rond-Point Échangeur de Solaize, 69360 Solaize, France

**Abstract**— The phenomenon of powder segregation during the direct compression process can pose a significant challenge in controlling of content uniformity in blended powders, particularly when the powder exhibits characteristics of being free-flowing or easily flowing. Evaluating the level of segregation in powders at early formulation stage faces a significant challenge due to the scarcity of available samples. The utilisation of small bench-scale testers for an advanced segregation evaluation can provide valuable insights for making formulation decisions and recommendations for operational parameters in a process that has not been extensively studied previously. The objective of the study was to investigate the phenomenon of segregation using two different types of bench-scale testers, namely the air-induced segregation tester and the surface rolling segregation tester. Additionally, a pilot simulation process rig was employed to conduct a comparative analysis. The findings indicate that the assessment of segregation on bench-scale testers can effectively serve as an indicator of the level of segregation within a blend for a process, if the segregation intensity does not exceed 20%. The comparison also demonstrates that both the bench-scale testers exhibit a strong correlation with the process rig, indicating that any segregation tester can be utilised autonomously for the purpose of evaluation.

**Keywords:** Segregation in process; Formulated powders; Bench-scale testers; Harshness factors; Linear regression model

## 1. Introduction

Powder segregation in pharmaceutical manufacturing poses significant challenges for maintaining content uniformity, leading to substantial wastage [1]. For powder-based medications like tablets or capsules, segregation alters the distribution of active pharmaceutical ingredients (APIs), critical for meeting quality standard [2]. Differences in particle size, shape, or density among powders can cause segregation during handling, compromising content uniformity control [3]. Extensive research has explored batch and continuous blending processes involving various co-processed drug substances [4]. However, powder segregation is complex due to diverse material properties, mixing efficiencies, equipment designs, and operational methods. Prior studies predominantly focused on material properties and blending techniques [5], with less emphasis on segregation mechanisms and operational conditions. Direct assessment of powder segregation during processes remains challenging [6], highlighting the importance of pre-process evaluation and formulation adjustments. Although small bench-scale testers are commonly used for powder evaluation, their comparison with full-scale processes has not been thoroughly investigated. This study examines powder segregation in a direct compression process, evaluating segregation intensity using small-scale bench testers.

## 2. Materials and methods

One API and two Co-Processed Excipients (CPEs) were used to form eight formulations at different mixing ratios, as shown in

Table 1. The API/CPEs were supplied by various suppliers, as shown in Table 2, with the material codes used in the analysis and corresponding names with their formulations.

TABLE-1: A LIST OF THE FORMULATIONS STUDIED AND SUPPLIERS OF THE MATERIALS

Code	Materials & Compositions	Grade	Supplier
AD	Acetaminophen Dense	API	Mallinckrodt Pharma
EasyTab	Prosolv® EasyTab SP	CPE	JRS Pharma
Ludipress	Ludipress® LCE	CPE	BASF Pharma
AD40P	40% AD + 60% EasyTab	Formulation	-
AD20P	20% AD + 80% EasyTab	Formulation	-
AD10P	10% AD + 90% EasyTab	Formulation	-
AD05P	05% AD + 95% EasyTab	Formulation	-
AD40L	40% AD + 60% Ludipress	Formulation	-
AD20L	20% AD + 80% Ludipress	Formulation	-
AD10L	10% AD + 90% Ludipress	Formulation	-
AD05L	05% AD + 95% Ludipress	Formulation	-

### 2.1. Material Characterisation

Characteristics of the materials and the formulations studied are given in Table 3, which include particle sizes at D<sub>10</sub>, D<sub>50</sub> and D<sub>90</sub> (volume % measured on a Malvern MasterSizer 3000) and other physical properties, including size span, and angle of repose (AoR) measured using a heap on the flat surface created by a fixed funnel according to ASTM C1444-00.

TABLE-2: MATERIAL PHYSICAL PROPERTIES

Code	Particle Size (µm)			Size Span (D <sub>90</sub> -D <sub>10</sub> )/D <sub>50</sub>	AoR (°)
	D <sub>10</sub>	D <sub>50</sub>	D <sub>90</sub>		
AD	5.9 ±0.3	38.0 ±2.0	177.0 ±2.0	4.50	53.1 ±0.8
EasyTab	38.0 ±1.0	122.0 ±3.0	246.0 ±9.0	1.70	37.4 ±0.9
Ludipress	43.0 ±0.8	161.0 ±6.0	491.0 ±30.0	2.78	36.2 ±0.3
AD40P	12.5 ±0.2	79.0 ±0.9	198.0 ±2.0	2.35	51.3 ±1.0
AD20P	21.5 ±0.4	98.6 ±0.3	226.4 ±0.8	2.08	49.3 ±0.5
AD10P	26.4 ±0.2	106.0 ±1.0	232.0 ±8.0	1.94	42.3 ±0.5
AD05P	31.0 ±0.4	111.0 ±1.0	229.0 ±3.0	1.78	38.8 ±0.3
AD40L	12.6 ±0.6	85.0 ±5.0	294.0 ±10.0	3.32	48.8 ±0.8
AD20L	21.0 ±0.3	119.0 ±3.0	411.0 ±15.0	3.28	44.2 ±0.2
AD10L	26.2 ±0.6	129.0 ±5.0	420.0 ±20.0	3.05	37.1 ±0.6
AD05L	36.7 ±0.3	160.0 ±3.0	490.0 ±9.0	2.83	35.6 ±0.3

### 2.2. Method for measuring segregation

The air induced segregation measurements were undertaken using tester (Fig. 1(a)). In this study, 5 sample sections were used, as shown in Fig. 1(a). Surface rolling segregation tests were undertaken on a surface rolling segregation tester [6], as shown in Fig. 1(b), which can quantify segregation intensity in a heap formation where particles segregate due to surface rolling (including percolation) mechanism.

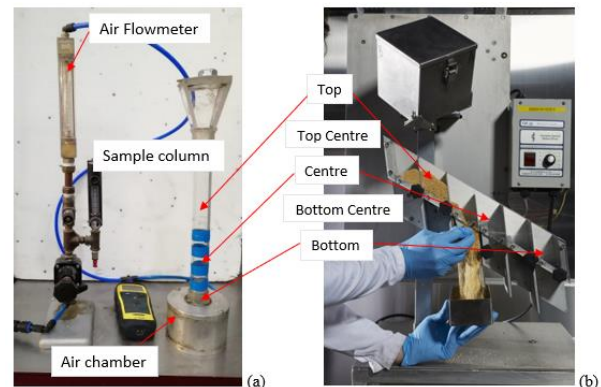


Figure 1. (a) Air-induced segregation tester, (b) Surface rolling segregation tester

To investigate powder segregation in the direct compression process of pharmaceutical formulations, an industrial-scale



simulation facility was constructed at the Wolfson Centre with Roche's support for in-process segregation assessment. Fig 2(a) presents a sketch (not to scale) of the rig without the sampling section, while Fig 2(b) shows a photo of the pilot simulation rig with the sampling section.

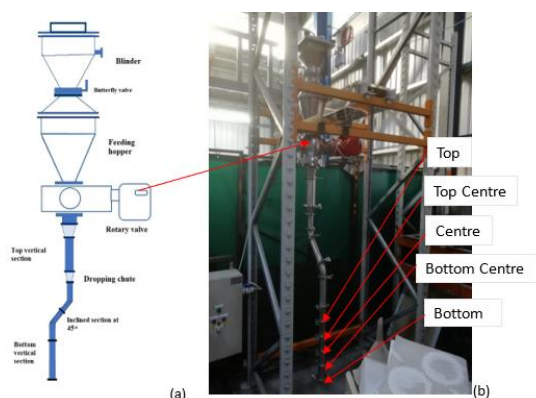


Figure 2. (a) Sketch of pilot rig at the Wolfson Centre, (b) a photo.

### 3. Results and Discussion

In this study, two continuous processing equipments (CPEs) and eight formulations containing Acetaminophen Dense as the API were utilized to investigate segregation. The study compared results from bench-scale tests and a pilot simulation process test rig to determine correlations. The results indicate that it is difficult to distinguish between the air-induced segregation tester and the surface rolling segregation tester, despite their different segregation mechanisms. Fig 3 shows a consistent trend in segregation across sample locations: fines accumulate in the top section and are deficient in the bottom section when the powder or formulation is less cohesive. As API content increases, the materials become more cohesive, leading to reduced segregation. However, further increasing the API content does not completely prevent segregation but results in a loss of fines in all sections. This may be due to other segregation mechanisms, such as electrostatic charge, which were not evaluated in this study.

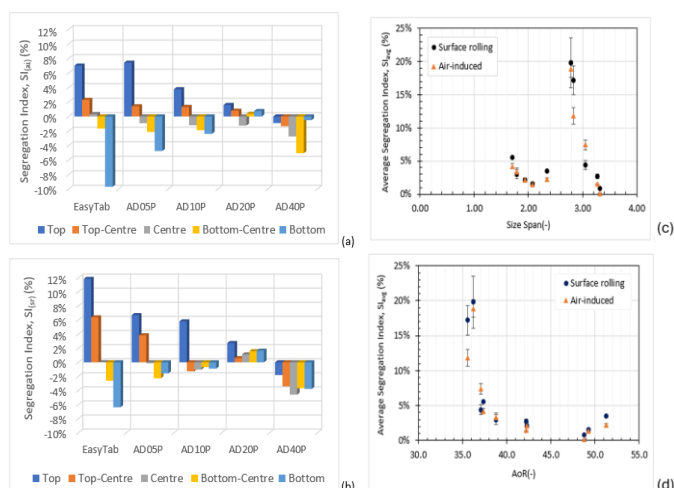


Figure 3. Segregation Index at the 5 sampling points for the EasyTab and the formulations on: (a) the air-induced segregation tester and (b) the surface rolling segregation tester. The averaged  $S_{avg}$  measured on the bench-scale testers versus (c) size span of particles, (d) the angle of repose

The results in Fig. 3(c) show the influences of particle size span clearly. Normally, a higher size span gives a higher risk of particle segregation, but it really depends on the cohesiveness of the powders. The results in Fig. 3(d) show a sharp drop in the

segregation when the angle of repose reaches about 37-38 degrees.

### 4. Conclusion

This study investigated segregation in eight formulated pharmaceutical powders using two types of small bench-scale testers (air-induced and surface rolling segregation) and a pilot simulation process rig for direct compression. The results revealed a linear correlation between segregation intensity measured by the bench-scale testers and that observed in the process, provided the maximum segregation index ( $S_{lmax}$ ) for the powders was below 20% as shown in Fig 4.

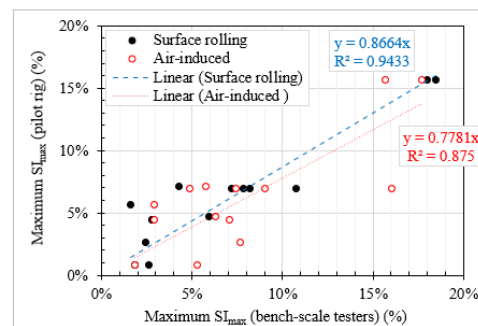


Figure 4. (a) Segregation Index at the 5 sampling points for the EasyTab and the formulations on: (a) the air-induced segregation tester and (b) the surface rolling segregation tester

Correlation coefficients exceeded 0.9, affirming the suitability of bench-scale testers for evaluating powder segregation in processes. However, powders with  $S_{lmax} > 20\%$  on bench-scale testers showed limited segregation in the process, likely due to insufficient kinetic energy. The study highlighted a consistent linear relationship between bench-scale testers and process equipment across different segregation mechanisms. A regression model accurately predicted segregation levels, although larger errors occurred for EasyTab and AD20P formulations. Overall, segregation mechanisms were found to have minimal impact on process segregation, emphasizing the utility of bench-scale testers for advanced segregation evaluation in pharmaceutical processes.

### Acknowledgment

We gratefully acknowledge the support of F. Hoffmann-La Roche Ltd for providing the data generated and the test materials as part of their project titled "Assuring powder-machine compatibility of direct compression formulations for continuous manufacturing processes, focusing on segregation and blend flowability." Roche also funded the construction of the pilot simulation process rig.

### References

- [1] Sapkota, B., & Pariatamby, A. (2023). Pharmaceutical waste management system—Are the current techniques sustainable, eco-friendly and circular? A review. *Waste Management*, 168, 83-97.
- [2] D. Schulze, *Powders and bulk solids: behavior, characterization, storage and flow*. 2008.
- [3] Deng, T., Garg, V., Salehi, H., & Bradley, M. S. (2021). An experimental study on free-surface rolling segregation and correlations with angle of repose and particle sphericity. *Powder Technology*, 379, 307-320.
- [4] Deveswaran, R., Bharath, S., Basavaraj, B. V., Abraham, S., Furtado, S., & Madhavan, V. (2009). Concepts and techniques of pharmaceutical powder mixing process: A current update. *Research Journal of Pharmacy and Technology*, 2(2), 245-249.
- [5] Jaspers, M., de Wit, M. T., Kulkarni, S. S., Meir, B., Janssen, P. H., van Haandel, M. M., & Dickhoff, B. H. (2021). Impact of excipients on batch and continuous powder blending. *Powder Technology*, 384, 195-199.
- [6] Bridle, I., Bradley, M. S. A., Reed, A. R., Abou-Chakra, H., Tüzün, U., & Farnish, R. J. (2004). Development of a test instrument to measure the segregation propensity of bulk materials. In *International Conference on Bulk Storage, Handling and Transportation*.

# Effects of Electrostatic Charge on Particle Adhesion, Cohesiveness and its Influences on Powder Flow Properties

Tong Deng, Vivek Garg, and Michael SA Bradley

The Wolfson Centre for Bulk Solids Handling Technology, University of Greenwich, Chatham, Kent, UK  
Email: t.deng@greenwich.ac.uk

**Abstract** — Characterising powder flowability can be challenging especially for pharmaceuticals when only a small quantity of samples is available. For the case, a novel method for powder flowability and other flow properties prediction has been developed using a few milligrams of powders, which applies Bond number to represent powder cohesiveness at median particle size. The prediction was promising for many powders, but a recent study on acetaminophen showed that the prediction did not match the results using a shear cell tester, which revealed that there must be other contribution forces in the cohesiveness measurements.

The subspinosus is believed to be the electrostatic charge on powders, which can significantly contribute to the particle adhesion. The current study focused on electrostatic charge measurements of acetaminophen dense and acetaminophen micronized with different particle sizes. The results have been compared to those other common materials such as Lactose, Avicel, and Calcium Carbonate, which all gives a good prediction of powder flow properties. The comparison shows that both acetaminophen dense and micronized can be charged significantly under handling conditions. The charge level of the acetaminophen can be 20 times higher than that of the common materials measured. If charge level in powders is significant, the electrostatic charge can strongly influence the adhesion measurement, but it will not appear in a shear cell test as the consolidation force overtakes it. It is concluded that the electric charge can strongly contribute particle adhesion that can affect powder flow at low consolidation stress but not the high consolidation stress.

**Keywords:** Powders; Flowability prediction; Electrostatic charge; Adhesion; Low consolidation stress.

## 1. Introduction

Powder flowability is an important characteristic in design of bulk solids handling processes and needs to be characterised prior to formulations developed especially for pharmaceuticals. It can be challenging when only a small quantity of samples is available, which conventional methods normally require 10s' to 100s' grams sample for one testing such as a shear cell test. For the case, a novel method to predict powder flow properties has been developed at the Wolfson Centre using a few milligrams of powders [1]. The technique applies Bond number to represent powder cohesiveness, which detects particle adhesion at median particle size using a mechanical surface energy tester [2]. The Bond number and the physical properties of sample powder are used for the prediction of powder flow. This method has shown very promising results of powder flowability and other flow properties prediction for a wide range of powders varying in particle properties such as particle size, particle shape and particle density. However, a recent study on different grades of acetaminophen showed that the predictions using Bond number did not match the results that were measured using a shear cell tester (Particle Flow Tester, Brookfield), which revealed that there must be other contribution forces in the Bond number measurements using the mechanical surface energy tester.

The suspected cause is believed to be the electrostatic charge on powders, as electrostatic force can significantly contribute to the measurement of particle adhesion. The current study focused on the charge measurements of two types of acetaminophens (dense and micronized) with different particle size distributions. The charge measurements have been compared to the charge measurement for other common materials such as Lactose, Avicel, and Calcium Carbonate, which all shows a good prediction of powder flow properties using the Bond numbers. The comparison identifies that both the acetaminophen dense and the acetaminophen micronized are significant charged under normal handling conditions compared to the other common materials. The study shows that electrostatic charge on powders can have strong influences on particle adhesion and alternative influences on powder flow at low consolidation stress, but it will not be significant in a shear cell test measurement due to the high consolidation stress applied.

## 2. Materials and Methods

### 2.1. Powders

The powders used for this study are acetaminophen dense and acetaminophen micronized, which proposed highly chargeable. As a comparison, three common powders were used, which are Lactose, Avicel, and Calcium Carbonate. Characteristics of the materials studied are given in Table 1 including particle size, size span, particle solid density and Bond numbers measured by a mechanical surface energy tester [2].

TABLE I. MATERIALS STUDIED AND MATERIAL PHYSICAL PROPERTIES

Materials	Particle Size ( $\mu\text{m}$ )			Size Span ( $D_{90}/D_{10}$ )	Solid Density ( $\text{kg/m}^3$ )	Bond Number
	$D_{10}$	$D_{50}$	$D_{90}$			
Acetaminophen dense	16	63	207	3.03	1356	8.9
Acetaminophen micronized	2	6	19	1.78	1380	9.1
Eskal 4 (CC)	2	4	13	2.76	2800	8.6
Granulac 70	19	90	118	1.10	1560	8.2
MCC-Avicel PH 200	59	180	337	1.54	1698	7.4

### 2.2. Powder flow properties and shear cell tests

Powder flowability is the ability of granular solids or powders to flow, which depend on the physical properties of the material including particle size, shape and internal friction of powders (cohesiveness). The flow properties used to be measured using shear cell testers or other conventional methods, which normally requires a significant quantity of samples such as 10-100 grams minimum [3]. In the study, a shear cell powder flow tester (PFT) (Brookfield, USA) was used to determine the flowability of the powders experimentally. In the meantime, a cohesive Bond number of the powders measured was used to predict the powder flowability by its representative of powder cohesiveness at a median size of the particles [1].

### 2.3. Sensing electrostatic charge of powders

Charge of powders was measured using a charge sensor [4].



The charge sensor is an inductive electrostatic charge sensor, which measures the electric charge on each individual particle or agglomerate and accumulates the charges according to the charge polarity over the total population of the particles [5]. The mass of the particles collected through the sensor is measured afterwards. Charge to mass ratio is calculated by the total charge and the mass of the particles as charge polarity and net charge.

### 3. Results

The measured and the predicted flow functions of the sample powders are given and compared. For the acetaminophen, the difference between the measurements and the prediction is clearly identified. Alternatively, charge levels of the powders are also measured.

#### 3.1. Flow functions measured and predicted

Instantaneous flow functions of the powders are measured using a shear cell tester and the results are shown in Fig. 1, which are compared to the predictions by the modelling [1].

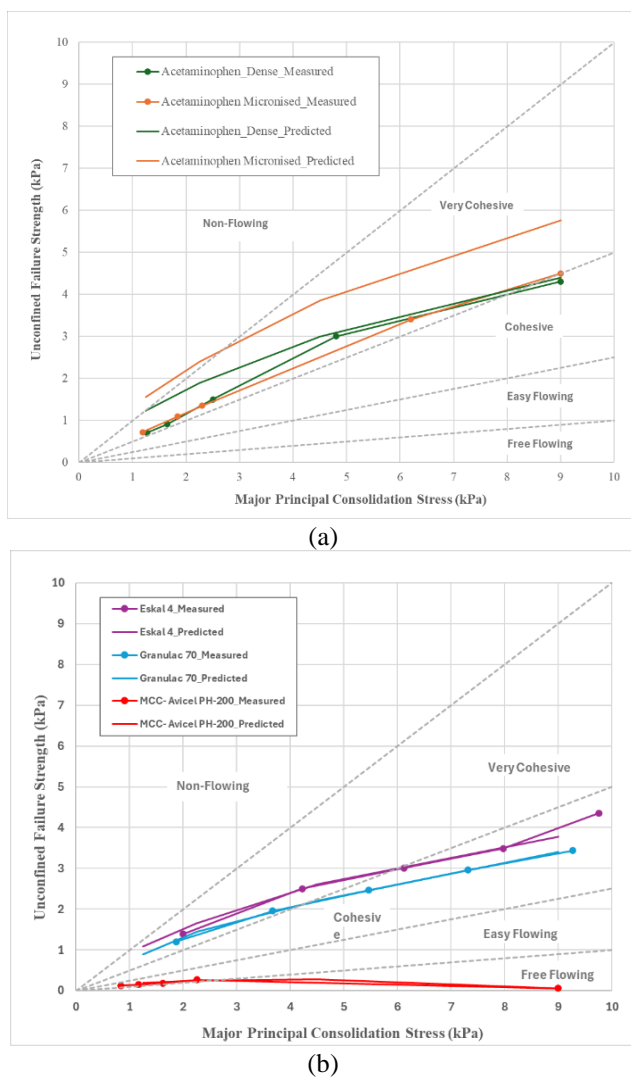


Figure 1. Instantaneous flow functions of the sample powders measured and predicted: (a) Acetaminophen dense and micronized, (b) Lactose, Avicel, and Calcium Carbonate

#### 3.2. Charge levels of the powders

In the case of the prediction of flowability for acetaminophen, electrostatic charge is thought to cause the difference in powder cohesiveness measurements due to different levels of particle adhesion at the different consolidation stress. Therefore, the charge levels and polarity distributions of the sample powders are measured by an inductive charge sensor and the results for all comparative materials are shown in Fig. 2.

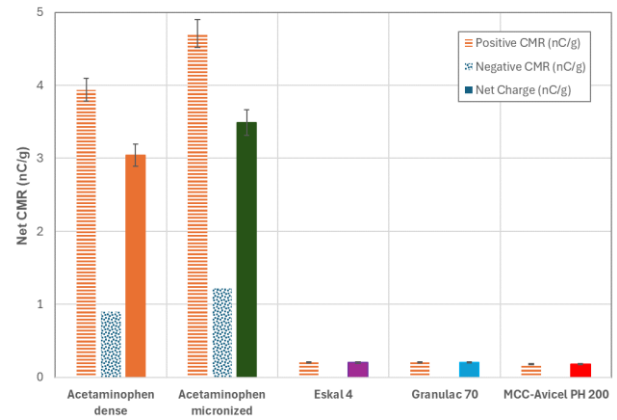


Figure 2. Charge levels and polarity distributions for the acetaminophen powders and the comparative materials.

### 4. Discussions

It is known that powder flowability is influenced by many factors including particle size and distributions, particle shape, friction between particles and storage conditions. The internal friction can be represented by powder cohesiveness which has a direct link with particle adhesion and been proved by previous studies [1]. However, this study discovered a difference in the measured flow functions and the predict flow function by using particle adhesions measured.

#### 4.1. The difference in predicted flow function

The results in Fig.1(a) clearly show that for acetaminophen micronized the predicted flow function is significantly higher than that measured using a PFT. For acetaminophen dense, it is noted that at the low consolidation stress the prediction is also higher than the measurement, but at the high consolidation stress the prediction is close to the measurement.

In comparison, the flow functions for three other common materials were predicted using the same method and compared to the measurements using a PFT. The results shown in Fig. 1(b) indicated a very good agreement between the predictions and the measurements. It reveals that there must be an influential factor in particle adhesion measurement, but it cannot contribute the powder flow properties at high consolidation stress. Considering the factors influencing particle adhesions, except capillary force, electrostatic force is thought that it is more likely the suspicious.

#### 4.2. The charge influences

The charge results in Fig. 2 identified the charge influences. It shows that the acetaminophens have much stronger bipolar charge compared to the other three materials as 20 times more.

### 5. Conclusion

Electrostatic charge is a strong donor to particle adhesion and alternative effects on powder cohesiveness at low consolidation stress. When the consolidation stress is high, the charge effect is negligible on powder flow properties.

### References

- [1] Garg, V., et al. (2022). A new method for assessing powder flowability based on physical properties and cohesiveness of particles using a small quantity of samples. *Powder Tech.*, 395, 708-719.
- [2] Deng, T., et al. (2021). A study of particle adhesion for cohesive powders using a novel mechanical surface energy tester. *Powder Tech.*, 391, 46-56.
- [3] Garg, V., et al. (2018). An investigation into the flowability of fine powders used in pharmaceutical industries. *Powder Tech.*, 336, pp.375-382.
- [4] Hussain, T., et al. (2012). Measurement of electrostatic charge on particles using a novel approach. *Int. Journal of Pharmaceutics*, 441(1-2), 781-789.
- [5] Deng, T., et al. (2023). Electrostatic charging of fine powders and assessment of charge polarity using an inductive charge sensor. *Nanomanufacturing*, 3(3), 281-292.

# Model predictive control simulation of pneumatic conveying of plastic pellets using nonlinear dynamics analysis and sparse identification of nonlinear dynamics with control

Osamh S. Alshahed<sup>1</sup>, Baldeep Kaur<sup>2</sup>, Michael S.A. Bradley<sup>2</sup> and David Armour-Chelu<sup>3</sup>

<sup>1</sup> Bradley Pulverizer, Kent, UK

<sup>2</sup> Wolfson Centre for Bulk Solids Handling Technology, University of Greenwich, Kent, UK

<sup>3</sup> School of Engineering, University of Greenwich, Kent, UK

**Abstract**—The study explores the integration of Model Predictive Control (MPC) and Sparse Identification of Nonlinear Dynamics with control (SINDYc) with nonlinear dynamics analysis to simulate the pneumatic conveying of plastic pellets. Nonlinear dynamics analysis measures were applied to data from a bottom arc-shaped electrostatic sensor of fully developed gas-solid flow in horizontal pipelines, including Lyapunov exponents, approximate entropy and recurrence rate. The study leverages SINDYc, a data-driven method, to identify sparse system models using the analysis measures. The MPC framework is then employed to optimise control inputs over a future horizon, ensuring desired nonlinear flow behaviour. The simulation framework assesses MPC's performance, using three distinct SINDYc models for each analysis measure to understand their control system's dynamics. Results showcase the ability to integrate MPC and SINDYc with the nonlinear dynamics analysis measures, highlighting improvements in system control.

**Keywords:** pneumatic conveying; model predictive control; sparse identification of nonlinear dynamics with control; chaos analysis; recurrence analysis.

## 1. Introduction

Pneumatic conveying systems are vital for transporting particulate materials as they provide dust-free and efficient material handling. However, these systems encounter challenges such as high energy consumption, material degradation, and pipeline blockages. Recent advancements in applying nonlinear dynamics analysis have shown promise in addressing these challenges by providing deeper insights into the complex behaviour of gas-solid flow systems near the pressure drop minimum curve (PMC) condition [1]. This analysis can extract invariant measures such as Lyapunov exponents (LE) for chaos, approximate entropy (AE) for unpredictability and recurrence rate (RR) for self-similar dynamics.

Classical control methods, like PID controllers, often struggle to maintain optimal conditions due to the complex nature of gas-solid flows [2]. In contrast, sparse identification of nonlinear dynamics with control (SINDYc) is a powerful data-driven method that identifies governing equations for dynamical systems from data, balancing complexity and prediction accuracy. When combined with model predictive control (MPC), SINDYc can effectively manage system nonlinearities and predict future states to optimise control inputs. This integrated approach is beneficial in scenarios with limited data and has demonstrated superior control performance [3].

This study uses the SINDY-MPC method with nonlinear dynamics analysis measures to conduct control simulations for each measure. By evaluating their control performance, the study seeks to identify the most appropriate measure to apply in a real-time control environment.

## 2. Material and methods

### 2.1. Pneumatic Conveying System Setup

The experimental setup for this study includes a pipeline cycle with a total length of 137 m and an inner diameter of 0.1 meters, a roots blower, a rotary feeder, a blow tank, and a receiving hopper, presented in Fig. 1. The conveyed material is plastic pellets with a mean diameter of 3.6 mm, a particle density of 910 kg/m<sup>3</sup>, and a bulk density of 560 kg/m<sup>3</sup>.

Five variables were measured to assess the pneumatic conveying characteristics: air and solids mass flow rates ( $\dot{m}_a$  and  $\dot{m}_s$ ), superficial air velocity ( $V$ ), pressure drop per unit length of a horizontal pipeline, and the bottom arc-shaped electrostatic sensor data.  $\dot{m}_s$  was measured at the receiving hopper using load cells and correlated with the rotary feeder speed. Four pressure sensors (P1, P2, P3, P4) were used, with P1 installed at the Roots blower exit to calculate  $\dot{m}_a$ , and P2, P3 and P4 downstream of the third bend for pressure drop. Assuming the flow is an ideal gas,  $V$  was calculated based on P2,  $\dot{m}_a$ , pipeline diameter and ambient temperature. The bottom arc-shaped electrostatic sensor was positioned at 1.62 m from P2.

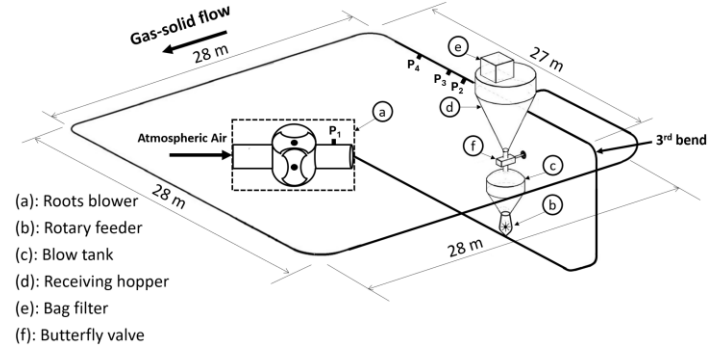


Figure 1. A schematic of a pneumatic conveying system setup.

### 2.2. Analysis and Modelling Methods

The nonlinear dynamics analysis starts by reconstructing a moving window of phase space from data collected using the bottom arc-shaped electrostatic sensor, then applying invariant measures (LE, AE and RR). Phase space reconstruction requires parameters such as moving data window, window step, time delay and embedding dimension, which are set to 10s, 2.5s, 1 and 2, respectively. LE quantify the rate at which nearby trajectories in phase space diverge or converge, which requires an expansion range, set to 5 steps. AE measure the unpredictability of time-series data by comparing the closeness of trajectories in phase space. RR is the ratio of recurrent points to the total number of points in a recurrence plot of a phase space, which requires a threshold radius, set to 0.1.

The SINDYc method identifies sparse equations of polynomial functions from input-output data, balancing complexity and prediction accuracy. SINDYc parameters include polynomial order set to 1 and balancing parameter  $\epsilon$  set to 0.01.

### 2.1. Control Simulation Framework

The control simulation framework used in this study provides a simulation environment that evaluates the performance and sensitivity of MPC models. The framework has two main components: a predictor to predict future states using a system model given initial inputs and an optimiser that uses a predictor that uses the same system model to optimise a sequence of inputs by minimising a cost function to reach a desired reference state and outputs the first control input. The MPC parameters are set to constants except for the weight of the input rate of change; multiple values were considered to compare different MPC models and choose the one with optimum control performance, ranging from 5 to 30. The other parameters include the prediction and control horizon steps set to 4 steps, the weights for the state deviation and the control effort for an input set to the constant of 1 and 0, respectively.

## 3. Results and Discussion

### 3.1. Data Collection

The acquired dataset contains large- and small-scale inputs, as shown in Fig. 2. Sinusoidal wave and Schroeder phased harmonic sequence functions were applied to the Roots blower speed, presented in Fig. 2a, and a square function was applied to the rotary feeder speed to change the solids mass flow rate, presented in Fig. 2b. The input frequencies of the blower and rotary feeder speeds are manipulated at 100Hz. The sampling frequencies for pressure sensors were collected at 4 Hz. The bottom arc-shaped electrostatic sensor was collected at 100 Hz, presented in Fig. 3a.

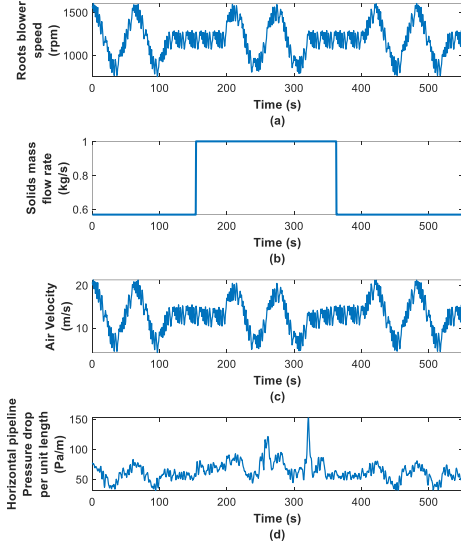


Figure 2. (a) Roots blower speed, (b) solids mass flow rate, (c) air velocity, and (d) pressure drop per unit length of horizontal pipeline.

### 3.2. Modelling and Control Performance Evaluation

The SINDYc method has been employed to construct three distinct system models. Each model incorporates two inputs: the Roots blower rpm control input and the solids mass flow rate disturbance input. Despite sharing the same inputs, the models differ in their outputs: LE, AE, and RR. Their predictions over the acquired dataset are illustrated in Figs. 3 a, b, c, and d. To assess their accuracy, the mean absolute percentage error was computed for each of the three models predicted and measured data, with the LE model having the lowest value of 1.4% and the RR having the highest value of 11.8%. The MPC simulation strategy is implemented to evaluate the control performance of the LE, AE, and RR system models using output reference step and disturbance step responses based on the output rise time and peak overshoot percentage. For each MPC model, the input rates

of change weight were selected at a 10% peak overshoot, presented in Fig. 4.

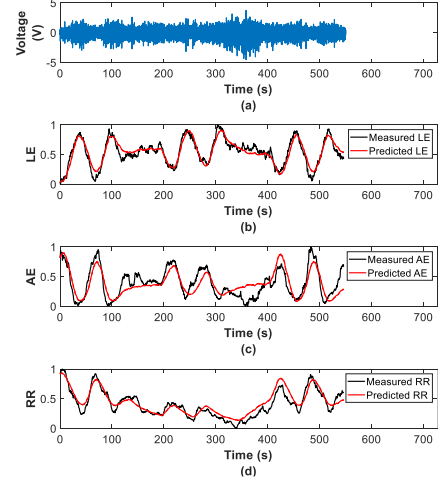


Figure 3. (a) The bottom arc-shaped electrostatic sensor measurement and the nonlinear dynamics analysis measures, including the (b) LE, (c) AE, and (d) RR, alongside their SINDYc system model predictions.

The LE MPC system model has the quickest reference step rise time at 20.7s, indicating a fast response to reference changes. The AE model shows the lowest disturbance input step peak at 4.5%, suggesting lower disturbance impact, but has nearly double the rise time of the LE model at 40.6s. The RR model, with a rise time of 22.3s, responds slower than the LE model but faster than the AE model. However, it exhibits the highest disturbance input step peak at 28.5%, indicating a significant sensitivity to disturbances. Thus, the LE measure is most suitable, offering a balance of quick response and moderate disturbance sensitivity, making it robust for real-time control applications.

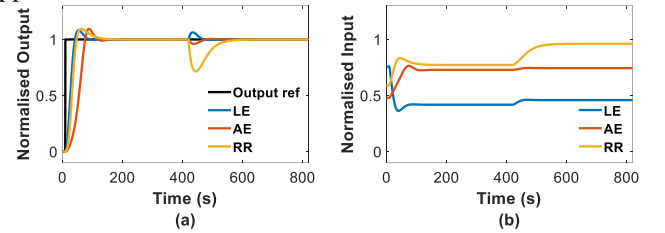


Figure 4. (a) Normalised output response at 10 % peak overshoot and (b) corresponding manipulated input.

## 4. Conclusion

The study effectively integrates MPC with SINDYc for simulating the pneumatic conveying of plastic pellets. LE, AE, and RR measures were evaluated, with LE proving most suitable for real-time control due to its fast response and moderate disturbance sensitivity, enhancing system robustness and control performance.

## Acknowledgement

The author acknowledges the financial support from the University of Greenwich through the Vice-Chancellor scholarship (VCS-ES-04-19).

## References

- [1] O.S. Alshahed, B. Kaur, M.S.A. Bradley, and D. Armour-Chelu, "Application of nonlinear dynamics analysis to gas-solid flow system in horizontal pneumatic conveying of plastic pellets," *Powder Technol.*, **428**, 118837, 2023. doi: 10.1016/j.powtec.2023.118837
- [2] R. Deloughry and E. Pickup, "Investigation of the closed-loop control of a pneumatic conveying system using tomographic imaging," *Process Imaging for Automatic Control*, 4188, 103, 2001. doi: 10.1117/12.417155
- [3] E. Kaiser, J. N. Kutz, and S. L. Brunton, "Sparse identification of nonlinear dynamics for model predictive control in the low-data limit," *Proceedings of the Royal Society A: Mathematical, Physical and Engineering Sciences*, 474(2219), 2018. doi: 10.1098/rspa.2018.0335

# On the effect of Powder Cohesion on the location of Geldart Group A to Group C Fluidisation boundaries

Hamed J. Sarnavi<sup>1</sup> and Michael S.A. Bradley<sup>1</sup>

<sup>1</sup> Wolfson Centre for Bulk Solids Handling Technology, FES, University of Greenwich, Chatham Maritime, Kent, ME4 4TB, UK

**Abstract—** This study explores the potential of enhancing the predictive capability of the Geldart chart for fluidisation behaviour in wet cohesive particles by incorporating additional flow properties beyond particle size and density. Focusing on a case study involving the flatbed drying of a highly cohesive food powder, the research emphasises the importance of achieving a near-fluidisation state to maximise the thermal energy efficiency of the drying process. Basic physical characterization was performed, and bulk cohesion were measured through shear testing. Fluidisation trials were conducted at both lab and full scales. The results provided insights into the aerodynamic behaviour of the bed, guiding the integration of wet-induced cohesiveness into the application of the Geldart chart. These findings are crucial for optimizing the design and operation of flatbed drying systems and have broader implications for other materials as well.

**Keywords:** Cohesion; Geldart chart; Fluidisation; Food

## 1. Introduction

Accurately predicting the hydrodynamic behaviour of cohesive powders during aeration is crucial in various industrial applications, including flatbed drying systems. The quality of the interaction between the air and particles at the minimum fluidisation point can ensure the highest drying rate or the shortest drying time, making it the optimal condition for drying wet particles. However, predicting this aerodynamic interaction in the sub-fluidisation and fluidisation regions has proven to be particularly challenging for wet materials [1]. There have been several attempts to devise theoretical and empirical classifications of these behavioural types. Of these, the most widely used is the empirical classification of Geldart, 1973, who divides fluidisation behaviour according to mean particle size and density difference between the solids and the fluidising gas [2,3]. It is crucial to consider the fact that the Geldart classification was developed by experimenting on dry particles for which the main cohesive force is the Van der Waals forces [1]. Therefore, attempts for reinforcing the current classification by incorporating further features of the particles beyond their size and density is sought. This study seeks to showcase how cohesion among wet particles influences a shift from Group A to Group C fluidisation boundaries, highlighting the importance of considering cohesive forces in the accurate prediction of fluidisation behaviour.

## 2. Material & Methods

### 2.1. Case study product: Cassava grits

The mechanically dewatered cassava mash was pulverised to produce cassava grits, which were then subjected to a drying process. These grits, which initially contain around 45% wet based water content, tend to form lumps easily.

### 2.2. Physical and Flow Characterisation

TM3030 Plus Benchtop Electron Microscope Hitachi and a Sympatec HELOS/RODOS laser diffraction particle size

analyser were employed to investigate the morphology and particle size distribution of the samples. A shear tester of PFT, Brookfield AMETEK was used to measure bulk flow properties.

### 2.3. Fluidisation characteristics

A series of aeration experiments were conducted at both full-scale and lab-scale. Full-scale trials involved a column with a diameter of 1m and a sample depth of 0.22m, while the lab-scale tests utilised a column with a diameter of 0.15m and a depth of 0.2m.

## 3. Results and Discussion

### 3.1. Physical properties

The morphological characterization results revealed that the cassava grits consist of aggregates of smaller entities, mainly starch granules, ranging from 10 to 20 microns in size. These are accompanied by coarser fibrous particles. The particle size distribution results indicated that the grits had particle size ranges of 141-227 $\mu$ m for D10, 456-473 $\mu$ m for D50, and 724-747 $\mu$ m for D90. The particle density, ranging from 1190 to 1230 g/cm<sup>3</sup>, showed a slight increase as the water content was removed.

### 3.1. Bulk flow properties

The shear test results indicated that the bulk density ranged from 370 to 580 g/cm<sup>3</sup>, with a decrease in density as the product dried. A significant increase of up to 80% in bulk density was observed when a consolidation load reached 4.8 kPa. This significant change in the packed structure of the particles was evident in the constructed failure envelopes, and it was also reflected in the cohesion values. The cohesion values are presented in Table 1.

TABLE I. COHESION VALUES OBTAINED FROM SHEAR TEST

Water Content (wet based)	Consolidation Load		
	482 Pa	1038 Pa	2237 Pa
46 %	289 Pa	483 Pa	1000 Pa
31 %	87 Pa	210 Pa	429 Pa
14 %	40 Pa	73 Pa	149 Pa

For the wet product, cohesion quantified as 289 Pa at the lowest consolidation load and increased to 1000 Pa under a consolidation load of 2237 Pa. However, after losing around one third of its water content, the cohesion values decreased significantly by a factor of 7.

### 3.2. Fluidisation Results

The sub-fluidisation behaviour of both wet and partially dry product was captured experimentally in light of the scale up effect. Figure 2 plots the experimental data for the five repeats of each trial.

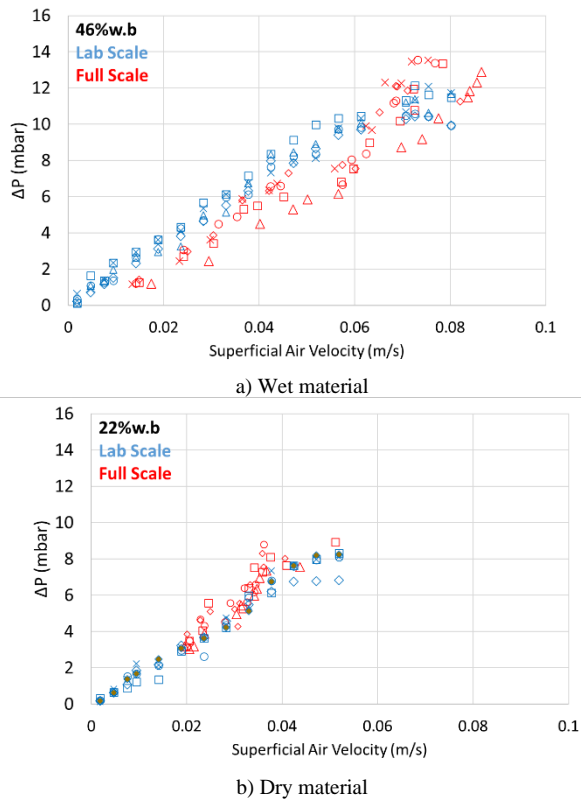


Figure 1. Experimental data of the fluidisation tests.

The superficial air velocity through the particles could reach up to 8.5 m/s for wet materials and 5.2 m/s for dry materials. At the same time, the gauge pressure beneath the material, just before fluidisation occurred, ranged between 10 and 14 mbar. In the lab scale trials, the material showed a slightly expansion before reaching the fluidisation point. But in the full-scale trials, the bed tends to bend due to the air back pressure beneath it rather than showing expansion and as a result a sudden loss of the static state of the bed happened. Nevertheless, no significant differences were obtained between the lab scale and full-scale trials for dry state of the material. This trend can also be linked to the decreasing magnitude of interparticle forces as the material dries. It is important to consider the impact of back pressure from the air beneath the material layer, which can be mimicked by applying a consolidation load during shear testing to measure cohesion. As shown in the shear test results in Table 1, the cohesion of the wet material was significantly affected by the consolidation load, whereas the dry material showed much less impact.

### 3.3. Cohesion in Geldart Classification

A significant deviation from Geldart classifications was observed when the case study material had higher water content level. A channelling behaviour occurred when the wet material reached the fluidisation stage while a smooth aeration with bubbling was expected according to the Geldart chart shown in Figure 2. Similar behaviour has been observed for products with starchy nature [2], reported channelling and agglomeration of dry corn-starch particles (15  $\mu\text{m}$ ), falls in Geldart Group C, during the attempts to fluidisation. It seems reasonable to interpret the boundary shift in Geldart classification as if it possessed finer particles in interaction with the flowing air. The wet surface of the freshly prepared cassava grits greatly enhances interparticle forces, similar to how a finer particle size distribution can lead to increased cohesion compared to coarser particles.

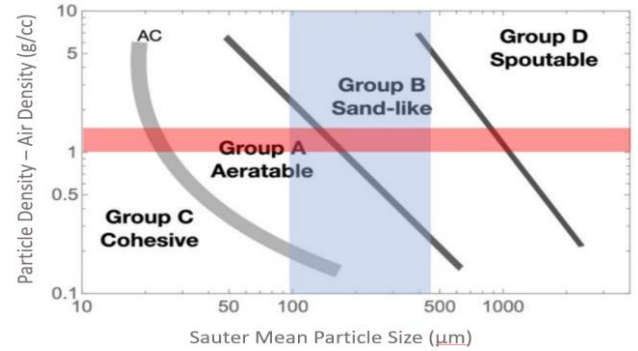


Figure 2. Geldart chart and classification; highlighting the expected region based on the physical properties of the product

Additionally, the hydrostatic pressure exerted by the stagnant air beneath the material layer served as a consolidating load, resulting in an increase in cohesion. Consequently, the particles began adhering together, forming agglomerates that ultimately blocked the existing air paths, thereby promoting the plunge lifting motion of the bed. Therefore, instead of exhibiting bubbling or slugging movement of air through the material layer, the fluidisation behaviour primarily showed channelling. However, the impact of this consolidating force on cohesion decreased as the material dried. This rationale finds support in the trend that emerged as the material became drier and gradually began to align more closely with the predictions presented in the Geldart graphs. This logical connection underscores the role of cohesion in predicting the fluidisation behaviour.

## 4. Conclusion

Despite the well-accepted utility of the Geldart classification, it should be used with an awareness of its limitations. This research showcases how incorporating the concept of cohesion can improve the prediction of fluidisation behaviour. Although cohesion, due to factors such as particle size or moisture content, is a complex concept and must be defined according to the measurement procedure, the study shows that cohesion measured through shear testing can be a promising indicator. Nonetheless, further investigation is needed to develop a systematic approach for incorporating cohesion into fluidisation predictions.

## Acknowledgement

The fieldwork of this research was funded by the FaNSI program, Natural Resources Institute, University of Greenwich, part of Research England 'Expanding Excellence in England' funding.

## References

- [1] T. Yehuda, and H. Kalman, Geldart classification for wet particles. *Powder Technology*, 362, 288–300, 2020.
- [2] Y. Zhou, T. Wang, J. Zhu., Investigation on minimum fluidization velocity in a modified Geldart's diagram. *Chemical Engineering Journal*, Vol 453, 2, 2023.
- [3] Cocco, R., & Chew, J. W. 50 years of Geldart classification. *Powder Technology*, 428, 118861, 2023.



# Application of Machine Learning to Granular Systems and Processes

Hugh Stitt<sup>1</sup>, Joe Emerson<sup>2</sup>, Carl Jackson<sup>1</sup>, Rob Gallen<sup>2</sup>

<sup>1</sup> Johnson Matthey, Technology Centre, Billingham, UK

<sup>2</sup> Johnson Matthey, Technology Centre, Sonning Common, UK

**Abstract**— The inherent statistical nature of granular systems and their behaviour is challenging to modelling in general but makes them well suited to Machine Learning approaches. This paper presents a series of case studies to illustrate some examples of successful use. The discussion will highlight also highlight good and poor practice in ML modelling, stressing that the latter can readily generate models that, albeit with a high correlation coefficient are (with a nod to George Box) are not useful.

**Keywords:** machine learning; feature selection, overfitting, powder properties, granular systems

## 1. Introduction

The application of Machine Learning (ML) methods and the associated Artificial Intelligence (AI) are gaining greater attention. What are the potential benefits and pitfalls of this approach to wider modelling and control of granular systems and processes?

Within the domain of granular systems, the predominant use to date has been in modelling and evaluating data deriving from DEM simulations. There are however a limited number of studies where ML methods are used to rationalise experimental data for flow and powder formation. It has to be said that the quality of these contributions is variable in terms of both the powder technology and the adherence to good ML practice.

This presentation will, through the use of case studies, illustrate how ML approaches can be used for granular systems and properties. This will include, *inter alia*, indications of the pitfalls of ML usage and some guidance as to good practice.

## 2. Why use ML for Granular Systems?

ML is, at its heart, statistical in nature; a logistical regression that is data driven. Many fundamental properties of granular systems are represented as statistical distributions; most fundamentally, particle size. Many other systems properties and process behaviours are dependent on particle size, and its distribution. Particle strength is related to size, commonly via a Weibull distribution; a probability distribution with an embedded size distribution. The residence time in a continuous rotating drum of a given particle is dependent on where it lies in the size distribution: the distribution residence time includes a particle size dependency. This behaviour is of course a result of particle segregation which is itself size difference or density driven. In summary, powder and granular system descriptions must incorporate multiple statistical distributions which may be nested. This is of course an underlying reason why continuum models that adequately describe powder systems are so difficult to realise. By contrast this does present an opportunity for mathematical approaches that more readily accommodate variance and variability such as machine learning.

## 3. Modelling Powder Property: “Slurryability”

### 3.1. ML for Feature Engineering

The wettability of a powder (its ability to be drawn into a high solids content slurry) is governed by many factors [1]. Univariate correlations on, for example, bulk density or wetting

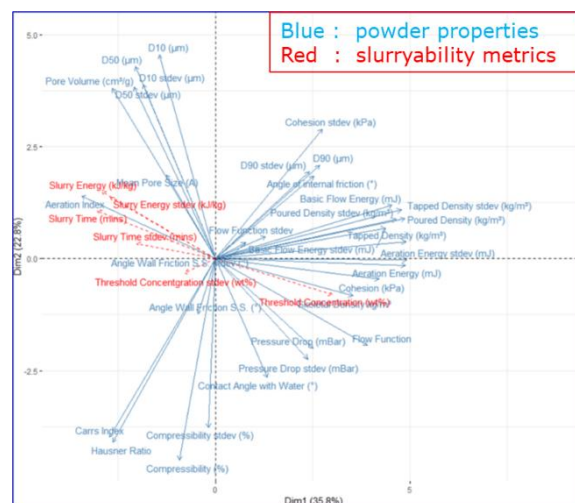


Figure 1: Principal Components Plot for Slurryability

contact angle) do not lead to satisfactory correlations. ML-based “feature engineering” using, in this instance, unsupervised Principal Components Analysis (PCA), Figure 1, to reveal cross correlation and low correlation of variables and supervised Partial Least Squares (PLS) to rank variable importance enables a data-driven reduction in the number of variables.

### 3.2. Correlation of Powder Wettability

The above data processing and feature engineering indicated that the optimal correlation of “slurryability” could be achieved using only 4 measured particle properties. Further, this correlation was validated by data for two unseen powders, demonstrating its “generalisation” – or predictive capability.

## 4. Modelling Powder Compaction

### 4.1. The Importance of Data Pre-processing

Data from a compaction simulator for over 350 single pellet compactions initially appear extremely untidy. Data wrangling methods can readily re-set all data sets to the same time scale, making the peak force event occur quasi-simultaneously [2]. This emphasises the data-preprocessing needs of ML – that are widely reported in the literature to demand over 80% of the total effort: the actual ML bit is simply “curve fitting”. Data pre-processing, how one looks at the data will influence the eventual modelling exercise – potentially disguising key features or amplifying minor ones. The feature engineering is again vital in reducing the number of parameters. This is a vital skill for the ML practitioner.

### 4.2. The Importance of the Data: the “Vs” of Data

The compaction data model fitting indicates that while pellet density can be readily correlated and predicted for unseen data, pellet hardness (crush strength) cannot. The reason for this lies however not in the property or modelling but rather in the reproducibility of crush strength data - reported in the literature to commonly have a scatter of  $\pm 25$ -30%. This leads to consideration of the “Vs” of data (Variety, Variance, Veracity, Volume ...) and that no modelling, other than overfitting, will conceal sparsity or unreliability of the input data. GIGO (garbage in – garbage out) remains a byword.



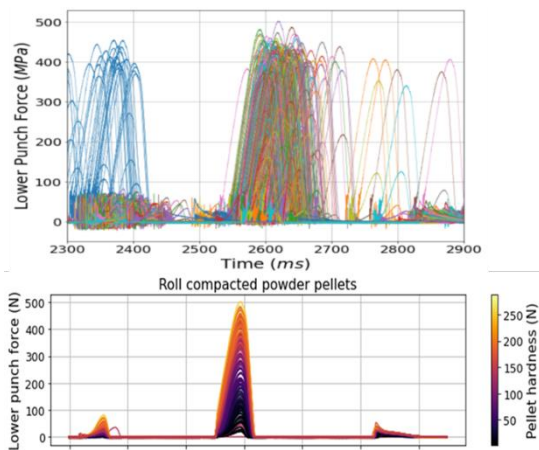


Figure 2: Raw and processed compaction data [2]

## 5. Modelling Jet Milling Data

### 5.1. Quality of Fit vs Overfitting

The vital and specific issue of overfitting (equivalent to over-parameterisation in deterministic equations) is addressed using jet milling data. It is shown that models with a high “correlation coefficient” are not necessarily good models. Rather, because of over-fitting (viz. tending to fit the scatter in the data beyond the physical features) they can lack generalisability – the ability to predict unseen data, Figure 3.

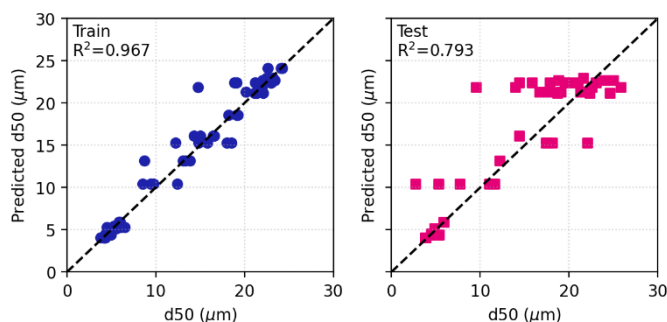


Figure 3: Training & Test Data Fits for an Overfitted Jet Milling Data Model

This emphasises the importance of cross-validation techniques (and quoting fitting values from unseen or test, not the training data) as well as techniques for specifically assessing quality of fit vs overfit, Figure 4, allowing optimisation of the model complexity and hyper-parameters.

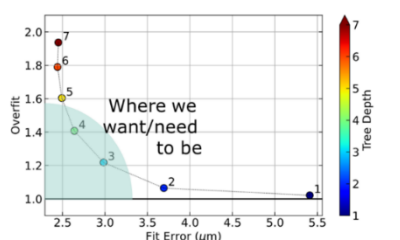


Figure 4: Random Forest Model Complexity vs Quality of Fit and Overfit

### 5.2. Over and Under Sampling

An interesting aside here is the selection of the size distribution “bin” sizes. More data (from small PBM-type bin sizes) do not always help. Citing only, say, a  $d_{10}$ ,  $d_{50}$  and  $d_{90}$ , can evidently under-represent a PSD: under-sampling. Using too small a bin size can be just as misleading, leading to an increase in “noise” and making the data prone to overfitting. The reason behind this is shown in Figure 5, that shows how, given only a moderate error bar on the data that adjacent and proximate bins have overlapping error bars and means indicating that they are not truly independent. This is exacerbated by the commonplace smoothing or regularisation of the data within the software of the PSD apparatus.

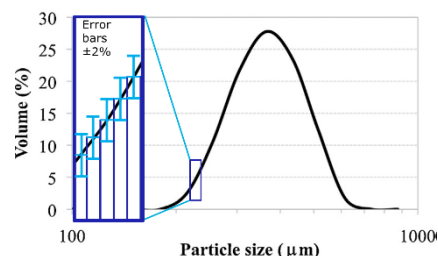


Figure 5: Data in PSD Bins may not be Independent and thus Prone to Over-sampling

### 5.3. ML Algorithm Selection

Similar over-fit vs quality of fit approaches can be exploited for ML algorithm selection once the number of input parameters or model depth is established, Figure 6 showing, in this instance, that the Support Vector Regression (SVR) should be favoured.

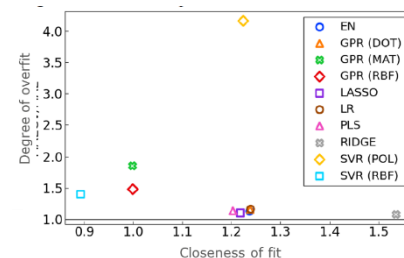


Figure 6: Use of Overfit Analysis in ML Model Selection

## 6. Hybrid Modelling Concepts

Finally, the concept of hybrid models: those combining both first principles and digital aspects. In this approach, data driven models can be built while retaining know physical principles. Of several actual viable model structures, one will be demonstrated – using theory as the prior to perform initial feature selection: in this case the fitting parameters from Druker Prager Cap compaction equation [3]. Variable importance ranking using PLS together with model complexity (number of parameters vs quality of fit and overfit) revealed that the data should be satisfactorily modelled using only two input parameters: maximum punch force and Youngs’ modulus. Quality of fit vs overfit was again used to compare 2-parameter ML algorithms leading to algorithm selection (Gaussian Process), which demonstrated good fit characteristics on both test and training data.

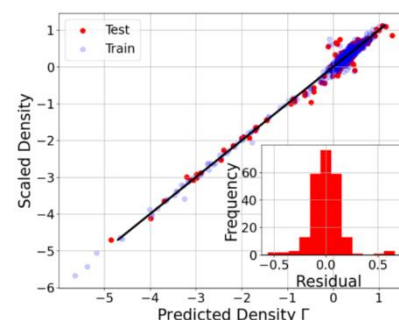


Figure 7: Pellet Density Hybrid 2-Parameter Gaussian Process Model [3]

## 7. Conclusions

Data driven or ML modelling approaches offer huge potential for application in particulate systems and processes. Successful application requires not only the requisite data processing and ML mathematical skills but also domain expertise. There are though many ways of producing poor, meaningless ML models which should be avoided. In deriving ML models data adequacy and model cross validation methods must be used. The latter with due consideration of overfitting and generalisation.

## References

- [1] T Wood, MJ Simmons, RW Greenwood, SA Turnbull, EH Stitt, *Ind. Eng. Chem. Res.*, 2019, 54, 14396.
- [2] JT Emerson, V Vivacqua, EH Stitt, *Johnson Matthey Technol. Rev.*, 2022, 66, (2), 154–163
- [3] M Trower, JT Emerson, M Yu, V Vivacqua, T Johnson, EH Stitt, G dos Reis, *Powder Technol.*, 2022, 427, 118745

# Exploring Predictive Laws for the Flowability of Powder Mixtures: the Case of UO<sub>2</sub> Powder

N. Blanc<sup>1</sup>, O. Laurent<sup>1</sup>, A.C. Robisson<sup>1</sup>

<sup>1</sup> CEA.DES.IRESNE.DEC.SA3E.LCU, Cadarache 13108 Saint-Paul-lez-Durance, France

**Abstract**— Dynamic behaviour of granular media is of crucial importance for many industrial processes. Better understanding of the powder rheology allows better control of the final properties of the manufactured product such as tablets or pellets and avoids specific problems occurring during powder conveying such as segregation or clogging of pipes and silos. In the nuclear field, powder flowability issues can lead to increased radiation exposure for workers who unclog pipes. Thus, in the context of nuclear fuel pellets fabrication, we explore flowability of mixtures of uranium oxides powders.

In this work, model powders were first developed to provide particles with "simplified" characteristics compared to conventional UO<sub>2</sub> powders. After determining particle physical characteristics of each powder, the flowability of these samples is studied by several indicators measured with a powder rheometer and other rheology characterization technics. The flow properties measured on these powders are analyzed in relation to the physical characteristics of the particles.

In a second step, binary mixtures were prepared using a cohesive model powder and a free flowing model powder. The flowability data was interpreted along three different axes: results analysis considering simple mixing laws, the use of correlation matrices to process data statistically, the use of models based on inter-particle forces and a multi-component population-dependent granular.

**Keywords:** flow; UO<sub>2</sub>; powder

## 1. Introduction

Nuclear fuel fabrication uses conventional powder metallurgy processes to produce the final fuel pellets. In order to improve the conditions under which actinide powders have been used in the manufacturing process, the CEA is studying their rheological behavior. Such laws could be used to predict the flowability of a UO<sub>2</sub> powder as a function of various stress conditions and the physical properties of the particles being studied. In particular, this type of law could help prevent tube clogging, thereby reducing radiation exposure to process maintenance personnel. In this context, UO<sub>2</sub> model particles have been developed to provide powders or granules with simplified characteristics. After characterizing their particle size, the rheological properties of these model particles are analyzed and interpreted in relation to their physical characteristics. In addition, binary mixtures were prepared using these model powders to verify the existence of mixing laws for predicting certain flow properties.

## 2. Préparation of model particles

### 2.1. Single model particles

Four batches of model particles were produced by granulation, crushing and sieving. Two batches of fine particles (less than 100  $\mu\text{m}$ , named FrF and GrF) and 2 batches of "small"

particles (between 100 and 300  $\mu\text{m}$ , named FrP and GrP) were thus produced. In order to obtain two distinct states of consolidation, 2 of the 4 batches (FrF and FrP) were treated at a temperature of 1600°C for 30 min under Ar/5%H<sub>2</sub>. This operation results in particles with a higher mechanical strength than GrF and GrP batches. These batches can also be used to simulate pellet scrap, which is industrially reintegrated into the fuel fabrication process.

### 2.2. Particles mixtures

The model powders FrP and GrF have been used to create binary mixtures, named M1, M2 and M3. M1 mixture is obtained by blending in a Turbula mixer. M2 mixture is obtained by adding GrF to the M1 mixture, followed by a new stirring for 10 min. The same applies to the M3 mixture, prepared from M2 (Tab. 1).

TABLE I. BINARY MIXTURES COMPOSITION

Binary mixture	Mass content FrP (%)	Mass content GrF (%)	Time mixing (min)
M1	75	25	10
M2	50	50	10 x 2
M3	25	75	10 x 3

a. Sample of a Table footnote. (Table footnote)

## 3. Particle characterisation

### 3.1. Physical characteristics

The physical characteristics correspond mainly to particle size distributions, which have been measured on single model powders and on powder mixtures. Particle densities were also determined for single powders.

Particle size distributions have been measured using a dry method with a Mastersizer 3000 laser particle sizer (Malvern). This method characterises the size of particles in conditions similar to those encountered during transport stages in a dry environment. Characteristic diameters and span values derived from the particle size distributions of model powders and mixtures were determined. The values measured are consistent with the batch preparation methods. It is also important to note that the batches can be distinguished by a difference in density, with values of approximately 10 and 6 g.cm<sup>-3</sup> for batches Fr and Gr, respectively.

### 3.2. Rheological properties

An FT4 powder rheometer (Freeman Micromeritics) was used to carry out 3 types of measurement: shear test, permeability measurement and compressibility measurement.

The shear test is used to assess the capacity of a powder to transition from a static to a dynamic state. The flow function coefficient  $ff_c$  is among the parameters that can be quantified by this test. Permeability is defined as the capacity of a porous material to be penetrated by a fluid. Compressibility is the rearrangement capacity of a powder bed.

### 3.3. First-level interpretation

The results obtained on single powders demonstrate that the powder flowability classification is specific to each rheological property measured. (Fig. 1). Indeed, these properties reflect different flow situations and depend on several physical characteristics. While size remains the dominant parameter for permeability, this is less clear for compressibility and flow function coefficient. In addition, the results on mixtures show the existence of a threshold effect around 30% fine particles for the flow function coefficient. Thus, in accordance with the literature for alumina powders, the flowability index of UO<sub>2</sub> powders is governed by the batch with the lowest flowability [1]. The results also indicate that the compressibility of a mixture can be deduced from the compressibility of the individual powders and the mass fractions corresponding to its composition. (Fig. 2).

## 4. Approaches for determining predictive laws

### 4.1. Use of correlation matrices

The construction of a correlation matrix is an initial step in identifying relationships between flow measurements and certain physical quantities [2]. Despite the limited number of samples, this methodology has been applied. Pearson correlation coefficients have been utilized, a method that identifies linear relationships between parameters. Using the logarithm of the data, it has also been possible to demonstrate the existence of correlations in the form of power laws. (Fig.4). The analysis of these matrices indicates that the flow function coefficient and the compressibility are correlated by a power law to the span and the powder d<sub>10</sub> characteristic diameter, respectively.

#### 4.1. Interpretation using the Bond number

A number of authors in the literature have identified a power law that links the flow function coefficient, obtained by shear tests, with the population dependent granular Bond number (1) [1, 3, 4].

$$ff_c = \alpha B o_G^{-\beta} \quad (1)$$

Based on the particle size distributions and the particle densities measured for UO<sub>2</sub> single model powders, the population dependent granular Bond number and the multi-component population dependent granular Bond number have been calculated. As in the literature for non-nuclear powders, a power law was deduced for UO<sub>2</sub> (2) with a good correlation coefficient (R<sup>2</sup>=0.96).

$$ff_c = 19.1 B o_G^{-0.19} \quad (2)$$

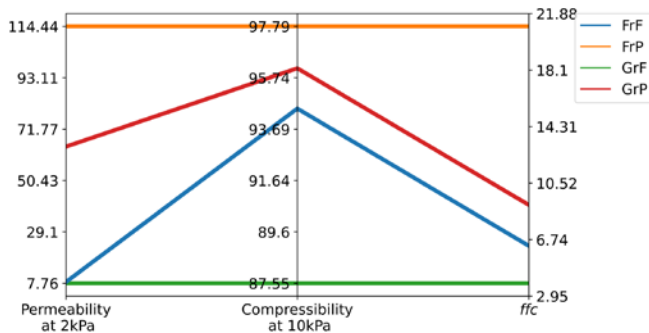


Figure 1. Permeability, compressibility and flow function coefficient for single model particles

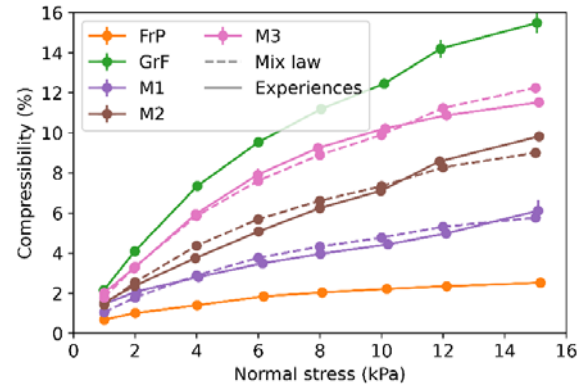


Figure 2. Compressibility of powder mixtures (mix law and experiences)

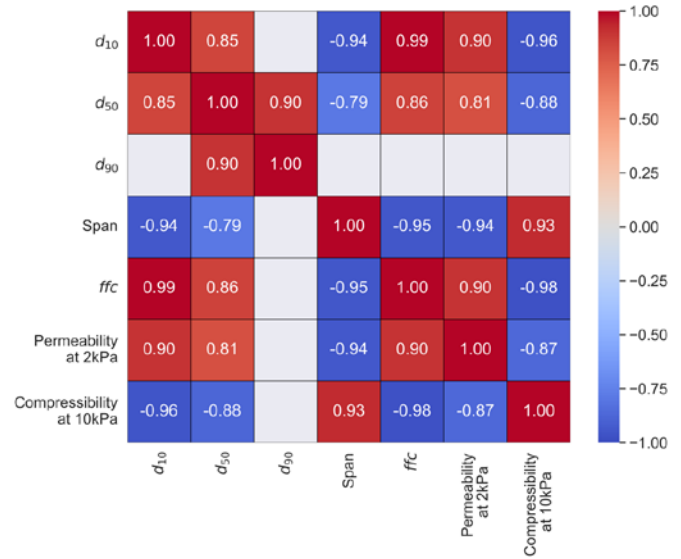


Figure 3. Absolute values of the Pearson correlation matrix taking into account the logarithms of various granulometric indices and FT4 flow properties (p-value ≤ 0,05).

## 5. Conclusion

This study shows that uranium oxide powders behave like other powders that have been more traditionally studied in the literature. It is therefore possible to determine certain flow properties of mixtures from their individual components. Furthermore, a power law relating to the flow function coefficient has been determined in accordance with the literature. Additionally, the use of correlation matrices has demonstrated the potential of this method for identifying the existence of other correlations for specific parameters. This work is continuing in order to refine existing correlations and predict the behavior of UO<sub>2</sub> powders as a function of their stress conditions.

## References

- [1] G. Bernard-Granger, M. Giraud et al., *Rheological properties of alumina powder mixtures investigated using shear tests*, Powder Technology, 2019.
- [2] A.P. Shier, A. Kumar et al. *Development of a predictive model for gravimetric powder feeding from an API-rich materials properties library*, International Journal of Pharmaceutics, 2022.
- [3] K. T. Kunnath, S. Tripathi, et al. *Selection of Silica Type and Amount for Flowability Enhancements via Dry Coating*, Pharm. Res., 2023.
- [4] M. Capece, K.Ruiz Silva, et al. *On the relationship of inter-particle cohesiveness and bulk powder behavior*, International Journal of Pharmaceutics, 2016.

# Machine Learning for the Calibration of Discrete Element Method Simulations

B.D. Jenkins<sup>1,2</sup>, A.L. Nicuşan<sup>1</sup>, A. Neveu<sup>2</sup>, G. Lumay<sup>3</sup>, F. Francqui<sup>2</sup>, J.P.K. Seville<sup>1</sup>, and C.R.K. Windows-Yule<sup>1</sup>

<sup>1</sup> School of Chemical Engineering, the University of Birmingham, Edgbaston, Birmingham, B15 2TT, UK

<sup>2</sup> Granutools, Rue Jean Lambert Defrene 107, 4340 Awans, Belgium

<sup>3</sup> Grasp laboratory, CESAM research unit, University of Liege, Place du 20 Aout 7, 4000 Liege, Belgium

**Abstract—** The calibration of Discrete Element Method (DEM) simulations presents difficulties and lacks a standardised procedure. One widely used technique involves deriving DEM particle properties from bulk measurements obtained via powder characterisation instruments, but it is presently a computationally intensive and demanding task for the individual performing the calibration. In this work, over 17,505 simulations of four powder characterisation tools were used to train a machine learning model that can accurately calibrate DEM simulations in seconds.

**Keywords:** DEM, calibration, machine learning, big data

## 1. Introduction

For an accurate simulation of the behaviour of granular materials in experimental systems using Discrete Element Method (DEM) simulations, accurate calibration of microscopic particle properties is essential. One of the most popular methods for calibrating particle properties in DEM simulation is the indirect method in which the particle properties of a real granular material are back-calculated from a bulk measurement or a set of bulk measurements [1]. However, this is a process that can take a person several weeks to complete due to the current time intensive nature of DEM simulations.

DEM is a very powerful tool that is capable of accurately modelling the bulk flow behaviour of many granular materials on a quantitative level [2]. However, to make DEM a practical tool for academia and industry to use, a novel approach to calibrating granular materials for DEM is required that is accurate and quick.

## 2. Method

The microscopic properties of particles in a granular material are closely linked to the material's bulk flow characteristics. For example, as shown in Figure 1 modifying the sliding friction coefficient between particles alters the dynamic angle of repose, highlighting the connection between particle ("micro") properties and bulk ("macro") behaviour. Understanding this relationship would enable direct determination of DEM particle properties from bulk behaviour measurements, but this relationship is complex due to numerous particle property interactions. To address this, a data-driven approach using machine learning was employed.

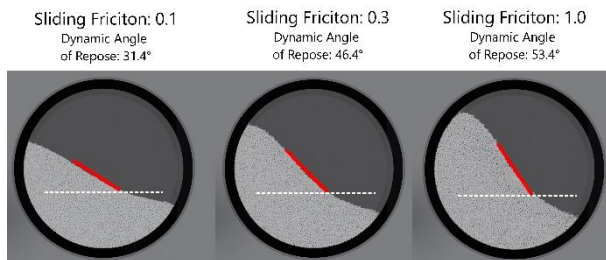


Figure 1. Sliding friction effect on the dynamic angle of repose in a rotating drum.

Given the extensive simulations required for this method, particles were assumed to be spherical, with rolling friction modelling surface roughness or non-sphericity. The selection

of contact laws was made by balancing speed and accuracy. In particular, the Hertz-Mindlin model [3] the CDT rolling friction model [4] and the Simplified-JKR (SJKR) model [5] were used.

### 2.1. Data Generation

To generate the data required to train the machine learning regression model to link bulk behaviour measurements to particle properties, more than 17,505 simulations of four different digital twins of common commercial powder characterisation tools were performed. The powder characterisation instruments used are detailed in Figure 2. Each instrument was simulated over 3000 unique combinations of particle properties, and the bulk behaviour measurements (dynamic angle of repose, angle of repose, Hausner ratio) were recorded.

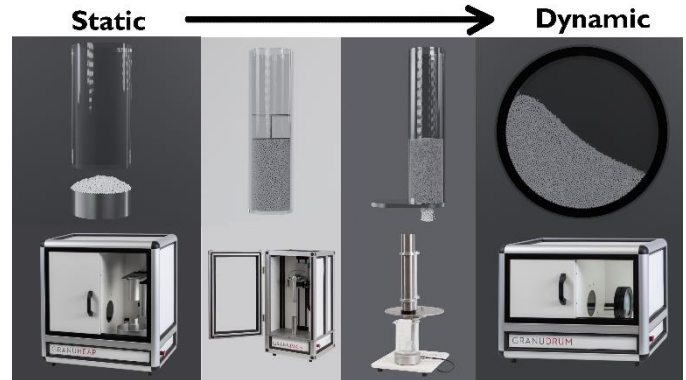


Figure 2. On the top, the digital twins of the powder characterisation instruments, on the bottom, the real instruments. From left to right the: GranuHeap, GranuPack, GranuFlow and GranuDrum.

### 2.2. Sensitivity Analysis

To enhance the training of the machine learning model, it is crucial to understand the impact of varying particle properties on bulk behaviour measurements. For this purpose, a sensitivity analysis was performed employing the RS-HDMR method. The outcomes of this study are depicted in Figure 3. The study revealed that the sensitivity of bulk behaviour measurements to particle properties varied significantly, with rolling friction and cohesive energy density generally being the most influential particle properties. The coefficient of restitution had minimal effect on bulk behaviour measurements meaning that it would be more difficult to calibrate [6].

### 2.3. Machine Learning Model

A benchmark of different machine learning models was conducted to determine which would give the most accurate model without overfitting. XGBoost [7] was found to provide the most accuracy for this data set. The hyperparameters of the XGBoost model were optimised using the Optuna [8] framework.

## 3. Results

The validation of the machine learning model is ongoing as the material complexity gradually being tested slowly increases, but the calibration methodology can already be



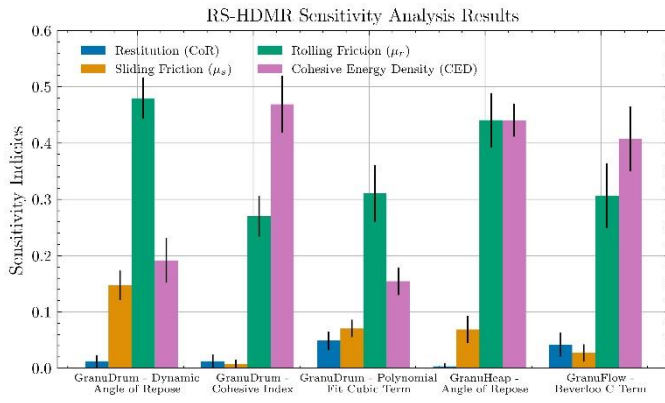


Figure 3. Results of RS-HDMR analysis study for the GranuDrum, GranuFlow and GranuHeap [6].

demonstrated. Experiments were conducted to measure the bulk behaviour of 1 mm glass beads using the GranuDrum and GranuHeap. The results of which can be seen in Table I. At this particle size, the glass beads can be considered cohesionless, necessitating the calibration of only three particle properties for a DEM simulation: the coefficient of restitution, sliding friction, and rolling friction.

TABLE I

BULK BEHAVIOUR MEASUREMENTS FROM THE REAL INSTRUMENTS.

Rotating Drum	10 RPM	30 RPM	50 RPM
Dynamic Angle of Repose	33°	41.2°	49°
Cubic Polynomial Fit	8.44e-7	7.86e-6	1.76e-5
<b>Angle of Repose Tester</b>			
Angle of Repose	16.92°		

These experimentally measured values were given to the machine learning calibration model which gave a set of calibrated values for the three particle properties in Table II.

TABLE II

PARTICLE PROPERTIES OF 1 MM GLASS BEADS CALIBRATED BY THE MACHINE LEARNING MODEL.

Particle Properties	Values
Coefficient of Restitution	0.74
Sliding Friction	0.78
Rolling Friction	0.094

As with any calibration, it is essential to validate the results. For this case, a straightforward validation was performed by running three rotating drum simulations at 10, 30, and 50 RPM, using monodispersed 1 mm spheres with the machine learning calibrated particle properties. Figure 4 presents a comparison of the dynamic angle of repose measured for the 1 mm glass beads in a rotating drum, contrasting the

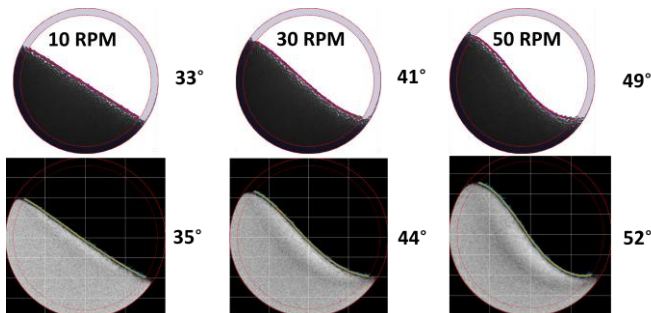


Figure 4: Comparison of rotating drum experiment dynamic angle of repose and the machine learning calibrated DEM simulation dynamic angle of repose.

experimental results with those from a DEM simulation calibrated with the machine learning derived particle properties. The results were within 1-2 of degrees of the experimental results across several rotational speeds showing there is still some room for improvement.

## 4. Conclusion

A machine learning approach was developed using XGBoost to link bulk behaviour measurements from commercial powder characterisation instruments with the particle properties necessary for accurate DEM simulations of granular materials. The model training data consisted of more than 17,505 simulations of four common powder characterisation instruments. Validation using monodispersed 1 mm glass beads demonstrated that the calibrated values could reproduce the dynamic angle of repose within a few degrees, confirming the method's effectiveness but also potential for further improvement.

## Acknowledgement

Authors acknowledge financial support received from the Centre for Doctoral Training in Formulation Engineering (EPSRC grant number EP/S023070/1) and Granutools. Computational resources have been provided by the Sulis Tier 2 HPC platform hosted by the Scientific Computing Research Technology Platform at the University of Warwick and the University of Birmingham BlueBear facility (see <http://www.birmingham.ac.uk/bear> for more details).

## References

- [1] C. R. K. Windows-Yule and A. Neveu, "Calibration of DEM simulations for dynamic particulate systems," *Papers in Physics*, vol. 14, p. 140010, 7 2022. [Online]. Available: <https://www.papersinphysics.org/papersinphysics/article/view/795>
- [2] C. R. K. Windows-Yule, D. R. Tunuguntla, and D. J. Parker, "Numerical modelling of granular flows: a reality check," *Computational Particle Mechanics*, vol. 3, no. 3, pp. 311–332, 2016. [Online]. Available: <https://doi.org/10.1007/s40571-0150083-2>
- [3] C. J. Coetzee, "Review: Calibration of the discrete element method," *Powder Technology*, vol. 310, pp. 104–142, 2017.
- [4] J. Ai, J. F. Chen, J. M. Rotter, and J. Y. Ooi, "Assessment of rolling resistance models in discrete element simulations," *Powder Technology*, vol. 206, no. 3, pp. 269–282, 1 2011.
- [5] M. Ajmal, T. Roessler, C. Richter, and A. Katterfeld, "Calibration of cohesive DEM parameters under rapid flow conditions and low consolidation stresses," *Powder Technology*, vol. 374, pp. 22–32, 9 2020.
- [6] B. D. Jenkins, A. L. Nicusan, A. Neveu, F. Francqui, J. P. K. Seville, D. Weston, D. Werner, and C. R. K. Windows-Yule, "The Sensitivity of Powder Characterisation Tool Measurements to Particle Properties," 2024.
- [7] T. Chen and C. Guestrin, "XGBoost," in *Proceedings of the 22nd ACM SIGKDD International Conference on Knowledge Discovery and Data Mining*. New York, NY, USA: ACM, 8 2016, pp. 785–794.
- [8] T. Akiba, S. Sano, T. Yanase, T. Ohta, and M. Koyama, "Optuna," in *Proceedings of the 25th ACM SIGKDD International Conference on Knowledge Discovery & Data Mining*. New York, NY, USA: ACM, 7 2019, pp. 2623–2631.

# Insights from DEM Simulations for Shear Cell Experiments with Wooden Spheres

Salvatore la Manna<sup>1</sup>, Klidi Qyteti<sup>2</sup>, Sina Zinatlou Ajabshir<sup>1</sup>, Diego Barletta<sup>1</sup>, Enric Illana<sup>2</sup>, Massimo Poletto<sup>1</sup>

<sup>1</sup> Department of Industrial Engineering, University of Salerno, Via Giovanni Paolo II, 132, 84084 Fisciano, SA, Italy

<sup>2</sup> Department of Energy Plant Technology, Ruhr-University Bochum, Universitätsstraße 150, 44780 Bochum, Germany

**Abstract**— The flow of solid particulates is governed by several factors, including granular density, bulk density, size distribution, stiffness, and cohesion. While powder flow testers are effective for fine powders, they are inadequate for coarse particles. Continuum-based methods also prove insufficient for particles larger than a few millimetres. However, the Discrete Element Method (DEM) shows considerable promise for these systems, particularly in reactive environments such as iron ore reduction, where particle properties evolve during conversion.

This research aims to verify the feasibility of extracting reliable data from a standard Schulze ring shear tester and comparing it with a DEM model using wooden spheres. Experimental tests at the University of Salerno involved monodisperse wooden spheres of 6 and 10 mm diameters. The Schulze rotational shear tester measured stress components, and the data were used to calibrate a DEM model. The results showed high similarity between the model and experiments, confirming the potential of using raw data from shear testing equipment to calibrate DEM models for large particles.

In summary, the study demonstrates that the Schulze ring shear tester can provide valuable data for calibrating DEM models, even for larger particles. This finding is significant as it opens up new possibilities for accurately modelling and predicting the behaviour of coarse particulate systems in various industrial applications. The successful calibration of DEM models using shear testing data could lead to more efficient and effective processes in industries where the handling and processing of large particles are critical.

**Keywords:** rotational shear cell, coarse particles, wooden spheres, cohesion, DEM simulation.

## 1. Introduction

Various factors affect the flow of solid particulates, such as granular density, bulk density, size distribution, stiffness, and cohesion. Established methods and standardized devices, such as powder flow testers, are effective for characterizing granulates and fine powders but cannot be directly applied to coarse particles. In fact, continuum-based methods are inadequate for interpreting the flow behaviour in laboratory settings for particles larger than a few millimetres. On the other hand, simulations using the Discrete Element Method (DEM) are appropriate for these systems and particularly promising when applied to reactive environments, such as the iron ore reduction processes, in which the particle properties, including the occurrence of interparticle adhesive forces, can evolve with particle conversion. Therefore, an alternative approach to take advantage of the controlled conditions of shear testing equipment with DEM simulation might be the direct interpretation of raw data obtained with conventional shear testing equipment to calibrate DEM models properly. The primary objective of this research is to verify the possibility of

extracting reliable data from a standard Schulze ring shear tester equipment and compare them with a DEM model system made of wooden spheres.

## 2. Experiments

Experimental tests were conducted at the University of Salerno (UniSA) using the standard Schulze rotational shear tester. Two monodisperse samples of spherical wooden spheres, with diameters of 6 and 10 millimetres and a powder density of approximately 0.79 kg/m<sup>3</sup>, were selected to reduce mathematical complexity and for the similarity with the shape of iron pellets used in direct iron reduction. The Schulze rotational shear tester, designed to measure stress components in bulk materials, compresses the material vertically and measures shear stress due to particle rotation. The cell of the tester is made of two elements: the lid and the trough. During testing, the trough (containing the sample) remains in rotation, while the lid vanes induce internal friction as they create two distinct regions within the sample. One upper region contains static particles between the vanes, and the other includes particles in motion from the trough rotation and shearing against the static particles of the upper layer. The relative motion between static and moving particles allows for quantifying friction phenomena between particles and evaluating the shear stress at the surface of transition between the two regions.

For experimental tests, a standard M-type rotation shear cell was used. The lid has an annular section with an inner diameter of 102 mm and an outer diameter of 198 mm. Additionally, 20 rectangular sectional vanes are radially positioned on the surface in contact with the material. The trough, where the sample is located, has dimensions of 40 mm (thickness) x 100 mm (inner diameter) x 200 mm (outer diameter). The experimental data necessary to calibrate the DEM model were obtained by subjecting wooden spheres to a two-step characterization procedure generally used for fine powders. Three values of normal force (15 N, 25 N, and 50 N) were investigated during particle compression.

## 3. DEM Simulation

The two components of the shear cell were replicated in a 3D model (Fig. 1) and meshed using tetrahedral elements.

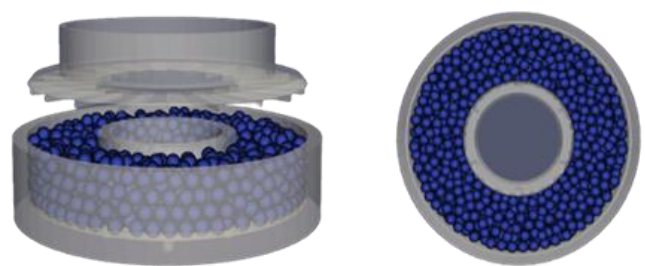


Figure 1 Shear cell in the simulation approach.



The simulation begins with wooden particles positioned above the shear cell, and approximately 950 and 4000 particles are used for 6mm and 10mm wooden spheres, respectively. Gravity causes the spheres to fall into the bottom ring of the shear cell, resulting in a random arrangement that mimics real loading conditions.

Table 1 Parameters used for the interaction between wooden pellets and the shear cell surface for the two simulations.

Parameter	Particle-particle interaction	Particle-surface interaction
Rolling friction coefficient	0.002	0.002
Sliding friction coefficient	0.3	0.6
Coefficient of restitution	0.3	0.7
Collision time	0.001	0.001
Particle density	720 kg/m <sup>3</sup>	

The model used for computing the forces is a linear spring-dashpot. The model parameters (tangential and normal spring stiffness as well as the tangential and normal damping coefficients) can be specified directly or calculated. In this work, the alternative of calculating the mass-related model parameters was chosen. For this purpose, the restitution coefficient, the tangential to normal spring stiffness ratio and the contact time are required as input variables for the linear spring-dashpot model [1-3]. In addition, the coefficient of rolling and sliding friction is specified. The value of these parameters is given in Table 1.

In the simulation, the lid is lowered onto the spheres until the desired normal force is exerted upon them. Once positioned, the normal force remains constant. Adjusting the vertical position of the lid allows for the setting and maintenance of all normal force levels required for the shear test. Fig. 2 compares the model and the experimental results regarding normal stress (Fig. 2a) and shear stress Fig. 2b) for a 50 N normal load and 6 mm particles.

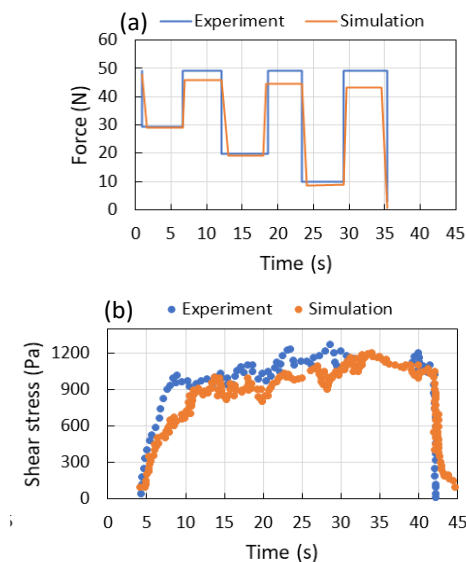


Figure 2 (a) Normal force and (b) shear stresses verified with the simulation compared with an experiment with an applied normal load of 50 N.

## 4. Conclusion

In conclusion, this research demonstrates the feasibility of using raw data from conventional shear testing equipment to calibrate DEM models for coarse particles. The high correlation between experimental results and DEM simulations underscores the potential of this approach. By leveraging the controlled conditions of shear testing equipment, it is possible to obtain

reliable data for DEM model calibration, even for particles larger than a few millimetres. This method offers a promising alternative for characterizing the flow behaviour of large particulates, particularly in reactive environments like iron ore reduction processes.

## Acknowledgement

The research presented in this paper was conducted as part of the project “Maximise H<sub>2</sub> Enrichment in Direct Reduction Shaft Furnaces” (Ref. MaxH2DR), GA No. 101058429, funded by the Horizon Europe EU framework programme. We gratefully acknowledge this support. The authors bear sole responsibility for the content of the paper; the Commission is not liable for any use of the information contained herein.

## References

- [1] J. Schäfer, S. Dippel, D.E. Wolf, *Force Schemes in Simulations of Granular Materials*, Journal de Physique I 6 (1996) 5–20. <https://doi.org/10.1051/jp1:1996129>.
- [2] H. Kruggel-Emden, E. Simsek, S. Rickelt, S. Wirtz, V. Scherer, *Review and extension of normal force models for the Discrete Element Method*, Powder Technology, Volume 171, Issue 3, 2007, Pages 157-173, <https://doi.org/10.1016/j.powtec.2006.10.004>.
- [3] H. Kruggel-Emden, S. Wirtz, V. Scherer, *A study on tangential force laws applicable to the discrete element method (DEM) for materials with viscoelastic or plastic behavior*, Chemical Engineering Science, Volume 63, Issue 6, 2008, Pages 1523-1541, <https://doi.org/10.1016/j.ces.2007.11.025>.

# Study of the infiltration of non-spherical slurry particles in a sand stratum during slurry shield tunnelling by CFD–DEM simulations

Jiayuan Liu<sup>1</sup> and Kevin J Hanley<sup>1</sup>

<sup>1</sup> University of Edinburgh, Scotland, UK

**Abstract**—Slurry infiltration and filter cake formation play key roles in maintaining excavation stability in slurry shield tunnelling. This paper presents a numerical model for slurry pressure balance (SPB) tunnelling, designed to simulate slurry infiltration in a horizontal orientation. It uses coupled computational fluid dynamics (CFD) and discrete element method (DEM) simulations to contrast the SPB tunnelling approach with a laboratory column test model. The analysis highlights variations in infiltration distance, fluid characteristics, and permeability. The SPB model demonstrates a broader infiltration range and distance, along with increased permeability. Fluid pressures in the SPB model dissipate more rapidly, resulting in quicker drops in velocity. Overall, the SPB tunnelling model offers a more accurate representation of slurry infiltration dynamics compared to the commonly used laboratory column test model.

**Keywords:** Coupled CFD–DEM simulation; Slurry pressure balance; Filter cake formation; Non-spherical particles

## 1. Introduction

Slurry pressure balance (SPB) machines are increasingly employed in urban tunnel construction projects [1]. Laboratory column tests for slurry infiltration have been widely used over recent decades to explore the macroscopic aspects of the infiltration process [2]. The CFD–DEM approach, which can provide an understanding of the interaction between slurry and soil particles, has been applied to simulate these laboratory column tests [3]. Previous studies have typically modelled a basic column infiltration device, confining slurry particle infiltration to a cylindrical apparatus and presupposing a distinct boundary between infiltrated and non-infiltrated soil [4]. In contrast, real-world SPB tunnelling sees slurry infiltration extending over a wider stratum range. This variation, which influences the infiltration properties of slurry particles, remains under-investigated in existing research. Limited studies have examined the horizontal infiltration of slurry particles using CFD–DEM. This paper aims to fill this gap by analysing slurry particle infiltration, filter cake properties, and fluid characteristics through more realistic CFD–DEM simulations.

## 2. Methodology and simulation setup

Three codes were used to conduct the coupled CFD–DEM simulations for this research study: the commercial DEM code Asphex, the open-source CFD code OpenFOAM (Open-Source Field Operation and Manipulation), and the non-spherical form of the CFDEM coupling module. This study utilises the standard CFD–DEM coupling procedure, which has been thoroughly established and documented for its application to non-spherical slurry particles [4].

In this study, bentonite slurry particles are modelled as oblate spheroids with an aspect ratio of 7 using superquadrics, while sand particles are represented as spheres. The drag force, lift force, pressure gradient force, viscous force and pitching torque were considered. The implementation of these forces and pitching torque, along with the validation for a laboratory column test model, was detailed in the authors' previous work

[4]. Sand particle diameters range between 1.8 mm and 4 mm. The size ratio between slurry and sand particles is established at 1:4. The simulation models are depicted in Fig. 1.

The simulation methodology previously outlined in [4] for a laboratory column test model is utilised. The numerical SPB tunnelling procedure involves four stages. First, sand particles are allowed to settle within a water-filled column due to gravity. Following this, a “slurry shield machine” represented by a cylinder is connected to the sand column, into which slurry particles are introduced at random orientations. Infiltration of slurry particles begins when they contact the sand column under applied pressure. A simulation stops when it reaches a steady state, characterised by stationary suspended particles and stable values of both porosity and pressure drop across a column. A total system energy threshold of  $10^{-7}$  J is set as the criterion to terminate a simulation.

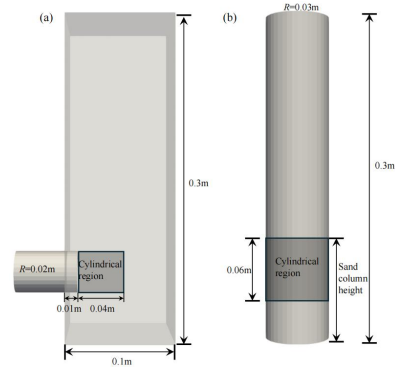


Figure 1. Simulation models of (a) SPB tunnelling and (b) the laboratory column test.

## 3. Results and discussion

### 3.1. Infiltration properties of slurry particles

The distributions of slurry particles in the sand columns for both the SPB tunnelling model and the laboratory column test model are depicted in Fig. 2. Internal filter cakes have formed in both models, yet there are notable differences in the infiltration ranges of slurry particles between two models. Fig. 2(a) highlights that a significant number of slurry particles exceed the “cylindrical” pipe region in the SPB tunnelling model due to the absence of boundaries in the sand column: a point of difference from the laboratory column test model. It is important to note that such boundary constraints on slurry infiltration are also absent in actual SPB tunnelling operations. Furthermore, Fig. 2 illustrates the radial symmetry of the slurry particle distribution within the sand column in the SPB tunnelling model. Some slurry particles infiltrated in the reverse direction (indicated by the red highlighted regions in Fig. 2(a)) because the fluid surrounding the tunnel boundary tends to flow in reverse. This phenomenon, which is not captured by laboratory column tests, has been observed experimentally [5].

The relative mean infiltration distance ( $D_{relative}$ ) and pressure direction infiltration distance ( $D_{pressure}$ ) are adopted to quantify the infiltration distances of slurry particles in the sand columns.  $D_{relative}$  represents the average distance from the centre of slurry particles to the centre of the tunnel surface after infiltration, relative to the tunnel radius.  $D_{pressure}$  indicates the infiltration distance in the pressure direction. In the SPB

tunnelling model,  $D_{relative}$  is higher (0.7865) than for the laboratory column test model (0.6798). Similarly,  $D_{pressure}$  is also higher in the SPB tunnelling model (0.0015 m) than in the laboratory column test model (0.0008 m). This indicates a more extensive permeation of slurry particles within the sand column in the SPB tunnelling model, as illustrated in Fig. 2.

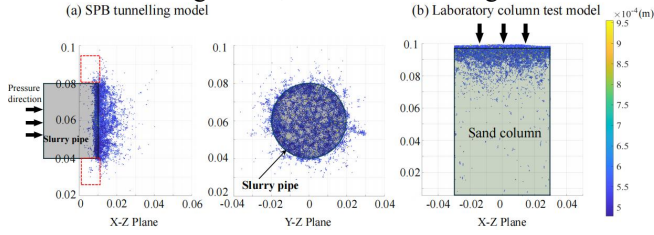


Figure 2. Distributions of slurry particles in sand columns for (a) the SPB tunnelling model and (b) the laboratory column test model. The colour bar shows the diameters of slurry particles.

### 3.2. Pressure and velocities

In each model, a cylindrical region of length  $L$ , equivalent to twice the tunnel radius, extending from the tunnel face was studied, as shown in Fig. 1. The broader slurry infiltration area in the SPB tunnelling model was omitted due to quantification challenges. Fig. 3(a) shows the fluid velocity within the cylindrical region extending from the tunnel face in each model. In the laboratory column test model, the fluid velocity initially increases with distance from the tunnel face, experiences a slight drop after 0.02 m, and then stabilises until reaching the bottom of the sand column. Conversely, in the SPB tunnelling model, fluid velocity near the tunnel face sharply increases, followed by a rapid decrease to 0 m/s. Fig. 3(b) illustrates the contours of fluid velocity in the sand columns both before and after infiltration, highlighting a more marked reduction in mean fluid velocity in the SPB tunnelling model compared to the laboratory column test model. This greater velocity dissipation in the SPB model is due to the fluid flowing into a broader area after exiting the slurry pipe. Fig. 3(c) displays the pressure distributions within the cylindrical regions, with the total pressure drop from the tunnel face to the end of each sand column maintained at a uniform 7.5 kPa. The fluid pressure in the SPB tunnelling model declines more rapidly than in the laboratory column test model. Notably, during actual tunnelling, the fluid flow velocity and pressure conditions ahead of the tunnel face are more comparable to those observed in the SPB tunnelling model, where fluid flow dissipates rapidly within the sand stratum.

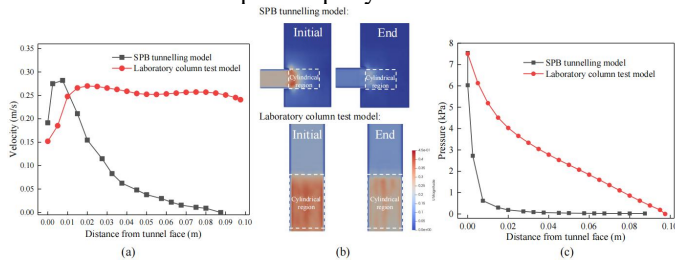


Figure 3. (a) Fluid velocities; (b) contours depicting fluid velocities within the sand columns before and after the infiltration of slurry; (c) fluid pressures in the SPB tunnelling model and laboratory column test model.

### 3.3. Permeability

To further explore filter cake properties and the effects of slurry particle infiltration ahead of the tunnel face, the permeability of each sand column was examined. The normalised permeability ( $k/k_0$ ) of the sand column after infiltration was calculated based on Darcy's law [6]:

$$q = -\frac{k}{\mu L} \cdot \Delta P$$

$k$  represents the permeability of a sand column within the defined cylindrical region.  $\Delta P$  denotes the pressure drop across this region of length  $L$ ,  $\mu$  signifies the dynamic viscosity of the fluid, and  $q$  denotes the superficial velocity.  $k_0$  is the permeability of a sand column in the same region prior to slurry infiltration. The normalised permeability  $k/k_0$  of the sand column in the SPB tunnelling model is 0.3255, which is lower than that of the laboratory column test model at 0.3911. As detailed in Section 3.1, slurry particles have penetrated further into the sand column in the SPB tunnelling model. Moreover, the proportion of slurry particles within the cylindrical region in the SPB tunnelling model is 53.6%, compared to 45.3% in the laboratory column test model, further supporting this observation.

## 4. Conclusion

This paper employs a CFD–DEM numerical approach to study non-spherical slurry particle infiltration in a more realistic model. Infiltration range, distance, and filter cake properties were analysed. SPB tunnelling simulations provide insights into slurry particle behaviour and filter cake properties within an unbounded sand column.

Internal filter cake formations were observed for both the SPB tunnelling model and the laboratory column test model. However, the infiltration range of slurry particles in the SPB tunnelling model is larger than that in the laboratory column test model due to the absence of the pipe boundary.

More slurry particles permeated a wider area in the sand column for the SPB tunnelling model, leading to a greater infiltration distance from the tunnel centre ( $D_{relative}$ ) as well as infiltration distance in the pressure direction ( $D_{pressure}$ ) compared to the laboratory column test model.

Comparing to the laboratory column test model, fluid velocity increases much more quickly near the tunnel face, then sharply drops to zero in the SPB tunnelling model. More rapid dissipation of fluid pressure was observed in the SPB tunnelling model.

Lower normalised permeability within the sand column was observed for the SPB tunnelling model, indicating a greater infiltration of slurry particles into the sand column and more pore throats in the sand column being sealed by slurry particles in the SPB tunnelling model.

## Acknowledgement

The authors would like to acknowledge DCS Computing GmbH for providing the licenses needed for the commercial simulation software.

## References

- [1] F. Min, J. Liu, J. Chen, T. Liu, C. Yu, J. Ji, and J. Liu, A study on the excavation face failure of pressurized slurry shield, *Tunn. Undergr. Sp. Tech.*, 132, 104900, 2023.
- [2] T. Xu and A. Bezuijen, Bentonite slurry infiltration into sand: filter cake formation under various conditions, *Géotechnique*, 69, 1095-1106, 2019.
- [3] T. Yin, Z. Zhang, X. Huang, T. Shire, and K. J. Hanley, On the morphology and pressure-filtration characteristics of filter cake formation: Insight from coupled CFD–DEM simulations, *Tunn. Undergr. Sp. Tech.*, 111, 103856, 2021.
- [4] J. Liu and K. J. Hanley, CFD–DEM modelling of the infiltration of non-spherical slurry particles in granular soils, *Comput. Geotech.*, 164, 105845, 2023.
- [5] X. Hu, Y. Fang, G. Walton, and C. He, Laboratory model test of slurry shield tunnelling in saturated sandy soil, *Géotechnique*, 73, 885-906, 2023.
- [6] H. Xiong, Z. Zhang, X. Sun, Z.-Y. Yin, and X. Chen, Clogging effect of fines in seepage erosion by using CFD–DEM, *Comput. Geotech.*, 152, 105013, 2022.

# Terminal Velocity and Drag Coefficient of Falling Particles in Newtonian Fluids

Haim Kalman, and Dmitri Portnikov

Ben-Gurion University of the Negev, Israel

**Abstract—** In a couple of recently published papers, the terminal velocity and drag coefficient of free falling of spherical and non-spherical particles in Newtonian fluids were investigated. Hundreds of experiments with various materials, sizes, shapes and fluids were conducted to found reliable correlations of the  $U_T$  vs  $Re$ ,  $C_D$  vs  $Re$  and  $C_D$  vs  $Ar$ . The terminal velocity of non-spherical particles was found to be affected by the particle sphericity. Therefore, a map of seven flow modes was developed.

**Keywords:** Terminal velocity; drag coefficient; particle shape;

## 1. Introduction

When an individual body moves at a velocity different from that of its surrounding fluid, the body experiences a drag force applied by the fluid. The drag force is commonly defined by the dimensionless drag coefficient ( $C_D$ ). For over 120 years, considerable work has been done to determine the terminal velocity and  $C_D$  of falling spheres, with numerous attempts to relate the  $C_D$  with the terminal Reynolds number,  $Re_T$ . Since 1960, hundreds of studies have been conducted and published, and tens of correlations have been developed. Kalman and Matana [1] reviewed the known experimental works and published correlations for spherical particles.

Non-spherical particles move in a more complex manner, as their terminal velocity and drag coefficients also depend on the particle shape and final orientation. Moreover, during the acceleration and final stages, orientation may vary depending on the initial orientation and other effects. Despite the complexity, many experiments and correlations can be found in the literature, which were reviewed recently by Kalman and Portnikov [2].

## 2. Experimental

Two types of experiments were conducted to measure the terminal velocities of various particles in various fluids. In addition, the particles and fluids were characterized using a number of standard measuring devices.

### 2.1. Materials

Spherical particles of seven different materials were tested [1]. Several sizes were examined for some of the materials. Six fluids were used in the tests: air, tapped water, glycerol (analytical grade), and three mixes of glycerol and water.

In addition, 85 experiments with non-spherical particles (irregular, discs and cylinders) free falling in various Newtonian fluids were conducted. The following analysis was based on the volume equivalent diameter of the non-spherical particles. Although, in some cases, as will be shown later, the velocity is fluctuating, we used here the average terminal velocity.

### 2.2. Experimental Apparatus

The terminal velocity was measured using two test rigs for acceleration in liquid and acceleration in air. Most of the measurements were conducted using a high-speed video camera

OPTRONICS- CR3000x2, with frame rates of up to 5000 frames per second.

Both experiments were conducted in a square column of 100 mm × 100 mm with Perspex walls of 600 mm height for liquids and 4000 mm for air. The column dimensions were sufficient, in most cases, to neglect wall effects. The particles were released from a small horizontal shelf mounted at the top of the column, below the liquid interphase. The tested particle was first immersed in the liquid for 24 h to separate any air bubble and then placed on the shelf. The measurements showed that the velocity increased as a function of location and time until it stabilized at the terminal velocity. Particle acceleration will be analysed in another work.

Clearly, the column height was not sufficient for the particle to reach the terminal velocity in air. Therefore, the acceleration of the particles was measured by positioning the camera at various heights along the column and repeatedly dropping the same particle. These measurements enabled the estimation of the terminal velocity by extrapolating the data in the acceleration region.

The non-spherical discs and cylinders were tested twice with two initial orientations – horizontal and vertical.

## 3. Results and Analysis

### 3.1. Terminal Velocity

Based on 73 new experiments [1] added to those found in the literature, it was shown [1] that the correlation of Haider and Levenspiel [3] fit the best (with a maximum error of 8.3%) the measurements for spherical particles. Further experiments with non-spherical particles showed, that the same correlation can be used by defining the coefficients as sphericity functions, as presented in Eqs. (1-3). The accuracy of the calculations is presented in Fig. 1.

$$Re_T = \left( \frac{R_1}{Ar} + \frac{R_2}{4Ar^{0.5}} \right)^{-1} \quad (1)$$

$$\begin{aligned} R_{1NS} &= 37 - 22\varphi \text{ for } \varphi > 0.87 \\ R_{1Flat} &= 45.55 - 31.84\varphi \text{ for } \varphi < 0.87 \\ R_{1Long} &= 93.44 - 86.89\varphi \text{ for } \varphi < 0.87 \end{aligned} \quad (2)$$

$$\begin{aligned} R_{2NS} &= 6.935 - 4.52\varphi \text{ for } \varphi > 0.87 \\ R_{2Flat} &= 11.09 - 9.30\varphi \text{ for } \varphi < 0.87 \\ R_{2Long} &= 7.71 - 5.40\varphi \text{ for } \varphi < 0.87 \end{aligned} \quad (3)$$

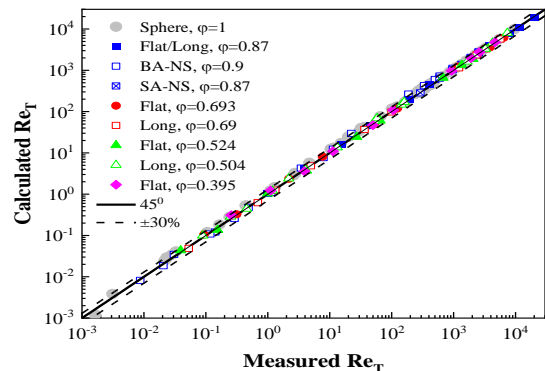


Figure 2. Calculated vs. measured terminal Reynolds number.



The results showed three zones of affecting shape. Sphericity of 0.87 is the case when disc is the same as cylinder (having the same height and diameter). Sphericity larger then that is considered as a particle having three dimensions of the same order (including sphere) and can be generalized as Nearly Spherical (NS). Disc is related to a particle having two dimensions at the same order and one is smaller and can be generalized as Flat. Cylinder is a particle having two dimensions of the same order and one is higher and can be generalized as Long.

### 3.2. Drag Coefficient

The most researched and analysed parameter is the  $C_D$ . The correlation reported by Hölzer and Sommerfeld [4] was found to best describe the new and previous experiments with some modifications to the empirical constants, for spherical particles. Analysing also the experiments with non-spherical particles resulted with two of the constants being functions of the sphericity, as presented in Eqs. (4-6). Fig. 2 presents comparison between the correlations and the experiments.

$$C_D = \frac{C_1}{Re_T} + \frac{5}{Re_T^{0.6}} + C_2 \quad (5)$$

$$\begin{aligned} C_{1NS} &= 51.8 - 27.8\varphi \text{ for } \varphi > 0.87 \\ C_{1DI} &= 24.4\varphi^{-0.91} \text{ for } \varphi < 0.87 \\ C_{1CY} &= 21.3\varphi^{-1.84} \text{ for } \varphi < 0.87 \end{aligned} \quad (6)$$

$$\begin{aligned} C_{2NS} &= 2.94 - 2.5\varphi \text{ for } \varphi > 0.87 \\ C_{2DI} &= 42.1(1 + \varphi)^{-6.4} \text{ for } \varphi < 0.87 \\ C_{2CY} &= 17.5(1 + \varphi)^{-5} \text{ for } \varphi < 0.87 \end{aligned} \quad (7)$$

In order to calculate the drag coefficient of any spherical particle, first  $Re$  has to be calculated using Eq. (1) or any other correlation and only then, Eq. (5) can be used. Therefore, it looks better to use a direct correlation between  $C_D$  and  $Ar$ , as presented previously [1, 2].

### 4. Particle Fall Mode

The final fall mode of a particle depends on the forces acting during acceleration and the steady state. Some of the forces also depend on particle orientation, which may change during the fall. As a result of the experiments with non-spherical particles, seven fall modes were identified. Fig. 3 presents two of the fall modes using a velocity-falling distance figure for two initial orientations (horizontal and vertical) and the orientation visualizations. The flow mode of each test was identified through the velocity figure and strengthened by visualization. A detailed explanation of the seven flow modes can be found in [2]. All experimental flow modes are presented as flowcharts of sphericity versus  $Ar$ , as shown in Fig. 5.

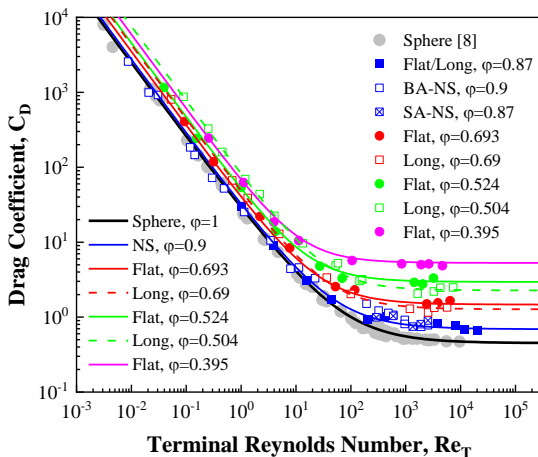


Figure 2. Drag coefficient as a function of Reynolds number.

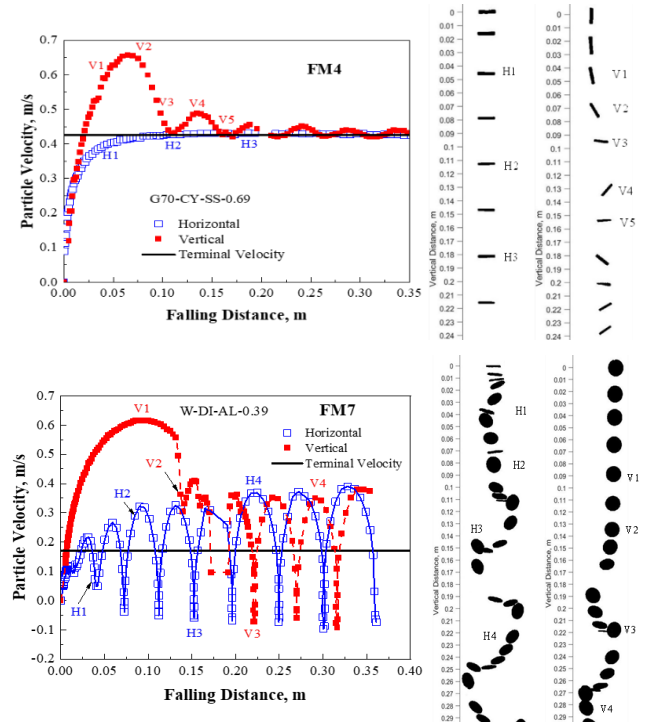


Figure 4. Velocity as function of the falling distance and orientation visualization during fall of two of the flow modes.

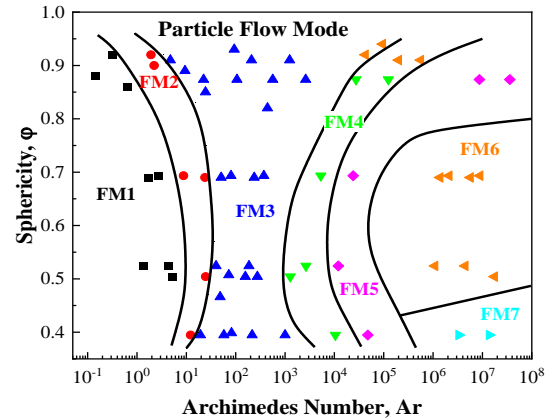


Figure 5. A map for seven flow modes in terms of sphericity vs.  $Ar$ .

### 5. Conclusion

Experiments with spherical and non-spherical particles at a wide range of  $10^{-3} < Re < 10^4$  and  $10^{-2} < Ar < 10^8$ , enabled to develop new correlations for  $Re$  vs  $Ar$  and  $C_D$  vs  $Re$  or  $Ar$ . The correlations based on appropriate ones developed for spherical particles defining two of the constants (for each) as functions of the sphericity. Seven flow modes were identified affecting the terminal velocity and presented as flow charts.

### References

- [1] H. Kalman, E. Matana, Terminal velocity and drag coefficient for spherical particles, Powder Technol. 396 (2022) 181–190. <https://doi.org/10.1016/j.powtec.2021.10.053>
- [2] H. Kalman, D. Portnikov, Free falling of non-spherical particles in Newtonian fluids, A: Terminal velocity and drag coefficient, Powder Technology 434 (2024) 119357. <https://doi.org/10.1016/j.powtec.2023.119357>
- [3] A. Haider, O. Levenspiel, Drag coefficient and terminal velocity of spherical and nonspherical particles, Powder Technol., 58 (1989) 63 – 70. [https://doi.org/10.1016/0032-5910\(89\)80008-7](https://doi.org/10.1016/0032-5910(89)80008-7)
- [4] A. Hölzer, M. Sommerfeld, New simple correlation formula for the drag coefficient of non-spherical particles, Powder Technol. 184 (2008) 361–365. <https://doi.org/10.1016/j.powtec.2007.08.021>

# Acceleration and Acceleration Length of Falling Particles in Newtonian Fluids

Haim Kalman, and Dmitri Portnikov

Ben-Gurion University of the Negev, Israel

**Abstract—** In three recently published papers, the acceleration process and acceleration length of free falling of spherical and non-spherical particles in Newtonian fluids were investigated. Hundreds of experiments with various materials, sizes, shapes and fluids were conducted to found reliable correlations for the acceleration. In addition, the history force was defined in a new way. The forces and acceleration length were defined as functions of a number of non-dimensional numbers including Ar and the sphericity.

**Keywords:** Terminal velocity; drag coefficient; particle shape; history force

## 1. Introduction

When an individual body accelerates in a surrounding fluid, the body experiences a number of forces (weight, buoyancy, drag, added mass and history). Much less has been published on particle acceleration, as comparing to the steady-state movement, although practically, particles usually undergo unsteady motion. The most problematic part is the Basset-history term, which is applied to a particle starting from a low velocity and describes the extra momentum transfer required to move the fluid in the flow field around the particle. This is commonly defined by a complex integral.

Recently, the acceleration of spherical particles was analysed, based on many experiments at a wide range of Re by Kalman and Portnikov [1]. A simple exponential function for the particle acceleration was found to fit all the experiments, describing the acceleration as a function of distance. Consequently, a simple exponential equation was developed for the velocity. This enabled a simple definition for the history force completing accurately the force balance. Using the simple model, Kalman and Portnikov [2] calculated the acceleration length (reaching 99% of  $U_T$ ). Results indicated that the acceleration length can be well described by a function of the Archimedes number, density ratio, and particle diameter.

Non-spherical particles move in a more complex manner, as the velocity, acceleration and forces also depend on the particle shape and final orientation. Moreover, during the acceleration and final stages, orientation may vary depending on the initial orientation and other effects. In a recent paper, Kalman and Portnikov [3] generalized the equations, originally developed for spherical particles to fit also non-spherical particles considering sphericity.

## 2. Experimental

The experiments with the same materials, fluids, particle size and shape used to the work related to the steady-state terminal motion, were used also here to analyse the particle acceleration. Therefore, it is not presented here in details.

## 3. Results and Analysis

### 3.1. Particle Velocity and Acceleration

An exponential function for the particle acceleration was found to fit the many experiments [1]. The acceleration should

start with the initial acceleration  $a_0$  for  $y=0$ , and approach zero at the terminal velocity.

$$a = a_0 e^{-Dy} \quad (1)$$

where  $D$  is currently unknown. Defining the acceleration in terms of the velocity gradient, the differential equation can be solved to define the velocity.

$$U = U_T(1 - e^{-Dy})^{0.5} \quad (2)$$

Applying the boundary condition,  $U_{y=\infty}=U_T$ , gives the empirical parameter  $D$  as a function of the initial acceleration and terminal velocity.

$$D = \frac{2a_0}{U_T^2} \quad (3)$$

Fig. 1 presents an example for the velocity and acceleration of a glass sphere of 2.9 mm in diameter falling in water.

### 3.2. Initial Acceleration

The new model [1] depends on the initial acceleration, which is defined based on the force balance, that will be presented later. For the case of accelerating in air, where it is reasonable to assume that the added mass and the history forces are negligible, the initial acceleration can be simply calculated.

$$a_0 = \frac{\rho_p - \rho_f}{\rho_p} g \quad (4)$$

However, for other surroundings, they are not negligible and affect the initial acceleration.

$$a_0 = \frac{\rho_p - \rho_f}{\rho_p + 0.5\rho_f + H\rho_f} g \quad (5)$$

where  $H$  is the history force parameter and found for spherical particles to be a function of Ar number [1] and for non-spherical particles also function of the sphericity [3], (the history force will be presented later) as presented in Eq. (6) and Fig. 2.

$$H = 700Ar^{-0.75} + H_1Ar^{-0.1} + H_2 \quad \text{for } Ar < Ar_{crit} \quad (6)$$

where the first term is the only term required for spheres, and  $H_1$  and  $H_2$  are functions of the sphericity. At  $Ar_{crit}$ , which is a function of the sphericity,  $H$  drops to nearly zero and the history force has no effect.

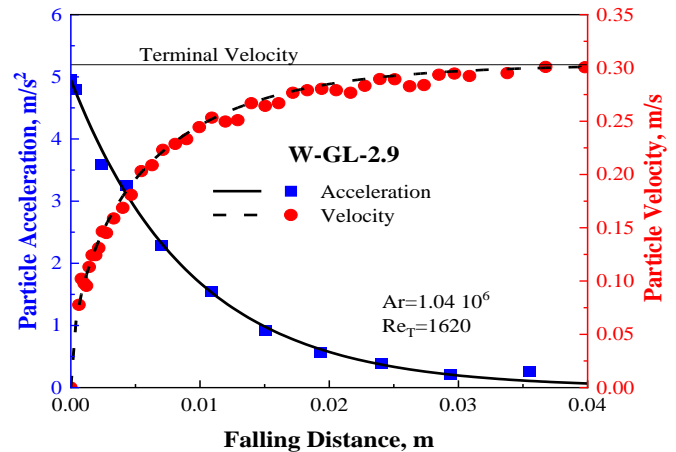


Figure 1. Comparing the model to an experiment.



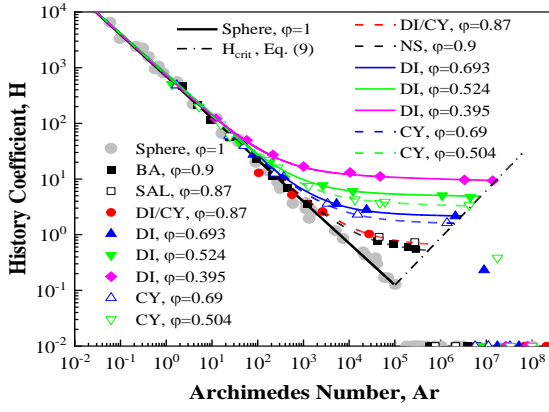


Figure 2. History force coefficient as function of Ar and sphericity.

$$\begin{aligned} H_{1NS} &= 3.85(1 - \varphi) \text{ for } \varphi > 0.87 \\ H_{1DI} &= H_{1CY} = 0.3\varphi^{-3.7} \text{ for } \varphi < 0.87 \end{aligned} \quad (7)$$

$$\begin{aligned} H_{2NS} &= H_{1NS} = 3.85(1 - \varphi) \text{ for } \varphi > 0.87 \\ H_{2DI} &= 35 \cdot 0.028^\varphi - 1 \text{ for } \varphi < 0.87 \\ H_{2CY} &= 12.2 \cdot 0.09^\varphi - 1 \text{ for } \varphi < 0.87 \end{aligned} \quad (8)$$

$$H_{crit} = 7 \cdot 10^{-6} Ar_{crit}^{0.85} \quad (9)$$

### 3.3 Force Balance

The model in this work, in which  $a_0$ ,  $C_D$  and  $H$  are correlated, enabled to overcome one of the most difficult aspects of particle motion, that is, calculating the history force. Here, the relevant forces are defined and analyzed based on the findings of this study. The general force balance can be rewritten as follows [3]:

$$\frac{\pi}{6} \rho_p d^3 a_0 e^{-\frac{2a_0 y}{U_T^2}} = \frac{\pi}{6} d^3 (\rho_p - \rho_f) g - \frac{\pi}{8} d^2 C_D \rho_f U_T^2 \left( 1 - e^{-\frac{2a_0 y}{U_T^2}} \right) - \frac{\pi}{12} \rho_f d^3 a_0 e^{-\frac{2a_0 y}{U_T^2}} - H \frac{\pi}{6} \rho_f d^3 a_0 e^{-\frac{2a_0 y}{U_T^2}} \quad (10)$$

where the terms stand for acceleration, weight-buoyancy, drag, added mass, and history. For this equation, the particle movement can be easily solved (mainly because the new definition for the history force). Since  $C_D$  and  $H$  are generalized to include non-spherical particles [3, 4], the force balance is relevant also to non-spherical particles. The forces as a function of the falling distance are presented in Fig. 3. The example of Fig. 3 has all forces relevant at the start of moving. For other cases the added mass and history forces may be negligible (see Fig. 2), as for falling in air. It is important to note, that  $C_D$  during acceleration was found to be constant, as for the terminal [1].

## 4. Acceleration Length

The acceleration length was determined using a previously developed model for spherical and non-spherical particles acceleration and velocity as functions of location and subsequently analysed. The acceleration length is defined as the distance required for the particle to reach 99% of the terminal velocity.

$$U = 0.99U_T = U_T(1 - e^{-DL_a})^{0.5} \quad (11)$$

where  $L_a$  denotes the acceleration length. Solving the equation for  $L_a$ , substituting the definition of  $D$  (Eq. 3), and normalizing the acceleration length by the particle diameter  $d$  yields

$$\frac{L_a}{d} = \frac{1.959U_T^2}{da_0} \quad (12)$$

Using the definitions for  $U_T$  [1] and for  $a_0$  (Eq. 5), which depends on  $H$  (Eqs. 6-9), the acceleration length can be

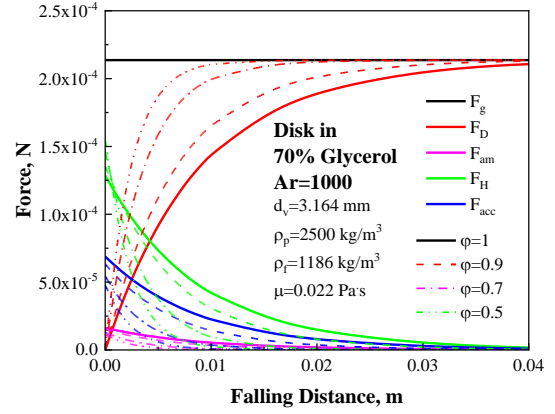


Figure 3. Forces along acceleration for various sphericities and one particle example.

calculated. Since,  $Re_T$  and  $H$  are valid for both spherical and non-spherical particles, the acceleration length should also be valid for both spherical and non-spherical particles (Fig. 4).

The reliability of the prediction of non-spherical particles is limited and depends on the particle flow mode, since the present model for the velocity does not consider velocity overshooting or fluctuations. Therefore, it may be valid for flow modes 4-7, but less for flow modes 1-3.

## 5. Conclusion

Experiments with spherical and non-spherical particles at a wide range of  $10^{-3} < Re < 10^4$  and  $10^{-2} < Ar < 10^8$ , enabled to develop a new exponential correlation for the history force. The new history force definition enabled to correlate a reliable initial acceleration, describe well the velocity and acceleration of spherical and non-spherical particles and to easily solve the force balance. Solving the force balance showed the effect of each force during the acceleration and the ranges in which some of them might be neglected. Based on the velocity function, the acceleration length was reasonably calculated.

## References

- [1] H. Kalman, D. Portnikov, New model to predict the velocity and acceleration of accelerating spherical particles, Powder Technology 415 (2023) 118197. <https://doi.org/10.1016/j.powtec.2022.118197>
- [2] H. Kalman, D. Portnikov, Acceleration length and time of falling spherical particles, Powder Technology 425 (2023) 118612. <https://doi.org/10.1016/j.powtec.2023.118612>
- [3] H. Kalman, D. Portnikov, Free falling of nonspherical particles in Newtonian fluids, B: Acceleration, Powder Technology 439 (2024) 119659. <https://doi.org/10.1016/j.powtec.2024.119659>
- [4] H. Kalman, D. Portnikov, Free falling of non-spherical particles in Newtonian fluids, A: Terminal velocity and drag coefficient, Powder Technology 434 (2024) 119357. <https://doi.org/10.1016/j.powtec.2023.119357>

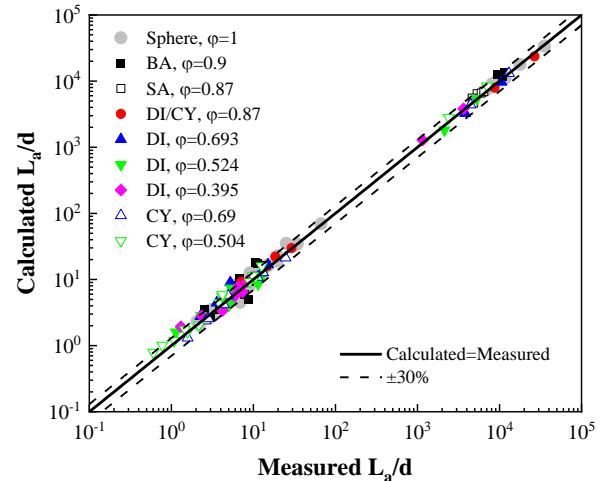


Figure 4. Comparison between calculated and measured acceleration length over particle diameter.

# Applying DEM-CFD coarse graining strategies to fluidized particle systems with geometrical constrictions

V.Brandt<sup>1</sup>, J. Grabowski<sup>1</sup>, N. Jurtz<sup>1</sup>, M. Kraume<sup>1</sup> and H. Kruggel-Emden<sup>1</sup>

<sup>1</sup> Technische Universität Berlin, Germany

**Abstract**—The discrete element method is a widely used technique for modelling granular materials, which is often coupled with computational fluid dynamics to account for fluid-phase interactions. However, simulating granular systems with a few million particles quickly exceeds the computational capabilities of modern computers, even with highly parallelized and optimized software. To overcome this problem, coarse graining strategies, which bundle multiple original particles into large-sized particles called grains, are well established. Coarse graining simulations are less computationally demanding due to the reduced number of granular entities considered. In many industrial applications, such as coating apparatus, circulating fluidized beds and other systems geometric constrictions prevail and the maximum grain size is locally restricted. In multi-level coarse graining, the coarse grain factor represents the resolution of particles, which is adapted in critical regions of the treated system. The goal of the investigation here is to perform multi-level coarse graining simulations of a circulating fluidized bed consisting of riser, cyclone and standpipe subsystems and to compare the results with conventional coarse graining and the unscaled particle simulation. In conclusion, the use of multi-level coarse graining in the simulation of circulating fluidized beds leads to a more efficient computation compared to conventional coarse graining because the resolution of particles can be adapted locally in the different subsystems.

**Keywords:** circulating fluidized bed, discrete element method (DEM), computational fluid dynamics (CFD), coupled DEM-CFD, multi-level coarse graining (MCG)

## 1. Introduction

Circulating fluidized beds (CFBs) are widely used in the chemical, process, agricultural and pharmaceutical industries due to their efficient mass transfer, good mixing performance, large solids throughput and continuous operating capability [1]. Notable examples include the gasification or combustion of coal and biomass, fluid catalytic cracking (FCC), CO<sub>2</sub> capture processes and ethylene polymerization as the Fischer-Tropsch synthesis [2,3]. Usually, a CFB consists of a riser, cyclone and standpipe. Between the standpipe and riser, a mechanical or non-mechanical valve is employed to regulate the solids recirculation and maintain the pressure balance of the CFB. The L-valve is a popular non-mechanical valve in the context of CFBs due to its simple structure, reliable sealing capability, and high temperature stability.

Despite the geometrical simplicity of a CFB, complex fluid-solid flow structures form out, leading to a heterogenous spatial distribution of solids on the mesoscale such as cluster and bubble formation. An approach that is frequently employed to model the fluid-solid flow of CFBs is to couple the discrete element method (DEM) to the unresolved computational fluid dynamics (CFD), referred to as DEM-CFD. In the DEM-CFD, interaction forces between the solid and fluid phases are computed by drag force closures. However, simulating granular systems with a few million particles or more quickly exceeds the computational capabilities of modern computers, even with highly parallelized and optimized DEM-CFD codes.

To overcome this issue, coarse graining (CG) strategies [4,5], which bundle multiple original particles into large-sized particles called grains, are well established especially for industrial applications. CG-DEM is less computationally demanding due to the reduced number of granular entities considered. Thereby, the goal is to maximize the CG factor  $l$  (ratio of coarse grain diameter to particle diameter) to reduce the computational cost, while maintaining the quality of results compared to the unscaled particle simulation ( $l = 1$ ). In common industrial applications, such as coating apparatus, circulating fluidized beds and other systems geometric constrictions locally limit the maximum applicable CG factor. Applying this maximum grain size uniformly throughout the system often results in an inefficient computation. Multi-level coarse graining (MCG) addresses this issue by using more than one grain size in the simulation domain. In MCG, the CG factor represents the resolution of particles, which is adapted in critical regions of the treated system. The MCG approach was first considered by [6] and later by [7]. Both studies applicate MCG in DEM simulations of a hopper, where the maximum grain size is limited by the size of the orifice to obtain reasonable results. The use of large-scale grains at a sufficient distance from the orifice and subsequent refinement close to the orifice enabled a significant reduction of computation time while maintaining comparable results to the simulation without CG. Recently, [8] extended the MCG approach to fluidized particle systems as part of the DEM-CFD using both a coarsening and a refinement step in the circulating solids flow of a Wurster coater system. Additionally, the influence of the placement of coarsening and refinement zones and commonly used contact force scaling models on the obtained results was analysed.

The goal of the investigation here is to apply MCG as part of DEM-CFD simulations to a circulating fluidized bed. The system consists of a riser, a cyclone and a standpipe subsystem. The results are compared with conventional CG and the unscaled particle simulation.

## 2. Multi-level coarse graining

When using CG techniques, scaling rules must be applied to at least hydrodynamic and contact forces to achieve reasonable results [5]. In contrast to conventional CG, which uses a fixed grain size, MCG uses multiple grain sizes in the simulation. The transition between different CG factors is realized by two essential steps (see Fig. 1). In the coarsening step, particles or grains are bundled together. In the refinement step, grains are refined to particles or grains with a lower diameter, i.e. lower CG factor. In the preprocessing stage, the coarsening and the refinement zones are defined as three-dimensional domains in which the coarsening and refinement steps are carried out. Well-placed coarsening and refinement zones are significant, because they

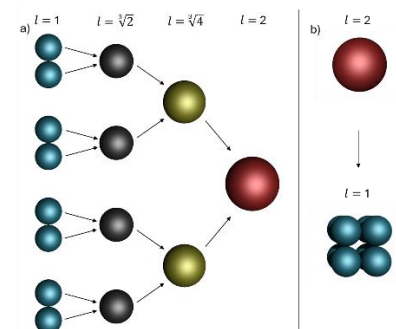


Figure 1. Example of adapting the CG factor from  $l = 1$  to  $l = 2$  and reverse considering a) a coarsening and b) a refinement step.

affect not only the results quality obtained from MCG simulations but also the computation time. The coarsening step is performed in the coarsening zone and bundles the nearest neighbours of either particles or grains to obtain a higher CG factor. The bundling is always done pairwise and can take place in multiple steps. The nearest neighbour search considers only particles / grains with the same CG factor. The coarsening procedure, which bundles particles with  $l = 1$  into a grain with  $l = 2$  in three intermediate steps, each performed in separate DEM time steps using the nearest neighbour search, is shown in Fig. 1a. The refinement step is the opposite of the coarsening step and is performed in a single step. In Fig. 1b, the refinement of a grain with  $l = 2$  into 8 particles with  $l = 1$  is shown. The particles are placed in a cubic pattern around the centre of the grain to be replaced to ensure that the centre of mass is unchanged. Further details regarding the coarsening and refinement step can be found in [8].

### 3. Simulation conditions

The geometric properties of the CFB consisting of a riser, cyclone and standpipe are shown in Fig. 2. A batch size of 0.35 kg was simulated which corresponds to an overall number of approx.  $1.17 \cdot 10^6$  particles. The simulation conditions used in this study are summarized in Tab. 1.

TABLE I. SIMULATION CONDITIONS

Unscaled particle simulation ( $l = 1$ )			
Particle diameter in m	0.000871	Fluidization inlet in m/s	2.67
Particle density in kg/m <sup>3</sup>	863	Aeration 1 in m/s	0.0493
Number of particles	$1.17 \cdot 10^6$	Aeration 2 in m/s	0.197
DEM time step in s	$1.5 \cdot 10^{-6}$	Pressure outlet in Pa	0
CFD time step in s	$1.5 \cdot 10^{-4}$	Simulated time in s	30

For the simulations, the motion of the particles was solved with a parallelized DEM code using the linear-spring-dashpot model as in previous studies (see e.g. [8]). For modelling the fluid-solid interaction, the DEM was coupled to the commercial CFD software Ansys Fluent 2022, where the fluid (air) was

assumed to be incompressible. Two-way coupled DEM-CFD simulations were performed using the particle-fluid interaction forces as the momentum source in a cell-based way according to [9]. CG was applied to the CFB with different CG factors ( $l = 2, l = 3, l = 4, l = 6, l = 8$ ) to determine the maximum global CG factor of the system. Obtained results were compared to experimental data from [10]. Subsequently, the CFB was modelled with MCG, utilizing the coarsening and refinement step to realize an appropriate grain size in each subsystem.

### 4. Results

The simulation model is capable of accurately predicting the experimental measured solids circulation rate when utilizing unscaled particles with  $l = 1$  (see Fig. 3a). When CG is employed with

$l \leq 3$ , the discharge rate exhibits only minor discrepancies. For higher CG factors ( $l \geq 4$ ), there is an observable increase in the deviations of the solids circulation rate see Fig. 3a). The MCG simulation with  $l = 6/3$  (Fig. 3c), comprising  $l = 3$  grains in the lower part of the riser and  $l = 6$  grains in the upper part of the riser, cyclone and standpipe (Fig. 3c), is capable of accurately predicting the solids circulation rate. With regard to the computation time, conventional CG with  $l = 3$  (see Fig. 3b) results in approximately 25 times fewer granular entities than the unscaled particle simulation. The use of MCG with  $l = 6/3$  leads to a reduction of the number of granular entities by a factor of 50.

### 5. Conclusion

In conclusion, conventional CG is able to correctly predict the solids circulation rate of the CFB up to a CG factor of  $l = 3$ . The utilization of MCG with  $l = 6/3$  enables the computation to be performed twofold more efficiently while maintaining the quality of the results in comparison to conventional CG, because the resolution of particles can be adapted locally in the different subsystems.

### Acknowledgement

Financial support was provided by the Deutsche Forschungsgemeinschaft (DFG, German Research Foundation) – Project-ID 456827728. Computing resources were funded by the DFG – Project-ID 463921749.

### References

- [1] Grace, Bi, et al., *Essentials of Fluidization Technology*, Wiley **2020**.
- [2] Wang, Shao, et al., *Chem. Eng. J.* **2020**, 386, 121951. DOI: 10.1016/j.cej.2019.121951.
- [3] Steynberg, Dry, et al., *Chapter 2 - Fischer-Tropsch Reactors, Studies in Surface Science and Catalysis*, 152, 64–195, Elsevier **2004**.
- [4] Sakai, Koshizuka, *Chem. Eng. Sci.* **2009**, 64, 533–539. DOI: 10.1016/j.ces.2008.10.003.
- [5] Brandt, Grabowski, et al., *Powder Technol.* **2023**, 426, 118629. DOI: 10.1016/j.powtec.2023.118629.
- [6] Queteschiner, Lichtenegger, et al., *Powder Technol.* **2018**, 338, 614–624. DOI: 10.1016/j.powtec.2018.07.033.
- [7] De, Chakraborty, et al., *Powder Technol.* **2022**, 398, 117058. DOI: 10.1016/j.powtec.2021.117058.
- [8] Brandt, Grabowski, et al., *Powder Technol.* **2024**, 436, 119447. DOI: 10.1016/j.powtec.2024.119447.
- [9] Kruggel-Emden, Oschmann, *Powder Technol.* **2014**, 268, 219–236. DOI: 10.1016/j.powtec.2014.08.033.
- [10] Xu, Musser, et al., *Ind. Eng. Chem. Res.* **2018**, 57, 740–750. DOI: 10.1021/acs.iecr.7b03817.

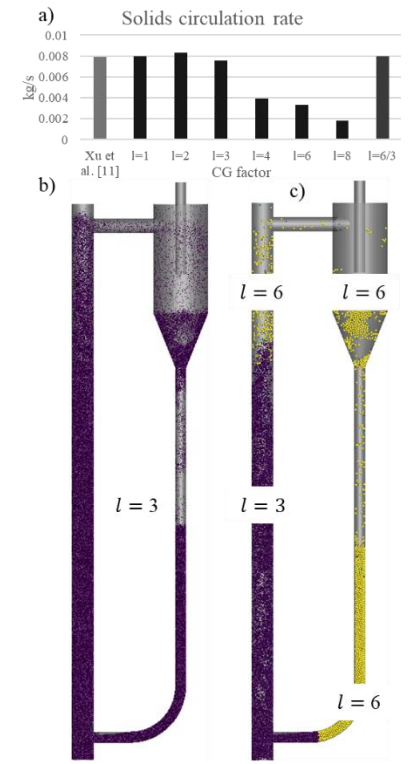


Figure 3. DEM-CFD simulation of a CFB showing a) the solids circulation rate of experiment, unscaled particle, CG, and MCG simulation, b) CG with  $l = 3$  and c) MCG with  $l = 6/3$ .

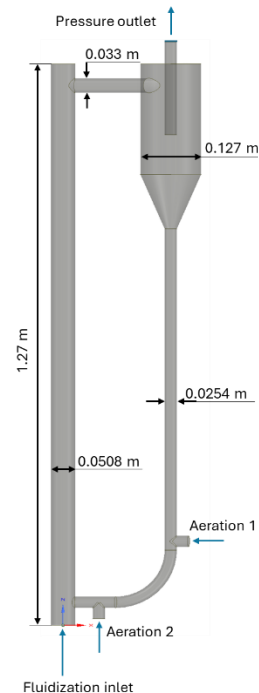


Figure 2. Geometric properties of the CFB.



# Drying Dynamics of Acoustically Levitated Wet Porous Agglomerates: Incorporating Nonisothermal Absorption Effects

A. Levy<sup>1</sup>, Y. David Pour<sup>1</sup>, B. Krasovitev<sup>1</sup>, A. Fominykh<sup>1</sup>, Z. Hashemloo<sup>2</sup>, A. Kharaghani<sup>2</sup>, E. Tsotsas<sup>2</sup>

<sup>1</sup> Ben-Gurion University of the Negev, Beer-Sheva, Israel

<sup>2</sup> Otto von Guericke University, Magdeburg, Germany

**Abstract—** In this work, we created a transient model for drying acoustically levitating slurry droplets at the stage at which solid particles have formed a wet porous agglomeration. At this drying stage, a slurry droplet can be viewed as composed of two regions: a central wet porous core and a dry porous crust. The complete model considers the effects on the drying intensity of wet porous agglomeration of acoustic streaming, forced convection, soluble gas absorption/desorption, filtration, and compressibility of the gas-vapor mixture inside the porous crust. The model applies the theory of heat and mass transfer during slurry droplet evaporation in conjunction with a gas absorption/desorption model accompanied by a chemical dissociation reaction. Anelastic approximation is used to describe the model through a series of transient conjugate nonlinear energy and mass conservation equations. It is demonstrated that the drying rate is accelerated with increasing intensity of the applied acoustic field and concentration of active gas. The desorbing gas's entrainment of water vapor molecules explains an increase in the wet porous particle drying rate in the presence of a soluble gas. As shown by numerical calculations, a gas mixture containing air with ammonia allows the residual moisture to be reached during the drying process in a much shorter time than that in a gas mixture not having an active gas. The predictions of the developed model are in good agreement with the experimental results available in the literature.

**Keywords:** slurry droplet; acoustic levitation; porous shell; gas absorption/desorption.

## 1. Introduction

Increased interest in acoustically levitated slurry droplet evaporation/drying processes during the last years can be explained by numerous reasons. The most essential is the possibility of investigating the drying process by holding the droplet in a stationary position, which distinguishes the acoustic levitation method from the falling drop method. Several decades ago, most experimental data on single-droplet evaporation were obtained using the glass-filament method. The main disadvantage of this method is that the droplet is in physical contact with the filament, which affects the evaporation process. Thus, the measurement setup disturbs the information obtained on the slurry droplet's drying process. One of the main disturbing effects is the heat exchange between the droplet and the filament, which becomes more pronounced for studying complex droplets, such as slurry droplets. In contrast, the recently developed acoustic levitation technique is free from the drawbacks above (see Fig. 1). This fact also explains the increased interest in acoustically levitated slurry droplet drying.

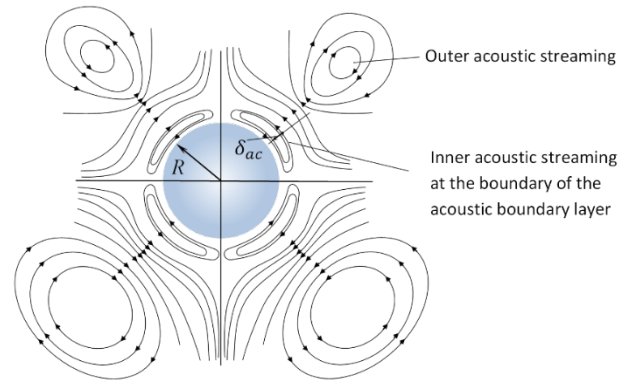


Figure 1. Acoustic streaming field around a small spherical droplet.

Acoustic levitation can be considered a contactless tool for studying slurry droplet drying. The present work is devoted to the analysis of the stage of slurry droplet drying when solid particles form an agglomerate.

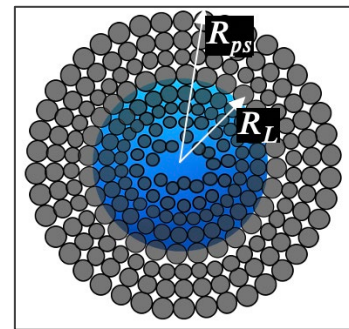


Figure 2. Schematic view of wet particle drying.

## 2. Model description

At a drying stage after shell formation, the acoustically levitated slurry droplet can be viewed as composed of two regions: a central wet porous core and a dry porous crust (see Fig. 2). At this stage, the formed porous agglomerate is characterized by the average porosity  $\epsilon$  and permeability  $K(d_p, \epsilon)$ ; the latter is a function of the particles' average diameter and porosity. Thus, the mass and energy conservation equations can be formulated in two domains. For the wet core where  $0 \leq r < R_L(t)$ , the system of equations is as follows (see Pour et al. [1]):

$$(\rho c_p)_{\text{eff}} r^2 \frac{\partial T^{(L)}}{\partial t} = k_{L,\text{eff}} \frac{\partial}{\partial r} \left( r^2 \frac{\partial T^{(L)}}{\partial r} \right)$$

$$\varepsilon r^2 \frac{\partial w_A^{(L)}}{\partial t} = D_{L,eff} \frac{\partial}{\partial r} \left( r^2 \frac{\partial w_A^{(L)}}{\partial r} \right)$$

Here,  $T^{(L)}$  is the temperature of the wet core,  $w_A^{(L)}$  is the mass fraction of the soluble species in the liquid,  $k_{L,eff}$  is the effective thermal conductivity of the wet core,  $D_{L,eff}$  is the effective diffusion coefficient of the soluble species in the liquid in the wet core, and  $\varepsilon$  is the porosity of the porous structure inside the wet core. In the porous shell ( $R_L(t) \leq r \leq R_{ps}$ ) the nonstationary heat and mass conservation equations for water vapor and active gas contain the convective term, which arises due to Darcy flow in a porous shell. Both domains' heat and mass transfer equations are supplemented by initial and boundary conditions at the center of a wet core, gas-liquid interface, and porous shell surface.

### 3. Results and discussion

The results of numerical calculations for the temporal evolution of the interfacial temperature for the first (see [2]) and second stages of slurry droplet drying for different mass fractions of ammonia in the gas phase are shown in Fig. 3. During the first stage when the droplet absorbs the soluble gas, the temperature reaches a temporal maximum owing to the thermal effect of absorption. The maximal temperature increases as the mass fraction of soluble gas in the gas phase increases. The droplet then reaches the wet-bulb temperature, i.e., until the second drying stage begins. The temperature drops to the wet-bulb temperature quite quickly because the droplet becomes saturated with ammonia in a short amount of time. As a result, the droplet's process of absorbing gas ends, and the heat release is stopped. Formation of a porous shell at a second drying stage causes an increase in hydrodynamic resistance to vapor flow in a shell. So, the evaporation rate decreases, and the liquid temperature in a wet core increases. The solubility of dissolved gas decreases with temperature increase. Gas dissolved in a wet core starts to desorb and liberate. Desorbing gas entrains water molecules - the rate of evaporation increases.

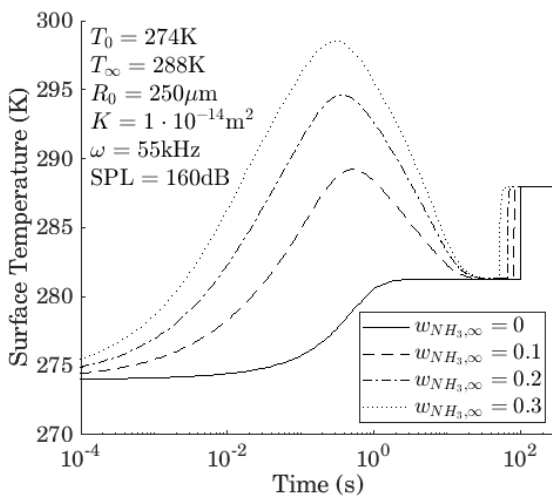


Figure 3. Temporal evolution of the temperature of the gas-liquid interface during the first and second drying stages for different mass fractions of ammonia in the surrounding gas.

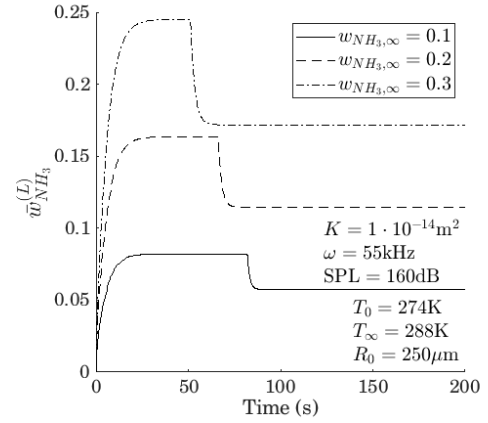


Figure 4. Temporal evolution of volume-averaged dissolved ammonia concentration inside an acoustically levitated slurry droplet evaporating in a gaseous mixture of  $N_2/NH_3/H_2O$  for different mass fractions of ammonia in the surrounding gas.

In Fig. 4, the volume-averaged mass fraction of ammonia is shown as a function of time for three values of the mass fraction of ammonia in the gaseous phase. During the first drying phase, the droplet collects ammonia, as seen in Fig. 4. As a result, the liquid's ammonia content rises until the gas concentration hits its saturation point. Due to the rising liquid temperature, as the second stage progresses, ammonia's solubility in water diminishes. As a result, the gas is desorbed from the wet core, and the mass fraction of the dissolved gas drops. Further, according to Henry's law, the mass fraction of dissolved ammonia reaches saturation at the temperature and concentration of the active gas in the ambient gas mixture as the particle temperature approaches the ambient temperature.

### 4. Conclusion

1. The drying rate of acoustically levitated slurry droplets at a second drying stage increased with the concentration of soluble gas in the gaseous phase. The desorbing gas's entrainment of water vapor molecules explains an increase in the droplet evaporation rate in the presence of a soluble gas.
2. The drying rate of an acoustically levitated porous agglomerate increases by ten percent with increasing intensity of the applied acoustic field from 158 dB to 162 dB and decreases with an increase in frequency.

### 5. References

- [1] Y. D. Pour, B. Krasovitev, A. Fominykh, Z. Hashemloo, A. Kharaghani, E. Tsotsas, A. Levy, 2022, Intensification of spray drying granulation process by gas absorption accompanied by chemical dissociation reactions, Chemical Engineering Journal. 433, 133566. doi.org/10.1016/j.cej.2021.133566.
- [2] Y. D. Pour, B. Krasovitev, A. Fominykh, Z. Hashemloo, A. Kharaghani, E. Tsotsas, A. Levy, 2023 Combined effect of acoustic field and gas absorption on evaporation of slurry droplet, Drying Technology. 41, 767-782, doi.org/10.1080/07373937.2022.2116583.

### Acknowledgment

This study was supported by the German-Israeli Foundation (Research Grant Agreement Number: I-1484-405.10/2019).

# Study on Density Segregation under Vertical Vibration —Mechanism of Inverse and Sandwich Segregations—

Haruhi Konno<sup>1</sup>, Tomoki Katayama<sup>1</sup>, Shusaku Harada<sup>1</sup>, and Koichiro Ogata<sup>2</sup>

<sup>1</sup> Hokkaido University, Sapporo, Japan

<sup>2</sup> National Institute of Technology, Oita College, Oita, Japan

**Abstract—** The mechanism of density segregation of fine particles under vertical vibration was investigated. The role of permeation air flow on inverse segregation (low-density particles accumulate at the bottom and high-density particles at the top) and sandwich segregation (low-high-low density profiles) was examined quantitatively. The air pressure in the vibrated particle bed was measured directly under various vibration conditions. The numerical analysis on coupling motion of particle bed and permeation flow was also performed. It was found that air pressure inside the particle bed changed periodically, which was due to relative motion of the particle bed to the vessel caused by vertical vibration. This periodic pressure change has a significant effect on the mechanism of density segregation.

**Keywords:** density segregation; fine particles; vibration

## 1. Introduction

The separation process of different-typed granular materials, i.e., particles of different sizes and densities, is important in various engineering fields such as recycling and material engineering. On the other hand, granular materials show interesting behaviors different from those of solids, liquids, and gases. Therefore, understanding of dynamic characteristics of granular materials is essential for handling them.

As one of the peculiar behaviors of granular materials, segregations have been of interest. The phenomena are utilized as dry separation process of mixed granules. In principle, these separation processes are based on the relative motion of different-typed particles excited by external energy sources such as vibration or fluid flow, causing the same particles to accumulate. When the vertical vibration is applied, heavy particles move upward and light particles sink to the bottom (inverse segregation) [1,2]. Interestingly, sandwich segregation is sometimes observed depending on the vibration conditions. The mechanism of inverse segregation was discussed qualitatively as the response of air flow, more specifically, the pressure force acting on different-inertia particles [2]. Although the mechanism of sandwich segregation was also discussed, it has been still qualitative and controversial.

The purpose of this study is to quantitatively examine the effect of air flow on the inverse and sandwich segregations under vertical vibration. Specifically, air pressure in vibrated particle bed was measured directly. We also conducted the numerical simulation on relative permeation flow through the moving particle bed under vertical vibration.

## 2. Experimental and Numerical Method

### 2.1. Experimental Method

Figure 1 indicates the schematic diagram of experimental system. The system mainly consists of a test vessel, a vibrator, a function generator, an amplifier, sensors and data processing systems. The almost equal size and different densities of steel particles (density  $\rho_s = 7450 \text{ kg/m}^3$ , diameter  $d_s = 125\text{--}180 \text{ }\mu\text{m}$ )

and glass particles (density  $\rho_g = 7450 \text{ kg/m}^3$ , average diameter  $d_g = 153 \text{ }\mu\text{m}$ ) were used in this study. The steel and glass particles were mixed at a volume ratio of 1:3 and were filled in a 50 mm diameter cylindrical vessel for a given bed height  $L$ .

We measured the interstitial air pressure in the particle bed under various vibration conditions with frequency  $f$  and amplitude  $a$ . Several pressure holes were placed vertically on the side of the test vessel. Each pressure hole was connected to a pressure sensor through a tube covered with a mesh through which particles cannot pass.

### 2.2. Numerical Method

The numerical analysis was conducted for understanding the fluctuation of air pressure in the vibrated particle bed. In the model, one-dimensional motion of particle bed and compressible flow was assumed. The basic equation is expressed as follows [3].

$$\frac{\partial p}{\partial t} = \alpha \frac{\partial^2 p}{\partial z^2}, \quad \frac{\partial s}{\partial t} = -\frac{\epsilon \alpha}{p_0} \frac{\partial p}{\partial z} \Big|_{z=L}, \quad \alpha = \frac{p_0}{180\mu} \left( \frac{\epsilon d_p}{1 - \epsilon} \right)^2 \quad (1)$$

where  $p$  is a vertical pressure,  $t$  is time,  $z$  is a depth of the particle bed,  $s$  is a length of the gap between vessel base and particle bed,  $\epsilon$  is a porosity,  $p_0$  is atmospheric pressure,  $d_p$  is a diameter of particle and  $\mu$  is a viscosity of air. For the dynamics of the particle bed, we assumed that the entire particle bed moves vertically like a porous piston inside the vessel. The equation of motion is expressed as a balance of inertial force, gravity, and the pressure difference between the top and bottom of the bed as follows.

$$\frac{d^2 s}{dt^2} = -g + \frac{1}{(1 - \epsilon)\rho_p} \frac{p_L - p_0}{L} - \frac{d^2 x}{dt^2} \quad (2)$$

where  $g$  is a gravity acceleration,  $p_L$  is the pressure beneath the bed,  $\rho_p$  is the particle density. The above equations were solved numerically using the orthogonal collocation method [3].

## 3. Results and Discussion

### 3.1. Segregation Pattern

Figure 2 shows the experimental results of segregation patterns under various vibration conditions for the bed height  $L = 50 \text{ mm}$ .  $\Gamma (= (2\pi f)^2 a / g)$  represents the vibration intensity. The results indicate that inverse segregation occurs at low frequencies and sandwich segregation occurs at high frequencies. The occurrence of these density segregations were already reported

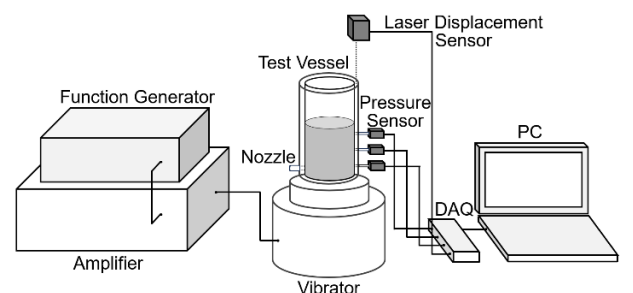


Figure 1 Schematic apparatus of experimental system.



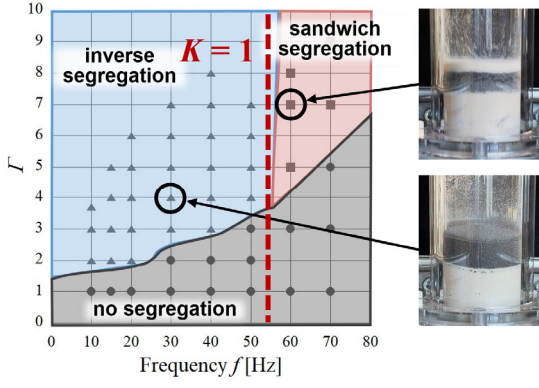


Figure 2 Segregation pattern in vibrated particle bed for bed height  $L = 50$  mm.

in previous studies [1,2]. They reported that the density segregation in vibrated particle bed causes by the interstitial air flow.

### 3.2. Pressure Change in Particle Bed

Figure 3 and Figure 4 shows the experimental and numerical results of vertical pressure distribution in the particle bed for one vibration period under the inverse and sandwich segregation conditions, respectively. The solid lines indicate the numerical results for each phase (see the upper right inset), and the circles indicate the measured results of air pressure in the particle bed. The same color indicates the same phase. The experimental and numerical results of pressure distribution are in good agreement.

As can be seen in the figure, air pressure in the particle bed changes synchronized with the motion of the particle bed. The pressure at the bottom of the bed becomes negative as the particle bed jumps off the vessel by vibration, as if a porous piston is being pulled. In contrast, when the particle bed falls into the vessel, the pressure in the bed becomes positive, as if a piston is pushed. These complicated pressure changes in the bed contribute to the segregation of particles of different densities.

### 3.3. Mechanism of Segregation

Firstly we discuss the mechanism of the inverse segregation. Focusing on the pressure distribution during the jumping phase of the particle bed, where the relative position of particles can easily change, the pressure at the bottom of the bed becomes negative, and the particles are subjected to a downward force due to the pressure difference. In this case, low-density particles with small inertia are more affected by the fluid force and move downward more than high-density particles. Such changes in the relative positions of particles are periodically repeated, resulting in inverse segregation.

Next we discuss the role of air pressure on the sandwich segregation. Under the condition that sandwich segregation occurs, the pressure distribution has inflection point during the jumping phase, i.e., low-high-low pressure distribution is formed instantaneously. Therefore, when the pressure distribution has inflection point in vertical direction, low-inertia particles moves upward and downward and high-inertia particles remain at the middle relatively. The results shown here suggest that the sandwich segregation occurs mainly by complicated change in air pressure in the particle bed.

The pressure distribution in the particle bed at each instant is determined by 1) the pressure fluctuations at the bottom of the bed caused by the jumping motion (piston effect) and 2) the propagation of pressure variance which obeys the diffusion equation (Eq.(1)). As shown in Figure 3 and Figure 4, air pressure increases and decreases twice in one period of the vibration. Therefore, the time scale (frequency) of pressure changes at the bottom  $f_p$  [Hz] is roughly estimated as follows.

$$f_p = 2f \quad (3)$$

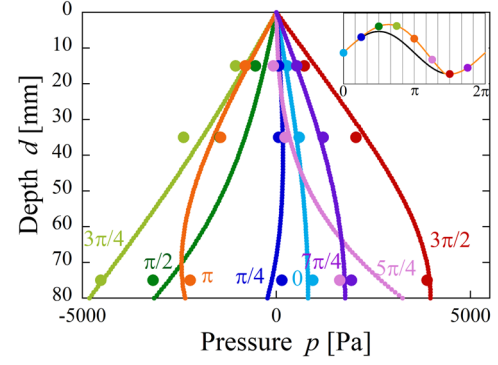


Figure 3 Air pressure profile in vibrated particle bed under an inverse segregation condition ( $f = 20$  Hz,  $\Gamma = 3.29$ ,  $L = 80$  mm).

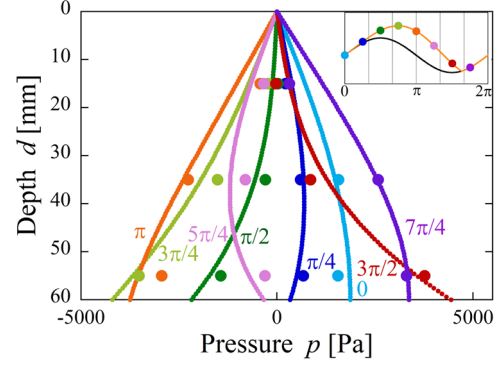


Figure 4 Air pressure profile in vibrated particle bed under a sandwich segregation condition ( $f = 40$  Hz,  $\Gamma = 3.89$ ,  $L = 60$  mm).

On the other hand, the time scale (frequency) on which the pressure propagates to the top by diffusion  $f_D$  [Hz] is expressed as follows.

$$f_D = \frac{\alpha}{L^2} = \frac{p_0}{180\mu L^2} \left( \frac{\epsilon d_p}{1 - \epsilon} \right)^2 \quad (4)$$

where  $\alpha$  is the diffusion coefficient in Eq.(1). The dimensionless number representing the transition from inverse to sandwich segregations can be defined as the ratio of these two time scales.

$$K = \frac{f_p}{f_D} = \frac{2fL^2}{\alpha} = \frac{360f\mu L^2}{p_0} \left( \frac{1 - \epsilon}{\epsilon d_p} \right)^2 \quad (5)$$

The frequency corresponding to  $K = 1$  under the present experimental conditions are indicated by the red line in Figure 2. As shown in Figure 2, inverse segregation appears in the region of  $K < 1$  and sandwich segregation in the region of  $K > 1$ .

## 4. Conclusion

The density segregation in vibrated particle bed was investigated experimentally and numerically. Focusing on the motion of permeation air flow through the particle bed, we measured and simulated the air pressure in the bed.

From the experimental and numerical results, it is found that the pressure distribution in the particle bed plays an important role on the density segregation. The relative motion of the particle bed to the vessel brings about various pressure distributions in the bed. Furthermore, the dimensionless parameter which describes the transition from inverse to sandwich segregations were proposed. The parameter can be predict well the transition frequency obtained from the experiment.

## References

- [1] N. Burtally, P.J. King and M. R. Swift, *Science*, 295, 1877-1879, 2003.
- [2] C. Zeilstra, M. A. van der Hoef and J. A. M. Kuipers, *Phys. Rev. E*, 77 031309, 2008.
- [3] T. Akiyama and T. Naito, *Chem. Eng. Sci.*, 42, 1305-1311, 1987.

# Quantifying cohesive, frictional and interlocking effects for universal powder flow characterisation

Amalia L. Thomas

Freeman Technology, 1 Miller Court, Severn Drive, Tewkesbury GL20 8DN, UK

**Abstract**— Powder flow behaviour is the result of countless combinations of interparticle forces of different natures: frictional, interlocking, cohesive and adhesive forces. We identify the rheological tests where one mechanism is most likely to dominate over the rest, and we propose the best descriptors of uniquely cohesive or frictional effects. We describe the procedure for a fluidisation test and the features of the results linked to powder cohesivity. We contrast these features against shear test results to determine powder frictional properties, explaining the conditions and limitations of the analysis. We use solid volume fraction and compressibility measurements to assess the extent to which the different mechanisms influence natural packing and forced flow in intermediate stress regimes. The proposed experimental protocol and framework of interpretation is applied to a wide range of powdered materials, representing typical industrial issues. The qualities of the characterisation are discussed and compared to those associated with traditional rheological testing methods. The framework successfully differentiates the effects of the various interparticle interaction mechanisms on powder flow, enabling a comprehensive prediction of powder behaviour in a variety of handling and processing settings. The metrics used are all normalised, allowing for a universal direct comparison of flowability across completely different materials.

**Keywords:** Powder flow; Cohesion; Fluidisation; Shear

## 1. Introduction

The infinite combinations of powder processing and handling conditions make it difficult for a single powder flow characterisation instrument or testing methodology to accurately simulate how a material will perform in any flow pattern in any combination of energy, shear-rate and stress regimes. While traditional and newer rheological testing methodologies can facilitate a quantitative and sensitive differentiation of powder samples, the root morphological cause of behavioural differences between the samples is often unknown, and the various testing methodologies can lead to conflicting results when extrapolating to processing in conditions beyond those in which the testing was performed.

We explore a new approach to powder flow characterisation based on the quantitative description of the mechanisms that oppose the motion of particles past each other: cohesion, friction and mechanical interlocking. The degree to which each mechanism contributes to ‘flowability’ scales differently with the normal force between particles and with the shear rate induced, and the different mechanisms lead to different flow-related issues: while a highly cohesive powder will tend to form clumps and agglomerates and loosely packed structures, a highly frictional and interlocking powder will form strong force chains than can arch and jam at openings. By quantifying the intrinsic strength of cohesive bonds, the effective coefficient of friction and the packing efficiency under different consolidating loads, the degree to which each mechanism contributes to

‘flowability’ can be predicted in terms of process parameters. This information can complement other rheological testing by rationalising differences in sensitivity and ‘flowability’- ranking obtained through other methodologies, it can support a more accurate understanding and prediction of how the powder will perform or behave in different conditions, and it can inform on the best course of action for solving flow-related issues.

## 2. Experimental methods

### 2.1. Fluidization test

We propose characterising the relevance of cohesive forces in a powder through features in the pressure drop curves during fluidisation and subsequent defluidisation. The tests performed for this purpose were modified from a standard aeration test in an FT4 Powder Rheometer® following the procedure described by Affleck et al. (2023), using 160 mL of powder samples in an aeration 50 mm-diameter vessel. Air supply was controlled via an aeration control unit (ACU) and distributed across the base of the vessel via a stainless-steel sintered wire mesh of 60 mm pore size. For each powder sample, a standard FT4 Aeration test was performed beforehand to estimate the minimum fluidisation velocity, and the air speeds for each fluidisation test ranged in steps from zero to roughly double  $U_{mf}$ , with extra steps around this point for added resolution.

### 2.2. Shear tests

Shear testing involves representing the relationship between shear and normal stresses between two layers of a powder. There exist several geometries for the cells that execute this measurement (translational/rotational, annular/circular), but they all apply a sequence of loads to consolidate a volume of powder, and a mechanism for trapping a layer of powder that is made to shear against another layer within the sample at each normal load step.

Using the fact that the effective frictional force resisting the shearing of powder layers scales with applied normal stress, the gradient of this graph represents the powder effective internal coefficient of friction. For ease of measurement and interpretation, we present this information as the Angle of Internal Friction, which is measured as the angle the yield locus makes with the x-axis.

The powder effective internal frictional force is expected to increase with normal load, which is not expected to be the case as significantly for cohesive forces. We therefore expect friction to become the more relevant interparticle interaction mechanism between shearing powder planes for higher normal loads.

### 2.3. Bulk tests

To assess powder behaviour at intermediate consolidating stresses, we propose to measure the conditioned solid volume fraction to assess how particles pack under the influence of gravity, and the compressibility to evaluate the effect of a controlled and repeatable external force on powder flow.

Assuming packing efficiency depends on the combination of cohesive and frictional forces relative to particle weight but also on the particle size distribution, while weak forces can be

overcome by an external compressing load, we expect that interlocking due to shape effects will limit the maximum possible packing efficiency, up to the point where compacting forces cause attrition of particles.

Forced flow behaviour is evaluated through a standard FT4 compressibility test (Freeman, 2007). 85 ml of conditioned powder are compressed in a 50 mm diameter glass cylindrical vessel using a vented piston in steps up to a normal load of 15 kPa. As the load increases, the powder compacts to smaller volumes, which are calculated from the position of the piston. The result of this test is the percentage volume change when the sample is compressed from its initial 85 ml volume at 0 kPa normal load to the final volume when compressed with 15 kPa.

### 3. Materials

We consider three CarTech® 316L Stainless steel powders (Carpenter Technology) used in laser powder bed fusion and direct energy deposition additive manufacturing.

- Produced by gas atomisation, so its particles are spherical with a relatively smooth surface texture with occasional agglomerates and satellites. Particle sizes are quoted by the supplier to be 16-45  $\mu\text{m}$
- Produced by water atomisation, with particles of irregular shapes and rough surface texture. The supplier comments that particle shapes are highly variable and have equivalent diameters in the range 25-100  $\mu\text{m}$ .
- Produced by gas atomisation, so particles are spherical with a relatively smooth surface texture but with occasional agglomerates and satellites. Particle sizes are quoted by the supplier to be 46-105  $\mu\text{m}$

### 4. Results and discussion

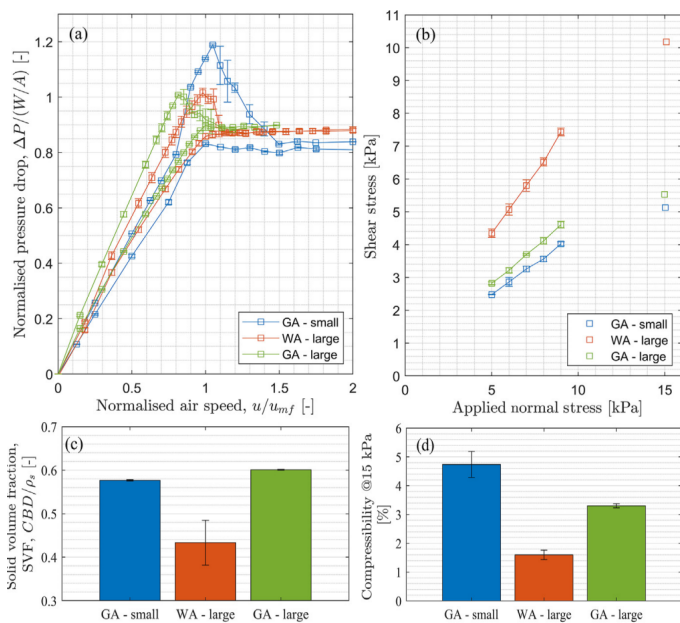


Figure 1. (a) Fluidisation curves, (b) shear vs normal stress relationships, (c) the solid volume fraction, and (d) the compressibility, for stainless steel samples of different shapes and size distributions: two spherical and smooth gas atomised samples separated into small and large grades, and a water atomised sample made of a wide distribution of rough and irregular particles.

The hysteresis, overshoot and steady-state pressure drop of the GA samples capture the increased cohesivity of the smaller grade due to the increased relevance of average interparticle force relative to particle weight. On the other hand, we do not observe significant differences in the overshoot, size of the

hysteresis and steady-state pressure drop for the two large grades, regardless of their differentiating morphological features, suggesting cohesion plays a similarly small role in interparticle interactions for these two samples.

Shear test data suggests little difference in the frictional properties of the two GA powders. The GA large-grade sample produces a slightly larger angle of internal friction, which we conjecture may be due to higher satellite content. The WA powder, in contrast, stands out for its significantly higher angle of internal friction, as expected from this atomisation process.

For the WA powder, particle roughness and shape irregularity clearly plays a more significant role than cohesion in the arrangement of particles. The low compressibility despite the loose packing of this sample suggests high friction and interlocking prevent particle flow despite its relatively low cohesivity. In this sample set, we differentiate between the GA small grade being the most cohesive and therefore the powder most likely to form clumps and agglomerates to resist flow in low-stress systems, and the WA sample as the most frictional and therefore predicted to be the most problematic in flows at high consolidating stresses, where both GA powders may behave similarly.

### 5. Conclusion

We propose a framework for universal powder flow characterisation based on a reduced number of tests that provide complementary information about interparticle interaction mechanisms in a range of shear-rate and consolidating stress regimes. The novelty of this work is in the selection of testing methodologies and fundamental metrics to isolate the characterisation of the different relevant interparticle interaction mechanisms: cohesive forces, friction and mechanical interlocking.

The comprehensive understanding of powder behaviour offered by the framework of interpretation proposed in this work supports the prediction of powder performance in handling and processing operations, as well as for quality control, with unprecedented insight. Rather than characterising powder flow through a metric of ‘success’ in a specific flow pattern, we propose to quantify powder flow in terms of the likelihood of exhibiting issues related to each of the interparticle interaction mechanisms. Cohesive powders tend to form clumps and agglomerates, they pack inefficiently and perform filling operations inconsistently; frictional powders require high levels of energy to be sheared at high consolidating stresses, and they may exhibit arching and intermittent jamming through narrow gaps or orifices; while irregularly-shaped particles lead to inefficient and inconsistent packing and low compressibility. The framework proposed for the characterisation of particle interactions allow for the quantification of fundamental mechanisms and formalise a sorely-needed link between different aspects of particle morphology, and powder flow behaviour and performance in relevant manufacturing processes.

### References

- [1] Affleck, S., Thomas, A. L., Routh, A. F., & Vriend, N. M. (2023). Novel protocol for quantifying powder cohesivity through fluidisation tests. *Powder Technology*, 415, Article 118147D.
- [2] Freeman, R. (2007). Measuring the flow properties of consolidated, conditioned and aerated powders—a comparative study using a powder rheometer and a rotational shear cell. *Powder Technology*, 174(1-2), 25-33.



# A robust indicator for the dense to dilute phase transition under horizontal moving bed flow during Fluidized Dense phase Conveying of Geldart A powders by Eulerian modelling

Prabu Balasubramanian<sup>1</sup>, Andrew Cowell<sup>1</sup>, and Don McGlinchey<sup>1</sup>

<sup>1</sup> Glasgow Caledonian University, Scotland, UK

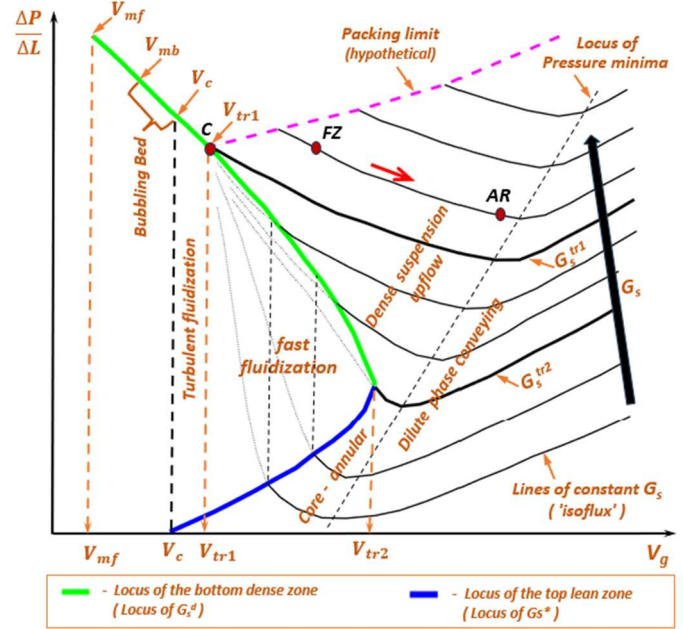
**Abstract**— Fluidized dense phase conveying of fine powders typically operates at high solids flux, 1000 – 3000 kg/m<sup>2</sup>s. The predominantly horizontal flow is characterised by a moving bed of solids at the bottom of the pipe cross-section coexisting with dilute phase flow at the top. Superficial gas velocity in the feed zone is typically 3–4 m/s at a pressure of up to 4 bar, increasing to 9–12 m/s at the ambient receiver, as the air expands along the conveying pipeline for the incurred pressure drop. If and where along the pipeline the flow transitions to dilute phase is significant for system design and there is no reliable macroscopic indicator. Eulerian modelling with the Granular Kinetic Theory suggests that the granular temperature at the dense bottom is 3–4 orders of magnitude lower than that at the dilute top, getting gradually uniform across the pipe cross-section towards the ambient receiver, as the moving bed gets suspended. With measurement techniques emerging for granular temperature, it may offer a reliable indicator for the transition. Besides a long pipe 3D model, this study has utilized a ‘pseudo-3D’, axially periodic 3D model with a single layer of axial cells (disk), to study the gradients in the radial and azimuthal directions by highly resolved simulations.

**Keywords:** granular temperature; pseudo-3D

## 1. Introduction

Fluidized Dense phase Conveying (FDC) typically operates at high solids flux ( $G_s$  of 1000 – 3000 kg/m<sup>2</sup>s) and loading ( $m \leq 300$  kg of solids / kg of air). The predominantly horizontal flow is characterised by a moving bed of solids at the bottom of the pipe cross-section coexisting with dilute phase flow at the top. Superficial gas velocity ( $V_g$ ) in the Feed Zone (FZ) is typically 3 – 4 m/s at a pressure of up to 4 bar and solids volume fraction ( $\varepsilon_s$ ) is 0.09 – 0.38; as the air expands for the incurred pressure drop along the pipeline to the Ambient Receiver (AR),  $\varepsilon_s$  decreases (0.03 – 0.18) and  $V_g$  increases (9 – 12 m/s). If and where along the pipeline the flow transitions to dilute phase is significant for system design (especially for abrasive and friable products) and is an area of active research.[1–3]

Although it is clear that the transition occurs where the moving bed of solids get fully suspended, there is no reliable macroscopic indicator. The locus of the pressure minima (the broadly accepted indicator for vertical up flow, dominated by static head of solids, Figure 1) may be suitable at low  $G_s$ , especially with larger particles wherein it marks the sharp saltation to the unstable zone; however, it may not be suitable at the high  $G_s$  of FDC wherein the unstable zone is irrelevant, and the pressure minima are rather shallow, determined largely by frictional losses. In fact, experimental data [4] (Figure 2) suggests that a large fraction of FDC, especially in shorter pipelines, occurs at higher  $V_g$  than at pressure minima. Other proposed ad hoc criteria such as  $m < 30$  or  $V_g > 10$  m/s or  $\varepsilon_s < 0.02$  may not be robust either.



$\Delta P/\Delta L$  – Pressure gradient;  $V_{mf}$  – Minimum fluidization velocity;  $V_{mb}$  – Minimum bubbling velocity;  $V_c$  – Onset of turbulent fluidization;  $V_{tr1}$  – Lower transport velocity,  $V_{tr2}$  – Upper transport velocity;  $G_s^*$  – Saturation carrying capacity;  $G_s^d$  – Gross upflow flux;  $G_{s,tr2}$  –  $G_s$  corresponding to  $V_{tr2}$ , the threshold  $G_s$  for Dense Suspension Upflow;  $G_{s,tr1}$  –  $G_s$  corresponding to  $V_{tr1}$

Figure 1. Phase map of Wirth adapted for Geldart A powders [5]

This study has explored by Eulerian modelling with Granular Kinetic Theory under the Two Fluid Model framework, the cross-sectional variation in granular temperature ( $\theta$ ) along the length of the pipeline. As  $\theta$  decreases by 3–4 orders of magnitude between dense and dilute phase flow conditions, it may offer a robust indicator for the transition. Furthermore, measurement techniques for  $\theta$  are emerging (e.g. [6]).

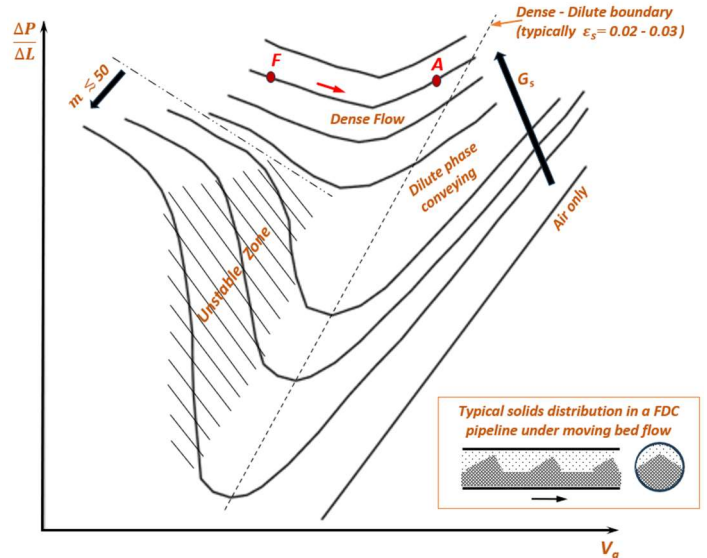


Figure 2. Typical horizontal characteristics of FDC on the phase map of Zenz

TABLE I. MODELLING OPTIONS AND CONDITIONS

Description	Long pipe model	Disk model
Code	MFiX-TFM (version 22.3.1)	
Particle diameter	70 $\mu\text{m}$ (monodisperse)	
Particle density	1400 $\text{kg} / \text{m}^3$	
Viscous stress model	Simonin	
Turbulence model	k-epsilon	
Frictional stress model	Srivastava-Sundaresan	
Drag model	Di Felice	
Inlet & Outlet BC	MI - PO	Periodic
Wall BC – Gas	No slip wall (wall functions)	
Wall BC – Solids	Free Slip Wall	
Pipeline diameter ( $D$ )	0.04 m	
Pipeline length ( $L$ )	10 m	Cell size <sup>a</sup>
Coordinates	Cartesian Cut-Cell	
Grid (Nominal / Fine)	18x4500x18 / --	18x1x18 / 54x1x54
Cell size in particle diameters	32	21 / 11
Maximum time step	1.5 – 3 E-5 s	1.0 E-5 s
Parallel processing	DMP (1-28-1)	DMP (2-1-2 / 4-1-4)

a. Same as the radial dimension of the cells

## 2. Methodology and methods

Simulations are carried out with the open-source MFiX-TFM code; model options have been chosen to cover the coexistent dense and dilute phases (TABLE I). Besides a long pipe model, an axially-periodic pseudo-3D (disk) model (inspired by [7]) with a single layer of axial cells is used, to capture the strong gradients in the radial and azimuthal directions by highly resolved simulations.

Simulation results are visualised, as well as post-processed to obtain the averages and deviations in the distributions of  $\theta$ ,  $\varepsilon_s$ ,  $V_g$ ,  $V_s$ , macroscopic pressure and the solids phase pressure to identify the transition.

### 2.1. Limitations

Resolved experimental data for solids distribution within horizontal pipelines is scarce; the study has used the long pipe model validated for vertical flow; the results of the disk model have been compared with that of the long pipe model. The model does not include slip shear lift force. Whereas typical powders handled by FDC are polydisperse with significant fraction of fines ( $<45\mu\text{m}$ ), a monodisperse 70  $\mu\text{m}$  powder is modelled; for the chosen powder, gravity is expected to be dominant over van der Waals forces, and hence a cohesion model is not essential. While this study (and [5]) covers straight pipes, the profound influence of bends on the flow is not covered. Findings of the study are based on a single, narrow pipeline diameter, and hence validation for additional / larger diameters may be required.

## 3. Results and discussion

Visualisation of a typical long pipe run is shown in Figure 3 and that of disk model runs, comparing a denser and relatively leaner emulsion are shown in Figure 4. Results indicate that the flow may not transition to dilute phase at the AR, for the conditions simulated. Further simulations to cover wider operating conditions would be required to ascertain conditions at which dilute phase flow at AR is probable.

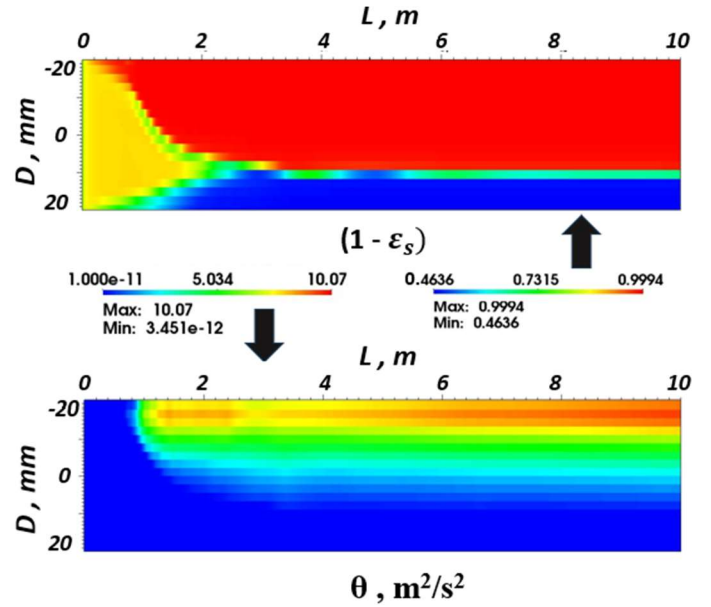


Figure 3. Visualization of a typical long pipe results

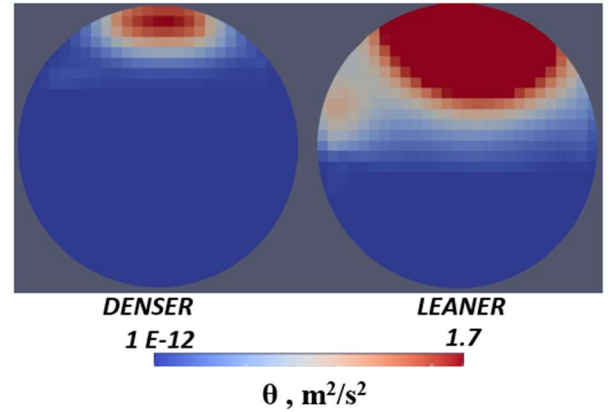


Figure 4. Comparison of disk model results for denser and leaner cases

## 4. Conclusion

The study outcome suggests that granular temperature may offer a robust indicator for if / where along the conveying pipeline the flow transitions to dilute phase; the indicator could be deployed when measurement techniques emerge. The pseudo-3D, ‘disk’ model enables highly resolved 3D simulations for cross-sectional profiles at an affordable cost.

## References

- [1] N. Behera, V. K. Agarwal, M. G. Jones, and K. C. Williams, “Transient parameter analysis of fluidized dense phase conveying,” *Powder technology*, vol. 217, pp. 261–268, 2012.
- [2] K. C. Williams, M. G. Jones, and A. A. Cenna, “Characterization of the gas pulse frequency, amplitude and velocity in non-steady dense phase pneumatic conveying of powders,” *Particuology*, vol. 6, no. 5, pp. 301–306, 2008.
- [3] J. S. Shijo and N. Behera, “Prediction of flow mode transition in pneumatic conveying of fine particles using CFD,” *Particulate Science and Technology*, 2022.
- [4] D. Mills, *Pneumatic conveying design guide*, 2nd ed. Amsterdam: Elsevier, Butterworth Heinemann, 2004.
- [5] P. Balasubramanian, A. Cowell, and D. McGlinchey, “Adaptation of the vertical upflow phase map of Wirth to fluidized dense phase conveying of Geldart A powders and validation of the transition boundaries by Eulerian modelling with MFiX-TFM,” presented at the NETL 2024 Workshop on Multiphase Flow Science, Aug. 2024.
- [6] Z. Maranic, F. Guillard, J. Baker, I. Einav, and B. Marks, “A granular thermometer,” *Granular matter*, vol. 23, no. 2, 2021.
- [7] S. Benyahia, M. Syamlal, and T. J. O’Brien, “Study of the ability of multiphase continuum models to predict core-annulus flow,” *AIChE Journal*, vol. 53, no. 10, pp. 2549–2568, 2007, doi: 10.1002/aic.11276.

# Intra-Particle Stresses: Insights into SAG Mill Mechanics

Tahir A. Jauhar<sup>1</sup>, Michael J. Carr<sup>1</sup>, Craig A. Wheeler<sup>1</sup>, Paul W. Cleary<sup>2</sup>, Dean Ellis<sup>3</sup>, Dasun Balasooriya<sup>1</sup>, Stephan Chalup<sup>1</sup>

<sup>1</sup> The University of Newcastle, Callaghan NSW, Australia

<sup>2</sup> CSIRO Data61, Private Bag 10, Clayton South, VIC 2168, Australia

<sup>3</sup> Bradken Resources Pty Limited, 20 McIntosh Drive, Mayfield West, NSW, Australia

**Abstract—** Semi-Autogenous Grinding (SAG) mills are used in mineral processing due to their simple design, straight forward production, strong adaptability, and reduced dust production. However, the internal mechanics of a SAG mill cannot be analysed in detail during production due to particle breakage and fluid flow. SAG mills are designed based on impact tests and attrition tests, which address two extremes of energy impacts within the mill. Rocks inside the SAG mill may experience multiple impacts while being immersed within a substantial volume of material. This unique scenario places varying stress levels on the rocks, depending on their spatial location within the mill. To study this phenomenon, this paper investigates a pilot mill equipped with sixteen lifters using Discrete Element Method (DEM) simulations. By injecting particles of varying sizes into the flow, intra-particle stresses and the particles' trajectories are analysed. For the same size particles, these follow similar trajectories over the mill cycles, leading to similarities in their intra-particle stresses. Evaluation of single particles inside the SAG mill is difficult therefore, a single particle simulation is proposed to match the intra-particle stresses experienced in the SAG mill.

**Keywords:** SAG; grinding mill; intra-particle stresses; pilot SAG mill;

## 1. Introduction

In mineral processing, crushed rocks undergo size reduction to liberate ore and gangue. The ore is then used for mineral extraction whereas gangue is the material of no commercial value. There are three main types of equipment that may be used for size reduction. These include High Pressure Grinding Rolls (HPGRs), Autogenous Grinding (AG) Mills and Semi Autogenous Grinding (SAG) mills. SAG mills are often preferred for their simple design, straight forward production, reduced dust production and smaller footprint to name a few [1]. SAG mills constitute site specific design using several tests for the SAG mill sizing. These tests may be divided into two main categories: (1) single particle impact breakage tests and (2) attrition tests. These tests include the SAG Power Index (SPI) test, Julius Kruttschnitt Mineral Research Centre (JKMRC) Drop-weight test [2] and the Steve Morrel Comminution (SMC) test [3] etc. These sizing tests correspond to a subset of rock mechanics inside the SAG mill. The rocks inside the SAG mill undergo impact breakage and attrition [4]. In the attrition paradigm, the rocks may be submerged within or under a substantial volume of material, that makes the scenario different from the attrition tests used for mill sizing. Therefore, further investigation of intraparticle stresses is required. A pilot scale SAG mill is simulated in a dry environment to analyse the intraparticle stresses.

## 2. Materials and Methods

### 2.1. Pilot SAG mill setup

A sixteen-lifters pilot mill with 1800 mm effective diameter, 138 mm lifter height, 40 mm lifter top width and 22.5° lifter face angle is simulated with the segment length of 430 mm at 2.44 radians/second. Mill load distribution is provided in Table 1.

TABLE I. MILL LOAD DISTRIBUTION

Type	Shape	Size (mm)	Mass (kg)	Density (kg/m <sup>3</sup> )
Rocks	Polyhedral	20	270	2930
		50.8	200	
		101.6	250	
Balls	Sphere	127	230	7800

For simulation, the hysteretic linear spring model is used for normal force, whereas the linear spring coulomb limit model is used for tangential force. The rolling resistance is resolved by the linear spring rolling limit model.

### 2.2. Particle tracking

Material is loaded with a surface inlet in one second and another second is utilized for settling down of the input material. The simulation is run for eight seconds to attain the developed flow as shown in Fig. 1. In this state, particles with three different sizes are added. Their intra-particle stresses are analysed along with their trajectories. The material flow can be broadly divided into three categories: cataracting stream, cascading stream, and lifting. In the cataracting stream, the material detaches from the lifter and follows a parabolic path inside the mill. In the cascading stream, the material particles roll over the bulk of the material. The lifting action happens when the material is lifted by the lifters. In Fig. 2, the graph on the left shows the cataracting and cascading streams, and the one on right shows lifting of the material for 20 mm particles.

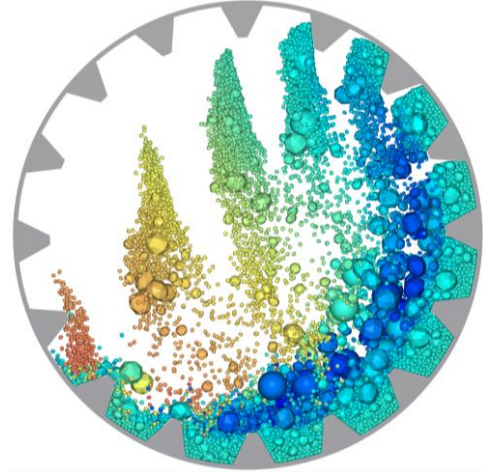


Figure 1. Pseudo Steady state of the SAG mill.

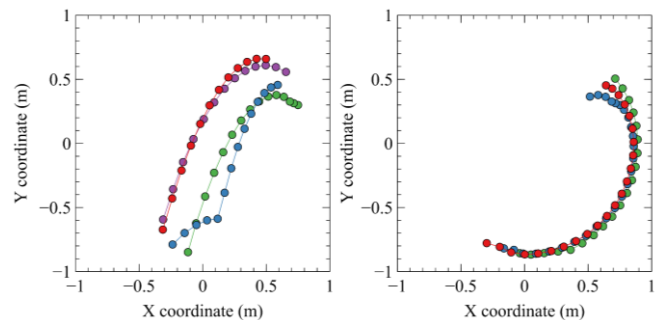


Figure 2. Cataracting and cascading streams (left) and lifting action (right).



### 3. Intraparticle stresses and breakage

The intraparticle stress module is turned on for this simulation. Similar values of maximum stress are observed. Stress variations are observed for two 20 mm particles as shown in Fig. 3 with red diamond and green circular markers. For detailed analysis, the stress values in different time are plotted for two different particles in Fig. 4. Similar trends are observed with maximum stress for the particle in the top graph being ~69 kPa and the stress for particle in bottom graph being ~88 kPa.

#### 3.1. Single particle setup

For single particle stress modelling, two surfaces are modelled with one being stationary and other moving. The movement of the top plate is adjusted to meet the intraparticle stress values. The setup is shown in Fig. 5. During single particle stress response, the particles are assumed not to rotate. Thus, in the simulation their rotation is turned off. The top plate is moved at a very slow speed to meet the required maximum stress value of the particle in Fig. 4.

#### 3.2. Breakage response

After matching the stress values, the breakage model is activated to understand the breakage behaviour at the maximum stresses in Fig. 4. Thus, predicting what may happen inside the mill in terms of breakage. The breakage is modelled using Tavares breakage model in Rocky2024R1 [5]. The breakage parameters used are available in literature [6]. Two breakage simulations were conducted at ~69 kPa and ~88 kPa. However, the breakage response was similar in both the cases. The PSD of the fragments is shown in Fig. 6.

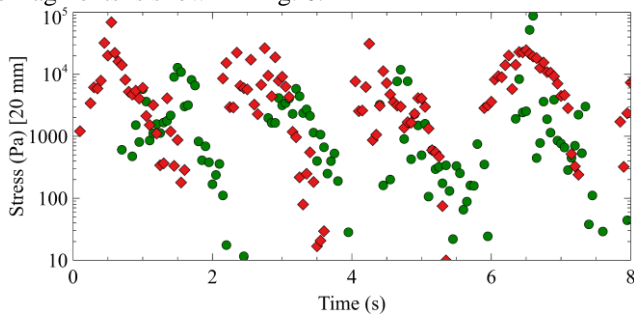


Figure 3. Intraparticle Stresses.

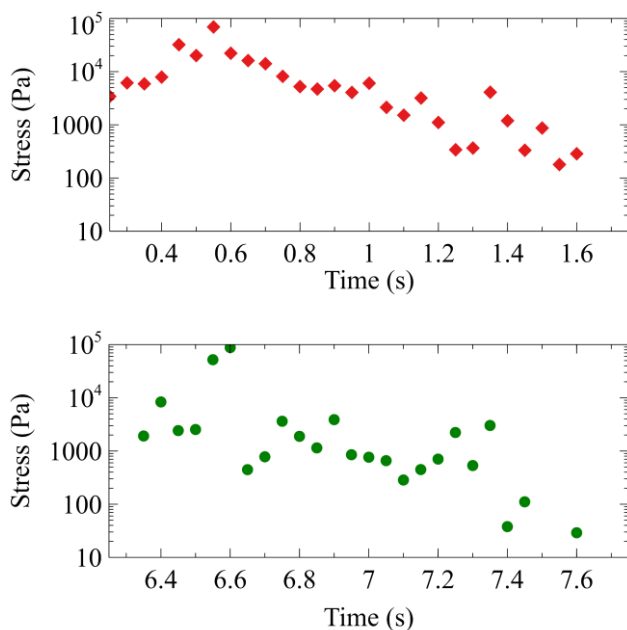


Figure 4. Intra particle stresses of 20 mm particles.

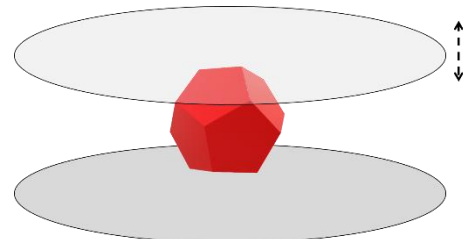


Figure 5. Setup for single particle.

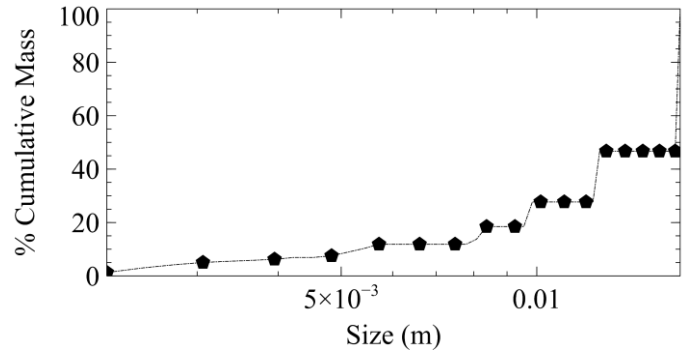


Figure 6. PSD of Single Particle at Maximum stress.

### 4. Conclusion

This study concludes that various particles may undergo a variety of stress distributions during the mill revolution. Their stress distributions may differ by a few kilopascals. However, for the particles undergoing a difference of ~19 kPa stress, their breakage behaviour remained the same. The minimum fragment size is adjusted in this case. Moreover, the stresses observed for the single particle were slightly higher than those observed in the mill. In future work, the experiments are to be conducted to quantify the breakage behaviour of various ore particles in accordance with their stresses inside the simulated mill.

### Acknowledgement

The authors are thankful to the Australian Research Council for funding this research through Linkage Project (LP190100378).

### References

- [1] M. Jahani Chegeni and S. Kolahi, "An Investigation on Effect of Shell Liner Type on Performance of Industrial SAG Mills Using DEM," *Journal of Mining and Environment*, vol. 11, no. 2, pp. 387-404, 2020.
- [2] C. Bailey, G. Lane, S. Morrell, and P. Staples, "What can go wrong in comminution circuit design," in *Proceedings of the 10th Mill Operators' Conference, Adelaide, SA*, 2009.
- [3] S. Morrell, "How to Formulate an Effective Ore Comminution Characterization Program," *Proceedings of the MetPlant*, 2019.
- [4] P. W. Cleary and R. Morrison, "Comminution mechanisms, particle shape evolution and collision energy partitioning in tumbling mills," *Minerals Engineering*, vol. 86, pp. 75-95, 2016.
- [5] "Ansys Rocky Particle Dynamics Simulation Software." <https://www.ansys.com/products/fluids/ansys-rocky> (accessed 11/06/2024, 2024).
- [6] R. Carvalho, "Mechanistic modelling of semi-autogenous grinding," Department of Metallurgical and Materials Engineering, (PhD Dissertation) Universidade Federal do Rio de Janeiro, 2013.

# 3D Reconstruction and Morphological Characterization of Falling Non-Spherical Particles

A. Bauer<sup>1</sup>, H. Kruggel-Emden<sup>1</sup>

<sup>1</sup> Technische Universität Berlin, Chair of Mechanical Process Engineering and Solids Processing, Berlin, Germany

**Abstract**— Real time bulk characterisation is essential in solids handling. Precise knowledge of size and shape of the processed particles is crucial, since they often determine the properties of subsequent process steps. To this day, particles are often characterised by means of 2D images in dynamic image analysis. 3D information is then obtained by statistical analysis under certain assumptions, which leads to systematic deviations. In our approach, we demonstrate the feasibility of obtaining accurate 3D models by reconstruction from images of as few as three cameras. Images of the particles are obtained in free fall from different perspectives at different times. A visual hull method as well as a data driven 3D-reconstruction model are utilized to obtain the shapes, which are then morphologically characterized. The reconstructed models yield good results in terms of the evaluated descriptors.

**Keywords:** 3D dynamic image analysis, 3D reconstruction, morphological analysis, process monitoring

## 1. Introduction

Monitoring disperse systems plays an important role in many industries such as chemical industry, pharmaceutical industry or food processing. Here, information about size and shape of particles in the bulk is crucial, since the properties determine the effectiveness and required process parameters of consecutive processes [1]. As the aspects flow velocity, accuracy and fast yield of results are of importance for process monitoring, dynamic image analysis (DIA) has proven to meet these requirements [2]. Additionally, there has been an increased understanding for the relevance of the particle shapes being present in the processed bulk material [2]. Currently, relevant measures of large particle systems (>10,000) are obtained by statistical evaluation of 2D images: each object is tracked over a period from different perspectives. From these images, several measurements of the same property are acquired. Obviously, those measurements are carried out on random projections of the object. However, it has been shown that 2D DIA induces an error depended on the object shape by estimating the 3D information by 2D statistics [3], as seen in Fig. 1. Therefore, obtaining the 3D information directly from the imaging system would largely benefit all facets of solids processing.

We address this shortcoming of currently used dynamic image analysis techniques by directly obtaining the 3D models of the particles via 3D reconstruction. In the presented work, an experimental test rig was set up to simultaneously capture images of falling objects from three different perspectives with high-speed cameras. From these images, the original shapes of the objects were reconstructed by making use of conventional and data-driven reconstruction techniques. The reconstructed shapes were compared to ground-truth data obtained by  $\mu$ CT-scans by morphological analysis of each particle. Three different materials with around 60 particles per material were analysed and compared. The proposed work contributes to the development of real time 3D analysis devices, basing on available 2D-image analysis and extending it towards accurate, fast and automated reconstruction of particle morphology.

## 2. Experimental Setup

### 2.1. Materials

Three different types of materials were used for 3D-reconstruction and subsequent morphological analysis. Brick particles with a maximum Feret diameter of 16 mm were used. The second material was lithium aluminate slag with maximum Feret diameters of 55 mm. As the third material, limestone with maximum diameters of 50 mm was analysed. 60 particles were considered for each material.

### 2.2. Hardware

Three monochrome industrial cameras with a Sony IMX252 Pregius CMOS sensor of size 7.1 x 5.3 mm were used to capture the falling particles. The cameras yield maximum FPS of 218. The resulting pictures have a resolution of 2064 x 1544 pixels. The cameras were equipped with a Kowa LM16JC10M lens with a focal length of 16 mm. Three HEDLER Profilux LED1000 were used to provide flicker-free lighting from each perspective. Software triggering was used to obtain simultaneous images. The camera control was implemented in Python.

### 2.3. Test Rig

All hardware components were mounted to a test rig of aluminium profiles. The cameras were aligned horizontally and were positioned at a 45° angle to each other. The distance to the falling object was around 350 mm for the middle camera and around 440 mm for the outer cameras. The middle camera was aligned with a vibrating feeder, which was positioned 565 mm above the focus point of the cameras. The feeder was used for dropping the particles into the field of view of the cameras.

## 3. Methods and Evaluation

### 3.1. 3D-Reconstruction

Two methods to reconstruct the 3D mesh from 2D images with known camera positions were utilized and compared in this study. The main difficulty was to incorporate the images from consecutive time steps into the reconstruction, since the relative pose between the cameras and the object changed for each frame. Traditional methods which rely on feature detection for estimating the camera position were not applicable to our setup, since we observe a moving object in front of a static background.

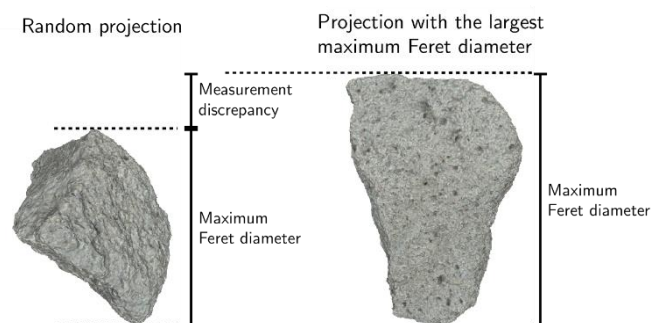


Figure 1. Illustration of measurement discrepancy of a measured property between a random projection and knowledge of the overall geometry.

The masked object without the background yielded to few features for those methods. Instead, we ran the reconstruction on a single frame, i.e. 3 images from 3 perspectives at the same time. We used two different reconstruction methods: A visual hull algorithm, which computes the shape from the binary masks of the images and a data-driven neural radiance field (NerF) approach.

The visual hull algorithm computes 3D shapes from the object masks of each camera and the respective camera positions for each image by projecting the binary images into a volume. The mesh is then obtained by a marching cube algorithm. A MATLAB implementation was used for the computation [4].

As a NerF implementation, ZeroRF [5] was chosen. A NerF represents a 3D scene radiance field by a Multi-Layer Perceptron, where given an input 3D location  $x$  and the view direction, it outputs the volume density and view-dependent color [5]. ZeroRF was optimized for sparse views, i.e. for scenes where only parts of an object are visible.

### 3.2. Morphological Descriptors

A list of morphological descriptors computed for each reconstructed particle is provided in Table I. The descriptors were evaluated for each material separately and results depicted as distributions for bulk characterisation.

TABLE I. MORPHOLOGICAL DESCRIPTORS.

Type	Descriptor	Explanation	Formula
Size descriptors	Surface area $A_s$ [mm <sup>2</sup> ]	Particle surface area	-
	Volume $V$ [mm <sup>3</sup> ]	Particle volume	-
	$d_{ESD}$ [-]	Diameter of sphere with equivalent particle volume	$\sqrt[3]{6V/\pi}$
	Longest $d_{Flength}$ , intermediate $d_{Fwidth}$ , shortest $d_{Fthickness}$ axes [mm]	Side lengths of oriented bounding box	-
Shape descriptors	Aspect ratio 3D [-]	Ratio of shortest to longest axes	$\frac{d_{Fthickness}}{d_{Flength}}$
	Flatness index, Elongation index [-]	Ratio of shortest to intermediate axes, Ratio of intermediate to longest axes	$\frac{d_{Fthickness}}{d_{Fwidth}}$ , $\frac{d_{Fwidth}}{d_{Flength}}$
	Sphericity 3D [-]	Ratio of the surface area of a volume equivalent sphere to the real surface area	$\frac{\pi d_{ESD}^2}{A_s}$
	Convexity 3D [-]	Ratio of the particle volume to convex hull volume	$\frac{V}{V_{convex}}$

Evaluation is carried out by comparing the computed descriptors from the reconstructed particle models with the descriptors calculated for  $\mu$ CT ground truth models of each particle.

## 4. Results

The evaluation is shown for an exemplary particle of slag. Fig. 2 shows a qualitative comparison of the two reconstructed models with the ground truth. As can be seen, the model reconstructed by ZeroRF is more detailed and faceted, while the model obtained by visual hull is bulkier and more convex. Qualitatively, the shape of the ZeroRF model is closer to the real object.

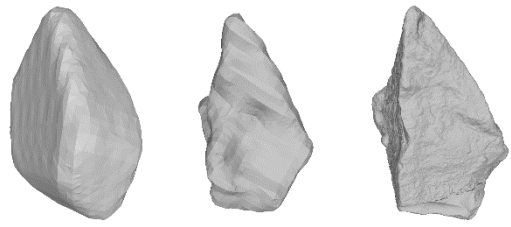


Figure 2. Qualitative comparison of models reconstructed by visual hull (left), ZeroRF (middle) and ground truth (right).

In Table II, the deviation from the ground truth is shown for the particles from Fig. 2 for selected size descriptors. While the object reconstructed by the visual hull in terms of surface area and volume is closer to the real object, the axes lengths are captured mostly more accurately in the model reconstructed with ZeroRF.

TABLE II. DEVIATION OF MORPHOLOGICAL PARAMETERS IN % FOR A SLAG PARTICLE (FIG. 2).

Method	$A_s$	$V$	$d_{Flength}$	$d_{Fwidth}$	$d_{Fthickness}$
Visual Hull	35.2	3.83	11.96	4.12	8.05
Zero RF	42.9	32.50	0.14	7.04	1.13

## 5. Conclusion

We have shown that a 3D-reconstruction of freely falling objects is feasible with the presented setup. The quality of the reconstructed objects depends on the chosen method, which must be investigated in more detail. As a next step, the parameters of all particles from each material will be evaluated and discussed.

Further improvements of the presented approach are the incorporation of the time dependent frames, to improve the quality of the reconstructed models by use of more perspectives. This can be achieved through camera pose estimation for the individual frames, for example. Also, the hyperparameters of the data-driven model will be tuned to enhance the output.

In terms of inference speed, the visual hull method clearly outperformed ZeroRF with an inference of <1 seconds vs ~20 minutes per particle, respectively. The cost of computation and the speed of inference will be the subject of further investigation.

## Acknowledgement

The research project IGF 22901 N/1 was funded by the Federal Ministry for Economic Affairs and Climate Action based on a resolution of the German Bundestag as part of a program for promoting industrial collective research (IGF).

## References

- [1] J. Emmerich et al., *Optical inline analysis and monitoring of particle size and shape distributions for multiple applications: Scientific and industrial relevance*, Chinese J. Chem. Eng. 27(2), 257-277, 2019. <https://doi.org/10.1016/j.cjche.2018.11.011>.
- [2] U. Ulusoy, *A Review of Particle Shape Effects on Material Properties for Various Engineering Applications: From Macro to Nanoscale*, Minerals 13(1), 91, 2023. <https://doi.org/10.3390/min13010091>.
- [3] R. D. Beemer et al., *Comparison of 2D Optical Imaging and 3D Microtomography Shape Measurements of a Coastal Bioclastic Calcareous Sand*, Journal of Imaging 8(3), 72, 2022. <https://doi.org/10.3390/jimaging8030072>.
- [4] <https://github.com/maximm8/VisualHull> (accessed 19.07.2024).
- [5] S. Ruixi et al., *ZeroRF: Fast Sparse View 360° Reconstruction with Zero Pretraining*, IEEE/CVF Computer Vision and Pattern Recognition Conference (CVPR) 2024, Seattle, US. <https://doi.org/10.48550/arXiv.2312.09249>.

# Deep Learning-Based Measurements of Segregation of Iron Ore Pellets, Sinter and Coke

Wessel de Jonge, Ahmed Hadi, Yusong Pang and Dingena L. Schott

Department of Maritime and Transport Technology, Faculty of Mechanical Engineering, Delft University of Technology, Delft, The Netherlands

**Abstract**— Segregation of materials (iron ore pellets, sinter and coke) within the blast furnace charging system is a significant challenge since it can have a negative effect on the burden permeability. Therefore, understanding and assessing segregation is highly important for optimising the charging process. Typically, segregation can be measured through invasive (sampling) and non-invasive (e.g. image analysis) methods. However, harsh environmental conditions within the blast furnace charging system make sampling challenging. Consequently, taking images of the material flow and measuring segregation using image analysis is preferred. However, as iron ore pellets, sinter and coke particles have similar colours, the measurements of their fraction using conventional image processing are not accurate. Here, we propose an innovative approach using deep learning (DL) to overcome this challenge. We systematically measured the segregation through several steps. First, we created the dataset by taking a number of photos of the mixture of the three materials, followed by labelling each material. Next, we selected and trained three DL models, namely Mask R-CNN, Cascade R-CNN and End-to-end instance segmentation with transformers (ISTR). After comparing these DL models' performance, Cascade R-CNN was selected. Finally, we leveraged the Cascade R-CNN to accurately segment the image and measure the materials' fraction. We also demonstrated that size segregation can be simultaneously analysed. Our findings show that deep learning can serve as an accurate and efficient method for analysing the segregation of materials with similar colours in bulk handling industries.

**Keywords:** deep learning; segregation; granular materials; artificial intelligence; image segmentation

## 1. Introduction

Segregation of granular materials happens when particles with similar characteristics, such as size, density, or shape, accumulate in certain areas of the mixture. This phenomenon is mostly viewed as unfavourable because it reduces the uniformity of the granular mixture. For instance, in the blast furnace charging system, segregation of iron ore mixture negatively impacts the distribution of materials on the burden surface, which can, in turn, adversely affect bed permeability [1]. Therefore, it is important to investigate granular segregation to enhance our understanding of this phenomenon.

Segregation can be measured and quantified through in-situ measurements or lab-scale experiments, using either intrusive or non-intrusive techniques [2]. Physical sampling, an intrusive method, not only disturbs the structure of the mixture but is also impractical in certain situations, such as the blast furnace charging system, due to the harsh environment. In contrast, image analysis is a simple, cost-effective, and non-intrusive method that provides an alternative approach to quantifying segregation [3].

Image analysis involves capturing photos of the granular mixture and performing image processing to segment the photo and then measure the fraction of materials at the pixel level. While conventional image processing methods are generally effective for segmentation, they struggle with accuracy when components have similar colours [4]. Although colour contrast can be achieved by coating the components, it may change the frictional properties of the materials and is only suitable for lab-scale experiments [5]. Therefore, more advanced techniques are needed to tackle this challenge.

In this study, we propose an innovative approach based on deep learning (DL) to address this challenge. We apply this method to a mixture of iron ore pellet, sinter and coke, which is used in the blast furnace charging system.

## 2. Methods

### 2.1. Establishing Dataset

To create the dataset for training the DL models, a mixture of iron ore pellets, sinter and coke was placed into an open-ended cylinder. A heap was then formed on a white cloth by lifting the cylinder vertically. Then, we took images from a top-down view of the heap at a fixed vertical distance. An example of such an image is shown in Fig.1. This process was repeated, resulting in a total of 215 images. We then annotated the images using Roboflow [6] to label and prepare them for model training.

### 2.2. Model Training

We selected three DL models for segmentation to train: Mask R-CNN [7], Cascade R-CNN [8], and ISTR [9]. Out of 215 images, 180 were used for training and 35 for testing. Each model was trained for 40,000 iterations corresponding to approximately 222 epochs. The learning rate was set at 0.001 for both Mask R-CNN and Cascade R-CNN, while ISTR required a much lower learning rate of  $5e-5$  to prevent divergence during training.

### 2.3. Quantifying DL Model Performance

The performance of DL models in image segmentation can be evaluated from two perspectives: 1) precision, which measures the accuracy of the model's predictions (i.e. correctly identifying the particle type), and 2) recall, which assesses the model's ability to detect all instances (i.e. all particles). To capture both aspects, we used the F-measure [10], which combines precision (P) and recall (R) into a single, unified formula:



Figure 1. An example of the image taken from top-down view of the heap.



$$F - measure = \frac{2PR}{P + R} \quad (1)$$

A higher F-measure indicates a better performance of the model.

#### 2.4. Quantifying Segregation

We employed a segregation index (SI) to quantitatively measure segregation in the segmented image. To calculate the SI, the image is first divided into  $N$  sections. Then, the concentration (pixel ratio) of each component in section  $i$ , denoted as  $\chi_i$ , is determined. The SI is finally calculated using the following equation [11]:

$$SI = \sqrt{\frac{\sum_{i=1}^N (\chi_i - \bar{\chi})^2}{N - 1}} \quad (2)$$

where  $\bar{\chi}$  is the arithmetic mean of  $\chi_i$  across all sections. SI ranges between 0 and 0.5, indicating perfectly mixed and fully segregated mixtures, respectively.

### 3. Results and Discussion

#### 3.1. Comparison of DL Models

We trained three selected DL models to identify the one with the best performance. Fig. 2 presents the qualitative segmentation results. It shows that ISTR underperforms in detecting all the particles. For a quantitative comparison, Table I provides the F-measure. Although Mask R-CNN slightly outperforms Cascade R-CNN in terms of the F-measure, we chose Cascade R-CNN because Mask-R-CNN struggles with detecting coke particles, often misclassifying some sinter particles and even parts of the background (see Fig. 2(a) on the right edge) as coke.

#### 3.2. Measuring Segregation

Once the image is segmented using the chosen model, Cascade R-CNN, we proceed with quantifying segregation using the segregation index (SI) defined in (1). To calculate the SI, we used a circular grid system to divide the image into bins. This analysis resulted in SI values of 0.22 for coke, 0.17 for sinter, and 0.11 for pellets, indicating a higher degree of segregation of coke particles, which is in good agreement with Fig. 2(b).

Since the model processes the image on a particle-by-particle basis, it can effectively isolate individual particles. This allows for precise size measurement of each particle. To determine particle size, we used the area-equivalent diameter, which is the diameter of a circle that has the same area as the particle. This method enabled us to classify the particles based on their sizes into small, medium and large particles, as illustrated in Fig. 3.

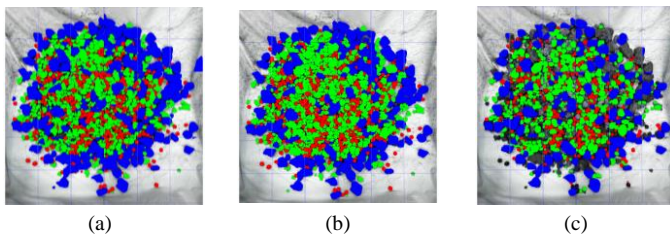


Figure 2. Segmentation results using a) Mask R-CNN, b) Cascade R-CNN, and c) ISTR. Blue, green and red colours correspond to coke, sinter and pellets, respectively.

TABLE I. F-MEASURES FOR THE SELECTED DL MODELS

	Mask R-CNN	Cascade R-CNN	ISTR
F-measure	0.69	0.66	0.25

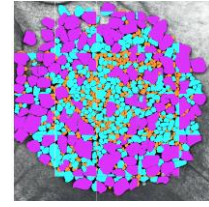


Figure 3. Classification of particles based on their size. Purple, cyan and orange colours represent large, medium and small particles, respectively.

### 4. Conclusion

The proposed DL method for quantifying segregation shows great potential. In our case study, Cascade R-CNN effectively segmented the image of a mixture with similar-coloured materials, including pellets, sinter and coke. Moreover, the DL model can simultaneously quantify size segregation. While the model's performance was promising, further accuracy can be achieved by optimising the model's hyperparameters as well as expanding the dataset. Notably, the images used for training were taken without specialised lighting, indicating the method's applicability in diverse environments and suitability for in-site applications in bulk handling industries.

### Acknowledgement

This research was carried out under project number T18019 in the framework of the Research Program of the Materials innovation institute (M2i) (www.m2i.nl) supported by the Dutch government. The authors would like to acknowledge dr.ir. Jan van der Stel and dr. ir. Allert Adema from Tata Steel IJmuiden for their valuable insights and support.

### References

- [1] Y. Yu and H. Saxén, "Experimental and DEM study of segregation of ternary size particles in a blast furnace top bunker model," *Chem. Eng. Sci.*, vol. 65, no. 18, pp. 5237–5250, Sep. 2010, doi: 10.1016/j.ces.2010.06.025.
- [2] A. N. Huang and H. P. Kuo, "Developments in the tools for the investigation of mixing in particulate systems - A review," *Adv. Powder Technol.*, vol. 25, no. 1, pp. 163–173, 2014, doi: 10.1016/j.appt.2013.10.007.
- [3] A. Hadi, R. Roelap, Y. Pang, and D. L. Schott, "DEM Modelling of Segregation in Granular Materials: A Review," *KONA Powder Part. J.*, 2023, doi: 10.14356/kona.2024017.
- [4] M. Asachi, E. Nourafkan, and A. Hassanpour, "A review of current techniques for the evaluation of powder mixing," *Advanced Powder Technology*, vol. 29, no. 7, pp. 1525–1549, 2018, doi: 10.1016/j.appt.2018.03.031.
- [5] A. H. Hadi, Y. Pang, and D. L. Schott, "Calibration of DEM Parameters for Multi-Component Segregation," in *ICBMH 2023: 14th International Conference on Bulk Materials Storage, Handling and Transportation*, 2023.
- [6] B. Dwyer, J. Nelson, and J. Solawetz, "Roboflow (version 1.0)[software]," *URL https://roboflow.com. Comput. Vis.*, 2022.
- [7] K. He, G. Gkioxari, P. Dollár, and R. Girshick, "Mask R-CNN," *IEEE Trans. Pattern Anal. Mach. Intell.*, vol. 42, no. 2, pp. 386–397, 2020, doi: 10.1109/TPAMI.2018.2844175.
- [8] Z. Cai and N. Vasconcelos, "Cascade R-CNN: Delving into High Quality Object Detection," in *Proceedings of the IEEE Computer Society Conference on Computer Vision and Pattern Recognition*, 2018, pp. 6154–6162, doi: 10.1109/CVPR.2018.00644.
- [9] J. Hu *et al.*, "Istr: End-to-end instance segmentation with transformers," *arXiv Prepr. arXiv2105.00637*, 2021.
- [10] Y. Sasaki, "The truth of the F-measure," *Teach Tutor mater*, pp. 1–5, 2007, [Online]. Available: <http://www.cs.odu.edu/~mukka/cs795sum09dm/LectureNotes/Day3/F-measure-YS-26Oct07.pdf>
- [11] D. Shi, A. A. Abatan, W. L. Vargas, and J. J. McCarthy, "Eliminating segregation in free-surface flows of particles," *Phys. Rev. Lett.*, vol. 99, no. 14, p. 148001, 2007, doi: 10.1103/PhysRevLett.99.148001.



# Comparing Aspherix against open-source DEM frameworks for simulations of common bulk processes

Marcel Kwakkel<sup>1</sup>, Balázs Füvesi<sup>1,2</sup>, Augusto F. Moura<sup>1</sup>, Christoph Goniva<sup>1</sup>, and Christoph Kloss<sup>1</sup>

<sup>1</sup> DCS Computing GmbH, Linz, Austria

<sup>2</sup> University of Twente, Enschede, The Netherlands

**Abstract—** While the physical realism of simulation results is often the primary reason for selecting a specific modeling approach, the computational cost is also crucial. Recently, a comparison between multiple open-source software frameworks was published, applying each package to three predefined case studies. To extend that study and include commercial software, this work solves the same cases using Aspherix. The comparison includes the commonly used CPU version, as well as a GPU version currently under development. The benchmark results indicate that Aspherix is usually faster, and never slower, than its open-source predecessor.

**Keywords:** DEM; GPU; performance benchmark; bulk processes; parallelization;

## 1. Introduction

There is a wide range of Discrete Element Method (DEM) based software for modelling the dynamics of granular materials. Their commonality is that they all track the behavior of particles by iteratively solving the equations of motion via explicit time integration. During each time step all particles in contact are detected, after which the calculated interaction forces and torques are used to integrate their motion. Despite such similarities, there is a significant difference between their efficiency, usability and applicability. These are directly affected by aspects like: data structure selection, parallelization techniques, physical model availability, convenience of (graphical) user interfaces and documentation quality.

A recent benchmark study by Dosta et al. [1] compares the performance of nine widely-used DEM frameworks: BlazeDEMGPU, ESyS-Particle, GranOO, Kratos Multiphysics, LIGGGHTS, MercuryDPM, MFIX, MUSEN and YADE. Only open-source software packages were considered, since these are freely available and their underlying algorithms can be reviewed and tested. In addition to analyzing the simulation results, also the performance of the DEM software was compared.

In this work, Aspherix, a commercial DEM software package developed by DCS Computing, is applied to the same cases as Dosta et al. [1]. The comparison includes the commonly used CPU version, as well as a Graphics Processing Unit (GPU) version that is currently under development.

## 2. Aspherix characteristics

### 2.1. Software aspects

Aspherix is build on the foundations of LIGGGHTS [2], and can therefore be seen as its direct successor. Compared to LIGGGHTS it offers many improvements and bug fixes. First of all, there is a graphical user interface (GUI) with preview window which allows users to set up cases in a more convenient

way. As was common with LIGGGHTS, cases can also be set up via input scripts. Although Aspherix introduced a more natural input scripting language, it is still fully backward compatible with the LIGGGHTS scripts.

Aspherix provides an application programming interface (API) with Python bindings, which allows users to extend, control and access simulation data. Where both DEM packages allow coupling with fluids (CFD-DEM), Aspherix additionally supports a finite element coupling interface (DEM-FEM) with the Elmer package [3]. Simulation data is exported in the VTK file format and can be easily analyzed in ParaView using provided Python-based post-processing scripts.

Compared to LIGGGHTS, Aspherix supports several additional non-spherical particle shapes like convex, concave and fibers. There is also a wider selection of contact models, mesh modules, and physical models for heat transfer, electrical conductivity, and powder compaction. Finally, Aspherix Calibration can be used to adjust the model parameters to match the experimental data as closely as possible. Thanks to improvements like these, Aspherix is able to simulate more complex problems with physical realism.

### 2.2. Implementational aspects

Just as LIGGGHTS, both CPU and GPU versions of Aspherix are written in the C++ programming language. To decrease computational time, Aspherix has optimized its parallel algorithms more effectively than LIGGGHTS. This optimization is the primary reason why Aspherix outperforms LIGGGHTS in parallel simulations, as demonstrated here.

Both CPU and GPU versions use the Message Passing Interface (MPI) for parallelization on multinode systems with distributed memory. The GPU version is hardware agnostic, meaning that it can run on both CPU (serial and OpenMP) and GPU (CUDA and ROCm/HIP) platforms. This choice makes Aspherix performance portable: the same source code can be repurposed across several hardware generations / architectures without having to provide specific instructions for one hardware type versus another.

## 3. Case studies

The work of Dosta et al. [1] covered three common bulk processes: (i) emptying of a silo, (ii) mixing in a rotating drum and (iii) impact of a particle on a particle bed. In all three cases, the standard formulation of the visco-elastic Hertz-Mindlin model for dry contacts was used and only spherical particles were modelled. For a more detailed discussion on the case setups, please see the work of Dosta et al. [1]. All benchmark cases were run on a personal computer equipped with one multi-core CPU and one GPU. Although not shown here, it was verified that all simulations produced consistent results.

### 3.1. Case study 1: silo emptying

This case simulates the discharge of particles from a cylindrical silo with varying orifice sizes, see Figure 1 (setup) and Figure 2 (benchmark results).

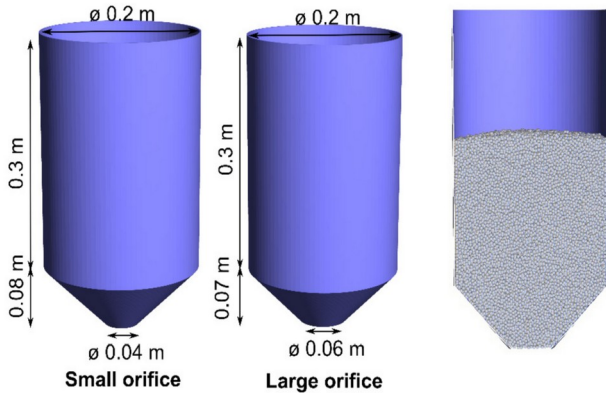


Figure 1. Case study 1: dimensions of silos with small (left) and large (centre) orifice, and a cross-cut of the silo at the initial state of the case study (right), copied from [1].

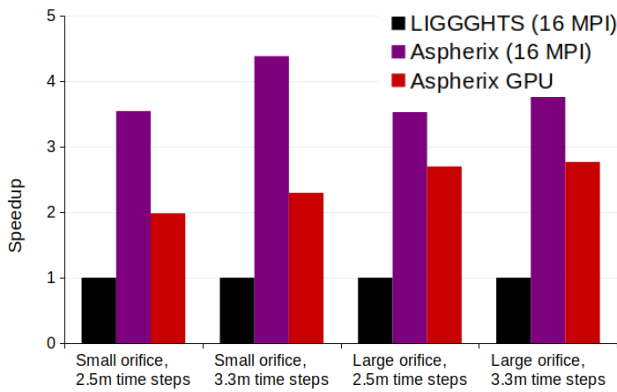


Figure 2. Case study 1: speed up of Aspherix CPU and Aspherix GPU compared to LIGGGHTS.

### 3.2. Case study 2: drum mixer

This case simulates the motion of two types of particles (M1 and M2) in a rotating drum mixer, see Figure 3 (setup) and Figure 4 (benchmark results).

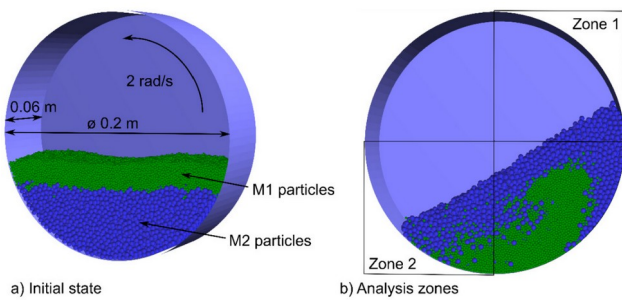


Figure 3. Case study 2: particle dynamics in a rotating drum. a) initial state; b) after 3 seconds of rotation., copied from [1].

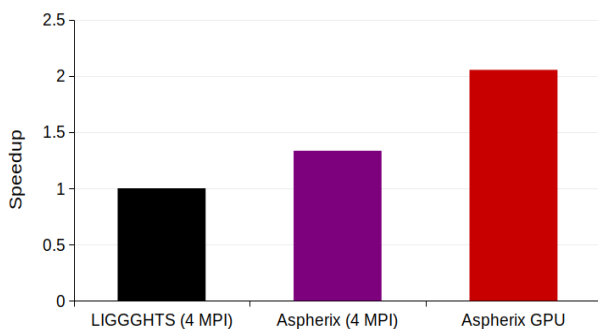


Figure 4. Case study 2: speed up of Aspherix CPU and Aspherix GPU compared to LIGGGHTS.

### 3.3. Case study 3: particle impact

This case models the impact and penetration of a steel particle with a diameter of 20 mm on a static bed, see Figure 5 (setup) and Figure 6 (benchmark results).

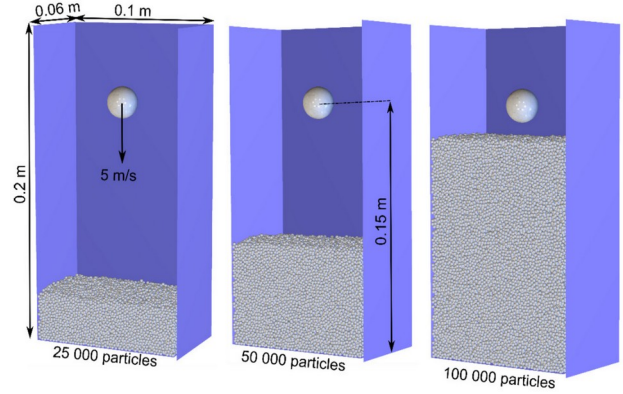


Figure 5. Case study 3: initial state of the impact test with a varied number of bed particles., copied from [1].

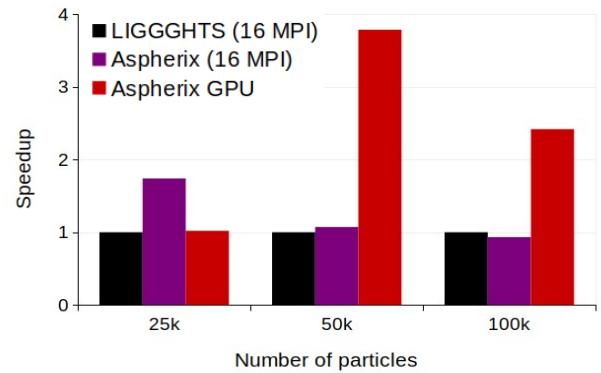


Figure 6. Case study 3: speed up of Aspherix CPU and Aspherix GPU compared to LIGGGHTS.

## 4. Discussion

The benchmark results indicate that Aspherix generally outperforms LIGGGHTS, though the speedup is problem dependent. Case study 1 shows a large speed up across all setups, while case study 3, with a high number of particles, shows no speed up. This effect is caused by the optimized parallel algorithms available in Aspherix, which are able to enhance the overall efficiency under specific circumstances.

The Aspherix GPU version, still under development, shows potential by outperforming the CPU version in certain scenarios, although it is not yet consistently superior. However, the GPU version has not been as extensively optimized as the CPU version, which has been under development for over a decade and utilized in numerous industrial setups.

## References

- [1] Dosta, M., D. Andre, V. Angelidakis, R.A. Caulk, M.A. Celigueta, B. Chareyre, J.-F. Dietiker, et al. "Comparing Open-Source DEM Frameworks for Simulations of Common Bulk Processes." *Computer Physics Communications* 296 (March 2024): 109066. <https://doi.org/10.1016/j.cpc.2023.109066>.
- [2] Christoph Kloss, Christoph Goniva, Alice Hager, Stefan Amberger, Stefan Pirker. "Models, algorithms and validation for opensource DEM and CFD-DEM." *Progress in Computational Fluid Dynamics, An Int. J.* 2012 - Vol. 12, No.2/3 pp. 140 - 152
- [3] M. Malinen and P. Råback, Elmer finite element solver for multiphysics and multiscale problems. In book: *Multiscale Modelling Methods for Applications in Material Science*, pages 101-113. Chapter: Elmer finite element solver for multiphysics and multiscale problems, Forschungszentrum Juelich, Editors: Ivan Kondov, Godehart Sutmann, 2013.

# A DEM-FEM coupling approach to model wheel loader bucket loading

Anita Ullrich<sup>1</sup>, Johannes Quist<sup>1</sup>, and Christoffer Cromvik<sup>1</sup>

<sup>1</sup> Fraunhofer-Chalmers Centre, Gothenburg, Sweden

**Abstract**— A coupling of the Discrete Element Method and the Finite Element Method is presented to demonstrate its value in wheel loader simulations, particularly focusing on the simulation of a wheel loader bucket loading granular material. This approach enables the evaluation of stresses on the bucket during loading, expanding the possibilities for assessing bucket designs. Different bucket filling strategies are compared based on key metrics, including the loaded material mass, the work done by the bucket, and the resultant stress responses within the bucket.

**Keywords:** DEM; FEM; wheel loader; bucket; coupling;

## 1. Introduction

In the past decade, simulations coupling Multi-Body Dynamics (MBD) with the Discrete Element Method (DEM) have been applied in the heavy machinery industry. With the DEM-MBD simulations, the interaction between machinery and soil or granular material can be analysed, such as in modelling wheel loader operations [1-3]. The coupled simulations accurately depict how machinery interacts with granular materials, thereby effectively capturing the impact on machine movement during operation. This enables trade-off analyses and optimisations for the wheel loader operations, as done by [2,3].

With the capability to model both machine-granular material interactions and the detailed behaviour of granular materials themselves, the next logical progression involves considering stresses and strains within machine components during operation. This can be accomplished, for example, through the application of the Finite Element Method (FEM). While a combined MBD-DEM-FEM approach for simulations poses computational challenges, we introduce a DEM-FEM coupling for heavy machinery, marking an initial step toward comprehensive MBD-DEM-FEM modelling.

## 2. Method

### 2.1. Numerical approach

The DEM-FEM surface coupling is based on the GPU-based state-of-art explicit solver Demify® for DEM and an in-house solver for FEM simulations. Both solvers have a C++ backend and provide a Python interface, which is accessed within the DEM-FEM coupling algorithm.

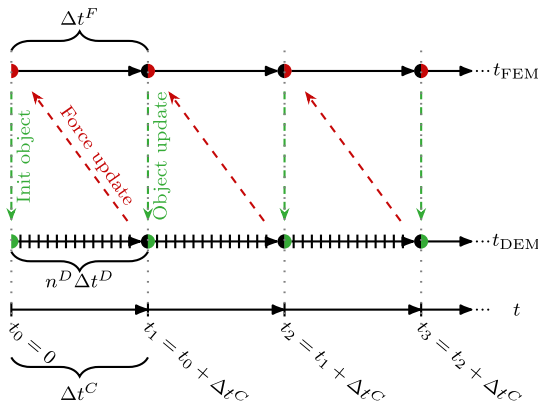


Figure 1. Schematic of the DEM-FEM coupling algorithm, modified from [4]. (figure caption)

A schematic for the coupling algorithm is depicted in Figure 1. At the beginning of the coupled simulation, the FEM object is initialised in the DEM domain for co-simulation to resolve the interaction with the particles. After some timesteps in the DEM simulation, the forces arising from the interaction between the bucket and the granular material are gathered from DEM and given as point load boundary conditions on the bucket in FEM. Then, after one timestep in FEM, the positions, velocities and accelerations of the FEM object nodes are applied as motion to the co-simulated bucket object in DEM.

For brevity, details of the implementations are omitted, and the interested reader is referred to [5] for DEM and [6] for FEM.

### 2.2. Simulation of wheel loader bucket loading

The bucket is modelled as a tetrahedral volume mesh in FEM, based on the design of a Volvo L180 bucket, with material properties corresponding to quenched and tempered steel. Boundary conditions for the bucket's motion are applied to a set of nodes at the typical positions of the attachment brackets.

In this study, five different load cases are considered and compared. The trajectories for these load cases, shown in Figure 2, follow the same rotational motion but vary in their starting positions. All motions simulate the action of loading rocks from a pile of granular material.

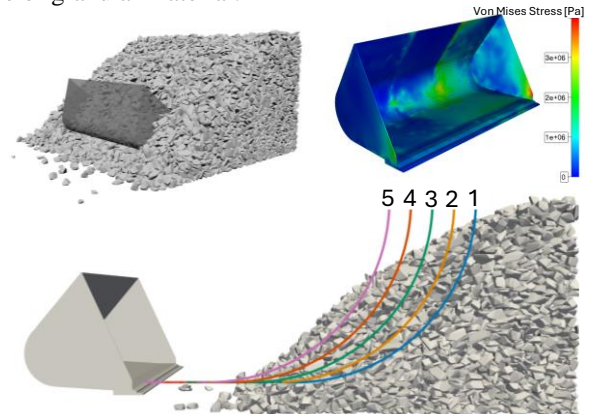


Figure 2. Illustration of the simulated particle pile (top left), the stresses on the bucket during a load operation (top right) and the bucket trajectories corresponding to the five load cases considered in this study (bottom). (figure caption)

The rocks are simulated as convex dilated polyhedral particles based on six scans from real rocks. The Hertz-Mindlin-Deresiewicz interaction model is used to resolve interactions both between the particles and between the particles and the bucket. The particle sizes are uniformly distributed between 90 and 150 mm, and the material properties of the rock particles correspond to those of granite.

## 3. Results

The five load cases are evaluated based on the loaded mass of rocks at the end of the motion, the total work done by the bucket, and the maximal von Mises stress on the bucket tip measured during the load operation. The work done by the bucket is calculated at each timestep as the product of the interaction forces and the distance travelled by the bucket. This work is accumulated over all timesteps to determine the total work done.

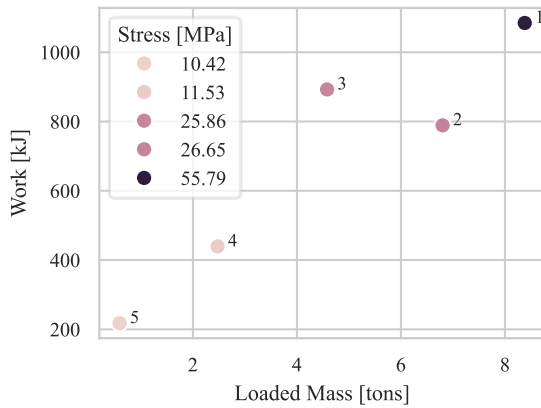


Figure 3. Evaluation of the 5 load cases (load case number indicated by label for each data point) with the total loaded mass on the x-axis, the total work done on the y-axis and the colour indicates the maximal measured von Mises stress on the bucket tip during the load scenario. (figure caption)

Figure 3 presents the results of these three metrics for each load case, with the loaded mass on the x-axis, the total work done on the y-axis, and the maximal von Mises stress on the bucket tip indicated by colour. The labels on the data points denote the load case number, according to Figure 2. The total mass ranges from 0.5 tons for load case 5 to 8.3 tons for load case 1, showing a linear increase correlated with the starting position of the motion. Similarly, the von Mises stress on the bucket tip increases correlated to the starting position. Further, the total work done increases as well from 200 kJ for load case 5 to 1080 kJ for load case 1. However, load case 3 is an outlier, as it shows a total work done of 900 kJ, which is higher than the 800 kJ for load case 2, despite load case 3 having a lower loaded mass than load case 2.

In Figure 4, the maximal von Mises stress from the bucket nodes on the tip over time is presented for the five load cases. The von Mises stress increases for all cases as soon as the bucket reaches the pile of granular material. Load case 1, being closest to the pile, shows the earliest increase and the highest stress response, followed by load cases 2, 3, 4, and 5, respectively. Load case 5 shows the latest and smallest stress response increase. Specifically, load case 1 peaks at 55 MPa, load case 2 at 26 MPa, load case 3 at 25 MPa, load case 4 at 11 MPa and load case 5 at 10 MPa. The maximal von Mises stress response tends to decrease as the starting position is farther from the pile. Interestingly, there is only a slight difference in the maximal stress response at the bucket tip between load cases 2 and 3, as well as between load cases 4 and 5. Additionally, load case 3 shows the highest stress response after 2.5 seconds, maintaining a stress level around 20 MPa until 5 seconds.

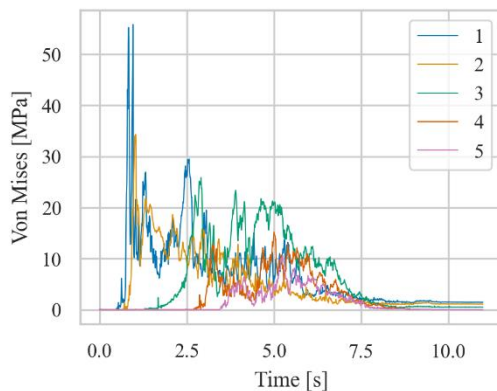


Figure 4. Maximal von Mises stress on the bucket tip over time for the 5 load cases from Figure 2. (figure caption)

## 4. Discussion

The observed increase in total mass loaded for starting positions closer to the pile aligns with expectations. This outcome is intuitive, as a shorter distance to the pile allows for more material collection, resulting in higher loaded.

An interesting result is the total work done by load case 3, which surpasses that of load case 2. This could partly be attributed to the simulation setup and the lack of statistical variance, as only a single specific pile and one simulation run were considered within the scope of this study. However, it might also be due to timing factors, where the bucket in load case 3 simultaneously starts a rotational motion as it begins to dig into the gravel pile. These two stress sources can contribute to the observed stress peak.

It is challenging to draw definitive conclusions from these specific results, since the DEM-FEM coupling, although generally verified and validated, still requires calibration and validation for the specific modelling of a wheel loader bucket. Therefore, the presented results should be viewed as a demonstration of the evaluation capabilities of DEM-FEM simulations for bucket operations rather than precise predictions.

The stress results from these simulations can be further utilised for fatigue analysis, which is an important aspect for optimising load operations and bucket design. Incorporating FEM in the analysis allows for a detailed examination of specific geometrical aspects of the bucket, particularly the stress on critical points such as welding joints. This enables more informed decisions in optimizing and conducting trade-off analyses between material loading capacity and bucket durability for different bucket designs and operational strategies.

## 5. Conclusion

This study demonstrates that the DEM-FEM coupling algorithm is effectively applicable for simulating the operations of a wheel loader bucket. By coupling DEM and FEM, this approach allows for a comprehensive analysis of the stress experienced by the bucket. The simulations account for various factors, including the bucket's geometries, material properties, and loading motions. This capability facilitates detailed evaluations that can inform the optimisation and design of wheel loader buckets, enhancing their performance and durability in practical applications.

## Acknowledgement

The authors gratefully acknowledge the Fraunhofer Gesellschaft Program for Affiliate Cooperation and Knowledge Transfer for their financial support of this research.

## References

- [1] Burger, M., Dreßler, K., Ekevid, T., Steidel, S., & Weber, D. (2017). Coupling a DEM material model to multibody construction equipment. *In Proceedings of the ECCOMAS Thematic Conference on Multibody Dynamics* (Vol. 2017, pp. 417-424).
- [2] Frank, B., Kleinert, J., & Filla, R. (2018). Optimal control of wheel loader actuators in gravel applications. *Automation in Construction*, 91, 1-14. doi: [10.1016/j.autcon.2018.03.005](https://doi.org/10.1016/j.autcon.2018.03.005)
- [3] Chen, G., Chang, R., Bai, J., Li, J., & Li, X. (2024). Shovel parameter sensitivity analysis and online optimization method for unmanned loaders. *Automation in Construction*, 157, 105149. doi: [10.1016/j.autcon.2023.105149](https://doi.org/10.1016/j.autcon.2023.105149)
- [4] Dratt, M., & Katterfeld, A. (2017). Coupling of FEM and DEM simulations to consider dynamic deformations under particle load. *Granular Matter*, 19(3), 49. doi: [10.1007/s10035-017-0728-3](https://doi.org/10.1007/s10035-017-0728-3)
- [5] Thornton, C. (2015). Granular dynamics, contact mechanics and particle system simulations. *A DEM study. Particle Technology Series*, 24.
- [6] Ottosen, N. S., & Petersson, H. (1991). Introduction to the finite element method. *TVSM*.



# An Investigation into Pneumatic Conveying Characteristics of Carbon Granules in Low Velocity Slug Flow

Chehan L.K.Y. Yapa Mudiyanse<sup>1</sup>, Atul Sharma<sup>1</sup>, and Michael S.A. Bradley<sup>1</sup>

<sup>1</sup> The Wolfson Centre for Bulk Solids Handling Technology, University of Greenwich, UK

**Abstract**— Low velocity slug flow is an important pneumatic conveying application due to its reduced particle degradation and pipeline wear. This study examines the low-velocity slug flow behaviour of two types of carbon granules (2-3mm and 3-8mm). Data was obtained from 30 conveying trials using an industry-scale pneumatic test rig at the Wolfson Centre in the University of Greenwich.

During the experiments, a transparent pipe section enabled the observation of flow patterns and the estimation of slug velocity through videography analysis. Particle size distribution analysis was conducted after each test run to assess degradation using particle size distribution data of the conveyed material, with samples obtained using a full-stream cross-cut sampler.

The analysis part focused on pressure drop across straight sections and bends, considering superficial air velocity, particle diameter(D50), solid loading ratio, and throughput. Videography-derived slug velocity was compared against predictions from the Legel and Schwedes (1984) equation to evaluate model accuracy. Additionally, the study also examined trends in particle degradation and their impact on pipeline pressure drop. Experimental data was used to evaluate the predictions of existing low-velocity slug flow models developed by Kofu and Ochi (2008), Mi and Wypych (1994), and Pan and Wypych (1997). It was concluded that Kofu and Ochi's model aligns relatively better with experimental data, although none of the models' predictions are sufficiently reliable for real-world applications.

**Keywords:** low velocity slug flow; pressure drop models;

## 1. Introduction

Pneumatic conveying can be categorised into two modes: dilute and dense phase. Dense phase conveying uses lower velocities, resulting in reduced particle degradation, less pipeline wear, and lower energy consumption compared to dilute phase. Low Velocity Slug Flow (LVSF), a subcategory of dense phase, is widely used to convey materials[1]. Hence, several researchers have made attempts to develop a reliable model to predict pressure drop and slug velocity in LVSF.

In this study, conveying data were obtained with two types of carbon granules having particle size ranges of 2-3mm and 3-8mm respectively. Conveying data including air mass flow rate, throughput, slug velocity and the pressure drop along the pipeline were analysed. Between each test, particle size distribution was also analysed to evaluate the effect of particle degradation towards the pressure drop and slug velocity. Data obtained from 30 conveying trials were used to evaluate LVSF models developed by Legel and Schwedes (1984) for predicting slug velocity, and pressure drop models developed by Kofu and Ochi (2008), Mi and Wypych (1994), and Pan and Wypych (1997)[2-4]. At the latter part of this study, the obtained data were analysed comparing the correlation coefficients and mean percentage errors.

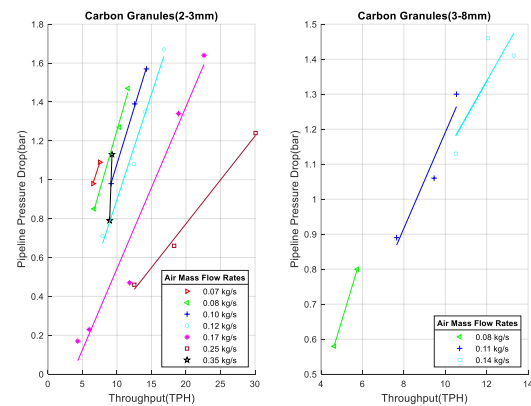


Figure 1. Conveying data of carbon granules 2-3 mm (left) and 3-8 mm (right)

## 2. Experimental Setup

### 2.1. Test Rig

The pneumatic conveying test rig consisted of a receiver hopper and a 1.5 m<sup>3</sup> blow tank, connected to a 120 m long, 4-inch pipeline containing three long-radius test bends and four straight sections. A transparent pipe section is utilised in the fourth straight section to measure slug velocity through videography analysis. Additionally, the test rig was equipped with a nozzle bank to control the air mass flow rate and 46 pressure transducers distributed throughout the straight sections to measure pressure drop. The solid mass flow rate was adjusted by varying the blow tank air ratio.

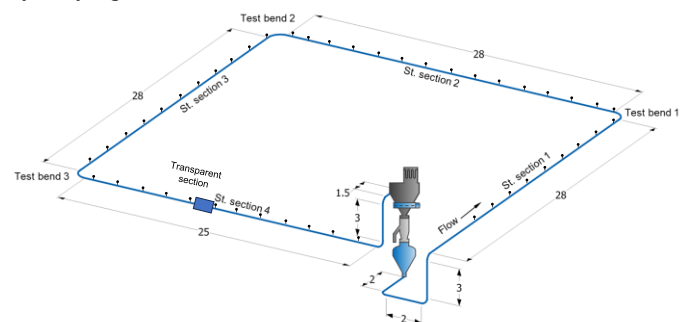


Figure 2. Pneumatic conveying test rig at the Wolfson Centre (all dimensions are in meters)

### 2.2. Particle Size Analysis

To evaluate particle degradation between trials, carbon granule samples were collected using the full-stream crosscut sampler installed between the receiver hopper and the blow tank. These samples were subsequently subjected to particle size distribution (PSD) analysis.

### 2.3. Videography analysis

Slug velocity was determined using a 136 cm long transparent pipe section through videography analysis. Videos were recorded at 60 FPS.



Figure 3. Transparent pipe section in the test loop

### 3. Results and Discussion

Using the data from the conveying trials, the average slug velocity from each trial was initially compared with the slug velocity calculated using the Legel and Schwedes equation. Subsequently, the average pressure drop observed at the fourth straight section during steady-state flow was compared against the pressure drop models by Kofu and Ochi (2008), Mi and Wypych (1994), and Pan and Wypych (1997).

#### 3.1. Results

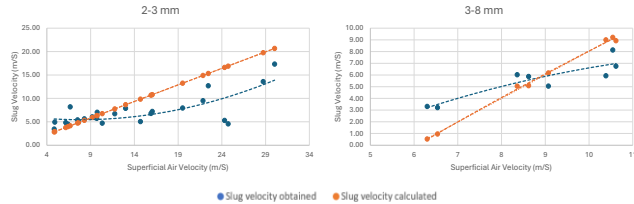


Figure 4. Experimental pipeline pressure drop data compared to predictions from the Legel and Schwedes model

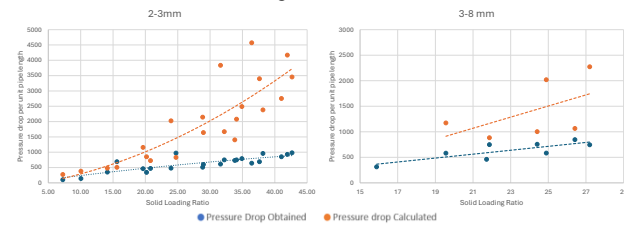


Figure 5. Experimental pipeline pressure drop data compared to predictions from the Mi and Wypych model

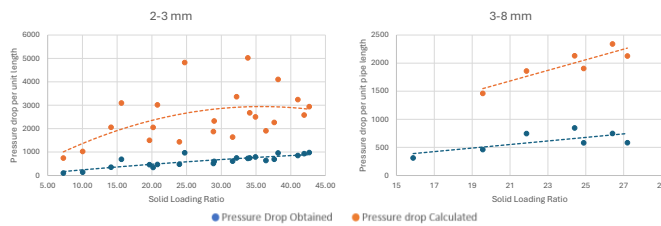


Figure 6. Experimental pipeline pressure drop data compared to predictions from the Pan and Wypych model

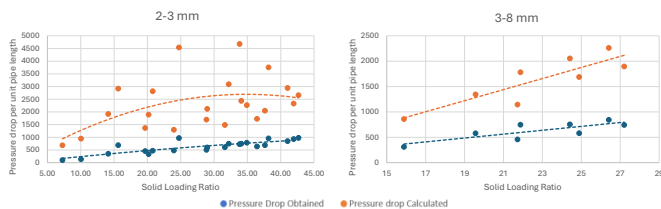


Figure 7. Experimental pipeline pressure drop data compared to predictions from the Kofu and Ochi model

#### 3.2. Discussion

The correlation coefficients and mean percentage errors derived from the experimental data and model predictions are presented in the Table 1.

TABLE I. CORRELATION COEFFICIENTS AND MEAN ERRORS

Comparison	Correlation Coefficient		Mean Percentage Error	
	2-3 mm	3-8 mm	2-3 mm	3-8 mm
Experimental vs predicted pressure drop using Legel and Schwedes equation	+0.71	+0.90	47.9%	37.9%
Experimental vs predicted pressure drop using Mi and Wypych equation	+0.56	-0.32	214%	105%
Experimental vs predicted pressure drop using Pan and Wypych equation	+0.73	+0.82	357%	179%
Experimental vs predicted pressure drop using Kofu and Ochi equation	+0.72	+0.97	321%	160%

The results clearly indicate that the calculations with Legel and Schwedes equation correlate well with the actual slug velocities obtained. Further, the experiments revealed that the equation can accurately predict velocity when the particles are larger.

Regarding the pipeline pressure drop predictions related to LFSF of carbon granules, the Mi and Wypych equation exhibits the lowest correlation coefficients and mean percentage errors, with predictions being more accurate at lower solid loading ratios. It was also noted that the Pan and Wypych equation shows better correlation, but lower accuracy compared to the Mi and Wypych equation. Additionally, both equations failed to provide accurate pressure drop predictions at low solid loading ratios for 3-8mm carbon granules conveying. Consequently, these data points were excluded when calculating the correlations.

Despite the considerable error, the Kofu and Ochi equation with its highest correlation coefficients, emerged as the most reliable among the three equations considered in this study. For smaller particle sizes (i.e., 2-3mm), the pressure drop prediction correlations closely resemble those of the Pan and Wypych equation. However, for larger carbon granule particles, the pressure drop predictions correlates better with the actual data.

None of the pressure drop prediction equations demonstrated both high correlation and low mean percentage error. All predictions exhibited at least a 105% error. However, it was evident that all predictive models showed higher accuracy when dealing with LVSF conveying of larger particles.

### 4. Conclusion

The main conclusions of this study are as follows:

- I. Legel and Schwedes slug velocity predictions are in a good agreement with the actual data.
- II. The Kofu and Ochi equation exhibits the highest correlation coefficient with the actual pressure drop data.
- III. The Mi and Wypych equation has the lowest correlation coefficient but also the lowest mean percentage error.
- IV. None of the predictive models in this study are not adequately reliable. But they can be used to predict the behaviour when the material properties such particle diameter, internal friction coefficient and wall friction coefficient are altered.

### Acknowledgement

The authors express their sincere appreciation to BASF SE, Germany, for their generous funding and provision of test materials, which made this study possible and to the technical support from the entire team at The Wolfson Centre for Bulk Solids Handling Technology, University of Greenwich.

### References

- [1] P. W. Wypych, D. B. Hastie, and J. Yi, "Low-Velocity Pneumatic Conveying Technology for Plastic Pellets," 2001.
- [2] B. Mi and P. W. Wypych, "Pressure drop prediction in low-velocity pneumatic conveying," 1994.
- [3] K. KOFU, M. OCHI, and M. TAKEI, "Derivation of Predicted Pressure Drop Equation on Granular Particle Plug Transportation in Horizontal Pipe," *Journal of Fluid Science and Technology*, vol. 3, no. 1, pp. 104–115, 2008, doi: 10.1299/jfst.3.104.
- [4] R. Pan and P. W. Wypych, "POWDER TECHNOLOGY Pressure drop and slug velocity in low-velocity pneumatic conveying of bulk solids," 1997.

# Simulating particle-structure interaction with *MercuryDPM*

Anthony R Thornton<sup>1,2</sup>, Jan-Willem Bisschop<sup>2</sup>, Luca Orefice<sup>2</sup>, Thomas Scrase<sup>2</sup> and Thomas Weinhart<sup>1,2</sup>

<sup>1</sup> University of Twente, Enschede, Netherlands

<sup>2</sup> MercuryLab BV, Enschede, The Netherlands

**Abstract** — Conveying and handling particulate materials involve the interaction of many particles with machinery. These machines can present complicated shapes and surfaces, such as screw feeders and vibrating screens. Moreover, packing granular materials, such as filling heterogeneous products into bags or pouches, can be a non-trivial process. In each of these operations, machinery and containers can bend under loading, warp due to heat, and eventually be worn down by the interaction with abrasive particles. All this can adversely affect the operations and potentially lead to failure.

While numerical models are valuable for troubleshooting and optimising these processes, such problems are hard to capture. The reason is that different modelling techniques are needed to simulate the different entities. Here we present how the open-source tools *MercuryDPM* (particle simulations, such as DEM and SPH) and *oomph-lib* (FEM) can be coupled to recreate all of these effects.

In this paper we show how *MercuryDPM* can replicate many of these processes efficiently and accurately: Firstly, complex geometries such as screw conveyors, secondly, the wearing down of machinery components leading to deformation and compromised efficiency. Finally, coupling *MercuryDPM* with *oomph-lib* allows the simulation of interaction with elastic bodies e.g. bags and pouches. We will explain how to successfully and realistically model such widespread industrial operations with *MercuryDPM*. Illustrative examples will include modelling screw conveying of cohesive powders, packaging of heterogeneous powders, and abrasion and wear of a vibrating screen.

**Keywords:** Open-source, virtual prototypes, simulation

## 1. Introduction

Particulate materials are extensively conveyed and handled across various industries, among which we usually find construction, pharmaceutical and food industries. In the construction industry sand and gravel are crushed to create concrete and asphalt. In the pharmaceutical industry, precisely dosed and mixed powders with very different properties are combined into blends and compacted into tablets. The food industry sees many ingredients in particulate form mixed and packaged, such as pasta sauces and instant soups. The chemical industry also handles huge amounts of particular materials. Finally, the mining industry has to convey and process ores to extract the valuable components. Thus, understanding how to convey and handle particulates is essential for optimising efficiency and quality in many industries.

The main problem is that each of these particulates is completely different, varying in size, shape, cohesion, friction etc. Therefore it is complicated to create one-size-fits-all solutions and often a lot of trial-and-error is required to get a known process working for a new material. Due to this variability of materials, and the time-consuming nature of

trial-and-error experiments, computer simulations and virtual prototyping are an attractive alternative.

## 2. Introduction to *MercuryDPM* and *Moomph*

Currently, the problem of simulating conveying and handling in the industry is even more difficult as the machines are often complex in shape, can be moving and vibrating or even flexible or wearable. Here we present *MercuryDPM*: An open-source code dealing with all of these many aspects.

*MercuryDPM* [1,2,3] uses the discrete particle method (DPM, a.k.a. discrete element method - DEM) to simulate the motion and interaction of discrete grains. It has been successfully used to understand and predict many granular processes. However, solving complex interactions with flexible structures requires the coupling of *MercuryDPM* with a structural FEM solver. *Moomph* was created to solve this complex particle-structure interaction problem.

*Moomph* [4] is a general framework for modelling multiscale/multiphysics processes. It combines two powerful open-source packages, *MercuryDPM* for discrete particle simulations and *oomph-lib* [5] for solving continuum equations, into one, easy-to-use coupled solver. Both codes are integrated into a single executable, allowing efficient data transfer. The software utilises one of the core features of *MercuryDPM*, coarse-graining, to improve the coupling accuracy and its flexibility. It is also directly installable from within the *MercuryDPM* build system.

We will now demonstrate this powerful open-source code using three industrial relevant problems: (i) screw conveying, (ii) powder packing and (iii) wear of a vibrating screen.

## 3. Screw conveying: Complex geometries in *MercuryDPM*

*MercuryDPM* can deal with contact detection with arbitrarily curved surfaces. This is highly advantageous for modelling complex industrial machinery such as screw conveyors as it is both more accurate and faster than using a triangulated STL-style geometry. Triangulated walls can introduce numerical artefacts from particles colliding with the vertices of the triangles, and to improve the accuracy a finer triangular mesh is needed. This increases the number of triangular vertices, thus increasing the number of objects with which particles can interact, leading to more potential interactions to be checked and a lower computational efficiency.

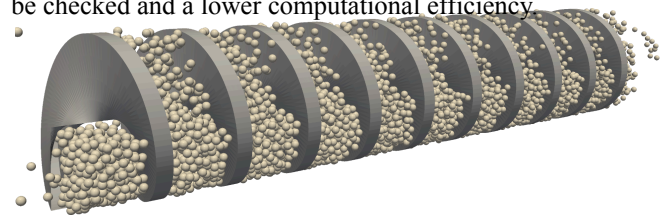


Fig. 1: A shaft-less single-flight auger screw.



The geometry shown in Figure 1 is obtained in *MercuryDPM* with a single wall, meaning that for each particle there is only a single surface to check for possible contact. The normal vector to particle-surface collisions is a function of the particle position, meaning all force directions are computed exactly.

There are many different types of complex walls in *MercuryDPM* and we refer the interested reader to the discussion in [2]. The screw wall shown in Figure 1 can be recreated via the driver *Demos/ScrewDemo.cpp*.

#### 4. Powder packing: Particle-structure interaction in *Moomph*

As stated in section 1, to solve more complex problems *MercuryDPM* is now directly coupled with *oomph-lib*: The *Moomph* project. The coupling can be directly enabled from the *MercuryDPM* framework simply by selecting the build option ‘*MercuryDPM\_OOMPH\_COUPLING*’ to ‘ON’. The code will then automatically download *oomph-lib* and on the next build step will build in *Moomph* mode. This is a very direct coupling, that is, it is built as a single code; there is no data transfer at run-time resulting in a very efficient code.

There are three types of coupling available via the *Moomph* framework. Using surface-coupling the user can model the interaction of the granular material with soft geometries [2,4]. With volume-coupling one can model parts of the granular material with a continuum model, while other parts are resolved with the discrete particle model, allowing for efficient but accurate simulations of large amounts of granular materials [2,4]. Finally, using particle-fluid-thermal coupling, one can model the interaction with a background fluid or with a thermal field [2]. Here we focus on surface-coupling and show a process of filling an elastic pouch/bag, an important application in many industries.

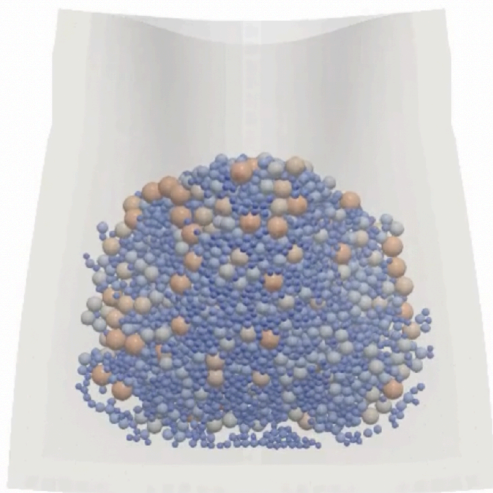


Fig. 2: A granular material poured into an elastic bag.

Figure 2 shows a screenshot of granular material inside an elastic bag after it was poured from an inlet and let settle under gravity. In this simulation, the bag was squeezed from the sides to let it open and was closed after the material was inserted. This is a two-way coupled simulation where the granular material affects the bag and vice-versa. Depending on the material properties of the particles and the bag, the pouch either folds and closes around the material or the material is pushed out and the bag cannot close. The pouch in Figure 2

and the opening process by side squeezing can be demonstrated via the driver *Oomph/SCoupling/SolidBag.cpp*.

#### 5. Wear of a vibrating screen: Wearable surface in *MercuryDPM*

*MercuryDPM* also contains the Reye–Archard–Khrushchov wear model [6], stating that the volume of material removed from a surface due to wear is proportional to the work done by the friction forces exerted by the material impacting the surfaces. The proportionality is usually set to higher values than for the real material to accelerate the process and reduce the simulation time.

Currently, this model can only be applied to *MercuryDPM*'s triangulated walls, but it will be extended to all types of walls including coupled *oomph-lib* elastic walls.

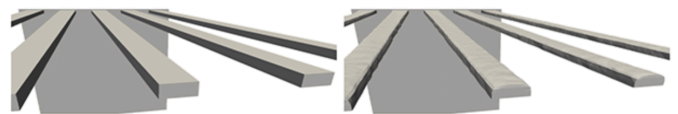


Fig. 3: A vibrating screen before (left) and after (right) particle flow of an abrasive granular material.

Figure 3 shows a vibrating screen before and after an abrasive granular flow has passed through it, where the rounding of the bars due to abrasion is clearly visible. This is a key problem in various industries as it can lead to a change in the particle sizes that pass through the screen. A similar wear pattern as shown in Figure 3 and the feature can be demonstrated via the driver *Demos/TriangulatedSurfaceWearDemo.cpp*.

#### 6. Code availability

Both *MercuryDPM* ([mercurydpm.org](http://mercurydpm.org)) and *oomph-lib* ([oomph-lib.org](http://oomph-lib.org)) are fully open-source and free to use.

#### 7. Conclusion

Simulating industrial particulate handling and conveying is a complex problem. Here we have shown a few industrially relevant case studies modelled with the open-source framework of *MercuryDPM* and *Moomph*. Both *MercuryDPM* and *Moomph* are often applied to many industrial problems via the official support company *MercuryLab* ([mercurylab.org](http://mercurylab.org)).

#### References

- [1] *MercuryDPM* website: [mercurydpm.org](http://mercurydpm.org).
- [2] A. R. Thornton, T. Plath, I. Ostanin, H. Götz, J. Bisschop, M. H. Hassan, R. Roeplal, X. Wang, S. Pourandi, T. Weinhart, *Recent Advances in MercuryDPM, Mathematics in Computer Science* **17:13** (2023).
- [3] T. Weinhart, L. Orefice, M. Post, M. P. van Schrojenstein Lantman, I.F.C. Denissen, D.R. Tunuguntla, J.M.F. Tsang, H. Cheng, M.H. Shaheen, H. Shi, P. Rapino, E. Grannonio, N. Losacco, J. Barbosa, L. Jing, J.E. Alvarez Naranjo, S. Roy, W. den Otter, A.R. Thornton, *Fast, flexible particle simulations — An introduction to MercuryDPM, Computer Physics Communications* **107129** (2019).
- [4] H. Cheng, A.R. Thornton, S. Luding, A.L. Hazel, T. Weinhart, *Concurrent multi-scale modeling of granular materials: Role of coarse-graining in FEM-DEM coupling, CMAME* **403:115651** (2023).
- [5] M. Heil, A.L. Hazel, *oomph-lib – An Object-Oriented Multi-Physics Finite-Element Library*. In: Bungartz, HJ., Schäfer, M. (eds) *Fluid-Structure Interaction. Lecture Notes in Computational Science and Engineering*, vol. 53. Springer, Berlin, Heidelberg (2006).
- [6] J.F. Archard, *Contact and rubbing of flat surfaces, Journal of Applied Physics* **24:981** (1953).



# On the Difference in Pneumatic Conveying Properties of the Same Product from Different Manufacturers; a Case Study Based on Quicklime

Atul Sharma, Michael S A Bradley, and Baldeep Kaur

The Wolfson Centre for Bulk Solids Handling Technology, University of Greenwich, Chatham, Kent, UK

**Abstract**— Quicklime plays a crucial role in infrastructure projects such as soil stabilisation, modifying soil properties and optimising moisture content. It is often handled pneumatically due to its hazardous nature and reactivity. However, the design of pneumatic conveying systems must carefully consider the specific conveying characteristics of the bulk material. These characteristics can be obtained by undertaking conveying trials in a laboratory. Experience has shown that industrial systems designed for a specific grade of a material may experience unreliable performance when handling material of nominally the same specification, obtained from different sources. This occurs due to variations in the material's conveying characteristics, leading to challenges such as low throughput, pipeline blockage, particle degradation.

Conveying trials were undertaken using an industrial-scale pneumatic conveying test rig that has 120 metre long, 100 mm NB (nominal bore) pipeline. Five grades of quicklime were tested, showing that each grade exhibits a different conveying behaviour.

When the conveying data was applied to design an industrial conveying system, it was observed that for the same airflow and pipeline pressure drop, throughput for different grades varies from +19% to -15% as compared to the benchmark grade. This study demonstrates the importance of testing the material in the conveying test pipeline and obtaining the conveying characteristics in determining key design parameters for reliable pneumatic conveying systems.

**Keywords:** pneumatic conveying characteristics; pressure drop; blow tank

## 1. Introduction

An accurate prediction of the pressure drop in the pneumatic conveying pipelines is a key factor to design efficient and reliable conveying systems [1]. Inaccurate prediction of the system pressure drop can lead to issues like pipeline blockages and reduced throughput [2]. Most conveying systems are designed based on the designer's previous experience or by using conveying data which is also known as conveying characteristics. If this data is not available, it can be generated by undertaking conveying trials on a sample of the product to be handled [3, 4]. Different materials behave differently in the conveying pipeline, resulting in distinct conveying characteristics unique to each material [5]. It is interesting to note that the conveying characteristics of the materials sourced from the different suppliers can have very different conveying characteristics that can influence the system performance.

This study aims to compare the conveying performance of five quicklime grades obtained from different suppliers when transported through a system designed for a specific quicklime grade.

## 2. Test Setup and Materials

The main test programme was performed using a bottom discharge blow tank, in conjunction with a pipeline of 100 mm

NB schedule-40 pipe, with a total run of 120 m, incorporating 8 bends and a vertical section of 6 m. The test pipeline was instrumented to gather data on pressure drops in straight sections and bends, overall pressure drop, and flow rates of solids and air. Details of the test rig are shown in the Fig. 1.

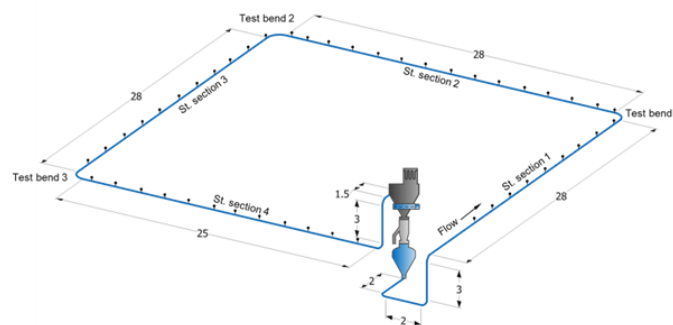


Figure 1. Layout of the 120 m long test pipeline

Five grades of quicklime were tested in the test program. These five grades were taken from five different sources, having similar particle size distribution and same chemical composition.

## 3. Experimental Programme

Conveying trials were undertaken on five grades of quicklime at three different air flow rates: 0.30, 0.32, and 0.35 kg/s. A minimum of 12 conveying trials were conducted for each grade to achieve a wide range of dilute phase conveying conditions, with inlet air velocities from 9 to 15.5 m/s, conveying pressures up to 2.4 barg, and throughputs up to 32 tonnes per hour. A desiccant dryer, installed immediately downstream of the compressed air supply, was employed to supply the dry air (nominally -40°C dew point) to avoid the build-up of lime inside the pipelines during testing.

## 4. Experimental Results and Discussion

Fig. 2 illustrates a comparison of the pressure drop and throughput achieved for the five grades of quicklime conveyed under 0.3 kg/s airflow in the test pipeline.

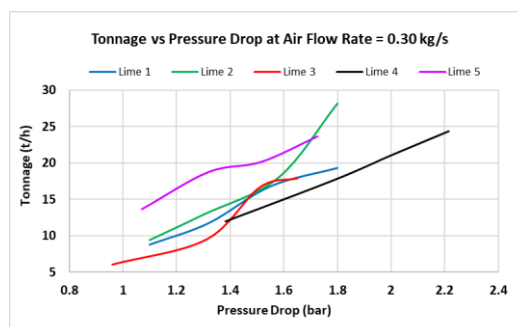


Figure 2. Tonnage vs pressure drop for lime grades in the test pipeline at an airflow of 0.30 kg/s

It can be seen that, with the same pressure drop and air flow rate, each grade yields a different tonnage in the test pipeline. This highlights how different grades of the same material can affect the system performance.

From an industrial installation perspective where the material may change or sourced from different suppliers, it is important to adjust the total airflow and operating pressure when switching between lime grades. Some quicklime grades yield the desired tonnage at a given airflow and pressure drop, however, handling a different grade in the same system will give a lower tonnage at the same operating conditions. To achieve the required duty, introducing more material in the conveying pipeline can lead to a higher pressure drop, reducing the conveying velocity and resulting in pipeline blockage.

Fig. 3 shows the effect of the blow tank air percentage on the tonnage for an airflow of 0.30 kg/s across different grades of lime.

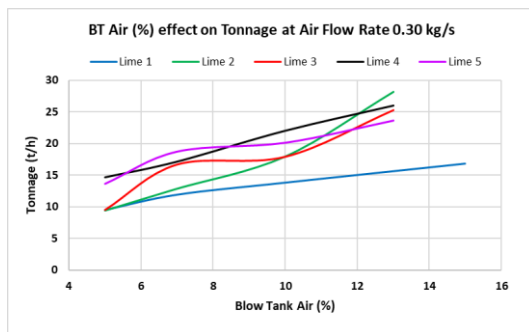


Figure 3. Tonnage vs blow tank air ratio for lime grades in the test pipeline at an airflow of 0.30 kg/s

It can be seen that each lime grade responds uniquely to blow tank air ratios and yield different tonnages in the test pipeline. This clearly shows that the materials with similar physical and chemical characteristics may respond differently to the blow tank air, thereby affecting the system performance.

This highlights the importance of adjusting blow tank air distribution when switching between lime grades in an industrial installation. Some quicklime grades demonstrate positive responsiveness to a given blow tank air ratio, potentially leading to higher tonnage. However, overfeeding of the material could lead to higher pressure drop, ultimately reducing conveying velocity and causing blockages in the pipeline.

The conveying characteristics of the five lime grades in terms of the bend and straight pipe loss coefficients in the test loop are shown in the Figures 4 and 5.

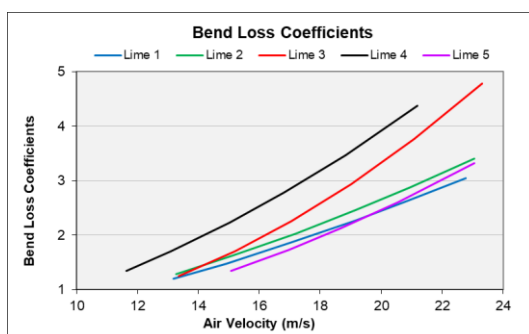


Figure 4. Bend loss coefficients as a function of air velocity

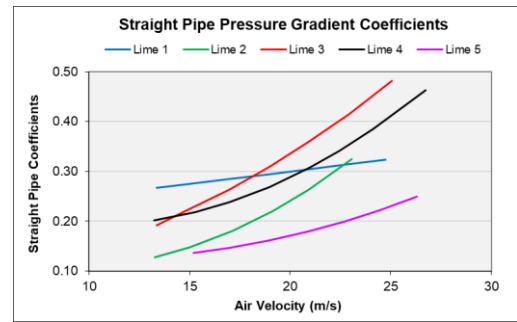


Figure 5. Straight pipe loss coefficients as a function of air velocity

It can be seen from the Figures 5 and 6 that all the lime grades exhibit different conveying characteristics for straight and bend pressure loss, which means that their throughput will vary if handled in the same system under identical operating conditions.

Conveying characteristics of the Lime 1 was used to design an industrial system. Figure 6 illustrates the effect of lime grade on throughput performance of the system at constant airflow and pressure drop for all five lime grades.

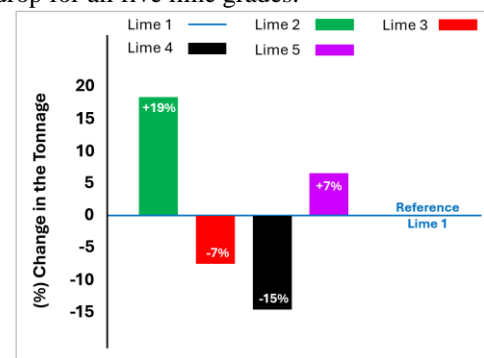


Figure 6. Comparison of system performance for different lime grades

It can be seen that Lime 2 performs the best, giving 19% more tonnage, whereas Lime 4 performance is worst, with 15% reduction in the tonnage compared to the reference Lime 1.

## 5. Conclusion

There are many conveying systems in the field that suffers from the poor performance that occur due to a change in the grade of the handled product. The result of this study highlights the need for undertaking conveying trials to determine the unique conveying characteristics of the various grades of the same product which serve as the foundation for a robust and efficient system design.

## Acknowledgement

The authors express their sincere appreciation to Hargreaves Industrial Services, Barnsley, UK for their generous funding and provision of test materials, which made this study possible.

## References

- [1] M. S. A. Bradley, "Prediction of pressure losses in pneumatic conveying pipelines," Thames Polytechnic, 1990.
- [2] G. Setia, S. S. Mallick, and P. W. Wypych, "On improving solid friction factor modeling for fluidized dense-phase pneumatic conveying systems," *Powder Technol.*, vol. 257, pp. 88–103, May 2014.
- [3] M. S. A. Bradley, L. M. Hyder, R. J. Famish, and A. R. Reed, "Latest development of the direct technique for measurement of the pneumatic conveying characteristics of bulk materials," in *Handbook of Powder Technology*, Elsevier, 2001, pp. 319–328.
- [4] C. R. Woodcock and J. S. Mason, *Bulk solids handling: an introduction to the practice and technology*. Springer Science & Business Media, 2012.
- [5] D. Mills, *Pneumatic Conveying Design Guide*. 2016.

# Influence of non-isothermal sorption processes on evaporation of acoustically levitated slurry droplet

A. Levy<sup>1</sup>, Y. David Pour<sup>1</sup>, B. Krasovitev<sup>1</sup>, A. Fominykh<sup>1</sup>

<sup>1</sup> Ben-Gurion University of the Negev, Beer-Sheva, Israel

**Abstract**— In this study, we developed a convective heat and mass transfer model of an acoustically levitated slurry droplet with a definite initial volume fraction of the solid phase that evaporates in an atmosphere of air, water vapor, and soluble gas. The advanced model considered the effects of acoustic streaming, forced convection, non-isothermal gas absorption, and adsorption on the evaporation rate of a liquid droplet containing small active solid particles. The model integrates the theory of heat and mass transfer during slurry droplet evaporation with a gas absorption/adsorption model. The problem was solved numerically using the d03ph function of the NAG Toolbox for MATLAB. Adsorption of dissolved in a droplet soluble gas leads to decreased dissolved gas concentration in a liquid droplet. A reduction in dissolved gas concentration in a liquid droplet causes an increase in the mass flux of active soluble gas from a gaseous phase to a slurry droplet, which causes a rise in the heating effect of absorption and an increase in evaporation rate of a droplet. The heat effect of adsorption also intensifies the evaporation rate. It is shown that the time of porous shell formation is essentially shorter when solid particles in slurry droplets are active compared to inert particles. Also, we found that the time of porous shell formation decreases with the increased sound pressure amplitude and increases with the increased frequency of the applied acoustic field. This proposed model serves as a basis for alternative drying technologies.

**Keywords:** slurry droplet; acoustic levitation; gas adsorption; gas absorption; evaporation.

## 1. Introduction

The present investigation is a continuation of a cycle of our works devoted to analyzing the influence of active soluble gases on the rate of slurry droplets drying. In the present work, we consider the adsorption of dissolved in liquid soluble gas by porous solid particles. In a previous work [1], solid particles were assumed to be inert, but in the present work, we analyze particle activity's influence on the slurry droplet drying rate. The present work is restricted by studying the process during the first drying stage, which starts when a slurry droplet enters a drying chamber. The gas adsorption mechanism influencing the slurry droplet drying rate is the following: Adsorption of dissolved in droplet soluble gas by solid particles leads to decreased dissolved gas concentration in a liquid droplet. A reduction in dissolved gas concentration in a liquid droplet causes an increase in the mass flux of active soluble gas from a gaseous phase to a slurry droplet, which causes a rise in the heating effect of absorption and an increase in interfacial temperature of a droplet. The rise of a droplet's interfacial temperature increases the droplet evaporation rate. The heat effect of adsorption also intensifies the evaporation rate. The main disadvantage of all slurry droplet drying study methods is a disturbance of the evaporation process by the measuring setup. This disadvantage

can be overcome by comparing the results of experiments with the results of mathematical modeling. Acoustic levitation is an effective tool for studying the drying process of a slurry droplet because the difficulties of modeling the acoustic streaming around the levitated droplet have mainly been overcome (see, e.g. [2]).

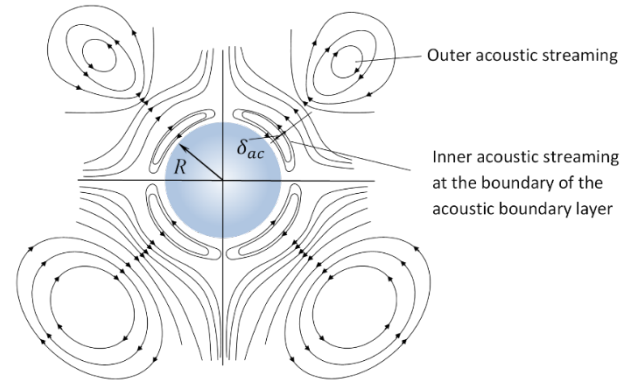


Figure 1. Acoustic streaming field around a small spherical droplet.

## 2. Model description

Consider a single acoustically levitated spherical droplet with an initial radius of  $R_0$  at an initial temperature of  $T_0$ , containing active solid particles with an initial volume fraction of the solid phase  $\Phi_{s0}$ . The surrounding gas mixture contains soluble gas. This study investigated the drying of acoustically levitated slurry droplets accompanied by gas absorption at or near room temperature. Gas absorption is accompanied by heat release at an interphase of a droplet. Gas, dissolved in liquid, is adsorbed by porous solid particles [3]. The heat effect of adsorption accompanies the process of adsorption. Diffusion of dissolved in liquid active gas, adsorbed by solid particles, can be described by transient diffusion equation in the spherical coordinates with a sink term:

$$\frac{\partial w_A^{(L)}}{\partial t} = \frac{1}{r^2} \frac{\partial}{\partial r} \left( r^2 \frac{D_A^{(L)}}{(1 - w_A^{(L)})} \frac{\partial w_A^{(L)}}{\partial r} \right) - \Lambda_c w_A^{(L)}.$$

Similarly, heat transfer in the same domain  $0 \leq r \leq R(t)$  is described by a transient heat transfer equation with a source term:

$$\frac{\partial T}{\partial t} = \frac{1}{(\rho c_p)_d r^2} \frac{\partial}{\partial r} \left( k_d r^2 \frac{\partial T}{\partial r} \right) + \Lambda_T T,$$

where  $w_A^{(L)}$  mass fraction of dissolved absorbate in a liquid phase,  $T$  is the temperature,  $k_d$  is the effective thermal conductivity of a droplet containing solid particles,  $D_A^{(L)}$  – coefficient of diffusion of dissolved gas in a liquid droplet,  $c_p$  –

specific heat capacity at constant pressure,  $r$  - radial coordinate,  $t$  - time. The formula for the scavenging coefficient  $\Lambda_C$  is as follows [4]

$$\Lambda_C = \frac{m\phi_s \tau_D^{-1} \exp\left(-\frac{(1+m\phi_s) \cdot t}{\tau_D}\right)}{1 - \frac{m\phi_s}{1+m\phi_s} \left[1 - \exp\left(-\frac{(1+m\phi_s) \cdot t}{\tau_D}\right)\right]}$$

where  $\Lambda_C = -w_A^{(L)-1} \cdot \partial w_A^{(L)} / \partial t$ ,  $\tau_D = (a \cdot m) / (3K_L)$ ,  $K_L = D_A^{(L)} / a$ ,  $m$  - Henry's law constant of adsorption,  $K_L$  - mass transfer coefficient,  $\phi_s$  - a volumetric fraction of a solid phase in a droplet,  $a$  - radius of a particle. Correspondingly, the rate of heat transfer, caused by the heat effect of gas adsorption  $\Lambda_T = -T^{-1} \cdot \partial T / \partial t$ ,  $s^{-1}$ , is determined by the following formula:

$$\Lambda_T = \frac{\frac{\Delta H \phi_s}{\rho_{\text{eff}} c_{\text{peff}}} \frac{m \rho_L w_A^{(L)}}{\tau_D} \exp\left(-\frac{(1+m\phi_s) \cdot t}{\tau_D}\right)}{T_0 + \frac{\Delta H \phi_s}{\rho_{\text{eff}} c_{\text{peff}}} \frac{m \rho_L w_A^{(L)}}{(1+m\phi_s)} \left[1 - \exp\left(-\frac{(1+m\phi_s) \cdot t}{\tau_D}\right)\right]}$$

where  $\rho_{\text{eff}}$  - density of a slurry droplet,  $c_{\text{peff}}$  - effective specific heat capacity of a slurry droplet,  $\Delta H$  - heat of adsorption. Heat and mass transfer equations are supplemented with initial and boundary conditions at the center of a slurry droplet and gas-liquid interphase.

### 3. Results and discussion

This section presents the results of the numerical simulations performed based on the developed slurry droplet drying model. Ammonia and activated carbon were chosen for our calculations as the highly soluble gas and solid phase. The temporal evolution of the interfacial temperature of a slurry droplet for different mass fractions of ammonia is calculated based on the developed model is shown in Fig. 2. An analysis of the plots presented in Fig. 2 shows that when solid particles are active and adsorb dissolved gas, the interfacial temperature of the droplet is higher than in the case of inert particles.

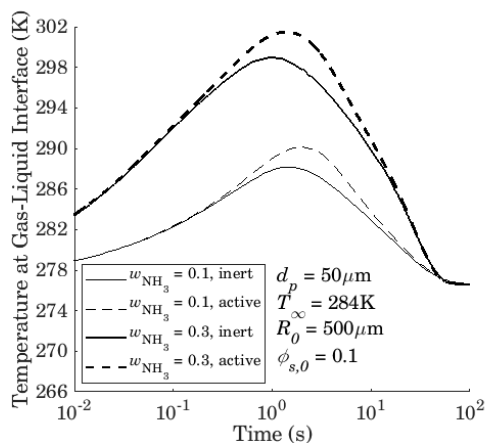


Figure 2. Influence of gas adsorption on the temporal evolution of surface temperature of an acoustically levitated slurry droplet evaporating in a gaseous mixture of  $N_2/NH_3/H_2O$  at different values of mass fraction of ammonia. RH = 50%,  $u_0 = 0.02$  m/s, frequency of acoustic field  $\omega = 2\pi \cdot 45$  kHz, SPL = 160 dB.

Results of numerical calculations of the temporal evolution of the volume fraction of solid particles inside an acoustically levitated slurry droplet are shown in Fig. 3. It follows from Fig. 3 that when solid particles are active, the rate of volume fraction

of solid particles growth with time is higher than when particles are inert.

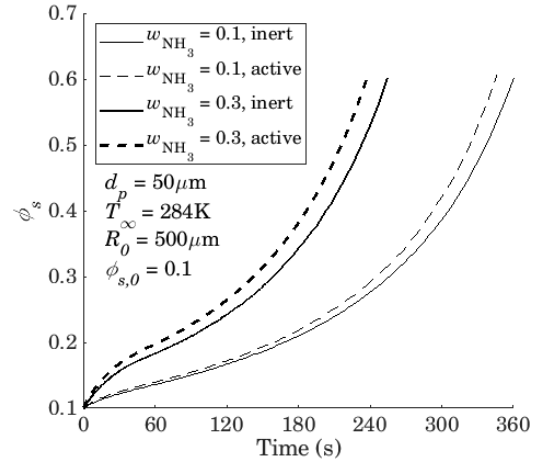


Figure 3. Influence of gas adsorption on the temporal evolution of the volume fraction of solid particles inside an acoustically levitated slurry droplet evaporating in a gaseous mixture of  $N_2/NH_3/H_2O$  at different mass fractions of ammonia; frequency of acoustic field  $\omega = 2\pi \cdot 45$  kHz; SPL = 160 dB.

### 4. Conclusion

1. The interfacial temperature of the evaporating slurry droplet absorbing soluble gas is higher when solid particles are active.
2. Solid particle adsorption activity leads to droplet evaporation rate enhancement. It is shown that at a mass fraction of ammonia in a gaseous phase equal to 0.1 at temperature 284 K and a humidity of 50% with an acoustic field frequency of  $\omega = 2\pi \cdot 45$  kHz and an SPL of 160 dB neglecting of adsorption process by activated carbon particles leads to underestimation of the rate of slurry droplet drying on 7%.
3. When solid particles are active, the rate of volume fraction of solid particles growth with time is higher than when particles are inert.
4. The rate of slurry droplet evaporation increases with the increase of Henry's constant of adsorption.
5. The time of porous shell formation decreases with increasing non-dimensional Henry's adsorption constant.

### 5. References

- [1] Y. D. Pour, B. Krasovitev, A. Fominykh, Z. Hashemloo, A. Kharaghani, E. Tsotsas, A. Levy, Combined effect of acoustic field and gas absorption on evaporation of slurry droplet. *Drying Technology* 2023 41, 767-782.
- [2] M. Doss, N. Ray, E. Bänsch, Modeling and simulation of single droplet drying in an acoustic levitator. *Drying Technology* 2023, 41, 2088-2104.
- [3] A. Fominykh, I. Katra, B. Krasovitev, A. Levy, Adsorption of active trace gases by ensemble of ultrafine porous particles with impermeable cores. *Process Safety and Environmental Protection* 2019, 131, 189-196.
- [4] T. Elperin, A. Fominykh, B. Krasovitev, I. Katra, Modeling of gas adsorption by aerosol plumes emitted from industrial sources. *Process Safety and Environmental Protection* 2017, 111, 375-387.



# Developing Sustainable Granulation Technologies

Y.Karunanayake<sup>1</sup>, L. Brutsch<sup>2</sup>, V. Meunier<sup>2</sup> and A. Salman<sup>1</sup>

<sup>1</sup> University of Sheffield, England, UK

<sup>2</sup> Nestle Research, Lausanne, Switzerland

**Abstract—** The key to developing sustainable granulation technologies is to better understand the energy efficiency of existing granulation technologies and the root causes behind them. This project evaluated the energy efficiency of four of the most common granulation technologies. The energy efficiency of the granulators was found to increase in the following order: Twin Screw Granulator, Fluidised Bed Granulator, High Shear Granulator and Roller Compactor. The wet granulators were found to be far less energy efficient due to the presence of the drying stage. The drying stage was found to consume most of the energy required by the production pathway. This was especially the case for the High Shear Granulator where drying encompassed 78% of the total energy consumed by the pathway. The different technologies were also found to produce granules of varying morphologies which highlights how the end application and granule suitability must also be considered when deciding on a production pathway.

**Keywords:** granulation; energy; sustainability;

## 1. Introduction

Process sustainability is something that has experienced renewed interest of late in the drive to combat global warming, reduce pollution and conserve resources. Nowhere is this more apparent than in the food sector which generates 30% of the world's greenhouse gases [1]. In addition to its role as a major driver of climate change, the food sector has an equally pivotal role of feeding society. However, rising global food prices has seen this sacrosanct duty threatened as essential goods become too expensive for consumers. The development and optimisation of sustainable manufacturing processes are essential if the food sector is to rise to this new challenge.

Granulation is a common size enlargement mechanism which is used throughout the food industry. It's widespread presence in the industry makes it a critical technology therefore to target in the drive to improve overall sustainability. Granulation can be grouped into two main categories: Wet and Dry. Wet granulation occurs with the aid of a liquid binder to stick powder together. Comparatively, Dry Granulation uses high compaction pressures to cause adhesion. The High Shear Granulator, Twin Screw Granulator and Fluidised Bed Granulator are the three main wet granulators used in industry. The Roller Compactor is the most common dry granulator used in industry.

Despite being well established, little research into the sustainability of these competing technologies has been carried out. The aim of this study is to investigate and compare the sustainability of these processes in a comprehensive and complete manner by looking at the complete production pathway going from dry powder to dry granule. In order to do this, the Energy Efficiency will be judged by evaluating the Specific Energy (kWh per kg of granules produced) of each process. A lower Specific Energy will indicate that less energy

is needed to produce the product. A lower energy requirement means lower costs which can be passed onto consumers. It also means that the process will have a smaller carbon footprint

## 2. Materials and Methods

### 2.1. Materials

Maltodextrin (Glucidex IT29, Roquette, France) was chosen as the model material for this work due to its commonplace use in the food industry. The chosen binder for the wet granulation technologies was distilled water at 20°C.

### 2.2. Methods

Four granulation technologies were evaluated. They include the Fluidised Bed Granulator (Glatt, GPCG3, Glatt, Germany), High Shear Granulator (Eirich, EL1, Eirich, Germany), Roller Compactor (WP120 Pharma, Alexanderwerk, Germany) and Twin Screw Granulator (EuroLab 16 mm, ThermoFisher, UK). All the technologies underwent an optimisation stage based on maximising yield. This was done to ensure that each technology was being presented in its best light. Once optimised parameters had been identified, the corresponding production times and energy consumption data were measured after which the produced granules were characterised.

The method to measure the energy consumption of the process is visualised in Figure 1. All the equipment involved in each pathway was connected to the mains via custom built power readers. The power consumed by the machine could be then be recorded manually or automatically by connecting the reader to a computer.

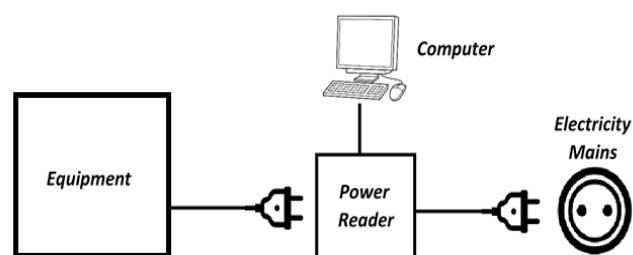


Figure 1. Energy consumption measurement method

## 3. Results

### 3.1. Sustainability (Energy Consumption)

Figure 1 shows the Specific Energy for each granulation pathway where a lower specific energy indicates a more energy efficient process. The energy efficiency was found to improve in the following order: Twin Screw Granulator, Fluidised Bed Granulator, High Shear Granulator and Roller Compactor.

The wet granulation technologies were found to be the least energy efficient. This can be attributed to the energy intensive nature of the drying step. Figure 3 shows example energy consumption distribution data for each unit involved in the production pathway. It is evident that when looking at the wet granulators, the drying step heavily dominates the energy consumption distribution. This is especially true when considering the Twin Screw Granulator and High Shear Granulator, where in both cases, the energy consumed by the drying step was over 3 times greater than that consumed by the granulator itself. Furthermore, wet granulation technologies were found to have far more processing steps and units involved in the production pathway compared to the Roller Compactor which only has 1. This increased processing complexity also results in the greater energy consumption requirement for wet granulators.

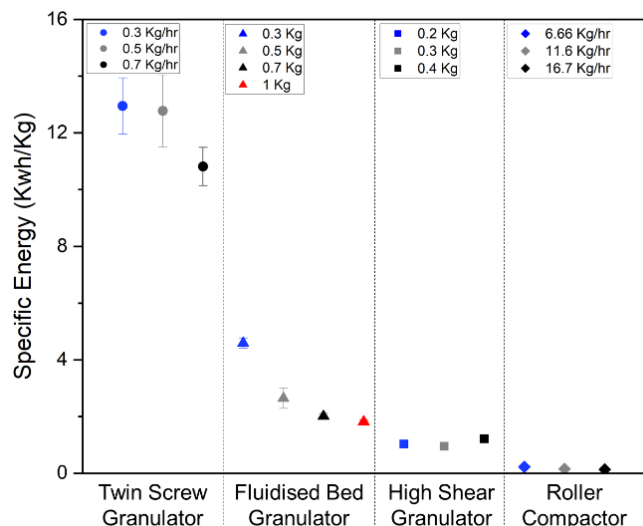


Figure 2. Energy consumption data for each granulation pathway going from dry powder to dry granule

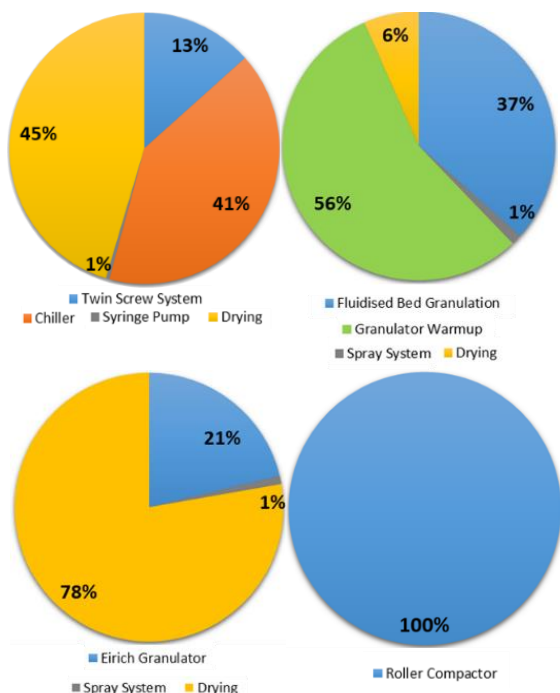


Figure 3. Sample energy consumption distribution data for each unit involved in the different production pathways

### 3.2. Suitability

The different granulation technologies were found to produce very different granules. These differences are highlighted in Figure 4 which displays X-Ray scans of the granules. The scans show that there are significant variations, both in terms of porosity and shape. Image analysis using ImageJ indicates that the average granule porosity from the different technologies was 14% (High Shear), 25% (Twin Screw), 28% (Roller Compactor) and 41% (Fluidised Bed). This difference in porosity is due to the varying extent of consolidation that granules experience in each unit and can lead to significant differences in granule properties such as strength and reconstitution [2].

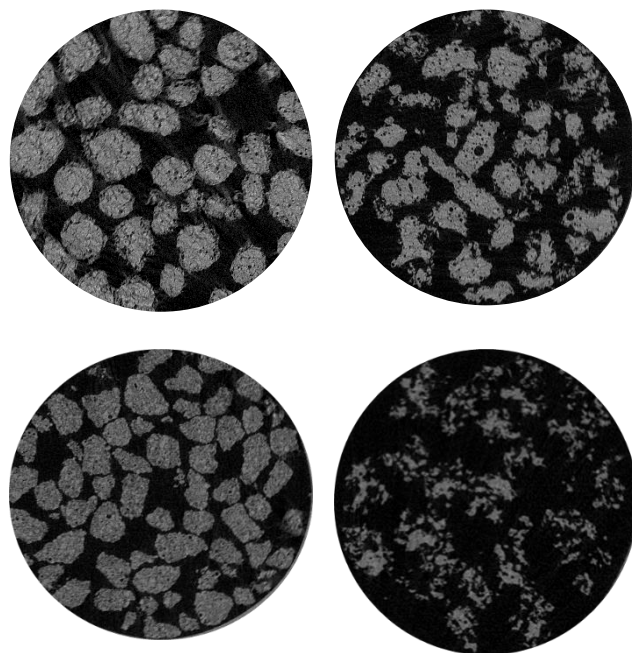


Figure 4. X-Ray Scans of granules produced from the competing technologies: High Shear Granulator (top left), Twin Screw Granulator (top right), Roller Compactor (bottom left) and Fluidised Bed (bottom right).

## 4. Conclusion

This work highlights the notable variations in sustainability between competing granulation technologies. The need for a drying step as well as an increased number of process steps has been found to increase the energy consumption and therefore decrease the energy efficiency of the process. Granule morphology was shown to differ between the technologies. This will lead to the production of granules with different properties making them more or less suitable for different applications. This underlines how a 'big picture' approach considering both the efficiency of the process alongside how suitable for use the granules are is essential if food manufacturers are to choose the optimum manufacturing pathway.

## References

- [1] A. Ladha-Sabur, S. Bakalis, P.J. Fryer, E. Lopez-Quiroga, Mapping energy consumption in food manufacturing, *Trends in Food Science & Technology*. 86 (2019) 270–280
- [2] G. Morin, L. Briens, A Comparison of Granules Produced by High-Shear and Fluidized-Bed Granulation Methods, *AAPS PharmSciTech*. 15 (2014) 1039–1048

# Food Phantom Packaging: Prolonging Product Shelf Life via Microstructure Engineering of Tableted Granular and Powdered Consumer Foods

Luc Dewulf<sup>1</sup>, Michael K. Hausmann<sup>2</sup>, Annabel Bozon<sup>3</sup>, Gerhard Niederreiter<sup>2</sup>, Agba D. Salman<sup>1</sup>.

<sup>1</sup> University of Sheffield, Sheffield, UK

<sup>2</sup> Nestlé Research, Lausanne, CH

<sup>3</sup> Nestlé Product Technology Centre Food, Singen, DE

**Abstract**— Many consumer food products such as confectionary or culinary seasonings are particle-based systems containing varying amounts of lipids such as oils, fats, and greases. Lipid migration leads to quality defects such as fat bloom on chocolate or oil stains on fibrous paper packaging. We identified drivers of oil migration in particle systems and developed a novel approach of microstructure engineering to reduce detrimental oil migration down to 2% and thus prolong shelf life of particle-based foods. Raman spectroscopy and automated image quantification were used to monitor oil retention performance. Fluid-mechanical modelling is used to model the oil migration phenomena as a predictive tool between food, packaging, and shelf-life.

**Keywords:** lipid migration; particulate foods; Raman; Image analysis; modelling;

## 1. Introduction

A recent review by us [1] identified lipid migration in foods as a major shelf-life challenge for consumer food manufacturers of particle-based foods, such as chocolate or seasoning products. The driver for oil migration is inherent thermodynamic instability of multiphasic particulate food systems. Despite prior research, the challenge to kinetically slow this metastable phase separation process is ongoing. Novel mitigation, monitoring, and modelling approaches are needed.

We developed a novel microstructural engineering approach for a model bouillon tablet, based on increasing the capillary pressure within the food system, enabling to retain the oil within the food. Oil mobility on the tablet surface was monitored for the first time with Raman Laser Spectroscopy and Chemical Imaging. The oil imbibition into paper packaging was measured via automated image quantification. A modelling approach based on fluid mechanics in porous media was constructed to link for the first time food microstructure with oil retention performance and the effect on packaging.

## 2. Methodology

### 2.1. Materials and Tableting

Model food tablets were made using 95 w/w% table salt of coarse and fine particle size, and 5 w/w% sunflower oil, mixed in a beaker. For each food tablet, 4 g of salt+oil mixture was tableted to a cube of 14 mm side length using a universal testing machine (Instron 3367). Compressed salt+oil tablets were subjected to oil-release measurements within 30 minutes of tableting. To model fibrous packaging material, Whatman 3mm blotting paper was used and cut to square pieces of 10 x10 cm, mimicking a typical single-serve wrapper size.

### 2.2. Raman Chemical Imaging and Automated Image Quantification

For Raman Chemical Imaging, the salt+oil/fat tablet was placed in a self-constructed Raman set up (Oxxius Laserboxx, 100 mW

laser power, 532 nm continuous wave diode). The signal was acquired daily over 4 days over the course of 1 hour by scanning the table surface in a grid pattern of 500  $\mu\text{m}$  spacing for 15 s at each location. The resulting 812 spectra were acquired with a CCD spectrometer (Horiba, iHR320, 1800 groves/mm, 500 nm blaze grating), and reconstructed using a self-written MATLAB code into 2D chemical images (Fig. 1).

Oil stain development on paper packaging was monitored via automated image acquisition using a flat-bed scanner and quantification using a self-written imageJ script.

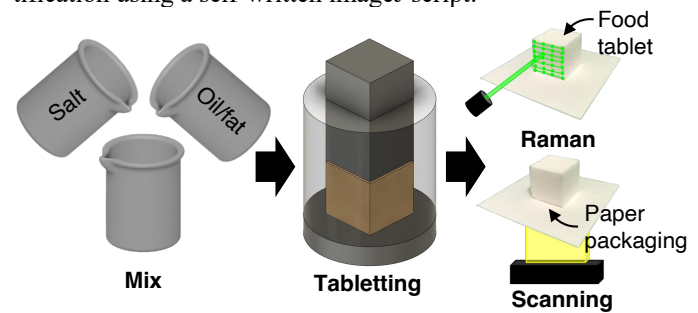


Figure 1. Experimental procedure for tablet preparation and oil migration monitoring (Raman Chemical Imaging and automated image quantification).

### 2.3. Modelling

A first-principle model was constructed to physically explain and predict the microscale phenomena occurring during oil migration (Fig. 2). Liquid flow in porous bodies is affected by the interstitial capillary size and overall permeability, and thus the Washburn and Darcy equation were used to evaluate capillary pressure  $P_{cap}$  (Pa) and permeability  $K$  ( $\text{m}^2$ ) [2, 3]. Microstructural information was gathered for each tablet formulation from x-ray computer tomography (ScancoMedical  $\mu\text{CT}$  35. 1.5  $\mu\text{m}$  voxel size, 45 kVp, 88  $\mu\text{A}$ , 0.5 mm Al filter, 10 s exposure time per projection). Oil wicking tests to obtain sorption parameters were performed in a tensiometer (Krüss K100, 10 mm cylindrical sample size), and the linear slope fitted with the Washburn equation [4].

The model was set up as two porous capillary bodies in direct contact, with the continuity of pressure equation governing the driving or retention force and frictional pressure loss of liquid oil between the bodies.

$$(p_t - p_0) + (p_i - p_c) + (p_p - p_i) + (p_0 - p_p) = 0 \quad (1)$$

where  $(p_t - p_0)$  is the capillary pressure between the oil in the tablet and air,  $(p_i - p_c)$  is the pressure drop due to friction in the tablet,  $(p_p - p_i)$  is the pressure drop due to friction in the paper, and  $(p_0 - p_p)$  is the capillary pressure between oil in the paper and air. Applying Washburn and Darcy definitions of  $P_{cap}$  and  $K$  for each body and constructing the model to display oil stain radius (cm) vs time (days), a differential equation is obtained of the form

$$\frac{dr_p}{dt} = - \frac{\Delta PK}{\mu r_p \left[ \ln \left( \frac{r_p}{r_i} \right) + \frac{2\pi h \epsilon_p}{S \epsilon_t} - \frac{2\pi h^2 \epsilon_p^2 r_p^2}{S^2 \epsilon_t^2 r_i^2} \right]} \quad (2)$$



where  $r_p$  is the radius of oil stain on paper packaging (m),  $\Delta P$  is the difference in Laplace pressures between tablet and packaging (Pa),  $\mu$  is the viscosity of oil (Pa.s),  $r_i$  is the radius of the tablet (m),  $h$  is the height of paper (m),  $\epsilon_p$  and  $\epsilon_t$  are the void fractions of paper and tablet respectively, and  $S$  is the side length of the tablet (m).

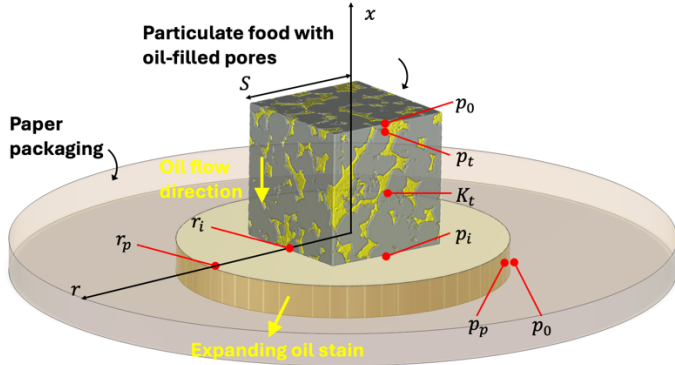


Figure 2. Modelling setup of oil migration from model bouillon tablet into paper packaging.

### 3. Results and Discussion

#### 3.1. Oil Migration Monitoring

Raman Chemical Imaging proved a successful technique for spatiotemporal monitoring of oil migration from model food tablets into paper packaging (Fig. 3). Surface oil concentration behaved differently for the different particle size formulations. Oil mobility was more pronounced for tablets containing coarse particles as can be seen from the faster colour change. Oil migration was less pronounced for tablets made from fine salt.

Congruently with Raman Chemical Imaging, automated oil stain imaging recorded a faster oil stain development on the paper packaging for the tablets made from coarse salt (Fig. 4). Tablets made from fine salt developed virtually no oil staining (2%), meaning the majority of oil was retained in the porous salt tablet structure. As such, our particle engineering approach proved successful in retaining the oil within the capillaries of the food.

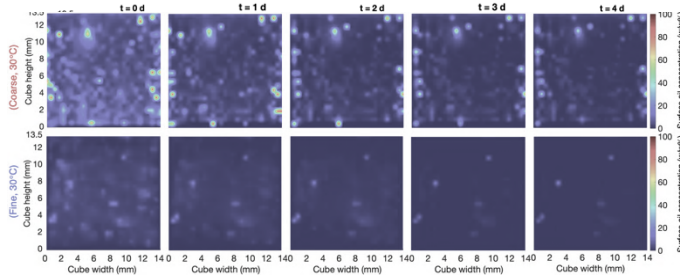


Figure 3. Raman Chemical Imaging of surface oil concentration with time for 2 different model bouillon tablet formulations.

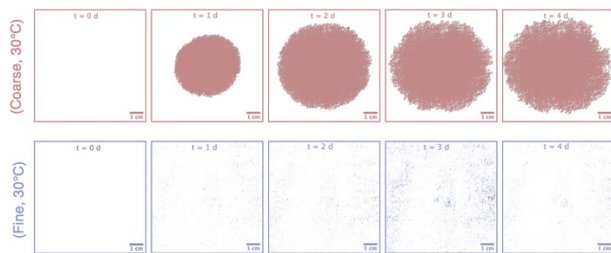


Figure 4. Oil stain images on paper packaging for the same 2 model bouillon tablet formulation acquired via automated image quantification.

#### 3.2. Modelling

X-ray tomography of the coarse and fine salt+oil tablets provided microstructural data (Fig. 5 a-c), while wicking tests

provided sorption data. For brevity, auxiliary measurements to evaluate  $\Delta PK/\mu$  in eq. 2 were omitted. Fig. 5 d) shows the experimental and data and model of oil stain radius of oil migrated out of the salt+oil tablets into paper packaging with time. The fit is less precise initially likely due to the modelling setup that captures less well the vertical flow of oil into paper. With prolonging time and better capture of the radial oil flow, the fit between model and experiments improves. With a more refined model, mechanistic explanation of microstructure effects on oil migration are possible, alongside future predictions on food and packaging compatibility for shelf life.

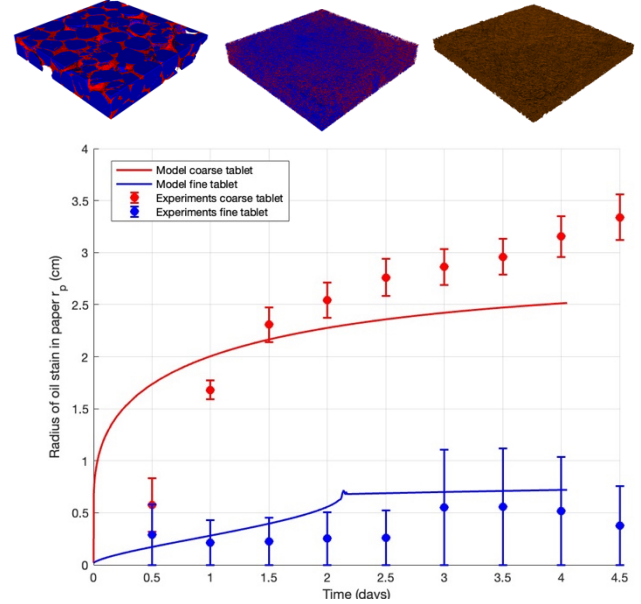


Figure 5. X-ray CT scans of a) coarse salt tablets, b) fine salt tablets, and c) paper packaging; d) model and experimental data of mass of oil migrated from tablet into paper packaging over time.

### 4. Conclusion

We provide an effective method to reduce and virtually stop oil migration from particle-based food structures into paper packaging, by engineering the food microstructure to increase the internal capillary pressure. The increased oil retention was monitored via Raman Chemical Imaging for the salt tablet, and via automated image quantification on the paper packaging side. The physical phenomena were modelled via a fluid-mechanical approach based on capillary pressure inherent to the tablet and paper, and frictional pressure loss of oil flow. Future work will entail a wider variation of tablet formulation parameters such as a broader particle size range, and further refinement of the model to attempt a better fit, especially at the early time scales.

### Acknowledgement

L. D. thanks EPSRC (grant 2602203) and Nestlé for funding this research, and Prof. Arnulf Materny and Dr. Patrice Donfack from Constructor University Bremen, Germany, for free Raman training in their spectroscopy lab.

### References

- [1] L. Dewulf, M. K. Hausmann, A. Bozon, G. Niederreiter, S. Palzer, and A. D. Salman, "Particle-based food systems subject to lipid migration – A review of measurement, modelling, and mitigation approaches," *Powder Technology*, vol. 445, p. 120097, 2024/09/01/ 2024, doi: <https://doi.org/10.1016/j.powtec.2024.120097>.
- [2] E. W. Washburn, "The dynamics of capillary flow," *Physical Review*, vol. 17, no. 3, pp. 273-283, 03/01/ 1921, doi: [10.1103/PhysRev.17.273](https://doi.org/10.1103/PhysRev.17.273).
- [3] H. Darcy, *Les fontaines publiques de la ville de Dijon*. Paris: Dalmont, 1856.
- [1] M. F. Pucci, P.-J. Liotier, and S. Drapier, "Capillary wicking in a fibrous reinforcement – Orthotropic issues to determine the capillary pressure components," *Composites Part A* vol. 77, pp. 133-141, 2015/10/01/ 2015, doi: <https://doi.org/10.1016/j.compositesa.2015.05.031>.



# Laboratory Evaluation of Wear Properties for Targeted Applications of Wear-Resistant Liners through First Principles Calculations and DEM Simulations

Kurt Naugler<sup>1</sup>, Eric Bengston<sup>2</sup>, Corin Holmes<sup>3</sup> and John Carson<sup>1</sup>

<sup>1</sup> Jenike & Johanson, Inc., Tyngsboro, MA, USA

<sup>2</sup> Jenike & Johanson, Inc., San Luis Obispo, CA, USA

<sup>3</sup> Jenike & Johanson, Inc., Perth, WA, AU

**Abstract**— As industry continues to focus on sustainability and obtaining the longest practical lifespan for material handling equipment, wear resistant liners have grown in popularity. Use of laboratory wear testing combined with predictive modelling of high wear locations within a system, allows for targeted use of wear resistant materials in critical system components and locations. A novel abrasive wear tester has been shown to provide accurate determination of wear rates based on the particle-to-surface interaction of materials flowing against a wall surface under varying levels of applied normal stress. Accurate prediction of high wear locations within both storage vessel and transfer chute applications allows a significant reduction in the requirement for high-cost wear resistant materials through targeted application in critical system locations.

**Keywords:** wear; abrasion; silo; chute; liner

## 1. Introduction

One of the many challenges faced in industrial applications that involve handling of granular solids is that of abrasive materials and their impact on the systems used to store and transport this class of material. Studies support the use of wear resistant liners to increase longevity of handling systems with correlations being drawn between the relative hardness of materials being handled and liner material of construction [1]. Building upon these general correlations, laboratory methods, including a novel test device, have been developed to quantify expected wear rates based on particle-to-surface interaction of material flowing against a wall surface under varying levels of applied normal stress.

With applications involving material flow through a silo, bin, hopper, or other storage vessel, surface wear rates can be calculated based on forces determined by Janssen's side-wall pressure distribution and Jenike's radial stress theory, material flow properties, and vessel geometry [2, 3]. In transfer chute applications, where dynamic interaction between the particles and system geometry is more complicated, DEM models can provide the information needed to correlate wear test results with expected wear rates at various points in the system.

Use of laboratory wear testing, combined with predictive modelling of high wear locations within a system, allows for targeted use of wear resistant materials in critical system components and locations.

## 2. Abrasive Wear Testing

### 2.1. Test Apparatus

Evaluation of wear within a system relies on a test apparatus (Fig. 1) which applies a range of pressures that particles exert on wall surfaces when flowing through full-scale production systems. High levels of loading in the normal direction to a wall surface are achieved through regulation of a linear pneumatic piston applying pressure to a coupon of the existing or proposed

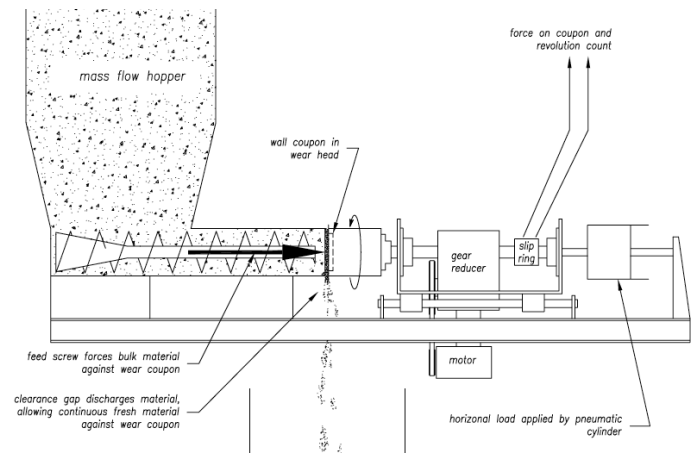


Figure 1. Abrasive wear test apparatus

wall surface[4].

The sample of material in contact with the wall coupon is continually refreshed by a hopper and screw feeder arrangement, while linear travel of material within the system is simulated by the controlled and measured rotation of the wall coupon.

### 2.2. Test Procedure and Results

Prior to running material against wall coupons, each surface is weighed and measured to serve as a reference point against which wear rate calculations can be based following testing. With pre-test values recorded, material is then run through the system under specified flow rates, coupon rotational speeds, and applied normal forces. Following each test, the coupon weight and thicknesses are recorded for calculation of wear rate specific to the unique test run. Results can then be compiled that give insight into wear rate as a function of material flow rate within the system and expected forces exerted on the walls of the silo or chute.

## 3. Correlation to Silo and Chute Applications

Due to the direct relationship between tested wear rates and loading of the granular material against wall surfaces, it is necessary to calculate expected loads within the handling system [5]. The approach for this evaluation is dependent on the nature of the application: silo (hopper) or transfer chute.

### 3.1. Silo Loading Analysis

Loading analysis for material forces in a silo can be completed based on a first principals approach using material flow properties (bulk density, internal friction, wall friction). With these flow properties, Janssen's side-wall pressure distribution is used to calculate pressures on the walls of the silo in the non-converging portions of the system. In the hopper portion of the silo, Jenike's radial stress theory is used to calculate expected material-induced loads.

### 3.2. Chute Modelling

Due to the dynamic interaction between the particles and system geometry in transfer chute applications, DEM models provide the information needed to correlate wear test results with expected wear rates at each point in the system where material is in contact with the chute surface [6]. Note that impact points typically exhibit high wear, but the mode of this impact wear is different than that of material sliding against a surface. Therefore, wear rates are not measured by the test apparatus described above or calculated by the methods described herein.

Calibration and post processing of DEM models representing material flow through a chute is used to show typical force profiles within the system that are combined with test results to predict wear rates.

### 3.3. Wear Calculations

Wear rates empirically measured in the wear test apparatus are a function of both the forces between the granular solids and wall materials and also the flow rates at each point within the system. With each of these variables defined, wear profiles can be calculated and applied to specific system geometries and liner configurations. In order to perform estimates of wear within a system, three items need to be defined and specified for each point of interest within the specific arrangement: (1) Wear rate test results, (2) loading calculation or DEM modelling, and (3) area specific expected flow rates.

## 4. Case Study – Silo Failure due to Wear

In addition to increased maintenance requirements and replacement of worn geometry within a system, wear can lead to premature failure of silos and chutes [7]. Such was the case for a silo handling relatively coarse ( $>1\text{mm}$ ), free-flowing aggregate material. Excessive wear at the transition point between the cylinder portion of the silo and the hopper section caused structural failure. Following this failure, analysis was done to evaluate expected wear rates and determine optimal locations for wear resistant liners to be added to other silos handling the same material.

Testing was conducted to evaluate expected wear rates of the current silo material of construction (carbon steel) and of a potential wear resistant liner (similar to AR500). Fig. 2 shows the material loading profile, calculated wear rates, and actual measured wear rates for this handling application. Note that the depicted stress profile is approximated, and units are omitted intentionally.

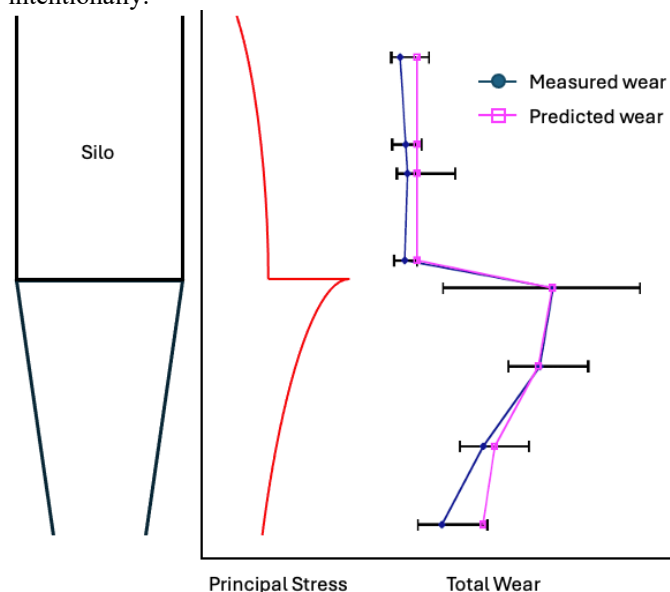


Figure 2. Silo application with accurately predicted wear profile

Measured wear rates were taken from similar silos handling the same material and the range shown represents the variability in measurements taken at multiple locations radially around each silo.

Following validation of the model and predicted wear rates, alternate surfaces were evaluated to determine optimal liner placement in targeted areas most impacted by material-induced wear. Instead of constructing the whole silo out of abrasion resistant material, a small section around the transition point was reinforced to drastically increase the usable life of the silos. Fig. 3 shows the impact of an abrasion resistant liner on the expected wear rate for this aggregate handling application. The liner covered less than one vertical meter of the silo height yet was able to improve overall wear rate to an acceptable level.

## 5. Conclusion

Abrasive wear in silos and transfer chutes is a difficult challenge that can have a negative impact on commercial operations. Understanding the driving forces behind abrasion and being able to quantify wear rates allows system operators to better predict system lifecycles and plan maintenance activities. To do this, expected wear rates must be determined empirically over the range of forces expected in a specific application. Calculation or modelling of the forces from material-to-surface interaction and determination of location specific flow rates provides the inputs needed to correlate test results with real world systems.

This systematic approach has been applied to multiple systems including both failure mode analysis and predictive evaluation with validation of accuracy through ultra-sonic thickness measurements. While methods described herein limit analysis to contact bed applications in silos and portions of chute systems where material is in contact with the chute surface, additional work is being done with computational modelling of dynamic particle-to-surface interactions such as those at impact points and with fluidized systems.

## References

- [1] V. Gopi, R. Sellamuthu and S. Arul, "Measurement of Hardness, Wear Rate and Coefficient of Friction of Surface Refined Al-Cu Alloy," *Procedia Engineering*, vol. 97, pp. 1355-1360, 2014.
- [2] A. Jenike, "Storage and Flow of Solids," vol. Bulletin 123 of the Utah Engineering Experimentation Station, 1980.
- [3] H. Janssen, "Experiments on Corn Pressure in Silo Cells," *Engineer in Bremen, Germany*, 1895.
- [4] T. Royal and J. Johanson, "Abrasive Wear Tester". United States of America Patent 4,446,717, 8 May 1984.
- [5] T. Royal and J. Johanson, "Predicting Wear due to Solids Flow," in *Powder & Bulk Solids Conference*, Rosemont, IL, May 1982.
- [6] A. D. Orlando and E. P. Maynard, "Using discrete element method software to design bulk solids handling equipment," *Powder & Bulk Engineering*, vol. 30, no. 6, pp. 41-44, 2016.
- [7] J. Carson, "Silo Failures: Case Histories and Lessons Learned," *Handbook of Conveying and Handling of Particulate Solids*, vol. 10, pp. 153-166, 2002.

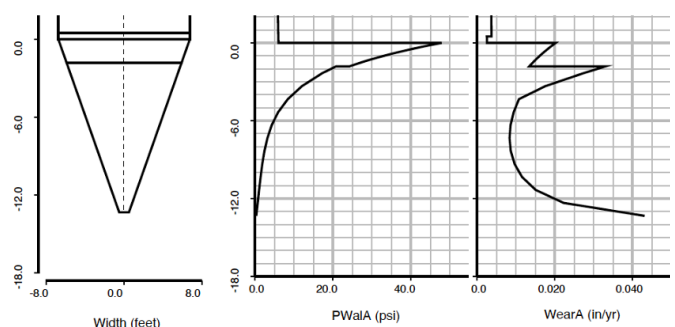


Figure 3. Wear management with targeted liner

# An Experimental Investigation into Sifting and Fluidization Segregation Characteristics for Coal Fly Ash

R. Poddar<sup>1</sup> and S S. Mallick<sup>1</sup>

<sup>1</sup> Thapar Institute of Engineering & Technology, India

**Abstract**—Sifting and fluidisation segregation characteristics were determined for six different fly ash samples (particle size ‘d<sub>50</sub>’ ranging from 68 µm to 141 µm) using two different testers as per ASTM standards, D6940 and D6941, respectively. The results have shown that the coarser particles have a greater tendency to sifting segregation, and the finer powders respond more to fluidisation segregation. The angle of repose for the fine ash and coarse ash were 55° and 38°, respectively, which indicated poor to good flowability conditions. The flow function test shows that all the samples were in an easy-flowing to a free-flowing zone under the major principal consolidating stress ranging from 0 to 10 kPa. The angle of repose and material flow function correlates well with the sifting segregation index. In contrast, cohesion between particles, the ratio of free terminal velocities and diameters for coarse to fine particles have shown a good fit with the fluidisation segregation index.

**Keywords:** Sifting and fluidisation segregation; segregation index; angle of repose; cohesion; terminal settling velocity

## 1. Introduction

Coal fly ash mainly comprises spherical particles ranging from less than 1 µm to 600 µm [1]. The chemical composition and physical characteristics of fly ash may vary significantly for different power plants and even within the same power plant, depending on the field of ESP from where the ash has been collected [2, 3]. Due to the differences in the particle and bulk properties (in terms of size, shape, bulk density etc.), it is possible to have content inhomogeneity of fly ash during the filling and discharge from silo/hopper because of sifting and fluidisation segregation [4]. This paper investigates into the segregation characteristics of powders which are in borderline between the Geldart Group A to B materials. In the author's understanding, very limited experimental data for segregation characteristics of powders are available in this size range (Geldart Group A to B borderline) and there seems to be no other available study on linking powder segregation to its flow properties.

## 2. Experimental methods

### 2.1. Physical properties

Six different coal fly ash samples (A-F) were obtained as test samples from a thermal power plant to investigate the physical properties such as particle size distribution, particle morphology, and particle and loose poured bulk densities as per ASTM standards.

### 2.2. Angle of repose

The angle of repose of an inverted cone whose surface is equivalent to the projected image of the powder heap was measured using the GranuHeap instrument of Granutools.

### 2.3. Annular shear testing

The flow properties of powder samples were evaluated using a powder flow tester-PFT (Brookfield, Middleboro, USA) built on Jenike's methodology. The PFT system was used with software (Powder Flow Pro) for data processing.

### 2.4. Sifting and fluidisation segregation tester

A lab-scale sifting segregation tester was developed at the Powder Flow Laboratory of Thapar Institute of Engineering & Technology as per the ASTM standard (ASTM Standard, D6940-10. 2010) [5]. The tester consists of three hoppers (one funnel flow and two mass flow hoppers), two slide gates and two guide cylinders. The segregation tendency due to the air resistance or induced by air flow on different fly ash samples (A-F) was evaluated using a fluidisation segregation tester (developed at the Powder Flow Laboratory of Thapar Institute of Engineering & Technology) based on ASTM Standard (ASTM Standard, D6941-12. 2012) [6]. The entire setup has been separated into three sections: the expansion chamber, the testing chamber, and the air chamber.

## 3. Results and discussions

### 3.1. Physical and flow properties of fly ashes

It can be seen from the SEM images that most of the fly ash samples have provided similar and spherical shapes (with a small presence of irregularly shaped particles). In the current study, fine ash refers to an ash sample with a median size of less than 100 µm, and coarse ash refers to that having a median size equal to and above 100 µm. Results show median sizes, loose poured bulk densities, and particle densities have varied from 68 to 141 µm, 648 to 1096 kg/m<sup>3</sup> and 1523 to 1761 kg/m<sup>3</sup>, respectively. Particle size and loose poured bulk densities have varied by factors of 2.07 and 1.69, respectively, which were considered to be considerable to demonstrate differences in segregation characteristics. The angle of repose for the fine ash (sample A) and coarse ash (sample F) were 55° and 38°, respectively. Figure 1 shows the flow function curves for the six fly ash samples.

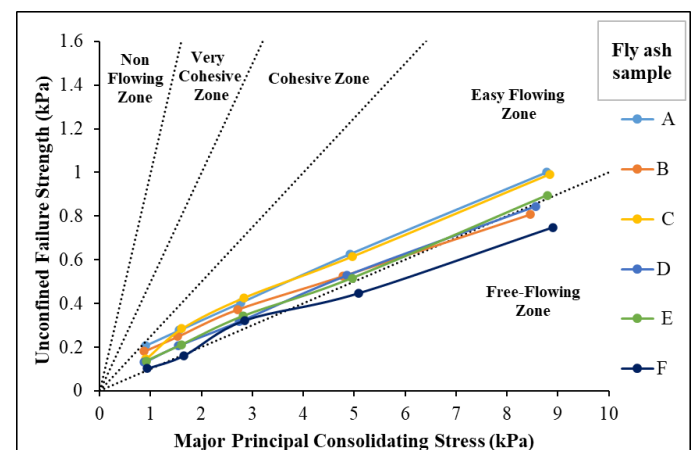


Figure 1. Flow function curve for fly ash samples

### 3.2. Assessment of segregation behaviour

In this study, the segregation index is based on the first (or top) and last (or bottom) batches retrieved after the segregation tests. Figures 2 and 3 show the comparison of their loose poured bulk densities between the first/top and last/bottom batch in case of sifting and fluidisation segregation. The results show that the

first/top batches for all the fly ash samples (A to F) have a higher percentage of fines than the last/bottom batches. Also, it can be seen that the first/top batch samples are heavier (represented by higher loose poured bulk density values) than the last/bottom batch.

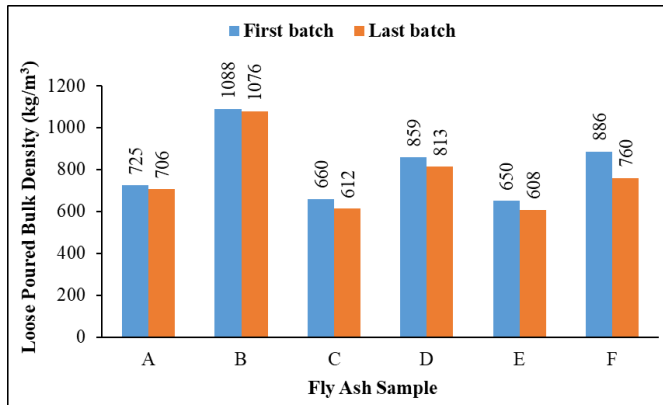


Figure 2. Comparison of loose poured bulk densities of ash between first and last batch (sifting segregation)

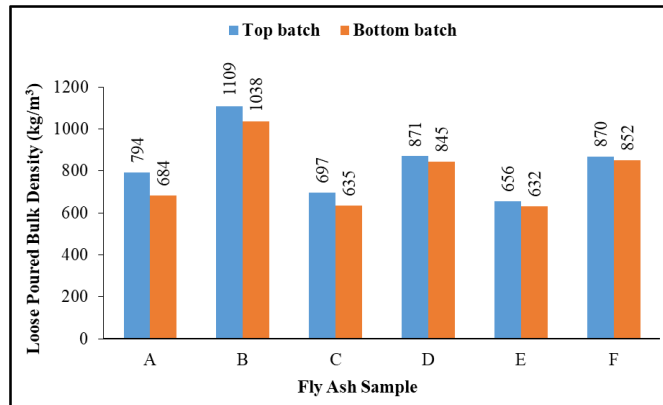


Figure 3. Comparison of loose poured bulk densities of ash between top and bottom batch (fluidisation segregation)

### 3.3. Segregation index

The segregation index,  $I_{S(k)}$ , is defined as the ratio of mass content (%) difference between the first/top and last/bottom batch to the average of mass content (%) in the first/top and last/bottom batch in the particle size range of 'k'. The mean segregation Index,  $\bar{I}_S$ , is defined as the sum of segregation index values for the entire size range.

Table 1. Sifting and fluidisation segregation index for ash samples

Fly ash sample	$d_{50}$ ( $\mu\text{m}$ )	$\rho_b$ ( $\text{kg/m}^3$ )	$\rho_p$ ( $\text{kg/m}^3$ )	$\bar{I}_{SS}$ (%)	$\bar{I}_{FS}$ (%)
A	68	744	1761	5.03	26.25
B	85	1096	1750	9.11	19.9
C	97	648	1605	30.74	20.14
D	102	853	1653	21.10	17.05
E	105	643	1523	31.95	17.04
F	141	860	1575	47.24	10.68

For sifting segregation, the relative movement amongst the powders under gravity has been considered to be a key contributor. The movement of smaller particles through the voids of coarser particles is expected to depend on the relative flowability of particles. Therefore, powder flowability would be an essential property contributing to sifting segregation tendencies. In view of this, the material flow function (1/ffc) has been included in representing sifting segregation in this study. The angle of repose (AOR) has been used in several studies as

an indicator of flowability. Since better powder flowability would cause enhanced segregation tendencies under gravity and the angle of repose is an indicator of flowability; hence the angle of repose has also been used in this study to represent sifting segregation tendencies. The leading cause of fluidisation segregation (also called air-induced segregation) is due to the differences in upper and lower particle size (in terms of  $d_{10}$  and  $d_{90}$ ) and/or particle density that can cause the particles to remain suspended in the air for different periods of time while filling a silo/bin from the top. Ultimately, they settle down at different rates causing segregated settlement [7]. Thus, wide particle size distribution and a higher ratio of  $w_{f90}$  to  $w_{f10}$  (i.e., the ratio of terminal settling velocities for coarse and fine particles) cause a greater chance of powder segregation due to the effect of fluidisation. It is quite likely that the particles would be sticking together due to cohesion and being together, the particles are not subjected to air entrainment and differential rate of settlement. Thus, cohesion would restrict fluidisation segregation at the first place. Therefore, cohesion (C) has been included in this study as a parameter to represent fluidisation segregation.

## 4. Conclusion

The results from their sifting and fluidisation segregation characteristics have shown that with an increase in median particle size, the sifting segregation tendencies have increased and are represented by higher values of segregation indices. The first batches of all fly ash samples A to F have shown higher loose poured bulk density, thus further confirming that fine particles have occupied the interstitial spaces between coarser particles, resulting in higher packing density. The finer ash samples have provided greater fluidisation segregation tendencies than the coarser samples. This has occurred in spite of the higher value of cohesion in finer ash samples. The higher values of the fluidisation segregation index for finer ash show that the difference in particle settling velocities (which promotes segregation) dominates over the particle-particle cohesion (which suppresses segregation).

**Acknowledgement:** The authors would like to acknowledge the collaboration between Thapar Institute of Engineering & Technology (TIET) and Granutools (Belgium) for using the GranuHeap instrument.

## References

- [1] Kazys, R., R. Sliteris, L. Mazeika, L. Van den Abeele, P. Nielsen, and R. Snellings. 2021. Ul-trasonic Monitoring of Variations in Dust Concentration in a Powder Classifier. *Powder Technology* 381 (March): 392–400. <https://doi.org/10.1016/j.powtec.2020.11.072>.
- [2] Antoni, J. Satria, A. Sugiarto, and D. Hardjito. 2017. Effect of Variability of Fly Ash Ob-tained from the Same Source on the Characteristics of Geopolymer. *MATEC Web of Conferences* 97 (February 1): 1-6. <http://www.mateconferences.org/10.1051/mateconf/20179701026>.
- [3] Kiattikomol, K., C. Jaturapitakkul, S. Songpiriyakij, and S. Chutubtim. 2001. A Study of Ground Coarse Fly Ashes with Different Finenesses from Various Sources as Pozzolanic Materials. *Cement and Concrete Composites* 23, no. 4–5 (August): 335–343. <https://linkinghub.elsevier.com/retrieve/pii/S0958946501000166>.
- [4] Marucci, M., B. Al-saigh, C. Boissier, M. Wahlgren, and H. Wikström. 2018. Sifting Segregation of Ideal Blends in a Two-Hopper Tester: Segregation pro Files and Segregation Magnitudes. *Powder Technology* 331: 60–67. <https://doi.org/10.1016/j.powtec.2018.01.070>.
- [5] ASTM Standard, D6940-10. 2010. Standard Practice for Measuring Sifting Segregation Tendencies of Bulk Solids, West Conshohocken, PA, USA: ASTM International ([www.astm.org](http://www.astm.org)).
- [6] ASTM Standard, D6941-12. 2012. Standard Practice for Measuring Fluidization Segregation Tendencies of Powders, West Conshohocken, PA, USA: ASTM International ([www.astm.org](http://www.astm.org)).
- [7] Schulze, D. 2008. *Powders and Bulk Solids*. Springer. <https://doi.org/10.1002/cite.201090034>.



# A robotic solution for autonomous weighing of powder materials

Shruti Chakraborty<sup>1</sup>, Alison Griffiths<sup>1</sup>, and Charles Williams<sup>3</sup>

<sup>1</sup> Staffordshire University, UK

<sup>2</sup> Promtek Ltd. UK

**Abstract—** This paper presents a robotic powder weighing solution with an adaptive control algorithm for automating the critical and error-prone task of manual weighing. Leveraging classical powder characterisation tests, data on 10 industrial-grade materials were collected and used to train an unsupervised clustering algorithm, classifying powders into cohesive, free-flowing, and moderately flowing categories. Integrating this classification into the control algorithm allows the robotic system to dynamically adjust its movements for optimal pouring and weighing.

**Keywords:** robot; control; flow; powder

## 1. Introduction

Although robots are used in manufacturing processes in various industries, few applications have focused on applying robots for handling of particulate solids[1, 2]. This study developed a robotic powder weighing solution to automate manual powder weighing, a time-critical step in manufacturing of products whose quality is recipe controlled and must comply with government regulations. Manual weighing is repetitive, error prone and hazardous, where operators use a scoop to weigh a target material on bench scales. Powder weighing also presents several challenges for robotic manipulation due to the complex dynamics and variable flow behaviour of powders which depends on their intrinsic and bulk properties, forces arising from inter-particle interactions and contact with handling equipment.

Here proposed is an adaptive robotic motion control algorithm for weighing powder materials. 10 industrial grade materials were used to develop a powder material database and study parameters that could affect the weighing process. This data was used to train an unsupervised prediction algorithm to cluster powder materials by flow type (cohesive, free flowing and moderately flowing) which was then used to adjust the pour of the material.

## 2. Materials and Methods

### 2.1. Robotic Weighing System Setup

The setup consists of a FANUC CRX-10iA/L 6 degree of freedom (DOF) collaborative robot connected with industrial grade weighing scales from OHAUS and a custom 3D printed scoop shaped end effector. To emulate factory setup there are two sets of containers to collect and pour the target powder as shown in Figure 1.

The weighing process is shown in Figure 3. Three motions were designed for the task: scooping, pouring and emptying. For each of these motions, a safe starting and approach pose for the robot was defined by manually guiding the robot and using its in-built controller for trajectory generation, such that these motions could be repeated exactly by the robot. These motions are executed by a finite state machine type controller that was designed for the robot with 4 states: Ready, Scooping, Pouring and Emptying. The robot enters Ready State at the start and the first Scooping state is triggered when a target weight and material is input via the HMI. Feedback from the scales was used to transition between the Pouring and Scooping states; a timeout function was implemented which monitored rate of change of scale readings. If no change was detected in scale readings within the timeout period and the target weight had not

been achieved, the scoop was deemed to be empty, and the Scooping state was triggered where the robot then returned to refill the scoop. On achieving the target weight, the robot transitioned to the Emptying state, where excess material remaining in the scoop is returned to the container. Finally, the robot returns to the Ready state for the next weighing.

This study is focused on the pouring state of the robot. Many different combinations of motion are possible for the robot to achieve a pour into the recipient container. To simplify this, a safe start pouring pose was defined above the recipient container. Once the robot reaches the pose, the powder is poured by changing the incline of the scoop. This is the relative pitch angle of the scoop or the 5th joint of the robot which can be controlled to change the incline of the pour and must be adapted to the flow type of the target material.



Figure 1. Robotic weighing setup

### 2.2. Powder Flow Characterisation

In weighing the amount of material poured depends on the incline of the scoop, the amount of material contained in the scoop and the flow type of the material. Data was collected using 10 different industrial grade powder materials of different flow types. Here, the parameters considered were physical properties such as aspect ratio, particle diameter and roundness, obtained from microscopy image analysis and particle size distribution, obtained using the Mastersizer-S Long Bench (Malvern Instruments Ltd., Malvern, UK). The angle of repose (AOR)[3] was experimentally obtained for the materials. According to [4], the magnitude of forces necessary to cause the flow of bulk material is a measure of the flowability of the material itself. In robotic weighing process, the mechanical forces arise from gravitational forces on changing the incline of the scoop, cohesive forces due to inter-particle interactions and adhesive forces due to friction between particles and the scoop surface. To characterise this, two parameters were introduced, the flow index  $\phi$ , which measures the ratio of the weight of powder dispensed to the weight of powder scooped and  $\theta_{min}$  the minimum angle of incline required to initiate flow. This definition is based on the hypothesis that for the same incline of the end effector, the amount of material poured is smaller for poor flowing materials with high cohesive and adhesive forces, compared to a freely flowing material.

Unsupervised clustering was performed on the obtained data using Matlab. Z-score normalization was applied due to the differing dimensions of the material properties. Clustering analysis in unsupervised learning partitions unlabelled data into groups based on similarity, aiming for high intra-cluster similarity and low inter-cluster similarity. This allows hidden

patterns in high dimensional datasets by creating a multilevel tree, as shown in Figure 2. , illustrating hierarchical relationships between the data clusters. In the resulting dendrogram, the horizontal axis contains the materials and vertical lines represent distance in similarity between two materials. Each material is most closely related to the material (or the cluster) on its immediate left. Three major clusters were created clearly distinguishing the materials.

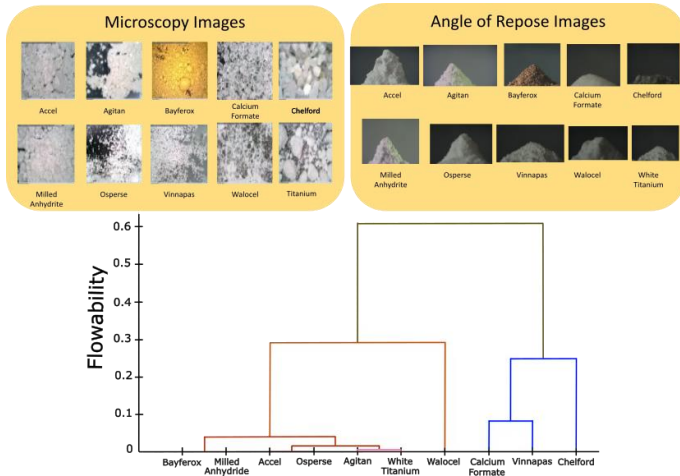


Figure 2. (a) – Cluster tree created from hierarchical clustering.

### 2.3. Proposed Control Algorithm

The angle of inclination  $\theta$  of the end effector is controlled using a simple P controller, where the starting angle  $\theta_0$  and the proportional constant  $P$  are chosen based on the flow type classification and the previous experimental results.

$$\theta = \theta_0$$

$$\frac{d\theta}{dt} = P((m_d - m_e) - m_a) \quad \text{when } m_a \leq m_d - m_e$$

Here,  $m_d$  is the desired target measurement,  $m_e$  is a set measurement error threshold and  $m_a$  is the current scale readings. The range of angles permitted lie between  $0^\circ - 90^\circ$  which corresponds to the 5<sup>th</sup> joint of the robot being completely horizontal to vertical. Practically, the angles were restricted within  $18^\circ - 70^\circ$ . The proportional constant acts as a speed coefficient at which the incline of the effector is changed. For instance, for a free-flowing material, both a low starting angle  $\theta_0$  and a low proportional constant  $P$  are required for a slow controlled pour and to avoid overshoot of the target measurement. Similarly, for a material with poor flow and a tendency to fall in clumps, a higher starting angle  $\theta_0$  and higher proportional constant  $P$  is required. As established, materials with lower flowability require a higher starting  $\theta_0$  to trigger flow, however, they also often tend to fall in clumps, thus controlling the pour is more difficult as the tendency to overshoot is higher. To improve the control algorithm to handle this case, the starting angle  $\theta_0$  and the proportional constant  $P$  were progressively reduced as measurement error exceeded a set measurement threshold  $m_e$ . This value scales with the target weight to be achieved and the amount of material that can fit in the scoop during a pour, which varies for different types of materials.

### 3. Discussion and Conclusion

The algorithm was deployed and tested using materials, of known flow types: free flowing, moderate flowing and poor flowing respectively. A target of 35 grams was set and five repetitions were carried out. The best results were obtained in the case of the free and moderate flowing materials, which

showed a standard deviation of 0.57g and 1.03g respectively. This demonstrates good repeatability and acceptable accuracy for batching processes. The mean cycle time of the process was 1.30 minutes with the robot in collaborative mode. For the poor flow type material, the standard deviation achieved was 2.683g and showed a high tendency to agglomerate on the scoop, requiring extremely high incline angles to initiate powder flow. Due to high cohesive forces the powder also flowed in large clumps which increased the tendency to overshoot. Reducing the angle of the end effector as the scale measurement got closer to the target gave more control over the flow but further testing must be carried out with a larger number of test materials and for a larger number of target weights to further validate the efficacy of the proposed algorithm for such type of materials. Additionally, in this study only the incline of the scoop is controlled, whereas certain materials might require more fine shaking motions in combination with changing of the incline. Different designs for the scoop could be considered to make it more suitable for different types of materials.

TABLE I. ROBOTIC WEIGHING CONTROL ALGORITHM RESULTS FOR A TARGET WEIGHT OF 35G

Material	Free flowing Material	Moderate Flowing Material	Poor Flowing Material
STDEV (g)	0.570	1.025	2.683
Mean (g)	34.800	35.400	38.800

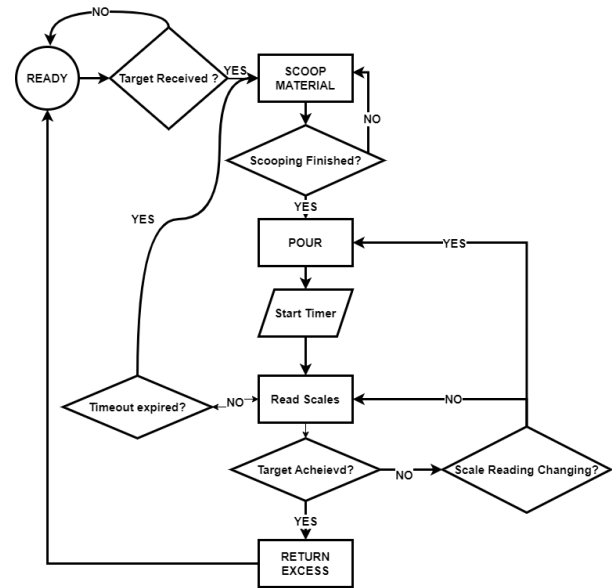


Figure 3. Workflow for the robotic weighing control algorithm

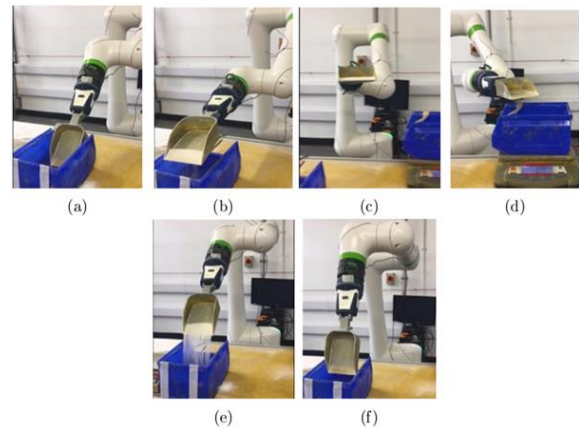


Figure 4. (a) - scooping state, (a) – (c) the scooped material is transported to the recipient container, (d) – robot reaching pouring pose. (e) – (f) robot returns excess material.

## Acknowledgement

The authors gratefully acknowledge the support received from Staffordshire Advanced Manufacturing, Prototyping, and Innovation Demonstrator (SAMPID) that is part funded through the European Regional Development Fund 2014–2020, project reference No: 32R19P03142.

## References

- [1] [1] Y. Kadokawa, M. Hamaya and K. Tanaka, "Learning Robotic Powder Weighing from Simulation for Laboratory Automation," in 2023 IEEE/RSJ International Conference on Intelligent Robots and Systems (IROS), pp. 2932-2939, 2023.
- [2] Y. Nakajima, M. Hamaya, Y. Suzuki, T. Hawai, F. von Drigalski, K. Tanaka, Y. Ushiku and K. Ono, "Robotic powder grinding with a soft jig for laboratory automation in material science," in 2022 IEEE/RSJ International Conference on Intelligent Robots and Systems (IROS), pp. 2320-2326, 2022.
- [3] G. Lumay, F. Boschini, K. Traina, S. Bontempi, J. Remy, R. Cloots and N. Vandewalle, "Measuring the flowing properties of powders and grains," Powder Technol, vol. 224, pp. 19-27, 2012.
- [4] D. Schulze, *Powders and bulk solids: behavior, characterization, storage and flow*. 2008.

# Simulation of UO<sub>2</sub> particles behavior in a powder rheometer

L. Cayla Arianer<sup>1,2</sup>, M. Leturia<sup>2</sup>, E. Daouk<sup>2</sup>, A-C. Robisson<sup>1</sup>, C. Ablitzer<sup>1</sup>, K. Saleh<sup>2</sup>

<sup>1</sup> : CEA, DES, IRESNE, DEC, Cadarache, France

<sup>2</sup> Université de technologie de Compiègne, ESCOM, TIMR, Compiègne, France

**Abstract**— The accurate simulation of powder rheometer is crucial for understanding the flow behavior of particulate materials in various industrial processes. This study presents a comprehensive approach to simulate the powder rheometer, starting with spherical particles to establish the numerical tools. Initially, simulations were conducted using spherical particles to validate the numerical framework and ensure the reliability of the simulation tools. Following this, the focus shifted to the simulation of non-spherical particles, achieved through calibration. Two methods were tested and compared. Finally, the study extended to simulating 'real' particles, represented here by uranium oxide model particles.

**Keywords:** DEM; calibration; uranium;

## 1. Introduction

The aim of this study is to develop a predictive model for hopper discharge in nuclear fuel manufacturing processes, focusing on the influence of powder flow properties. We try to establish a link between physical characteristics such as size, shape, and density [1], and powder flow behavior. To do so, we employ a methodology based on numerical modeling of a FT4 powder rheometer, widely used for assessing powder flowability [2].

## 2. Simulation of spherical particles

The considered FT4 geometry corresponds to a rotating blade passing through a powder bed (VFR test configuration). The system is simulated using the discrete element method (DEM), often used to analyze granular materials by calculating contact forces or particle velocity fields [3].

The developed model was first tested for millimeter-sized spherical glass particles. The implementation of digital tools was carried out using data from the literature. Then, the flow behavior of spherical particles in a geometry identical to that of the VFR test (cell size, filling, blade trajectory) was simulated.

## 3. Simulation of non-spherical particles

The simulation of non-spherical particles was then performed. Prior calibration of simulation parameters is required for non-spherical particles application [4]. A sensitivity study was conducted to determine which parameters best adjust the resulting force and torque in the rheometer. The influence of the Poisson's ratio, restitution coefficient, friction coefficient, and rolling friction on the flow energy was evaluated (Fig. 1).

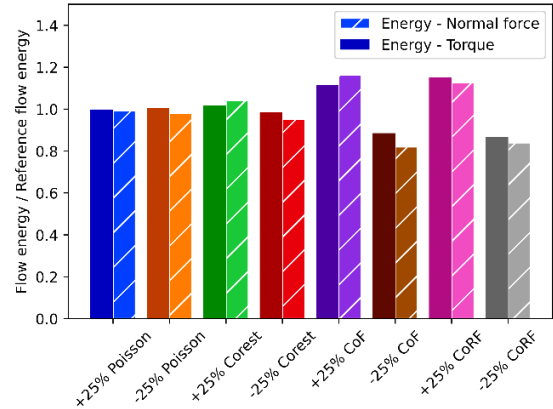


Figure 1. Influence of simulation parameters on normal force and torque

First, the calibration was performed using a trial-and-error method by adjusting only the rolling friction coefficient, as it is commonly used to account for particle morphology [5]. This calibration was carried out by comparing numerical results with experimental data, focusing on the force and torque measured on the blade during VFR tests. While this method is precise, it allows the adjustment of a single coefficient only. This method was compared to the LHS-Kriging-EGO method [6], which was used to calibrate both the friction and rolling friction coefficients. The results obtained with this calibration seem representative of the experimental behavior (Fig. 2).

By comparing the flow energy for both methods (Tab. 1), we can conclude that this second method is less precise than the previous one. However, LHS-Kriging-EGO enables the calibration of several parameters simultaneously, which is particularly important when simulating materials whose parameters are not available in the literature or are difficult to measure.

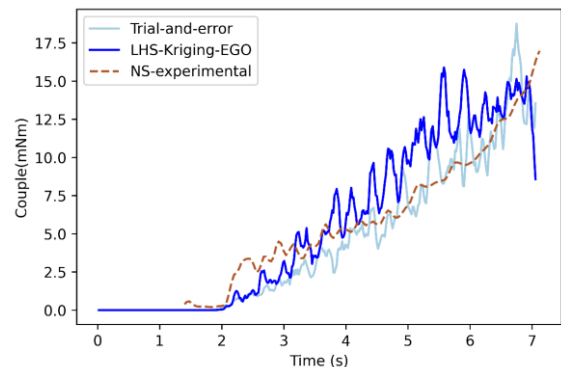


Figure 2. Comparison of the two calibrations methods for the simulation of glass particles

TABLE I. COMPARISON OF FLOW ENERGY FOR 2 CALIBRATIONS METHODS

	Flow energy (mJ)
Experimental	273
Trial-and-error	290
LHS-Kriging-EGO	360



## 4. Simulation of UO<sub>2</sub> particles

The next step is to apply this methodology to simulate the behavior of nearly spherical millimeter-sized uranium oxide particles (Fig. 3) in the studied geometry. Calibration is necessary to determine the parameters required for the simulation process since there is no data available on these powders.

Parameters determined by calibration are then applied for the VFR simulation of these UO<sub>2</sub> particles.

The parameters obtained through calibration are not consistent with the material properties. However, the simulation seems to reproduce the flow behavior of the powder in this geometry (Fig. 4).

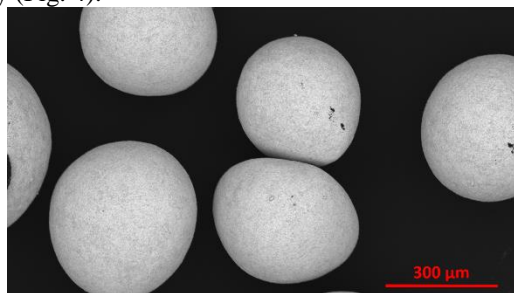


Figure 3. UO<sub>2</sub> model particles

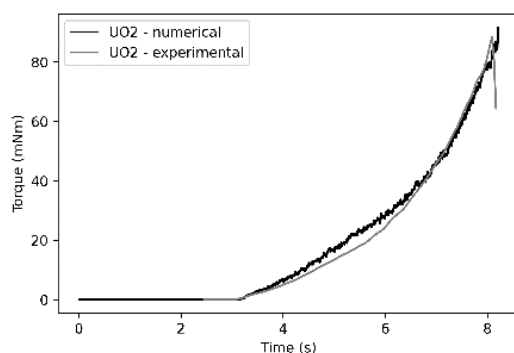


Figure 4. Force and torque after parameter calibration for the simulation of UO<sub>2</sub> particles

## 5. Conclusion

This study has demonstrated a successful approach to simulate the powder rheometer, beginning with spherical particles and advancing to the simulation of non-spherical and UO<sub>2</sub> model particles. The initial phase, validate the numerical tools required for accurate simulations. The calibration for non-spherical particles enabled the simulation of more realistic particle behavior. The comparison of the two calibrations methods highlights the pros and cons of each method.

Finally, simulating UO<sub>2</sub> particles provided a comprehensive understanding of the rheological properties of 'real' particles.

Future work will focus on further refining these models and exploring their applicability to a wider range of particulate systems, potentially incorporating additional factors such as particle cohesion or polydisperse size distribution. Validation by comparison with experimental data through PIV study can also be considered.

The simulation of other unit operations, such as hopper flow, can be useful to describe the flow behavior throughout the fabrication process.

## References

- [1] J. Petit, J. Burgain, C. Gaiani, and J. Scher, "Aptitude à l'écoulement de poudres alimentaires : impact des propriétés physicochimiques des particules," *Ind. Aliment. Agric.*, pp. 26–30, 2017.
- [2] X. Fu, D. Huck, L. Makein, B. Armstrong, U. Willen, and T. Freeman, "Effect of particle shape and size on flow properties of lactose powders," *Particuology*, vol. 10, no. 2, pp. 203–208, Apr. 2012, doi: 10.1016/j.partic.2011.11.003.
- [3] W. Fang, X. Wang, D. Han, and X. Chen, "Review of Material Parameter Calibration Method," *Agriculture*, vol. 12, no. 5, Art. no. 5, May 2022, doi: 10.3390/agriculture12050706.
- [4] C. J. Coetzee, "Calibration of the discrete element method and the effect of particle shape," *Powder Technol.*, vol. 297, pp. 50–70, Sep. 2016, doi: 10.1016/j.powtec.2016.04.003.
- [5] C. M. Wensrich and A. Katterfeld, "Rolling friction as a technique for modelling particle shape in DEM," *Powder Technol.*, vol. 217, pp. 409–417, Feb. 2012, doi: 10.1016/j.powtec.2011.10.057.
- [6] E. Beaunac, "Étude du lien entre les caractéristiques physico-chimiques des poudres et leur comportement lors des phases de transfert," Doctorat en Génie des procédés, Université technologique de Compiègne, 2021.

# Predictive Analysis for Ingredient Weighing Cycle Time in Manufacturing Industries

Ashwanth Vivakanantha<sup>1</sup>, Alison L Griffiths<sup>2</sup>, Mohammad M Ardekani<sup>3</sup>, and Charles Williams<sup>4</sup>

<sup>1</sup> Staffordshire University, Stoke-on-Trent, UK

<sup>2</sup> Promtek Ltd, Stoke-on-Trent, UK

**Abstract—** This study leverages big data and machine learning techniques to optimize the ingredient weighing process, enhancing predictability and control over production in line with Industry 4.0 principles. Collaborating with Promtek Ltd and Duffields South West Ltd, six months of data points were collected. Initial findings revealed intriguing insights, particularly the varying prediction accuracy for different ingredients, highlighting the potential for automation and AI in manual processes. This research highlights the importance of predictive analysis in strategic decision-making and process optimization.

**Keywords:** industry 4.0 and digitalisation; machine learning; ingredient weighing; smart manufacturing; big data

## 1. Introduction

In the realm of manufacturing industries specialising in ingredient handling and weighing, production output and time efficiency stand as pivotal metrics for generating profit. However, the inherently complex environment of ingredient handling plants necessitates continual optimisation of processes to enhance productivity, aligning with the principles of Industry 4.0 and digitalisation. A reservoir of untapped data exists that contains diverse features that are useful for gaining insights into ingredient handling optimisation and ripe for exploration through big data and ML techniques. The utilisation of machine learning and advanced data analysis techniques enables the optimisation of the ingredient weighing process, thereby achieving a more predictable outcome and ensuring greater control over productive output, all in line with the objectives of Industry 4.0. By harnessing this wealth of data, predictive models can be developed to anticipate variations in ingredient weighing, identify potential bottlenecks, and streamline operations.

This study aims to create predictive machine learning models to investigate patterns in different ingredients and their weighing cycle times. By identifying these patterns, managers can better detect slowdowns or irregular cycle times in future batches. Additionally, this analysis enables the identification of ingredients that could be optimised to improve the weighing cycle time, which would enhance overall production productivity and reduce costs. This is achieved through collaboration with Promtek, an ingredient handling systems specialist and Duffields South West Ltd an animal feed manufacturer, thereby gaining access to their extensive real-world dataset.

The paper begins with a concise literature review to provide context and highlight relevant research in the field. This is followed by a detailed explanation of the methodology employed to obtain the results. Subsequently, the results are discussed, and finally, the paper concludes with a summary of the findings and their significance.

## 2. Literature Review

[1]The current era of food manufacturing is supercharged with Big data and becoming essential in the advancement of new product development (NPD). As businesses need to

consistently adapt to raw material prices, operational costs and customer demand, developing new products or reformulating current products can be complicated. By leveraging Big data that captures all the production operations, companies can reduce NPD costs and time without affecting the quality of the product.

Apart from that, [2]leveraging big data and machine learning to forecast production planning by focusing on predicting energy consumption at the batch level can be a strategic method for increasing productivity in a manufacturing plant.

A traditional company located in Yorkshire, specializing in the production of water crackers and biscuits, was experiencing poor financial performance due to underutilized capacity and inconsistencies in product quality and taste across technically identical production lines. [3]By utilizing a large dataset of approximately 250,000 real-time data points collected over a six-month period, the company was able to fine-tune product quality by identifying the 'perfect conditions' that lead to consistent, high-quality products and identify the casualty of the inconsistencies. This approach significantly reduced inconsistencies between batches, leading to improved product quality and operational efficiency.

## 3. Methodology

Due to the nature of the real-world dataset, data preprocessing is required to prepare it for machine learning. This preprocessing is necessary because some data points have abnormal values, which can be attributed to machine failures or operator errors in data entry.

### 3.1. Data collection

Six months of data were collected, encompassing approximately 200,000 data points with various features relevant to determining the weighing cycle time of ingredients. These features included the date and time, ingredient information, target weight, and the final measured weight of the ingredients. Additionally, operator data were considered to investigate potential performance differences between operators and the impact of their shift times on the weighing cycle time.

### 3.2. Preprocessing and outlier removal method

The next step involved preprocessing and outlier removal, as illustrated in Figure 1. The dataset was initially grouped by ingredient ID and target weight. This grouping was crucial to ensure that the outlier filtration process was based on target weight rather than the entire dataset, which would have skewed the filtration. This method demonstrated improved performance in noise reduction compared to applying outlier filtration directly to the whole dataset.

Following this, Tukey's method for outlier removal was applied to the grouped dataset, focusing on the weighing cycle time. This approach removed data points with weighing cycle times outside the interquartile range, which were considered noise. Grouping by target weight was essential as the interquartile range values differ between target weights. Additionally, data points where the measured weight was 0 kg

despite a non-zero target weight were removed, indicating faulty data.

### 3.3. Machine learning Modal

After filtering the data, machine learning models were applied. Three supervised regression models were tested: Linear Regression, XGBoost, and Random Forest. Random Forest and XGboost regression exhibited the best performance in predicting the cycle time. However, Random Forest had a greater computational efficiency among the algorithms used. Consequently, Random Forest was selected to interpret the results, which will be elaborated further in the next section.



Figure 1. Flow Chart of preprocessing and outlier removal method used

## 4. Discussion

This experiment was conducted using three different weighing methods: automatic weighers, bagged weighing, and manual weighing. Automatic weighing was used for ingredients in very large quantities, typically above 100 kg. This process involves trucks loading ingredients into bins that store various ingredients, as illustrated in Figure 2, where the yellow colour in the bins indicates the capacity of ingredients. Once ready, the automatic weighers signal which ingredient to dispense from the bin onto the weigher. The dispensing continues until the target weight is reached, and the cycle time is recorded. For manually weighed ingredients, an operator pours the ingredient onto a weighing scale and interacts with a user interface, as shown in Figure 3. When the indicator changes from red to green, the target weight is reached, and the cycle time is recorded. Bagged weighing is performed in 25 kg increments, with an operator directly pouring the ingredient into the weigher, as shown in Figure 4. For batches requiring weights slightly offset from the 25 kg increment, such as 27 kg, the process involves manually weighing the additional 2 kg before adding the 25 kg bagged weight.

### 4.1. Results

Initial findings reveal intriguing results, particularly in the prediction accuracy for different ingredients. Ingredients, primarily weighed using automatic weighing machines, exhibit overall good prediction accuracy as shown in Figure 2 which indicates automatic weighing exhibits a linear cycle time with target kg. Furthermore, insights examined from the study highlight poorer prediction accuracy for manually weighed as seen in Figure 3 and bagged ingredients Figure 4, indicative of inconsistencies in human operator efficiency, highlighting the potential for automation and AI assistance in enhancing manual processes within digitalised manufacturing settings. Although the prediction accuracy is low, patterns can be identified between the manually weighed and bagged ingredients and the operator handling the ingredients, paving the way for continuous improvement.

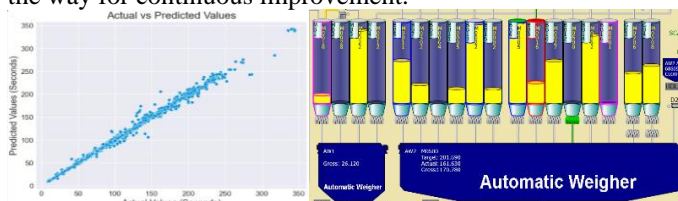


Figure 2 Bulk weighed ingredient

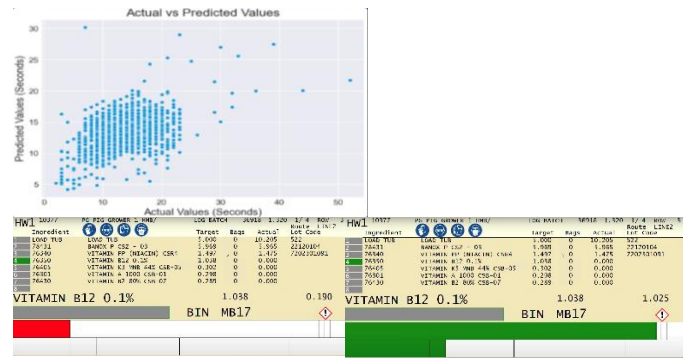


Figure 3 Manually weighed ingredient

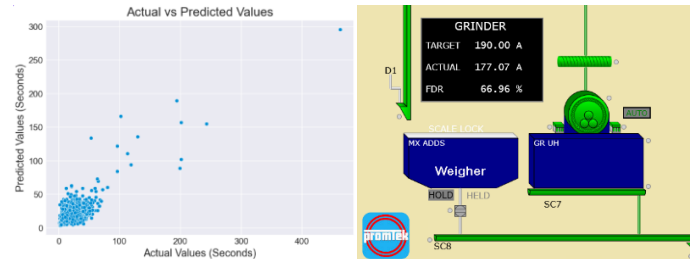


Figure 4 Bagged weighed ingredient

## Conclusion

In conclusion, these insights can prompt the client to explore avenues for optimising the weighing process, aligning with the objectives of Industry 4.0 and digitalisation. Equipped with a deeper understanding of which ingredients or processes warrant priority optimisation, the ingredient handling manufacturing plants can effectively enhance profitability and productivity while mitigating excessive costs, energy usage and carbon emissions, showcasing the tangible benefits of integrating AI and ML into manufacturing workflows. This study highlights the significance of predictive analysis in guiding strategic decision-making and process optimisation, ultimately fostering a more agile and adaptive environment within manufacturing industries, in line with the transformative vision of Industry 4.0.

## Acknowledgement

The authors gratefully acknowledge the support received from Knowledge Transfer Partnership(KTP), funded through the UK Research and Innovation (UKRI), project reference No: 10063959. As well as Promtek Ltd an ingredient handling systems specialist that provided support and execution of the project, Duffields South West Ltd for providing their dataset information that was used for the project and finally Staffordshire University for their academic experts.

## References

- [1] S. Jagtap and L. N. K. Duong, 'Improving the new product development using big data: a case study of a food company', *Br. Food J.*, vol. 121, no. 11, pp. 2835–2848, Jan. 2019, doi: 10.1108/BFJ-02-2019-0097.
- [2] C. Morariu, O. Morariu, S. Răileanu, and T. Borangiu, 'Machine learning for predictive scheduling and resource allocation in large scale manufacturing systems', *Comput. Ind.*, vol. 120, p. 103244, Sep. 2020, doi: 10.1016/j.compind.2020.103244.
- [3] S. K. et al, 'Towards design and implementation of Industry 4.0 for food manufacturing Jan 2021 doi=10.1007/s00521-021-05726-z

# 3D graphical representation technique for complex-shape particles and DEM modelling

Yani Alhaddad<sup>1</sup>, Álvaro Ramírez-Gómez.<sup>1,2</sup>

<sup>1</sup> Departamento de Ingeniería Mecánica, Química y Diseño Industrial. Escuela Técnica Superior de Ingeniería y Diseño Industrial. Universidad Politécnica de Madrid. Ronda de Valencia, 3. Madrid, Spain.

<sup>2</sup> Centro Tecnológico de Seguridad y Calidad en Industrias Energéticas y Minas (TECMINERGY). Madrid, Spain.

**Abstract—** The shape of complex particles is often approximated in DEM simulations, in part because implementing realistic shapes remains a challenge. This research proposes a procedure for simplifying the representation of complex shapes using structured light scanning technology, with a focus on minimizing computational cost. The method provides an approximated shape using the minimum bounding box volume, followed by a simplified triangulation. A batch of woodchip particles, ranging in size from approximately 1 to 8 cm, was used in this study. The procedure begins by obtaining point clouds that accurately represent the real shapes of the particles. These data are then processed using 3D point cloud editing software and a numeric computing platform for the analysis and algorithm development. Initially, the dimensions of the minimum volume of the bounding boxes surrounding the scanned particles are determined. The next stage involves simplifying the point clouds by reducing the number of points, thereby minimizing the computational cost of processing large datasets. Simplification is achieved by applying the convex hull method to the three projections of the point clouds across each coordinate plane of the bounding box, reducing the number of nodes and faces based on the desired minimum distance between nodes. Subsequently, a hierarchical approach is employed, using triangular tessellation to represent the simplified particle shapes. The differences in volume and surface area between the original and simplified particle representations are analyzed. This research provides valuable insights into the challenges of representing complex particle shapes for DEM modelling.

**Keywords:** particle shape; computational cost; point cloud; triangulation; DEM.

## 1. Introduction

The simulation of particle interactions is an option when trying to understand phenomena in many industrial processes, such as storage, conveying, transport, milling, mixing, and many others. The discrete element method (DEM) is a numerical technique introduced by Cundall and Strack in 1971 that allows to simulate the interactions of particles and predict their behaviour [1]. In DEM simulations, the efficiency of the simulation is heavily influenced by the geometric complexity of the particles, as more complex shapes require more computational resources to determine interactions and monitor the particle movements during the simulation. DEM provides several approaches that can be followed to represent the particle shape, but these methods could also require high computational costs, especially with complex shapes. Therefore, developing the representation methods to simplify complex particle shapes without highly affecting accuracy is essential for practical applications to achieve the balance between representation, accuracy, and DEM simulation efficiency. Different approaches and methods can be used in the discrete element method, starting

from the simplest representation with spheres, advancing through polyhedral shapes, and reaching triangulation for a highly realistic representation [2-4]. Several triangulation methods can be considered, beginning with Delaunay triangulation, which maximizes the minimum angle of triangles to prevent acute triangles [5, 6], and alpha shapes, which generalize the concept of convex hulls to more accurately capture the shape of a point set [7]. The  $\alpha$ -shape depends on the value of  $\alpha$ , which determines the level of detail captured. When  $\alpha$  is small, fine details are captured, and concave shapes become apparent. When  $\alpha$  is large, the  $\alpha$ -shape approximates the regular convex hull that encloses all points. This produces a complex hull that can capture finer details with higher complexity than a simple convex hull. Although these methods can represent shapes with higher detail, they also demand significant computational resources due to the extensive data sets involved. The data sets from identifying numerous nodes with short triangle edges and a large number of particles are real obstacles for the DEM simulation.

This research proposes a method to represent complex-shaped particles that reduces the data required for shape representation, thereby overcoming the limitations of DEM modelling software. The approach provides a systematic process for DEM, automatically controlling points based on triangle lengths in the convex hull using fewer points.

## 2. Methodology

The method includes shape detection using a structured light scanning technology to extract 3D point clouds. A sample of woodchips with complex shapes ranging from 1 to 8 cm has been used. The selected scanning technology detects surface details with an accuracy of 2 mm. The method utilizes software for editing and processing and a custom code for auto-shape representation using a numeric computing platform. The code will implement the desired commands and functions on the data sets of the particle shape to obtain the particle's representation. The code provides two representations of the complex shape, starting from the minimum volume of a bounding box (MVBB) to a simplified triangulation based on the minimum distance desired between the nodes in the convex hull of the 2D projection [8, 9]. The methodology is divided into two main stages: particle scanning and post-processing, followed by shape approximation and simplification.

### 2.1. Stage 1: Particle scanning and post-processing

Fig.1 illustrates the steps followed for particle scanning and post-processing. The process begins with scanning a batch of 5-15 particles, which takes approximately 3-4 minutes to capture the intricate details. After scanning, the captured data undergoes several post-processing steps as point clouds form where the coordinates of each point on the particle surface can be found.

The first step consisted of reconstructing the point clouds by checking the layers' overlapping and filling the gaps produced at the bottom of the particles. The point cloud is then segmented



to obtain individual particle data, with each point's coordinates stored in the Polygon File Format format (PLY).

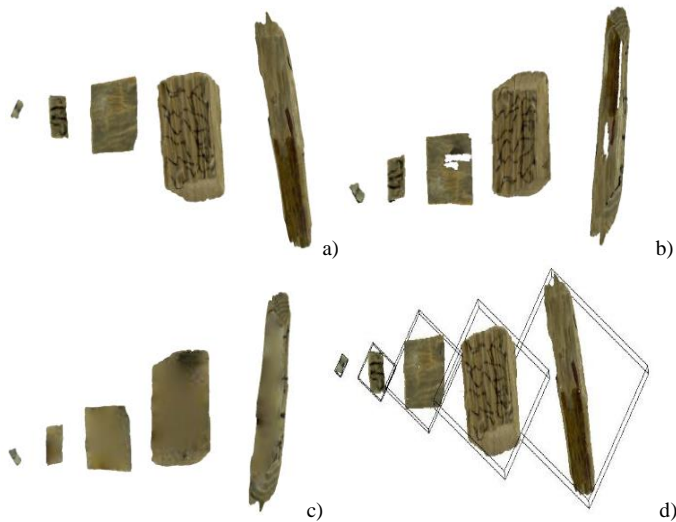


Figure 1. Scanned particles and post-processing, a) scan of five woodchips particles, b) first post-processing step with gaps detection, c) gaps filling, d) particles' segmentation.

## 2.2. Stage 2: Shape approximation and simplification

### Minimum volume of a bounding box

The first representation in this approach begins with the minimum volume of a bounding box, which is considered the simplest method. This technique detects the smallest box that can enclose the point cloud of each scanned particle. It is highly efficient for the automated detection of a large number of particles and allows for automated computation and data export to DEM software. While this method results in fewer points for modelling, it comes at the cost of reduced accuracy.

Fig.2 illustrates the particle before and after detecting the minimum volume of the bounding box. The first step in this approximation is to measure the approximate mean center and the longest length of the point clouds. The second step is to align the longest length of the particle on a center axis. Then, a 360-degree rotational view around the three center axes was implemented to detect the minimum volume of the bounding box, which includes all the points of the particle.

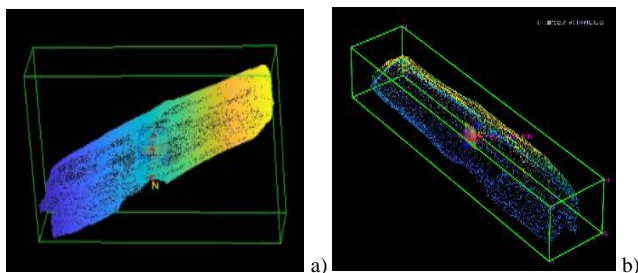


Figure 2. Detection of the minimum volume of the bounding box: a) the initial bounding box, b) the minimum volume of a bounding box was detected.

### Simplified triangulation

The second approach uses hierarchical triangular tessellation to represent a simplified particle shape and extract meaningful geometric structures of three-dimensional point clouds.

This approach begins by detecting the 2D projection of the minimum bounding box for the particle's points and identifying the convex hull with a reduced number of points. Initially, point clustering is performed in three orthogonal 2D projections (XY, XZ, and YZ planes).

A threshold distance is then applied to control the minimum distance between points in the convex hull. This clustering step simplifies the point cloud. The algorithm calculates a distance matrix for the points, clustering those closer than the specified threshold. Clusters are merged iteratively by selecting the maximum x and y coordinates among clustered points. The algorithm continues to detect and exclude undesired points, ensuring that all remaining clusters have a minimum distance greater than or equal to the threshold. The code keeps detecting all the distances after excluding any point to ensure that all undesired points are excluded.

Each projection undergoes a clustering phase to capture its boundary, where points are iteratively merged based on their coordinates. Unique points from all projections are then consolidated, ensuring no duplication, and used to construct a 3D triangulation through triangulation techniques.

This triangulation of the extracted points gives a good representation, facilitating visual analysis and shape simplification of the original point cloud for DEM simulation. The approach also supports automated computation and data export, eliminating the need for manual intervention to simplify and detect each particle separately.

Fig.3 shows the particle shape and original convex hull of one scanned particle (left) and the simplified 2D projection with a minimum distance of 5 mm between any two points (right). Providing a desired distance between nodes reduces the data extracted, and controls shape representation based on modelling limitations.

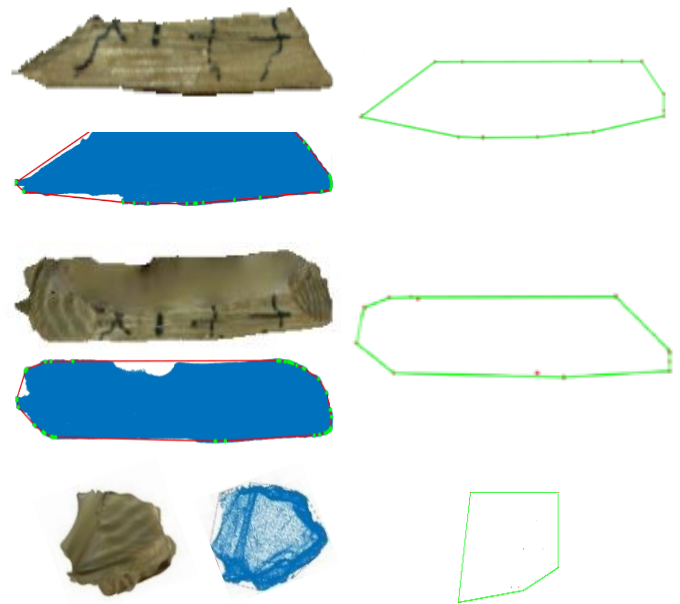


Figure 3. The particle shape and original convex hull of points clouds in the (left) and the simplified convex hull with a 5 mm minimum distance for the three "2D points projections" of the minimum volume of the bounding box (right).

By excluding undesired distances between nodes, the code generates a prism shape, along with the nodes, triangles, and connectivity matrices needed for further DEM modelling steps, providing the necessary particle shape data.

Fig.4 shows the original triangulation for one particle and the level of simplification achieved. The three results displayed have minimum distances between points in the convex hull set at 2 mm, 5 mm, and 10 mm, respectively. The exclusion of points reduces the data required to model the particles while maintaining a high representation of the general shape boundaries, with the desired simplification based on the threshold value.

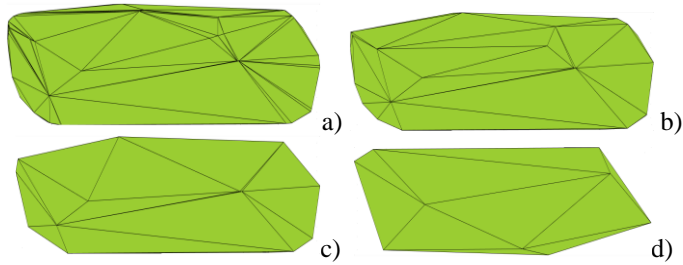


Figure 4. Original and simplified triangulation. a) Delaunay triangulation of points with the original convex hull, b) 2 mm minimum distance between the nodes, c) 5 mm minimum distance between the nodes, d) 10 mm minimum distance between the nodes.

### 3. Results and discussion

Table I compares the original triangulation with the shape approximation and simplification implemented with the code. The first approximation involves the minimum volume of the bounding box, followed by various minimum distances in the convex hull (Min D) for the simplified triangulation: 0 mm, 2 mm, 5 mm, and 10 mm. The table includes the time (T) required to obtain each representation, the volume (V), and the particle's surface area, along with differences from the original point cloud representation. Table II shows the differences in overall processing and detection of the shape representation, whether it was manual or automated processes, starting from data importing and exporting (Data Imp, Exp), segmentation, and the accuracy of the original segmented points with (MVBB), in addition to the accuracy of the shape simplification, also the numbers of points were included. The code showed better data importing and exporting through an automated approach for the original points and high accuracy with the simplification method for both the minimum volume of the bounding box and the simplified triangulation. The code required more time with lower commands but with the desired simplification of the point cloud. The code showed high detection accuracy of the minimum volume of the bounding box without being affected by the original vertices. As expected from the differences in volume (V) and surface area (SA), the MVBB showed the highest values compared with the original triangulation of the particles. The code achieved 0% differences from the original triangulation with a 0 mm threshold value. The other values with 2 mm, 5 mm, and 10 mm showed lower values of (V) and (SA). These variations can be attributed to the complexity of the particles, including the presence of sharp edges, surface concavities, roughness, and the threshold value used.

TABLE I. COMPARISON BETWEEN ORIGINAL AND SIMPLIFIED TRIANGULATION

Type	Original triangulation, MVBB, and simplification for one particle with 59064 points, with 2, 5, and 10 mm as minimum D						
	T (s)	Min D	V cm <sup>3</sup>	$\Delta V$ %	SA cm <sup>2</sup>	$\Delta SA$ %	#P
Original	2.09	-	9.224	-	33.397	-	96
MVBB code	20	0mm	17.17	46.2	52.36	36.2	8
Convex hull - code	25.28	0mm	9.224	0%	33.397	0%	96
Convex hull - code	37.15	2mm	8.401	8.92	32.073	3.96	39
Convex hull - code	35.26	5mm	7.266	21.2	30.732	7.98	22
Convex hull - code	34.32	10mm	6.973	24.4	28.739	13.9	13

TABLE II. OVERALL COMPARISON BETWEEN THE TWO APPROACHES

Type	Original triangulation and the simplified methods					
	Data Imp, Exp	Segmentation	MVBB Accuracy	Min D Accuracy	No. Points	Simplification
Original	Manual	Manual	Low	High	Higher	No
Code	Automated	Automated	High	High	Lower	Yes

### 4. Conclusion

This research introduced a method to improve the detection and simplification of particle shape for (DEM) simulations using structured light scanning technology. By employing the minimum volume of the bounding box, combined with the convex hull and triangulation, the study proposed an approach to simplify complex geometries and reduce the computational cost. A cluster detection algorithm, ensuring a minimum distance threshold between points, is applied to the "2D projections" of the orthogonal planes of the minimum bounding box. This approach gave a simplified 3D triangulation that maintains the outer shape boundaries of the particles while reducing the number of representation points. The method demonstrates lower complexity for the simplified shapes, making it more suitable for DEM simulation than other methods. The simplified point cloud shows significant differences in the number of points, with consideration of the desired minimum distance between nodes. An automated code streamlines the entire process, eliminating the need for manual intervention and user interface for shape simplification in each particle. The method exhibits high detection capability and rapid determination times while adhering to software limitations and effectively removing clustered points.

This study emphasizes both simplicity and practicality, making it valuable for various industrial applications involving large particles, simplified shapes, and modelling processes in the simulation stage. Future work will focus on reducing the time required, improving the segmentation of scanned particles with an automated technique, and enhancing the detectability of smaller particles using more advanced scanning technology.

### References

- [1] P. A. Cundall and O. D. L. Strack, "A discrete numerical model for granular assemblies," *Géotechnique*, vol. 29, no. 1, pp. 47–65, Mar. 1979, doi: 10.1680/geot.1979.29.1.47.
- [2] U. Radvilaitė, Á. Ramírez-Gómez, D. Rusakevičius, and R. Kačianauskas, "Semi-analytical models of non-spherical particle shapes using optimised spherical harmonics," *Chem. Eng. Res. Des.*, vol. 137, pp. 376–394, Sep. 2018, doi: 10.1016/j.cherd.2018.07.031.
- [3] F. Alonso-Marroquín et al., "Experimental and numerical determination of mechanical properties of polygonal wood particles and their flow analysis in silos," *Granul. Matter*, vol. 15, no. 6, pp. 811–826, Dec. 2013, doi: 10.1007/s10035-013-0443-7.
- [4] J.-P. Latham, A. Munjiza, X. Garcia, J. Xiang, and R. Guises, "Three-dimensional particle shape acquisition and use of shape library for DEM and FEM/DEM simulation," *Miner. Eng.*, vol. 21, no. 11, pp. 797–805, Oct. 2008, doi: 10.1016/j.mineng.2008.05.015.
- [5] "B. Delaunay, 'Sur la sphère vide,' *Izvestia Akademii Nauk SSSR, Otdelenie Matematicheskii i Estestuentzyka Nauk*, vol. 7, pp. 793–800, 1934. (In French)."
- [6] B. Joe, "Construction of three-dimensional Delaunay triangulations using local transformations," *Comput. Aided Geom. Des.*, vol. 8, no. 2, pp. 123–142, May 1991, doi: 10.1016/0167-8396(91)90038-D.
- [7] H. Edelsbrunner and E. P. Mücke, "Three-dimensional alpha shapes," *ACM Trans Graph*, vol. 13, no. 1, pp. 43–72, Jan. 1994, doi: 10.1145/174462.156635.
- [8] J. O'Rourke, "Finding minimal enclosing boxes," *Int. J. Comput. Inf. Sci.*, vol. 14, no. 3, pp. 183–199, Jun. 1985, doi: 10.1007/BF00991005.
- [9] "F. P. Preparata and M. I. Shamos, 'Computational Geometry: An Introduction,' 1st ed., Springer-Verlag, 1985, pp. 95–149., 1985, pp. 95–149.

# A simulation model development for moisture migration in glass beads under oscillations

V. Gurung<sup>1</sup>, K. Williams<sup>1</sup>, D. Ilic<sup>1</sup>, A. Lavrinec<sup>1</sup>

<sup>1</sup> School of Engineering, The University of Newcastle, Callaghan NSW 2308, Australia

**Abstract—** This study aims to develop a calibration procedure for coupled Discrete Element Method (DEM) and Smoothed Particle Hydrodynamics (SPH) simulation of moisture migration. A simulated parametric study is conducted to determine the influencing parameters affecting the movement of moisture in a bed of glass beads. The results indicate fluid viscosity as the prominent parameter affecting the flow of moisture in the simulations.

**Keywords:** moisture migration; modelling; DEM; SPH

## 1. Introduction

In the bulk material handling industry, moisture migration presents significant challenges, especially during maritime transport. Oscillations due to a ship's motion, caused by ocean waves, can mobilize moisture within the granular-bulk material during transport. This mobilization can result in a slurry-like or wet and sticky bulk solid state, with variability in moisture profile during unloading. This heterogeneity within the bulk solid complicates material handling process and poses safety risks, including potential ship capsize due to liquefaction [1].

Particle and moisture interactions can be examined in detail using numerical modelling. However, real materials contain particles of various shapes and sizes, making full Particle Size Distribution (PSD) computationally intensive to model. This study uses a coupled DEM and SPH approach to model moisture migration, with DEM representing solid particles and SPH representing liquid. The model is simplified by using spherical glass beads representing the bulk solid material, eliminating PSD complexities and model materials at the experimental scale. An initial parametric study identifies influencing parameters. Subsequently, moisture migration under oscillations will be modelled using the developed calibration method.

## 2. Experimental Method

### 2.1. Material Characterization

The material properties of the glass beads, including PSD, particle density, and free-drained saturated (FDS) moisture content, were determined experimentally. PSD was analysed by mechanically sieving the beads through 4 mm and 3.5 mm aperture sieves, with the material retained in the 3.5 mm sieve used for experiments. Particle density was measured using a nitrogen gas pycnometer. The FDS moisture content, indicating the maximum water retention capacity under static gravitational conditions, was determined using the setup shown in Fig. 1.

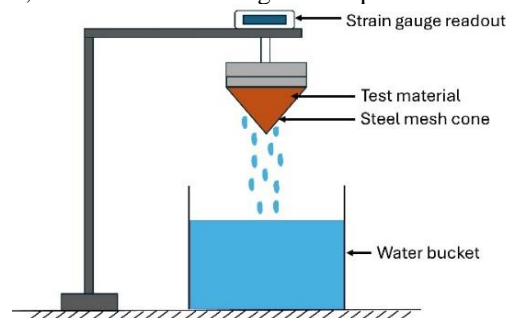


Figure 1: Schematic diagram of the FDS moisture content test

This involved filling a steel mesh cone with 500 grams of dry glass beads, then fully submerging it in water for 30 minutes. After soaking, the cone was lifted, and the weight of the material was recorded every 15 minutes until the variation in weight was  $\leq 1\%$ . The FDS moisture content was calculated based on the amount of water retained in the sample. Results from the characterization tests are summarized in TABLE I.

TABLE I: Material characterization test results for glass beads

Material property	Experimental values
Particle size	(3.5 – 4) mm
Particle density	2510 kg/m <sup>3</sup>
Free-drained saturated (FDS) moisture content	2.39 %

### 2.2. Calibration Experiment

The calibration experiment involved a static water drainage test, as shown in Fig. 2, to measure the water retained by the glass beads for validation. Approximately 8 grams of water were added to 20 grams of glass beads in a tube measuring 100 mm in length and 20 mm in diameter. A perforated steel mesh at the bottom of the tube held the glass beads while allowing water to drain when the rubber stopper was removed. Once drainage ceased, the amount of water retained by the glass beads was recorded.

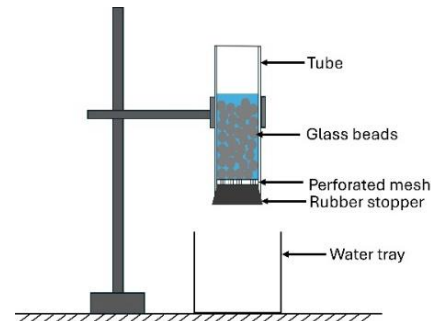


Figure 2: Static water drainage experiment

## 3. Modelling and Simulations

Simulations were performed using Ansys Rocky 2024 R1. The DEM phase utilized the Hertz-Mindlin model with Type C rolling friction to calculate contact forces between particles. For SPH elements, the Wendland kernel function estimated local fluid properties based on neighbouring SPH elements. Coupling between the DEM and SPH models was achieved through solid-fluid no-slip boundary conditions [2].

### 3.1. Calibration simulations

To reproduce the experiments, we need specific simulation parameters. Typically, DEM particle calibration uses the Bulk Calibration Approach (BCA), adjusting particle sliding friction (PF) and rolling friction (RF) coefficients [1]. This method validates simulation results based on the material's bulk flow behaviour. However, current study focuses on assessing moisture flow within bulk materials, requiring an understanding of the simulation parameters affecting SPH element movement within DEM particles. The simulation setup is shown in Fig. 3. For the static water drainage test, 8 grams of SPH elements were



added to 20 grams of mono-sized 3.5 mm spherical DEM particles in a tube with dimensions matching the calibration experiment. The mixture was allowed to settle for 5 seconds before the bottom lid was opened to let the SPH elements to drain.

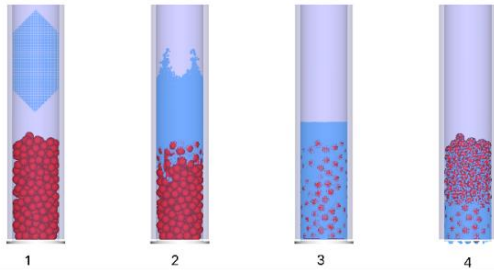


Figure 3: Calibration simulation

A parametric study was conducted to analyse the effects on SPH element flow. Table II summarizes the model parameters and iteration values for the study. The ratio of DEM to SPH was varied by adjusting the size of SPH elements in the simulations.

TABLE II: Simulation model parameters iteration values

Model parameter	Parameter iteration	Units
SPH Element Size (DEM/SPH ratio)	3: 1: 8	[-]
Particle sliding (PF) and rolling friction (RF) coefficients	0.1: 0.1: 0.9	[-]
Fluid viscosity	1: 50: 200	[cP]

## 4. Results

### 4.1. Simulation Results

This section presents the simulation results for 25 seconds using the parameters listed in Table II. The graphs illustrate the mass of water, represented by SPH, retained within the DEM particle assembly after the bottom lid was removed.

#### 4.1.1. DEM/SPH ratio

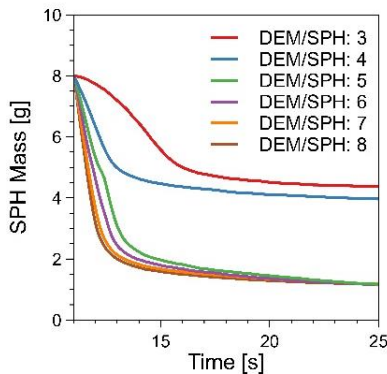


Figure 4: Moisture migration curves for varying DEM/SPH ratio

#### 4.1.2. Particle Sliding and Rolling Friction Coefficients

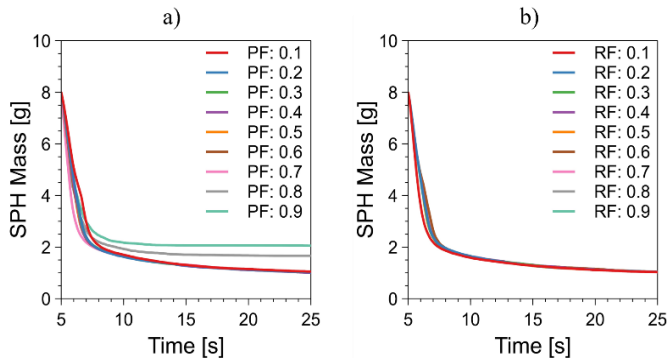


Figure 5: Moisture migration curves for varying particle a) sliding friction and b) rolling friction coefficients

### 4.1.3. Fluid Viscosity

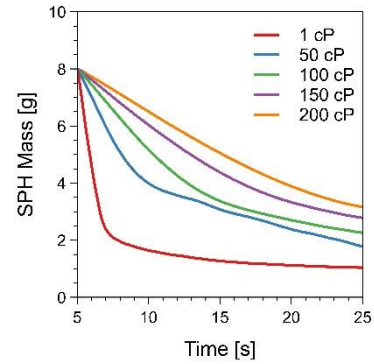


Figure 6: Moisture migration curves for varying fluid viscosities

The results from the parametric study suggest maintaining a minimum DEM to SPH size ratio of 5 to mitigate the effects of SPH element size. Additionally, the effects of particle sliding and rolling friction are minimal. Fluid viscosity, however, significantly impacts water retention in DEM particles.

### 4.1. Calibration Experiment Test Results

This section shows the experimental test results of the static water drainage test, where the mass of water retained by the glass beads were measured.

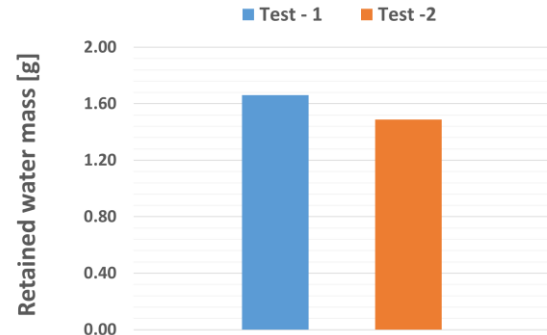


Figure 7: Retained water mass in glass beads

## 5. Conclusion

The effects of particle sliding and rolling friction, used in the BCA approach, appear minimal on SPH element flow. A full factorial simulation results of these parameters are needed for a conclusive assessment. Materials like glass beads, which have low water retention capacity and smooth water flow, maybe simulated by adjusting only sliding and rolling friction, which will be assessed. However, fluid viscosity could be a crucial parameter showing possibilities to model complex materials like coal and iron ores.

## Acknowledgement

The authors acknowledge the funding support from the Australian Research Council for the ARC Centre of Excellence for Enabling Eco-Efficient Beneficiation of Minerals, grant number CE200100009.

## References

- [1] J. Chen, O. Orozovic, K. Williams, J. Meng, and C. Li, "A coupled DEM-SPH model for moisture migration in unsaturated granular material under oscillation," *International Journal of Mechanical Sciences*, vol. 169, p. 105313, 2020/03/01/ 2020, doi: <https://doi.org/10.1016/j.ijmecsci.2019.105313>.
- [2] A. V. Potapov, M. L. Hunt, and C. S. Campbell, "Liquid-solid flows using smoothed particle hydrodynamics and the discrete element method," *Powder Technology*, vol. 116, no. 2, pp. 204-213, 2001/05/23/ 2001, doi: [https://doi.org/10.1016/S0032-5910\(00\)00395-8](https://doi.org/10.1016/S0032-5910(00)00395-8).



# Investigating the influence of ultrasonic waves on the wall friction of bulk solids

Rike Pfeufer<sup>1</sup>, Hans Schneider<sup>1</sup>

<sup>1</sup> Zeppelin Systems GmbH, Friedrichshafen, Germany

**Abstract**— In today's industry, the handling and storage of bulk materials play an important role but pose challenges due to the diverse properties of particulate solids. Traditional silo designs focus on mass flow, but funnel flow remains problematic. Avoiding funnel flow often requires expensive and space-consuming solutions. Discharge aids like vibration and ultrasound are employed, though their impact is not fully understood. A novel method for measuring wall friction using a translational shear tester and ultrasound device has been developed, showing promising results in reducing wall friction for limestone powder. These findings suggest potential industrial applications for improved silo design with ultrasonic-assisted discharge. The initial tests indicate that the frequency and intensity of ultrasonic waves are key parameters, and additional experiments to determine their impact are necessary. Further research is needed to optimize energy consumption and efficiency, as well as to validate the effectiveness of ultrasound in enhancing flow profiles and reducing space requirements for silos.

**Keywords:** silo; flow; powder; ultrasound; discharge

## 1. Introduction

In modern day's industry, production processes rely heavily on bulk solids. Whether they form the raw material, an intermediate or the final product, storage and handling of bulk material is an indispensable part of most production processes. However, challenges arise from the variety of properties of particulate solids. Especially flowability poses issues in material storage. Although the theory behind silo design is well established, there are still numerous effects concerning flowability that have yet to be investigated. One of the key challenges in designing silos is the prevention of funnel flow. To mitigate this effect, one approach involves utilizing steep cones with preferably smooth surfaces for discharge. However, this solution requires additional space and results in higher investment costs. Alternatively, the implementation of discharge aids is common practice, though proper rules for silo design are missing. Different discharge aids for cohesive powders have been developed, but the applications rely mostly on experience rather than the knowledge on physical mechanisms. [1,2]

## 2. Vibration as a discharge aid

Some efforts have been made to understand the effects of discharge aids. Kollmann [3] and Haack [4] have already investigated the effect of vibration of fine and cohesive powders. In their work they used a vibration-induced translational shear tester to study the attenuation of the vibration in the bulk solid.

Schwenke [5] and Kache [6] studied vibration-induced flow of powder material from silos. Using vibration cones and vibrational shear tests helps to understand the effect of vibration on powder flowability.

However, vibration cones are not the only discharge aids based on vibrations. Ultrasound is already established in industry as a discharge aid to improve gravity flow in silos and hoppers. While the aforementioned studies focus on vibration

with a frequency up to 200 Hz, ultrasound operates with frequencies above 20 kHz [7, 8]. Therefore, more research on the impact of these high frequencies is needed.

## 3. Experiments on ultrasonic impact on wall friction

In response to this challenge, a novel method for wall friction measurements has been developed. The set-up consists of a translational shear tester with an ultrasound device. This allows the evaluation of the ultrasonic impact on effective wall friction across different combinations of bulk solids and wall samples. By positioning the ultrasound converter directly on the wall sample, ultrasonic waves penetrate the wall and interact with the bulk material, thereby reducing effective wall friction. The extent of this effect could depend on several factors, such as the materials used in the experiments, their flow properties, and their capacity to attenuate ultrasonic waves.

First experiments for limestone powder show promising results which could enable a potential industrial application for improved silo design that already considers the effect of ultrasonic-assisted discharge. It was possible to reduce the wall friction by applying ultrasound during the shear tests. The intensity (amplitude) and therefore the energy input into the system plays a significant role and might be a key parameter for upscaling the shear tests to a cone with ultrasonic discharge.

### 3.1. Methodology

For these first shear tests the wall friction of limestone powder eskal500 from KSL Staubtechnik GmbH was measured on a translational shear tester (TSG-70/140 from AVT Anlagen- und Verfahrenstechnik GmbH). The ultrasound was produced with a converter (C35-GD2) and generator (DGS35-200-T) from Artech Ultrasonic Systems AG. The converter was attached to the wall sample (stainless steel 1.4301, thickness 6 mm). Fig. 1 shows the set-up of the shear test with the ultrasound converter screwed to the wall sample and the hanger, which is then loaded accordingly, placed on top of the shear cell.

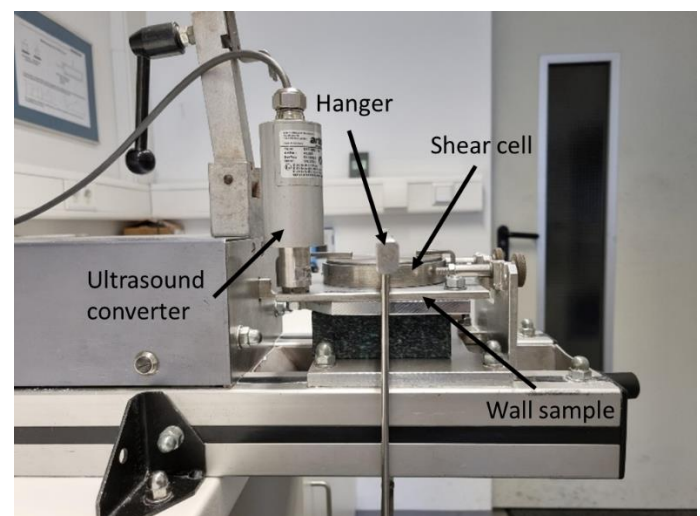


Figure 1. Set-up of the translational shear tester with the ultrasound converter.

The wall friction was measured first without ultrasound and afterwards at different energy input levels with ultrasound. All measurements were conducted at least in triplicate. The powder was filled into a shear ring placed on the wall sample and the bulk material was twisted 15 times under a load of 12 kg (plus weight of hanger). After smoothing the surface of the compacted powder, the lid and the hanger with the load is placed on top. The shear ring is lifted to measure the friction between wall and powder, rather than wall and shear ring. Under a load of 12 kg the set-up is sheared until steady state is reached. The ultrasound is then activated, and the load gradually reduced (from 12 kg to 10 kg, 8 kg, 6 kg, 4 kg, 2 kg, 1 kg, 0.5 kg and 0 kg).

### 3.2. Results

For graphical display and evaluation, the software SV95 (Version 2.3.0.3) from Dietmar Schulze is used. Fig. 2 illustrates the wall yield locus of limestone powder under the impact of ultrasound of different amplitudes. Under normal conditions (black line), the tested limestone powder forms a linear wall yield locus. At 5 W ultrasonic input, a parallel shift of the wall yield locus towards smaller shear stresses can be observed. While the measurements without ultrasound lead to a linear wall yield locus (black line), shear stress decreases under ultrasonic impact, especially for small normal stresses, leading to curved wall yield loci for the data with 10 W (blue line) and 15 W (green line) ultrasound input, respectively.

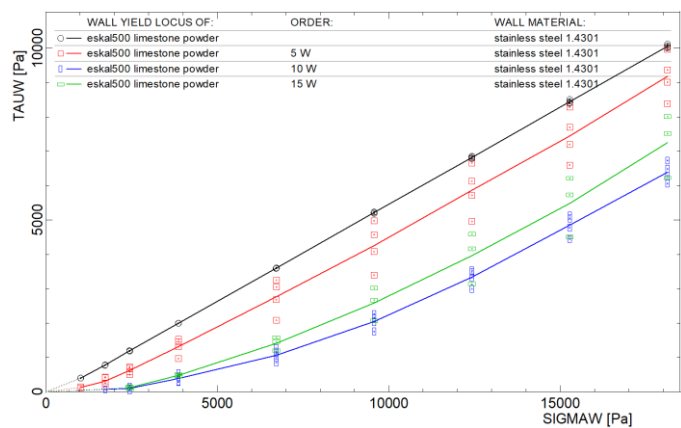


Figure 2. Wall yield locus of limestone powder with different ultrasonic amplitudes applied.

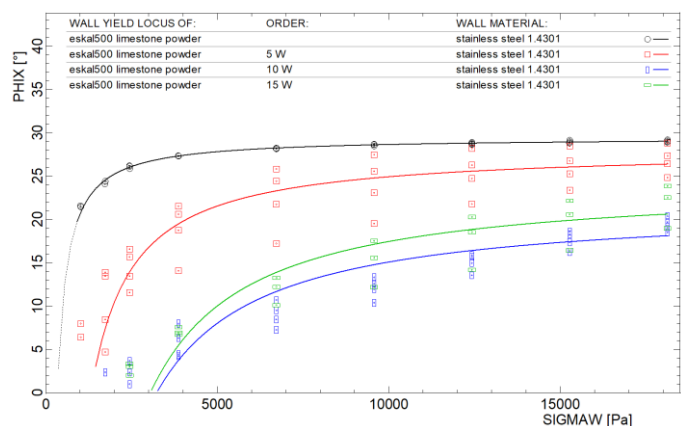


Figure 3. Wall friction angle of limestone powder with different ultrasonic amplitudes applied.

As can be seen in Fig. 3, even at a normal stress of 18 000 Pa wall friction could be reduced by 10°, from 29° to 19°, depending on the intensity of the applied ultrasound. Apparently, the reduction of wall friction angle is impacted by the intensity of the applied ultrasound, though for this set-up an optimum in ultrasonic intensity exists.

Varying the set-up parameters, could potentially minimize the wall friction even further. One key parameter being the frequency of the ultrasonic waves. Resonance intensity analysis at frequencies between 30 kHz and 40 kHz showed diverse responses, with elevated resonance around 36 kHz and 37 kHz. As the ultrasound generator identifies the optimal frequency for the system, current data is not at a constant frequency. Consequently, more precise data on the influence of frequency is required.

## 4. Conclusion

A novel method for shear testing has been developed, using ultrasonic-induced wall samples. Current results from these shear tests show that wall friction can be reduced significantly. If these results align with Jenike's theory, flatter cones for ultrasound discharge could be designed accordingly, reducing space requirements while maintaining or even improving flow profiles.

Although the data is still limited, it suggests the existence of an optimum of energy input, where further increase in power does not automatically reduce wall friction but might lead to its increase instead. Further research can help explain the extend of this phenomenon and its underlying reasons. Thereby optimizing the energy consumption and efficiency of these discharge aids.

A crucial influence on the wall friction in this kind of set-up is the frequency of the ultrasound generated. Some first analysis show that the system resonates stronger for some frequencies. Leading to the assumption that at these frequencies the desired effect on the wall friction might be stronger. If so, for each combination of wall sample and bulk material in each environment (shear tester or hopper) a frequency analysis should be done.

To validate the efficacy of this discharge aid on the flow profile in the future, the acquired data will be used to compare flow patterns of fine, cohesive powders in silos with varying cone angles with and without ultrasound. This comparative analysis serves to ascertain the effectiveness of the ultrasound-assisted approach in mitigating funnel flow and optimizing powder handling processes.

## References

- [1] D. Schulze, *Powders and bulk solids: behavior, characterization, storage and flow*, 2008.
- [2] A. Levy and H. Kalman, *Handbook of Conveying and Handling of Particulate Solids*, 2001.
- [3] T. Kollmann, *Schwingungsinduziertes Fließen feinstkörniger, kohäsiver Pulver*, 2002.
- [4] A. Haack, *Dämpfungsverhalten ultrafeiner, kohäsiver Pulver beim langsamen, reibungsbehafteten Fließen*, 2009.
- [5] C. Schwenke, *Modellierung und experimentelle Validierung des Schwerkraftaustrags ultrafeiner kohäsiver Pulver*, 2018.
- [6] G. Kache, *Verbesserung des Schwerkraftflusses kohäsiver Pulver durch Schwingungseintrag*, 2009.
- [7] B. Pollet, *Power Ultrasound in electrochemistry – from versatile laboratory tool to engineering solution*, 2012.
- [8] M. Kaps, *Ultraschall in der Neurologie*, 2005.

# Heat transfers in a flowing granular material: towards efficient cooling for agrofood applications

F.Rioual<sup>1,2</sup>, M.Galoppin<sup>1,2</sup> and R.Khirallah<sup>1,2</sup>

<sup>1</sup> National Research Institute for Agriculture, Food and the Environment, France

<sup>2</sup> University of Paris-Saclay, France

**Abstract**— Indirect cooling processes as mobile bed heat exchangers (MBHE) are promising technologies for an efficient cooling of a granular material. We propose a new MBHE in a rotating drum *FRISEDNUM* whose main asset is compactivity and we analyse the flow patterns in this device. We show by modelling (DEM) and experiments the existence of a flow pattern called “Biflow” which may be favourable to transfers. More generally, we expose the scientific challenges that have to be faced in order to progress in this field for the description of the heat transfers in such diphasic media composed of biobased particles.

**Keywords:** Mobile bed heat exchanger; granular material; heat transfer; biobased material

## 1. Introduction

The cooling of a granular material represents an important challenge in terms of energy efficiency in numerous applications of the agrofood industry (biosolids or wood pellets for a safe storage and conveying of the material, cereals and seeds in silos for an improved conservation....).

Direct processes as air ventilation and fluidised beds are largely used and enable an efficient cooling by an intimate contact between the refrigerant fluid and the particles but usually at the expense of high energy costs. As an alternative, indirect processes are an interesting approach for cooling because of the limited volume of refrigerant fluid to be used in the process: in mobile bed heat exchangers (MBHE), the working fluid (for instance water) is usually confined in an array of tubes (tube and shell) or through a plate (plate and shell) and the granular material flows along this boundary by gravity and cools by indirect transfer of heat with the fluid. We present a new type of mobile bed heat exchanger based on a rotating drum whose main asset is compactivity and which enables a maximized transfer compared to previous MBHE.

A supplementary level of complexity arises from the particular thermal properties of biobased particles as encountered in agrofood applications. We expose the scientific challenges that have to be faced to model accurately the heat transfers in this range of processes for agrofood applications involving a flowing diphasic media which we believe is the key for possible innovative solutions in this field of thermal engineering of granular matter.

## 2. The new mobile bed heat exchanger *FRISEDNUM*

The new mobile bed heat exchanger consists in a horizontal rotating drum (radius  $R_d$ , length  $P$ ) and a fixed pipe (radius  $R_p$ ) located along the rotation axis of the drum. The drum is filled with a granular material (particle radius  $r$ ) at a certain height  $h_0$  measured from the centre of drum as a fraction of the pipe radius  $R_p$ . The rotation of the drum at a velocity  $\Omega$  will generate a granular flow at the surface that we wish to study in order to

maximize the heat transfer between the granular material and the pipe. *Figure 1* shows the principle of the classical tube and shell exchanger and the new exchanger *FRISEDNUM*.

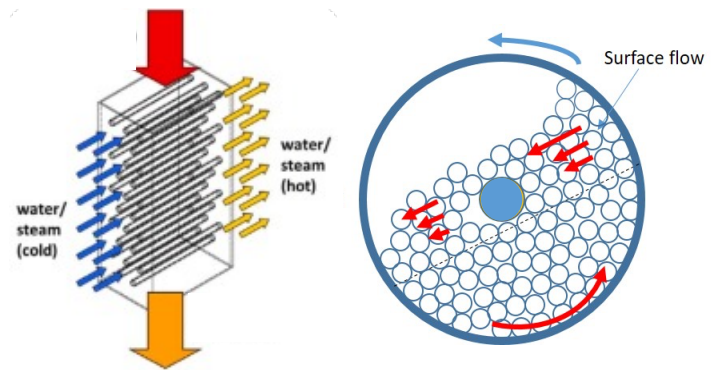


Figure 1: Classical Tube and Shell MBHE (left); the new MBHE *FRISEDNUM* based on a rotating drum (right)

### 2.1. Numerical modelling

The granular flow around the pipe in the device is studied by the discrete element method [1] as a function of the main control parameters of the problem: Froude Number  $Fr$  where  $Fr = (R_d \Omega^2) / g$ , the Diameter Ratio  $R_d/R_p$  and the effective height of the packing  $h_0 = \beta R_p$  where  $\beta$  is a scale parameter.

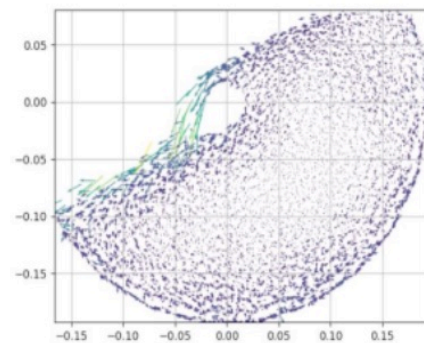


Figure 2: Numerical simulation (DEM) of the flow – Velocity field in the Biflow regime

We identify in particular a flow regime that we called *Biflow* (*Figure 2*) where the flow of particles occurs at the top as well as the bottom of the pipe. This may be relevant for the transfer as it maximizes convection of particles at the boundary despite the presence of a depletion zone on the downstream side of the pipe and a stagnation zone on the upstream side of the pipe as a consequence of an obstruction effect of the pipe in the flow.

In a second part, we precise the properties of the contact in the *Biflow* regime through the calculation of the packing fraction and the velocity field at the contact with the pipe. We observe in particular that the initial height is a crucial factor in order to determine the magnitude of the velocities on the top side and the bottom side of the pipe and the properties of the *Biflow* regime: As the height increases the velocity on the top of the pipe increases and the velocity at the bottom decreases. The depletion zone is also larger for lower heights.



## 2.2. Experiments by image analysis

Experiments have been conducted with glass beads of average radius  $r = 4\text{mm}$ . at a velocity  $\Omega = 40\text{ rpm}$ .,  $R_d = 20\text{ cm}$ . ;  $R_p = 4\text{ cm}$ . by image analysis with a long exposure time. They confirm previous numerical observations on the *Biflow* regime (Figure 3).

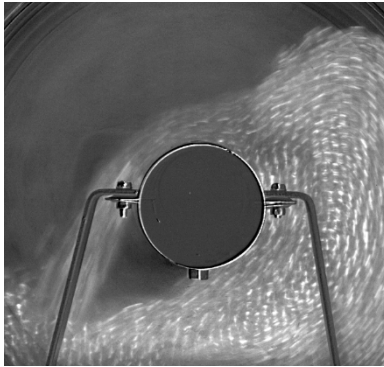


Figure 3: Experimental evidence of "Biflow" regime

The convective motion of the beads along both side of the pipe induced by the rotation of the drum is potentially favourable to transfers.

In real applications, classical gravity driven mobile bed heat exchangers have a limitation for the transfer in terms of the total height of fall of the particles in the process (see Figure 1). In the new device *FRISEDREDUM* [2], the continuous motion of recirculation of the particles along the pipe, generated by the rotating drum, allows to maximize the amount of heat transferred towards a reduction of the temperature differential between the fluid in the pipe and the particles. Simplicity of installation and energy savings may also be more reachable compared to indirect rotary coolers for instance because a simple pipe embedded in the granular flow along the drum axis is necessary and there is no need to dive the entire drum in a thermostated bath.

However a quantitative characterisation of the transfers in such flowing diphasic media for agrofood applications requires a deeper analysis at the grain scale.

## 3. Heat transfers involving biobased particles

The description of the heat transfers involving biobased particles include further peculiar levels of complexity in a multiphysics context depending on the time scale considered:

- Low conductivity of the grain material

The consequence is that the conduction through the interstitial air in MBHE can be a non negligible thermal path. In particular, at the contact or close distance between grains, the role of air remains to be clarified [3].

- Heterogeneity of the bulk material of the grain

Biobased grains can have a specific heterogeneous microstructure which has consequences in terms of internal thermal transfer: For wood pellets, the microstructure depends on the process of agglomeration of the saw dusts in the pellet fabrication process. For biological grains, germ, endosperm and the surrounding bran compose the microstructure with eventually different thermal properties for each part. What is the effect of the microstructure of the grain on the effective heterogeneous cooling of its different parts? In particular, is there a critical region of the grain structure or surface to cool for conservation purposes in applications ?

- Hygroscopic properties of the material

Porous biobased Grains or wood and chip pellets are usually hygroscopic such that they can exchange moisture with the surrounding air as a function of local temperature and hygrometry. This mass transfer is combined to heat transfers consecutive to the phase change of water which has to be quantified, in particular in the dynamic regime considered here.

- Respiration phenomena (living grains)

Respiration is a physiological process generating energy to carry out various metabolic functions. This process involves the consumption of reserve substances of seeds (carbohydrates) and results in the release of byproducts such as  $\text{CO}_2$ , water and heat [4] which thus come into play in the energy balance and is coupled with previous properties.

Thermal data at the scale of the process are based usually on the introduction of thermocouples in the bulk of the flow which are scarce, localised and intrusive inducing a local perturbation of the flow. It can be thus difficult to establish direct comparisons with models at this scale.

Our alternative strategy to capture the heat transfers in 3D will be based on the development of basic experiments which mimic elementary processes encountered in the 3D process and allow us to explore the complexity of the transfers at the grain scale by being accessible to experimental measurements at this scale. These different model experiments can guide us to new paths for heat transfer enhancement in biobased granular materials. They will represent also severe tests for the benchmarking of the model in 3D which should integrate the physics at this scale before any comparison with 3D experiments at the scale of the process.

## 4. Conclusion

We show the potentiality of a new mobile bed heat exchanger *FRISEDREDUM* for cooling applications through DEM modelling and image analysis. Further improvements for such range of processes involving mobile beds or silos require the description of heat transfers in a diphasic particulate media composed of biobased particles. For biobased particles, the low conductivity of the material induces the essential role of heat transfers through the gas phase. Furthermore, hygroscopicity of the biobased material can lead to further heat exchanges with the environment. The heterogeneity of the material in the bulk of the grain can also lead to specific heterogeneous conduction properties. At last, for living grains, respiration phenomena are associated to heat release notably which have also to be accounted for in future studies.

## Acknowledgement

"F.R. would like to thank A.Denis, Y.Paviet-Salomon and S.Saavedra for technical assistance in the experimental setup".

## References

- [1] F.Rioual and P.E.E.Gbehe, *Characterisation of the granular dynamics at the interface between a pipe and a granular flow in a rotating drum*, Particuology, vol.86, p.117-125 (2024)
- [2] F.Rioual, A.Denis, S.Saavedra *Procédé et installation de transfert thermique entre un matériau granulaire et un fluide*, France, Patent n° : FR2302630 (2024)
- [3] M.Hobbs, R.P.Goodrich, J.Y.Ooi, *Numerical and experimental investigation of the effect of interstitial gases on conductive heat transfer for dense particulate systems*, Chemical Engineering Science, vol.230, 116145 (2021)
- [4] Lehninger Principles of Biochemistry (4th Ed.): Nelson, D., and Cox, M.; W.H. Freeman and Company, New York, 1216 pp. (2005)



# Evolution of pore geometry and flow properties of polyhedral particles discharged from a model silo

J. Wiącek<sup>1</sup>, R. Kobyłka<sup>1</sup>, J. Horabik<sup>1</sup>, and N. Govender<sup>2,3</sup>

<sup>1</sup> Institute of Agrophysics, Polish Academy of Sciences, Lublin, Poland

<sup>2</sup> University of Johannesburg, Department of Mechanical Engineering, Johannesburg, South Africa

<sup>3</sup> Research Center Pharmaceutical Engineering, Graz, Austria

**Abstract**— The effect of particle shape on flow from a cylindrical flat-bottomed model silo was studied using the Discrete Element Method (DEM) on GPU. The study considered mono-sized spheres and equi-volume polyhedral particles, represented by octacontahedron, icosahedron, octahedron and hexahedron respectively. The Mass Discharge Rate (*MDR*) was found to be strongly affected by particle shape, reaching the highest values for spheres and the lowest for octahedrons and hexahedrons, which exhibit the highest degree of angularity. A strong effect of particle shape on flow behavior was observed, with spheres, octacontahedrons, and icosahedrons exhibiting a mass flow behaviour, and octahedrons and hexahedrons being prone to core flow.

**Keywords:** polyhedra; DEM; silo discharge; granular flow

## 1. Introduction

Granular materials play an important role in agriculture, as well as in food, chemical, and pharmaceutical industries, where they are subject to diverse processes such as conveying, storage and comminution. Conducting each of these processes requires knowledge of the resulting changes in bulk behavior that arise from interactions between the individual grains of the bulk material, which possess a range of geometrical and morphological properties. Among these properties, the shape of the grains is a parameter that strongly affects the bulk behavior of the material [1, 2]. Thus, understanding the influence of particle shape on the structural and mechanical properties of granular packing allows for selection of appropriate conditions for given granular material processes. The tortuosity of the pores and changes in their geometry play a crucial role in the storage and processing of granular materials, influencing air permeability, density, stability, and the rate of discharge from storage tanks [3]. Over the last few decades many investigations have been conducted to study the mass discharge rate (*MDR*), which is one of the crucial parameters for the design and control of processes involving flow of granular materials [4]. A steady and precisely controlled flow rate is indispensable for preparing mixtures of materials in agriculture and many industries. The flow rate through the orifice was found to be determined by, among other, the shape of particles [5]. A more comprehensive understanding of the effect of grain shape on the discharge rate is of high importance for many industries and the design of devices and processes involving granular materials. Therefore, the objective of the reported project was a numerical analysis of the influence of shape of polyhedral particles on flow characteristics and the evolution of structural and micromechanical properties of material discharged from a model silo.

## 2. Simulations setup

The DEM simulations [6] were conducted for a monodisperse assembly of spheres with a diameter ( $d_p$ ) of 5.95 mm, or

polyhedral particles represented by octacontahedron, icosahedron, octahedron, and hexahedron (Fig.1). The volume of particles remained constant irrespective of their shape. The number of particles was 15,000.



Figure 1. Shapes of particles used for DEM simulations.

The input parameters of the particles were: solid density of  $2212 \text{ kg}\cdot\text{m}^{-3}$ , Young's modulus of 0.88 GPa, and Poisson's ratio of 0.25. The coefficient of friction between particles ( $\mu_{pp}$ ) was 0.1, 0.3 and 0.5, and the coefficient of friction between particle and the wall of cylinder was 0.3. No rolling friction was applied for simulations. The coefficient of restitution was 0.3.

A flat-bottomed cylindrical container with a diameter ( $d_o$ ) of 150 mm (equivalent to 25 times the diameter of a sphere) and a height ( $H$ ) of 450 mm (yielding an  $H/D$  ratio of 3.0) was modelled. The density of the silo wall was  $7800 \text{ kg}\cdot\text{m}^{-3}$ , Young's modulus was 200 GPa, and Poisson's ratio was 0.25, which are material parameters of steel. The particles were generated inside the model silo and subsequently discharged through a centrally located circular orifice with a diameter ranging from 4.71 to 10.08 times the mean particle diameter (equivalent to 28 to 60 mm). The Hertz-Mindlin contact model, including the damping term introduced by Tsuji *et al.* [7], was employed. The simulations were conducted using GPU-based DEM software (Blaze-DEM) [8].

## 3. Results and discussion

### 3.1. Packing characteristics

Fig. 2 shows the evolutions of the bulk density of the assemblies composed of particles with various shapes and coefficients of interparticle friction. The bulk densities were determined after silo filling when the kinetic energy of the system was less than  $10^{-7} \text{ J}$ . The lowest bulk densities were obtained for spheres, which increased with an increase in the degree of particle angularity. The face-to-face contacts in polyhedral particle beds enhanced packing density by promoting more organized and compact arrangements and reducing void spaces. For all particle shapes, the bulk density decreases as the coefficient of interparticle friction increases from 0.1 to 0.3, followed by a slight change in the bulk density as the coefficient of friction increases to 0.5. These results indicate the presence of a certain threshold value of the coefficient of interparticle friction above which the packing structure is more strongly affected by the shape factor than the frictional factor.

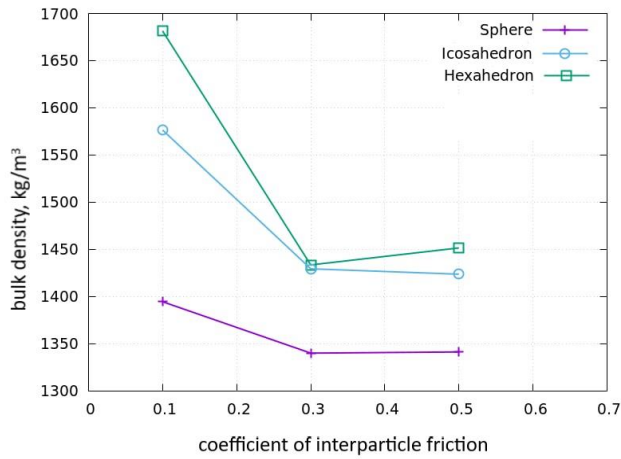


Figure 2. Initial bulk densities of beddings of spheres and polyhedral particles for various coefficient of interparticle friction.

### 3.2. Granular flow characteristics

The relationships between the mass discharge rate and the orifice diameter for various particle shapes at  $\mu_{pp}=0.3$  are shown in Fig. 3. The *MDR* values increase monotonically with an increase with the orifice size. The highest *MDR* values were obtained for spheres due to their smooth, rounded surfaces and efficient packing, which minimize friction and interlocking, facilitating smoother and more consistent flow. A change in particle shape from spherical to octahedral decreased the *MDR* by above 60% across the entire range of orifice diameters. The lowest mass discharge rates were obtained for octahedrons and hexahedrons, which are the most prone to interlocking or developing face-to-face contacts that can resist torque and decrease flowability.

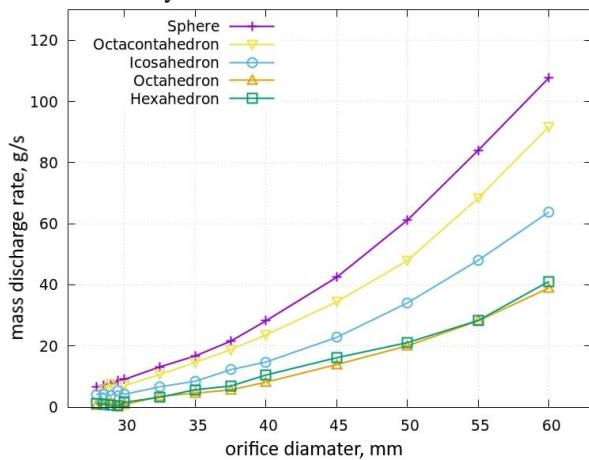


Figure 3. The *MDR*( $d_o$ ) relationships for different particle shapes at  $\mu_{pp}=0.3$ .

Fig. 4 shows the profiles for the vertical velocities of spheres, icosahedrons, and hexahedrons during silo discharge across the cross section of the bin, with the orifice diameter equal to 60 mm. The coefficient of interparticle friction was 0.3. The velocity profile is highly sensitive to particle shape. The widest flame-like area of particles with increased velocity was observed in the sphere bedding (Fig. 4a) and became significantly smaller as the particle shape approached that of hexahedron (Fig. 4c). Spherical and icosahedral particles developed a V-shaped flow across the hopper, with significant movement reaching to the side walls, indicating mass flow behaviour. A core flow, with particle movement mainly localized in the centre of silo, was observed for octahedrons and hexahedrons. The sphere bedding had the smallest stagnant zone; meanwhile, this area differed only slightly for non-spherical particles.

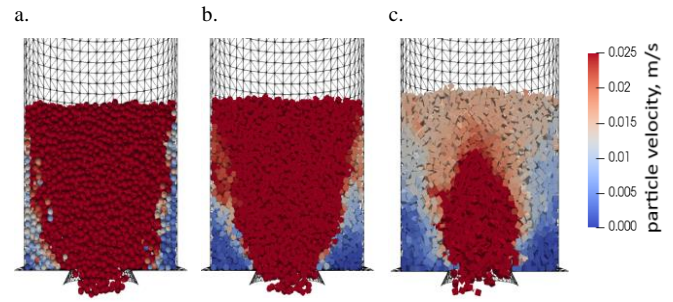


Figure 4. Profiles of particle vertical velocities for spheres, icosahedrons and hexahedrons at  $\mu_{pp}=0.3$ .

## 4. Conclusions

The packing and flow characteristics of spherical and polyhedral particles with varying degree of angularity have been investigated by using a numerical Discrete Element Method. The discharge of the granular material from a flat-bottomed model silo was simulated, providing critical insight for optimizing processes involving its handling and storage. Polyhedral particles are common in natural materials such as minerals and crystals, as well as in industrial applications like pharmaceuticals, food processing, and construction materials. This project addresses a significant knowledge gap concerning the packing structure of assemblies of polyhedral particles. The study results indicate that particle shape significantly affects the flow behavior of granular materials, with particles exhibiting greater angularity, such as polyhedral particles, showing more complex flow patterns and lower discharge efficiency compared to spherical particles. Furthermore, the relationship between the orifice-to-particle diameter ratio and bulk density, as determined by interparticle friction, is crucial for optimizing processes related to the handling and storage of bulk materials.

By investigating the effects of particle shape and friction, this research aims to improve the efficiency and predictability of processes involving polyhedral particles, thereby enhancing the design and operation of silos and other bulk handling equipment.

## References

- [1] J. Wiącek, M. Molenda, J. Horabik and J.Y. Ooi, *Influence of grain shape and intergranular friction on material behavior in uniaxial compression: experimental and DEM modelling*, Powder Technology 217, 435–42, 2017. <https://doi.org/10.1016/j.powtec.2011.10.060>.
- [2] N. Govender, *Study on the effect of grain morphology on shear strength in granular materials via GPU based discrete element method simulations*, Powder Technology 387, 336–347, 2021. <https://doi.org/10.1016/j.powtec.2021.04.038>.
- [3] M. Li, H. Chen, X. Li, L. Lin and J. Lin, *Permeability of granular media considering the effect of grain composition on tortuosity*, International Journal of Engineering Science 174, 103658, 2022. <https://doi.org/10.1016/j.ijengsci.2022.103658>.
- [4] J. Wiącek, J. Horabik, M. Molenda and R. Kobyłka, *Discharge rate influenced by friction and shape of dimers: Numerical study*, Tribology International 193, 109421, 2024. <https://doi.org/10.1016/j.triboint.2024.109421>.
- [5] M.A. Madrid, K. Asencio and D. Maza, *Silo discharge of binary granular mixtures*, Physical Review E 96, 022904, 2027, <https://doi.org/10.1103/PhysRevE.96.022904>.
- [6] P.A. Cundall and O.D. Strack, *A discrete element model for granular assemblies*, Geotechnique 29, 47–65, 1979. <https://www.science.org/doi/10.1126/science.109301>.
- [7] Y. Tsuji, T. Tanaka and T. Ishida, *Lagrangian numerical simulation of plug flow of cohesionless particles in a horizontal pipe*, Powder Technology 71, 239–250, 1992.
- [8] N. Govender, D.N. Wilke and S. Kok, *Blaze-DEMGPU: modular high performance DEM framework for the GPU architecture*, SoftwareX 5, 62–66, 2016. <https://doi.org/10.1016/j.softx.2016.04.004>.

# Analysis and optimization of failures during transport and processing of Solid Alternative Fuels (SAFs) for combustion in a heating plant

D. Žurovec<sup>1</sup>, J. Rozbroj<sup>1</sup>, J. Hlosta<sup>1</sup>, J. Diviš<sup>1</sup>, K. Pokorná<sup>1</sup>, J. Zegzulka<sup>1</sup> and J. Nečas<sup>1</sup>

<sup>1</sup> VSB - Technical University of Ostrava, Faculty of Mining and Geology, Ostrava, Czech Republic

**Abstract**— Protecting the environment is in the interest of all global powers. Reducing the burning of fossil fuels is one of the main priorities of the Green Deal adopted by the European Commission. Another area of environmental protection is minimizing the dumping of municipal waste in open landfills. A European Union regulation requires member states to recycle 55% of municipal waste by 2025. The energy industries are forced to react to these facts and is gradually converting their coal-fired power plants and replacing them with new specialized technologies, e.g. for burning wood chips or SAF (solid alternative fuels). These bulk materials have diametrically different mechanical and physical properties compared to pulverized coal. They are formed from sorted municipal waste and are characterized by different grain shapes, different grain sizes, and very low bulk density. This fact is strongly reflected in their behaviour during processing, from stacking to entry into the combustion chamber. In this study, failure conditions during the transport, handling, and storage of SAFs were identified. SAFs designed for incineration were subjected to a detailed analysis in the form of measurements of mechanical and physical properties and the study of their behaviour along the transport route. In the next step, structural modifications of the problematic nodes were proposed in a virtual 3D environment. Subsequently, dynamic simulations were carried out using the DEM method to confirm the correctness of the proposed measures. Based on the validation of these DEM simulations, the proposed solutions were applied to real-world technology.

**Keywords:** fuel; bulk density; DEM; simulation

## 1. Introduction

Handling waste through processing and recycling materials from various industrial sectors remains a relevant global issue. Waste management practices differ among EU countries. The European Union aims to promote waste prevention and product reuse as much as possible. When this is not feasible, recycling and subsequent use of waste for energy production is prioritized. Despite the increase in waste generated per capita, waste management has improved. Recycling is increasing, while landfilling is decreasing. The proposed measures aim to preserve, protect, and improve the quality of the environment, protect human health, ensure the prudent, efficient, and rational use of natural resources, strengthen the principles of the circular economy, increase energy efficiency, and reduce the European Union's dependence on imported resources [1-3]. As part of the Green Deal, European countries have committed to gradually replacing coal-fired power plants with clean energy sources. In the Czech Republic, the deadline for the cessation of coal power plant operations is set for the end of 2033 [4].

Therefore, energy and heating companies in the Czech Republic and beyond have begun transitioning to other fuel sources. Solid alternative fuels (SAF) are one option for replacing fossil fuel energy sources. This type of waste

material (SAF) has drastically different mechanical-physical properties compared to pulverized coal. This difference significantly affects their behaviour during processes of transport, storage, or processing from initial unloading to entry into the combustion chamber. The Discrete Element Method (DEM) simulation tool was used to analyse problematic areas in the transport and storage process. DEM is currently widely used for various industrial applications. The main application areas of this method are the transportation, handling, and storage of bulk and piece materials. The DEM method is based on evaluating the mutual interactions between individual particles and the interactions of particles with contact surfaces, which can be, for example, a transport chute or the wall of storage facilities. The interactions are evaluated for a chosen time interval individually, resulting in a continuous simulation of the investigated process [5-8].

## 2. Material and methods

### 2.1. Fuel Transport Technology Line

The technology line includes equipment for transporting fuel from a roofed fuel reservoir to a pair of operational reservoirs of the combustion chamber. The performance capacity of the line is 15 t/h. The fuel transport line consists of a double belt conveyor, a standalone belt scale, an upward belt conveyor with a sampler, a discharge scraper, and a short conveyor above the operational reservoir of the combustion chamber. The fuel transport line is controlled by a control system based on the requirements of the combustion process. The most problematic part of the entire transport process is currently the discharge scraper (position A, see Figure 1). At this point, there is problematic fuel accumulation, and the scraping efficiency is very low. This operational malfunction often stops the entire transport line, requiring technical personnel to manually clear the filled scraper area. This problem prompted optimization research and the design of a new technical solution for this problematic node.

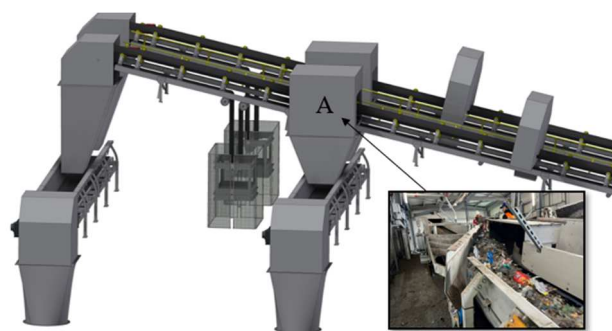


Figure 1. Depiction of the problematic part of the fuel transport line

### 2.2. Material Characterization

Before any optimization application of transport, storage, or processing equipment that handles bulk materials, it is essential to conduct material characterisation to understand its behaviour during movement. Material characterization is also necessary to create a virtual material for the DEM simulation



environment. The fuel was subjected to measurements of its mechanical-physical properties. A sample of the material was taken from the fuel reservoir at the entry point of the entire technological line. A second sample was taken at the exit of the upward belt conveyor. The mechanical-physical properties of the collected samples are compared in Table I. Notably, from the measured bulk density, it is evident that the properties of the bulk fuel change during transport. The material compacts during movement on the transport route, increasing its bulk density, while the flow function does not change significantly. Moisture measurements showed that the material dries out during transport.

TABLE I. FLUEL PROPERTIES

			INPUT	OUTPUT
Angle of internal friction	$\varphi_{cf}$	[°]	49,26	37,31
Initial shear stress	$\tau_c$	[kPa]	4264	4008
Flow function	$ff_c$	[-]	1,4	1,5
Bulk density	$\rho_s$	[g/cm <sup>3</sup> ]	99	124
Wall friction (stainless steel )	$\varphi_w$	[°]	25,01	20,04
Wall fiction (plastic Murtfeld)	$\varphi_w$	[°]	17,05	16,35
Wall friction (rubber)	$\varphi_w$	[°]	24,02	22,76
Angle of repose	$\alpha_r$	[°]	34,35	34,8
Size of particle 50%	$d_{50}$	[mm]	<20	<20
Size of particle 90%	$d_{90}$	[mm]	<40	<40
Moisture	$v$	[%]	37,88	27,72

### 3. Results and discussion

In the first phase of the optimization process, a DEM simulation of the current problematic state was conducted, confirming the problematic fuel discharge. This is illustrated in Figure 2, where areas with zero fuel movement velocity are shown in red.

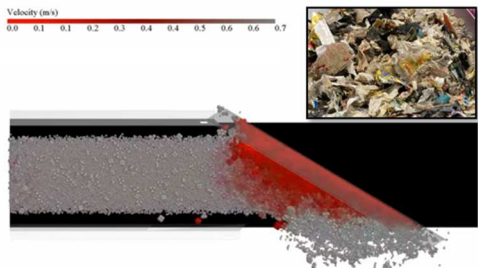


Figure 2. DEM simulation of the scraper issues

In the second phase of the optimization process, two design proposals for the discharge scraper were developed and subjected to simulation verification to observe fuel behaviour during discharge from the belt conveyor. The first variant focused solely on optimizing the shape of the static scraper (see Figure 3). However, this optimization solution did not bring any improvement.

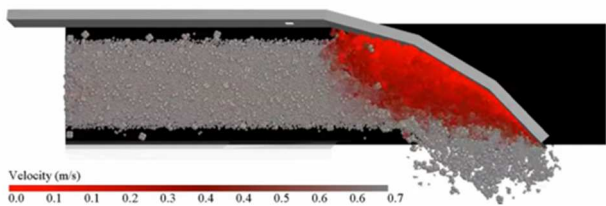


Figure 3. Simulation of the optimized static scraper

The second technical solution was a movable belt scraper designed to guide the fuel into the discharge section using a continuous moving belt. Essentially, this involves a short belt

conveyor positioned perpendicular to the main upward belt conveyor. The results of the DEM simulation are shown in Figure 4. This solution revealed the optimal movement parameters for the fuel during the required discharge into the hopper.

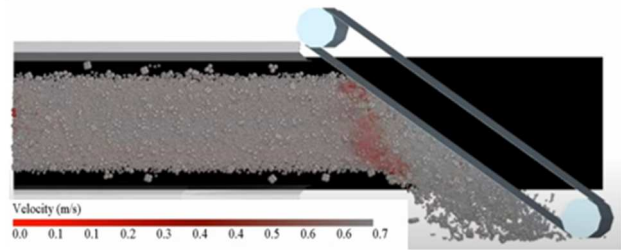


Figure 4. Simulation of the movable belt scraper

### 4. Conclusion

In this research project, malfunctioning conditions were identified in the process of transporting solid alternative fuel on a technological line in a newly built Thermal Power Plant intended for combustion. A detailed analysis of the fuel was carried out by measuring its mechanical-physical properties. Subsequently, design optimisation solutions for the problematic discharge scraper were proposed. Dynamic simulations using the DEM method were carried out, which confirmed the effectiveness of the proposed design solution, making it applicable to real operations.

### Acknowledgement

This paper was created as part of the projects No. CZ.02.01.01/00/22\_008/0004631 Materials and technologies for sustainable development within the Jan Amos Komensky Operational Program financed by the European Union and from the state budget of the Czech Republic and the European Just Transition Fund supported this work within the Operational Programme Just Transition under the aegis of the Ministry of the Environment of the Czech Republic, project CirkArena, number CZ.10.03.01/00/22\_003/0000045.

### References

- [1] A. Kumar, *A novel framework for waste management in smart city transformation with industry 4.0 technologies*. Research in Globalization, 2024. doi: <https://doi.org/10.1016/j.resglo.2024.100234>.
- [2] N.P. Adriyanti, A. Gamal, O. C. Dewi, *Solid Waste Management Models: Literature Review*. ICSGSC, 2018. doi: <https://doi.org/10.1109/ICSGSC.2018.8541350>.
- [3] D. Kannan, S. Khademolqorani, N. Janatyan and S. Alavi, *Smart waste management 4.0: The transition from a systematic review to an integrated Framework*. Waste Management, 2024. <https://doi.org/10.1016/j.wasman.2023.08.041>.
- [4] European Parliament [online], *European Parliament*, 2024. <https://www.elections.europa.eu>.
- [5] L. Zhao, X. Jin and X. Liu, *Numerical research on wear characteristics of drum based on discrete element method (DEM)*. Engineering Failure Analysis, 2020. <https://doi.org/10.1016/j.engfailanal.2019.104269>.
- [6] R. Xia, X.W. Wang, B. Li, X. Wei and Z. Yang, *Discrete Element Method- (DEM-) based study on the wear mechanism and wear regularity in scraper conveyor chutes*. Mathematical Problems in Engineering, 2019. <https://doi.org/10.1155/2019/4191570>.
- [7] D. Forsström and P. Jonsén, *Calibration and validation of a large scale abrasive wear model by coupling DEM-FEM Local failure prediction from abrasive wear of tipper bodies during unloading of granular material*. Engineering Failure Analysis, 2016. <http://dx.doi.org/10.1016/j.engfailanal.2016.04.007>.
- [8] Q. Xu, H. Yu, J. Chong, J. Xie, X. He, Y. Li and J. Li, *The analysis for characteristic of particles movement and pressure balance stability in the shield soil chamber during the EPBS excavation in weathered diorite stratum*. Engineering Failure Analysis, 2024. <https://doi.org/10.1016/j.engfailanal.2024.108029>



# Liquid-gas flow around resolved densely-packed objects in CFDEMcoupling

Martin Niemann<sup>1</sup>, Dennis Heinrich<sup>2</sup>, Giovanni Viciconte<sup>1</sup>, Christoph Goniva, Jürgen Grabe<sup>2</sup>, and Christoph Kloss<sup>1</sup>

<sup>1</sup> DCS Computing GmbH, Linz, Austria

<sup>2</sup> Technische Universität Hamburg-Harburg, Hamburg, Germany

**Abstract**—This contribution presents recent solver enhancements in CFDEMcoupling for two-phase liquid-gas flows in the presence of resolved solid objects modeled by the Immersed Boundary Method (IBM). The method is very versatile and allows using all particle shapes as well as triangulated surface meshes. Particular focus is given to solver validation using various validation examples. Ensuring the impermeability of solid objects is crucial in this regard and paramount to mass conservation. Moreover, the handling of contact angles of the liquid-gas interface at the particle surface modeled by the IBM is discussed. A suitable test case to quantify the impact of the contact angle is the force exerted by a liquid bridge between two adjacent particles.

**Keywords:** CFD-DEM, non-spherical particles, IBM

## 1. Introduction

Many applications in soil mechanics deal with unsaturated particle packings that exhibit a water saturation below 100%. Consequently, capillary effects arise that influence the material's hydro-mechanical behavior. Highly detailed simulations of these applications require resolving the inter-particle pore space and the liquid-gas interface within these pores. When using body-fitted meshes, simulations of these problems become quite demanding in terms of mesh generation, especially when considering finite volume approaches. Additionally, it is even more demanding when allowing particle motion and, thus, requiring mesh deformation. Modeling the particle surface with the IBM is one solution to this problem.

## 2. Numerical Method

The presented method is implemented in a Volume-of-Fluid (VoF) solver from the CFD-DEM simulation framework CFDEMcoupling. The solver is derived from the OpenFOAM solver interFoam and couples with the discrete element method (DEM) Aspherix. The DEM calculates particle collisions and integrates the particle trajectories in time. Coupling to the fluid is implemented by the interaction forces between fluid and particles.

On the fluid side, the particles are represented in a resolved manner, i.e. extending over several cells. The fluid inside the region occupied by the particle is forced to the particle velocity, resulting in an IBM. The transport for the liquid phase is modeled by a VoF method and solved for by OpenFOAM's implementation of the Multidimensional universal limiter for explicit solution (MULES). The method is improved to account for immersed boundaries when propagating the liquid-gas interface and ensure mass conservation. Moreover, an additional contact angle condition is enforced on the immersed boundaries.

The implementation allows the usage of arbitrary surface shapes. This means that surface meshes on a user-specified trajectory are a valid input as well as particles of arbitrary shape.

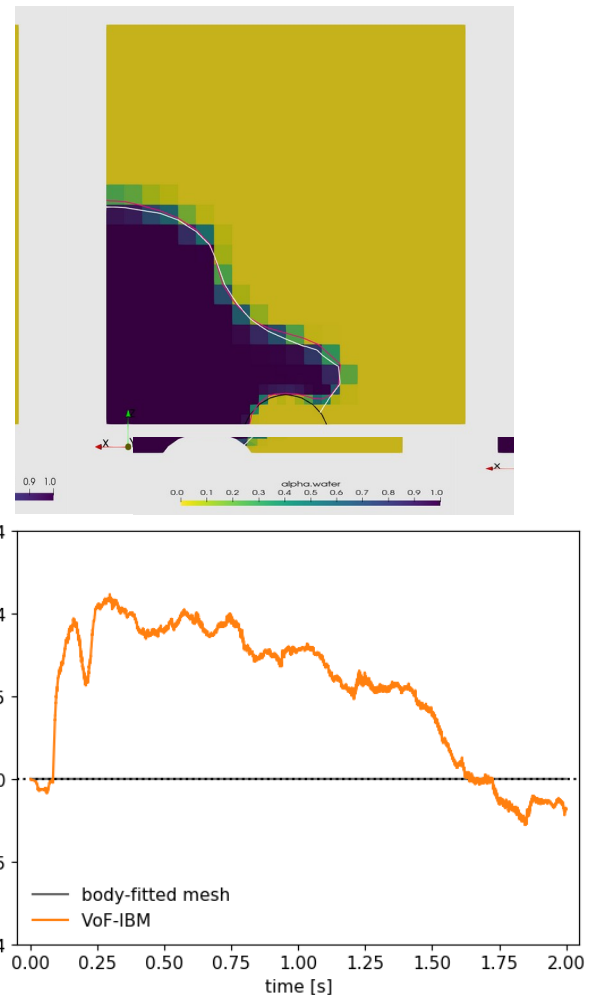


Figure 1: Top: Liquid distribution in the dam break case with obstacle for the VoF-IBM solver. The liquid volume fraction in each cell is shown along with the liquid-gas interface indicated by the white line. The liquid-gas interface from the simulation using a body-fitted mesh is indicated by the magenta line. The body-liquid interface is shown as a black line. Bottom: Mass conservation for the dam break case. The change of liquid mass relative to the initial liquid mass is plotted for both body-fitted mesh and VoF-IBM.

## 3. Application Examples

### 3.1. Dam Break

The method is validated in a dam break setup – where a rectangular sub-domain filled with liquid is released by opening or removing a wall inside a larger container and, subsequently, sloshes inside this container – that contains an additional cylindrical obstacle at the bottom. Simulations are conducted for a reference setup using a body fitted mesh and the solution by the VoF-IBM compared to that reference. As shown in Figure 1, very good agreement between the two solutions as well as a negligible error in mass conservation for the VoF-IBM is found.

In a second step, the obstacle can be moved using the IBM and the impact of motion of the immersed boundary is assessed. Slightly larger mass errors in liquid mass are found than for the stationary case.

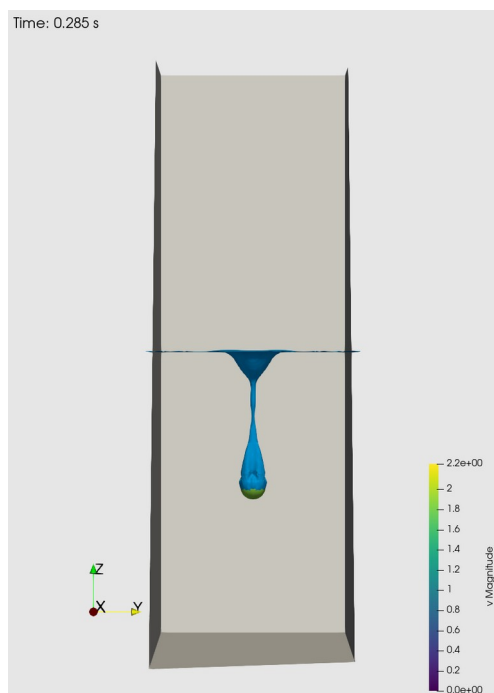


Figure 2: Liquid-gas interface for a single sphere dropping into water. The snapshot captures the time about 0.07 seconds after impact and directly before pinch-off of the particle's gas wake. Interface shape and this timing are in good agreement with experimental data from [1].

### 3.2. Water Entry of Particles

Experimental data for particles dropping into water is available, see e.g. [1]. The case of a steel sphere with diameter 2.54 cm was chosen. The initial height was chosen such that the impact velocity onto the surface (about 2 m/s) matches the experimental conditions. A snapshot of the results is shown in Figure 2. Very good agreement in terms of shape of the liquid-gas interface as well as particle motion is found.

Similar to the previous case, several particles of convex shape are dropped from the same height. The particles differ in shape and initial rotational velocity. They hit the surface at slightly different times due to differences in experienced drag force and create waves corresponding to their individual shape, see Figure 3.

### 3.3. Imbibition of a Packed Sand Grains

The imbibition of a packed sand bed is investigated as an application case for the developed set of models. The particle packing is extracted from in-situ X-ray computed tomography data of a corresponding laboratory experiment. The shape of each individual particle is approximated as a purely convex body to reduce computational complexity. The imported and initially dry bed of sand particles is filled with water from the bottom, and

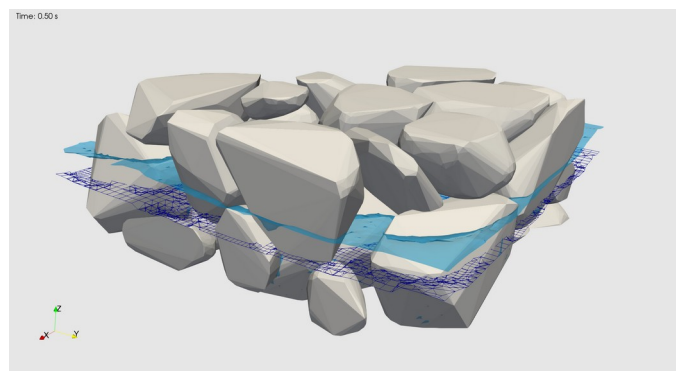


Figure 4: Water surface for the imbibition of packed sand grains for a body-fitted mesh approach (blue wire frame) and the presented VoF-IBM (transparent light blue).

simulation results from the presented VoF-IBM approach are compared to those of a similar setup using a body-fitted mesh.

Figure 4 shows the comparison between the water surface for the body-fitted simulation and calculated by the VoF-IBM. Good agreement in terms of shape and overall behavior is found. However, the interface travels with a slightly larger velocity. This behavior corresponds to larger fluid velocities being observed in that case and requires further investigation.

In a further step, particle motion is allowed for the VoF-IBM simulation. This setup requires an additional relaxation step for the particles to avoid overlaps between particles that would lead to large velocities and, consequently, destabilize the coupled simulation. The resulting particle packing is close to the measured packing but not identical. As the simulation domain is rather small and restricted by walls on all sides, most particles cannot move due to geometric constraints. However, motion can be observed on a few particles.

## 4. Conclusion

This contribution presents an IBM for immersed objects like resolved particles in CFD-DEM simulations in the presence of liquid-gas interfaces. This method was recently implemented in the CFD-DEM framework CFDEMcoupling. Several validation and application examples are discussed and compared to available reference data. Very good agreement is found for the cases of a breaking dam and a sphere dropping onto a water surface. These test cases are then extended into cases using several particles of convex shape with the imbibition of packed sand being the most complicated one. The latter case will be considered in more depth in the future, especially for larger domains and, thus, packings with more particles.

## Acknowledgement

Work on this project was funded by FWF Project I 5374-N "Micro mechanical modeling of unsaturated particle packings using CFD-DEM and computed tomography".

## References

- [1] J. M. Aristoff, T. T. Tadd, A. H. Techet, and J. W. M. Bush, *The water entry of decelerating spheres*. in *Physics of Fluids* 22, 2010. doi: 10.1063/1.3309454

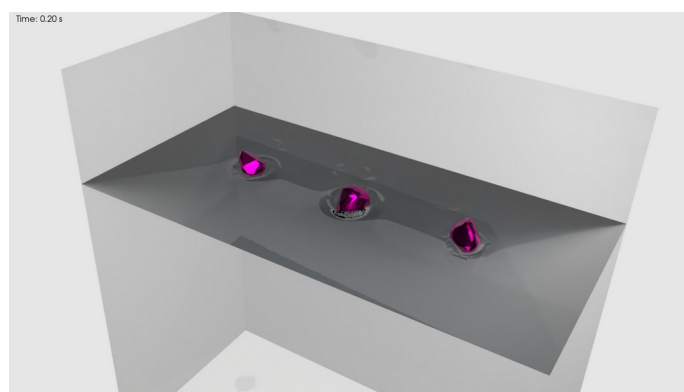


Figure 3: Three differently shaped convex particles at the moment of impact onto the water surface. Except for particle shape and count the simulation setup is identical to the one shown in Figure 2.

# Design principles for composite wear liners with inserts

Daniel Grasser<sup>1</sup>

<sup>1</sup> TUNRA Bulk Solids, Newcastle, Australia

**Abstract**— Reducing wear in bulk materials handling is critical for an effective production and to reduce costs. Raw materials often include hard solid particles that cause significant wear on the handling equipment; this wear is being influenced by the mode of particle motion (sliding or rolling) and the sliding velocity. Today, however, design principles for wear liners utilising these fundamentals are limited. To tackle this gap of knowledge, this study was focused on composite wear liners with reinforcing inserts. Based on two design elements of the composite, namely the base plate and the inserts, design principles targeted to foster a less severe particle flow regime were derived. A comprehensive overview of micro scale principles, such as the application of the Rule of Mixture (ROM), was conducted and the principles upscaled to macro scale composites, where applicable. The particle flow and wear were assessed by experiments and calibrated numerical models using the Discrete Element Method (DEM). The effect of the design parameters, namely the spacing, exposure height and the diameter of the inserts on wear performance of the liners was investigated systematically. Importantly, these design parameters are formulated in respect to the size of the abrasive particles, enabling scalable wear solutions. An optimal designed composite wear liner with inserts can significantly increase the service life, when compared to a conventional wear liner.

**Keywords:** Discrete Element Method (DEM); Dry Sand Rubber Wheel (DSRW) test; composite, abrasive wear.

## 1. Introduction

Composites can perform significantly better than their constituents. The Rule of Mixture (ROM) is a tool to predict the performance, for example the wear performance, of a multi-constituent component [1]. Deviations from the ROM indicate secondary effects, which need to be understood and offer optimisation potential. To the best of knowledge, the ROM has not been utilised to assess and optimise composites wear liner with inserts for bulk handling applications. The present investigations are based on previous experimental [2] and numerical studies [3, 4]. Interestingly, composites can retain a geometrical pattern and exposure height of reinforcing inserts due to different wear rates between the constituents (inserts and base plate). This is an important benefit of composites over conventional single-phase wear plates. This study is targeted to investigate the effect of spacing, exposure height and diameter of the inserts on the wear performance, while comparing the results with conventional wear liners and the ROM prediction.

## 2. Methodology

Table 1: Overview of all investigated wear liners.

Methodology	Number of investigated wear liners	Comment
Dry Sand Rubber Wheel (Experiment)	5	Laboratory scale
Dry Sand Rubber Wheel (Simulation)	23	Laboratory scale
Transfer chute (Simulation)	37	Full-scale
–	65	All investigations

The composite wear liner designs were tested experimentally and numerically. Experimentally, the Dry Sand Rubber Wheel (DSRW), similar to the ASTM G65 [5], was used to test the composites under controlled conditions. Numerically, the DSRW was implemented as a Discrete Element Method (DEM) model and the results were validated against the experimental results. Additionally, a numerical DEM model of a transfer chute was implemented; 35 composite wear liners and two references (conventional wear liners) were simulated. An overview of all investigated wear liners is shown in (Table 1).

In the experiments, in the DSRW, hard inserts with 1 mm diameter were placed in a soft (less wear resistant) base plate and this resulted in different wear rates between the two constituents (Figure 1). In the simulations, in the DSRW, the investigated insert diameters were 1 mm, 2 mm and 4 mm. The abrasive particle size distribution possessed a  $d_{50}$  value (50% sieve size passing) of approximately 0.5 mm. Size, size distribution and particle shape were consistent with the experimental dimensions. For the transfer chute, the insert diameter was 20 mm and the particles were mono-sized with a sieve size of 20 mm. Additionally, four case studies with size distributions between 3.5–32 mm were implemented for the simulations of the transfer chute. All particles were non-spherical for all investigations (an example of particles in the DSRW test are illustrated in Figure 2).

The inserts were placed in an equi-distant pattern (Figure 1). The important parameters were the spacing,  $\lambda$ , diameter,  $\delta$ , and exposure height,  $\varepsilon$ , of the inserts (Figure 4). Where the spacing and diameter of the inserts depend on the vol% of the inserts and a wide range of combinations was investigated (Table 1). The exposure height (at steady-state) was a result of the wear rate ratio between the inserts and the base plate [2]. The resulting wear rate and wear pattern were compared to the wear performance of conventional (flat) wear liners.

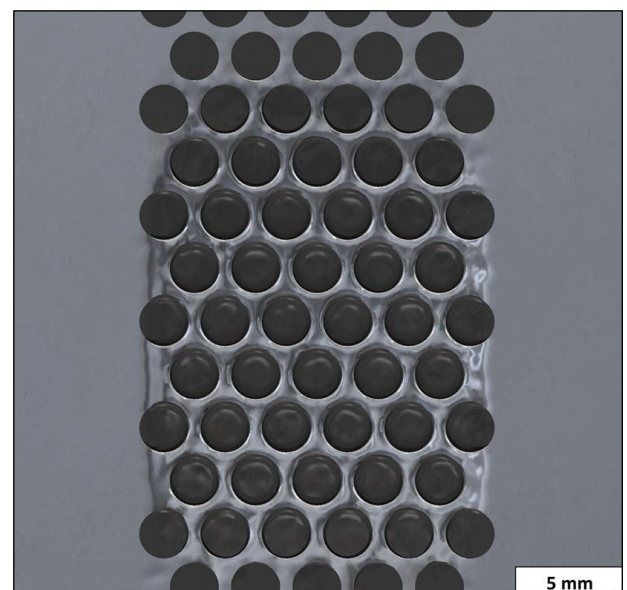


Figure 1: Example of a simulation result of a composite wear liner with inserts in the DSRW test.



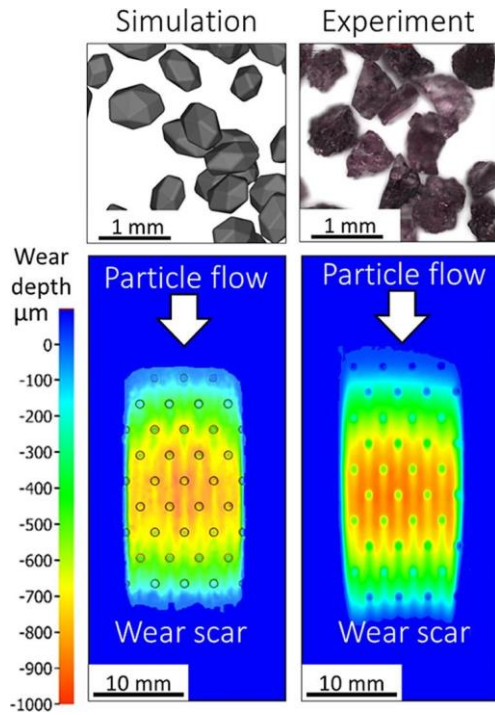


Figure 2: Example of an experimental and a corresponding simulation wear pattern and abrasive particles in the DSRW test.

### 3. Results

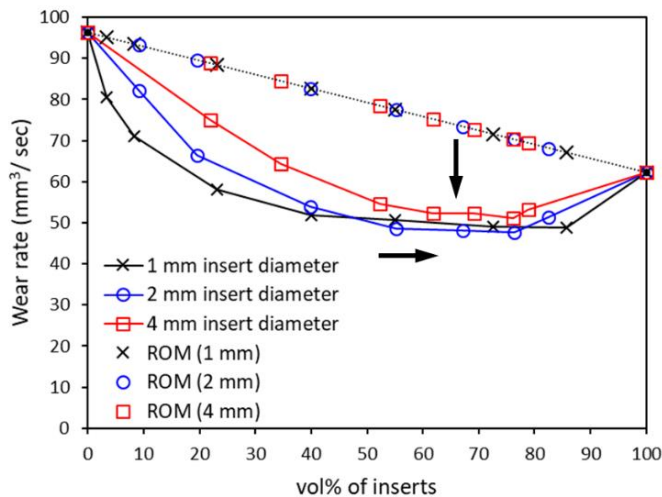


Figure 3: Simulation results of the DSRW test. Wear rates as a function of the vol% of inserts and different insert diameters. *Note:* The black arrows indicate the optimum (lowest wear rate). ROM indicates the Rule of Mixture prediction.

Good agreement was found between the wear pattern and wear rates of the experiments and simulations for the Dry Sand Rubber Wheel (DSRW) abrasion wear test (Figure 2).

On the laboratory scale, in the DSRW test, the optimum (lowest wear rate) occurred for a shift into a regime of high vol% of inserts, however, for further increasing vol% a tendency towards a reverse trend was observed (Figure 3). Moreover, the reduction of wear rate was different for each insert diameter; smaller insert diameter showed the lowest wear rate (most beneficial) of a wide range (Figure 3). Summarising, the lowest wear rates were seen for vol% leading to spacing and insert diameter combinations, causing a spacing/ particle size ratio,  $\tilde{\lambda}$ , close to 1, the exposure height/ particle size ratio,  $\tilde{\epsilon}$ , larger than 0.5 and a diameter/ particle size ratio,  $\tilde{\delta}$ , smaller than 5 (Figure 4). Importantly, a deviation (improvement) of up to 42% was found for optimum composite designs, when compared to a conventional wear liner and the ROM prediction (Figure 3).

On the full-scale, in a transfer chute, similar beneficial size ratios and mechanisms were found (Figure 4 (b)). However, while the shear intensity was lower for an optimum design composite wear liner ( $\tilde{\lambda} \approx 1$ ,  $\tilde{\epsilon} > 0.5$ ,  $\tilde{\delta} < 5$ ), the impact intensity was higher (especially for the inserts) for non-optimum designed wear liners. Interestingly, the lowest particle velocity, highest rotational velocity and the build-up of a protective particle layer (rock-box) [6] was observed for the optimum designed wear liner with inserts (Figure 4).

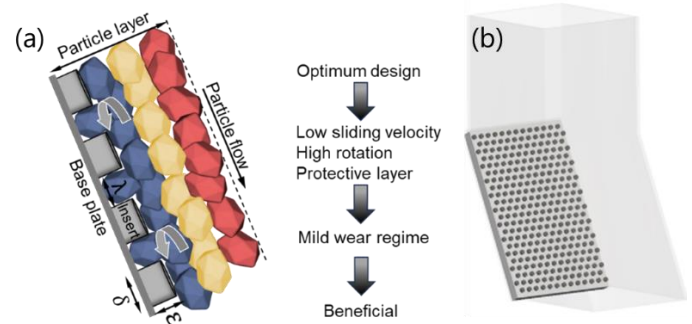


Figure 4: (a) Schematic of the design parameters ( $\lambda$ ,  $\epsilon$  and  $\delta$ ) and important particle flow mechanisms (blue=slow, orange=intermediate, red=fast). (b) Example of a transfer chute with a composite wear liner with inserts.

### 4. Conclusions

For the experiments and simulations, good agreement was found for the wear pattern and wear rate of the composite wear liners with inserts. Similar mechanisms were observed on different size scales (laboratory scale and full-scale transfer chute). For the optimum design, the quantities associated with wear were reduced. Importantly, for an optimum designed wear liner, a change from sliding to rolling particle motion occurred. Additionally, a protective particle layer (similar to a rock-box) and reduced particle velocity were observed. Paradoxically, the abrasive particles can be utilised as reinforcing elements. To reduce abrasive wear, optimum composite wear liners with inserts can be designed for specific particle size ranges, such as known size ranges after a crushing process. An optimum composite wear liners with inserts can significantly increase the service life of bulk materials handling equipment.

### Acknowledgement

TUNRA Bulk Solids, University of Newcastle (Australia) is acknowledged for their support. Additionally, parts of this research were conducted during the affiliation with Deakin University (Australia) and the ARC Industrial Transformation Training Centre in Alloy Innovation for Mining Efficiency.

### References

- [1] M. M. Khrushchov, Principles of abrasive wear, *Wear* 28(1) (1974) 69–88.
- [2] Daniel Grasser, Santiago Corujeira Gallo, Michael Pereira, Matthew Barnett, Experimental investigation of the effect of insert spacing on abrasion wear resistance of a composite, *Wear* 494–495 (2022) 204277 <https://doi.org/10.1016/j.wear.2022.204277>
- [3] Daniel Grasser, Santiago Corujeira Gallo, Michael Pereira, Matthew Barnett, Wear simulation and validation of composites (insert-reinforced matrix) in the dry sand rubber wheel test, *Minerals Engineering* 207 (2024) 108583 <https://doi.org/10.1016/j.mineng.2024.108583>
- [4] Daniel Grasser, Santiago Corujeira Gallo, Matthew Barnett, Michael Pereira, Design principles for wear liners with inserts in mining chutes, *Powder Technology* 436 (2024) 119450 <https://doi.org/10.1016/j.powtec.2024.119450>
- [5] Standard test method for measuring abrasion using the dry sand/ rubber wheel apparatus, ASTM International, USA, 2017.
- [6] Daniel Grasser, Understanding Mining Equipment Wear, *Australian Bulk Handling Review (ABHR)*, Volume 29, Issue 3 (May/ June 2024).



# RFID-based Early Failure Detection for Composite Idler Rollers for Belt Conveyors

Dietrich Trepnau<sup>1</sup>, Andre Katterfeld<sup>1</sup>, Yevhen Redka<sup>2</sup>, Rolf Schwandtke<sup>2</sup>

<sup>1</sup> Chair of Material Handling, University of Magdeburg, Magdeburg, Germany

<sup>2</sup> Artur Küpper GmbH & Co. KG, Bottrop, Germany

**Abstract**— The paper will present the first results of a research project where composite idlers for belt conveyors are investigated. The used idler rollers consist out of a glass fiber tube which is covered with a PU layer. The development of a wear sensor is the focus of research. The wear sensor is integrated into the PU layer and is based on RFID technology. This allows an easy and efficient detection of the wear state of the PU cover without integrating additional electronics in the idler. Due to the non-metallic structure of the idler, the RFID technology can be used. The first test results for the RFID technology is shown and it is explained how this wear sensor is applied in a more complex setup to monitor the condition of the composite idlers as well as to predict the end of the lifetime of such rollers.

**Keywords:** belt conveyor; composite idler; RFID

## 1. Introduction

Belt conveyors are one of the most important conveying systems used in mining and bulk material handling. The research in this field is dedicated to increase the efficiency and reduce power consumption of belt conveying systems. Another aim is the more and more detailed condition monitoring of each component of such systems to reduce unplanned down times.

Composite idlers can reduce the total motion resistance of the conveyor plant due to lower dead weight. The reduced weight of the idler rollers requires less massive support frames and reduces the effort of installation. At the same time, this type of idlers often shows lower material build-up probability on the idler shell in comparison to classical steel shells. However, the life time prediction of composite idlers regarding damages of the shell such as fatigue or wear is much more challenging than for idlers out of steel. Hence, in a joint research project of the Artur Küpper GmbH & Co. KG (AKT) and the University of Magdeburg a wear sensor and a methodology for the life time prediction should be developed.

## 2. General Idler Design

While several composite idlers are on the market, the so-called xForce idler design of AKT consist of a carrying roller shell made of fiberglass-reinforced plastic tubing with a PU coating, lightweight roller ends, and a torsion-resistant hollow axle (see Fig. 1). These idlers are primarily used when the following requirements are placed on the idlers:

- Weight reduction (up to 40% less total mass compared to steel idlers)
- High load capacity (50% higher load-bearing capacity compared to standard plastic carrying idlers)
- Chemical resistance
- Heat resistance
- Low noise emission levels
- Excellent concentricity properties (TIR <0.2 mm/m)
- Durability

- Self-cleaning properties (prevention of material build-up)

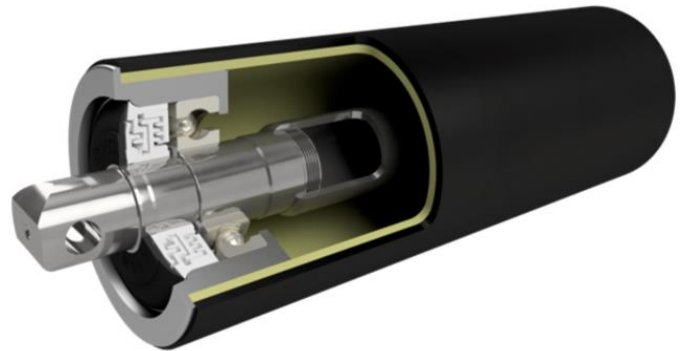


Figure 1. xForce composite idler design by Artur Küpper GmbH & Co. KG

## 3. First Idea of Wear Sensor

The abrasive wear of the composite shell is one main parameter which is limiting the lifetime of such idlers. Whereas the PU cover is relatively resistant to wear and the decrease of the thickness of this layer has no structural importance for the idler, the fiberglass shell is not designed to withstand abrasive wear and its damage severely influences the structural integrity of the whole idler. Hence, it is important to monitor the wear rate of the PU cover.

Since, manual measurements of the cover thickness are no option if higher amounts of composite idlers are used, the integration of a simple wear sensor was one main aim of the research project. For (distance) measurements from outside it must be considered, that material build-up on the idler may influence the result. Hence, the first idea was to implement a simple electric circuit in the cover and a measurement device in the idler which analysis the wire resistance as shown in Fig. 2. If the wire is broken due to wear, the measured resistance should increase. If wires could be integrated in several depth within the PU cover, a detection of wear at several levels should be possible.

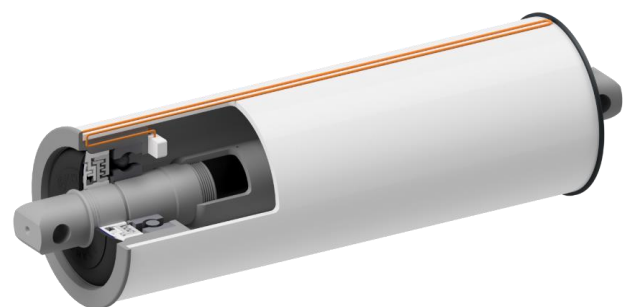


Figure 2. Wire sensor in the PU cover and resistance measurement within in the idler.

Integrating electronics in the idlers itself is often challenging due to conflicting requirements [1]. The costs of the components

should be very low and at the same time the reliability very high. The integration of a battery as the power supply for the electronics is usually the cheapest solution. Than the lifetime of the battery should be longer than the average lifetime of the idler. Another problem is the sending of the data out of the idler. Whereas this is not simple for standard idlers out of steel, it should be easy for the composite idler without a metal shell.

#### 4. RFIDs as Wear Sensors

The non-metallic shell generated the idea to use passive RFID tags as the wear sensor. The RFID application at a fibreglass matrix could already be proven by [2]. While such tags cannot be used on a metal surface, they can be applied on and within the PU cover of the composite idler. Depending on the size of the RFID tags several could be applied over the whole length of the idler. The RFID tags could be read by an antenna outside the idler, installed e.g. on the supporting frame. Fig. 3 is showing the application idea.

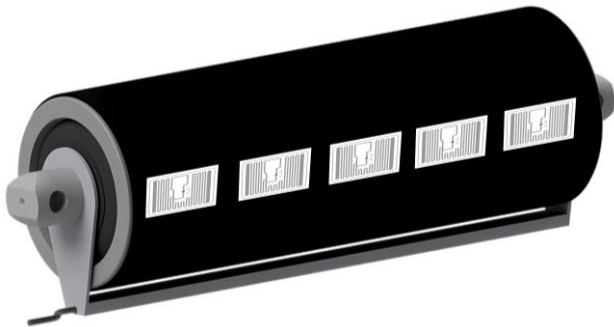


Figure 3. RFID tags as wear sensors along the idler length

To identify the limitation of the RFID use, a set of standard RFID tags e.g. RFID Smartrac Dogbone Impinj Monza R6 (costs per tag approx. 0.2 €) and a standard UHF antenna (860-960 MHz with a gain of 6dBi, costs approx. 45€) where used to study the reading possibility of the tags depending on the

- Distances between several tags
- Distances between tags and antenna
- Positioning on a rotating composite idler
- Disturbance due to metallic objects between tags and antenna
- Cutting failures on the tags
- Wear failures on the tags (simulated by sanding of the tags, see Fig. 4)
- Heat resistance of the tags up 150°C (due to the manufacturing process of the PU cover)

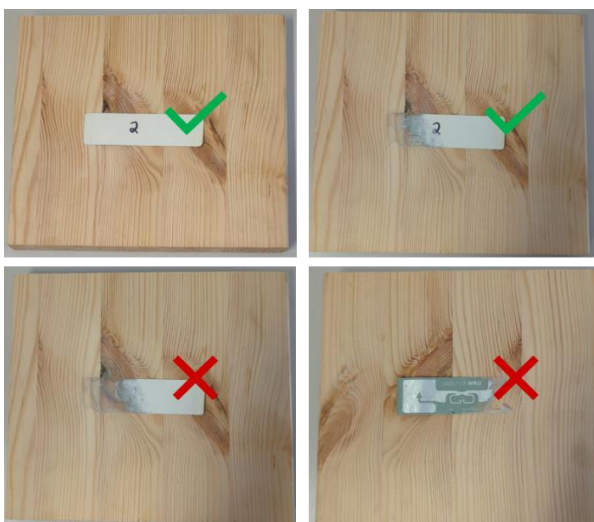


Figure 4. Readability test of RFID tags with different levels of sanded surfaces

In all tests the RFID tags could prove their applicability of the given task. Reading problems were detected when

- RFID tags are overlapping each other,
- antenna is more than 1.5-2 m away from rotating idlers (100 rpm was tested),
- a high number of massive metal objects are placed between tags and antenna,

Further we found, that cutting of the RFID tags does not destroy the function but negatively influence the reading range. The sanding tests showed, that only severely damaged tags could not be read. Also, the RFID tags could be read continuously during and after the placement in a climate chamber and heating to 150°C.

#### 5. Conclusion and Outlook

Ongoing manufacturing test will explore how the tags could be precisely positioned in a certain depth of the PU cover as well as the influence of the tags to the overall properties of the PU cover.

With the developed RFID sensor it is possible to detect the decrease of the PU cover. However, the lifetime of composite idlers is also limited due to the fatigue in the fibreglass core. The main influencing factors on this process are frequency and size of the load as well as boundary conditions such as operating temperature. The development of holistic prediction models for the composite idler lifetime as well as its validation is another part of the ongoing research project.

#### Acknowledgement

This research project (ZIM project number: 16KN074760) is supported by the Federal Ministry for Economic Affairs and Climate Action (BMWK) on the basis of a decision by the German Bundestag. The authors would like to thank for the financial support.

#### References

- [1] A. Katterfeld; C. Richter; K. Fessel; M. Ajmal; R. Schwandtke; Y. Chumachenko: 3iS - intelligent IoT idler stations for the identification of damaged idler bearings. In: Proceedings of the ICBMH 2019, Gold Coast, Australia, Institution of Engineers Australia, 10 S., 2019
- [2] Pecho P, Hruz M, Novak A, Trsko L. Internal Damage Detection of Composite Structures Using Passive RFID Tag Antenna Deformation Method: Basic Research. Sensors (Basel). 2021 Dec 9;21(24):8236. doi: 10.3390/s21248236. PMID: 34960329; PMCID: PMC8705414.

# Design and simulation of a powder feeding system for LP-DED process under zero gravity

Matthias Pusch<sup>1</sup>, Andre Katterfeld<sup>1</sup>, Niklas Hoffmann<sup>1</sup>, Marvin Raupert<sup>2</sup>, Christoph Lotz<sup>2</sup>, Ludger Overmeyer<sup>2</sup>

<sup>1</sup> Chair of Material Handling, University of Magdeburg, Magdeburg, Germany

<sup>2</sup> Institute of Transport and Automation Technology, Leibniz University Hanover, Hanover, Germany

**Abstract**— Laser powder directed energy deposition (LP-DED) is an additive manufacturing process where the metal powder is transported by a carrier gas to the processing point. There, a concentrated laser beam melts the metal powder and builds up material on the workpiece by moving the workpiece or the processing unit. A powder feeder is required to generate the powder carrier gas mixture, which mixes the concentrated metal powder with the carrier gas flow. Due to several advantages the LP-DED process is interesting technology for space research. Hence, the LP-DED process under zero gravity conditions is currently investigated in the so-called Einstein Elevator at the University of Hanover. The Einstein Elevator allows short-term zero gravity or better microgravity conditions. For this research facility a powder feeder that also works under zero gravity conditions was developed. The functionality of the feeding principle was investigated with the help of DEM and coupled CFD-DEM simulations. The experimental results regarding the function of the feeding system are compared with the predictions of the simulation. Finally, an outlook on the further experiments under short-term zero and reduced gravity conditions in the Einstein Elevator is given.

**Keywords:** additive manufacturing; LP-DED; metal powder; CFD-DEM simulation; microgravity

## 1. Introduction

Several additive manufacturing technologies are tested for the use in space missions to provide universal repairing and manufacturing possibilities on longer mission to Moon and Mars. In comparison to wire based methods, the use of the laser powder directed energy deposition (LP-DED) belonging to the group of laser metal deposition (LMD) technologies brings additional challenges, since powder need to be stored and feed continuously during the process within a microgravity ( $\mu g$ ) condition. However, LP-DED has several advantages including the production of near-net-shape parts, coating, joining, adding features and, unlike all other additive manufacturing processes, components can also be repaired. Hence, the LP-DED in  $\mu g$ -condition is the focus of joint research project between the universities of Hanover and Magdeburg. To investigate the LP-DED a new device for generating short-time (up to approx. 4s)  $\mu g$ -condition is used: the Einstein-Elevator (see Fig. 1).

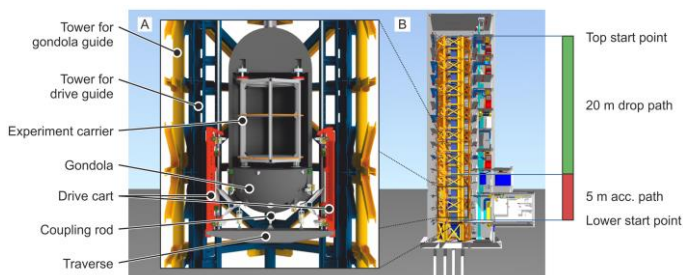


Figure 1. Einstein-Elevator with gondola [1]

The primary aim of the joint project is to study the properties of seed sticks manufactured under  $\mu g$ -condition. To enable this, a device was required which allowed the feeding of metal powder without the help of gravity. Two devices were developed with the help of coupled CFD-DEM simulations. Two metal powders were used for the investigations: titanium (Ti-6Al-4V) and nickel alloys (Inconel 625).

## 2. LP-DED process and powder properties

The LP-DED uses a laser beam to melt a thin layer of the base material in a controlled manner. This ensures that a metallurgical bond is formed between the coating and the base material. The metal powder is then injected with six jet nozzle through a gas stream containing inert gas. The flexible positioning of the nozzle makes the process very versatile. As described in more detail in [2] for optimal manufacturing with the LP-DED process, various parameters must be adjusted to the environmental and production conditions before and during the process. This includes the laser power, the powder mass flow, the shielding gas flow, the laser spot diameter, the focus diameter of the powder, the vertical feed rate and the material properties of the powder. Due to the properties of the used metal powders (nickel and titanium alloys), the inert gas argon is used as the shielding gas.

The Inconel 625 powder, which is an alloy on nickel base with 22 % of chromium, around 9 % of molybdenum, around 4 % of niobium and tantalum and several other elements of less than 0.5 % each. The powder Ti64-G23-E (or short Ti64), also known as Ti-6Al-4V is an alloy on titanium base (89 %) with around 6 % of aluminium and around 4 % of vanadium. Other elements are only present in traces. Important properties of the metal powders are shown in Table 1.

TABLE I. PROPERTIES OF THE USED METAL POWDERS

Properties	Inconel 625	Ti64
Bulk density	4.16 kg/l	2.38 kg/l
d(50)	36 $\mu m$	70 $\mu m$
Angle of Repose	27.1°	29.5°
$\phi_p$ from ring shear tests	33°	32°
Wall friction vs. stainless steel X5CrNi18-10	0.45	0.39
Wall friction vs PE	0.33	0.32

Although angle of repose as well as the frictional values from shear test are quite similar, Ti64 can be characterised as a free flowing powder due to the almost spherical particle visualised by SEM imaging in Fig. 2. Inconel 625 particles have a much less spherical shape. Interlocking between Inconel 625 particle is very easy. Hence, Inconel 625 behaves more cohesive.



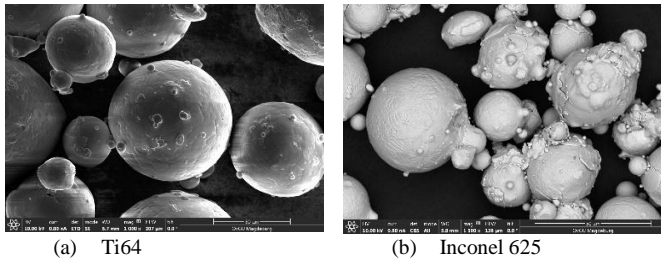


Figure 2. SEM images of the used metal powders

The volumetric flow rate of the shielding gas is at minimum 8 l/min, better around 15 l/min. Into the stream of gas the powder has to be uniformly feed. Higher gas velocities may contribute to an undisturbed conveying process of the powder.

In the first trials of the LP-DED process under earth gravity two powder mass flow rates were successfully tested: 13.3 g/min for Inconel 625 and 7.4 g/min for Ti64. Because of their different bulk density, it is around the same volumetric flow rate of 3.2 ml/min. The mass flow rate of the powder and hence the mixture rate of powder in the carrier gas stream has to be easily and precisely adjusted. A blocking or jamming of the powder inside the powder feeding system has to be avoided at all times. The generation of a stable constant material flow rate is an important requirement.

### 3. Developed powder feeders for $\mu g$

The identified volumetric flow rate of just 3.2 ml/min can be characterised as very small. The precise feeding under earth gravity is typically done by filling a small volume which is then exposed to the gas flow. For  $\mu g$  conditions several concepts for the powder feeder were developed and tested with DEM and coupled CFD-DEM simulations. However, the fine particle size distribution and the small openings limited the usage of the simulations for a prediction of the mass flow rate. Two designs for the powder feeder were selected for build and experimental testing.

The first idea for the feeder was simple: create artificial gravity by centrifugal forces within a centrifuge as shown in Fig. 3. To prevent blocking of the pipeline the bins in the centrifuge should have an opening of 1-3 mm only.

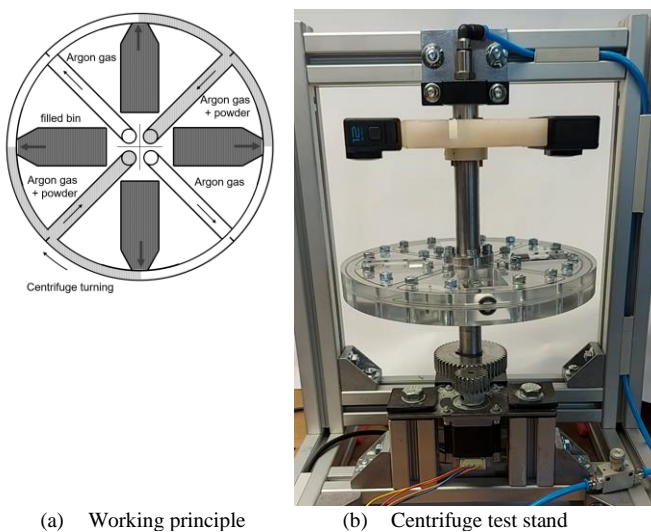


Figure 3. Centrifuge powder feeder

The working principle was tested successfully in first prototypes. However, the manufactured test stand (Fig 3 b) could not provide reproducible mass flow rates. Also, the necessary 131 rpm of the 250 mm centrifuge disk could have an effect on the artificial  $\mu g$  environment of the Einstein-Elevator.

Therefore, a powder feeder with very small working speeds was developed. The design includes a scraper blade with sits on top of a bucket filled with the metal powder. The bucket itself rotates and lifts slowly.

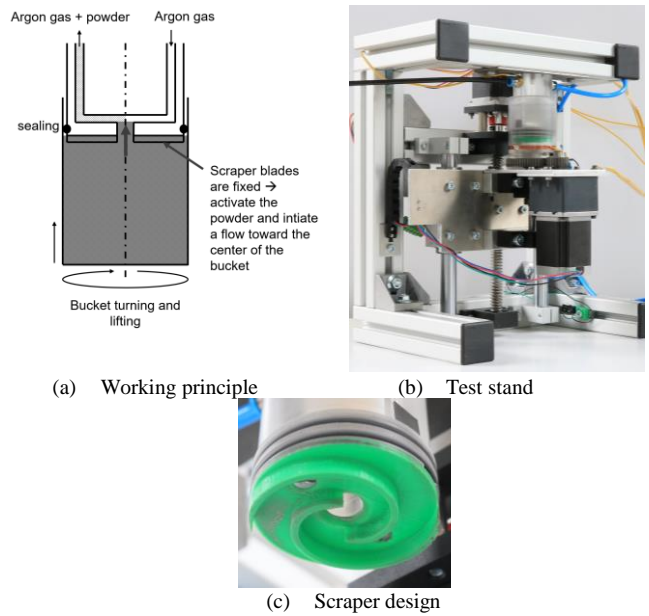


Figure 4. Scraper bucket powder feeder

With the scraper bucket design a powder mass flow rate with good reproducibility could be reached depending on a corresponding speed set of bucket lifting and rotation and the gas flow rate (see Fig 5).

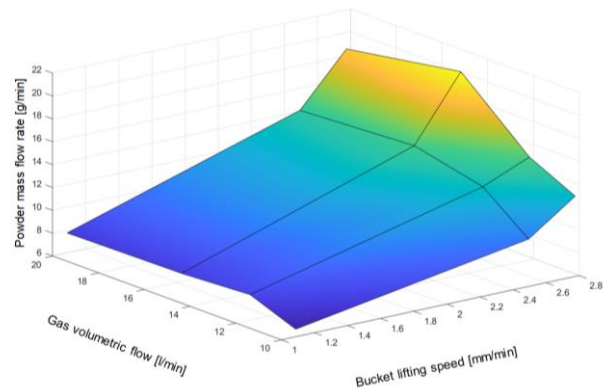


Figure 5. Powder mass flow rate depending of gas flow and bucket lifting speed.

During the tests under  $\mu g$  condition in the Einstein-Elevator the achieved powder mass flow rates must be measured with special mass flow rate sensors.

### Acknowledgement

This research project (project number: 456663377) is funded by the Deutsche Forschungsgemeinschaft (DFG). The authors would like to thank the DFG for their financial support. In addition, the authors would like to thank the DFG and the Lower Saxony state government for their financial support for building the Hannover Institute of Technology (HITec) and the Einstein-Elevator (NI1450004, INST 187/624-1 FUGB).

### References

- [1] C. Lotz, T. Froböse, A. Wanner et al. (2017) Einstein-Elevator: A New Facility for Research from  $\mu g$  to 5g. Gravitational and Space Research, Vol 5, No 2, S. 11-27. ISSN 2332-7774.
- [2] M. Raupert, M. Pusch, E. Tahtali, R. Sperling, A. Heidt, C. Lotz, A. Katterfeld, L. Overmeyer: *Laser Metal Deposition with Metal Powder in Microgravity*. Conference Proceedings Deutscher Luft- und Raumfahrtkongress 2022 Dresden, doi: [10.25967/570466](https://doi.org/10.25967/570466)



# The Spontaneous Liquid Flow On The Small Particle Moving Pattern

Zheng Wang<sup>1</sup>, Constantijn Sanders<sup>2</sup> and Agba D Salman<sup>1</sup>

<sup>1</sup> Department of Chemical and Biological Engineering, University of Sheffield, Mappin Street, Sheffield, S1 3JD, UK

<sup>2</sup> Nestlé Product Technology Centre, Nestlé Strasse 3, CH-3510 Konolfingen, Switzerland

**Abstract**— The homogeneity of milk products has attracted more attention, such as rehydrated infant milk formula and milk beverages. The addition of the water-insoluble nutrients, such as vitamin and minerals, has brought some problem on the product appearance and bioaccessibility. The water-insoluble particles with different size may trigger several issues. For example, the big particles would settle down to the bottom driven by gravity, while some fine particles might stick on the wall of the container or floating on the liquid surface. All of them could reduce the concentration of the nutrients intentionally added by the manufacturer and the homogeneity of the milk suspension. This work focus on the natural convection in a rectangular enclosure. The development of the wall plume is visualized by recording the motion of the particles.

**Keywords:** natural convection; particle floating; suspended particles;

## 1. Introduction

In infant milk formula, water-insoluble ingredients have currently drawn more concerns, because stability and homogeneity of the particle suspension can strong affect bioaccessibility of the insoluble nutrients. Previous work in our group reveals that the calcium carbonate particle within a certain size range can be suspended in water more than a week without external interference [1]. This work has been inspired to understand how the particles move in a static bulk liquid and its dynamic mechanism of a dilute particle suspension.

Some fine particles might stick on the wall of the container due to the adhesion force ( $F_A$ ). And the big particles settle down reaching to the bottom due to the large gravity force. The sticking and floating particles cannot be dispersed into the liquid and will reduce the concentration of the water-insoluble nutrients in milk suspension.

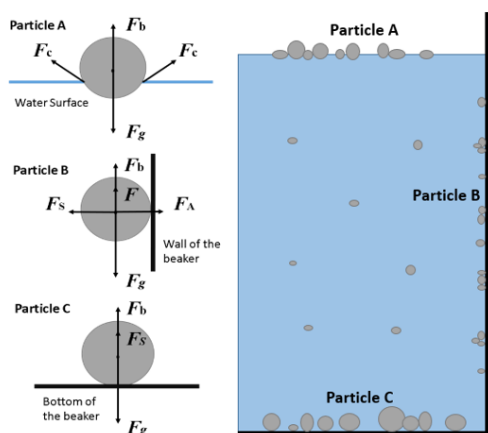


Figure 1. The problem faced when suspending solid particles into liquid. Particle is floating on the liquid surface. Particle B is sticking on the wall of the beaker. While particle C settles down to the bottom.

Natural convection has been wildly reported theoretically and experimentally. It is a self-motivated liquid movement as the results of temperature gradient. The convection currents will

form when the cooler and denser liquid tends to settle down, while warmer and lighter liquid expands to the top. To be more specific, the wall-source buoyant plume has been investigated in details. Caudwell et al. [1] report the turbulent liquid flow along the isothermal hot wall. And the wall plumes are described in details and modelled by involving the entrainment coefficient. Hölling and Herwig [2] firstly pointed out the three layers of the wall plume, namely viscous sublayer, overlap layer and fully turbulent layer. They also provided the equations describing the temperature and velocity profiles in the three different layers respectively. Parker et al. [3] compare the difference of the entrainment coefficients in a convection plume created by forcing dense salt water solution through a porous wall with those of other canonical buoyancy-driven free and wall-bounded flows. It shows that the bulk mixing of the wall-source plumes can be expressed by the characteristic vertical velocities and a constant entrainment coefficient.

In this work, the temperature gradient is identified and the development of the wall plume is visualized. On the other hand, the effect of particles on natural convection is preliminary discussed.

## 2. Methods

### 2.1. Natural convection system

The container is separated into three different heights close to the wall, top middle and bottom. The temperatures of the wall and the liquid far from the wall are measured separately. The heat is insulated from the top and bottom and water fills the entire enclosure to reduce evaporation. The water or the suspension are heated up to 22°C and the room temperature is controlled at 20°C.

### 2.2. High quality image capture

High resolution CCD camera and transmitted LED light were used for video capture. The camera is capable of recording 4K video with resolution of 3860×2090 pixels. Pixel size is reduced to 1.1  $\mu\text{m}$  per pixel. The camera is fixed on a stand that can move in three dimensions with high accuracy of 10  $\mu\text{m}$ . The light source was only on when it was recording or focusing and would be turned off when the camera stopped. The duration of recording is 1 s. During the experiments, the camera can be placed at 5 different heights, bottom, medium bottom, middle, medium top and top. The focal plane also can be moved inside the liquid, where the distance to the wall can be adjusted from 1 mm to 5 mm inside.

### 2.3. Particle size characterization

The samples from different parts are measured using Camsizer (X-Flow, Retsch, Haan, Germany). Then, the particles at the bottom were dry using a hot plate and the dried sediment was gently crushed. The size of sediment was also tested using Camsizer Samples were clearly labelled and tested three times. Small amount of colloid was gently taken following the order of the top, middle and bottom by using a syringe with a rubber pipe on its tip. Sample was placed on glass slide and heated to accelerate evaporation of water. The dried particles were observed under the Light Microscopy (Keyence, Osaka, Japan).

### 3. Results and discussion

#### 3.1. Particle size distribution at different locations

Figure 2 show the picture of different particles captured by microscope and Figure 3 is the cumulative particle size distribution measured by Camsizer. As the results, the particles suspended in the liquid are the smallest among these four followed by the sticking particles collected on the wall. Bigger particles with hydrophobic surface float on liquid surface. And the largest particles tend to settle down at the bottom.

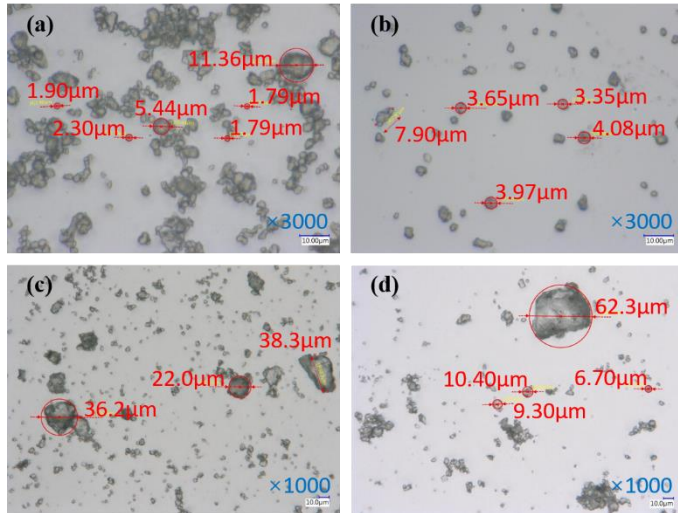


Figure 2. Pictures taken by Microscope for the particles from different places. (a) and (b) taken under 3000 magnification show the sticking particles and suspended particles respectively. (c) and (d) taken under 1000 magnification show the floating particles and particles from sediments.

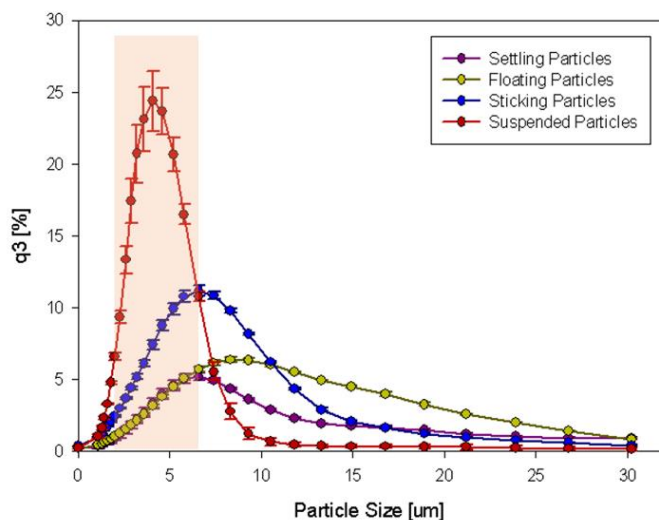


Figure 3. Size distributions of different particles.

#### 3.2. The effects of water evaporation on particle velocity

The suspended particles follow the movement of the surrounding fluid. The flow pattern will be investigated in future work. Figure 4 show the particle moving direction in a thin layer close to the wall. The suspension was prepared by combining calcium carbonate powder (Longcliffe, UK) in distilled water. In order to evaluate the effects of heat transfer, the suspensions were prepared at uncontrolled room ( $20 \pm 2^\circ\text{C}$ ) and controlled room  $20^\circ\text{C}$  individually. In the controlled group distilled water was conditioned at  $20^\circ\text{C}$  and the videos were obtained after transporting the suspension to a  $22^\circ\text{C}$  room. The container is sealed to reduce the effects of water evaporation. All the videos

are analysed through the PIV software individually to calculate the particle velocities. The results are shown in Figure 5.

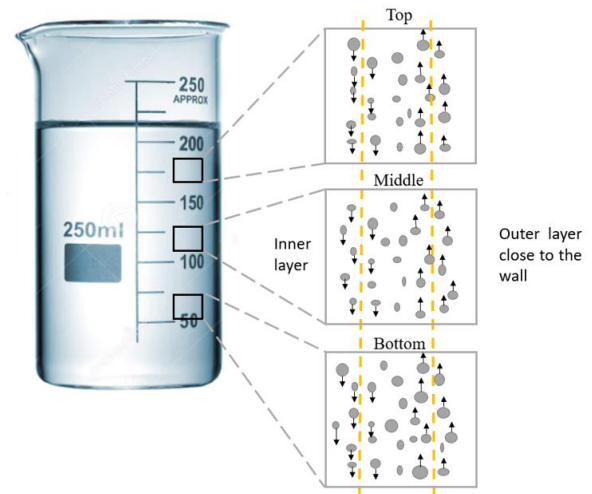


Figure 4. The schematic results of observation.

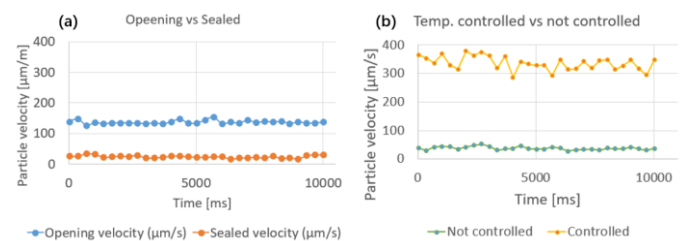


Figure 5. The difference between particle moving velocity. (a) a sealed container vs an opening container and (b) Temperature controlled vs room temperature.

The results are shown in Figure 5. In Figure 5a, the particles move in a higher speed with water evaporation compared with the particles in the sealed container in the room temperature. That is because water evaporation will absorb more heat from the surrounding environment leading to inhomogeneous temperature distribution in the suspension. To be more specific, the temperature measured at the top layer is slightly higher compared with the middle and bottom with the difference of  $0.1 - 0.2^\circ\text{C}$ . The layer with higher temperature tends to go upward due to its lower density. In the temperature controlled group (Figure 5b), the temperature difference of air and suspension is enlarged to  $2^\circ\text{C}$ . The particle velocity increase with an intense heat exchange and transfer from ambient to liquid.

### 4. Conclusion

In this work, the size of suspended particles is measured. And the particle moving speed is calculated in the thin layer close to the wall.

### References

- [1] Wang, Z. et al. (2024) 'Investigation of the homogeneity of particle suspension', Chemical engineering research & design, 205, pp. 280–291.
- [2] Caudwell, T., Flór, J.-B. and Negretti, M. E. (2016) 'Convection at an isothermal wall in an enclosure and establishment of stratification', Journal of fluid mechanics, 799(799), pp. 448–475.
- [3] Hölling, M. and Herwig, H. (2005) 'Asymptotic analysis of the near-wall region of turbulent natural convection flows', Journal of fluid mechanics, 541(1), pp. 383–397.
- [4] Parker, D. A. et al. (2020) 'A comparison of entrainment in turbulent line plumes adjacent to and distant from a vertical wall', Journal of fluid mechanics, 882(1).

# Simulation and validation of a highly cohesive paste inside a storage bin

Daniel Grasser<sup>1</sup>, Shaun Reid<sup>1</sup>, and David Bradney<sup>1</sup>

<sup>1</sup> TUNRA Bulk Solids, Newcastle, Australia

**Abstract**— Predicting and simulating the flow behaviour of highly cohesive slurry is a challenge. In this study, a cohesive multi-phase bulk material (coal tailings and water) was simulated. The phases consist of high moisture, paste-like ultrafine coal tailings and a coarse reject. The goal was to model the bulk material flow when discharged from a storage bin. To address the feasibility of modelling a large volume of paste, a coupled Discrete Element Method (DEM) and Smoothed Particle Hydrodynamics (SPH) model was implemented using ANSYS Rocky 2024. Experimental trials on two different size scales were conducted to calibrate and validate the model; firstly, a simplified bin consisting of a straight tube combined with a plunger to simulate the head pressure of the bin, secondly, a scaled bin with a head height of 2.5 m. The DEM-SPH model was calibrated based on different head pressures applied to the tube and two bins with 65° and 80° wall angles, respectively. Several important simulation parameters affecting the two-phase flow were examined. Good agreement between the numerically predicted bulk particle flow and the experiments was achieved. Eventually, a full-scale bin with a head height of approximately 20 m was implemented in the DEM-SPH model. The full-scale bin design was tested using the calibrated parameters, applying approximately 30 million combined DEM-SPH particles. This allowed the prediction of the bulk material flow, however, at high computational efforts. Based on this numerically validated design, the full-size bin is going to be manufactured and commissioned on the mine site.

**Keywords:** Discrete Element Method (DEM); Smoothed Particle Hydrodynamics (SPH); storage bin; cohesion; bulk material.

## 1. Introduction

Bulk materials equipment, such as storage bins, often is of a large-scale and handles significant volume of material. This equipment is expensive to design and manufacture, but also incurs significant operating costs if the equipment fails, for example, due to lost time and remediation of a blocked storage bin. To address this and to validate the design process of bins for high density paste-like slurries, Discrete Element Method (DEM) and Smoothed Particle Hydrodynamics (SPH) was used. The goal was to model the bulk material flow behaviour of a highly cohesive two-phase material (coal and water) and to assess the predicted discharge behaviour of a storage bin on an Australian mine site, while assessing the feasibility of the simulation approach with respect to computational demand.

## 2. Methodology

### 2.1. Simulation: DEM-SPH model

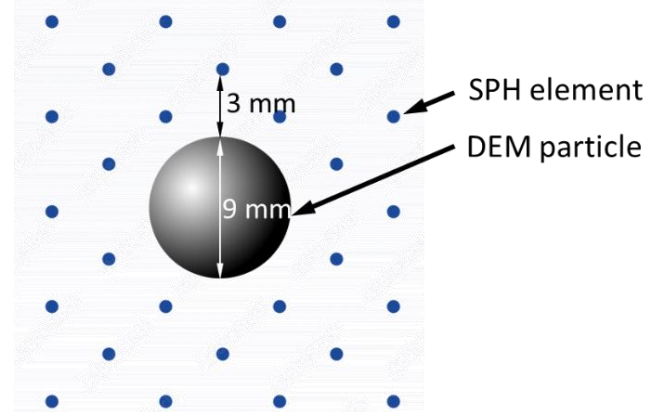


Figure 1: Illustration of a DEM particle and several SPH elements.

The Discrete Element Method (DEM) and Smoothed Particle Hydrodynamics (SPH) were used to model the cohesive bulk material paste (Figure 1). For this, the commercially available software Rocky 2024 R1.1 provided by ANSYS was utilised. The DEM particles represented the coarse fraction and the SPH elements the liquid fraction, respectively, of the cohesive two-phase bulk material. To represent the bulk particle flow, while still having reasonably short computational times, the particles in DEM are commonly upscaled. The size of the DEM particles was 9 mm (mono-sized spheres). The SPH elements possessed a distance of 3 mm and this was consistent for all setups; resulting in a constant DEM particle to SPH element ratio of 3 (Figure 1). Different cohesive models were applied to simulate the cohesive bulk properties of the DEM particles, and the resulting bulk particle flow was compared (constant adhesion model, linear adhesion model, JKR adhesion model). Good agreement was achieved using the linear cohesion model and it was used for all investigations. The other important DEM parameters, for example, the coefficient of friction and rolling resistance were chosen based on best practices. The viscosity of the liquid SPH phase was 100 Pa·s.

### 2.2. Experiment: simplified laboratory scale bin

The first experimental setup, was based on a straight PVC pipe with a height of 350 mm and a diameter of 100 mm, representing a simplified storage bin and was conducted under laboratory conditions (Figure 2). Importantly, the pipe diameter was more than 10× larger than the DEM particle size (see previous section). The bulk material was filled into the tube. A polymer plunger was loosely fitted inside the tube. Then, to discharge the bulk material, the load on the plunger was incrementally increased up to 350 N, resulting in a head pressure of up to 44 kPa. To assess the bulk particle discharge behaviour, a video camera was placed horizontally to the discharge location of the tube and images of the videos were taken at set time intervals. The required computational time was 3 h.



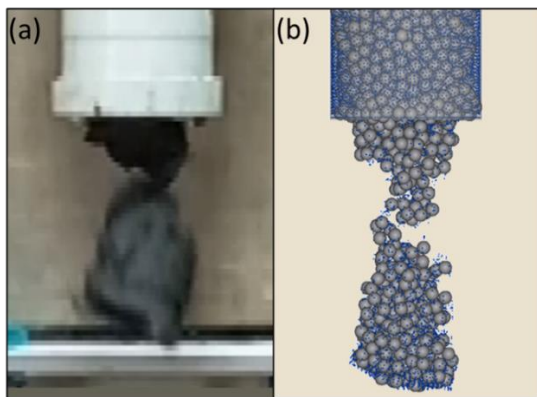


Figure 2: Simplified laboratory scale bin (Tube-plunger).  
(a) Experiment, (b) DEM-SPH model.

### 2.3. Experiment: scaled bin on mine site

The second experimental setup was conducted on a mine site and consisted of two scaled storage bins. For both bins, the height of the bins was approximately 2.5 m and the top diameter was 0.7 m (Figure 3). The wall angles were 65° and 80° to the horizontal, respectively, resulting in a diameter of the discharge opening of 0.35 m for the steeper case (Figure 3). The bulk material was filled into the bins using a forklift. After the material was filled in, the bulk material was discharged from the bin by opening the gate at the bottom. The computational time was 12 h.



Figure 3: Scaled bin on mine site with a wall angle of 80° and a height of 2.5 m. (a) Experiment, (b) DEM-SPH model.

## 3. Results

Good agreement was found between the results of the DEM-SPH simulations and the experimental results (Figure 2, Figure 3). Qualitatively, the bulk material flow agreed well, replicating consolidation effects near the transition zone between the straight and angled region of the bin. Quantitatively, the mass flow rate (Figure 2) and the shape of the discharged pile (angle of repose) (Figure 3) was quantified at consistent time intervals and the shape showed good agreement with the experiments.

Finally, the full-size bin with a height of approximately 20 m was implemented. Consistently, the calibrated DEM-SPH parameters were used, as described previously. This resulted in approximately 30 million particles and a required simulation time of 30 days. Qualitatively, a sufficient discharge of the highly cohesive two-phase bulk material was indicated by the calibrated simulation model for a particular bin design (Figure 4). Moreover, important quantities such as the particle velocity and wall pressure can be extracted from the simulations and compared with existing analytical models.

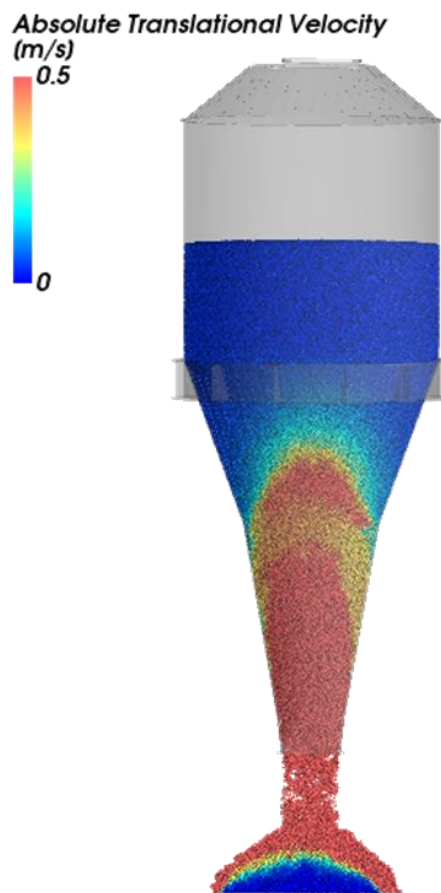


Figure 4: DEM-SPH model of the full-size bin with a height of 20 m. The colour scale indicates the velocity of the discharging particle stream (red=fast, blue=slow).

## 4. Conclusion

A coupled Discrete Element Method (DEM) and Smoothed Particle Hydrodynamics (SPH) numerical model was used to study the bulk material flow of a highly cohesive, paste-like material. After the calibration of the model, using observations from laboratory scale experiments and scaled bins on the mine site, the DEM-SPH model was validated. Good agreement was observed for several quantities associated with the bulk particle flow, for example the angle of repose. A full-scale bin was implemented using the calibrated bulk material, and a large volume of material consisting of approximately 30 million particles was simulated. The design process of the storage bin was accelerated by successful simulation of the cohesive bulk material. The DEM-SPH model can be applied to optimise the design process of similar bulk material applications. However, further research targeted to reduce the computational efforts is suggested.

## Acknowledgements

TUNRA Bulk Solids, University of Newcastle (Australia), is acknowledged for the opportunity to publish this research.



# Alternative Measures in DEM Calibration of Cohesive Materials via Angle of Repose Test

Aleksej Lavrinec<sup>1</sup>, Ognjen Orozovic<sup>1</sup>, Vincent Hamilton<sup>1</sup>

<sup>1</sup> University of Newcastle, Australia

*Discrete Element Method (DEM) simulations require calibration, usually accomplished through simple experimental measurements that are then matched in simulations by varying the relevant parameters. A systematic and consistent calibration methodology for achieving this mapping between experiments and simulations is largely solved for cohesionless materials, however, this is not the case for calibration of cohesive materials. Most cohesionless materials are calibrated through experiments that visually measure various angles. However, when applied to cohesive materials, the measurement of angles in these experiments are ambiguous, resulting in researchers developing more intricate tests that are too complicated or specific and do not see wide adoption as a result.*

*The study presented employed the conventional cylinder lift angle of repose test, arguably the simplest of all experiments but with a very high sensitivity to the ambiguity of measuring angles when applied to cohesive materials. However, instead of only measuring the angles, a number of alternative quantification techniques were employed in this study. Coarse sand was used as the material for experiments which was then simulated in Rocky DEM. Various parameters were calculated, but fractal dimension proved to be the most useful for material calibration. Cohesive materials tend to form complex patterns on the surface and fractal dimension is an applicable measure of the complexity of these patterns.*

**Keywords:** DEM; calibration; cohesive bulk material;

## 1. Introduction

Handling cohesive materials is a challenge. Wet and sticky materials tend to adhere to equipment surfaces, leading to build-up and blockages in hoppers, chutes, screens and mixers. Reducing the probability of these events occurring is important simply because these blockages can be extremely costly.

Using discrete element method (DEM) simulations is one of the most popular tools when optimising bulk material handling systems and processes. DEM is certainly capable of simulating the behaviour of cohesive materials through implementing additional tensile forces between the particles, however the challenge lies in calibrating DEM simulations.

DEM calibration is usually done by conducting a small scale and simple experiment and then matching the results in the simulations. The most popular way of achieving that is by doing an angle of repose test, measuring the angle in an experiment and then simulating a range of rolling and sliding frictions to find the combinations that match the. If a more accurate calibration is required, more complicated experiments can be used: dynamic angle of repose, rotating drum, draw-down – the advantage of these tests is that they allow to measure and match multiple parameters simultaneously. In general, the calibration experiment should represent the problem being solved by DEM, but also needs to be small enough in scale to be solved quickly.

In general, these procedures work well for cohesionless materials, however they are not as applicable for cohesive ones. The main issue is that measuring various angles, parameters that are arguably the most useful in the case of cohesionless materials, is either challenging or entirely impossible when it comes to cohesive materials. The reason for that is that cohesive

materials simply do not form an objectively measurable angle and even when they do, the angle that is formed is not unique or unambiguous. What is more, it can be argued that the main characteristic of cohesive materials is the clumping and formation of agglomerates as well as significant asymmetry, and not the angles that are formed.

In any case, the problem of calibrating cohesive materials remains and has been around for a number of years now with researchers applying various alternative experiments and measures to calibrate for cohesion. Some examples include:

- Lifting a cylinder slowly and measuring the cracks and curvature that the material forms. [1]
- Lifting a plate from underneath the material and measuring the angles of the resulting clump. [2]
- Rotating a small sample in a centrifuge and measuring the angle the material forms due to lateral forces. [2]
- Using a rotating drum, but measuring centre of gravity instead of the angle. [2]
- Consolidation-penetration, measuring bulk density after consolidation and accumulative penetration of a wedge-shaped tool. [3]

Most of these alternative ways to calibrate are relatively complicated and stray too far away from the tried and tested simple angle of repose. This paper uses a simple angle of repose test to look at two new parameters to help with calibrating cohesive materials: fractal dimension and symmetry.

## 2. Fractal dimension

Firstly, it is assumed that the concept of symmetry is generally understood and will not be addressed in this discussion. Instead, a more detailed explanation of fractals and fractal dimension will be provided. The first step on the way to understanding how fractal dimension can be applied to measure a bulk solid is to dispense of the notion that fractals are necessarily self-repeating or self-similar. There are many definitions of a fractal, some more pedantic than others, however, the generally accepted one is that a fractal is a geometric shape whose fractal dimension is higher than its topological dimension. [4,5]

Without going into the mathematical definition of topological dimensions, it is more important to understand that the topological dimension of any line is 1. The fractal dimension definition is actually closely related to the well-known coastline paradox and is easier understood through an example of one of the ways to calculate it – the box counting method. The procedure is as follows:

- Overlay the shape with a grid of boxes sized  $\epsilon$  and count the number of boxes  $N(\epsilon)$  that contain at least a part of the object (object being a line in this case)
- Decrease the box size  $\epsilon$  and repeat the counting process.
- Plot  $N(\epsilon)$  against  $1/\epsilon$  on a log-log scale and use linear regression to find the slope of the line which is the negative of the fractal dimension:

$$D = - \frac{\log(N(\epsilon))}{\log(\epsilon)} \quad (1)$$

For example, the coastline of Norway is very rough and its fractal dimension is 1.52. Great Britain and Australia are much smoother with  $D$  of 1.25 and 1.13 respectively.

### 3. Methodology

RockyDEM was used to make a simulation of the cylinder lifting test. The target material was coarse sand that was simulated as 4-5 mm in particles. Hertz-Mindlin contact model with type C rolling friction and JKR cohesion model were used.

Both simulations and experiments were then evaluated by taking a number of snapshots of the final state. The simulated case was rotated 360 degrees with 360 screenshots taken, one for every degree. The experimental setup was treated similarly, by rotating the sample on a turntable and then only keeping the frames that are unique – unique being a relative term here, but approximately 300 frames were selected.

The frames were then image-processed to output a line that describes the perimeter of the bulk material. This line was then processed using the box-counting method to calculate the fractal dimension. Naturally, the fractal dimension varied depending on the angle the pictures were taken, therefore the mean of all the points was taken to represent the fractal dimension of that case.

Symmetry was processed in a similar way. The images were processed similarly to the fractal dimension calculation and then the centre of mass was calculated to split the shape into vertical and horizontal halves. The horizontal symmetry might be useful for calibrating cohesive materials, however, is outside of the scope of this paper. The Vertical symmetry, however, is useful, but since the object is rotated 360 degrees, naturally the mean relative centre of gravity is exactly at 0.5. In order to use this to quantify how symmetrical the pile of sand is, the standard deviation of the normalised symmetry is calculated instead.

### 4. Results

The case was simulated varying sliding and rolling friction between 0.2 and 0.9 in increments of 0.1. Cohesion energy density was varied from 0.0 to 3.0 with smaller increments closer to zero and larger after. Sample results are presented in Figure 1 and Figure 2. A number of experiments were conducted, however the ones presented here are the extremes of very dry and nearly saturated sand.

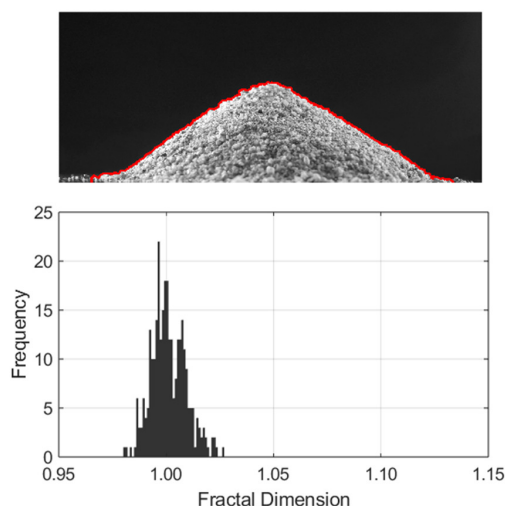


Figure 1: Dry sand perimeter and distribution of fractal dimensions. Mean fractal dimension of 1.001.

Simulation results were compiled in a similar fashion and show similar trends with the highest cohesion tests having a fractal dimension of approximately 1.10 and the cohesionless

ones of approximately 1.00. The symmetry about the vertical axis was useful as well, since low cohesion tests had a narrow distribution with low standard deviation and standard deviation increased with cohesion. Additional corrections needed to be applied to experimental measurements as material was not centred perfectly on the turntable.

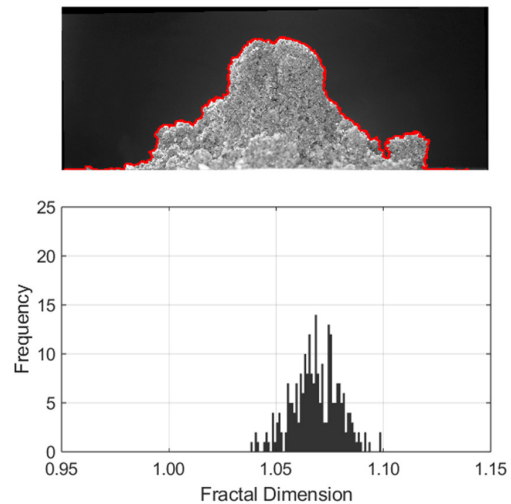


Figure 2: Wet sand perimeter and distribution of fractal dimensions. Mean fractal dimension of 1.069.

### 5. Conclusion

Simple angle of repose tests were performed experimentally and in simulations. Fractal dimension has proved to be a useful metric to help alleviate ambiguity when it comes to calibrating cohesive bulk solids. The key findings from this investigation are as follows:

- Fractal dimension can be used to quantify the complex surfaces that cohesive materials form.
- Multiple measurements are required as fractal dimension can vary drastically from one viewing angle to another.
- In future work, the actual distribution of fractal dimensions can be used to further enhance calibration.
- In the current work fractal dimension varied between 1.00 and 1.10.
- Measuring variations in symmetry is useful, but care needs to be taken in experiments to make sure the material is in the centre of the turntable.

### Acknowledgement

We would like to thank Ansys for providing a research license of RockyDEM.

### References

- [1] T. Roessler and A. Katterfeld, "DEM parameter calibration of cohesive bulk materials using a simple angle of repose test", *Particuology*, vol. 45, pp. 105–115, 2019.
- [2] O. C. Scheffler and C. Coetzee, "DEM calibration for simulating bulk cohesive materials", *Computers and Geotechnics*, vol. 161, p. 105476, 2023.
- [3] M. J. Mohajeri, C. van Rhee, and D. L. Schott, "Replicating cohesive and stress-history-dependent behavior of bulk solids: Feasibility and definiteness in DEM calibration procedure", *Advanced Powder Technology*, vol. 32, no. 5, pp. 1532–1548, 2021.
- [4] B. B. Mandelbrot and B. B. Mandelbrot, *The fractal geometry of nature*, vol. 1. WH freeman New York, 1982.
- [5] Grant Sanderson (3Blue1Brown). "Fractals are typically not self-similar," *YouTube*, 28 Jan 2017 [Video file]. Available: <https://www.youtube.com/watch?v=gB9n2gHsHN4>

# Investigating the Impact of Expansion and Bubble Explosion on Particle Size Variation in Single Droplet Drying and Spray Drying Processes

Xuqian Li<sup>1</sup>, Constantijn Sanders<sup>2</sup>, and Agba D. Salman<sup>1</sup>

<sup>1</sup> University of Sheffield, UK

<sup>2</sup> Nestec Ltd., Nestlé Product Technology Centre, Switzerland

**Abstract**—Single droplet drying constitutes a fundamental process across a myriad of drying industrial sectors, where meticulous control over individual droplets is imperative for optimizing product quality and process efficiency. Within this multifaceted realm, the formation and subsequent collapse of bubbles emerge as significant phenomena profoundly influencing particle size variation. This study aims to find the relationship between bubble explosion and the changes in particle size during the single droplet drying process. Employing a multidisciplinary approach, advanced experimental analysis is combined with high-speed camera to capture the dynamic evolution of bubbles within drying droplets with high temperature. Concurrently, particle tracking methodologies are utilized to precisely monitor changes in particle size distribution throughout the drying process. These experimental observations provide invaluable insights into the complex interplay between bubble dynamics and particle size variation during single droplet drying at different temperature. Furthermore, the experimental observations serve as a foundation for optimizing single droplet drying processes and ensuring consistent product quality across various industrial applications. The results shows that bubbles generation and explosion phenomenon happen in the spray drying process, which effect the traditional size distribution prediction. This research gives a new size prediction method for spray drying processes with high drying temperature conditions.

**Keywords:** Spray drying; Bubble expansion; Bubble explosion; Single droplet drying;

## 1. Introduction

Spray drying is a widely used technique in the food and pharmaceutical industries to produce powders from liquid feedstocks. This continuous process involves atomizing a liquid into droplets, which are then rapidly dried by hot air or inert gases to yield fine powders. It is favored for its ability to control particle size, ensure product consistency, and enhance shelf stability.

The drying kinetics of single droplets are influenced by factors such as droplet size, composition, temperature, and surrounding gas conditions. These parameters affect moisture diffusion and heat transfer rates, which in turn influence internal moisture migration and shell formation dynamics. Particle shrinkage, cracking, and collapse can occur, impacting final particle morphology and powder characteristics.

Despite controlled outlet temperatures being below the boiling point, uneven droplet sizes due to atomizer design can cause some droplets to reach or exceed boiling temperatures. This leads to vapor build-up and increased internal pressure within droplets. The behavior of particles upon boiling depends on the permeability and mechanical characteristics of the formed crust or shell. Particles can inflate, crack, or explode, depending on the shell's properties.

Charlesworth and Marshall's earlier study illustrated different morphology development routes above boiling, based on the

shell's mechanical properties [1]. In open porous systems, low resistance to internal mass transfer prevents the particle temperature from reaching boiling. Less permeable crusts result in internal pressure build-up, with morphology depending on the crust's rigidity. Rigid crusts cause fractures, while plastic shells may stretch and puff or rupture and collapse.

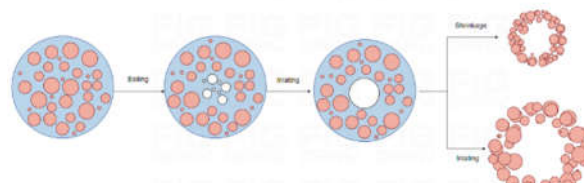


Figure 1. Morphology development routes when drying at temperatures above the droplet boiling temperature.

## 2. Literature review

The nature of the skin is still a matter of debate, it can be defined as a specific region with viscoelastic behavior, a layer of soft gels, or a film of glassy polymers [2]. Tran et al. carried out an intriguing investigation that assessed the drying kinetics of lactose/water droplets at air temperatures above and below boiling point [3]. Although an IR was added to detect the humidity of the exit air and, consequently, the mass loss from the droplet, this investigation still used a filament SDD. This study assessed the locking point at and above boiling as well as the frequency of cycles of inflation and deflation. Locking was defined as the minimal diameter before the droplet enters the boiling stage above boiling and as the point at which the diameter becomes constant below boiling. The final particle's morphology verified that puffing had occurred. In order to account for the impact of the inflation/deflation cycles on changes in particle diameter and the drying curve, the experimental data gathered from drying experiments—specifically, conditions of skin formation, locking point, and inflation/deflation parameters—were compiled and applied in an empirical submodule.

A few studies have also documented the impact of boiling on the ultimate size and shape of dried particles. Paramita et al. (2010) used confocal laser scanning microscope (CLSM) and scanning electron microscopy (SEM) to examine the effects of additives like ethanol, gelatin, or decaglycerol monolaurate as well as outlet air temperature on the morphology of spray-dried gum Arabic/maltodextrin systems[5]. It was noted that a greater percentage of hollow particles was produced during spray drying at higher air temperatures. Furthermore, because of their involvement in the early stages of skin creation, the additives also contributed to the rise in the fraction of hollow particles.

Using a monodisperse spray dryer, Rogers et al. (2012) also looked at the effects of drying skim milk at temperatures exceeding boiling [6]. No puffing was seen at 124°C for the inlet air temperature, and all of the particles were buckled and had surface folding. Fifty percent of the particles exhibited puffed structure with thin shells and bigger diameters at 181 °C, the higher air temperature. The diameters of the final dried particles were greater than those of the original droplets.

### 3. Materials and methods

#### 3.1. Material

Whole fat milk powder used in this research is from Nestle and the content is shown in following table, the raw size D50 is 78.9  $\mu\text{m}$ . Powders were reconstituted at 20°C in de-ionized water with magnetic stirrer with 40% w/w solid content.

#### 3.2. Methods

Different solid content whole fat milk single droplets are dried in three different methods. Dino-lite Digital Microscope and high-speed camera are used to capture the drying process. 2.5  $\mu\text{l}$  volume droplets are generated by Eppendorf pipettes manually. The distance between camera and droplet is 20cm and the magnification rate is set at 40x.

Single droplet is attached to a filament and placed in a drying chamber as shown in Figure 2. The droplets were attached to the filament by Eppendorf pipettes and hold by friction and capillary force. X-ray and SEM were used to observe the surface and structure of droplet.

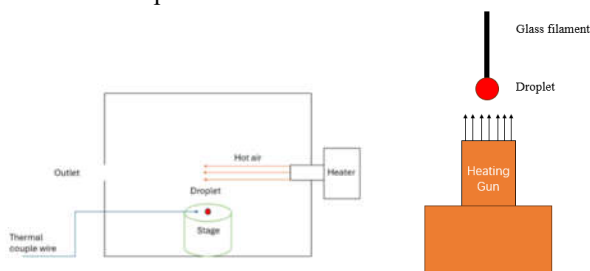


Figure 2. Sketch and set up of sessile drying and filament drying

### 4. Results

#### 4.1. Sessile drying

The size reduction of different solid content droplets dried in room temperature is shown in Fig. 3. Generally, the drying rate increases with the decrease of solid content. The shell is not formed or not well formed, which result in the low concentration droplet drying curves (pure water, 10%, 20%) are overlapped. The end point is little bit higher than the solid content, which may because of the bubble area inside the droplet. 10% and 20% droplets are in low viscosity and the shell formation is slow, so that the components hardly hold the water evaporation so that cause the overlapping with pure water, but with time after 30 mins, the 10% and 20% droplet form a tiny shell, so they did not end at 0. Because of their high viscosity and shell formation speed, 30% and 40% droplets drying curve are overlapped. The limitation of this method is for low viscosity droplet, high contact angle and high hydrophobic surface is necessary.

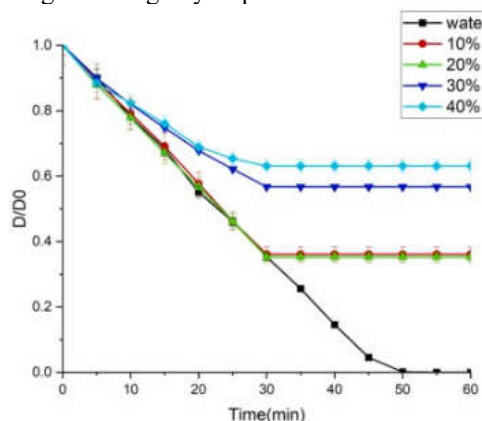


Figure 3. The drying rate curve of different concentration milk droplets of sessile drying droplets.

#### 4.2. Filament drying

The size reduction rate is decreasing with the increase of concentration but need more time until total dried as shown in Fig. 4. The drying rate is obviously increases with the decrease of solid content. The shell is well formed that all the end point is much larger than the solid content. The milk droplet of 40% solid content end around 0.8 which refers to high porosity.

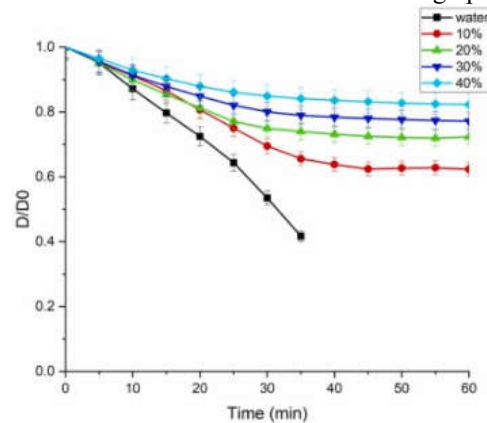


Figure 4. The drying rate curve of different concentration milk droplets of filament drying droplets.

### 5. Conclusion

For low temperature drying the shrinkage is taken the main place. However, for high temperature, the occurrence of bubble boiling and explosions in droplets within spray dryers highlights the need for improved particle size prediction models. Traditional size prediction methods do not account for the dynamic behaviours observed at and above boiling temperatures. By incorporating the effects of vapor bubble formation, shell characteristics, and multiple bubble generations, predictive models can be refined to better forecast final particle sizes and morphologies under various drying conditions.

### References

- [1] D. H. Charlesworth and W. R. Marshall, "Evaporation from drops containing dissolved solids," *AIChE Journal*, vol. 6, no. 1, pp. 9–23, Mar. 1960, doi: <https://doi.org/10.1002/aic.690060104>.
- [2] K.Y. Ozawa, T Okuzono, M Doi, Diffusion process during drying to cause the skin formation in polymer solutions. *Japanese journal of applied physics*. 2006 Nov 8;45(11R):8817.
- [3] T. T. H. Tran, M. Jaskulski, J. G. Avila-Acevedo, and E. Tsotsas, "Model parameters for single-droplet drying of skim milk and its constituents at moderate and elevated temperatures," *Drying Technology*, vol. 35, no. 4, pp. 444–464, Apr. 2016.
- [4] V. Paramita, K. Iida, H. Yoshii, and T. Furuta, "Effect of Additives on the Morphology of Spray-Dried Powder," *Drying Technology*, vol. 28, no. 3, pp. 323–329, Mar. 2010, doi: <https://doi.org/10.1080/07373931003627098>.
- [5] S. Rogers, W. D. Wu, S. X. Q. Lin, and X. D. Chen, "Particle shrinkage and morphology of milk powder made with a monodisperse spray dryer," *Biochemical Engineering Journal*, vol. 62, pp. 92–100, Mar. 2012, doi: <https://doi.org/10.1016/j.bej.2011.11.002>.



# Hydrodynamic and Heat Transfer Investigation of A Fluidised Bed Solar Receiver

Farid Jalili Jamshidian<sup>1</sup>, Jhuma Sadhukhan<sup>1</sup>, Charley Wu<sup>1</sup>, and Dimitrios Tsaoulidis<sup>1</sup>

<sup>1</sup> University of Surrey, Guildford, UK

**Abstract**—Fluidised beds have been introduced as a promising option to act as the receiver of Concentrating Solar Power (CSP) plant. To investigate the performance of the receiver during the air-solid interaction under heating, a laboratory-scale fluidised bed was built, and pressure and temperature were measured at different levels in the centre of the bed. Different scenarios were defined to assess the effect of particle material, particle size, bed aspect ratio and air velocity on hydrodynamics and heat transfer along the bed. Results showed that the as the size increased, thermal efficiency could attain highest value at 57%.

**Keywords:** fluidised bed; thermal receiver; CSP;

## 1. Introduction

Commissioning Concentrating Solar Power (CSP) plants all over the world have experienced a considerable rise during the last 2 decades. A host of them use molten salts as the heat transfer medium. However, to overcome limitations such as high melting temperature and decomposition at higher temperatures, a lot of attention was given to other promising alternatives such as solid particles, which are inexpensive and abundant. Taking advantage of solid-gas Fluidised Beds (FBs) as a solar thermal receiver in heliostat solar fields has been introduced as a prominent option for both transferring and storage of heat in a solar power plant.

Several works were conducted on the integration of heliostat fields, fluidised beds as receivers or heat exchangers and a power cycle to generate electricity. In a relevant study to confirm the feasibility of FBs utilized as a direct or indirect HTF in a power cycle, Zhang et al. [1] suggested particle suspension as heat carriers in FBs to increase the efficiency and reduce the capital and operating costs of CSPs. They carried out experiments on both a single tube and a bundle of 16 parallel tubes with Silicon Carbide (SiC) and Cristobalite particles at the CNRS 1 MW plant. Results proved that heat transfer coefficients up to 1100 W/(m<sup>2</sup>K) for bare tubes and 2200 W/(m<sup>2</sup>K) for finned tubes were achievable at low superficial gas velocities under 0.2 m/s.

Even though different coupling configurations of fluidised beds and solar power plants have been studied so far, a deeper understanding at the working conditions of the particle solar receiver including solid material, bed geometry, particle size and air mass flow rate is essential. This study aims to investigate experimentally the performance of a laboratory-scale fluidised bed using different particle types and sizes at various fluidisation velocities at 2 states (with and without heating). Delving into the multiphase behaviour of air-particle at the first step and investigating the thermal efficiency of the bed, can shed light on reaching the optimum performance of a particle-based solar power plant.

## 2. Facility and Experiments

The setup of this study is comprised of a pressure regulator, a ball valve, a rotameter to control the air flow, and an acrylic bed, as shown in Fig. 1. Air is blown into the bottom conical part of the bed for a more uniform and developed flow and then

passes through a perforated plate along with a stainless steel mesh to assure the minimum 30% required pressure drop due to the bed mass is maintained for a distributed air flow across the cross-sectional area of the bed [2]. The bed is equipped with ports at different heights to measure the pressure drop and the temperature of the bed, as well as inlet and outlet air. A thermal pad along with a temperature controller was attached to the bottom half circumference of the bed to simulate the solar radiation on one side of the receiver. Therefore, the remaining parts were insulated to prevent heat loss, as shown in Fig 2.



Figure 1. Fluidised bed rig without heating elements

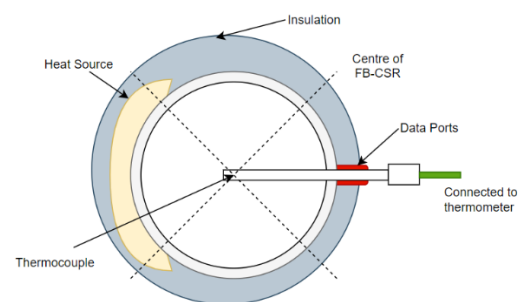


Figure 2. Schematic top view of the heated fluidised bed

The first part of the experiments is related to the hydrodynamic behaviour of the bed without heating. Three different particles of sand, Cristobalite (SiO<sub>2</sub>) and SiC were chosen and sieved to provide a diverse size distribution. One sample of sand and SiC each with the average particle diameter of 310 microns and 3 samples of SiO<sub>2</sub> with the average diameter of 310, 440 and 575 microns were prepared. The minimum fluidisation velocity ( $U_{mf}$ ) was calculated experimentally by the conventional method of measuring the pressure drop across the bed. The aspect ratio (defined as the ratio of the height to the diameter of the bed) changed from 0.5 to 1.5 for each sample and the bed expansion was logged. The bed diameter was set at 71 mm.

The second part of the experiment is dedicated to the thermal performance. The thermal pad is adjusted to heat the bottom 20

cm of the external wall of the bed at constant temperatures of 60, 80 and 100 °C. Heating at each wall temperature continues until the bed and outlet air temperature reach constant temperatures at steady state, then the wall temperature is adjusted to a higher one. This process was replicated for all samples at various air velocities of 1, 1.5 and 2  $U_{mf}$  while the aspect ratio was 1.

### 3. Results and Discussion

The effect of different parameters on the performance of the bed was investigated. To test different air velocities, minimum fluidization velocity ( $U_{mf}$ ) was obtained as shown in Table 1. SiC with the highest density and smallest size, experienced higher pressure drops, while it started fluidisation at the lowest velocity. On the contrary, the coarse SiO<sub>2</sub> with the mean diameter of 575 micron, represented low pressure drop while the fluidisation velocity was the highest.

TABLE I. PARTICLE PROPERTIES AND THEIR WORKING CONDITIONS

Material	Size (micron)	Density (kg/m <sup>3</sup> )	Bed Pressure Drop (Pa)	$U_{mf}$ (m/s)
Sand	310	2630	160	0.12
SiC	310	3210	190	0.08
SiO <sub>2</sub>	310	2350	140	0.1
SiO <sub>2</sub>	440	2350	100	0.12
SiO <sub>2</sub>	575	2350	120	0.17

#### 3.1. Effect of Particle Properties on Bed Expansion

Fig. 3 indicates the expansion of bed under different velocities for 3 samples of SiO<sub>2</sub>. Expansion of bed was defined as the difference between the initial static level and the highest level where some particles could reach. The smallest size of SiO<sub>2</sub> could not only be fluidised at lower velocities but also benefited from highest bed expansion.

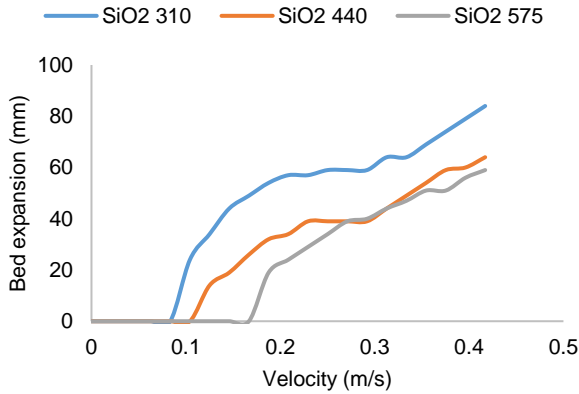


Figure 3. Bed expansion for different sizes of SiO<sub>2</sub>

#### 3.2. Effect of Fluidisation on Heat Transfer

Under constant conditions of aspect ratio 1 for SiO<sub>2</sub> particles with an average diameter of 310 microns, heating was conducted at packed and fluidised conditions at velocities slightly lower and higher than  $U_{mf}$ . Fig. 4 depicts filtered graphs meaning that steady time has been cut from the graphs at each constant external wall temperature of 60, 80 and 100 °C to show the highest steady temperature and its required period during each heated wall temperature. Although outlet air at packed condition could reach approximately the same temperature at half period compared to the fluidised condition, packed bed temperature saw a slight decrease while external heating started at 60 and ended in 100 °C. This fact could show the importance of fluidisation for more uniform heat distribution thanks to air-particle interaction.

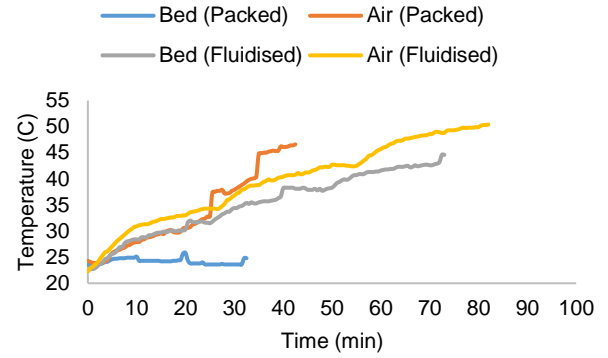


Figure 4. Temperature gradient for the bed and air when packed and fluidised

#### 3.3. Bed Thermal Efficiency

To obtain the bed efficiency, equation (1) was used as following:

$$\eta_{th} = \frac{Q_{air}}{Q_{in}} = \frac{\rho_g U_g A c_{p,g} (T_{g,out} - T_{g,in})}{Q_{in}} \quad (1)$$

$Q_{air}$  and  $Q_{in}$  are the transferred heat to air and power consumption in (W).  $\rho_g$ ,  $U_g$  and  $c_{p,g}$  are density, velocity and heat capacity of air,  $A$  is the cross-sectional area of the bed.  $T_{g,out}$  and  $T_{g,in}$  also indicate the outlet and inlet temperature of air. Table (2) shows different values of bed efficiency for different particles at various velocities and wall temperatures. According to Table (2), increasing the heating temperature from 60 to 80 °C caused a considerable rise in thermal efficiency while this was not significant enough when ascending from 80 to 100 °C. Increasing the flow rate to double could lead to 23% and 30% rise in thermal efficiency at heating temperature of 100 for Sand and SiO<sub>2</sub> 440, respectively. Despite being less efficient at 1  $U_{mf}$ , SiO<sub>2</sub> 440 could stand at the peak at higher flow rates of 1.5 and 2  $U_{mf}$  compared to other materials in terms of thermal efficiency reaching the highest value at 57%.

TABLE II. BED THERMAL EFFICIENCY (%) AT VARIOUS CONDITIONS

Air Velocity (m/s)	$U_{mf}$			1.5 $U_{mf}$			2 $U_{mf}$		
	60	80	100	60	80	100	60	80	100
Wall Temp. (°C)									
Sand 310	22	25	31	37	46	47	42	53	54
SiC 310	22	27	29	34	41	40	39	46	47
SiO <sub>2</sub> 310	27	33	35	37	45	45	45	51	53
SiO <sub>2</sub> 440	17	24	27	43	52	52	48	56	57

### 4. Conclusion

In this work, a tubular fluidised bed was built. Different particles at various sizes were prepared to assess the performance of the bed while exposed to heating. Results showed that by heating a half circumference of the bed, thermal efficiencies above 50% are achievable. To optimize the performance of the bed as a thermal receiver, it is recommended to use a circulating FB to benefit from both lower power consumption and utilising particles as heat storage medium.

### References

- [1] H. Zhang, H. Benoit, I. Perez-Lopèz, G. Flamant, T. Tan, and J. Baeyens, "High-efficiency solar power towers using particle suspensions as heat carrier in the receiver and in the thermal energy storage," *Renewable Energy*, vol. 111, pp. 438-446, 2017/10/01/ 2017, doi: <https://doi.org/10.1016/j.renene.2017.03.101>.
- [2] D. Kunii and O. Levenspiel, *Fluidization engineering*. Elsevier, 2013

# Electrostatic removal of CaCO<sub>3</sub> particles using dielectric barrier discharge

Francisco Pontiga<sup>1</sup>, Helena Moreno<sup>1</sup>, Carlos Soria-Hoyo<sup>1</sup>, Francisco J. Durán-Olivencia<sup>2</sup>,  
Manuel A. Martín-Alfonso<sup>1</sup>, and José M. Valverde<sup>1</sup>

<sup>1</sup> Universidad de Sevilla, Seville, Spain

<sup>2</sup> Universidad Loyola Andalucía, Seville, Spain

**Abstract**— The electrostatic removal of calcium carbonate particles from a glass epoxy surface has been investigated. A surface dielectric barrier discharge has been used to electrically charge the particles. The mass of particles ejected from the surface has been continuously recorded as a function of time for different operating frequencies of the electrical discharge. In all tests, complete particle removal was achieved. However, the results have shown that, in the frequency range considered, the higher the frequency, the faster the particle removal. In contrast, the energy efficiency of the cleaning process is little affected by frequency.

**Keywords:** particle removal; surface cleaning; surface dielectric barrier discharge.

## 1. Introduction

Powder flowability is of prime importance for the development of reliable concentrated solar power (CSP) plants based on the calcination-carbonation reaction of CaCO<sub>3</sub>/CaO, the so-called Calcium-Looping (CaL) process. The CaL process involves the transport of CaCO<sub>3</sub> and CaO granular solids between the calciner, the carbonator and the storage reservoirs [1]. Pneumatic conveying is usually proposed as a viable solution for the transport of high temperature granular solids. However, as particle size decreases (which is beneficial to increase the reactive surface) cohesive forces dominate over inertial ones, turning the granular flow from inertial to cohesive. Therefore, powder build-up starts forming at the walls, increasing the pressure drop in the conveying pipes, favouring the development of intermittent flows and, eventually, interrupting the powder supply.

Particle accumulation on solar panels and mirrors is also a major operational challenge for technologies using solar energy, since dust blocks a significant portion of incident sunlight and reduces the efficiency of solar energy conversion. To mitigate this problem, different cleaning systems that use electric forces have been proposed. In these systems, particles are usually charged by triboelectricity [2] or charge induction [3]. However, in very low humidity conditions, such as those present in the CaL process, charge induction may not be effective. Instead, charging the particles using a surface dielectric barrier discharge may be a suitable alternative [4]. In this work, this last procedure will be applied to investigate the removal of CaCO<sub>3</sub> particles from a horizontal plane surface, with the perspective of its possible future expansion to pipelines.

## 2. Materials and Methods

A FR-4 glass epoxy board, 1.5 mm thick, was used as dielectric substrate of the surface dielectric barrier discharge (sDBD) reactor. The glass epoxy board was cut according to the geometry shown in Fig. 1. On the upper side of the board, 14 copper strips, 22 mm long and 1 mm wide, were arranged in parallel, separated by a distance of 3 mm (red lines, Fig. 1).

Similarly, on the lower side, 15 analogous parallel copper strips were arranged, so that each strip on the upper side was equidistant from two strips on the lower side (blue lines, Fig. 1). The lower side of the reactor was covered with a second FR-4 board, with identical geometry, but without copper strips.

The copper strips on the upper side of the board were connected to a high-voltage amplifier (20/20C-HS, Trek Inc.), which amplifies the signal supplied by an arbitrary waveform generator. Here, a sinusoidal waveform with a frequency between 2 and 50 Hz was used to trigger the electrical discharge. On the other hand, the copper strips on the lower side of the board were connected to ground. A 1μF capacitor was inserted in the path to ground. Therefore, the current intensity of the electrical discharge was determined by measuring the voltage drop across the capacitor.

The CaCO<sub>3</sub> powder used in the experiments was supplied by KSL staubtechnik (Eskal 45), which has a typical particle size between 30 μm and 60 μm. In each measurement, a mass of 1 gram of CaCO<sub>3</sub> was distributed on the upper side of the board, within the rectangular region where the copper electrodes are located. Just beneath the board, a large lightweight container was placed on an analytical balance (AB204-S/FACT, Mettler Toledo, resolution of 0.1 mg).

When a high voltage is applied to the reactor, a surface dielectric barrier discharge develops on the upper side of the board. Thus, the CaCO<sub>3</sub> particles are charged, and they are progressively ejected by the effect of the Coulomb force and collected in the container below. As the CaCO<sub>3</sub> particles fall inside the container, the cumulated mass of ejected particles is registered by the balance and the data is transferred to a computer.

## 3. Results and Discussion

Figure 1 shows, for different operating frequencies of sDBD, the evolution in time of the mass of CaCO<sub>3</sub> particles collected in the container, after being ejected from the board by the action of electrical forces. A small portion of the mass ejected from the board (about 5%) is not collected in the container, but remains adhered to nearby surfaces. Therefore, to facilitate the comparison between the different measurements, the cumulated

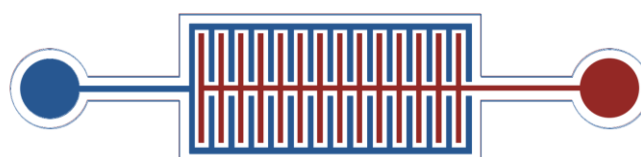


Figure 1. Schematic picture of the dielectric barrier discharge reactor used in the experiments. Copper electrodes on the upper (lower) side of the dielectric substrate are shown in red (blue) colour.

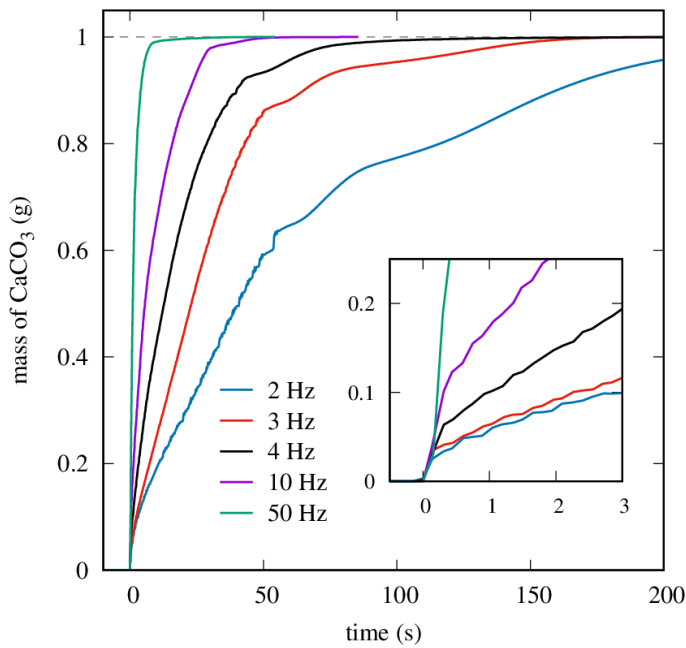


Figure 2. Temporal evolution of ejected  $\text{CaCO}_3$  mass for an applied voltage of 18 kVpp and different ac frequencies.

mass registered by the balance has been normalized to 1 gram. As clearly seen, the particle removal from the board is not a perfectly smooth curve, particularly at low frequencies. The irregularities can be attributed to inevitably non-uniformities of the mass deposited on the board.

Immediately after applying the high voltage, and for a short time (a few fractions of a second), the collected mass grows very rapidly, although the total mass of the ejected particles does not exceed 10% of the mass initially deposited on the board. This behaviour is more clearly observed at low frequencies (see inset in Fig. 2). During this short initial phase, charge induction probably plays a predominant role in the charge acquired by the particles that are being ejected from the board.

Subsequently, the rate of particle ejection decreases, although it is always faster the higher the operating frequency of the discharge. This is because the number of microdischarges in each period of the ac cycle is approximately independent of the frequency. Therefore, the higher the frequency, the more charge is deposited on the particles per unit of time. During this phase, the growth of the mass collected by the balance is approximately linear.

Finally, for longer times, the rate of particle ejection decreases significantly, until the total removal of the particles deposited on the board is complete.

To investigate the efficiency of the cleaning process at different frequencies, it is convenient to define a characteristic sweep time, for example, the time required to remove half of the mass initially deposited on the board. The averaged power over an ac cycle can be obtained by evaluating the area of the Lissajous figure that is generated when the instantaneous capacitor charge is plotted against the instantaneous voltage applied to the reactor [5]. The dependence of the characteristic sweep time with the averaged power dissipated in the sDBD is shown in Fig. 3. As can be readily seen, in the range of frequencies considered in this work, the characteristics sweep time is inversely proportional to the sDBD power. Therefore, the energy required to remove the particles from the surface of the

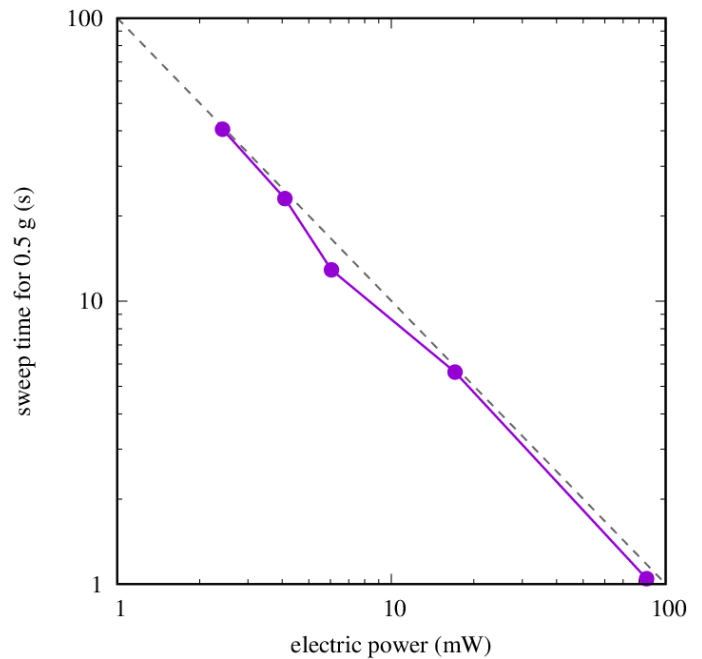


Figure 3. Characteristic sweep time as a function of the electric power dissipated in the sDBD.

board is roughly independent of the frequency of operation of the electrical discharge, and has a value  $E \sim 0.1$  J. However, at high frequencies the cleaning process could be less efficient, since the particles might not acquire a sufficient charge to be ejected.

## 4. Conclusion

The results of this study have confirmed the ability of a sDBD to completely remove the accumulation of  $\text{CaCO}_3$  particles from a surface, with an energy efficiency roughly independent of the operating frequency. At the highest frequency considered in the experiments (50 Hz), the complete elimination of particles was achieved in about 20 s. Further experiments are underway to investigate the effect of using higher frequencies, and powders with smaller or larger particle sizes than those considered in this study.

## Acknowledgement

This research is part of the project PID2022-138943OB-I00, funded by MICIU/AEI/10.13039/501100011033/ and by FEDER, EU.

## References

- [1] M. Alvarez Rivero, D. Rodrigues, C. I. C. Pinheiro, J. P. Cardoso, and L. F. Mendes, "Solid-gas reactors driven by concentrated solar energy with potential application to calcium looping: A comparative review", *Renewable and Sustainable Energy Reviews*, vol. 158, 2022. Art. no. 112048.
- [2] C. I. Calle, C. R. Buhler, J. L. McFall, and S. J. Snyder, "Particle removal by electrostatic and dielectrophoretic forces for dust control during lunar exploration missions", *Journal of Electrostatics*, vol. 67, pp. 89–92, 2009.
- [3] S. Panat and K. K. Varanasi, "Electrostatic dust removal using adsorbed moisture-assisted charge induction for sustainable operation of solar panels", *Science Advances*, vol. 8, 2022. Art. no. eabm0078.
- [4] P. Atten, H. L. Pang, and J.-L. Reboud, "Study of Dust Removal by Standing-Wave Electric Curtain for Application to Solar Cells on Mars", *IEEE Transactions on Industry Applications*, vol. 45, pp. 75–86, 2009.
- [5] D. E. Ashpis, M. C. Laun, and E. L. Griebeler, "Progress Toward Accurate Measurement of Dielectric Barrier Discharge Plasma Actuator Power", *AIAA Journal*, vol. 55, pp. 2254–2268, 2017.



# The future - CO<sub>2</sub> Absorption (Carbonation) and Bulk Materials Handling

Baldeep Kaur, and Michael S.A. Bradley

The Wolfson Centre for Bulk Solids Handling Technology, University of Greenwich, Kent, UK

**Abstract—** The industry is working towards achieving the aim to neutralise CO<sub>2</sub> emissions by 2050. This is accelerating the development of new technologies to capture carbon and hence reduce carbon emissions. These innovative techniques involve processes handling the challenging bulk materials. These bulk materials may include added moisture, elevated temperature, or by-products of ongoing chemical reactions. All these factors affect the handling properties of bulk materials. This research aims to study the handleability of the bulk materials going through various process stages in the process plant.

**Keywords:** carbon capture; characterisation; bulk flow properties.

## 1. Introduction

Carbon capturing is one of the burning issues across the industry to neutralise CO<sub>2</sub> emissions. Carbon capture and storage (CCS) involves three steps: (i) carbon capture, (ii) transportation, and (iii) storage of captured carbon in rocks or deep under the ground. The advanced iteration of CCS is Carbon capture utilisation and storage (CCUS) [1]. CCUS is a step further to utilise the captured carbon by finding suitable applications or converting it into plastics, concrete or biofuels etc. CCUS is strongly supported by the Governments across the developed nations. Heavy industries such as cement, steel, and chemicals are often seen as the major producers of greenhouse gasses, therefore, the flue gases produced from processes are mixed with waste byproducts to create a useful product. Flue dust is also one of the waste products for the cement industry, which is engineered to be recycled by forming a new product out of waste product generated from the cement manufacturing process, also known as the end of waste (EoW) product [2]. The process of carbon capturing generates numerous challenges in handling bulk materials during carbonation processes [3]. This research aims to highlight some of the challenges and discusses mitigation strategies to safely and efficiently handle bulk materials during carbonation processes.

## 2. Experimental Procedure

### 2.1. Carbonation

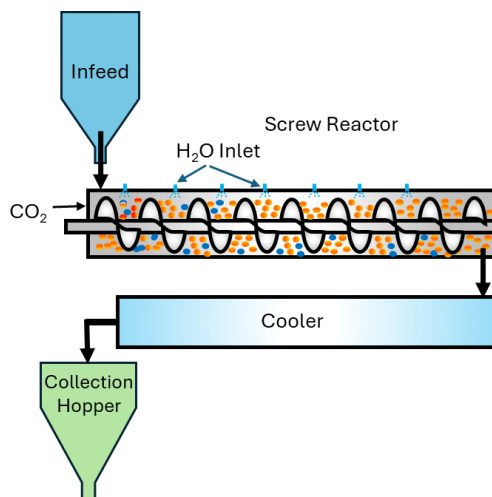
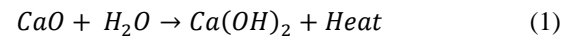


Figure 1: A schematic of a carbonation process.

The carbonation process involves hydration of the bulk material, interaction of hydrated bulk material with the CO<sub>2</sub>, and drying and cooling of carbonated bulk material, as illustrated in Fig. 1. EoW products used for carbonation may contain mineral oxides, such as calcium oxide which reacts with water during hydration process and generates heat [1].



The heat generated during the hydration process needs to be dissipated before it causes structural damage to the constraining equipment. The dissipation capacity of different bulk materials varies; therefore, it is vital to study the heat generation and dissipation properties of the bulk material being handled.

During the carbonation process, there are a few unknown parameters that need to be investigated for the bulk material to maximise the CO<sub>2</sub> absorption: (i) moisture content to fully hydrate the bulk material, (ii) concentration of CO<sub>2</sub> in the flue gas, and (iii) residence time of bulk material in the reactor.

The moisture content of the bulk material has an impact on the flowability of bulk material, thus affecting the handling and storage of the bulk material in the process. This led to investigate flow properties of bulk material at different moisture content levels. Also, heat generation during the reaction process is another aspect that needs to be investigated further.

### 2.2. Bulk materials

Flue dust (FD), a waste by-product of cement manufacturing, has been used as a bulk material to study its handling properties during the carbonation process. Table 1 shows the moisture content of samples of FD. Three samples of FD have been tested for their flow properties to determine the effect of the flowability of FD during different stages of handling during the carbonation process.

Table 1: Free moisture content of flue dust samples.

Synod	Sample	Free Moisture Content (%)
1.	FD (as supplied)	0.4
2.	Carbonated FD	0.43
3.	Double Carbonated FD	0.43

The temperature of bulk material during hydration may reach 120°C or beyond, and if the dissipation of heat is poor then this temperature may increase further.

## 3. Results and Discussions

The structural integrity of storage silos depends on the bulk density, effective internal friction and wall friction of bulk materials. This section examines the variability in the flowability, bulk density and angle of wall friction of the FD during the carbonation process.

### 3.1. Flowability

The flowability of bulk materials is defined by a relationship between major principal consolidation stress and unconfined

yield strength [3]. Fig. 2 compares the flowability of the as supplied sample of FD, carbonated (singly carbonated sample), double carbonated, hydrated samples of FD at 10%, 11.6% and 20% free moisture content.

As supplied FD with a moisture content 0.4% exhibits easy flowing flowability characteristics, as the moisture content of FD increases, the flowability shifts towards a very cohesive region. This indicates during the hydration process; the bulk material would be difficult to handle.

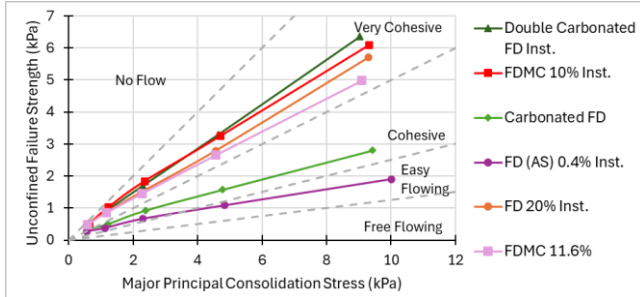


Figure 2: Unconfined failure strength versus consolidation stress for the samples of FD.

### 3.2. Bulk Density

Bulk density and compressibility curve provides an indication of the increase in the bulk density of bulk material across the consolidation stress range. Fig. 3 shows double carbonated sample of FD exhibits 50% increase in bulk density as compared to 'as supplied' sample of FD. Also, the samples of FD are highly compressible, and the bulk density increases considerably as the consolidation stresses increase. This indicates the requirement of structural integrity of the storage and handling equipment when handling FD in bulk.

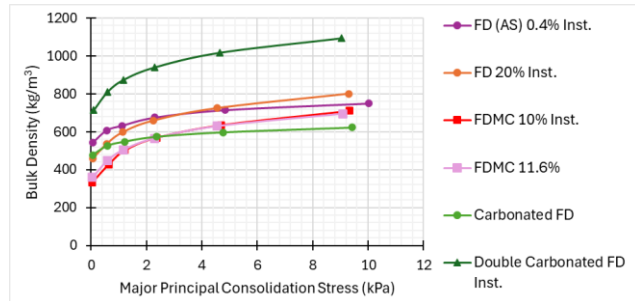


Figure 3: A variation in bulk density of FD as a function of consolidation stress.

### 3.3. Wall Friction

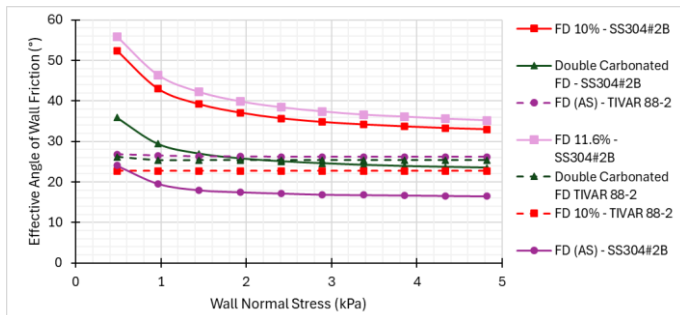


Figure 4: Effective angle of wall friction as a function of consolidation stress.

Fig. 4 represents the comparison of wall friction of FD samples with different moisture contents against stainless steel 304 with 2B satin finish (SS304#2B) and ultrahigh molecular weight (UHMW) polyethylene TIVAR 88-2 wall samples. TIVAR 88 and TIVAR 88-2 works well as a constraining wall sample when samples have moisture content. These specially design materials are hydrophobic and repel sticky material, thus reduce the adhesion of bulk material to the constraining walls.

On the other hand, wet bulk materials exhibit wall adhesion against stainless steel which may cause flow disruptions for the mass flow discharge. Fig. 3 shows the samples of FD with elevated moisture content exhibited significant wall adhesion when tested against SS304#2B finish.

## 4. Structural Loading Considerations

### 4.1. Stress Distribution in Mass Flow Silos

Stress distribution in bulk solid silos along the depth does not follow hydrostatic pressure distribution law (as a function of bulk density, acceleration due to gravity and depth). The stress distribution ( $\sigma_1$ ) in the vertical section of silos is a function of bulk density  $\rho_b$ , angle of wall friction  $\phi_w$ , lateral stress ratio ( $K$ ) and acceleration due to gravity ( $g$ ) and fill depth ( $D$ ), and given by Eq. 2 [3, 5]:

$$\sigma_1 = \frac{\rho_b g D}{4K \tan \phi_w} \left( 1 - e^{-\frac{4K \tan \phi_w Z}{D}} \right) \quad (2)$$

The lateral stress ratio is a function of angle of internal friction ( $\delta_j$ ). It can be measured experimentally using the procedure stated in Eurocode standard EN1991-4 or can be estimated using  $K = 1.1(1 - \sin \delta_j)$ .

### 4.2. Effect of Bulk Material Temperature

AAC1 silos does not have significant effect of high temperature of its contents, whereas if the bulk material is being handled in larger quantities, then structural loading calculations needs to be revisited to eliminate any risks associated with the structural aspects of the storage equipment's [5].

### 4.3. Other considerations

The research shows the presence of  $\text{CO}_2$  affects the strength of the concrete and also increase the rate of corrosion in the metals used for structural stability during construction. This limits the applicability of usage of carbonated FD for the wider applications [2].

## 5. Conclusion

Carbonation of bulk materials is a way forwards to minimise or ideally neutralise the greenhouse, particularly,  $\text{CO}_2$  emissions from the industrial processes. Carbonation involves hydration of the bulk material which can generate significant heat. The handling and storage equipment's should be designed keeping in view the variation in the properties of bulk material to improve the efficiency and safety of the processes. The measurement of flow properties and identifying the variations in the material properties have significant impact on the structural integrity of the storage equipment.

## Acknowledgement

The authors acknowledge the technical support from the Wolfson Centre for Bulk Solids Handling Technology, University of Greenwich.

## References

- [1] *Carbon capture, usage and storage (CCUS): business models*, Department for Energy Security and Net Zero, HM Government, April 2024. <https://assets.publishing.service.gov.uk/media/661530cdc4c84d6602346a13/ccus-iccc-business-models-update-april-2024.pdf>
- [2] Q. Qiu, *Construction and Building Materials* 247, 118503, 2020.
- [3] D. Schulze, *Powders and bulk solids: behaviour, characterization, storage and flow*. 2008.
- [4] J. M. Rotter, *Guide for Economic Design of Circular Metal Silos*. in Civil Engineering Series. Taylor & Francis, 2001.
- [5] *Eurocode 1- Actions on Structures – Part 4: Silos and Tanks*, European Committee for Standardization, EN 1991-4:2006, 2006.

# Heat Transfer Augmentation in Horizontal Dilute-Phase Pneumatic Conveying

A. Ratzabi<sup>1</sup>, G. Ziskind<sup>1</sup>, and H. Kalman<sup>1</sup>

<sup>1</sup> Ben-Gurion University of the Negev, Israel

**Abstract**— Wall-suspension and particle-gas heat transfer were investigated in horizontal dilute-phase pneumatic conveying. One correlation for gas-only and two correlations for wall-suspension Nusselt number were developed for the fully developed flow regime. In addition, we found that gas-particle Nusselt number is higher in the particle acceleration zone compared to the fully developed flow regime, due to greater relative velocity of the particles.

**Keywords:** pneumatic conveying; heat transfer; accelerating particles;

## 1. Introduction

Pneumatic conveying is a common method for transporting particulate materials and powders over relatively short distances in industrial plants. This method transfers particles between units where mechanical, thermal, and chemical processes occur. Efficiency can be enhanced by integrating part of the process into the conveying system, such as heating a pipe section to warm particles before they enter an oven or dryer. This approach can also be used in thermal energy storage (TES) systems based on particulate materials.

Several papers [1-4] review pneumatic conveying systems combined with a heating test section. Most experimental work focuses on wall-suspension heat transfer in the fully thermally developed region, using a uniform heat flux with particles under 350  $\mu\text{m}$ . This study develops quantitative models predicting heat transfer to a particle-gas suspension and between its components in horizontal dilute-phase pneumatic conveying. We analyze experimental data from different hydrodynamic and thermal flow regimes, particularly comparing accelerating and fully accelerated particles.

## 2. Experimental Test Rig

The experimental test rig comprises two main parts: (1) the flow system, which allows to convey particles and determine different flow regimes, and (2) the heat transfer test section, which allows to supply heat and measure gas and particle temperatures. These two parts are next described.

### 2.1. Flow System

Compressed air passes through a pressure regulator and two-in-a-row calibrated hot-wire flowmeters, adjustable by a valve to a maximum flow rate of 290  $\text{m}^3/\text{h}$ . Particles stored in a hopper enter a mixing chamber via a screw feeder, controlled to adjust the particle mass flow rate. The mixed suspension flows through a 52.5 mm internal diameter (ID) galvanized steel along vertical and horizontal sections. The particles then enter a bag house separator and free-fall through a weighing bin back to the hopper. The weighing bin is mounted on a load cell and has a pneumatic valve at the bottom, allowing for online, though not continuous, measurement of the particle mass flow rate.

A high-speed camera positioned in front of a 0.5 m transparent glass pipe and allows to monitor the particles' velocity before the heated test section. This camera, along with image processing software, was previously used in [5-6], though for very dilute flows.

All data are collected by a multifunction data acquisition system and displayed online on a dedicated computer. This setup enables detection of experimental issues (e.g., blockages), control of air and particle mass flow rates, monitoring of pressure drop along the pipe, and conveyance of various particle types, sizes, and shapes.

### 2.2. Heat Transfer Test Section

A 1.02 m test section module was specially designed to be mounted at different positions along the pipeline. It includes four 25 cm long tubular Mica Band heaters encircling a steel pipe of the same type as discussed above. Each heater enables to supply 1950 W or 5  $\text{W}/\text{cm}^2$  and is connected to a separate PID controller, enabling uniform wall temperature or heat flux. Another safety PID controller prevents the wall temperature from exceeding 215°C (or any chosen value). The module and one meter of the pipe on each side are insulated with glass-wool ( $k=0.04 \text{ W}/\text{mK}$ ), approximately 20 cm in outer diameter.

A single Chromel-Alumel (type K) thermocouple ( $T_{in}$ ) is mounted at the pipe's center, half a meter upstream from the first heater. Another 13 thermocouples ( $T_1 - T_{13}$ ) of the same type are equally spaced along the upper side of the test section wall, with each pair spaced 8.5 cm apart. The inner and outer pipe walls are assumed to have the same temperature. An additional thermocouple, protected by a ceramic sleeve, is mounted 0.75 m from the test section entrance ( $T_{out}$ ). This thermocouple can be moved horizontally within the pipe cross-section to obtain the bulk temperature by reconstructing the gas temperature profile. A single type K thermocouple measures the ambient temperature,  $T_{\infty}$ .

A specially designed particle withdrawal unit for measuring particle temperature is located immediately after the last heater. This unit collects a small amount of particles, which cover a thermocouple. Previous oven tests calibrated the thermocouple readings to accurately reflect the particle temperature for each particle type.

## 3. Experimental Procedure

Each experiment begins with an air-only test, where the air flow rate and total heat supplied to the test section are adjusted. Inlet, wall, and ambient temperatures, as well as air flow rate and pressure readings along the pipeline, are monitored online. After waiting 2-4 hours for temperatures to stabilize, azimuthal temperatures are measured at four positions around the central cross-section (0.5 m from the test section entrance). In addition, 11 equally spaced temperature readings of  $T_{out}$  are taken along the pipe cross-section.  $T_{out}$  is positioned away from the test section outlet to avoid edge effects.

Next, particles are introduced into the flow stream at an adjusted rate. The procedure for air-particle tests is similar to the air-only test process, with particles collected three times by the withdrawal unit. Particle mass flow is measured, and particle trajectories are briefly filmed by the high-speed camera.

All raw data is processed based on previous calibrations and analyses, including wall temperature correction from azimuthal measurements, and estimations of heat loss and gas backflow.

#### 4. Physical Model

The heat transfer coefficient  $h_g(x)$  and gas temperature  $T_g(x)$  for the gas-only case are calculated as follows:

$$h_g(x) = \frac{q_w''}{T_w(x) - T_g(x)} ; \quad T_g(x) = T_{in} + \frac{q_w'' \pi D x}{\dot{m}_g c_{pg}}. \quad (1)$$

The heat transfer coefficient  $h_{mix}(x)$  and mixed mean temperature  $T_{mm}(x)$  for the particle-gas suspension are calculated as shown in [7-8]:

$$h_{mix}(x) = \frac{q_w''}{T_w(x) - T_{mm}(x)} ; \quad T_{mm}(x) = T_{in} + \frac{q_w'' \pi D x}{\dot{m}_g c_{pg} + \dot{m}_p c_{pp}}. \quad (2)$$

The interphase heat transfer coefficient  $h_{pg}$  depends on the velocity and temperature of both phases. Therefore, a coupled system of mass, momentum, and energy conservation equations for each phase is solved numerically with initial condition  $[\rho_g, \varepsilon_g, u_g, u_p, T_g, T_p]_{x=0}$ :

$$\frac{\partial}{\partial x} (\varepsilon_g \rho_g u_g) = 0; \quad (3)$$

$$\frac{\partial}{\partial x} [(1 - \varepsilon_g) \rho_p u_p] = 0; \quad (4)$$

$$\frac{\partial}{\partial x} (\varepsilon_g \rho_g u_g^2) = -\beta_A (u_g - u_p) - \frac{\tau_{wg} \pi D}{A}; \quad (5)$$

$$\frac{\partial}{\partial x} [(1 - \varepsilon_g) \rho_p u_p^2] = \beta_A (u_g - u_p); \quad (6)$$

$$\frac{\partial}{\partial x} [(\varepsilon_g \rho_g u_g A) (C_{pg} T_g + \frac{u_g^2}{2})] = q'_{pg} + q'_{wg} - w'_{pg}; \quad (7)$$

$$\frac{\partial}{\partial x} [(1 - \varepsilon_g) \rho_p u_p A] (C_{pp} T_p + \frac{u_p^2}{2}) = q'_{gp} - w'_{gp}. \quad (8)$$

We estimate  $h_{pg}$  in the particle-gas heat transfer term  $q'_{pg}$  and solve the system iteratively using a Runge-Kutta scheme to match the measured values of  $T_g$  and  $T_p$ .

#### 5. Results

Thirty-two experiments were conducted with varying particle types, air flow rates, particle mass flow rates, and total heat power, all in the fully developed flow regime with fully accelerated particles. An additional 29 experiments were performed in the particle acceleration regime. In both cases, the wall temperature decreased in the last quarter of the heating section because of axial heat conduction through the pipe wall downstream of the test section. Consequently, we decided to focus on the first 3/4 of the test section, assuming a constant heat flux.

We calculated  $h_g(x)$  and  $h_{mix}(x)$  using (1) and (2), respectively, and fitted the results to the form  $y = a + b \cdot e^{-x/c}$  to obtain the extrapolated values "a" of  $h_{g,\infty}$  and  $h_{mix,\infty}$ . Subsequently, correlations for the Nusselt number were developed for the fully developed flow regime. For the gas-only case:

$$Nu_{g,\infty} = 0.079 Re_g^{0.68} Pr^{0.4}. \quad (9)$$

Correlation (9) ( $R^2 = 0.968$ ,  $err_{max} = 9.2\%$ ) aligns well with established literature correlations [9-10]. For the particle-gas suspension case, two correlations were developed:

$$Nu_{mix,\infty} = 0.082 (Re \cdot Pr)^{0.71} \left( \frac{c_{pp}}{c_{pg}} \eta + 1 \right)^{-0.11} Ar^{-0.027}; \quad (10)$$

$$Nu_{mix,\infty} = Nu_{g,\infty} - 2.62 \cdot 10^{-4} (Re \cdot Pr)^{0.73} \left( \frac{c_{pp}}{c_{pg}} \eta \right)^{0.53} Ar^{0.30}. \quad (11)$$

Correlation (10) ( $R^2 = 0.964$ ,  $err_{max} = 10.3\%$ ) is based on the form of other literature correlations [1,11], with the addition of

an  $Ar$  multiplier. Correlation (11) ( $R^2 = 0.961$ ,  $err_{max} = 15\%$ ) shows the relationship to  $Nu_{g,\infty}$  in (9). The results indicate a decrease in the wall-suspension Nusselt number compared to the gas-only case.

Fig. 1 displays the axial temperature profiles for the gas-only test (using (1)) and for the particle-gas test (using (3-8)) under the same operational conditions. Gas temperature profiles are similar in both the gas-only tests, whether in the fully developed or particle acceleration regimes. With particles added, some heat is transferred from the gas to the particles, causing a decrease in gas temperature. However, in the acceleration zone, the temperature difference between the phases is smaller than in the fully developed regime. This indicates a higher  $Nu_{pg}$  due to the greater relative velocity between the phases in the acceleration zone.

#### 6. Conclusions

One correlation for  $Nu_{g,\infty}$  and two correlations for  $Nu_{mix,\infty}$  in the fully developed flow regime were developed. For the particles tested, the wall-suspension heat transfer coefficient is lower compared to the air-only case. In addition, we found that particle-gas heat transfer in the particle acceleration regime is better than in the fully developed flow regime, due to higher interphase relative velocity.

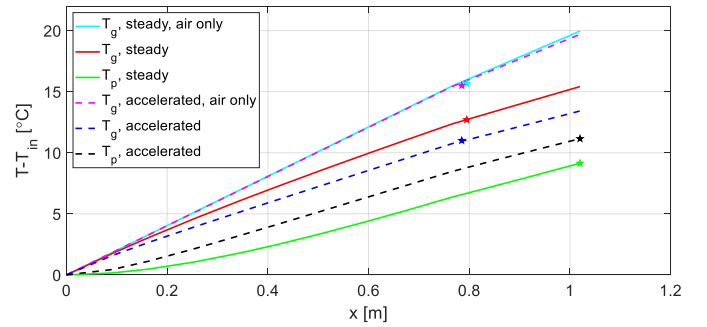


Figure 1. Example of gas and particle temperature profiles for gas-only and particle-gas tests. Fully developed flow regime (solid lines) vs. particle acceleration regime (dashed lines). Temperature measurements are marked with stars.

#### References

- [1] R. Pfeffer, S. Rossetti, and S. Lieblein, *Analysis and correlation of heat-transfer coefficient and friction factor data for dilute gas-solid suspensions*. NASA technical note. Lewis Research Center., 1966.
- [2] C. A. Depew and T. J. Kramer, *Heat transfer to flowing gas-solid mixtures*. Advances in Heat Transfer, 1973.
- [3] S. Banooni, E. Hajidavalloo, and M. Dorfeshan, *A comprehensive review on modeling of pneumatic and flash drying*. Drying Technology, 2018.
- [4] M. M. Shah, *A correlation for heat transfer to gas-solid suspensions flowing in pipes*. Journal of Thermal Science and Engineering Applications, 2020.
- [5] N. Santo, D. Portnikov, I. Eshel, R. Taranto, and H. Kalman, *Experimental study on particle steady state velocity distribution in horizontal dilute phase pneumatic conveying*. Chemical Engineering Science, 2018.
- [6] N. Santo, D. Portnikov, N. M. Tripathi, and H. Kalman, *Experimental study on the particle velocity development profile and acceleration length in horizontal dilute phase pneumatic conveying systems*. Powder Technology, 2018.
- [7] R. G. Boothroyd and H. Haque, *Fully developed heat transfer to a gaseous suspension of particles flowing turbulently in ducts of different size*. Journal of Mechanical Engineering Science, 1970.
- [8] C. A. Depew and E. R. Cramer, *Heat transfer to horizontal gas-solid suspension flows*. Journal of Heat Transfer, 1970.
- [9] W. M. Kays and M. E. Crawford, *Convective heat and mass transfer*. McGraw-Hill Education, 1993.
- [10] D. Taler and J. Taler, *Simple heat transfer correlations for turbulent tube flow*. EDP Sciences, 2017.
- [11] W. J. Danziger, *Heat transfer to fluidized gas-solids mixtures in vertical transport*. Industrial & Engineering Chemistry: Process Design and Development, 1963.



# Application of Principal Component Analysis (PCA) and Regression with Lagged Variables to Identify the Effect of Blower Speed and Feed Rate in Pneumatic Conveying

Chanaka Prasad Premarathna<sup>1</sup>, Baldeep Kaur<sup>1</sup>, Hamid Salehi Kahrizsangi<sup>1</sup>, Richard Ellis<sup>2</sup>, Michael S.A. Bradley<sup>1</sup>

<sup>1</sup> The Wolfson Centre for Bulk Solids Technology, University of Greenwich, Central Avenue, Chatham Maritime, ME4 4TB, UK

<sup>2</sup> Schenck Process UK Ltd, Doncaster, DN4 5FB, UK

**Abstract—** This study investigates the dynamic behaviour of particle velocity in a pneumatic conveying system for bird food, focusing on the effects of blower voltage and feed rate on system performance and stability. Particle velocities were recorded under blower input voltages ranging from 4.5 to 7 V (2310 to 3260 rpm) and feed rates from 30% to 70%, using a rotary feeder. Principal Component Analysis (PCA) revealed that the first two components accounted for most of the variance in particle velocity, indicating a significant but not exclusive impact of the studied variables. Autocorrelation analysis of detrended particle velocity showed substantial system inertia, with a decay rate of -0.046 over five 1-second intervals, highlighting the influence of historical conditions on current dynamics. This insight is crucial for refining control algorithms to manage temporal dependencies within the system. Cross-correlation analysis identified a time-lagged response in particle velocity following adjustments in blower voltage, with a peak correlation at a 1-second lag, underscoring the system's dynamic nature. The study identified optimal stability at specific voltage-feed rate combinations, such as 5.75 V and 30%, which exhibited a low standard deviation in particle velocity (0.63 m/s). In contrast, settings like 4.5 V and 70% led to significant fluctuations, indicating potential instability. The findings underscore the importance of understanding the interplay between blower voltage and feed rate in developing predictive models and advanced control strategies, thereby enhancing the efficiency and reliability of pneumatic conveying systems.

**Keywords:** Pneumatic Conveying; Closed-loop Control; PCA

## 1. Introduction

Pneumatic conveying is a widely used method of bulk material transport where a gas, typically air, is employed to move materials through a pipeline. This technique is common in various industries such as chemical, pharmaceutical, food processing, and power generation due to its flexibility, safety, and reduced maintenance costs[1]. Despite these advantages, the inherently complex and nonlinear nature of pneumatic conveying systems presents significant challenges in understanding and controlling their behaviour[2].

Historically, research on pneumatic conveying systems has focused on empirical and experimental approaches to understand their unpredictable behaviour[3]. While these studies have provided valuable insights, they often fall short in explaining the underlying system dynamics. Specially, there has been limited research evaluating the effects of blower speed and feed rate on pneumatic conveying systems, despite practical understanding within the industry, particularly regarding control aspects.

Previous studies, such as those by Klinzing [4], have explored unusual phenomena in pneumatic conveying, including reduced gravity effects and electrostatics. More recently, we conducted system identification and stability analysis based on key variables like blower input voltage and particle velocity[5]. Understanding these variables is crucial in the context of Industry 4.0, where minimizing energy consumption is a priority [6].

This study aims to investigate the dynamic behaviour of particle velocity in a pneumatic conveying system, focusing on the effects of blower speed and feed rate. Using PCA and regression with lagged variables, this research seeks to provide deeper insights into the system's performance and stability, ultimately contributing to the development of advanced control strategies for improved efficiency and reliability.

## 2. Methodology

### 2.1. Experimental Setup

The experimental setup consisted of a pneumatic conveying system approximately 26 meters long with four bends, designed for conveying bird food. The air mover in this system was a blower, whose rotational speed (rpm) could be controlled by adjusting the input voltage, ranging from 0 to 10 V. This input voltage was directly proportional to the rpm of the blower and, consequently, the inlet air mass flow rate. A rotary feeder was used to introduce the material into the system, with feed rates controllable as a percentage. The study did not measure inlet air velocity, pressure, or the feed rate in kg/s, as the primary focus was on analysing the effects of variations in blower voltage and feed rate on the system.

Particle velocity, a critical parameter in this study, was determined using electrostatic signals captured by two electrodes positioned at a known distance apart. By applying cross-correlation techniques in the time domain to these signals, the particle velocity was accurately calculated.

### 2.2. Data Analysis Techniques

To analyse the effects of blower voltage and feed rate on particle velocity, several statistical techniques were employed:

**Principal Component Analysis (PCA):** PCA was used to reduce the dimensionality of the dataset and to identify the principal components that account for the variance in particle velocity. The independent variables (blower input voltage and feed rate) were standardised and combined into a matrix, on which PCA was performed. The analysis aimed to capture the most significant features affecting particle velocity, thereby simplifying the data structure for further analysis.

**Autocorrelation Analysis:** Autocorrelation analysis was applied to the detrended particle velocity data to investigate the temporal dependencies within the system. This method assessed how current values of particle velocity were influenced by past

values, thus highlighting the inertia within the system. The decay rate over a specific number of time intervals was calculated to quantify this dependency.

**Cross-Correlation Analysis:** To understand the dynamic response of particle velocity to changes in blower voltage and feed rate, cross-correlation analysis was conducted. This technique helped identify time-lagged relationships between the independent variables and particle velocity, thereby providing insights into the system's dynamic nature and the time delay effects of input changes on particle velocity.

These methods collectively provided a comprehensive framework for understanding how variations in operational parameters influenced the system's behaviour, particularly in terms of particle velocity dynamics.

### 3. Results and Discussion

This study focused on the dynamic behaviour of particle velocity in a pneumatic conveying system for bird food, examining the effects of blower voltage and feed rate on system performance and stability. The results highlight several key findings.

Principal Component Analysis (PCA) indicated that the first two components accounted for a significant portion of the variance in particle velocity, with regression coefficients of 1.57 and 0.51. The PCA model explained approximately 52.8% of the variability in particle velocity, suggesting that while blower voltage and feed rate are influential, other factors may also affect system behaviour.

Autocorrelation analysis of the detrended particle velocity showed a substantial system inertia with a decay rate of -0.046 over five 1-second intervals. This slow decay rate underscores the influence of past conditions on the current state of the system, indicating persistent temporal correlations. The inability to reach 80% decay within the specified lags further highlights the prolonged impact of previous system states, which is crucial for refining control algorithms to manage these temporal dependencies effectively.

Cross-correlation analysis revealed a peak correlation at a 1-second lag between blower voltage changes and particle velocity, underscoring the system's dynamic nature and the delayed response of particle velocity to adjustments in blower voltage. This lag is critical for developing responsive control strategies that can anticipate and compensate for these delays.

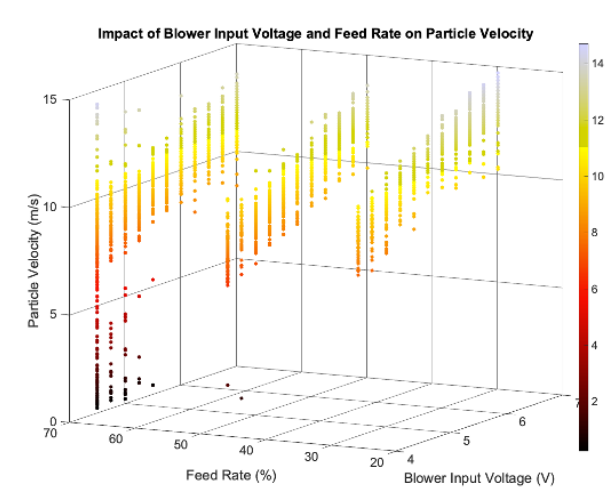


Figure 1. Impact of Blower Input Voltage and Feed Rate on Particle Velocity

The study identified optimal operating conditions at a blower voltage of 5.75 V and a feed rate of 30%, where particle velocity exhibited a low standard deviation of 0.63 m/s. In contrast, settings such as a blower voltage of 4.5 V and a feed rate of 70% resulted in significant fluctuations, with a standard deviation of 3.27 m/s, indicating potential instability. These findings emphasize the importance of carefully controlling blower voltage and feed rate to maintain stable and efficient system operation.

### 4. Conclusion

This study investigated the impact of blower voltage and feed rate on particle velocity in a pneumatic conveying system. PCA showed that the first two components accounted for significant variance in particle velocity, highlighting the influence of these operational parameters. Autocorrelation analysis revealed a decay rate of -0.046, indicating substantial system inertia, while cross-correlation analysis identified a 1-second lag in the response of particle velocity to changes in blower voltage.

Optimal stability was achieved at a blower voltage of 5.75 V and a feed rate of 30%, minimizing fluctuations in particle velocity. In contrast, settings like 4.5 V and 70% led to increased variability, indicating potential instability. The study emphasises the importance of precise control over blower voltage and feed rate, considering both immediate and delayed responses, to enhance system efficiency and reliability.

### Acknowledgement

The authors thank Schenck Process UK Ltd for providing their facility for the experiments. Special thanks to Amit Kumar and the team at their test centre for their support during the experiments. The authors also extend their gratitude to the Wolfson Centre for providing financial support for the conference.

### References

- [1] O. Molerus, 'Overview: Pneumatic transport of solids', *Powder Technol*, vol. 88, no. 3, pp. 309–321, Sep. 1996.
- [2] S. Kuang, M. Zhou, and A. Yu, 'CFD-DEM modelling and simulation of pneumatic conveying: A review', *Powder Technol*, vol. 365, pp. 186–207, Apr. 2020.
- [3] A. Rautiainen, G. Stewart, V. Poikolainen, and P. Sarkomaa, 'An experimental study of vertical pneumatic conveying', *Powder Technol*, vol. 104, no. 2, pp. 139–150, Sep. 1999.
- [4] G. E. Klinzing, 'Review of unusual and some unexplained phenomena in pneumatic conveying', *Particulate Science and Technology*, vol. 34, no. 4, pp. 424–431, Jul. 2016.
- [5] C. P. Premarathna, B. Kaur, H. S. Kahrizsangi, R. Ellis, and M. S. A. Bradley, 'System Identification and Stability Analysis of a Pneumatic Conveying Pipeline Based on Blower Input Voltage and Particle Velocity: Preliminary Study', in *ICBMH2023: 14th International Conference on Bulk Materials Storage, Handling and Transportation*, Wollongong, NSW: The Institution of Engineers, Australia, 2023.
- [6] C. P. Premarathna, 'Digital Twinning in Pneumatic Conveying', *Process Industry Informer*. Accessed: Aug. 02, 2024. [Online]. Available: <https://www.processindustryinformer.com/digital-twinning-in-pneumatic-conveying/>

# Quantifying Variability in Wall Friction Measurements – An EFCE Supported International Study

Don McGlinchey<sup>1</sup>, Diego Barletta<sup>2</sup>, Eddie McGee<sup>3</sup>, Salvatore La Manna<sup>2</sup> and Edward Agbonkhese<sup>1</sup>

<sup>1</sup> Department of Mechanical Engineering, Glasgow Caledonian University, Scotland, UK

<sup>2</sup> Department of Industrial Engineering, University of Salerno, IT

<sup>3</sup> Ajax Equipment Ltd, UK

**Abstract**—A statistical analysis of results from the most recent Working Party on Mechanics of Particulate Solids of the European Federation of Chemical Engineering supported international round-robin study on wall friction measurements of two powders and two wall materials shows significant variation in the values obtained by participating industrial and academic laboratories.

**Keywords:** wall friction; measurement; variability;

## 1. Introduction

Wall friction plays a principal role in the handling behaviour of bulk solids, exerting a significant impact on various aspects such as the flow patterns within hoppers, the stresses experienced by vessel walls, the performance of equipment involving sliding contact, including mixers, screw feeders, chutes, and for the calibration of DEM models and other simulation methods. The reliable measurement of wall friction is clearly of importance to the global bulk solids handling industry and as such has been the subject of investigation by the Working Party on Mechanics of Particulate Solids (WPMPS) of the European Federation of Chemical Engineering (EFCE) for many years. Reported here is a statistical analysis of the results of wall friction measurements made in 2021/22 by the test facilities of AJAX Ltd, (UK), Freeman Technology (UK), International Flavors & Fragrances (USA), Institute of Agrophysics, Polish Academy of Sciences (PL), Jenike & Johanson Inc. (USA), Schwedes + Schulze Schüttguttechnik GmbH (DE), Technical University of Delft (NL), Technical University of Ostrava (CZ), TUNRA Bulk Solids, University of Newcastle (AUS), University of Edinburgh (UK), University of Greenwich - Wolfson Centre (UK), University of Salerno (IT), University of Wollongong (AUS). Measurements using linear and rotational test apparatus are reported.

## 2. Uncertainty in Measurement of Wall Friction

### 2.1. Sources of Uncertainty in Measurement

According to the Guide to the Expression of Uncertainty in Measurement [1] there are many possible sources of uncertainty in a measurement, including:

- nonrepresentative sampling — the sample measured may not represent the defined measurand;
- inadequate knowledge of the effects of environmental conditions on the measurement or imperfect measurement of environmental conditions;
- approximations and assumptions incorporated in the measurement method and procedure.

### 2.2. Mitigation of Uncertainty in Measurement

Considerable care was given to ensure each lab received closely matched powder and wall material samples. Power samples supplied to each lab were sub-sampled from individual batches of limestone and HDPE powder and the wall material ‘coupons’ were cut from single sheets of stainless steel and aluminum. A detailed test procedure based on ASTM D6128 [2]

was provided to each group and all groups were experienced in powder flow measurement.

## 3. Test Output and Analysis

Measurements of wall friction were undertaken using either a linear [Jenike type] or a rotational shear cell. Twelve sets of results from individual labs using linear testers and three or four sets of results from labs using rotational testers were analysed. The test combinations were: HDPE/Steel, HDPE/Aluminium, Limestone/Steel and Limestone/Aluminium

### 3.1. Data Available for Analysis

The test results were provided for analysis as pre-processed data sets of shear and normal stress under prescribed loading conditions in tabular form. Initial calculation of friction angle was based on a best fit to a linear relationship between shear and normal stress passing through the origin. Values of wall friction at low normal stress (<5000 Pa) were highly irregular and although worthy of investigation were excluded from the analysis reported here. Limited sets of ‘raw’ data from the testers and testing environment temperature and air humidity data was also available.

### 3.2. Results from Linear Test Apparatus

Results from individual labs were assumed to conform to a Gaussian distribution and standard statistical measures were determined. A summary of the results from test with HDPE powder and the Steel wall material is given in Table 1. Similar results are available for the other test combinations. No evidence of experimental bias across the laboratories was observed.

TABLE I. SUMMARY OF HDPE/STEEL WALL FRICTION ANGLE RESULTS

Lab	Mean	Stdev	Min	Max
1	14.0	0.4	13.4	14.3
2	10.8	0.3	10.5	11.4
3	8.2	0.2	8.0	8.7
4	9.2	0.6	8.6	10.8
5	9.8	0.6	9.3	11.0
6	11.4	0.7	10.5	13.1
7	8.0	0.5	7.1	8.7
8	9.0	0.2	8.8	9.4
9	7.2	0.5	6.7	7.8
10	8.3	1.0	6.8	10.4
13	9.6	1.5	8.5	13.1
14	9.1	0.8	8.3	10.8

The standard deviation and range values suggest that the wall friction of HDPE powder on a steel wall can be measured by most labs to within one degree or so, however, there is a much greater variation in mean values as illustrated in Fig 1.

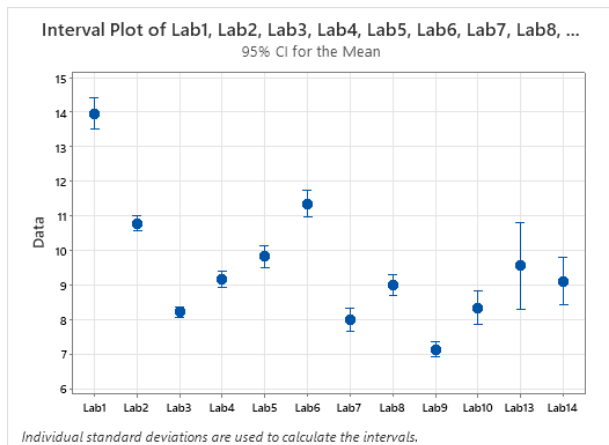


Figure 1. Interval plots of HDPE/STEEL wall friction angle results. (linear testers)

To quantify the variation between labs a F-test was used, where:

$$F = \frac{\text{Variance between lab results}}{\text{Variance within lab results}} \quad (1)$$

The F-test values, Table II, signifies significantly larger variance between the wall friction angles obtained from different groups than the variation in individual wall friction measurements obtained by each group for all test combinations.

The Levene's test was used to test the assumption of homogeneity of variances, see Table II, for material combinations where the p-value is less than 0.05, indicates a lack of homogeneity in variances across labs.

TABLE II F-TEST AND LEVENE'S TEST RESULTS

Material	ANOVA F-Value	Levene p-value
Limestone/Steel	10.5	0.0078
Limestone/Aluminium	31.9	0.3596
HDPE/Steel	63.4	0.0223
HDPE/Aluminium	53.6	0.0123

### 3.3. Results from Rotational Test Apparatus

Results from individual labs were assumed to conform to a Gaussian distribution and standard statistical measures were determined. A summary of the results from test with HDPE powder and the Aluminium wall material is given in Table III. Similar results are available for the other test combinations.

TABLE II. SUMMARY OF HDPE/ALUMINIUM WALL FRICTION ANGLE RESULTS

Lab	Mean	Stdev	Min	Max
11	10.2	0.9	9.2	12.1
12	7.3	0.2	7.0	7.6
9S	6.3	0.4	5.8	7.0
10S	6.4	0.4	5.7	7.1

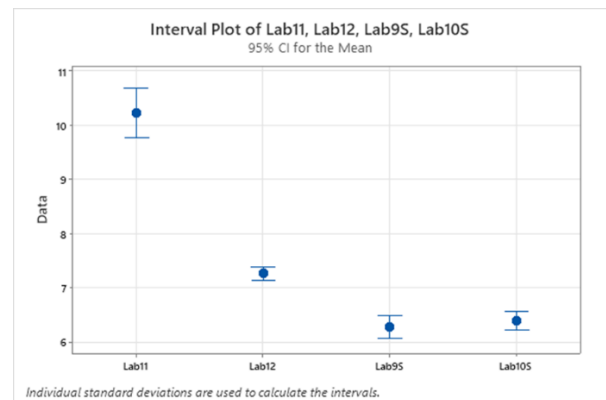


Figure 2. Interval plots of HDPE/ALUMINIUM wall friction angle results. (rotational testers)

As with the results from the linear testers, the standard deviation and range values suggest that the wall friction of HDPE powder on an aluminium wall can be measured by most labs to within one degree or so, however, there is a much greater variation in mean values as illustrated in Fig 2. No statistical comparison of variance was determined due to the limited number of data sets. Again, no evidence of experimental bias across the laboratories was observed.

## 4. Conclusion

The analysis presented here shows that despite considerable effort to mitigate the sources of variation in the measurement of wall friction through control of the powder and wall materials there is significant variation in the values obtained by participating industrial and academic laboratories. This is clearly of importance across a range of applications in both bulk solids design and process operations e.g. [3,4] where the difference in measured values of approximately seven degrees exceeds typical 'safety' factors in design calculations.

Further work is required to determine the causes of this variation.

## Acknowledgement

The authors thank the Working Party on the Mechanics of Particulate Solids of the European Federation of Chemical Engineering and in particular to all those who participated in the supply of test data. A special acknowledgement is due to Jenike and Johanson Inc., Zeppelin Systems GmbH, Schwedes + Schulze Schüttguttechnik GmbH and AJAX Ltd for the organisation and supply of test materials.

## References

- [1] BIPM, IEC, IFCC, ILAC, ISO, IUPAC, IUPAP, and OIML. *Evaluation of measurement data — Guide to the expression of uncertainty in measurement*. Joint Committee for Guides in Metrology, JCGM 100:2008. URL: <https://www.bipm.org/documents/20126/2071>
- [2] ASTM D6128-00 *Standard Test Method for Shear Testing of Bulk Solids Using the Jenike Shear Cell*, Am. Soc. Test. Mater, West Conshohocken, PA (2000)
- [3] Technical Report: *Storage and flow of solids*. Bulletin No. 123 of the Utah Engineering Experiment Station; Vol. 53, No. 26, November 1964
- [4] J. M. Rotter, *Guide for Economic Design of Circular Metal Silos*. in Civil Engineering Series. Taylor & Francis, 2001.



# Verification of the Contact Mechanics Calculation of Superquadrics in the Discrete-Element-Method

Fabian Krull, Sergiy Antonyuk

Institute of Particle Process Engineering, University of Kaiserslautern-Landau (RPTU), Germany

**Abstract**— The Discrete Element Method is widely used to simulate granular processes, such as silo discharge, pneumatic transportation and compaction. By using experimentally calibrated contact models, the mechanical particle interactions can be analysed and the particles dynamics in these processes can be obtained. The DEM originated by using spheres to represent the particles, however, by adjusting the model parameters, the flow behaviour and bulk density of non-spherical particles can also be described. This work deals with the verification of the contact mechanics of superquadrics in the DEM. Therefore, ten different non-spherical particles were generated in the DEM domain as superquadrics and the corresponding shapes were produced using a 3D printer. These particles were investigated by compression tests to obtain the force-displacement curves for a range of loads. The experiments were then replicated in the DEM simulation using an elastic-plastic contact model to verify and identify the limitations of the superquadric approach for calculating real contact mechanics.

**Keywords:** Discrete Element Method, superquadrics, compression tests, elastic-plastic contact model, plastic deformation

## 1. Introduction

The simulation of the real particle shape in the DEM is becoming increasingly important, given the impact of particle shape on the behaviour of granular materials, such as packing and flow. The particle shape can be reproduced in the DEM by using a multi-sphere approach [1], bonded particle models [2], triangulated shapes [3] and by a description via superquadrics [4]. The superquadric approach [4] has been used to study various granular processes and scenarios, such as shear flow and silo discharge [5], fluidization [6] and segregation in rotating drums [7]. However, processes with high stresses on the particles have rarely been investigated using this approach. Therefore, in this study, a contact detection method of superquadrics of varying particle shapes was investigated across a broad force range (500  $\mu$ N – 500 N) with compression tests to verify and to identify the limits of this approach.

## 2. Material and Methods

A mathematical description of superquadrics can be provided through an approach developed by Barr [8] as

$$f(x) = \left( \left| \frac{x}{a} \right|^{n_2} + \left| \frac{y}{b} \right|^{n_2} \right)^{\frac{n_1}{n_2}} + \left| \frac{z}{c} \right|^{n_1} - 1 = 0, \quad (1)$$

where  $a, b, c$  are the radii of the particles along the principal axes and the blockiness parameters  $n_1$  and  $n_2$ , which become more box-like as these parameters increase. Based on this formula, ellipsoidal, box-like and cylinder-like particles can be modeled in the DEM (for  $n_x \geq 2$ ) [4].

### 2.1. Manufacturing of non-spherical particles

Eleven different superquadric shapes (one sphere and ten non-spherical particles) were selected for the mechanical study, which involved a variation of the radii (2 mm or 1 mm) and the blockiness parameters (2, 4, and 12). Firstly, a digital representation of the particles was generated using a MATLAB script [9], and the corresponding stl files were generated with a high resolution to reduce artefacts of the triangulated surfaces. The obtained stl files were used to 3D printed the particles using a Digital Light Processing (DLP) printer (Elegoo Saturn) with a photosensitive polymer (M58, Resione). In the slicer software (Chitubox), the particles were oriented with an angle (25° in x and y axis) and a single support structure was used to prevent defects of the particle shape due to overexposure of the first layers. After the 3D printing, the particles were washed three times with isopropanol (technical grade) and dried in a paper towel. After drying, the particles were post-cured under UV light for 8 minutes. The produced particles and their digital representation are shown in Figure 1. The numbers in the upper brackets are the radii ( $a, b, c$ ) in millimetre and in the lower brackets are the blockiness parameters ( $n_1, n_2$ ).

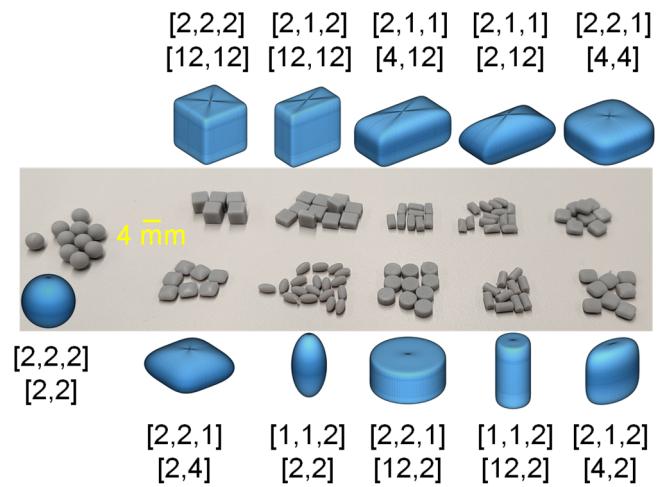


Figure 1. 3D printed superquadric particles with their digital representation. The upper brackets shown the radii in each direction (in millimetre) and the lower brackets are the blockiness parameters.

### 2.2. Compression tests

Single particle compression tests were performed with a Nanoindenter (TIPremier Hysitron) for low deformation and forces (300  $\mu$ N – 2N) and a Texture Analyser (Stable Micro Systems) for high forces (1 N to 500 N). Compression test were performed with a brass flat punch and a brass substrate for both systems. A cyclic compression test routine with increasing maximum force was used to determine the plastic deformation, elastic recovery, and change of stiffness. Depending on the contact situation, the brass substrate contained different grooves to investigate also the compression behaviour for edges and corners of the particles. The experimental setup with the Texture Analyzer is shown in Figure 2.

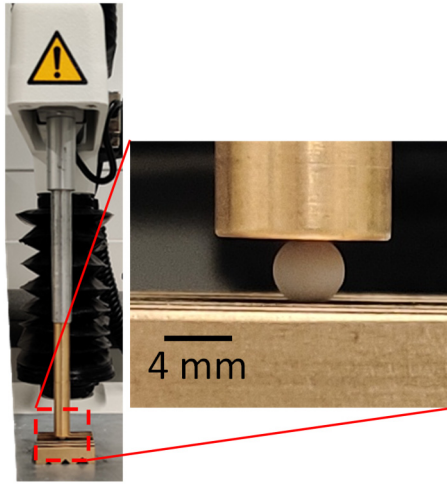


Figure 2. Compression tests of 4 mm sphere using the Texture Analyzer.

### 2.3. Discrete Element Method

An elastic-plastic contact model [10] was implemented in LIGGGHTS to investigate the contact mechanics of the compressed superquadric particles. This model can describe the contact mechanics of elastic-plastic particles with using only physical measurable parameters as shown in Equations 2-4:

$$F_{el-pl} = \left[ \frac{(2 - 2\kappa_A)}{\text{elastic}} + \frac{(3\kappa_A - 2)}{\text{plastic}} \right] \cdot \frac{(3\kappa_A - 1) \cdot \pi R^* \cdot s \cdot p_y}{\text{contact area } A_c} \quad (2)$$

with the area ratio  $\kappa_A$  according to Tomas [11]:

$$\kappa_A = \frac{2}{3} + \frac{1}{3} \left( \frac{r_{c,pl}}{r_{c,el-pl}} \right) = 1 - \frac{1}{3} \sqrt[3]{\frac{s_y}{s_n}} \quad (3)$$

and the displacement at the yield pressure according to Thornton and Ning [12]:

$$s_y = \frac{\pi^2 \cdot R^* \cdot p_y^2}{4 \cdot E^{*2}} \quad (4)$$

where  $R^*$  is the equivalent radius,  $p_y$  is the yield pressure and  $E^*$  is the equivalent Young's modulus.

The parameters required for the model were measured for the 3D-resin by gas pycnometer (density) and nanoindentation (Young's modulus and yield pressure). Due to the quasi-static behaviour of compression tests with particles  $> 2$  mm in radii, the coefficient of restitution, the friction coefficient and cohesion were less important in the context of the present investigation.

The model parameters were validated by comparing the compression curves for a spherical particle as shown in Figure 3 for a force range between 5 N and 300 N. It can be observed that the given model can describe the force-displacement behaviour of the sphere quite well for forces up to 200 N, which achieved a compression of 7.5% of the particle diameter and the predicted plastic deformation was predicted. At 300 N, the simulation differed greatly from the experiment in the unloading behaviour. Here, the creep behaviour of the polymer led to a bow shaped unloading curve, which the model could not describe. Therefore, a maximum force of 200 N was used for the investigation.

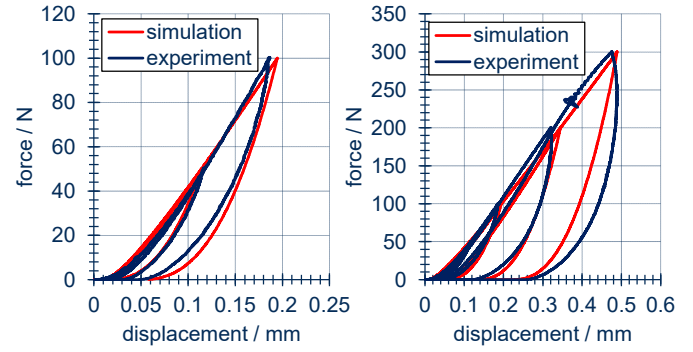


Figure 3. Comparison of compression tests with a 4 mm sphere between experiments using the Texture Analyzer and superquadric simulation with blockiness parameters 2,2.

With the obtained simulation parameters for the sphere, the compression experiments were simulated for the ten different non-spherical particles (Figure 1) and the resulting force-displacement curves were compared with the experiments for different contact scenarios such as compression on a flat surface or in grooves for edge compression.

### References

- [1] H. Kruggel-Emden, S. Rickelt, S. Wirtz, V. Scherer, A study on the validity of the multi-sphere Discrete Element Method, *Powder Technology* 188 (2008) 153–165. <https://doi.org/10.1016/j.powtec.2008.04.037>.
- [2] M. Wolff, V. Salikov, S. Antonyuk, S. Heinrich, G.A. Schneider, Three-dimensional discrete element modeling of micromechanical bending tests of ceramic–polymer composite materials, *Powder Technology* 248 (2013) 77–83. <https://doi.org/10.1016/j.powtec.2013.07.009>.
- [3] A.G. Neto, P. Wriggers, Discrete element model for general polyhedra, *Comp. Part. Mech.* 9 (2022) 353–380. <https://doi.org/10.1007/s40571-021-00415-z>.
- [4] A. Podlozhnyuk, S. Pirker, C. Kloss, Efficient implementation of superquadric particles in Discrete Element Method within an open-source framework, *Comp. Part. Mech.* 4 (2017) 101–118. <https://doi.org/10.1007/s40571-016-0131-6>.
- [5] B. Soltanbeigi, A. Podlozhnyuk, S.-A. Papanicopolulos, C. Kloss, S. Pirker, J.Y. Ooi, DEM study of mechanical characteristics of multi-spherical and superquadric particles at micro and macro scales, *Powder Technology* 329 (2018) 288–303. <https://doi.org/10.1016/j.powtec.2018.01.082>.
- [6] P. Grohn, L. Schaedler, A. Atxutegi, S. Heinrich, S. Antonyuk, CFD-DEM Simulation of Superquadric Cylindrical Particles in a Spouted Bed and a Rotor Granulator, *Chemie Ingenieur Technik* 95 (2023) 244–255. <https://doi.org/10.1002/cite.202200121>.
- [7] S. Yang, H. Wang, Y. Wei, J. Hu, J.W. Chew, 2020. Segregation behavior of binary mixtures of cylindrical particles with different length ratios in the rotating drum. *AIChE Journal* 66, e16799. <https://doi.org/10.1002/aic.16799>.
- [8] Barr, Superquadrics and Angle-Preserving Transformations, *IEEE Comput. Grap. Appl.* 1 (1981) 11–23. <https://doi.org/10.1109/MCG.1981.1673799>.
- [9] DGM, Plot Superquadratic Surfaces, 2018. <https://de.mathworks.com/matlabcentral/fileexchange/58413-plot-superquadratic-surfaces> (accessed 1 August 2024).
- [10] R. Hesse, P. Lösch, S. Antonyuk, CFD-DEM analysis of internal packing structure and pressure characteristics in compressible filter cakes using a novel elastic–plastic contact model, *Advanced Powder Technology* 34 (2023) 104062. <https://doi.org/10.1016/j.appt.2023.104062>.
- [11] J. Tomas, Assessment of Mechanical Properties of Cohesive Particulate Solids. Part 1: Particle Contact Constitutive Model, *Particulate Science and Technology* 19 (2001) 95–110. <https://doi.org/10.1080/02726350152772056>.
- [12] C. Thornton, Z. Ning, A theoretical model for the stick/bounce behaviour of adhesive, elastic-plastic spheres, *Powder Technology* 99 (1998) 154–162. [https://doi.org/10.1016/S0032-5910\(98\)00099-0](https://doi.org/10.1016/S0032-5910(98)00099-0).

# Integration of Spectroscopic Techniques and Machine Learning for Predictive Characterisation of Coal Tailings

E. Ergun Donohoe<sup>1</sup>, K. Williams<sup>1</sup>, and L. Bradney<sup>1</sup>

<sup>1</sup> University of Newcastle, NSW, Australia

This study investigates the integration of spectroscopic techniques and machine learning for predictive characterisation of coal tailings. Hyperspectral spectroscopy was utilised to analyse the mineral content and organic matter in coal tailings. This spectroscopic data was combined with laboratory test results to create a comprehensive dataset. Machine learning algorithms were then used to develop predictive models capable of discerning the complex composition of coal tailings.

The results show that the machine learning models can accurately predict the soil-enriching properties of coal tailings, demonstrating promising agreement with laboratory measurements. However, further research is needed to improve the model's accuracy by incorporating samples from a wider range of coal mines.

The combined approach of spectroscopy and machine learning enables accurate identification and quantification of key minerals, organic compounds, and potentially hazardous elements in coal tailings [1]. Additionally, feature importance analysis highlights the most influential spectral bands and chemical markers in tailings characterisation [2].

Overall, this integrated methodology provides a rapid, cost-effective, and efficient way to predict and characterise coal tailings compared to traditional analytical techniques [3].

**Keywords:** coal tailings; prediction; spectroscopy; machine learning

## 1. Introduction

This study explores the integration of spectroscopic techniques and machine learning for the predictive characterisation of coal tailings. Accurate characterisation of coal tailings is crucial for assessing their potential environmental impacts and their suitability for soil enrichment and rehabilitation [4]. By combining advanced analytical methods, this research aims to enhance the efficiency and precision of tailings evaluation, providing valuable insights for both environmental management and resource recovery [5].

## 2. Methods

### 2.1. Hyperspectral Spectroscopy

Hyperspectral spectroscopy was used to analyse coal tailings, providing detailed insights into mineral content and organic matter. Data were collected across various wavelengths to accurately identify and quantify minerals and organic compounds. For mineral analysis, spectral data were processed to determine composition, with key minerals identified and calibrated against standards. For organic matter, spectroscopy detected and characterised compounds, offering insights into the tailings' potential for soil enrichment.

### 2.2. Integration of Spectroscopic Data with Laboratory Test Results

Spectroscopic data were aligned with lab measurements to create a comprehensive dataset. This involved synchronising spectral and lab results to ensure accurate comparisons. The spectroscopic and lab data were then combined, enriched with detailed information, and normalised for consistency. Finally, the dataset was organised into features and tags, ready for machine learning analysis.

### 2.3. Integration of Spectroscopic Data with Laboratory Test Results

Machine learning algorithms were used to build predictive models from the integrated dataset. Different algorithms were tested for accuracy, with their performance comparisons shown below (see Table 1). The models were trained and validated on a dataset subset to identify patterns and relationships, with performance measured through cross-validation and accuracy metrics. Feature importance analysis identified key spectral bands and chemical markers influencing predictions. This approach effectively combined machine learning with spectroscopic and lab data to accurately characterise coal tailings.

TABLE 1. COMPARISON OF MACHINE LEARNING PREDICTION ALGORITHMS FOR COAL TAILINGS CHARACTERISATION

Model Type	Model Name	Performance
<i>LR*</i>	Linear	Fair
	Interactions Linear	Poor
	Robust Linear	Poor
<i>SLR*</i>	Stepwise Linear	Poor
<i>Tree</i>	Fine Tree	Good
	Medium Tree	Good
	Coarse Tree	Good
<i>SVM*</i>	Linear SVM	Poor
	Quadratic SVM	Poor
	Cubic SVM	Poor
	Fine Gaussian SVM	Poor
	Medium Gaussian SVM	Poor
	Coarse Gaussian SVM	Poor
<i>Ensemble</i>	Boosted Trees	Good
	Bagged Trees	Excellent
<i>GPR*</i>	Squared Exponential GPR	Poor
	Matern 5/2 GPR	Poor
	Exponential GPR	Poor
	Rational Quadratic GPR	Poor
<i>NN*</i>	Narrow Neural Network	Poor
	Medium Neural Network	Poor
	Wide Neural Network	Poor
	Bi-layered Neural Network	Poor
	Tri-layered Neural Network	Poor
<i>Kernel</i>	SVM Kernel	Poor
	Least Square Regression Kernel	Poor

\* LR: Linear Regression, SLR: Stepwise Linear Regression, SVM: Support Vector Machine, GPR: Gaussian Process Regression, NN: Neural Networks

## 3. Results

The machine learning models achieved high accuracy in predicting coal tailings properties, effectively analysing the integrated dataset and reliably predicting soil-enriching attributes. The prediction system ran under 12 different parameters, including pH, EC, acid neutralising capacity, total carbon, total nitrogen, exchangeable calcium, exchangeable magnesium, exchangeable sodium, cation exchange capacity, boron, potassium, phosphorus,

and sulfur. pH predictions and measured results can be found in Figure 1.

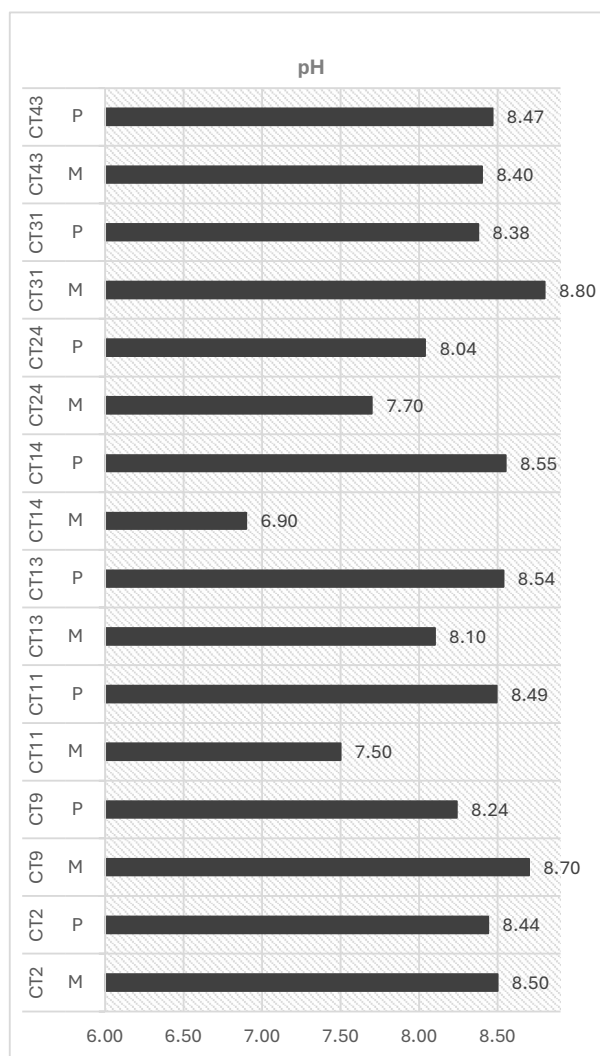


Figure 1. pH prediction results including measured values  
M: Measured P: Predicted

### 3.1. Comparison with Laboratory Measurements

Some predictions from the machine learning models closely matched lab measurements, validating their effectiveness in accurately characterising coal tailings. This alignment highlights the potential of combining machine learning with spectroscopic data for precise characterisation.

### 3.2. Need for Further Research

To improve model accuracy, further research is needed. Current models were trained on a limited range of coal mine samples, which may not represent the full diversity of coal tailings. Expanding the dataset to include samples from a broader range of coal mines is essential for enhancing model generalisability and performance.

### 3.3. Incorporation of Diverse Coal Mine Samples

Future research should focus on incorporating a wider variety of coal mine samples. Including samples from different locations and mining conditions will refine the models and improve their ability to account for variability in coal tailings composition, leading to more accurate and broadly applicable predictions.

## 4. Findings

The integration of hyperspectral spectroscopy with machine learning has proven effective for characterising coal tailings. This approach helped to identify and quantify key minerals, organic compounds, and hazardous elements in coal tailings. Hyperspectral data provided detailed composition insights, while machine learning models refined these assessments, crucial for evaluating environmental and agricultural potential. Feature importance analysis highlighted the most influential spectral bands and chemical markers, revealing the variables that most impact model accuracy and offering insights into the key factors driving tailings characterisation.

## 5. Additional Considerations

The combined use of hyperspectral spectroscopy and machine learning offers significant advantages over traditional methods. It provides a rapid, cost-effective, and efficient way to predict and characterise coal tailings, reducing time and expense while delivering precise and detailed insights. This methodology's ability to quickly process large datasets makes it a valuable tool for environmental management and resource recovery in the mining industry.

## Acknowledgement

I would like to thank Professor Kenneth Williams for his guidance and support throughout this research. I also express my gratitude to Lauren Bradney for her valuable contributions. I am grateful to the University of Newcastle's Institute for Energy and Resources and Newcastle Innovation for providing the necessary resources and facilities. Lastly, I appreciate the opportunity provided by the CHoPS 2024 conference to present this work.

## References

- [1] Carvalho, M., et al., Convolutional Neural Networks Applied to Antimony Quantification via Soil Laboratory Reflectance Spectroscopy in Northern Portugal: Opportunities and Challenges. *Remote Sensing*, 2024. 16(11): p. 1964.
- [2] Chen, T., et al., Rapid identification of soil cadmium pollution risk at regional scale based on visible and near-infrared spectroscopy. *Environmental Pollution*, 2015. 206: p. 217-226.
- [3] Angulo, A., et al., Machine learning enhanced spectroscopic analysis: towards autonomous chemical mixture characterization for rapid process optimization. *Digital Discovery*, 2022. 1(1): p. 35-44.
- [4] Sun, W., et al., An extensive review on restoration technologies for mining tailings. *Environmental Science and Pollution Research*, 2018. 25: p. 33911-33925.
- [5] Suppes, R. and S. Heuss-Aßbichler, Resource potential of mine wastes: A conventional and sustainable perspective on a case study tailings mining project. *Journal of Cleaner Production*, 2021. 297: p. 126446.



# Predicting Powder Flow from Containers with Flexible Walls

Mitch. Boots<sup>1</sup>, Shaun. Reid<sup>2</sup>, Mark G. Jones<sup>3</sup> and Craig. Wheeler<sup>1</sup>

<sup>1</sup> University of Newcastle, Newcastle, Australia

<sup>2</sup> TUNRA Bulk Solids, Newcastle, Australia

<sup>3</sup> Centre for Bulk Solids and Particulate Technologies, Newcastle, Australia

**Abstract**— Flexible Intermediate Bulk Containers (FIBCs), or ‘bulk bags’, are used to transport various materials but face common handling issues such as arching and ratholing. This project aims to model FIBCs using Discrete Element Method (DEM) numerical modelling to better predict powder discharge from these containers, and complement this approach with experimental and theoretical methods, to investigate flexible bin geometry and associated discharge regimes.

**Keywords:** FIBCs; flexible particles; DEM; flow; discharge;

## 1. Introduction

Known commonly as the ‘bulk bag’, Flexible Intermediate Bulk Containers (FIBCs) are used extensively in the transportation of food-grade materials, volatile chemicals, pharmaceutical powders, agrochemicals and more. Despite their widespread use, the industry users frequently face many issues with handling of FIBCs, problems such as arching, ratholing, and sensitivity to storage conditions are commonplace and are not well understood. These issues have resulted in an undesirable reliance on FIBC conditioners to promote flow. This project aims to address these issues by developing new methods to predict powder discharge from FIBCs, based on the properties of the bulk material being stored.

## 2. Flexible Intermediate Bulk Container (FIBC)

Flexible Intermediate Bulk Containers (FIBCs) are industrial containers typically made from woven polypropylene (PP) fabric, used for transporting a range of materials, from landscaping supplies to hazardous chemicals. Constructed according to international standards like ISO21898 or AS3668, FIBCs must meet minimum load criteria but lack specifics on stitching, elasticity, stiffness, and fabric thickness, which influence the bag’s rigidity and performance.

FIBCs vary in design, with different inlets, outlets, dimensions, and mounting loops. Dischargers for FIBCs range from pneumatic to gravity-based solutions, often with flow aids and conditioners utilized for loosening solidified materials—critical for low-flowability cohesive granular materials.

Recent studies have shown that in FIBCs, vertical stresses increase while lateral stresses decrease, correlating with the flow issues observed in the industry [1]. The AS3774 standard for bin loads includes an equation to calculate a flexibility factor,  $\alpha$ , this factor has been used in various studies on the impact of flexible walls [2].

$$\alpha = \frac{E_s \left( \frac{d_c}{2} \right)}{E_w t} \quad (1)$$

Where  $E_s$  is the Youngs modulus of the Bulk Solid,  $E_w$  is the Young’s modulus of the flexible wall,  $t$  is the thickness of the flexible wall and  $d_c$  is the diameter of the bin.

## 3. Discrete Element Model (DEM)

The Discrete Element Method (DEM) has become a leading approach in modelling granular systems. DEM provides for greater flexibility than continuum-based analyses by examining microscale interactions between particles and boundaries to predict flow through a system [3], however it involves complexities in calibration, particularly when predicting arching and ratholing. DEM is used in our study to simulate the discharge of a Flexible Intermediate Bulk Container (FIBC), representing both the bulk material and the flexible bag geometry. The simulations were conducted using ANSYS Rocky 2024R1.

### 3.1. Flexible Particle Model

Flexible particles are composite structures made by connecting simple-shaped elements. Despite the flexibility of the composite particle, each individual element remains rigid. It is the joint that allows flexibility, and the joint mechanics define the reaction of the flexible particle. Specifically focusing on flexible ‘shell’ particles, they are connected by a series of triangular prisms. When a joint is subjected to linear and angular deformations, it reacts by exerting forces and moments over the connected elements, opposing the deformations. These forces and moments hold the elements together, forming a singular particle.

The linear deformation of a joint, due to the relative translation, is quantified by  $d^{rel}$ . To write the model equations for the tensile and shear forces, the displacement is decomposed, as well as other magnitudes, into normal and tangential components. The normal direction for this decomposition is represented by (2) [4]:

$$\hat{n} = \frac{\widehat{B}_1 + \widehat{B}_2}{|\widehat{B}_1 + \widehat{B}_2|} \quad (2)$$

Where  $\widehat{B}_1$  and  $\widehat{B}_2$  are unit vectors aligned parallel to the direction of the two elements connected by the joint. The magnitude of  $d^{rel}$  is divided into the normal and tangential components. The (3-4) define their relationships.

$$d_n^{rel} = d^{rel} \hat{n} \quad (3)$$

$$d_t^{rel} = d^{rel} - d_n^{rel} \quad (4)$$

#### 3.1.1. Joint Model

The Joint Model primarily defines the deformation of the flexible particle. For this study, the bilinear elastoplastic model within Rocky was utilised. The bilinear model is an extension of the existing linear model that is applied by default in Rocky. The bilinear model was chosen because it allows permanent deformations to occur in the flexible geometry, whereas the linear model tends to revert to an elastic state. Fig 2 summarises the loads acting on each element.

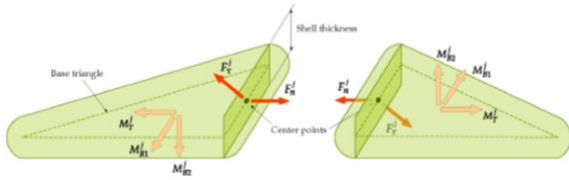


Figure 1. Force and Moments acting on each element [4].

Each force and moment are directly proportional to the linear or angular joint deformation of the particle. Further details on the calculation of the forces and moments, as well as explanations, are elaborated in the ANSYS Rocky Technical Manual [4].

#### 4. Simulation Results/Discussion

Preliminary simulations examined how changing the flexibility factor of an FIBC impacts discharge behaviour. A 90 cm x 90 cm x 90 cm bulk bag with an open top and spouted outlet was used to simulate a sand-like granular material. Effects of flowability were tested by adjusting the rolling resistance and adhesion of the material. Each bag contained 0.53 m<sup>3</sup> of bulk material and was allowed to settle for 1.5 seconds before discharge.

Fig 3 shows a visualisation of the simulated FIBC during discharge:

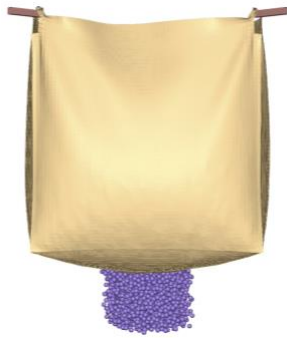


Figure 2. Simulated visualisation of FIBC during discharge.

The results of the simulations conducted are presented in Fig 4 & 5, with Fig 4 highlighting the impacts of a flexible boundary on discharge by varying the flexibility factor.

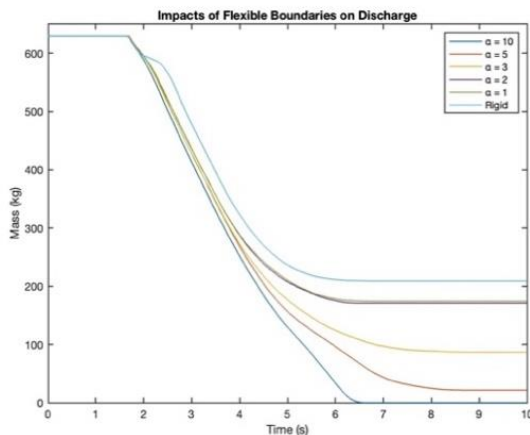


Figure 3. Impacts of Flexible Boundaries on Discharge.

The results in Fig 4 highlight the significant variation in discharged mass when only the flexibility factor is adjusted. In this scenario, the stiffness of the container is the sole variable modified. As the flexibility of the container increases, its ability to hold its shape decreases. The bulk material largely maintains the geometry of the container during discharge, but as the bulk solid discharges, the container begins to rapidly lose the structural integrity gained from the bulk solid. This transition

moves the container from a flat-bottomed bin to one with a large hopper half-angle.

Fig 5 illustrates the impact of flowability on a flexible wall container compared to a rigid wall container for various bulk material models.

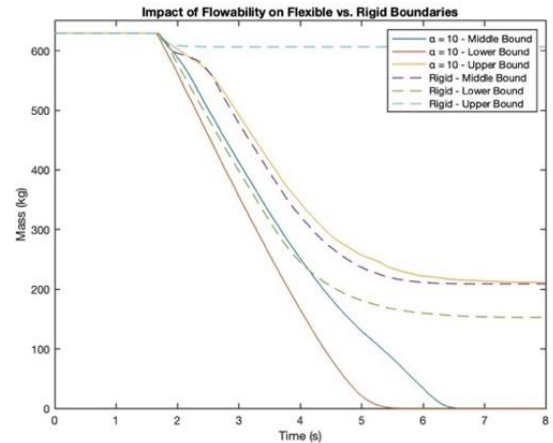


Figure 4. Impact of Flowability on Flexible vs Rigid Boundaries.

The three bulk material models are designated as upper, middle, and lower bound. The flow characteristics of each material were benchmarked using the Rocky Calibration Suite [4], with the outcomes reported in Table 1.

TABLE I. SIMULATED MATERIAL CHARACTERISTICS

Material	Poured AOR Trials		Drawdown AOR Trials	
	3 runs	Av.	3 runs	Av.
Upper	45.1°, 38.6°, 43.6°	42.4°	57.2°, 58.4°, 54.1°	56.6°
Middle	41.3°, 43.2°, 42.4°	42.3°	46.2°, 51.3°, 47.5°	48.3°
Lower	36.0°, 35.2°, 34.9°	35.4°	41.4°, 39.8°, 39.0°	40.0°

#### 5. Conclusion

Although preliminary, this DEM approach has provided valuable insights into visualising basic flow regimes from FIBCs. The simulations highlight the significant impact of flexible wall characteristics on discharge behaviour, laying a foundation for more detailed studies. Future work will refine the models and explore experimental validation to enhance prediction accuracy and reliability. This research has the potential to improve FIBC design and handling, reducing issues such as arching and ratholing, and optimising material discharge processes.

#### Acknowledgement

Thank you to the International Fine Particle Research Institute (IFPRI) and TUNRA Bulk Solids (TBS) for their generous support, feedback and guidance.

#### References

- [1] S. L. Pantaleev, S.-A. Papanicolopoulos and J. Y. Ooi, "Finite element analysis of stresses in flexible bulk solid container," *Advances in Structural Engineering*, 2018.
- [2] AS3774-1996, "Loads on Bulk Solids Containers," *Standards Association of Australia*, 1996.
- [3] P. A. Cundall and O. Strack, A discrete numerical model for granular assemblies, *Geotechnique*, 1979.
- [4] ANSYS, "Rocky Technical Manual," ANSYS, Inc, Southpointe, 2024.

# Investigating the effect of agitator dynamics on the twin-screw feeder performance for pharmaceutical powders

L. Naranjo<sup>1</sup>, K. Matsunami<sup>1</sup>, P. Van Liedekerke<sup>1</sup>, T. De Beer<sup>1</sup>, and A. Kumar<sup>1</sup>

<sup>1</sup> Ghent University, Belgium

**Abstract—** In continuous manufacturing of solid dosage forms precise and consistent feeding is crucial to ensure the quality of the final product. An important but often disregarded factor in this feeding process is the intermixing effect induced by the agitator, which modifies the bulk density, flow rate, and flow patterns of the powder. The purpose of this contribution is to propose a framework to assess feeding performance, combining Discrete Element Method (DEM) modeling and experiments for a commercial-scale feeder. The developed DEM model provides quantitative predictions for the feed factor and identification of zones prone to material accumulation while also properly capturing key flow features such as preferential flow patterns, stagnant zones, and bypass paths. Using scenario analysis, the impact of the screw-agitator ratio and screw speed is determined considering the cohesive properties of the powder. The findings suggest that powders with poor flow characteristics require restrictive operational constraints, as the screw-agitator ratio is susceptible to variations in mass feed rate. This contribution highlights the importance of appropriately choosing a screw-agitator ratio to determine an optimal operation window (achieve a minimum agitation needed to induce unhindered flow and reduce variability in the mass flow rate).

**Keywords:** powder; feeder; agitator; modeling;

## 1. Introduction

Powder feeding is crucial in continuous pharmaceutical manufacturing. It must provide precise and consistent material discharge to the subsequent manufacturing steps. Good flowing powders pose fewer handling issues, while challenging materials that tend to stick may need density conditioning and flow facilitation with an agitator. The agitation system is used to prevent bridging and ensure a stable and accurate mass flow rate.

Recent studies show that the agitator influences feeding behavior, affecting flow patterns (e.g., funnel flow), bulk density distribution, mass flow rate variability, and material traceability [1]. All these aspects suggest that controlling screws and agitator speed independently could be beneficial. This contribution uses a combination of experimental and predictive modeling tools-Discrete Element Method (DEM), to understand the impact of the agitator on flow and mixing behavior when changing the rotational speed ratio. The insight will enable the adequate selection of feeding operating conditions based on material characteristics.

## 2. Materials and methods

This contribution studies the effect of screw-agitator rotational speed changes on powder feedability using a twin-screw LIW feeder. The focus is on assessing the effect of changes in the screw and agitator rotational speed ratio on powders with different flowability levels. The model development steps include calibration, validation (i.e., emptying experiments with free-flowing colored powder and a cohesive powder), and modelling of feeding scenarios.

### 2.1. Materials and equipment

The materials used for the emptying experiments consider pink and white lactose-base free-flowing powder and a binary blend of paracetamol powder and 10% sodium saccharine as tracer material.

The Loss In Weight (LIW) feeder equipment used is a Brabender DDSR20-QR twin-screw that enables independent control over screw and agitator rotational speed.

### 2.2. Feeder characterization

The feeder is operated in volumetric mode (i.e., constant screw speed) to characterize the inherent feeding behavior under various operating conditions. Experiments run until the hopper is empty or unable to further deliver more material. Results, measured as mass change per unit time, are used to calculate the feed factor over time.

The experimental results are used to qualitatively validate the predictions of the main model. A lactose-based free-flowing colored powder is used to visualise flow characteristics such as bypass formation and preferential extraction, and paracetamol powder is used to provide information on the feeding of cohesive powders, focusing on feed factor values over time and zones of material accumulation.

### 2.3. Model implementation

The methodology used a simplified virtual replicate of the feeder, considering only a section of the real geometry but maintaining the general flow behavior, this in order to reduce the number of particles and the calculation time.

The DEM model uses scaled monodispersed bi-spheres and the Hertz-Mindlin with JKR [2] contact model, which is chosen for its consideration of elastic and adhesive particle interactions. DEM input values are selected based on a calibration approach specific to the powder being represented.

### 2.4. Model validation

The model results are validated by replicating the feeder emptying experiments with lactose-based free-flowing colored powder and paracetamol powder. The experimental results and model predictions are compared qualitatively (i.e., image comparison) and quantitatively (i.e., feed factor values) for the same cases experimentally studied.

### 2.5. Scenario analysis

The validated DEM feeder model is used to predict feeding performance, considering a set of scenarios for each material defined based on a three-level full factorial design of simulations. The parameters include powder screw-agitator ratio (3, 15, and 35) and screw rotational speeds (96, 170, and 243 RPM).

## 3. Results and discussion

DEM simulation results visualize the flow profiles for different powders and operating conditions. Three general observations about the feeding process are relevant (Fig. 1).

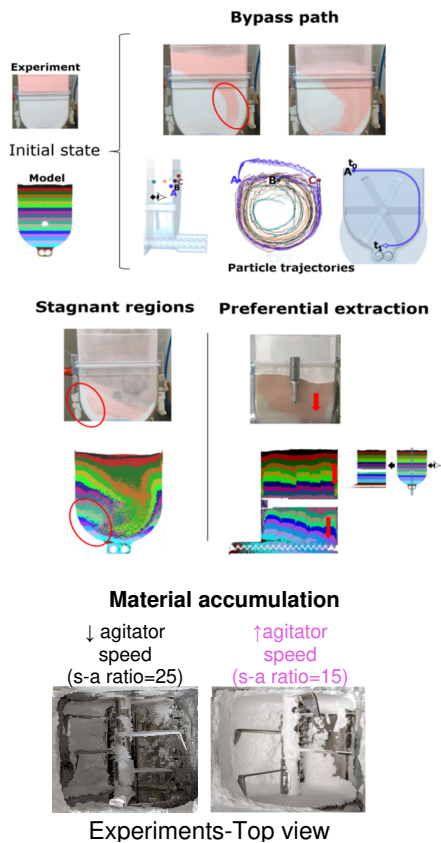


Figure 1. Validation considering experimental and modelling results. Main flow features bypass path, stagnant regions, and back preferential extraction. Experimental visualization of material accumulation zones

First, the feeder shows a non-uniform flow profile where the agitator induces a bypass trajectory i.e., the powder lying on top of the powder bed leaves first out of the system. Second, stagnant zones (e.g., feeder corners) are present during the emptying process, powder which, in some cases, does not manage to leave the feeder. Lastly, the screw design with a constant pitch affects powder draw-down patterns, leading to preferential extraction from the back region of the feeder.

The validation process for paracetamol powder allows for a quantitative comparison between experimental findings and model predictions for feed factor (i.e., the mass of material per screw revolution) and identification of material accumulation zones. The DEM model predicts the mean experimental feed factor value at an intermediate hopper level with a relative error of less than 7%. Besides, it is experimentally shown (Fig. 1) that some powder tends to remain in the left bottom region of the feeder. This zone is also identified in the model predictions by a regional comparison of normal forces, obtaining values up to 20 % higher for the average normal force in the left region compared to the right region.

### 3.1. Scenario analysis

The validated DEM model is used as a tool to predict feeding performance when taking into consideration different process operating conditions (Fig. 2): screw and agitator rotational speeds for powders with different flowability levels: free, intermediate, and poorly flowing (i.e., approximate flow function coefficients of 7, 3, and 1 respectively). This provides a general understanding of the process regarding the effect of screw-agitator ratio on powder feedability.

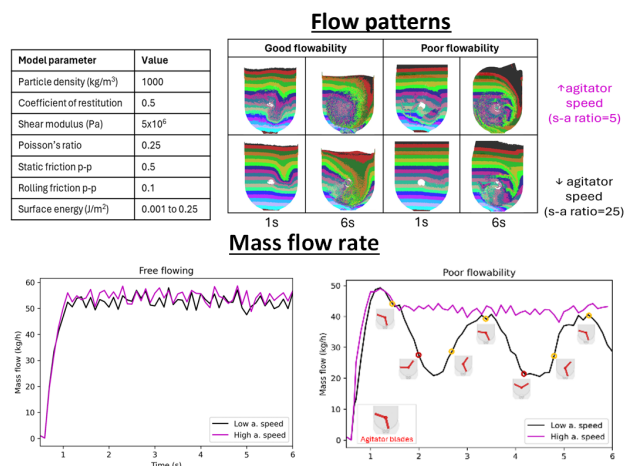


Figure 2. DEM input parameters and predictions: flow patterns and mass flow rate for free-flowing and cohesive powders

In Fig. 2 it is observed that the screw-agitator ratio influences the obtained flow patterns due to the mixing induced by the agitator, which in some cases can subsequently lead to variations in mass flow rate. This is particularly noticeable when dealing with poorly flowing powders at a high screw-agitator ratio (i.e., low agitator speed), as the mass flow rate experiences cyclical changes due to the rotating agitator. In contrast, powders that are free and intermediate flowing powders are less sensitive to variations in the screw-agitator ratio.

Using the previously acquired values together with an interpolation based on a PLS model, contour plots can be created and further used to illustrate the determination of a suitable feeder operating condition.

## 4. Conclusion

This contribution studies the effect of the screw-agitator rotational speed ratio using DEM. The results corroborate DEM's capability as a tool to provide detailed insight into the flow pattern development in a feeding system, considering different powder characteristics and operating conditions.

The results made it possible to visualize the main characteristics of the agitator-induced flow and to further analyze the areas prone to material accumulation, considering various operating conditions and powder flowability levels.

The modeling and experimental results confirm the relevance of an adequate selection of screw-agitator ratio for the feeding process. This is to ensure, in some cases (e.g. cohesive powders), a system less prone to feeding problems and to reduce mass flow rate variability. Furthermore, these results could be considered an initial step towards determining an adequate or optimal operation window (e.g., a minimum level of agitation required to induce unhindered flow or reduce mass flow rate variability from setpoint) rather than using a fixed ratio.

## Acknowledgement

The financial support for this research from BOF, Research Fund Ghent University and the experimental support from Fette Compacting Belgium are gratefully acknowledged.

## References

- [1] L. De Souter *et al.*, "Elucidation of the powder flow pattern in a twin-screw LIW-feeder for various refill regimes," *Int. J. Pharm.*, vol. 631, p. 122534, 2023.
- [2] S. Bin Yeom, E.-S. Ha, M.-S. Kim, S. H. Jeong, S.-J. Hwang, and D. H. Choi, "Application of the discrete element method for manufacturing process simulation in the pharmaceutical industry," *Pharmaceutics*, vol. 11, no. 8, p. 414, 2019.



# Ultrafine Air-Classification of Plant based Proteins: A step Towards Reducing Carbon Footprints

Zaki Hussaini<sup>1,2</sup>, Baldeep Kaur<sup>2</sup>, Atul Sharma<sup>2</sup>, Ian Hancock<sup>1</sup>, and Michael Bradley<sup>2</sup>,

<sup>1</sup> Bradley Pulverizer, Dartford, UK

<sup>2</sup> The Wolfson Center for Bulk Solids Handling Technology, University of Greenwich, Chatham Maritime, UK

**Abstract**— Air classification is vital for separating particles, with applications in industries such as food, pharmaceuticals, agriculture and many more. With the increased innovation and advancements of science, demands of smaller particle sizes, innovative and effective methods of classifications are needed. The performance of a rotor air classifier is effected by both its structural parameters which includes the design of the rotor cage, shell design, volute and much more, and operating parameters which include the classifier rotor speed, the feed rate and the air inlet velocity. With the increased demand of ultra fine classification of sub 10 micron the air classification method is within its limit of possibilities to achieve this range. Effect of change in rotor blade angle, rotor speed and feed rate are investigated. With extensive experimental work carried out and results are analysed to optimise the classification of sub 10 micron particle size.

**Keywords:** classification; efficiency; rotor cage; volute; blade angle;

## 1. Introduction

Powder classification divides raw feed material into fractions based on properties like size or density, ensuring uniformity. Various methods exist for size-based classification, each with pros and cons. Air classification using dynamic air classifiers is popular for meeting industrial demands, such as high throughput and low cut sizes. The cut size is the particle size with a 50% chance of being classified as fine or coarse fraction [1]. Perfect classification is theoretical, as factors like particle collisions and aerodynamic interactions can cause finer particles to form coarser ones or allow coarser particles into the fine fraction.

An improved uniform flow field inside the air classifier mainly in and around the classifier rotor blade can achieve fine cut size classification and improvement of separation efficiency. Studies have been conducted the performance of classifier. Adamcik studied the effect of performance parameter on classification mainly focusing on the feed rate, air flow and rotor speed [2]. Jia, et al. used Ansys-Fluent in order to conduct investigation on the effect of various rotor cage structure as well as diversion cone [3]. Shubo, et al. used Ansys-Fluent in order to obtain a discrete phase simulation between the single and double layer spreading plate [4]. The presented paper deals with the experimental investigation of the effect of various rotor cage structure design with varying feed rate and rotor speed.

This study uses a classifying system with a vertical rotor cage and no guide vane. Figure 1 illustrates such system whereby particles enter from the top, controlled by a rotary valve, while air from a fan enters from the bottom, rising into a conical chamber. The rotor cage, driven by an electric motor, whirls the air to create a centrifugal counter flow separation zone at the top. Around the blades, a centrifugal cross flow zone forms, enabling particle separation.

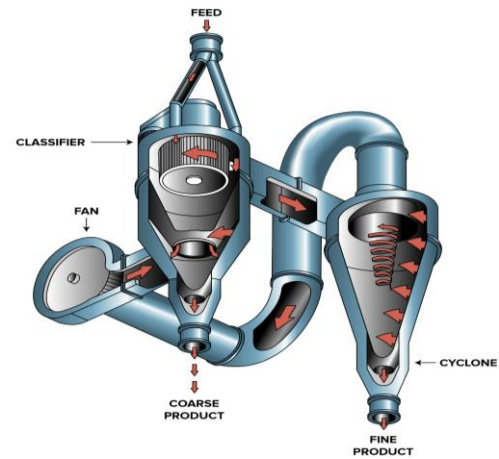


Figure 1. Schematic Illustration of Particle Flow in Classification System [5]

## 2. Rotor Classifier

### 2.1. Introduction of Rotor Classifier

Rotor air classifiers are vital in industries like mineral processing, pharmaceuticals, food processing, and agriculture for particle size classification. They use centrifugal and aerodynamic forces to separate particles by size and shape, ensuring the desired product specifications [6].

Rotor air classifiers come in various designs, from them the main design variations include the dimensions of the rotor cage, the characteristics of the rotor blade, the rotor orientation (horizontal or vertical), the use of guide vanes, the design of feeding inlets and methods, and the air inlet and volute design.

When the relative velocity angle matches the rotor blade angle, the incidence angle between the airflow and rotor blade becomes zero. This reduces the impact of airflow and particles on the rotor blade, resulting in a well-distributed flow field in the rotor cage, which is the primary focus of this study.

Sharpness of separation and cut size are key performance measures when evaluating rotor air classifier performance.

Sharpness of separation is the ratio of a selected particle size in the coarse selection compared to the infeed. This is illustrated by an efficiency curve. The ideal situation places particles below the selected size in the fine collection and those above in the coarse fraction. In reality, this is represented by an S-shaped efficiency curve [7].

In air classification, the cut size is the particle size at which fine and coarse particles separate. Controlling the cut size is essential for achieving the desired particle size distribution, affecting product quality, yield, and energy consumption. Factors influencing cut size include airflow rate, particle properties, classifier design, and feed material characteristics. Determining the appropriate cut size involves understanding and optimising these factors.

## 3. Experimental Methods

The general classification process in air classifier is of the initial in-feed material entering from above to the classification zone, where particles follow one of two paths. If gravitational

and centrifugal forces exceed the drag force, particles drop into the coarse fraction collection bucket. Alternatively, if particles overcome these forces, they are transferred via the fine fraction air stream to the filter. Clean air passes through filter cartridges, capturing the fines inside. These fines are cleaned with timed pulse jets, which disturb particles on the inner filter surface, causing them to drop into the fines fraction collection unit. The clean air then escapes into the atmosphere. Figure 4 shows the components of the air classifier in the experimental set up.

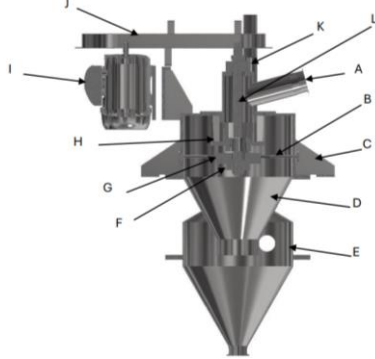


Figure 2. Main Components of an Air Classifier. (A) Rotor Housing; (B) Stay Bolt; (C) Upper Chamber; (D) Inner Cone; (E) Lower Chamber; (F) Lower Bearing; (G) Stay Bolt Ring; (H) Rotor Cage; (I) Electric Motor; (J) Drive Components; (K) Upper Bearing; (L) Shaft.

### 3.1. Experimental Measurements

The study examined the effect of rotor blade angle with varying operating parameters. A total of 27 experimental trials were conducted using three different rotor designs with blade angles of 0°, 30°, and 45°, varying feed rates of 15, 35, and 113 kg/s, and rotor speeds of 1600, 2000, and 2400 rpm. Each trial used 1 kg of pea powder, which was collected from both fine and coarse collection units, then weighed. Samples were analyzed using a Malvern Mastersizer 3000 to obtain particle size distribution curves. Classifier efficiency for each trial was calculated using the Bradley efficiency formula, considering yield, purity, and throughput of the desired particle size;

$$\eta = \frac{F_f}{F_t} \times \text{Percentage fines in the fine collection} \quad (1)$$

$F_f$  – mass of fines content in the fine collection  
 $F_t$  – mass of fines content in the in feed

## 4. Results

The classifier efficiency for each trial is plotted on graph to visualise the effect of rotor blade angle and the varying operating parameters.

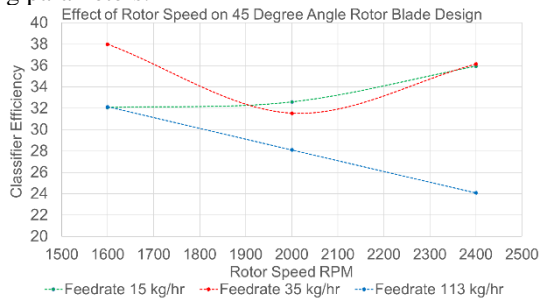


Figure 3. Graph Showing the Classifier Efficiency of 45° Rotor Blade Angle

Figure 3 shows the classifier efficiency with varying operating parameters for a 45-degree rotor blade angle. It indicates that as the feed rate increases significantly, the classifier efficiency reduces. However, at lower feed rates of 15 and 35 kg/hr, there is a crossover throughout the varying rotor speeds. Figure 4 illustrates that with a 30-degree rotor blade

angle, as the feed rate increases, there is a slight improvement in efficiency. Additionally, an increase in rotor speed results in a gradual improvement in efficiency. However, when the feed rate is 113 kg/hr, it follows a U-shaped parabola, with 1600 and 2400 rpm showing optimal efficiency and 2000 rpm being the most inefficient. Figure 5 demonstrates that for the 0-degree rotor blade angle, rotor speed has very little effect on efficiency. However, there is an improvement in efficiency when the feed rate is increased to 113 kg/hr.

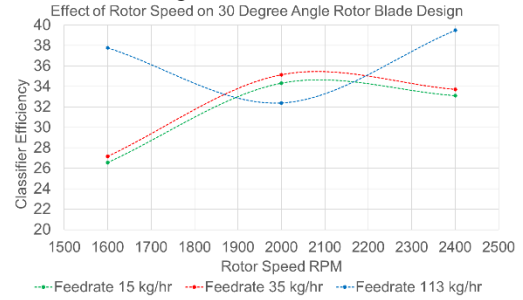


Figure 4. Graph Showing the Classifier Efficiency of 30° Rotor Blade Angle

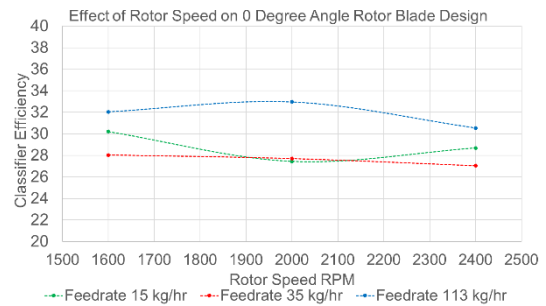


Figure 5. Graph Showing the Classifier Efficiency of 0° Rotor Blade Angle

## 5. Conclusion

The classifier efficiency was studied by using different rotor designs and varying operating parameters. The 30° and 45° rotor blade angles were identified as the most optimal designs, improving flow fields through the rotor cage compared to the 0° blade angle [8]. However, the 0° blade rotor showed a fairly consistent efficiency pattern. Further research with varied rotor speeds is needed to understand their impact on efficiency. Future work will focus on curved blade rotors to enhance the flow field.

## Acknowledgement

The authors appreciate the financial and technical support of Bradley Pulverizer and the Wolfson Centre, University of Greenwich. The project is partly supported by the University of Greenwich through VC Scholarship (VCS-FES-05-21).

## References

- [1] Y. Yuan, L. Jiaxiang and Z. Kai, "Establishment of a prediction model for the cut size of turbo air classifiers," *Powder Technology*, vol. 254, pp. 274-280, 2014.
- [2] M. Adamcik, "Limit Modes of Particulate Materials Classifiers," BRNO University of Technology, 2017.
- [3] F. Jia, X. Mou, Y. Fang and C. Chen, "A New Rotor-Type Dynamic Classifier: Structural Optimization and Industrial Applications," *Processes*, vol. 9, p. 6, 2021.
- [4] W. Shubo, L. Jiaxiang and Y. Yuan, "Design of a new double layer spreading plate for a turbo air classifier," *Powder Technology*, vol. 312, no. 1, pp. 277-286, 2017.
- [5] B. Pulverizer, "Bradley Pulverizer," 2024. [Online]. Available: <https://www.bradleypulverizer.com/windsifter-air-classifiers/>.
- [6] L. Guo, J. Liu, S. Liu and J. Wang, "Velocity measurements and flow field characteristic analyses in a turbo air classifier," *Powder Technology*, vol. 178, no. 1, pp. 10-16, 2007.
- [7] Q. Huang, J. Liu and Y. Yu, "Turbo air classifier guide vane improvement and inner flow field numerical simulation," *Powder Technology*, vol. 105, no. 1, p. 226, 2012.
- [8] Y. Yu, X. Kong and J. Liu, "Effect of rotor cage's outer and inner radii on the inner flow field of the turbo air classifier," *Materialwissenschaft und Werkstofftechnik*, vol. 51, no. 7, pp. 908-919, 2020.

# Particle levitation by ultrasound for on-orbit powder-based additive manufacturing

Anushanth Karalasingam<sup>1</sup>, Sina Haeri<sup>1</sup>

<sup>1</sup> Institute for Materials and Processes, University of Edinburgh, UK

**Abstract**— Powder-bed additive manufacturing (PBAM) presents significant potential for in-space manufacturing due to its versatility and material compatibility. However, terrestrial PBAM systems are ill-suited for microgravity, where powder distribution and manipulation are critical challenges. To address this, we investigated the use of ultrasound transducer arrays to levitate and control powder particles. By precisely controlling sound wave properties, we established stable zones for powder manipulation. Initial experiments successfully levitated and controlled various materials, including glass beads, validating the concept. While these results are promising, the levitation of denser metallic powders, commonly used in PBAM, necessitates further optimization. We are developing new array designs based on the Gorkov theory and exploring complementary control techniques. Our ultimate goal is a scalable, modular array capable of precise manipulation of metallic powders in microgravity, enabling on-demand additive manufacturing for future space missions. This technology holds the promise of revolutionizing in-space manufacturing by providing the capability to produce complex components directly on-site, reducing reliance on ground-based supply chains and accelerating space exploration.

**Keywords:** microgravity; ultrasound; levitation; metallic powders; additive manufacturing

## 1. Introduction

Powder-bed additive manufacturing (PBAM) has emerged as a promising technology for in-space manufacturing due to its versatility and compatibility with diverse materials. Unlike traditional manufacturing methods, PBAM offers the ability to create complex geometries and structures directly from digital models, making it an attractive solution for on-demand manufacturing in space exploration missions. However, the microgravity environment presents a critical challenge for PBAM, hindering the even distribution and manipulation of powder particles crucial for successful additive manufacturing. In terrestrial PBAM systems, gravity plays a significant role in maintaining the powder bed's stability and facilitating the spreading and distribution of powder particles. However, in the absence of gravity, these processes become significantly more challenging.

A novel method for manipulating powder particles in microgravity environments using ultrasound transducer arrays is deployed. This approach leverages the principles of acoustic radiation forces generated by high-frequency sound waves to levitate and control microscopic particles. Acoustic radiation forces arise from the transfer of momentum from sound waves to particles suspended in a medium. By designing the ultrasound transducer array and precisely controlling the properties, such as phase and amplitude, a stable zone can be created for controlled manipulation and distribution of powder within the PBAM system.

## 2. Experimental Validation

To validate the concept of ultrasound-based powder manipulation, initial experiments were conducted using an ultrasound transducer array designed based on simulations guided by the Gorkov theory. The Gorkov theory explains how sound waves interact with small particles in an acoustic field as shown in Equation (1 - 2) [1-3], providing a theoretical foundation for the design and optimization of the transducer array.

$$F^{\text{rad}} = -\nabla U^{\text{rad}} \quad (1)$$

$$U^{\text{rad}} = \frac{4\pi a^3}{3} (A - B)$$

Where,

$$A = \frac{1}{2} \left( 1 - \frac{K_p}{K_m} \right) K_m \langle p_{in}^2 \rangle \quad (2)$$

$$B = \frac{3}{4} \left( \frac{2 \left( \frac{\rho_p}{\rho_m} - 1 \right)}{2 \frac{\rho_p}{\rho_m} + 1} \right) \rho_m \langle v_{in}^2 \rangle$$

The acoustic radiation force, denoted as  $F^{\text{rad}}$ , is determined by the negative gradient of the acoustic potential  $U^{\text{rad}}$ . This force is significant when a spherical particle, smaller than the wavelength, is immersed in an ideal fluid. The expression for  $U^{\text{rad}}$  considers the particle's radius ( $a$ ), compressibility of both the particle ( $K_p$ ) and the surrounding medium ( $K_m$ ), as well as their respective densities ( $\rho_p$  and  $\rho_m$ ). Additionally, it accounts for the incident time-averaged pressure ( $p_{in}$ ) and velocity waves ( $v_{in}$ ), averaged over a full oscillation period. These factors collectively describe how the acoustic field exerts forces on the particle, crucial for understanding particle dynamics.

In the initial experiments, Expanded Polystyrene (EPS) particles with a density of 13.8 kg/m<sup>3</sup> were used. The experiment successfully demonstrated the ability of the array to levitate and control the EPS particles, validating the potential of this ultrasound-based powder handling approach.

Building upon this success, arrays capable of handling heavier and more diverse materials, including Isopropyl alcohol (0.8 mm, 786 kg/m<sup>3</sup>), sugar pearls (1590 kg/m<sup>3</sup>), and glass beads (0.1 mm, 2500 kg/m<sup>3</sup>) were developed. Notably, a layer of glass beads was levitated for the first time using an array of transducers, as shown in Figure 1.

TABLE I. PROPERTIES AND ACOUSTIC RESPONSE OF PARTICLES TESTED WITH ULTRASOUND TRANSDUCER ARRAY

Material	Styrofoam	Inconel	Glass
Radius (m)	$1 \times 10^{-3}$	$10 \times 10^{-6}$	$50 \times 10^{-6}$
Density (kgm <sup>-3</sup> )	25	8193	2500
Speed of sound (ms <sup>-1</sup> )	900	5700	4540



Surface Area (m <sup>2</sup> )	12.6×10 <sup>-6</sup>	1.26×10 <sup>-9</sup>	3.14×10 <sup>-8</sup>
Gravitational force (N)	1.03×10 <sup>-6</sup>	3.36×10 <sup>-10</sup>	1.28×10 <sup>-8</sup>
Acoustic force (N) [4]	14.8×10 <sup>-6</sup>	1.59×10 <sup>-11</sup>	1.99×10 <sup>-9</sup>

TABLE I. compares Styrofoam, Inconel, and Glass based on their physical properties and forces. Styrofoam, with the largest surface area (12.6×10<sup>-6</sup> m<sup>2</sup>), experiences the highest acoustic force (14.8×10<sup>-6</sup> N). In contrast, Inconel and Glass, having smaller surface areas, experience significantly lower acoustic forces of 1.59×10<sup>-11</sup> N and 1.99×10<sup>-9</sup> N, respectively. The greater acoustic radiation force on Styrofoam is due to its larger surface area compared to the other materials, despite variations in density and size.

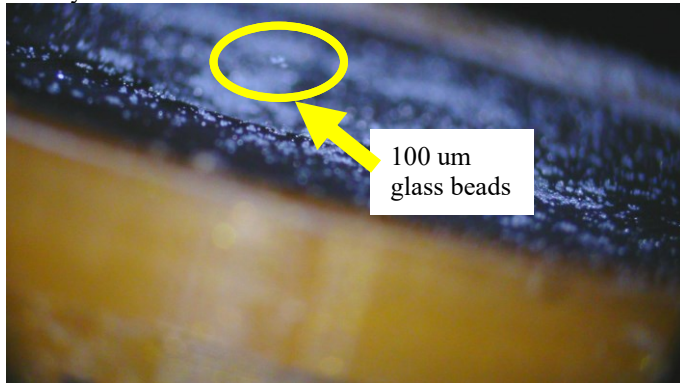


Figure 1. Levitation of 100 μm glass beads using ultrasound transducers.

There are few ways to visualize the generated acoustic fields using transducer arrays, such as schlieren imaging, laser Doppler velocimetry, and thermal imaging. We employed a thermal camera (FLIR 655C) to visualize the wave patterns created by the arrays on a thin cellulose layer positioned in the ultrasound field as shown in Figure 2. This method was used to verify the overall system performance as predicted by simulations due to its ease of use [5].

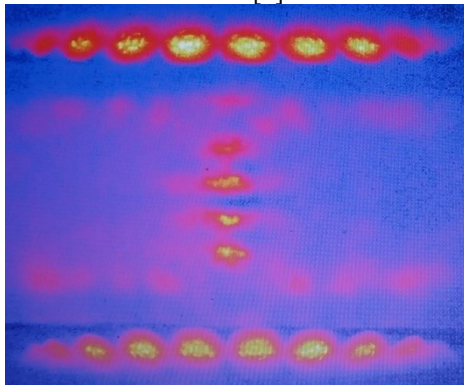


Figure 2. Image from FLIR 655C of the ultrasound standing wave.

While these initial results are promising, significant challenges remain to be overcome. Metallic powders commonly used in PBAM, such as Inconel (8193 kg/m<sup>3</sup>) and Stainless Steel (7850 kg/m<sup>3</sup>), are typically smaller and denser than the materials tested thus far. Manipulating these metallic powders requires more precise control and stronger levitation forces.

The current array design can vibrate the metallic powders, but levitation requires further optimization. To address this challenge, new array designs guided by the Gorkov theory are being developed. Additionally, complementary techniques are being investigated to achieve the necessary level of control over metallic powder manipulation in microgravity. For instance, hexagonally packed transducer arrays will be used. Since the top and bottom configuration of arrays are found to be effective and

the distance between the arrays would be maximised to accommodate manufacturing conditions.

One of the key developments in progress is the design of a scalable modular array that can levitate and move metal powders. This array will incorporate a microcontroller capable of generating individual signals for each transducer, enabling precise movement of the layers of powders used in additive manufacturing.

### 3. Conclusion

The successful implementation of ultrasound-based powder manipulation for Powder Bed Additive Manufacturing (PBAM) in space could revolutionize space exploration by enabling on-demand manufacturing. This capability would allow for the production of essential components, tools, and structures directly in space, reducing dependence on pre-manufactured and transported materials. Such technology would also facilitate the construction of habitats and infrastructure on other planetary bodies like the Moon or Mars, utilizing local resources and additive manufacturing techniques. This adaptability could lead to more efficient scientific experiments and exploration activities, as researchers could quickly prototype and refine designs.

However, several challenges must be addressed, including developing reliable control systems for the ultrasound transducer arrays. Accurate control over the phase and amplitude of sound waves is crucial for manipulating powder particles precisely. Any inconsistencies in the control system could compromise the quality of the manufactured products. Moreover, integrating this technology with existing PBAM hardware and software requires careful engineering to ensure compatibility and seamless operation. Continued research and development are essential to overcome these challenges and fully realize the potential of ultrasound-based powder manipulation in space, paving the way for more autonomous and capable space missions.

### Acknowledgement

The authors express their gratitude to the Electronics Lab technicians (TLD) at the University of Edinburgh, Dr. Martina Meisnar from the European Space Agency, and Mr. Yanzhen Li for their invaluable support and contributions.

### References

1. Горьков, Л.П., *О силах, действующих на малую частицу в акустическом поле в идеальной жидкости*. Доклады Академии наук СССР, 1961. **140**(1): p. 88-91.
2. Bruus, H., *Acoustofluidics 7: The acoustic radiation force on small particles*. Lab on a Chip, 2012. **12**(6): p. 1014--1021.
3. Settnes, M. and H. Bruus, *Forces acting on a small particle in an acoustical field in a viscous fluid*. Physical Review E, 2012. **85**(1): p. 016327.
4. Marzo, A., T. Corkett, and B.W. Drinkwater, *Ultraino: An Open Phased-Array System for Narrowband Airborne Ultrasound Transmission*. IEEE Transactions on Ultrasonics, Ferroelectrics, and Frequency Control, 2018. **65**(1).
5. Onishi, R., et al., *Visualization of airborne ultrasound field using thermal images*. arXiv preprint arXiv:2203.07862, 2022.



## **Investigating Pellet Durability in Storage and Pneumatic Conveying Systems**

Pablo Garcia-Trinanes<sup>1,2</sup>, Steffen Beitz<sup>3</sup>, Hans Schneider<sup>3</sup>, Stefan Zigan<sup>1</sup>

<sup>1</sup> Westsächsische Hochschule Zwickau (WHZ), Fakultät Physikalische Technik/Informatik, Zwickau, Sachs, Germany. <sup>2</sup>University of Surrey, Guildford, Surrey, United Kingdom. <sup>3</sup>Zeppelin Systems, GmbH, Friedrichshafen, Germany

### **Introduction**

The storage and transportation of pellets via pneumatic conveying systems are integral processes in various industries, including agriculture, food, pharmaceuticals, recycling, and energy. Furthermore, feeding problems often impede smooth operation [1]. Pellets are favoured for their high density and ease of handling, making them a versatile material for a range of applications. However, the durability of pellets during these processes is a critical concern due to potential abrasion, chipping, or attrition, which can lead to reduced product quality, increased maintenance costs, and operational inefficiencies. This study emphasizes the need to explore the pelletisation of plastics, considering their different behaviours in terms of structure and density, to meet the increasing recycling quotas mandated by regulations such as 94/62/EG, and invites collaboration from the scientific community to address these challenges.

### **Background and rationale**

Understanding pellet durability is essential for optimising handling systems and ensuring product quality. The degradation of pellets during handling and transportation can result from various mechanical stresses. This study aims to comprehensively analyse these degradation characteristics, focusing on three key experimental methods: single particle impact tests, centrifugal tests, and single-bend pneumatic conveying tests. By examining these aspects, we can identify the mechanisms and extent of pellet degradation, providing valuable insights for industries relying on pelletised materials.

### **Methodology**

#### **1. Review of Single Particle Impact Testers**

These tests assess the resistance of pellets to high-velocity impacts. By subjecting pellets to controlled impacts, their ability to withstand mechanical stress without significant degradation can be evaluated [2]. The forces experienced during pneumatic conveying and handling are simulated, helping to understand the mechanisms and conditions so that the pellets maintain their integrity throughout their lifecycle in industrial applications.

#### **2. Review of centrifugal testers**

Centrifugal tests [3] simulate abrasive conditions by exposing pellets to high rotational speeds and impacts. This method helps in understanding how pellets degrade under continuous abrasive forces, mimicking the wear and tear they undergo in storage and conveying systems.

#### **3. Review of single-bend pneumatic conveying testers**

These tests evaluate pellet performance in real-world conveying scenarios. By analysing the degradation that occurs when pellets navigate bends in conveying pipelines, e.g. the impact of pipeline design on pellet durability can be assessed [4].

Key parameters for analysis include monitoring changes in particle size distribution and degradation, examining surface morphology to identify damage types and extent, and measuring mass loss to quantify material loss and correlate it with pellet durability.

The findings of this study hold significant industrial importance as by understanding pellet degradation mechanisms and optimising pneumatic conveying systems, industries and practitioners can achieve enhanced process efficiency through smoother operations and reduced downtime. Additionally, minimising wear and tear on pellets and conveying equipment lowers maintenance frequency and costs [5]. Ensuring pellet integrity throughout handling and transportation processes maintains product quality, meeting regulatory standards and customer expectations. The test results applied to different industrial use cases can help optimise processes, reduce maintenance costs, and ensure product quality by understanding and mitigating pellet degradation mechanisms.

### Future research directions

The methodologies and results presented in this study serve as a foundation for future research in bulk solids handling and transportation. Further studies could explore the impact of environmental factors like humidity and temperature on pellet durability, the development of sophisticated materials and coatings to enhance pellet resistance, and the integration of real-time monitoring systems in conveying processes to dynamically detect and mitigate pellet degradation.

### Conclusions

This presentation emphasises the critical importance of investigating pellet durability in storage and pneumatic conveying systems. By exploring current experimental methods and conducting a thorough analysis, this study aims to provide valuable insights for optimising industrial processes, ensuring product quality, and guiding future developments in this essential research domain.

### References

- [1] J. Dai, J. R. Grace, Biomass granular screw feeding: An experimental investigation, Biomass and Bioenergy, Volume 35, 2, 2011, 942-955, <https://doi.org/10.1016/j.biombioe.2010.11.026>.
- [2] J. Jägers, P. Spatz, S. Wirtz, V. Scherer, (2021) Analysis of wood pellet degradation characteristics based on single particle impact tests, Powder Technology, 378, Part A, 704-715, <https://doi.org/10.1016/j.powtec.2020.10.017>.
- [3] Benjamin A. Kotzur, Robert J. Berry, Stefan Zigan, Pablo García-Triñanes, Michael S.A. Bradley, Particle attrition mechanisms, their characterisation, and application to horizontal lean phase pneumatic conveying systems: A review, Powder Technology, Volume 334, 2018, 76-105, <https://doi.org/10.1016/j.powtec.2018.04.047>.
- [4] J. Jägers, S. Wirtz, V. Scherer, M. Behr, Experimental analysis of wood pellet degradation during pneumatic conveying processes, Powder Technology, Volume 359, 2020, 282-291, <https://doi.org/10.1016/j.powtec.2019.10.004>.
- [5] Shalini Graham, Ibrahim Ogunfayo, Matthew R. Hall, Colin Snape, Will Quick, Susan Weatherstone, Carol Eastwick (2016) Changes in mechanical properties of wood pellets during artificial degradation in a laboratory environment, Fuel Processing Technology, 148, 395-402. <https://doi.org/10.1016/j.fuproc.2016.03.020>

# Compression behaviour of elastic-plastic microparticles in a centrifugal force field: Experiment and CFD-DEM simulation

A. Lier<sup>1</sup>, F. Krull<sup>1</sup> and S. Antonyuk<sup>1</sup>

<sup>1</sup> Institute of Particle Process Engineering, University of Kaiserslautern-Landau (RPTU), Germany

**Abstract**— Centrifuges are widely used to separate different phases by their density. During centrifugation, particles can be deformed or break due to acting forces resulting in a loss of product quality. In this study, the compression behaviour of elastic-plastic microparticles in a centrifuge was investigated by experiment and simulation. A suspension of spherical paraffin particles and ethanol was centrifuged in an analytical photocentrifuge (LUMiSizer, LUM GmbH) with variation in rotational velocity and temperature. The plastic deformation behaviour of the particles depending on their mechanical properties and acting centrifugal force was analysed. The change of the sediments height with increasing rotational velocity was measured inside the centrifuge. Additionally, the sediments were analysed using  $\mu$ CT imaging to obtain the porosity distribution inside the sediment. To understand the mechanics of the particle movement and sediment compression within a centrifuge, coupled computational fluid dynamics (CFD) - discrete element method (DEM) simulations were performed. A multiphase model was used to describe the liquid, gas and particle phases, with centrifugal, Eulerian and Coriolis forces implemented. The simulations and the experiments showed that a stronger plastic deformation of the particles is achieved with the increase in rotational speed and consequently centrifugal force.

**Keywords:** compression; centrifugation; elastic-plastic particles; multiphase CFD-DEM; elastic-plastic DEM model

## 1. Introduction

The sedimentation process in the centrifugal field is often employed to separate solid particles from a fluid. The particles sediment due to a difference in density and acting centrifugal force, forming a sediment layer over time. The acting forces can deform the particles plastically or break these. It is therefore important to know the mechanical properties and the sediment behaviour of the used material to avoid quality losses. The analytical photocentrifuge (LUMiSizer, LUM GmbH) enables the analysis of the sedimentation and compression behaviour of particles through space- and time-resolved extinction measurements (STEP-Technology) in a centrifugal field [1]. The centrifugal force can be set up to 2.300 times greater than that of the gravitational force. The rotational velocity and temperature can be adjusted to investigate the change in sedimentation and compression behaviour. To gain further insight into the particle movement during sedimentation within the centrifuge, the deformation and acting forces on particles, the coupled computational fluid dynamics (CFD) and discrete element method (DEM) can be used, where DEM describes the discrete phase and CFD the fluid phase. The developed elastic-plastic contact model [2] was used to describe the plastic deformation of the particles. The centrifugal field was implemented by adding the acting centrifugal, Coriolis and Euler forces into the CFD and DEM.

## 2. Materials and methods

Spherical paraffin particles in a size range of 100-250  $\mu$ m were produced by an emulsion formation method [3, 4] and subsequent sieving. The paraffin wax pastilles were melted while stirring in a water bath with emulsifiers and then subsequently emulsified with an ultrasonic sonotrode. The spherical droplets were then cooled with cold water, resulting in solidification. The particles were separated and dried (Fig. 1). The mechanical properties of the particles, such as yield pressure and Young's modulus, were measured with single particle compression tests using a Nanoindenter (TI Premier Hysitron, Bruker).

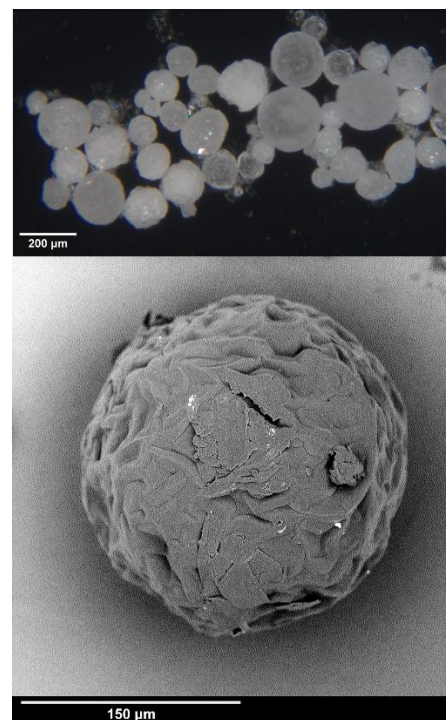


Figure 1. Images of the produced paraffin particles captured using an optical microscope and SEM.

The produced paraffin particles were dispersed in ethanol and subsequently subjected to centrifugation in the photocentrifuge while measuring the light transmission through the measuring cell over time and position. During centrifugation, the rotational velocity was increased with a speed ramp up to 4000 rpm and the temperature varied between 20°C and 40°C to investigate the plastic deformation of the particles depending on their mechanical properties and the acting centrifugal force. To analyse the plastic deformation and porosity distribution of the formed sediment,  $\mu$ CT imaging (TomoScope L, Werth Messtechnik GmbH) was used.

## 3. Results

Initially, during centrifugation the particles sediment rapidly due to the high rotational speed and large particles. Following the formation of the sediment layer, the rotational speed was

increased, resulting in the compression of the particle packing due to the increased centrifugal force. Fig. 2 shows the formed sediment in the measuring cell, its  $\mu$ CT image and coupled CFD-DEM simulation after centrifugation at 4000 rpm and 20°C.

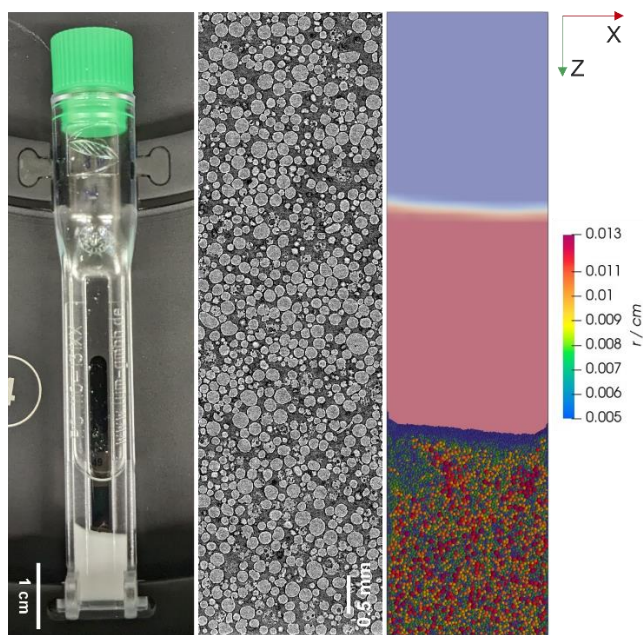


Figure 2. Measuring cell after centrifugation,  $\mu$ CT image of the sediment (voxel size: 2,45  $\mu$ m) and coupled CFD-DEM simulation after 4000 rpm at 20°C (blue phase: air, red phase: ethanol).

The experiments and the simulations showed that the sediment volume decreased at higher rotational speeds and therefore centrifugal force indicating that the centrifugal force exerted on the particles resulted in plastic deformation. The plastic deformation of the particles depends on the yield pressure, which was reached as a consequence of the increasing centrifugal pressure. As the centrifugal pressure increases with larger radial distances, more plastic deformation of the particles occurs at the sediment bottom. The low temperature-dependent mechanical properties of the paraffin particles resulted in a reduction in their yield pressure as the temperature was increased. The reduction in sediment volume at elevated temperatures is attributed to the enhanced plastic deformation. The porosity distribution in the sediment, which was analysed by  $\mu$ CT imaging after centrifugation, showed a reduction in porosity at a lower yield pressure of the particles. The porosity exhibited a greater decrease with increasing radial distance, as the cavities were reduced by the plastic deformation of the particles. Consequently, a radial pressure distribution occurs, whereby the particles at the sediment surface can exhibit reduced plastic deformations, while particles at the sediment bottom show strong plastic deformations. The influence of the Coriolis force is evident in both the experiments and the simulations (Fig. 2), as the sediment height at the surface is uneven due to the particles moving in a negative x direction. The polydisperse particle system, the surface topography and the wall friction have an influence on the compression process, which must be considered as these influences result in different packings and limit the particle movement and rearrangement during compression.

#### 4. Conclusion

The centrifugation of elastic-plastic particles showed a different compression behaviour of the sediment layer over the height due to the radial pressure distribution in a centrifugal field. As a result, particles located at the sediment bottom are

subjected to a greater degree of the stress than particles situated at the sediment surface. Upon reaching the yield pressure, the particles are deformed plastically and the sediment layer is compressed more strongly. Accordingly, the yield pressure of the particles was varied due to different temperatures in order to analyse the compression behaviour of the sediment. It was shown that stronger compaction occurs due to larger plastic deformations of the particles. Furthermore, a stronger compaction is also reached due to the increasing rotational speed and therefore centrifugal force. This different compression behaviour can have an influence on the subsequent process. By means of numerical simulations, the sediment compression and structure, the acting forces on the particles and the plastic deformation can be predicted in order to optimize the processes.

#### References

- [1] D. Lerche u. T. Sobisch: *Consolidation of concentrated dispersions of nano- and microparticles determined by analytical centrifugation*, Powder Technology 174, 2007.
- [2] R. Hesse, P. Löscher, S. Antonyuk, *CFD-DEM analysis of internal packing structure and pressure characteristics in compressible filter cakes using a novel elastic-plastic contact model*, Advanced Powder Technology 34, 2023.
- [3] Y. Pan, S. Sun, Q. Cheng, Y. Celikbag, B. K. Via, X. Wang u. R. Sun: *Technical Note: Melt Dispersion Technique for Preparing Paraffin Wax Microspheres for Cellulose Encapsulation*, Wood and Fiber Science 46, 2014.
- [4] K. G. K. Singh, S. Halder, S. Pati u. J. Wang: *Microencapsulation of Paraffin Wax Microspheres with Silver*, Defence Science Journal 68, 2018.



# Microdynamic Flowability to Characterize Die-filling Processes

David Blanco<sup>1</sup>, Anne Juppo<sup>1</sup>

<sup>1</sup> Division of Pharmaceutical Chemistry and Technology, University of Helsinki, Finland, david.blanco@helsinki.fi

**–Abstract–** Powder flow properties within the tablet press are yet to be understood and characterized. The challenge is to reproduce the processing conditions during the separation of the unit dose. Current knowledge on filling performance mostly originates from the analysis of bulk powder volumes and is, in practice, limited to iterative testing of the final product. Building quality into the development process can drastically reduce formulation and scalability times and costs.

Miniaturization of the pharmacopoeial measuring principle “powder flow through an orifice” integrated small-scale measurements (< 200 mg) in a machine vision-based testing setup. Relevance, sensitivity and practicality determined the quality of the novel method. Most extended filling geometries in formula development were evaluated and systematically compared to bulk flow measuring techniques. Understanding the impact of testing conditions and powder characteristics grounded the theoretical basis.

Flowability of powder volumes closer to the dosage unit –microdynamic flowability– strongly correlated with filling performance in R&D tablet presses. Cohesive forces and associated powder agglomeration largely governed the flow behaviour of small powder volumes and determined final product quality. Bulk flow analysis hindered measurements at such low stress environments: frictional contact forces dictated material behaviour and did not match in-process performance.

This presentation introduces the basic concepts behind the novel method and highlights recent applications in drug development. Process-relevant data can be generated from the lab to commercial production for enhanced understanding, monitoring and control of products and processes.

**Keywords:** Powder Flow; Small-scale; Filling processes; Early Assessment; Image-analysis.

## 1. Introduction

Many pharmaceuticals are produced in premeasured doses and effective filling is a prerequisite for successful processing. Despite significant advances in powder flow research over the last decades, flowability in these operations remains a frequently encountered challenge. Powder flow analysis has been focused on bulk powders, while an important aspect –powder flow in small volumes and confined spaces– has received less attention.

Powders do not behave the same when they are in bulk volumes as when they are separated from the mass. During filling processes, particle velocities are high, physical contacts are short lived, and small contact areas exist between particles, which are not sufficient to transmit solid pressure. Flowability under such small stresses cannot be treated as a contact powder bed [1, 2]. Frictional contacts are limited, and particle-level (cohesive) flow behaviour dominates over bulk behaviour [3].

Although effective filling of materials into cavities have been widely studied, there is no consensus on suitable test to characterize flow properties within the press. Few techniques can measure flowability at low stress environments, and even fewer do so under dynamic conditions [4]. The measuring principle or design of available testers hinders measurements at the very low stress range observed in tablet presses [5].

Early assessment of filling performance remains inaccessible during formulation development, and scale-up. Formulators and manufacturers heavily rely on extensive testing of the final product, with limited understanding of the process and considerable time and resources consumption. Particle-level understanding of flowability may be key in bringing increased flexibility and capacity to the manufacture of pharmaceuticals.

## 2. Materials and Methods

### 2.1. Compression Trials

R&D eccentric presses equipped with a gravity and a force feeder with multiple paddles were investigated (Type F3, Manesty Machines LTD, Liverpool; EK0, Korsch, Germany). Filling performance (Ph.Eur. 2.9.40 - Weight uniformity).

### 2.2. Powder Processing

Mechanical milling was applied to BCS class 2 drug candidate Palbociclib at small scale (250±0.1 mg; 15 min; 15 Hz; MM 200, Retsch, Haan, Germany). Pilot-scale fluidized-bed granulators (15 and 120 kg; Glatt WSG CD 15 and Niro-aeromatic S-5).

### 2.3. Bulk Flow Properties

Pharmacopoeial methods included flow rate through an orifice and tapping studies (Ph. Eur. 2.9.36). Dynamic test and shear cell analysis were conducted in a FT4 powder rheometer (Freeman Technology, WOR, UK).

### 2.4. Microdynamic Flow Properties

Miniaturized powder flow through an orifice involves small-scale flow testing in a horizontally positioned funnel-based geometry. The testing setup consists of a sample cuvette illuminated from below and monitored from above (Fig. 1). A precisely controlled stress (linear motion) is applied to discharge the powder sample, replacing gravity in conventional hopper discharge techniques. No additional stresses are introduced in the measurement. The powder sample (0.20 cm<sup>3</sup>) is placed in the left chamber (a) and the cuvette is subjected to a specific acceleration profile as it moves to the right. Deceleration-induced dynamics discharge the sample through the funnel into the opposite imaging chamber (c), where a pivot (b) disturbs the powder flow stream. The resistance of the powder to this displacement yields unique digital flow patterns, depending on the material properties. A three-step sample conditioning process eliminates powder's processing history and ensures a reproducible, loosely packed powder bed for analysis.

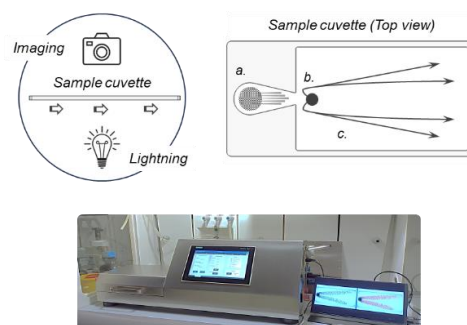


Figure 1. Scheme and picture of the measuring system and testing setup, including a detailed diagram of the sample cuvette and powder flow inside.  
a. Left chamber (funnel-based geometry). b. Pivot. c. Imaging area.

### 3. Results

#### 3.1. Consolidation stress and flow properties

Minitablets ( $\varnothing = 5\text{mm}$ ) and gravity feeding constituted a very basic filling geometry operating in the very low stress range and with high flow requirements. MCC direct compression grades, L200M and starch are shown as model compounds with clear differences on particle size.

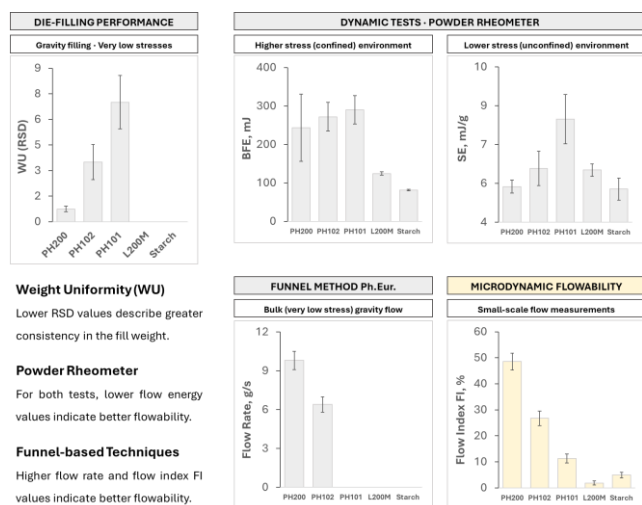


Figure 2. Effect of consolidation stress on dynamic flow props (n=3).  $Dv_{50}$  ( $\mu\text{m}$ ): PH200 (190), PH102 (102), PH101 (63), L200M (40), Starch (21).

Powder flow properties depended on the applied (or consolidation) stress. At the very low stress range observed in the press, frictional contacts were limited, and flow behaviour was governed by size-dependent cohesive forces. The miniaturized measuring principle closely reproduced such processing conditions. The lower stress limit depended on the specific tester and so the influence of frictional contact forces. In descending order:  $BFE > SE > \text{Funnel-based tests}$ . Cohesive materials in the press, such as lactose L200M, were overestimated at higher stresses.

#### 3.2. On the mechanisms of flow enhancement

Subtle changes on powder characteristics were evaluated from small increments on CSD (0.025% w/w). Standard tablets ( $\varnothing = 9\text{ mm}$ ) and a force feeder with multiple paddles constituted the selected filling geometry.

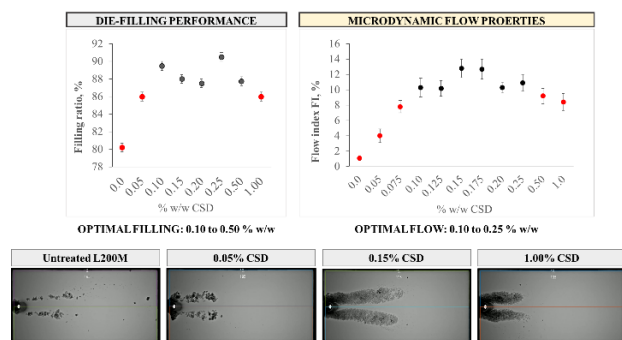


Figure 3. Lactose 200M modified with increasing amount of CSD (n=3). Right: Microdynamic flow data. Left: Die-filling performance.

Microdynamic flow studies captured important but often subtle differences in powder flow, and precisely determined the amount of glidant needed for optimal filling performance (Fig. 3). Digital imaging proved highly versatile for visualizing and interpreting results. State-of-the-art detection of powder agglomeration captured the effects of cohesion governing filling processes. This evidenced the mechanisms of flow enhancement that cannot be elucidated from numerical data.

#### 3.3. Tech transfer and process validation

Successful scale-up relies on adjusting the processing parameters for each unit operation to achieve the same quality as that observed in the R&D phase. Tech transfer between pilot-scale fluidized bed granulators was evaluated. Similar PSD data was found between batches, although Sample B presented a higher number of fines. Significant differences between flow testing methods highlighted the impact of consolidation stress on flowability.

At the very low stress range, cohesive forces dictated material performance. In Ph. Eur. funnel test, Sample A was good flowing (Flow rate,  $\text{g/s} = 9.8$ ) while Sample B did not flow. Similar results were found in microdynamic flow studies, largely overcoming the limitation for more cohesive powders (Fig. 4). Increased dynamics for cohesive Sample B highlighted agglomeration and spreadability of the powder specimen.



Figure 4. Microdynamic flow patterns. Left: Sample A. Centre: Sample B. Right: Sample B at higher speed. Same magnification for both samples. MCC (PH101, 102 and 200) as flowability reference.

In powder rheometer (Table I), at higher stresses (BFE data), no differences were detected between samples. At lower stresses, both samples were classified as good flowing powders [ $SE < 5$ ]. Bulk friction governed the flow energy values, and the fraction of fines acted as a lubricating agent.

TABLE I. DYNAMIC TEST · POWDER RHEOMETER

	<i>BFE, mJ</i>	<i>SE, mJ/g</i>	<i>SI</i>	<i>FRI</i>
Sample A · 15Kg	79.78±2.17	2.82±0.08	0.94±0.05	0.91±0.02
Sample B · 150Kg	81.92±3.36	3.28±0.08	0.95±0.05	1.42±0.04

### 4. Conclusion

Our findings demonstrate that the novel method characterizes dynamic flow properties at very low stresses, as observed in R&D tablet presses. This has far-reaching consequences for the manufacture of oral solid dosage forms (OSDs), now restricted to indirect sample-consuming flow tests and lengthy compression trials. Using less than 200 mg per measurement, microdynamic flow studies can be a cost-effective sustainable solution to identify potential manufacturing bottlenecks earlier in product development.

Beyond fast and reproducible measurements, machine vision offers new insights into powder flow analysis. Increased sensitivity (and visualization) to cohesive forces facilitated achieving a robust target flowability during formulation development and was decisive for process validation strategies. Early assessment of filling performance can support consistent product quality, minimize waste and reduce time-to-market.

### References

- [1] Prescott & Barnum. *On powder flowability*. Pharm Technol, 2000.
- [2] D. Schulze, 2008. *Powders and bulk solids: Behaviour, Characterization, Storage and Flow*. 2008.
- [3] S. Sogaard et al. *An experimental evaluation of powder flow predictions in small-scale process equipment based on Jenike's hopper design methodology*. Powder Technology, 2017.
- [4] M. Ghadiri et al. *Cohesive powder flow: Trends and challenges in characterisation and analysis*. KONA Journal, 2020.
- [5] A. Stavrou et al. *Investigation of powder flowability at low stresses: Influence of particle size and size distribution*. Powder Technology, 2020.

# DEM simulation comparative study of train wheel abrasive wear

Diviš, J.<sup>1</sup>; Hlosta, J.<sup>1</sup>; Rozbroj, J.<sup>1</sup>; Žurovec, D.<sup>1</sup>; Pokorná, K.<sup>1</sup>; Nečas, J.<sup>1</sup>; Zegzulka, J.<sup>1</sup>

<sup>1</sup> VSB – Technical University of Ostrava, Czech Republic

**Abstract.** High-speed railways are gaining popularity globally, introducing challenges like constructing railways through deserts. Railway wheel samples, 55MnSi44 and Class C materials, were tested for abrasion wear, and Discrete Element Method (DEM) simulations of railway wheels on tracks were conducted. Input parameters for these simulations were determined through calibration simulations of dynamic particulate material behaviour and wear rate for coupled geometry material and particulate material.

Simulated silica sand was modelled using spherical and polyhedral particles to compare input values. The calibration simulation of the simulated silica sand material combined static and dynamic calibration procedures for particulate materials. The wear rate calibration simulation for coupled geometry material and simulated silica sand was performed using the rubber wheel/sand test according to ASTM G65-00.

Four simulations were conducted for two different wheel materials, 55MnSi44 and Class C, and two simulated silica sand materials, with spherical and polyhedral particles. The simulations showed significant agreement with experimental data and measured wear rates. The nominal loading of the railway wheel was 12.5 tons, the rotational speed was 200 rpm, and the slip relative to the rail was 1%. Each simulation lasted 0.85 seconds, with wear exceeding 10,000 mm<sup>3</sup> for all four simulations.

These simulations confirm increased wear in regions with higher sand particle abundance, such as the Middle East and North Africa. The validated results of simulated abrasive wear can be used to investigate and predict the degree of abrasive wear under given operating conditions, adjust input parameters, or choose different construction materials.

**Keywords:** Railways; abrasion wear; DEM simulations; calibration; sand

## 1. Introduction

High-speed railways are gaining popularity globally, introducing challenges such as constructing railways through deserts. Engineering interest in windblown sand is driven by the harmful interactions between sand and various human infrastructures in arid environments. Notably, ongoing grand railway projects in the deserts of the Far East, Middle East, and North Africa require robust technical solutions to ensure efficient railway performance (1).

Today's manufacturers and operators of railway wheels aim to assess the properties and variables that can easily influence wheel wear. One of these factors is the wheel's properties, and wear tests have been developed to predict its lifespan. Wear tests are used to understand the formation and consequences of damage to materials that come into contact with each other. (2).

Extending the lifespan and efficiency of machine components is essential for reducing downtime related to repairs and maintenance, failures and accidents, material usage, and human resources (3). By selecting appropriate experimental equipment for testing resistance to abrasive wear, it is possible to achieve results that can predict the behaviour and long-term wear that will occur in operation. (4).

Today, the Discrete Element Method (DEM) is increasingly used as a tool for predicting the behaviour of particulate materials, optimizing processing equipment, and assessing the impact of particulate materials on their surroundings (5).

The development of numerical simulations and increasing computational power enables the study of abrasive wear. Today, the use of the Discrete Element Method (DEM) is often combined with the Finite Element Method (FEM). This simulation model merges the advantages of DEM, which excels in predicting the behaviour, movements, and contacts of particles, with FEM, which can modify the geometry of the observed functional surface during the simulation based on interactions with individual particles. (6).

There is a gap in research regarding the prediction of abrasive wear on railway wheels when impacted by sand. We filled this gap by our findings. We made comprehensive study using DEM-FEM simulations and the validated results can be used to investigate and predict the degree of abrasive wear under specific operating conditions, adjust input parameters, or choose different construction materials.

## 2. Materials and methods

For the study of abrasive wear, particulate material silica sand KPB supplied by Bonatrans Group a.s. (Bohumín, Czech Republic) was chosen. Railway wheel samples, 55MnSi44 and Class C materials, were tested for abrasion wear.

### 2.1. Particulate material DEM calibration

A suitable calibration method was developed to optimize the behaviour of virtual particulate material in the DEM simulation environment. The software Rocky DEM was used for calibration and subsequent simulations.

A method was chosen that combines several well-known calibration methods. This approach is rarely used because it is extremely time-consuming to align all parameters given the numerous combinations of input parameters. This method combines filling material into a container (volume filling calibration), emptying the container (validation of the calibration simulation using emptying time), material flow over an obstacle (calibration of the material's dynamic behaviour), static repose angle after emptying the container (calibration of the discharged repose angle), and static repose angle after piling up against an obstacle (calibration of the piled repose angle). In total, 10 parameters were monitored in the calibration simulations, which had to be calibrated to match (or at least closely approximate) the experimental measurements.

Simulated silica sand was modelled using spherical and polyhedral particles to compare input values.

### 2.2. Abrasive wear DEM-FEM calibration

A standardized laboratory apparatus, the ASTM G65-00 Dry Sand/Rubber Wheel Apparatus, was chosen for measuring the wear resistance on test samples. Two set of tests procedure E (ASTM G65-00) were performed for both railway wheel materials 55MnSi44 and Class C.

DEM-FEM calibration was conducted for both types of calibrated virtual silica sand materials: first with spherical particles and then with polyhedral particles. A 5-second

calibration simulation was conducted for the corresponding pair of railway wheel specimen material and silica sand.

### 2.3. Railway wheel abrasive wear DEM-FEM simulation

Four simulations were conducted for two different wheel materials, 55MnSi44 and Class C, and two simulated silica sand materials, with spherical and polyhedral particles. The nominal loading of the railway wheel was 12.5 tons, the rotational speed was 200 rpm, and the slip relative to the rail was 1%. Each simulation lasted 0.85 seconds.

## 3. Results

### 3.1. Calibrated DEM input parameters

KPB silica sand was calibrated using spherical and polyhedral particles. The input parameters are shown in TABLE I. calibrated Input parameters for virtual silica sand

DEM INPUT PARAMETERS	VIRTUAL SILICA SAND	
	spherical particles	polyhedral particles
coefficient of restitution	0.30	0.70
static friction	0.75	0.35
dynamic friction	0.85	0.30
rolling resistance	0.25	0.05
Young's modulus	0.0006 GPa	0.0006 GPa
Poisson's constant	0.30	
particle size distribution	350 – 750 µm	

### 3.2. Calibrated DEM-FEM abrasive wear

The DEM abrasion coefficient C was calibrated for each pair of railway wheel specimen material and silica sand. The resulting values of these coefficients C are listed in TABLE I.

TABLE I. THE DEM ABRASION COEFFICIENTS C

RAILWAY WHEEL SPECIMEN MATERIAL	VIRTUAL SILICA SAND	
	spherical particles	polyhedral particles
55MnSi44	3,50E-09	4,00E-10
Class C	2,30E-09	2,60E-10

### 3.3. Railway wheel DEM-FEM abrasive wear

Four simulations of a railway wheel running on a track were conducted. The simulated wheel had a triangular mesh element size of 0.6 mm. The resulting values of volume loss are listed in TABLE II. The results indicated noticeable wear. Abrasive wear simulations were conducted over a much shorter time period than would occur in industrial applications. The rate of abrasive wear is higher in the simulation, necessitating a conversion ratio between the experimental and simulated wear rates. The resulting wear values were consistent with each other, validating the calibration method for the behaviour of abrasive particulate material and the abrasive wear of particulate material.

The high wear values can be explained by the high contact force (load acting on the railway wheel) and the high dynamics of the railway wheel (rotation speed and slip). The higher simulated abrasive wear is also due to the infinite hardness of the virtual silica sand KPB particles in the DEM simulation environment. Overall, these simulations confirm increased wear in regions with higher sand particle abundance.

TABLE II. VOLUME LOSS OF RAILWAY WHEEL BY ABRASIVE WEAR IN THE SIMULATION

RAILWAY WHEEL SPECIMEN MATERIAL	VIRTUAL SILICA SAND	VOLUME LOSS [mm <sup>3</sup> ]
55MnSi44	spherical particles	10,144.5
55MnSi44	polyhedral particles	10,492.0
Class C	spherical particles	10,473.0
Class C	polyhedral particles	10,492.0

## 4. Conclusion

Future research on abrasive wear by particulate materials will focus on non-spherical particles, different contact models for these particles, and accurately determining input simulation parameters.

Advancements in discrete element simulation will include developing contact models for coupling different simulation methods. Currently, coupled DEM-MBD, CFD-DEM, or DEM-FEM simulations are common. The future potential lies in combining multiple simulation methods. The discrete element method will rapidly evolve, tackling complex problems by using multiple numerical models like DEM, MBD, CFD, and FEM. New mathematical contact models will be developed alongside new calibration and validation methods.

The comprehensive procedure for calibrating the behaviour and abrasive impact of simulated particulate materials has wide applicability. This study shows calibration procedure which is suitable for all abrasive processes involving particulate materials.

## Acknowledgement

This paper was created as part of the project No. CZ.02.01.01/00/22\_008/0004631 Materials and technologies for sustainable development within the Jan Amos Komenský Operational Program financed by the European Union and from the state budget of the Czech Republic.

The European Just Transition Fund supported this work within the Operational Programme Just Transition under the aegis of the Ministry of the Environment of the Czech Republic, project CirkArena, number CZ.10.03.01/00/22\_003/0000045.

## References

- [1] Bruno, L.; Horvat, M.; Raffaele, L. Windblown sand along railway infrastructures: A review of challenges and mitigation measures. *Journal of Wind Engineering and Industrial Aerodynamics*. Volume 177, June 2018, Pages 340-365. 10.1016/j.jweia.2018.04.021
- [2] Meneghetti G., Terrin A., Giacometti S. A twin disc test rig for contact fatigue characterization of gear materials. *21st European Conference on Fracture, ECF21*. 2016. 3185-3193. 10.1016/j.prostr.2016.06.397.
- [3] Holmberg K, Kivikytö-Reponen P, Härkisaari P, Valtonen K, Erdemir A. Global energy consumption due to friction and wear in the mining industry. *Tribol Int*. 115:116, 2017. doi.org/10.1016/j.triboint.2017.05.010.
- [4] Wahl, M. Verschleiss metallischer Gleitflächen-paarungen unter Mitwirkung fest-körniger Zwischenstoffe. *Aufbereitungstechnik*, 10, 1969.
- [5] Divis, J., Hlosta, J., Zurovec, D. et al. 3D printed laboratory equipment to measure bulk materials in extreme conditions. *Sci Rep* 12, 17331 (2022). DOI: 10.1038/s41598-022-22114-2
- [6] Katinas E., Chotěborský R., Linda M., Kuře J. Sensitivity analysis of the influence of particle dynamic friction, rolling resistance and volume/shear work ratio on wear loss and friction force using DEM model of dry sand rubber wheel test, *Tribology International*, DOI: 10.1016/j.triboint.2021.106853



# Experimental investigation of the fracture characteristics of bicomponent agglomerates using in-situ X-ray tomography

Y. Sinnwell<sup>1</sup>, K. Nikolaus<sup>1</sup>, and S. Antonyuk<sup>1</sup>

<sup>1</sup> University of Kaiserslautern-Landau, Institute of Particle Process Engineering, Kaiserslautern, Germany

**Abstract**— Agglomerates represent a significant element of the product portfolio across a wide variety of industrial sectors. During the production and transport agglomerates are exposed to a variety of stresses that can lead to premature breakage and unwanted loss of material quality. It is therefore of paramount importance for producers to be able to predict the mechanical strength of agglomerates with a high degree of accuracy. Due to the complex composition of agglomerates, it is not possible to make an exact prediction, given the limitations of the models that are currently available. The application of tomography-based in-situ stress tests for the investigation of breakage behavior of agglomerates provides access to high-resolution experimental data, which can promote the further development of models for the Discrete Element Method. This contribution presents the development and application of an experimental procedure that enables the systematic investigation of the fracture characteristics of agglomerates, with a particular focus on multicomponent agglomerates.

**Keywords:** Multicomponent agglomerates; strength analysis; X-ray in-situ compression test;

## 1. Introduction

In the chemical and pharmaceutical industries, the agglomeration of particles with a binder is an important production step in the manufacture of tablets or pellets. During handling and transportation, the agglomerates are exposed to high mechanical stresses, which can lead to their breakage. Knowledge of the breakage mechanisms is therefore important for optimizing the manufacturing and transport processes. The agglomerates are often produced from mixtures of several components. These compositions of these mixtures are becoming increasingly complex and the components used often differ significantly in terms of mechanical properties, particle size, porosity and wetting behaviour. The resulting mechanical strength of the agglomerates is yet not fully understood, particularly in relation to the structure formation process. The existing models that take into account the micro structure and adhesion mechanisms between primary particles are limited to some simplified cases [1-2].

## 2. Methods

### 2.1. Sample Preparation

The experimentally studied cylindrical agglomerates with a diameter of 15 mm and a height of 15 mm (Fig. 1), are produced from nearly monomodal spherical primary particles (2 mm in diameter) of two different materials. In order to represent different material properties, a ductile component, (in this case, polypropylene (PP)) and a brittle component (soda-lime glass, (GL)), are mixed with an aqueous hydroxypropyl methylcellulose (HPMC) solution, which serves as the binder. This mixture is then compacted in an aluminium die and dried. In order to cover a spectrum of different agglomerate compositions, the mass ratio (GL/PP) of the primary particles

are varied as follows: 100/0; 75/25; 50/50; 25/75; 0/100. To facilitate the segmentation of the agglomerate components in the computer tomography (CT) images, an aqueous KI-I<sub>2</sub> solution is added to HPMC binder solution. Due to the high atomic mass number of iodine, a clearly visible contrast enhancement in the CT-images is achieved. This facilitates the subsequent image analysis.

### 2.2. In-situ loading tests

To clarify the mechanism of crack propagation and fracture in agglomerates as a function of their composition single compression tests are carried out in an X-ray tomograph (Tomoscope L, Werth Messtechnik GmbH, min. voxel size of 500 nm) using an in-situ pressure measuring cell (Deben, CT500RT, Fig.1 a)). The pressure load is applied stepwise manner. Upon reaching the respective force level, the measuring cell is halted and the CT measurement is started after a short relaxation time. This stop-motion-measuring principle is applied until a macroscopic fracture occurs in the agglomerate, which is characterized by the previous occurrence of a maximum force (Fig.1 b)).

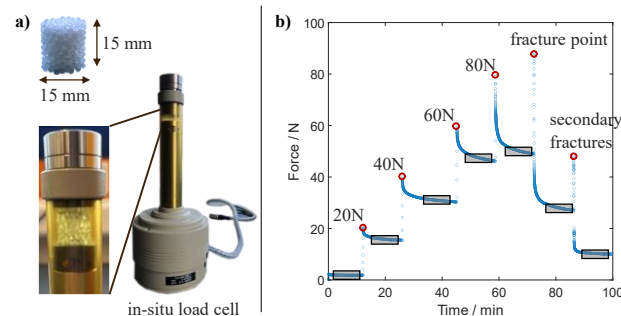


Figure 1. a) Representation of a cylindrical agglomerate and the in-situ loading cell. b) Exemplary representation of the force-time curve for the in-situ measurement principle with gradual pressure loading. The grey frames represent the time period of the CT measurement.

## 3. Image Analysis

To analyse the fracture characteristics, the radiographic images taken at the respective force levels are evaluated. The aim is to segment the individual components of the agglomerate (primary particles PP and GL as well as HPMC binder material) and reconstruct these components as a 3D model. By overlaying the 3D reconstructions (STL or point cloud) of the various loading steps a quantification of the fracture progression and crack initiation zones is possible.

### 3.1. Image processing

The CT measurements generate an image stack with around 1500 grayscale images at each force level. The grey values represent the different components of the agglomerate. In order to analyse the fracture behaviour, the individual components must be segmented. To prepare the grey value images for the segmentation, a noise filter, in this case a Gaussian Blur, is applied using the Fiji software [3]. The blurring allows for the

reduction of noise and radiation artefacts which are naturally present in radiographic images. Reducing the noise and artefacts facilitates the subsequent segmentation via thresholding (cf. Fig.2).

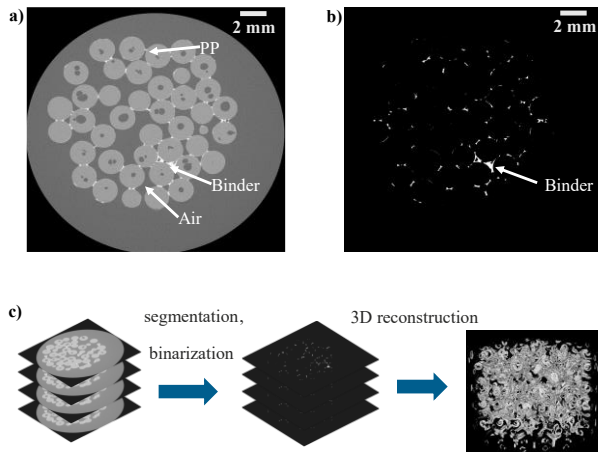


Figure 2. Representation of a grey value sectional image with a) the respective components PP, binder and air spaces and b) the segmented binder. c) illustrates the procedure for image processing of the grey value image stacks into component-specific 3D reconstructions.

Based on the chosen threshold grey value a segmentation for the respective components is possible. The binarized image stacks created in this way serve as a starting point for creating 3D reconstructions of the respective components. The 3D models of the segmented components can be transformed to the STL file format or in a point cloud format for further data analysis.

### 3.2. Analysis of the displacement fields

Typically, the agglomerates examined here show a fracture course that runs over the contact points of the primary particles cross-linked with binder. Fracture processes through the primary particles themselves cannot be observed. The analysis of crack initiation and crack propagation is therefore based on reconstructions of the binder matrix. In this study, the analysis of the binder matrix is based on STL reconstructions. The calculation of the displacement field of the binder matrix of two loading states is based on the comparison of the position of the center of gravity of the corresponding STL vertexes. In addition to the shift of the center of gravity in space, the change in the orientation of the corresponding vertexes can also be calculated. The analysis of the resulting displacement field between two loading states allows the identification of crack initiation points in dependance of the exact position in the agglomerate. This makes it possible to quantify the influence of the agglomerate composition on the fracture characteristics by analyzing the respective primary particle position (PP or GL) and comparing their position with crack initiation points and crack propagation paths. Figure 3 shows an exemplary representation of the analysis of the displacement field of the binder matrix between two loading states of an agglomerate. To simplify the representation, the binder matrix is shown in a) as a point cloud of the centroids of the vertexes. For evaluation, the volume object is divided into four regions of interest (ROI), which are marked in different colors. In b) the point clouds of the respective ROI are projected onto the length/width plane and the coloring of the points indicates the size of the shift in the height direction. For a better overview, only displacements that are bigger than 0.5 mm or smaller than -0.5 mm are shown. It is clear that there is no homogeneous shift of the individual points, but rather a strongly position-dependent distribution of the magnitude of the shift. The results in Figure 3 show that the experimental procedure described here enables a high-

resolution analysis of the fracture characteristics of agglomerates. This provides an excellent basis for correlating the agglomerate composition with the fracture characteristics.

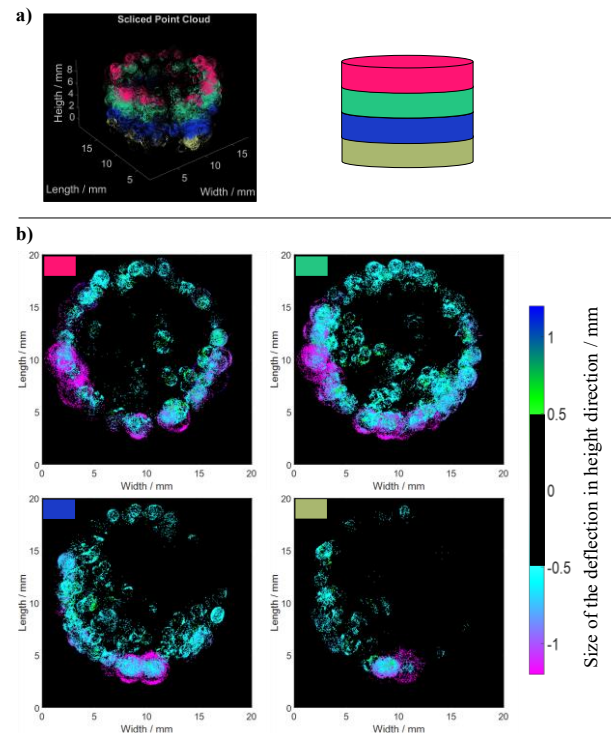


Figure 3. Representation of an exemplary point cloud divided into ROI (a)). b) shows the projection of the points of the ROI onto the latitude/longitude plane. The colour scale of the points shows the magnitude of the displacement of the points in the height direction.

## 4. Conclusion

Tomography-based analysis of the fracture characteristics of agglomerates using in-situ compression tests represents a promising experimental approach to improve the understanding of the fracture characteristics of agglomerates. The experimental procedure presented here enables the systematic analysis of fracture processes in multicomponent agglomerates. In the future, the here presented image analysis of the CT data will be enhanced by applying the discrete image correlation theory. It is a promising approach for the analysis of the fracture and deformation process of the individual agglomerate components as a discrete phase (single particle resolution). This enables the direct validation of DEM models based on high-resolution experimental data.

## References

- [1] Antonyuk, S.; Palis, S.; Heinrich, S., „Breakage behavior of agglomerates and crystals by static loading and impact“, *Powder Technol.* 206/1-2 (2011), 88-98.D. Schulze, *Powders and bulk solids: behavior, characterization, storage and flow.* 2008.
- [2] Antonyuk, S., Khanal, M., Tomas, J., Heinrich, S. and L. Mörl: Impact breakage of spherical granules: experimental study and DEM simulation, *Chemical Engineering and Processing* 45 (2006), 838-856.A. W. Bishop and D. J. Henkel, *The Measurement of Soil Properties in the Triaxial Test.* E. Arnold, 1957.
- [3] J. Schindelin, I. Arganda-Carreras, E. Frise, V. Kaynig, M. Longair, T. Pietzsch, S. Preibisch, C. Rueden, S. Saalfeld, B. Schmid, J.-Y. Tinevez, D.J. White, V. Hartenstein, K. Eliceiri, P. Tomancak, A. Cardona, Fiji: an open-source platform for biological-image analysis, *Nat. Methods* 9 (2012) 676–682. <https://doi.org/10.1038/nmeth.2019>.

# Modelling of metallurgical coke breakage to examine the influence of pore structure using X-ray computed tomography and discrete element method (DEM)

Masahiko Watanabe<sup>1,2</sup>, Zeynep Karatza<sup>3</sup>, Jin Y. Ooi<sup>1</sup>

<sup>1</sup> University of Edinburgh, Scotland, UK

<sup>2</sup> Nippon Steel Corporation, Tokyo, Japan

<sup>3</sup> National Technical University of Athens, Athens, Greece

**Abstract**— The large amount of CO<sub>2</sub> emissions is the biggest issue in the iron and steel industry. Therefore, it is necessary to decrease the amount of metallurgical coke usage, which is the primary source of CO<sub>2</sub>. However, this is difficult to achieve due to the coke's important functions in a blast furnace. A key attribute of metallurgical coke that controls the amount of coke usage in a furnace is coke strength. As coke is a very porous material, the pore structure could significantly influence its strength. This study investigates the coke's pore structure using X-ray computed tomography (XCT). The Brazilian split test is used to examine the mechanical properties of coke. Finally, a model capturing the characteristics of the coke pore structure obtained from the XCT is developed using the bonded Discrete Element Method (DEM). The model is shown to be able to successfully reproduce the experimental loading response. The results show that the stiffness and strength of the coke vary according to the pore structure of the fabric in the model, even though the porosity is the same. Finally, we found that the bond's density in the fabric of the model, which could reflect the connectivity of the matrix in coke, is the crucial factor in deciding its strength.

**Keywords:** metallurgical coke; bonded-DEM; XCT; breakage

## 1. Introduction

The iron and steel industry emits a significant amount of CO<sub>2</sub> with one of the largest sources of CO<sub>2</sub> coming from the use of coke in a furnace. It is therefore advantageous to reduce the amount of coke usage in a blast furnace to decrease CO<sub>2</sub> emissions. However, this presents a number of challenges, since coke plays several essential roles in ironmaking, including a porous permeable structure with sufficient strength to support the burdens in the blast furnace [1]. Researchers have tried to predict the response of coke in a blast furnace to develop strategies and reduce its use. Considering the microstructure is paramount since coke is a very porous material (porosity of approximately 50%), and it is well known that the porosity of a porous material will be the leading factor in its fracturing mechanism. In this paper, we built a model considering the influence of the pore structure using X-ray computed micro-tomography (XCT) and the Discrete Element Method (DEM) and then examined the governing factors in the coke strength.

## 2. Methodology

### 2.1. Materials

This work used raw hard coking coal to produce the coke sample. The entire raw coal was crashed so that 85% of the crushed samples were less than 3 mm in diameter. The crushed coal was charged into a pilot-scale oven [2], 420 mm wide, 600 mm long, and 400 mm high, with a bulk density of 0.85 t/m<sup>3</sup>. Then, the sample was carbonised into coke for 18.5 h by

applying heat from both sidewalls, replicating the conditions of a commercial coke oven operating at a flue temperature of 1250°C. After specimens were drilled out from the coke lump, cylindrical specimens with 20 mm and 10 mm in diameter and height were obtained. For 10 mm specimens, Brazilian split tests were carried out to evaluate the mechanical properties of the coke. On the other hand, XCT was performed on the 20 mm specimens.

### 2.2. X-ray Computed Tomography Imaging

To visualise the 3D nature of the pore structure of the cylindrical coke specimens. Using a scanner in Nippon Steel Technology Co., Ltd., scans were performed with a polychromatic cone beam at 59.0 keV acceleration. Each specimen was rotated 360° during the scans, acquiring radiographs at 1,200 equally spaced angular positions with an average of 2 images per angular position to enhance the signal-to-noise ratio. The voxel size is 12.8 μm, providing images of high resolution (more than 1,700 pixels per specimen diameter). The built-in software of the tomograph was used to reconstruct the 3D image.

Then, the pore structure was examined in detail using an image processing method. As the coke pores were highly interconnected, we developed a novel method to extract the salient feature of the structure, which discretises the pores at their necks. The details of the discretisation method are described elsewhere [3] and omitted here due to space limitations. The image processing was applied to the 3D image, and the size distribution of the pores was characterised. The information was reflected in a model mentioned in the next section.

### 2.3. Discrete Element Method

The breakage of individual particles was simulated using the bonded DEM. We used the Timoshenko beam model [4] to generate the coke particle model, as a cluster of bonded polydisperse spheres. Fabrics with various pore structures but with the same overall porosity, matching that measured from XCT, but also fabrics with multiple types of pore structure to match the bulk porosity were prepared as shown in Fig. 1. Firstly, the model was calibrated using the XCT fabric with the DEM model parameters as shown in Table I. Then, the remaining fabrics were simulated to study the effect of pore structure on the coke loading response. In this paper, the tensile splitting stress was calculated using the following equation,

$$\sigma_t = \frac{2P}{\pi LD} \quad (1)$$

where  $\sigma_t$  is the tensile strength,  $P$  is the applied load,  $L$  is the thickness of the specimen, and  $D$  is the diameter of the specimen, respectively.

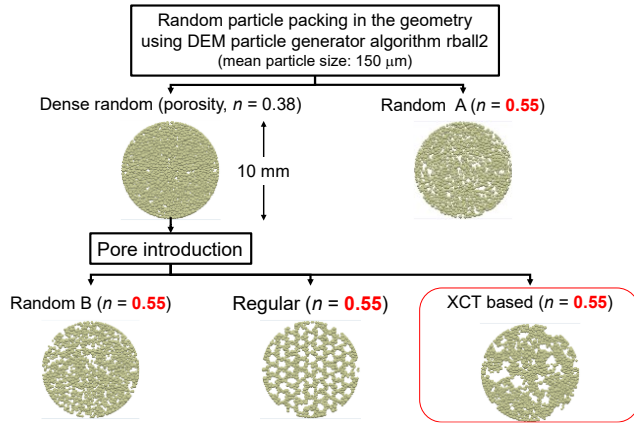


Figure 1. Fabric for the coke model in DEM

TABLE I. DEM MODEL PARAMETERS

Particle	Young's modulus	26 GPa
	Poisson ratio	0.21
Bond	Young's modulus	26 GPa
	Poisson ratio	0.21
	Bond radius multiplier	0.5
	Compressive strength	6 GPa (CoV 0)
Load	Tensile strength	1.2 GPa (CoV 0.8)
	Shear strength	1.2 GPa (CoV: 0.8)
Load	Loading speed	5 m/min (x10,000)

### 3. Results

#### 3.1. XCT observations

The coke specimens consist mainly of three materials: a) reactive, which is the main part of the solid; b) inertinite, which contains fewer pores in its texture and has more variable density/grey-scale value; and c) ash, which has the highest density. As shown in the Fig. 2, dark objects are voids/pores. The pore size widely varies from  $\mu\text{m}$  order to mm order. Also, the pores were highly interconnected in 3D, though the fact cannot be fully visualised in 2D images like in Fig. 2. As explained in the methodology section, the pore was discretised in 3D, and the pore size distribution was obtained.

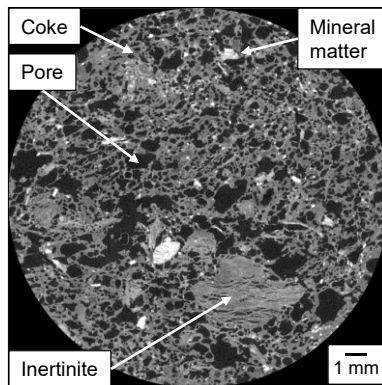


Figure 2. X-ray CT image of coke

#### 3.2. DEM modelling

The results of the Brazilian split test simulations are compared with the experiments in Fig. 3. The calibrated model (XCT based pore in Fig. 3) can successfully reproduce the experimental loading response, stiffness and ultimate strength. Specifically, the results show that all the fabrics can reproduce the brittle behaviour of the coke. The different pore structures, however, resulted in a change in strength and stiffness, though the overall porosity of those fabrics was the same. This change

indicates that the pore structure significantly influences the specimen's mechanical behaviour.

After various investigations, we defined a bond's density, which is the volume of bonds in the fabric divided by the volume of the fabric. Fig. 4 shows the relationship between the bond's density and the ultimate tensile strength, and a good correlation was confirmed between them even when the porosity of the fabrics was different. This correlation suggests that the bond's density would be the most critical factor to control the mechanical behaviour of the fabric. This index includes both information on particle density and the coordination number of particles in the fabric. We assume that the bond's density could reflect the connectivity of the matrix of the coke specimen.

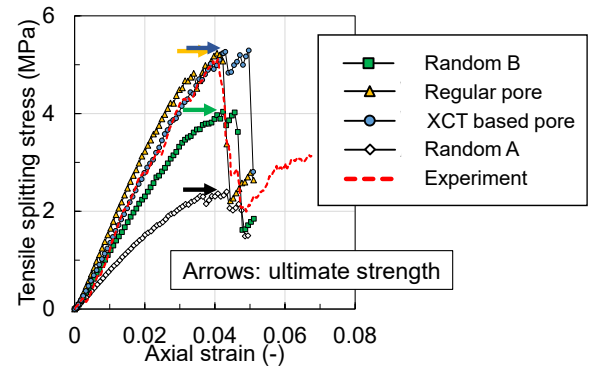


Figure 3. Mechanical behaviour in the model and the experiment

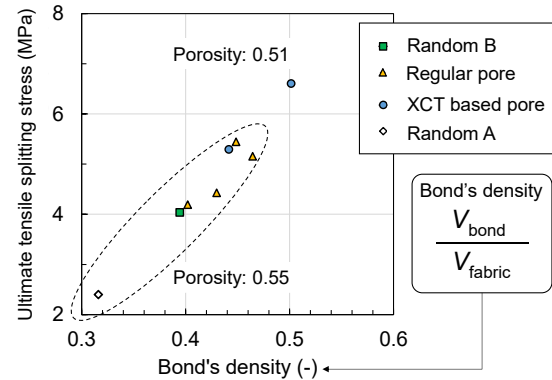


Figure 4. Relationship between bond's density and ultimate tensile splitting stress

### 4. Conclusion

The influence of the pore structure on coke breakage was investigated using the loading test and the bonded DEM modelling. The model reflects the salient feature of the coke specimen obtained using XCT and the image processing. We clarified that the pore structure significantly impacts coke strength, and the bond's density controls the strength of the fabric. The parameter could reflect the connectivity of the matrix in the coke specimen, and it would be essential to obtain the high strength coke, which leads to reduced  $\text{CO}_2$  emissions in the steelmaking industry.

### References

- [1] A. Babich and D. Senk, "Coal use in iron and steel metallurgy," in *The Coal Handbook: Towards Cleaner Production Volume 2: Coal utilisation*, Woodhead Publishing Limited, 2013.
- [2] S. Nomura, T. Arima, K. Kato, "Coal blending theory for dry coal charging process," *Fuel*, vol. 83, 13, pp. 1771-1776, 2004.
- [3] M. Watanabe, Z. Karatza, J. Y. Ooi, "Determination of porous microstructure of metallurgical coke using XCT," in *PARTEC 2023*, Nuremberg, GER, 2023.
- [4] N. J. Brown, J.F. Chen, J. Y. Ooi, "A bond model for DEM simulation of cementitious materials and deformable structures," *Granular Matter*, vol. 16, 3, pp. 299-311, 2014.



# CFD-DEM Simulation Validation of Metal Powder Conveying in Thin Pipes

Lorenzo Pedrolli<sup>1</sup>, Luigi Fraccarollo<sup>2</sup>, Beatriz Achiaga<sup>1</sup>, and Alejandro Lopez<sup>1</sup>

<sup>1</sup> University of Deusto, Bilbao, ES

<sup>2</sup> University of Trento, Trento, IT

**Abstract**— Directed Energy Deposition (DED) processes require consistent material flow to the melt pool, typically achieved through pneumatic conveying of metal powder via thin pipes. This study validates CFD-DEM (Computational Fluid Dynamics-Discrete Element Method) simulations of this process, with a focus on observed self-excited instabilities in particle flow. An experimental setup involving high-speed cameras and dedicated optics was developed to directly compare with simulation outcomes. This work discusses the experimental design, video analysis via Particle Tracking. Results confirm the predictive accuracy of simulations and offer insights into the dynamics of pneumatic conveying, with implications for improving DED processes.

**Keywords:** Pneumatic Conveying; CFD-DEM; Particle Tracking;

## 1. Introduction

In Directed Energy Deposition (DED), maintaining consistent pneumatic conveying of metal powder is essential for uniform material flow to the melt pool. Variations in powder feed can significantly impact deposition quality, as noted by Dadbakhsh et al. [1].

Previous research has typically focused on time-averaged powder flows [2], but variability in mass flow rates in pneumatic systems is well-documented [3, 4]. Factors influencing flow dynamics are extensively discussed in the literature [5, 6].

Self-induced flow variations can affect particle velocity and mass flow rate, impacting material deposition in DED. Zhou et al. [7] observed pulsating flows in larger pneumatic systems, while Zhao [8] demonstrated the significance of particle-fluid interactions in CFD-DEM simulations.

CFD-DEM simulations have shown that particle-particle interactions lead to clustering and flow rate fluctuations [9, 10].

This work presents the experimental setup used to capture the pneumatic conveying flow in the thin horizontal pipe, highlighting the flow fluctuation.

The primary goal of this study is to provide and analyse high-speed video data that captures the nuances of particle flow in horizontal pneumatic conveying systems. By making individual particles distinguishable and traceable, this work allows for a granular analysis of flow dynamics that is not possible with time-averaged data alone. This level of detail is essential for identifying and addressing issues such as particle clustering and flow irregularities in conveying systems.

## 2. Experimental methods

This work aims to record the particle trajectories in detail. This is achieved through the use of a Phantom 640L high-speed camera, coupled with a matching 2.5x-5x macro lens. The recordings at 10'000 fps have a pixel size between 4 and 2 micrometres. A shutter speed of less than 10 microseconds eliminates the streaks from the particles' movement.

Experiments were conducted with the three pipes at different gas flowrates, and using different materials, for a total of 60 combinations.

### 2.1. Experimental setup

The schematic of Fig. 1 shows the setup used to generate the pneumatic conveying flow to analyse. The central part of the circuit is the borosilicate glass pipe, through which the powder is conveyed, and which is filmed slightly after the central portion. The pipe is coupled with the rest of the circuit using custom-made couplers. These also present a pressure sensing port, which is interfaced on both sides to a differential pressure sensor. The conveying gas is a regulated flow of pure, dry nitrogen gas coming from a canister. The powder is put into the system by a custom-made rotary valve feeder. A cyclone separator is used to recover the powder.

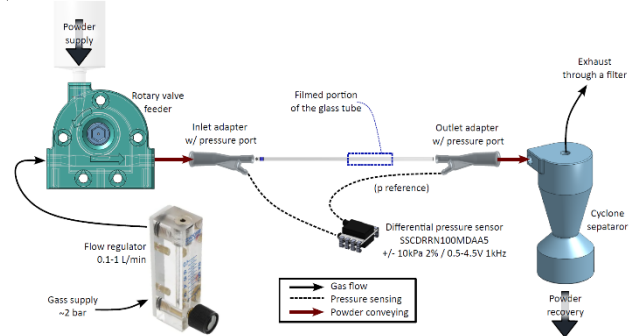


Figure 1. Schematic of the experimental circuit

The conveying system is held onto an adjustable platform, which can be oriented orthogonal to the camera. A 10W LED is powered using a linear regulator, ensuring flicker-free recordings, and illuminates the through the pipe directly across the camera. Using a diffuser, this results in a relatively uniform white background and clear images of individual particles, especially in dilute flow conditions.

### 2.2. Particle tracking

The video recordings show each particle sharply in black against a clear background. Fig. 2 shows an example of one frame. The full video is analysed as 8-bit image stack, in Fiji/ImageJ [11]. Particles are individually tracked using a custom version of the TrackMate plugin for ImageJ [12], available at: <https://github.com/trackmate-sc/TrackMate/pull/296>.

The recognized particles in each frame are identified as *spots*, two particles can be connected by an *edge*, which contains the information on particle velocity. Multiple consecutive edges form a *track*.

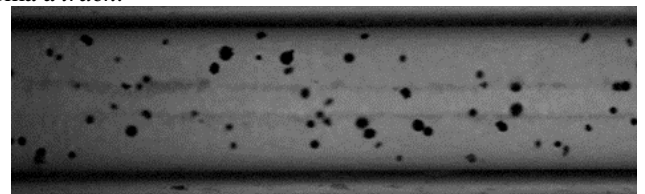


Figure 2. Example of one frame of the recordings

### 3. Results

The processed information can provide the Particle Size Distribution, for example the one reported in Fig. 3, which is compatible with the one declared by the supplier of the *MetcoAdd 316L-D* metal powder, who declares a  $D_{10}=45\mu\text{m}$ , and  $D_{90}=106\mu\text{m}$ .

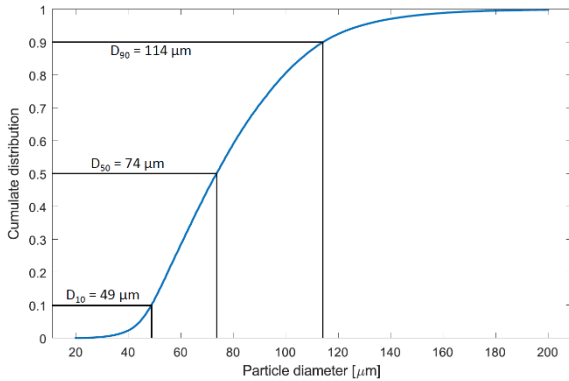


Figure 3. Example of the Particle Size Distribution (PSD), determined experimentally on 336'000 spots. The powder is *MetcoAdd 316L-D*.

Knowing the instantaneous particle concentration and average velocity at each frame, it is possible to determine the instantaneous mass flowrate, as shown by Fig. 4, which reports the results of the tracking for the conveying of the same metal powder in the circular pipe of diameter  $d=1.15\text{mm}$ , at a gas flowrate of  $0.8\text{ L/min}$ . In the presented case the flow is expected to be laminar, with a Reynolds Number calculated at  $Re=971$ .

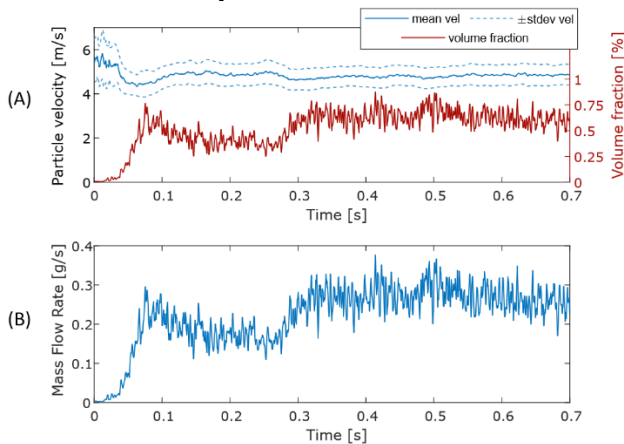


Figure 4. Particle average velocity and volume fraction (A) for the case of *MetcoAdd 316L-D* powder, in the circular pipe at  $0.8\text{ L/min}$  of conveying gas. The resulting mass flowrate over time is reported in (B).

#### 3.1. Comparison with simulation

The deviation from the average mass flow rate is expressed in terms of the Root Mean Square (RMS), a statistical measure of the variability of a set of values, in this case the mass flowrate, from the average. The RMS values of the mass flow fluctuations obtained in this work are compared with previous simulations [13]. The intensity of flow irregularities is close in magnitude to what was determined using CFD-DEM, though with an imperfect match.

#### 3.2. Data availability

Data is available as an open access repository [14]. This includes the particle tracking results of three levels of the conveying gas flowrate:  $[0.8; 0.6; 0.4]\text{ L/min}$ . For all cases the material is *MetcoAdd 316L-D*, and the pipe is circular with an internal diameter of  $d=1.15\text{mm}$ .

An extended dataset includes four different materials and two other pipe sections, but only the non-processed videos are made available [15].

### 4. Conclusion

This study successfully leveraged high-speed video analysis to capture the dynamics of particle flow in pneumatic conveying systems, crucial for LMD processes. Using advanced imaging techniques, we achieved precise tracking of individual particles, uncovering flow fluctuations and instabilities often overlooked in traditional time-averaged data.

Our experimental findings validated the predictive ability of CFD-DEM simulations, confirming the critical role of particle interactions in inducing flow irregularities. The availability of this experimental data provides a valuable resource for fostering collaboration and further improvements in pneumatic conveying and LMD processes.

### Acknowledgement



This project has received funding from the European Union's Horizon 2020 research and innovation programme under the Marie Skłodowska-Curie grant agreement No. 847624. In addition, a number of institutions back and co-finance this project.

This study received financial support from the Basque Government through the Research Group program IT1507-22.

### References

- [1] S. Dadbakhsh, L. Hao, and C. Kong, *Surface finish improvement of LMD samples using laser polishing*, Virtual and Physical Prototyping, 2010. doi: [10.1080/17452759.2010.528180](https://doi.org/10.1080/17452759.2010.528180).
- [2] S. Zekovic, R. Dwivedi, and R. Kovacevic, *Numerical simulation and experimental investigation of gas-powder flow from radially symmetrical nozzles in laser-based direct metal deposition*, Int. Journal of Machine Tools and Manufacture 2007. doi: [10.1016/j.ijmachtools.2006.02.004](https://doi.org/10.1016/j.ijmachtools.2006.02.004).
- [3] M. Mezhericher, T. Brosh, and A. Levy, *Modeling of Particle Pneumatic Conveying Using DEM and DPM Methods*, Particulate Science and Technology, 2011. doi: [10.1080/02726351003792914](https://doi.org/10.1080/02726351003792914).
- [4] S. Baraldo, A. Roncoroni, F. Palo, and A. Valente, *Multi-physics based methodology for evaluating powder feeding quality for Laser Metal Deposition*, Procedia CIRP, 2022, doi: [10.1016/j.procir.2022.05.036](https://doi.org/10.1016/j.procir.2022.05.036).
- [5] G. E. Klinzing, F. Rizk, R. Marcus, and L. S. Leung, *Pneumatic Conveying of Solids: A Theoretical and Practical Approach*, 3 ed. SPRINGER NATURE, 2010.
- [6] D. Mills, *Pneumatic Conveying Design Guide*. Elsevier Science and Technology Books, 2015.
- [7] F. Zhou, S. Hu, Y. Liu, C. Liu, and T. Xia, *CFD-DEM simulation of the pneumatic conveying of fine particles through a horizontal slit*, Particuology, 2014, doi: [10.1016/j.partic.2014.03.015](https://doi.org/10.1016/j.partic.2014.03.015).
- [8] H. Zhao and Y. Zhao, *CFD-DEM simulation of pneumatic conveying in a horizontal channel*, International Journal of Multiphase Flow, 2019, doi: [10.1016/j.ijmultiphaseflow.2019.06.003](https://doi.org/10.1016/j.ijmultiphaseflow.2019.06.003).
- [9] M. Mezhericher, T. Brosh, and A. Levy, *Modeling of Particle Pneumatic Conveying Using DEM and DPM Methods*, Particulate Science and Technology, 2011, doi: [10.1080/02726351003792914](https://doi.org/10.1080/02726351003792914).
- [10] M. Sommerfeld, *Analysis of collision effects for turbulent gas-particle flow in a horizontal channel: Part I. Particle transport*, International Journal of Multiphase Flow, 2003, doi: [10.1016/s0301-9322\(03\)00031-4](https://doi.org/10.1016/s0301-9322(03)00031-4).
- [11] J. Schindelin et al., *Fiji: an open-source platform for biological-image analysis*, Nature Methods 2012, doi: [10.1038/nmeth.2019](https://doi.org/10.1038/nmeth.2019).
- [12] J.-Y. Tinevez et al., *TrackMate: An open and extensible platform for single-particle tracking*, Methods, 2017, doi: [10.1016/j.ymeth.2016.09.016](https://doi.org/10.1016/j.ymeth.2016.09.016).
- [13] L. Pedrolli, B. Achiaga, I. Martinez de Arenaza, and A. Lopez, *Comparison of CFD-DEM and MP-PIC in the Simulation of Metal Powder Conveying for Laser Metal Deposition*, OpenFOAM® Journal, 2024, doi: [10.51560/ofj.v4.91](https://doi.org/10.51560/ofj.v4.91).
- [14] L. Pedrolli, *Optical Particle Tracking in the Pneumatic Conveying of Metal Powders through a Thin Capillary Pipe*, 2024. doi: [10.5281/zenodo.12806978](https://doi.org/10.5281/zenodo.12806978).
- [15] L. Pedrolli, *High-Speed Video Recordings of Metal Powder Pneumatic Conveying in Thin Capillary Pipes*, 2024. doi: [10.5281/zenodo.12938843](https://doi.org/10.5281/zenodo.12938843).

# On the Convergent Flow Property Behaviour of Different Fine Dry Powders Across Wide Size Ranges, and the Concept of Critical Particle Size

Michael SA Bradley<sup>1\*</sup> and Vivek Garg<sup>1</sup>

<sup>1</sup> Wolfson Centre for Bulk Solids Handling Technology, Faculty of Engineering & Science, University of Greenwich, Central Avenue, Chatham ME4 4TB, UK

**Abstract**— It is well known that fine, dry powders exhibit cohesive behaviour and that this increases with finer particle size. This is a very important phenomenon to industry because in many applications, it is desired to use fine particles, but the question of “how fine can we go before it becomes too difficult to handle?” is an important one in formulation design.

To date, no standardised model has been put forward that can be used to represent this variation, because even for the same particle size, each powder substance has a different Flow Function from others.

In this study, a substantial number of dry powders (not modified with glidants, surface coating, etc.) were subjected to shear testing to obtain their flow functions, each across a range of particle sizes. Plotting the data on the ratio of unconfined failure strength to compaction stress, versus particle size (for a given compaction stress) shows that they exhibit strikingly similar behaviour, except that they are shifted in terms of particle size.

The authors, therefore, propose the concept of “critical particle size” at which a powder transitions from free-flowing to non-free-flowing. Using this concept, it is found that when plotting the data on the basis of the ratio of median particle size to critical particle size for each powder, the data for all powders collapses onto a single curve.

This potentially makes the representation of the cohesive behaviour of powders simpler in that for any given substance, its entire flow behaviour across all size ranges can be represented by the single value of critical particle size. Once this critical particle size is determined, the flow functions of the same substance in different particle sizes can be predicted by referencing the one standard curve. This has great potential for use in digital assistance to the formulation of powders in many different industries, especially pharmaceuticals, foods and battery materials where particle size may need to be changed for the purposes of functionality, and the effect on handling and packing properties computed.

**Keywords:** Formulated powders; Cohesion; Critical Particle Size; Compaction Stress

## 1. Introduction

Finer powders confer many functional advantages to formulations. For example, the greater surface area gives better reaction rates, and higher bioavailability in pharmaceuticals. The smaller size lends a finer finish in additive manufacturing applications. The authors have found from experience that DEM models can have some predictive capability when the particles are large enough to be free-flowing. Therefore, the question of “how fine can we make our material before it becomes cohesive?” is a significant one in powder formulation. The Wolfson Centre has a rich database of flow properties measured from many different materials, from many years worth of undertaking powder characterisation testing.

## 2. Materials and methods

Eight materials were used to undertake the investigation. All tests were undertaken using the Brookfield Powder Flowability Tester, which is an automated annular shear cell commonly used in industry. From the measurement of the Flow Function for each powder sample, the unconfined failure strength  $\sigma_c$  of the powder was identified for a maximum principal normal consolidation stress  $\sigma_1$  of 8kPa. The cohesiveness, in terms of “specific strength”  $\sigma_c/\sigma_1$  was determined. This is also the reciprocal of the flow function coefficient  $ffc$ , which is sometimes used to characterise the cohesiveness of a powder.

## 3. Results and Discussion

Plotting specific strength ( $\sigma_c/\sigma_1$  or  $1/ffc$ ) against particle size, at a fixed compaction stress of 8kPa, gave the graph in fig. 1 below:-

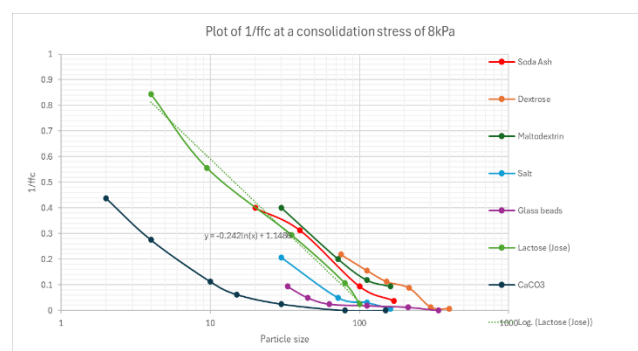


Figure 1. Specific strength versus particle size for seven different powder materials

The particle size at which there is the on-set of cohesion came out was identified as the size below which the powders were “easy flowing” ( $1/ffc > 0.1$ ) and above which the powders were “free-flowing” ( $1/ffc < 0.1$ ). The results are as in table 1 below:

TABLE-1: CRITICAL PARTICLE SIZE BELOW WHICH COHESION STARTS TO APPEAR

Substance	Critical particle size, microns
Calcium carbonate	10
Glass beads	31
Salt	53
Lactose	80
Soda ash	100
Maltodextrin	150
Dextrose	200

It is interesting to note their order. It is hardly surprising to see that the sugars (maltodextrin and dextrose) start to exhibit cohesion with the largest particle sizes; these naturally have a “sticky” surface (high surface energy), which is undoubtedly due to the presence of hydrogen bonding, which is essentially what makes sugar so sticky. The other materials are not known to exhibit hydrogen bonding, so the attraction between their surfaces would be dominated by van der Waals forces (electrostatics are negligible with the stresses involved in these

tests. However there seems to be a loose correlation between critical particle size and hardness with the harder materials (glass beads and calcium carbonate, i.e. ground limestone) having the lowest critical particle size, and the softer materials having progressively larger critical particle sizes. It is postulated that this is due to softer particles suffering more deformation at contact points therefore giving more contact area for the van der Waals forces to work upon.

### 3.1 Normalisation of Data

Normalising with respect to particle size, by dividing the particle sizes in each data set ( $D_{50}$ ) by critical particle size at which  $1/ffc = 0.1$  as shown in table 1 for that substance, the data all collapses onto one curve as shown in fig. 2:-

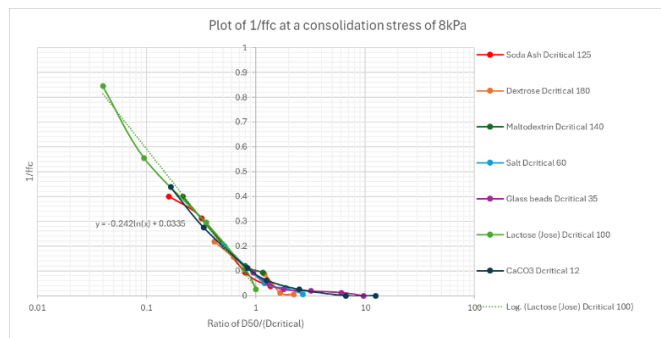


Figure 2. Analysis of data for all the materials

There is some scatter around the data points, but the closeness to a single curve over a relative size range of more than 100:1, is quite remarkable. The authors postulate that the scatter is due to the difficulties in classifying such fine (especially once there is some cohesiveness) to a desired median size and measuring that size accurately.

## 4. Conclusion

The concept of “critical particle size below which a powder exhibits cohesiveness” or conversely, critical particle size above which a powder is free-flowing, has been validated for a range of dry powders. The fact that the curves of cohesiveness versus particle size collapse onto a single line once normalised for critical particle size, means that if the cohesiveness of a substance is measured for a single particle size, reference to that curve can be used to predict the cohesiveness at other particle sizes. This is a useful shortcut for formulators desiring to select ingredients to have a controlled influence on the flow and handling through processing and use. It also offers a basis for a universal model for powder cohesion and, indeed, powder Flow Function, based only on a single measurement of effective surface energy, and median particle size.

## Acknowledgment

Powder samples were provided by a range of industrial sponsors and collaborators that were too wide to enumerate here. Various sources, including UK Engineering and Physical Sciences Research Council and the Department for Environment, Food and Rural Affairs, and a number of industrial sponsors, provided funding for the powder flow property measurement work. The flow property data was produced by Dr Jose Santana, the late Dr Robert Berry, and the authors.



# Modelling and Optimization of Scrap Flows for On-demand Metal Recycling

Yongli Wu<sup>1\*</sup>, Tijmen Oudshoorn<sup>2</sup>, and Peter Rem<sup>1</sup>

<sup>1</sup> Section of Resources & Recycling, Delft University of Technology, Delft, The Netherlands

<sup>2</sup> Myne Circular Metals, Harderwijk, The Netherlands

Contact: y.wu-7@tudelft.nl (Yongli Wu)

**Abstract—** Recycling is critical to enabling a circular economy and the sustainable use of metals. The efficient recycling of metals necessitates smart sorting technologies to obtain high-quality metal scraps that meet the demands of the subsequent users in the supply chain. To aid the development and optimization of the smart sorting technologies, a virtual experiment model is built, based on the discrete element method (DEM). The model considers particle-scale dynamics of complex-shaped scraps and mimics the automated operation of the sorting facility, which helped to realise the optimised scrap flows for particle-scale sorting operations. On such a basis, a full-scale digital recycling plant has been built, for the on-demand recycling and the circularity of metals.

**Keywords:** DEM; metal recycling; scrap sorting.

## 1. Introduction

The recycling of metals (*e.g.*, aluminium) is key to realising a circular economy and meeting the substantial metal demand in various applications such as construction, transportation, machinery, and electronics. Due to their use in extensive applications and the diversity of product functionality, more complex metal alloys and composites are increasingly produced. This raises the difficulty for efficient recycling while downcycling creates a loss of environmental/economic profits[1].

To sort specific metal alloy types for enabling on-demand recycling process, it is important to develop smart sorting technologies that generally integrate different high-tech technologies (*e.g.*, artificial intelligence (AI), sensors, and robotics) for materials characterisation and automated sorting. However, in recycling processes, those original input materials of metal waste are shredded into smaller scraps which can have diverse shapes and corresponding random flow behaviours in the processing line. Those random scrap flows with some undesired overlapping or clustering of scraps can result in problems or errors in the material characterisation by AI or sensors, as well as difficulties in robotic picking. Therefore, it is important to understand and optimize the scrap flows for realising an efficient smart sorting facility.

This work presents a numerical model based on the discrete element method (DEM) [2] for the modelling and optimisation of the scrap flows in the processing line. Based on the modelling, the optimal design and operation of the sorting facility are proposed and validated in pilot-scale tests, which aided the building of a full-scale digital recycling plant.

## 2. The virtual experiment model

### 2.1. Model development

To model the scrap flow behaviours in the sorting facility, a virtual experiment model is developed by the particle-scale

DEM [2, 3], based on the open-source program LIGGGHTS [4, 5].

As shown in Fig. 1, the non-spherical scrap shape is described through 3D scanning and represented by a multisphere method.

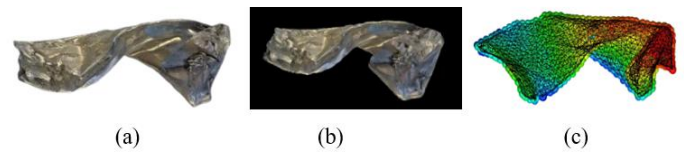


Figure 1. Description of scrap shapes: (a) original scrap; (b) 3D scanning; and (c) shape representation by multisphere method.

### 2.2. Realisation of the automated sorting facility

Based on DEM, the modelling of the proposed design and the automated sorting of scraps is realised, as shown in Fig. 2. The simulated model integrates the functions of scrap feeding, sensor characterisation, and automated ejection, thus allowing it to be a virtual experiment model.

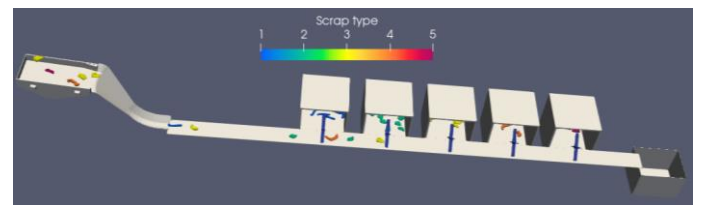


Figure 2. The automated sorting facility simulated by DEM.

## 3. Results

### 3.1. Testing on the effects of parameters

The developed DEM model is used to study various operation parameters. For example, the effects of varying vibratory frequencies and different feeding rates on the scrap flow behaviours (Fig. 3) and the sorting rates of scraps (Fig. 4) are studied. Besides, the effects on some other parameters like belt speed and scrap shape properties have also been tested recently [6].

Such qualitative and quantitative results helped to identify the feasible range of operational parameters for the optimal operation of the sorting facility.

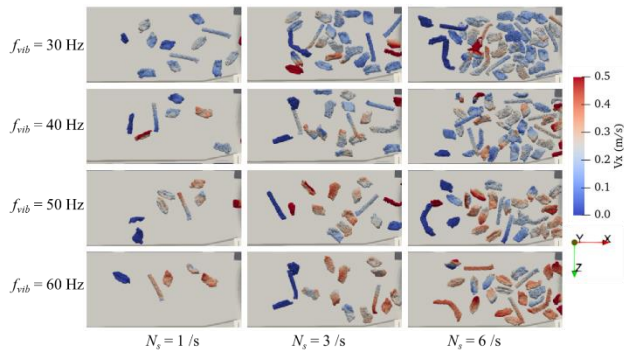


Figure 3. Effects of varying vibratory frequencies and different feeding rates.

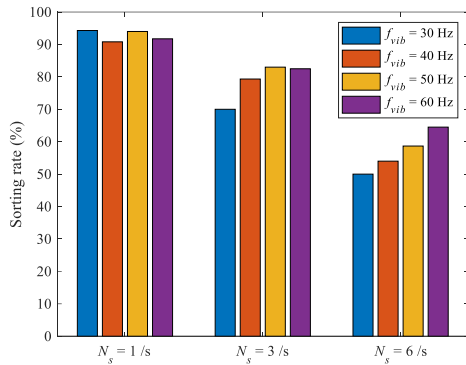


Figure 4. Sorting rates at varying vibratory frequencies and different feeding rates.

### 3.2. Implementation in the industry

The proposed design and results from DEM modelling were tested and implemented at Dutch company *Myne Circular Metals* [7]. A full digital recycling plant named “Xorter” (Fig. 5) has been built with 8 processing lines and 8 robotic ejectors for each line (64 robotics running at the same time), enabling the sorting of scraps into diverse metal alloys according to the demands of customers (e.g., various smelters and manufacturers).

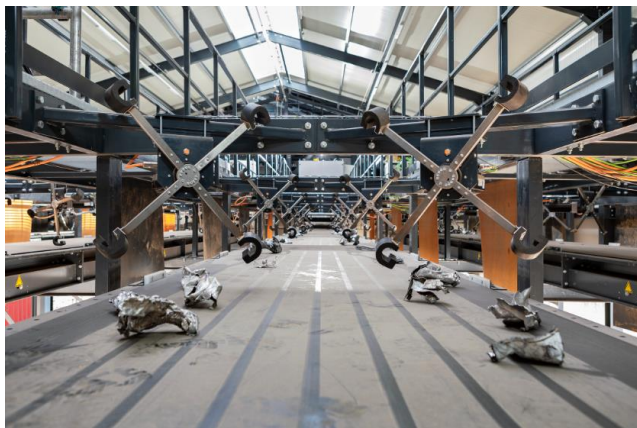


Figure 5. The full-scale digital recycling plant at *Myne Circular Metals* [7].

## 4. Conclusion

A computational model based on DEM is developed and applied for the simulation and optimisation of an automated scrap sorting facility. The simulated/proposed results have been used for aiding industrial implementation. So far, the study has been focused on the sorting of aluminium scraps, while the following work will be on the sorting of many other materials, including various metal scraps (e.g., steel, copper), composite materials, and electronic wastes. By such high-definition sorting

of waste materials, the goal is to realise the on-demand recycling of materials that can meet the demands of various manufacturers for making circular products, thus promoting a circular economy and the sustainability of manufacturing industries.

## Acknowledgement

We would like to acknowledge the support from Dutch company *Myne Circular Metals* (formerly *Reukema*) and EU Horizon Marie Skłodowska-Curie Project (SortCAS, No.101066062). Besides, this work made use of the Dutch national e-infrastructure with the support of the SURF Cooperative using grant no. EINF-3045, which is also acknowledged.

## References

- [1] E. Aluminium, *Vision 2050: European aluminium's contribution to the EU's mid-century low-carbon roadmap*, Brussels, Belgium, 2019.
- [2] P. A. Cundall, and O. D. L. Strack, “A discrete numerical model for granular assemblies,” *Géotechnique*, vol. 29, no. 1, pp. 47-65, 1979.
- [3] H. P. Zhu, Z. Y. Zhou, R. Y. Yang, and A. B. Yu, “Discrete particle simulation of particulate systems: Theoretical developments,” *Chemical Engineering Science*, vol. 62, no. 13, pp. 3378-3396, 2007.
- [4] CFDEM@project. “CFDEM@coupling Documentation, Version 3.X,” [https://www.cfDEM.com/media/CFDEM/docu/CFDEMcoupling\\_Manual.html](https://www.cfDEM.com/media/CFDEM/docu/CFDEMcoupling_Manual.html).
- [5] C. Kloss, C. Goniva, A. Hager, S. Amberger, and S. Pirker, “Models, algorithms and validation for opensource DEM and CFD-DEM,” *Progress in Computational Fluid Dynamics, an International Journal*, vol. 12, no. 2-3, pp. 140-152, 2012.
- [6] Y. Wu, T. Oudshoorn, and P. Rem, “Modelling and optimization of an innovative facility for automated sorting of aluminium scraps,” *Waste Management*, vol. 189, pp. 103-113, 2024.
- [7] “Myne Circular Metals,” <https://www.myne.eco/>.

# Accelerated DEM Simulations: An Improved Time-Series Model for Forecasting Particle Trajectories Using Machine Learning

Elis I. Bright<sup>1,2</sup>, John P. Morissey<sup>1</sup>, and Jin Y. Ooi<sup>1</sup>

<sup>1</sup> University of Edinburgh, Scotland, UK

<sup>2</sup> Astec Industries, Inc., Chattanooga, TN, USA

**Abstract**— The Discrete Element Method (DEM) is widely used for simulating granular materials but is computationally intensive, particularly for large particle systems. To address this, recent research has explored machine learning-based methods to accelerate DEM simulations. One such approach, the Recurrent Neural Network with Stochastically Calculated Random Motion (RNNSR) predicts particle trajectories to reduce simulation time. However, a recreation of the original model revealed issues with physical accuracy, such as predictions with solid fractions higher than unity and severe particle overlapping. This study presents an improved RNNSR model that incorporates geometric information into the time-series model to prevent unphysical particle behaviour, ensuring accurate solid fractions and boundary adherence in a rotating drum. Porting the prediction method to GPU increased computational speed, making it more practical compared to the current state of DEM technology.

**Keywords:** DEM; mixing; machine learning; prediction

## 1. Introduction

The Discrete Element Method (DEM) is a prevalent approach for simulating granular materials, but its computational intensity can be a barrier, particularly with large particle systems such as powders. Recent research has focused on a variety of machine learning (ML)-based approaches for accelerating and predicting particulate behaviour through a variety of different neural network architectures. Previously, convolutional neural networks [1, 2], and graph neural networks [3, 4] among other architectures have been utilised for particle position prediction based on datasets with multiple instances of physics simulations. Conversely, the recurrent neural network with stochastically calculated random motion (RNNSR) [5] uses a short, single simulation to learn particle trajectories and can be used to extrapolate particle positions quickly while decreasing the computational time of simulations.

In this study, an improved RNNSR model was developed to address some of the limitations of the original method in terms of physical accuracy and computational speed. The original method showed high accuracies for large DEM simulations of powder with over a million particles [5]. However, limitations of the original model's physical accuracy were revealed when applied to simulations with fewer particles in this study. Due to the model training purely on time-series of individual particle mean positions, predictions showed particles overlapping and crossing geometrical boundaries defined in the simulation. Notably, the geometric boundaries of the system or solid fraction are not discussed in the original RNNSR study [5], although the importance of encoding boundary information to ML-based models for particulate simulations has been highlighted previously [1, 4].

The proposed improvements to the RNNSR model in this study consist of encoding boundary information to the particle time-series, implementing correction logic for particles violating the boundary, and architectural changes. Furthermore, the computational speed of the model was increased by porting the method to GPU, offering a substantial reduction in

computational time and providing a more practical comparison to the performance of commercial DEM solutions. A comprehensive sensitivity analysis of the RNNSR model parameters was conducted, guiding the accurate and efficient deployment of the model.

## 2. Methodology

The model developed in the study follows the basic principles of the RNNSR model established by [5] and is illustrated in Fig. 1. A short DEM simulation of particles mixed in a rotating drum is first run for data acquisition, from which the data is pre-processed to get position and velocity data at particle-level. These values are used to calculate particle local mean components and construct the velocity variability grid used for the stochastic random effects used during prediction rollout. Additionally in this study, distances from a particle's local mean to both vertical walls and the curved boundary of the drum are calculated and encoded for each particle at each time step. Local mean position and boundary distances are then learned using the recurrent neural network (RNN), where  $n$  time steps are given as the input, with particle values at time step  $n+1$  as the output. The gated recurring unit (GRU) layer in the original RNNSR model was changed to long-short term memory (LSTM).

Once trained, the model can be used to predict particle positions, referred to as rollout. A stochastic velocity component is generated and added to the predicted particle local means based on their respective position in the variability grid to get the final particle position at  $n+1$ . Errant particles that are predicted by the RNN, or moved outside the boundaries by the local variability, are corrected to be inside the geometry based on their radial and axial vectors in reference to the centre point of the drum, as illustrated in Fig. 2. It should be noted that no particle correction logic is discussed by [5]. Finally, the actual distances from particles to the drum's three walls can be correctly adjusted and fed back into the RNN for the prediction of next time step.

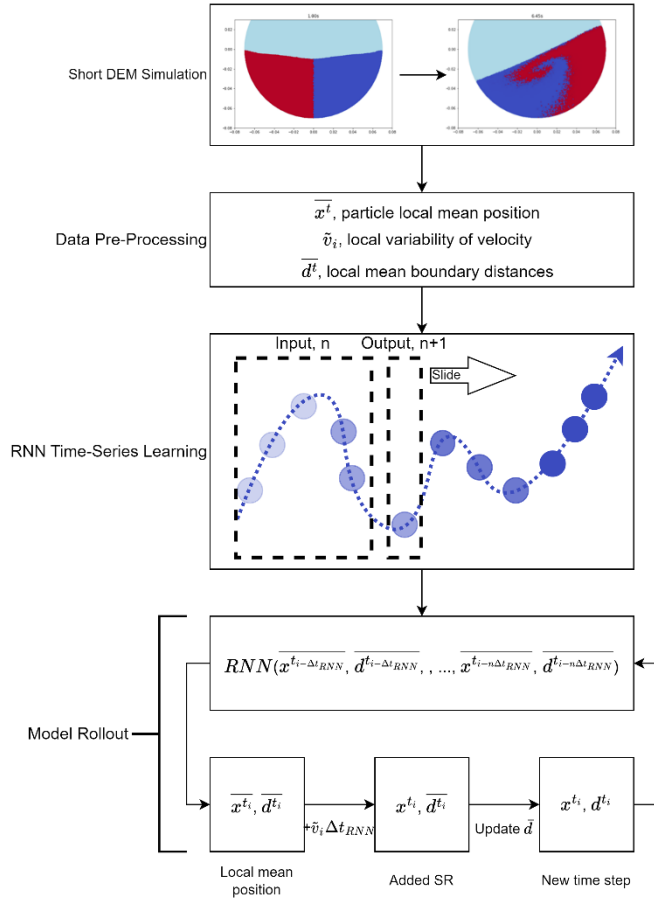


Figure 1. Improved RNNSR Model Overview

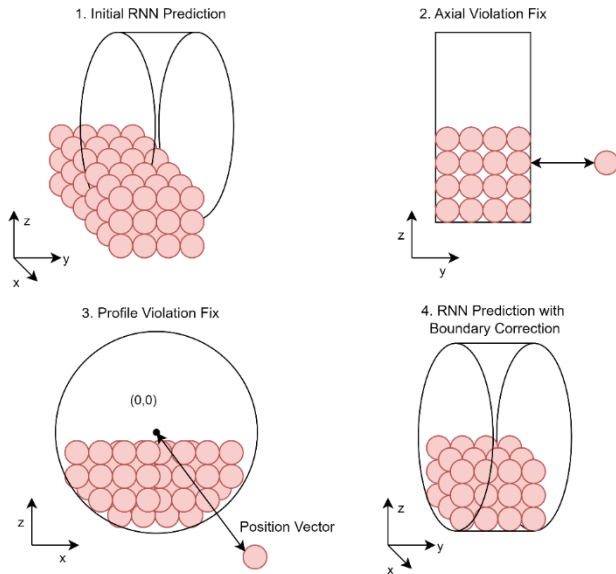


Figure 2. Boundary Particle Correction Logic

### 3. Results

The results showed that the improved model's particle rollout was able to predict the mixing quality with similar accuracy while keeping the solid fraction and mass distribution of the particles more in line with the ground truth simulation, as shown in Fig. 3, when compared to the predictions of the original model (Fig. 4). However, a slight increase in the solid fraction is still shown. Further improved performance was also seen using the LSTM layer in place of the GRU layer.

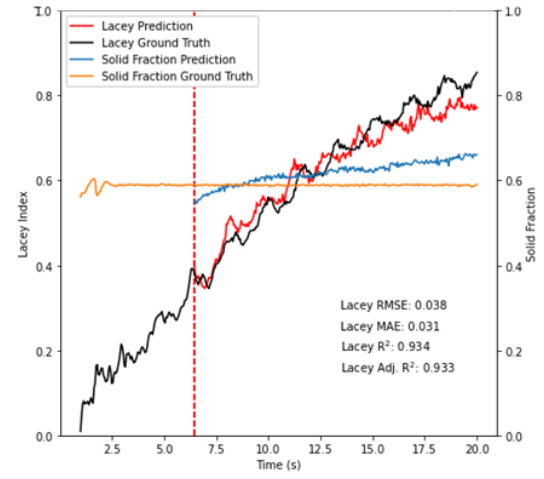


Figure 3. Improved RNNSR Model Results

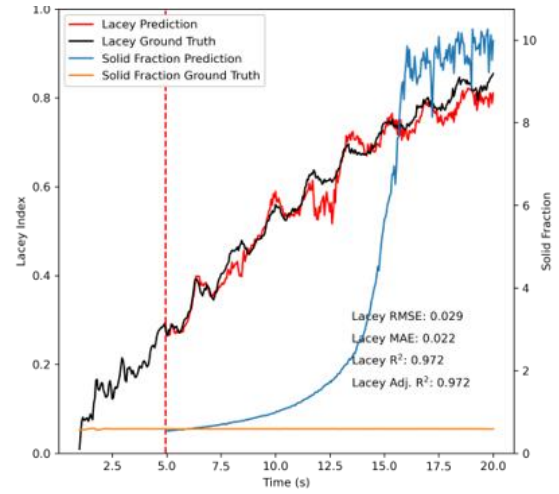


Figure 4. Original RNNSR Model with Physically Inaccurate Solid Fraction

The computational speed of the method was improved by porting it to GPU. While the original RNNSR method on CPU achieved a fivefold improvement in computational speed compared to its respective DEM simulation, our improved method on GPU predicted particle locations twice as fast as the original simulation. Although the computational acceleration is less than the original method, the improved model delivers better physical accuracy overall as a trade-off.

### 4. Conclusion

In conclusion, this study demonstrates significant improvements to the RNNSR model for accelerating DEM simulations of granular materials. The enhanced model successfully improves physical accuracy issues by incorporating geometric information and boundary constraints, resulting in more physically plausible particle behaviour. These improvements show the potential for the deployment of the RNNSR model for a wide range of dense granular systems.

### References

- [1] Xu, D. and Y. Shen, An improved machine learning approach for predicting granular flows. *Chemical engineering journal*, 2022. 450: p. 138036.
- [2] Lu, L., et al., Machine learning accelerated discrete element modeling of granular flows. *Chemical engineering science*, 2021. 245: p. 116832.
- [3] Sanchez-Gonzalez, A., et al., Learning to Simulate Complex Physics with Graph Networks. 2020.
- [4] Mayr, A., et al., Boundary Graph Neural Networks for 3D Simulations. *Proceedings of the AAAI Conference on Artificial Intelligence*, 2023. 37(8): p. 9099-9107.
- [5] Kishida, N., et al., Development of ultra-fast computing method for powder mixing process. *Chemical engineering journal*, 2023. 475: p. 146166.



## 4 TUSAIL SYMPOSIUM

# Strategies for CFD–DEM modelling of plug flow pneumatic conveying using meso-scale particles

Oguzhan Erken<sup>1,2</sup>, Kevin J. Hanley<sup>1</sup>, Jin Y. Ooi<sup>1</sup>, Prashant Gupta<sup>2</sup>, and Simon Greener<sup>2</sup>

<sup>1</sup> University of Edinburgh, Scotland, UK

<sup>2</sup> Procter and Gamble Technical Centre Ltd., Newcastle upon Tyne, UK

**Abstract—** CFD–DEM simulations of industrial-scale systems can be very computationally expensive. One potential solution is to use “coarse grained (CG)” or “scaled-up” particles in these simulations, which can significantly reduce computational costs while still capturing the essential physics. This study investigates various scaling methods for drag and contact forces in the context of horizontal plug flow pneumatic conveying to establish a clear methodology for similar operations. Comparisons are made between six contact force scaling methods and three drag force scaling methods. It is found that cubic drag force scaling provided the most accurate results, while linear and quadratic scaling led to unrealistic fluid velocities. Contact force scaling methods that involved scaling of the sliding friction coefficient resulted in inaccuracies, while the others produced similar results. Spatio-temporally averaged continuum fields showed that the constant relative overlap model better preserved contact stresses compared to the constant absolute overlap model, particularly at high CG ratios. Overall, the combination of cubic drag force scaling and constant relative overlap contact force scaling yielded the most reliable results, maintaining contact pressures and enabling larger DEM time steps.

**Keywords:** Coarse-graining (CG), Particle scale-up, Discrete Element Method, Computational Fluid Dynamics, Slug flow

## 1. Introduction

Computational Fluid Dynamics–Discrete Element Method (CFD–DEM) coupled simulations are widely used in industry to model multiphase particulate flows. DEM tracks each particle in the simulation individually, so it can easily become computationally infeasible when the number of particles in the simulation exceeds  $\sim 10^7$ . Considering billions of particles may be present in an industrial unit operation, different strategies are necessary to be able to apply this method to industrial processes.

Coarse grained (CG) CFD–DEM is one of those strategies proposed to decrease this computational expense. In this simulation method, a group of original particles are represented by a single representative particle (grain) by applying certain scaling rules.

Various studies have been conducted to compare and analyse different coarse graining methodologies in specific flow settings. Brandt et al. [1] examined hydrodynamic and contact force scaling models in fluidised beds, concluding that the cubic drag scaling approach outperformed the quadratic approach and that contact force scaling had limited influence in a full CFD–DEM simulation. Che et al. [2] compared three CG approaches, namely constant relative overlap ( $n^2$  scaling, where “ $n$ ” is the CG ratio, i.e., the size ratio between the CG and original particles), constant absolute overlap ( $n^3$  scaling) and non-dimensional number–based scaling methods, in their experimentally validated fluidised bed study. They found that the effectiveness of CG simulations decreased when the size ratio between the bed chamber and particles decreased below 20. The chosen CG approach for inter-particle contact

parameters had minimal impact on simulation outcomes in this hydrodynamic system. De Munck et al. [3] conducted a comparative study for a bubbling fluidised bed, comparing scaling methods based on preserving non-dimensional numbers and constant absolute overlap. They determined that the latter approach better described the original unscaled system.

Previous research has shown that coarse graining methodologies can perform differently in different simulation settings and flow regimes. Furthermore, the existing research on CG CFD–DEM has mostly focused on fluidised beds. In fact, to the best of our knowledge, only Sakai and Koshizuka [4] investigated coarse graining in the context of pneumatic conveying. Therefore, this study aims to fill this gap by evaluating six different contact force and three different drag force scaling methods, specifically in the context of plug flow pneumatic conveying. To simulate a developed flow section of an extended pipeline, a horizontal and circular pipe with periodic boundary conditions is utilised. The main goal of this study is to identify the most effective coarse graining approach for horizontal plug flow pneumatic conveying or similar flow conditions.

## 2. Methodology

CFD and DEM equations are solved using OpenFOAM (Version 8) and Aspherix (Version 6.1.0), respectively. They are linked via the CFDEMcoupling framework (non-spherical Version 6.1.0). The details of the formulation and numerical methods of CFD and DEM are omitted here for brevity, but an interested reader is referred to [5–7] for details.

The simulations are run in a horizontal and circular pipe with periodic boundary conditions as seen in Fig. 1 (which includes further details of the simulation setup). The simulations are run for a total duration of 5 seconds, and the system reaches a steady state after approximately 3 seconds. The response parameter values are calculated by averaging the results over the last 2 seconds of each simulation, exported at 0.05 second intervals.

In order to extract the continuum fields, such as solid volume fraction, momentum flux, and contact stresses, spatio-temporal averaging techniques are employed using the MercuryCG package of MercuryDPM. Spatio-temporal averaging is conducted over a  $40 \times 40 \times 400$  grid, utilising a D2C (discrete-to-continuum) coarse graining width of  $w = 2d_p$ .

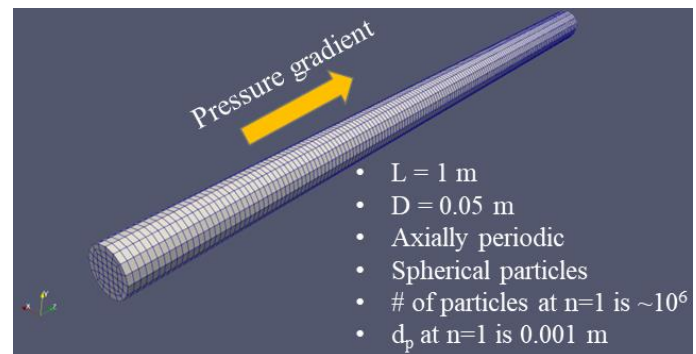


Figure 1. Pipe geometry with CFD mesh.

### 3. Results

Firstly, linear, quadratic, and cubic drag force scaling methods were compared by fixing the contact force scaling as the constant relative overlap method. This initially showed that there is not a prominent difference between these methods for plug properties, namely plug length, plug porosity, plug velocity, and rate of particle exchange (percentage of particles exchanged between the stationary particle layer and plug per second). However, a closer examination of the flow field revealed that the linear and quadratic drag force scaling methods produced artificially high fluid velocities which exceeded the benchmark simulation results. This is illustrated in Fig. 2 for the average interstitial fluid velocity within each plug.

Then, different contact force scaling methods were compared. This analysis showed that the methods including sliding friction coefficient scaling performed poorly compared to the other methods. The constant relative and absolute overlap methods performed indistinguishably, while the Simplified Dissipation Scaling (SDS) method agreed reasonably well with them, producing slightly lower plug velocities. These results are depicted in Fig. 3. The suffix “-fric” stands for the variations of the respective methods in which the sliding friction coefficient is scaled.

The  $n^2$ ,  $n^3$  and SDS contact force scaling methods were further investigated by employing spatio-temporally averaged continuum fields. The radial variation of the contact pressure, i.e., trace of the stress tensor, is presented in Fig. 4. It should be noted that these results were obtained by axially averaging the contact pressures along the plug. As the CG ratio increases, the contact pressures disappear in the  $n^3$  scaling and SDS methods, while they are conserved in the  $n^2$  scaling method.

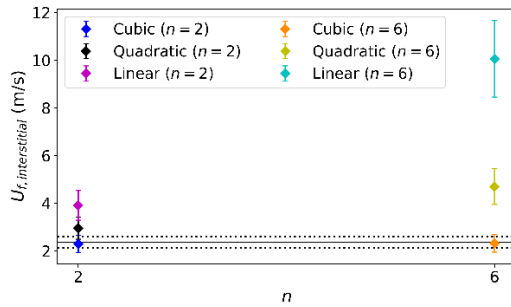


Figure 2. The average interstitial air velocities within the plugs for linear, quadratic, and cubic drag force scaling rules. The solid line represents the value for the benchmark simulation, while the dotted lines indicate deviations of  $\pm 10\%$  from this reference.

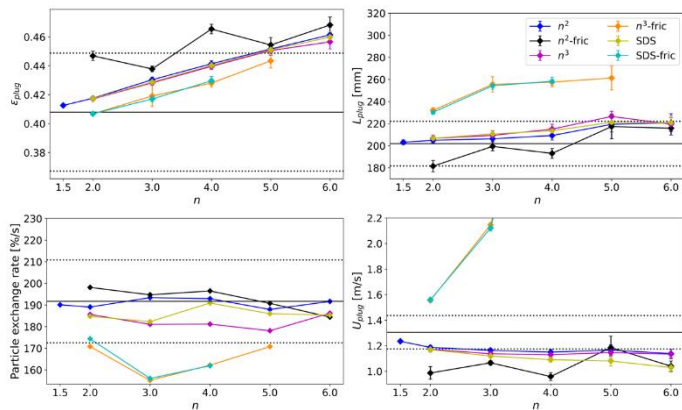


Figure 3. Variation of plug porosity (top left), plug length (top right), rate of particle exchange (bottom left), and plug velocity (bottom right) for different contact force scaling methods. The solid lines represent the values for the benchmark simulation, while the dotted lines indicate deviations of  $\pm 10\%$  from this reference.

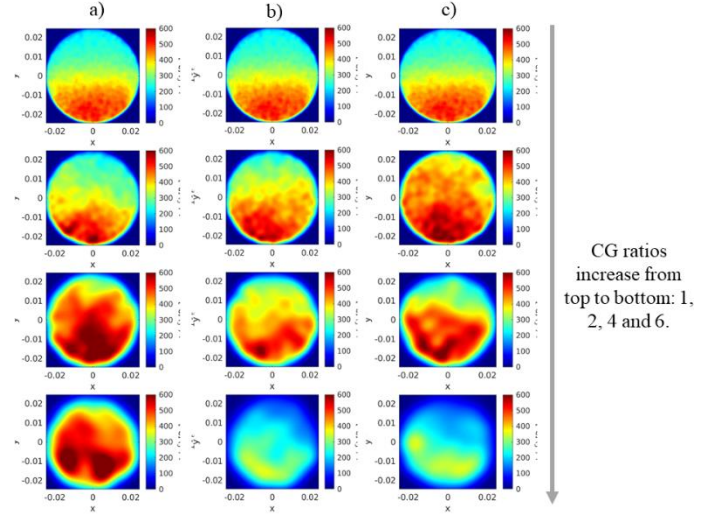


Figure 4. Time-averaged contact pressures within plugs for a)  $n^2$  b)  $n^3$  and c) SDS contact force scaling methods.

### 4. Conclusion

The combined implementation of cubic scaling for drag force and constant relative overlap scaling for contact forces demonstrated the best performance for the coarse-grained system. Furthermore, this contact force scaling method allowed for the utilisation of larger DEM time steps in the simulations, solidifying its status as the most advantageous choice among the assessed contact force scaling methods.

The variation of the computational time with the coarse graining ratio (omitted here for brevity) showed that the computational time reached a plateau after  $n=3$ . This implies a balance between computational expense and spatial resolution, necessitating a careful evaluation from a modeller to consider whether a further increase in the coarse graining ratio yields a worthwhile reduction in computational cost.

### Acknowledgement

This project has received funding from the European Horizon2020 Framework Programme for research, technological development and demonstration under grant agreement ID 955661. We would like to thank DCS Computing GmbH for providing the CFD-DEM software. We would also like to acknowledge Balázs Füvesi (University of Twente) for his help in converting Aspherix data to MercuryDPM data using Python.

### References

- [1] V. Brandt, J. Grabowski, N. Jurtz, M. Kraume, and H. Kruggel-Emden, “A benchmarking study of different DEM coarse graining strategies”, *Powder Technology*, vol. 426, p. 118629, Aug. 2023.
- [2] H. Che, D. Werner, J. Seville, T. K. Wheldon, and K. Windows-Yule, “Evaluation of coarse-grained CFD-DEM models with the validation of PEPT measurements”, *Particuology*, vol. 82, pp. 48–63, Nov. 2023.
- [3] M. J. A. de Munck, J. B. van Gelder, E. A. J. F. Peters, and J. A. M. Kuipers, “A detailed gas-solid fluidized bed comparison study on CFD-DEM coarse-graining techniques”, *Chemical Engineering Science*, vol. 269, p. 118441, Apr. 2023.
- [4] M. Sakai and S. Koshizuka, “Large-scale discrete element modeling in pneumatic conveying”, *Chemical Engineering Science*, vol. 64, no. 3, pp. 533–539, Feb. 2009.
- [5] Aspherix, DCS computing GmbH, 2021, <https://www.aspherix-dem.com/> (Accessed on 18 June 2024).
- [6] C. Goniva, C. Kloss, N.G. Deen, J.A. Kuipers, S. Pirker, “Influence of rolling friction on single spout fluidized bed simulation”, *Particuology*, vol. 10 no. 5, pp. 582–591, 2012.
- [7] O. Erken, J. Y. Ooi, P. Gupta, L. Capozzi, and K. J. Hanley, “Parameters affecting plug characteristics in dense phase pneumatic conveying of ellipsoidal particles,” *Powder Technology*, vol. 437, p. 119561, Mar. 2024.

# Discrete magnification lens: A new hybrid discrete-continuum method for simulating particle laden flows

Behrad Esgandari<sup>1</sup>, Daniel Queteschiner<sup>1</sup>, Stefan Pirker<sup>1</sup> and Simon Schneiderbauer<sup>1</sup>

<sup>1</sup> Department of Particulate Flow Modelling, Johannes Kepler University Linz (JKU), Linz, Austria

**Abstract—** We introduce a new hybrid multi-scale model, the "discrete magnification lens" method, which employs a computational fluid dynamic coupled to discrete element method (CFD-DEM) approach within a specific region of interest in a two-fluid model (TFM) simulation. We applied the discrete magnification lens to the crossing jet problem, where the TFM fails due to lack of considering bi-modal velocity distribution in its formulation. It was observed that the non-physical behaviour of the TFM can be effectively altered to conform to the behaviour observed in CFD-DEM simulations by incorporating the discrete magnification lens.

**Keywords:** Hybrid multi-scale modelling; Two-Fluid model; CFD-DEM; Particle laden flows; Particle-trajectory crossing;

## 1. Introduction

The presence of a dispersed phase (particle phase) gives rise to a broad range of length and time scales that needs to be considered in the modelling of fluid-particle flows. In addition, the large separation of scales observed in particle laden flows, wherein processes happen at the microscale, such as particle collisions and fluid-particle interactions, affect the structures at the macroscale. Therefore, a multiscale modelling strategy which can model fluid-particle flows at different time and length scales with different levels of detail was introduced [1].

The conventional multiscale modelling strategy is based on the off-line and one-way coupling between the PR-DNS, CFD-DEM and TFM methods. For instance, the PR-DNS is used to derive interphase momentum, heat and mass transfer correlations that can be used in CFD-DEM and TFM approaches. In recent years, the similarities between PR-DNS and CFD-DEM in treating the particle phase and CFD-DEM and TFM in treating the fluid phase and the momentum exchange closures has given rise to hybrid multiscale modelling approaches.

We introduce a new hybrid continuum-discrete method (discrete magnification lens) for simulating particle-laden. This hybrid model applies a CFD-DEM approach within a specific region of interest in a TFM simulation to magnify the continuum particle phase using discrete particles. In the boundaries of the region, the information from the TFM is used to initialize and derive the CFD-DEM simulations while in an inner region away from the boundaries, the CFD-DEM affects the TFM simulation. We examine the effectiveness of discrete magnification lens (DML) method, in case of particle jets.

## 2. Methodology

A detailed description of the numerical methodology and implementation of the DML method can be found in our recent publication [2]. Here we present a short explanation about the DML method.

The locally averaged mass and momentum equations for the fluid and the continuum particle (cp) phases in the TFM are written as,

$$\frac{\partial}{\partial t}(\alpha_q \rho_q) + \nabla \cdot (\alpha_q \rho_q \mathbf{u}_q) = 0 \quad (1)$$

$$\frac{\partial}{\partial t}(\alpha_f \rho_f \mathbf{u}_f) + \nabla \cdot (\alpha_f \rho_f \mathbf{u}_f \mathbf{u}_f) = -\alpha_f \nabla p + \nabla \cdot \alpha_f \boldsymbol{\tau}_f - \beta_{TFM}(\mathbf{u}_f - \mathbf{u}_{cp}) + \alpha_f \rho_f \mathbf{g} \quad (2)$$

$$\frac{\partial}{\partial t}(\alpha_{cp} \rho_{cp} \mathbf{u}_{cp}) + \nabla \cdot (\alpha_{cp} \rho_{cp} \mathbf{u}_{cp} \mathbf{u}_{cp}) = -\alpha_{cp} \nabla p - \nabla \cdot (\mathbf{S}_{cp}^{kc} + \mathbf{S}_{cp}^{fr}) + \beta_{TFM}(\mathbf{u}_f - \mathbf{u}_{cp}) + \alpha_{cp} \rho_{cp} \mathbf{g} + \Psi_{cp} \quad (3)$$

where in (1),  $\mathbf{u}_q$ ,  $\alpha_q$  and  $\rho_q$  are the velocity, volume fraction and density of phase  $q$ , where  $q$  represents either the particle phase or fluid phase. In addition,  $\beta_{TFM}$  is the drag coefficient in TFM simulations where the drag model of Beetstra et al. [3] is used in this study. It can be noted that in (3) solids stress tensor consists of kinetic-collisional,  $\mathbf{S}_{cp}^{kc}$ , and frictional solids stresses,  $\mathbf{S}_{cp}^{fr}$ . The variable  $\Psi_{cp}$  in (3) denotes a semi-implicit source term used in DML and will be discussed later. Moreover, for detailed explanations about the TFM constitutive relations, we refer to our previous paper [4]. Note that we do not discuss the equations related to the CFD-DEM approach in here, the interested reader is referred to our previous paper [2].

In the DML, the CFD-DEM is nested into a TFM simulation. In other words, the CFD-DEM acts like a magnification lens and magnifies the continuum particle phase by using the discrete particles in a specific region of interest. The schematic of the DML is illustrated in Fig. 1. The region indicated with the cyan color represents a TFM simulation and the region in the left-hand side of the overlapping boundary marked by the green color is the CFD-DEM domain. It can be deduced that the DML region is composed from different parts.

The *overlapping boundary* is the shared boundary between the TFM and the CFD-DEM domains. This boundary is utilized to quantify the inflow mass flux of the continuum particle phase into the CFD-DEM at each cell face. The number of discrete particles to be inserted into the CFD-DEM domain can be determined by utilizing the measured mass flux of the continuum particle phase at the cell faces. The *insertion region*, represents the region where the discrete particles are inserted. This region consists of the initial layer of cells that are located near the overlapping boundary. The initial velocity vector of the newly inserted discrete particles can be assigned by randomly sampling from the Maxwellian velocity distribution. In the *particle velocity controller region*, the deviation of the velocity of discrete particles compared to the continuum particle phase velocity in the cell corresponding to the particle's position is minimized. The velocity of discrete particles is controlled by adding a force on every discrete particle in the particle velocity controller region.



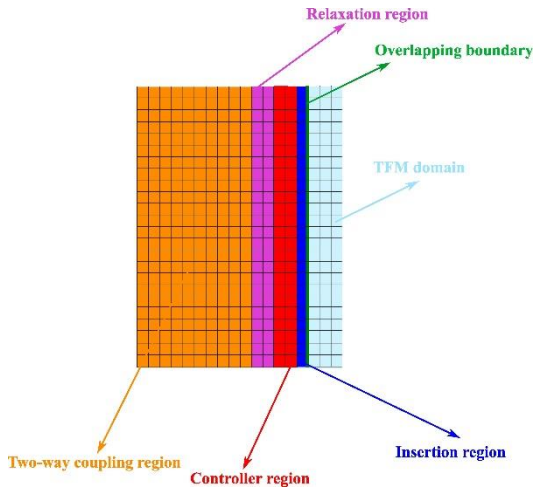


Figure 1. The schematic of the DML model.

The *relaxation region* is used to dampen the possible disturbances on the discrete particles caused by the imposed forces on the particles. In the two-way coupling region, the discrete particles' information is used to influence the underlying TFM simulation, resulting in a two-way coupling between the TFM and the CFD-DEM models. To do so, a semi-implicit source term,  $\Psi_{cp}$ , is added to the RHS of (3) which drives the continuum particle phase velocity of the underlying TFM towards the discrete particle velocity field. In addition to  $\Psi_{cp}$ , the interphase momentum exchange coefficient of the continuum particle and fluid phases,  $\beta_{TFM}$ , in (2)-(3), is replaced by the interphase momentum exchange coefficient obtained from the CFD-DEM simulations.

### 3. Results

In the simulations, two diagonal particle jets with 45-degree angle and velocity of  $14 \text{ m s}^{-1}$  were injected from the opposite sides of a channel. The particle volume fraction in jets were 0.02. The fluid flow entered with a velocity of  $25 \text{ m s}^{-1}$  and left through the top outlet. The simulation settings can be found in our previous work [2].

Fig. 2 illustrates the particle volume fraction profiles of the jets over time. It is evident that particle jets are crossing in CFD-DEM, exhibiting only minor interaction, a phenomenon that is not observed in the TFM. The absence of a bi-modal velocity distribution in the TFM approach's formulation is responsible for this defect. The behavior of the TFM simulation can be corrected by using DML approach, as shown by the particle volume fraction profile of the DML method.

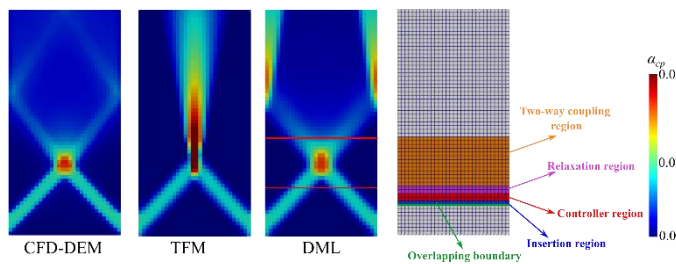


Figure 2. Time-averaged particle volume fraction profiles and Schematic of the DML region in dilute particle jets. The red lines on DML profile indicate the two-way coupling region location.

To quantitatively investigate the results, the time-averaged particle volume fraction obtained from the simulations is represented in Fig. 3. The particle volume fraction at  $z = 0.09 \text{ m}$

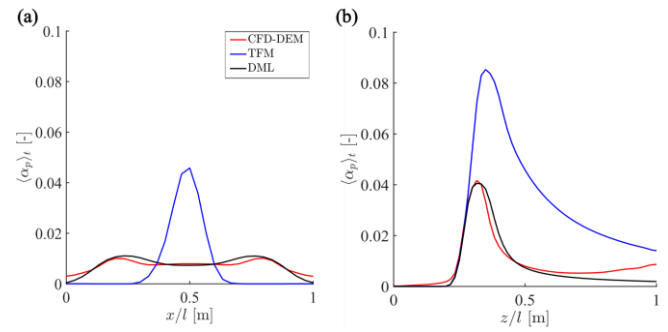


Figure 3. Comparison of the time-averaged particle volume fraction obtained from the simulations. The horizontal profile: (a)  $z = 0.09 \text{ m}$ , and the vertical profile: (b)  $x = 0.045 \text{ m}$ .

(outside the magnification region), indicates that the behaviour of the TFM simulation is wrong, while the CFD-DEM and the DML simulations predict particle jet crossing correctly. The particle volume fraction profiles along the channel height at  $x = 0.045 \text{ m}$  are depicted in Fig. 3b. Although the DML and the CFD-DEM simulations are predicting a similar trend, the TFM exhibits totally different trend with the highest discrepancy compared to the CFD-DEM results.

### 4. Conclusion

We introduced and successfully implemented a novel hybrid multi-scale modelling method for simulations of fluid-particle systems, referred to "discrete magnification lens" method. We adopted the discrete magnification lens method in case of dilute particle jets. It was observed that the CFD-DEM approach can successfully capture the particle trajectory crossing while the TFM failed, due to lack of considering bi-modal particle velocity distribution. However, it was demonstrated that applying discrete magnification lens model can improve the behaviour of the TFM to conform to the one observed in the CFD-DEM simulations.

### Acknowledgement

This project has received funding from the European Union's Horizon 2020 research and innovation programme under the Marie Skłodowska-Curie grant agreement No 955661 (TU SAIL ITN, <https://tusail.eu/>).

### References

- [1] S. Subramaniam and S. Balachandar, "Modeling Approaches and Computational Methods for Particle-laden Turbulent Flows," 2023.
- [2] B. Esgandari, D. Queteschiner, S. Pirker, and S. Schneiderbauer, "Discrete magnification lens model: A new hybrid multi-scale modelling method for fluid-particle systems," *Powder Technol.*, p. 120094, Jul. 2024, doi: 10.1016/j.powtec.2024.120094.
- [3] R. Beetstra, M. A. Van Der Hoef, and J. A. M. Kuipers, "Drag force of intermediate reynolds number flow past mono- And bidisperse arrays of spheres," *AIChE Journal*, vol. 53, no. 2, pp. 489–501, 2007, doi: 10.1002/aic.11065.
- [4] B. Esgandari, S. Rauchenzauner, C. Goniva, P. Kieckhefen, and S. Schneiderbauer, "A comprehensive comparison of Two-Fluid Model, Discrete Element Method and experiments for the simulation of single- and multiple-spout fluidized beds," *Chem Eng Sci*, vol. 267, 2023, doi: 10.1016/j.ces.2022.118357.

# Coupled CFD-DEM and PBM Framework for Wet Stirred Media Milling

Yeswanth S. Tanneru<sup>1,2,3,\*</sup>, Jan H. Finke<sup>1,2</sup>, Carsten Schilde<sup>1,2</sup>, Yogesh M. Harshe<sup>3</sup>, and Arno Kwade<sup>1,2</sup>

<sup>1</sup> Institute for Particle Technology, TU Braunschweig, Volkmaroder Straße 5, Braunschweig 38104, Germany

<sup>2</sup> Center of Pharmaceutical Engineering (PVZ), TU Braunschweig, Franz-Liszt-Straße 35A, Braunschweig, 38106, Germany

<sup>3</sup> Société des Produits Nestlé SA, Nestlé Research, Route du Jorat 57, Lausanne, 1000, Switzerland

**Abstract**— Wet Stirred Media Mills (WSMMs) are used in many industrial applications such as food, pharmaceutical and mineral processing for their ultra-fine grinding ability. Collisions in the system, such as bead-bead and bead-wall, cause breakage and particle size reduction in the slurry when product particles are caught in between the collision partners. A challenge with such systems is to identify the effective operating state for a given requirement, i.e., to maximize throughput at minimized specific energy consumption (which goes along with minimizing the product contamination by the wear from grinding media and mill internals). However, WSMMs are systems with several process parameters that affect the system performance, and only a limited information can be extracted via experimental analysis.

Numerical modelling such as coupled CFD-DEM simulations can be used to virtually represent the mill system, i.e., grinding chamber, grinding beads and slurry, to extract the quantitative information, i.e., stress energies of the collisions, stress frequency, the grinding bead distribution, and their velocities, etc. On this basis predictive population balance modelling (PBM) can be used to track the evolving particle size distribution of the product particles, with which the grinding state of the system at different intervals can be estimated. In the current work, we propose a framework to utilize the coupled CFD-DEM data as a machine function, which along with material information is given as an input to the PBM via an offline coupling approach.

**Keywords:** wet stirred media mills; CFD-DEM; population balance modelling; machine function; material function

## 1. Introduction

Mechanistic modelling can be applied to model and predict the fine grinding in Wet Stirred Media Mills (WSMMs). One of such mechanistic models, which was successfully applied for the ball milling application is the UFRJ mechanistic model [1]. Discrete Element Method (DEM), which serves as a function for machine behavior is used. The information from DEM, along with the material function (breakage behavior) is utilized by the population balance model (PBM) to evaluate the evolving particle size distribution (PSD).

In case of WSMM's, where grinding beads are dispersed in a fluid, DEM can be coupled with Computational Fluid Dynamics (CFD) to capture the multiphase physics i.e., to emulate the bead motion and thereby capture the collision-/stress energy distribution. An advantage of such mechanistic modelling approach is that it gives a scope for virtual process engineering i.e., the process parameter influence can be captured using a coupled CFD-DEM and PBM framework, which reduces the number of experimental trials.

## 2. Models and Methods

Fig. 1 shows the schematic of the mechanistic modelling approach followed in the present work.

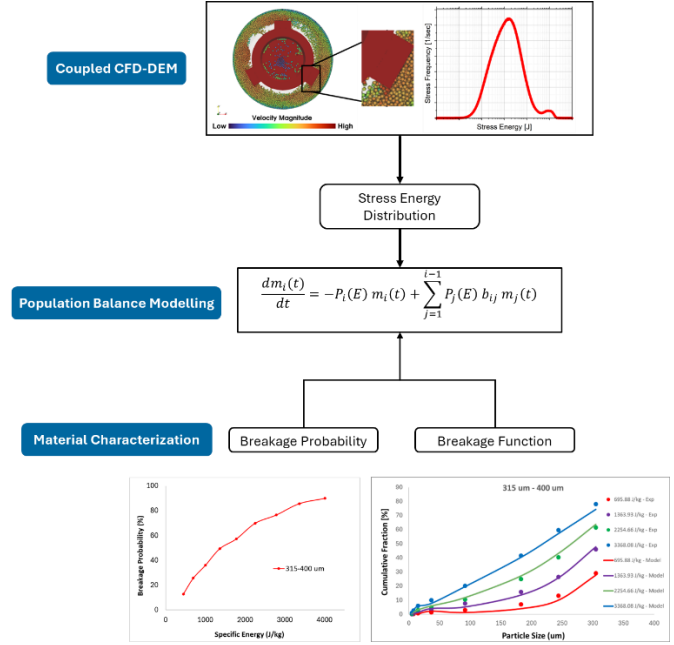


Figure 1. Schematic of the coupled CFD-DEM and PBM framework

### 2.1. Population Balance Modelling (PBM)

PBM in the current context, shown in (1) contains the breakage kernels which are ‘disappearance’ and ‘appearance’ terms of the particles in a batch system. The term ‘ $m_i$ ’ in the equation represents the mass of the  $i^{\text{th}}$  particle size in the system. The disappearance term signifies the mass lost in the class  $i$ , while the appearance term signifies the appearance of new mass in class  $i$  from classes  $j$  ( $j > i$ ).

$$\frac{dm_i(t)}{dt} = -P_i(E) m_i(t) + \sum_{j=1}^{i-1} P_j(E) b_{ij} m_j(t) \quad (1)$$

The term  $P(E)$  in (2) is the breakage probability with material parameter  $E_{50}$  and the machine parameter  $E$ . The convolution of the material and machine parameters for different particle classes and energy classes yields the breakage probability  $P(E)$ .

$$P(E) = \frac{1}{2} \left[ 1 + \operatorname{erf} \left( \frac{\ln E^* - \ln E_{50}}{\sqrt{2}\sigma^*} \right) \right]; E^* = \frac{E_{\max} E}{E_{\max} - E} \quad (2)$$

$$t_{10} = A \left[ 1 - e^{-b \frac{E}{E_{50}}} \right] \quad (3)$$

$$t_n(t_{10}) = \frac{100}{\int_0^1 x^{\alpha n-1} (1-x)^{\beta n-1} dx} \int_0^{t_{10}/100} x^{\alpha n-1} (1-x)^{\beta n-1} dx \quad (4)$$

$$B_{ij}(t_{10}) = B(x, t_{10}) = \operatorname{interp}(t_{10}, x) \quad (5)$$

$$b_{ij} = B_{i-1,j} - B_{i,j} \quad (6)$$

The term  $b_{ij}$  signifies the progeny distribution of particles in case of a breakage event i.e., how does the PSD of a given particle look after it has undergone breakage when a certain energy  $E$  is applied on it. To achieve this,  $t_{10}$ - $t_n$  approach, originally proposed by Narayanan and Whiten [2] is used. Equations (3), (4), (5) and (6) are used to reconstruct the progeny

distribution.  $A$ ,  $b$  are the fitting parameters in (3);  $\alpha_n$ ,  $\beta_n$  are the fitting parameters in (4) for user defined  $n$ -values, which sufficiently represent the progeny distribution.

## 2.2. Coupled CFD-DEM

To obtain the applied energy values ( $E$ ) i.e., the stress energy distribution which are one of the input parameters in (1) and (2), coupled CFD-DEM simulations are used. The obtained stress energy distribution with a given operating setting is used as the machine function.

The open-source software packages such as LIGGGHTS, OpenFOAM and CFDEMcoupling are used to simulate the grinding media motion in wet-operated stirred media mills. The unresolved coupling framework [3] is adopted in this work. In DEM, the Hertz-Mindlin contact model is used and the lubrication forces [4] are used in the non-contact model. Koch-Hill drag model is used, and the IB approach [5] is adopted to emulate the stirrer rotation on CFD domain. The  $k$ - $\varepsilon$  turbulence model was chosen to model the fluid turbulence. The simulation setup, modelling considerations, assumptions, and post-processing are detailed in [6].

## 3. Results and discussion

### 3.1. Fitting Parameters in Material Function

To fit the parameters in (2), (3) and (4), which define the material function, a model material of Calcium Carbonate (ESKAL) from KSL Staubtechnik GmbH was chosen. The particles of the material are sieved initially to obtain a narrow-sized distribution. Material breakage tests are performed on each sieved size using a centrifugal grinding device from Retsch (ZM 200). The tests are performed without sieving in the device, with an assumption that each particle introduced into the system is stressed with at least and exactly one high intensity collision with the rotating pins. The applied stress intensity on the particles is controlled by the rotation speed of the platform with pins. The specific energies are calculated using the tip speeds.

For parameter fitting, the breakage probabilities are calculated using the initial PSD (before breakage) and progeny distributions (after breakage, at different specific energies). The obtained breakage probability values are shown in Fig. 2. The  $E_{50}$  value of the particle class 314-400  $\mu\text{m}$  is then used to fit the  $A$  and  $b$  values in (3). Furthermore, the  $t_{10}$  values obtained using (3) are used to derive  $\alpha_n$  and  $\beta_n$  values in (4) for different  $n$ -values i.e., 1.2, 1.5, 4, 25, 50, 75. The obtained fitting parameters are used to represent the progeny distribution of other particle classes. The comparison of experimental and fitting results are shown in Fig. 3.

### 3.2. Coupled CFD-DEM Simulations

Fig. 4 shows the comparison of the stress energy distributions from DEM and coupled CFD-DEM simulations at same operating conditions. As it can be clearly seen that the simulations with DEM only have a less agitated system and doesn't yield a high stress frequency as compared to coupled CFD-DEM simulations. It can also be seen that the inclusion of the lubrication provided additional damping which resulted in a reduction in the stress frequency.

This shows that an adequate coupling along with other considerations like the inclusion of lubrication effect are necessary to obtain appropriate stress energy distributions [6]. Such stress energy distributions can be used as the machine function in the framework shown in Fig. 1.

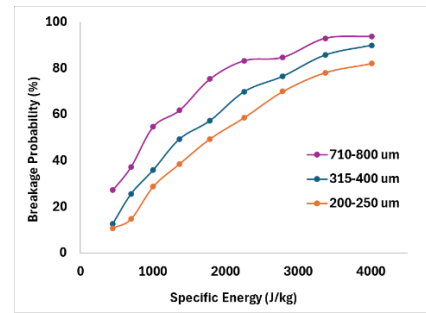


Figure 2. Breakage probabilities of ESKAL at various specific energies.

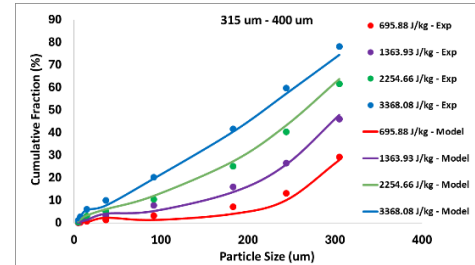


Figure 3. Comparison of progeny distributions, experimental vs model fit.

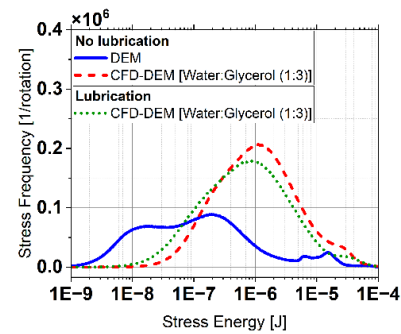


Figure 4. Stress energy distributions from DEM and coupled CFD-DEM.

## 4. Conclusion

A mechanistic framework is described in this study, to model the fine grinding in a WSMM. The coupled CFD-DEM simulations are proposed to derive the machine function (i.e., the stress energy distributions), which combined with the material function, can be used in PBM evolve the PSD.

## Acknowledgement

Thanks to the European Union's Horizon 2020 research and innovation programme who supported this work under the Marie Skłodowska-Curie grant agreement No 955661.

## References

- [1] Tavares, L. M., & Carvalho, R. M. (2010). A mechanistic model of batch grinding in ball mills. In XXV International Mineral Processing Congress (Vol. 1, pp. 1287-1297). AUSIMM Brisbane.
- [2] Narayanan, S. S. (1988). Determination of comminution characteristics from single particle breakage tests and its application to ball mill scale-up. Trans. Inst. Min. Metall. (Sec. C), 97, 115-124.
- [3] Kloss, C., Goniva, C., Hager, A., Amberger, S., & Pirker, S. (2012). Models, algorithms, and validation for opensource DEM and CFD-DEM. Progress in Computational Fluid Dynamics, an International Journal, 12(2-3), 140-152.
- [4] Kroupa, M., Vonka, M., Soos, M., & Kosek, J. (2016). Utilizing the discrete element method for the modeling of viscosity in concentrated suspensions. Langmuir, 32(33), 8451-8460.
- [5] Blais, B., Lassaingne, M., Goniva, C., Fradette, L., & Bertrand, F. (2016). A semi-implicit immersed boundary method and its application to viscous mixing. Computers & Chemical Engineering, 85, 136-146.
- [6] Tanneru, Y. S., Finke, J. H., Schilde, C., Harshe, Y. M., & Kwade, A. (2024). Coupled CFD-DEM simulation of pin-type wet stirred media mills using immersed boundary approach and hydrodynamic lubrication force. Powder Technology, 120060.



# Influence of particle shape on macroscopic rotational properties during shearing

Max Winkelmann<sup>1,2</sup>, Vanessa Magnanimo<sup>2</sup>, Stefan Luding<sup>2</sup>, and Stefanos-Aldo Papanicolopoulos<sup>1</sup>

<sup>1</sup> School of Engineering, The University of Edinburgh, Edinburgh, UK

<sup>2</sup> University of Twente, The Netherlands

**Abstract**— This study explores the influence of particle shape on macroscopic rotational properties in granular media, specifically focusing on the relationship between shape, rolling friction, and dissipation. The study uses Discrete Element Method (DEM) simulations within a planar split-bottom shear cell to analyse particles of different shapes, ranging from spherical to oblate or prolate forms. The question is: how do these shapes impact rotational behaviour at the macro scale?

**Keywords:** shape; rotations; dissipation; orientation;

## 1. Introduction

Granular media are made of discrete particles that interact with each other through normal and frictional contacts. Any change of properties at grain level, the microscale, affects the response of the material on the macro-scale. It has been shown that particle shape is one major factor that influences the rotational behaviour of the material [1, 2].

Through discrete-to-continuum (D2C) upscaling methods, the discrete particle data such as particle mass, particle velocity (momentum) and contact force can be mapped onto continuous fields like density, velocity, and stress. Following the approach by Goldhirsch [3] and Weinhart [4, 5], and using a smoothening function, we develop a D2C method to also transform particle properties related to rotations such as the discrete angular velocity, angular momentum, tangential forces, and contact torques to non-classical micropolar fields such as relative rotation, curvature, skew-symmetric stress, and couple stress.

Particles start to rotate when they are sheared, and hence those fields occur. On the example of a DEM simulation of a Cartesian (planar) split-bottom shear cell, we can understand via a parameter study the effect of microscopic contact parameters between spherical particles, namely that rolling friction is causing considerably strong relative rotation. Furthermore, the shape of particles plays a significant role for all micropolar phenomena such as relative rotation and non-classical stresses.

## 2. Methodology

We simulate a Cartesian (planar) split-bottom shear cell using the Discrete Element Method (DEM), with gravity pointing downwards. We populate the shear cell with approximately 20.000 particles. The walls are made of spherical particles and the simulation is periodic in the depth of the shear cell along the flow direction. We apply a constant shear velocity to the right wall and right bottom. A shear velocity with opposite sign is applied to the left wall and left part of the bottom. The shear velocity is chosen to be small to reach immediate steady state. The box is open and hence the granular material has a mostly horizontal free surface.

The shape of the particles is defined using the aspect ratio ( $\xi$ ), where  $\xi < 1$  represents oblate shapes,  $\xi = 1$  represents spherical shapes, and  $\xi > 1$  represents prolate shapes. The volume of the particles is kept the same for different shapes.

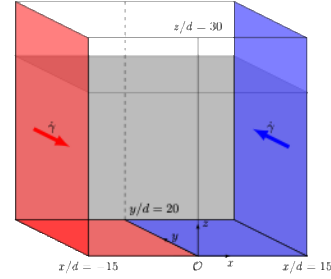


Figure 1. Schematic of the Cartesian (planar) split-bottom shear cell.

The discrete data is post-processed towards continuous fields using a D2C upscaling method using a smoothening function with a Gaussian kernel and a cut-off. The micro-rotation,  $\omega$ , is averaged using the discrete angular momentum of particles via

$$\omega(r) = \left( \sum_i I_i \phi(r - r_i) \right)^{-1} \cdot \sum_i I_i \cdot \omega_i \phi(r - r_i) \quad (1)$$

with  $I_i$  and  $\omega_i$  being the moment of inertia and angular velocity of particle  $i$ , respectively, while  $\phi(r - r_i)$  represents the smoothening kernel with  $r$  and  $r_i$  being the position vector and position of particle  $i$ , respectively.

The primary focus is on the relative rotation, defined as the difference between rotations in granular media on different scales (macro-rotation and micro-rotation) [6]. Macro-rotation represents the rotations of the surroundings as gradients (curl) of the velocity field. Micro-rotation represents the rotation of the particles around their own axis of rotation. Relative rotation serves as an objective measure of rotational kinematics and contributes to (angular) momentum exchange and dissipation via skew-symmetric stress (like strain and symmetric stress for translation). Hence, we define the upscaled relative rotation,  $h$ , as

$$h = w - \omega \quad (2)$$

with  $w$  being the axial vector to the skew-symmetric part of the continuum velocity gradient  $\nabla v$ . To compare the relative rotation for different shapes, we normalise it with the maximum macro-rotation in the flow profile which appears in the centre of the cell. In addition, we only consider rotations around the height axis because effects are stronger by several orders:

$$\widehat{h}_z = \frac{w_z - \omega_z}{\max w_z} \quad (3)$$

## 3. Key Findings

Particles far outside the centre are dragged along with the walls and the granular media does not rotate. Only in the centre of the shear cell, macro- and micro-rotation can be observed. Hence, relative rotation and all observed quantities can be found in this area as well. The comparison of the different particles shapes is done at heights of same pressure.



### 3.1. Effect of Rolling Friction and Shape

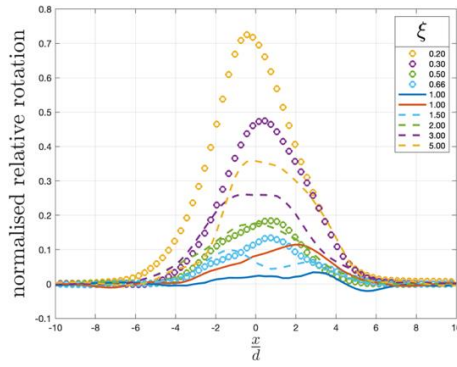


Figure 2. Normalised relative rotation,  $\hat{n}_z$ , along the width of the shear cell for different particle shapes: Prolates (dashed), spheres with rolling friction (solid red), spheres without rolling friction (solid blue), and oblates (circles). Corresponding aspect ratios are of the same colour.

Fig. 2 shows that rolling friction with  $k_r/k_n = 0.4, \mu_r$ , affects the rotational behaviour of spherical particles meaning that the relative rotation is stronger, and the micro-rotation is decreasing (solid lines) for  $\mu_r = 1$  (red). However, its influence is much smaller than the influence of particle shape (dashed lines for prolates and circles for oblates). The relative rotation is significantly increasing with the aspect ratio deviating from 1. High rolling friction of  $\mu_r = 1$  gives a relative rotation equal to those of particles with a small aspect ratio of  $\xi = \{0.66, 1.5\}$ . Furthermore, note that the exact shape is only relevant for particles that are strongly non-spherical ( $\xi < 0.5$  &  $\xi > 2$ ).

In all those cases of relative rotation, the rotation of the particles around their own axis of rotation (micro-rotation) is smaller than the rotation of the immediate surroundings which can lead to dissipation, as discussed next.

### 3.2. Effect of Elongation on Rotational Dissipation

Classically, symmetric stresses and strain rates are causing dissipation due to translation/shear. Analogously, relative rotation and non-symmetric stresses cause dissipation due to rotation. As shown before, shape dramatically influences rotational properties, thus leading to higher dissipation rates compared to spherical particles. Fig. 3 shows the dissipation due to rotation for spheres with rolling friction (solid lines) and elongated particles (dashed lines). It highlights a clear link between particle elongation and dissipation due to rotation, with dissipation increasing as particle shape becomes more elongated. Rolling friction for spheres (with the parameters used) might not be able to accurately represent the stronger dissipation due to large elongation.

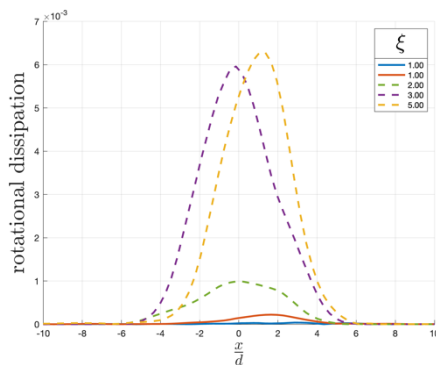


Figure 3. Dissipation due to rotation along the width of the shear cell for different particle shapes: Prolates (dashed), spheres with rolling friction (solid red), and spheres without rolling friction (solid blue).

## 4. Conclusion

Computing objective relative rotations allows us to understand rotations in granular media on different scales, from which micro-mechanisms they are caused, and how they influence dissipation. It demonstrates that particle shape, more than rolling friction, has a considerable influence on the rotational intensity of granular media, also causing stronger dissipation.

The studied shapes are rather simple. It is expected that more complex shapes could lead to even stronger effects – promoting the importance of shape and rotations in granular media.

This method can be used in future applications for the formulation of extended constitutive equations with respect to rotations. Furthermore, a study on contact fabric anisotropy is ongoing.

## Acknowledgement

This research is part of the project TUSAIL (Training in Upscaling Particle Systems: Advancing Industry across Length-scales, <https://tusail.eu>) and has received funding from the European Horizon2020 Framework Programme for research, technological development and demonstration under grant agreement ID 955661.

## References

- [1] Rorato, R., Arroyo Alvarez de Toledo, M., Andò, E.C.G. *et al.* Linking shape and rotation of grains during triaxial compression of sand. *Granular Matter* **22**, 88 (2020). <https://doi.org/10.1007/s10035-020-01058-2>
- [2] Ali, U., Kikumoto, M., Ciantia, M. *et al.* Systematic effect of particle roundness/angularity on macro- and microscopic behavior of granular materials. *Granular Matter* **25**, 51 (2023). <https://doi.org/10.1007/s10035-023-01341-y>
- [3] Goldhirsch, I. Stress, stress asymmetry and couple stress: from discrete particles to continuous fields. *Granular Matter* **12**, 239–252 (2010). <https://doi.org/10.1007/s10035-010-0181-z>
- [4] Thomas Weinhart, Remco Hartkamp, Anthony R. Thornton, Stefan Luding; Coarse-grained local and objective continuum description of three-dimensional granular flows down an inclined surface. *Physics of Fluids* 1 July 2013; **25** (7): 070605. <https://doi.org/10.1063/1.4812809>
- [5] Thomas Weinhart, Carlos Labra, Stefan Luding, Jin Y. Ooi, *Influence of coarse-graining parameters on the analysis of DEM simulations of silo flow*, *Powder Technology* **293**, 138-148 (2016). <https://doi.org/10.1016/j.powtec.2015.11.052>.
- [6] Jean Sulem, Ioannis Vardoulakis, *Bifurcation Analysis in Geomechanics*. Bifurcation Analysis in Geomechanics (1st ed.), CRC Press. (1995) <https://doi.org/10.1201/9781482269383>

# Upscaling mixing in rotating drum simulations

Balázs Füvesi<sup>1,2</sup>, Christoph Goniva<sup>2</sup>, Vanessa Magnanimo<sup>1</sup>, Stefan Luding<sup>1</sup>

<sup>1</sup> University of Twente, Enschede, Netherlands

<sup>2</sup> DCS Computing GmbH, Linz, Austria

**Abstract**— Mixing and segregation processes of granular materials are important and common steps in various industrial processes. The discrete element method is widely used to model granular flows and optimise particulate processes. Since it treats discrete particles, tracking their motion and collisions, it requires many particles, leading to high computational costs, making its usage impractical for large scale industrial applications.

Coarse graining presents a potential solution. This method replaces collections of small primary particles with larger virtual particles, significantly reducing the number of particles and computational load. However, applying it to mixing and segregation processes poses specific challenges, as the aim is to capture effects associated with the original, fully resolved particles.

Mixing in a rotating drum is studied with increasing coarse graining factors, across three operational regimes – rolling, cascading, and cataracting – to achieve flows with increasingly dynamic behaviour. Using 12 different mixing indices from three categories: grid-, contact-, and distance-based, mixing features and results are compared, across coarse graining factors and regimes.

Maintaining consistent mixing evaluation with coarse graining is more reliable in the rolling and cascading regimes but is more challenging in the cataracting regime. Higher coarse graining ratios, can be used with mixing indices less sensitive to coarse graining, enabling more significant reductions in simulation costs.

**Keywords:** discrete element method; coarse graining; rotating drum flow regimes; mixing index;

## 1. Introduction

Coarse graining (CG) applied to the discrete element method (DEM) [1] is a useful technique that can help simulating, and therefore optimising, mixing and segregation devices and processes on industrial scales. A variety of mixing indices [2] were derived to quantify the mixing in these devices, and studies [4,5] were conducted to compare some of their properties and test their effectiveness. Different CG models were proposed and investigated for mixing in rotating drums [5-7].

However, previous mixing index comparisons focus on mixing in unscaled simulations and in rotating drum studies considered the rolling regime only. There is a lack of investigations to compare mixing indices in coarse grained simulations combined with different regimes, where the system has both dense and dilute regions, as in the cataracting regime.

Therefore, we study the preservation of mixing and segregation features of the original scale drum simulation, in different operational regimes, and as the CG ratio increases.

## 2. Methodology

### 2.1. Discrete Element Method and Coarse Graining

We use Asphex 6.4.0 commercial DEM software, which comes with a wide variety of contact models and implemented methods. We use Hertz contact model, as it is scale independent with CG [8]. For up-scaled simulations we use the implemented

coarse graining command to set the CG ratio from 2 to 5, and compare with the original CG=1.

### 2.2. Rotating Drum Setup

We use a rotating drum to study particle mixing in different dynamic conditions.

The rotating drum diameter and depth/length are  $D=1.0$  m and  $L=0.4$  m respectively. We use a periodic boundary condition in the axial L-direction. We add wedges along the cylindrical wall of the drum to avoid particles sliding along the walls, especially at higher rotational speeds. There are 128 wedges with their inner angle being 90 degrees.

The particles and the drum have the same material, with material properties shown in Table I., set to represent glass like material and glass beads [9]. We only colour the particles differently based on their initial positions to make the two groups visually distinguishable. In the mixing cases, they are monodisperse with 4 mm diameter in the original scale. In the segregation cases, they are bidisperse with 3.8 and 4.2 mm diameter in the original case, which is enough to induce size-based segregation.

TABLE I. DEFAULT MATERIAL PROPERTIES

Youngs modulus	$63 \cdot 10^6$ Pa
Poissons ratio	0.21
Coefficient of restitution	0.95
Coefficient of friction	0.4
Density	2500 kg/m <sup>3</sup>

To achieve different dynamic conditions, we set the drum rotational speed to 5, 15, and 35 RPM for rolling, cascading, and cataracting regimes, respectively, as shown in Fig. 1 at the same time, 10 s of the original scale simulation. To avoid a sudden spike in acceleration, a continuous 3rd order smooth step function gradually increases the rotational speed to the desired level during the initial 1 second.

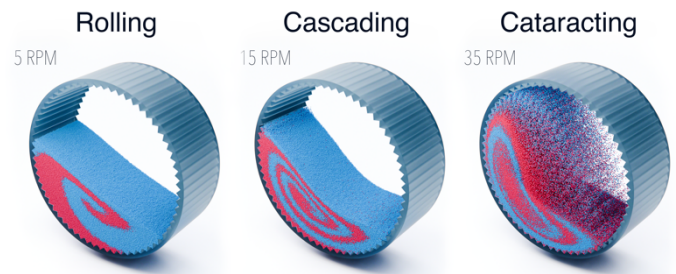


Figure 1. Mixing in rotating drum in three regimes – rolling, cascading, and cataracting – at 10 s of the original scale simulation.

## 3. Comparisons

### 3.1. Continuous fields and flow pattern

We average the discrete particle data along the axial direction of the drum with discrete to continuum mapping [10], yielding continuous fields, which allows us to compare the across the different CG ratios.

Fig. 2 shows the volume fraction of the original and CG simulations in the three regimes. We observe that the contour lines corresponding to the different CG ratios in the rolling and cascading regimes are very similar, with small differences in the lower right corner, where the avalanching particles meet the wall. However, the contour lines in the cataracting regime become increasingly different as the CG ratio increases. This suggest that the used contact model and CG method works satisfactory in the dense rolling and cascading regimes, but cannot represent well the original system in the dilute and more dynamic cataracting regime. We can make similar observations and conclusion when we compare the velocity fields and flow patterns, not included here for brevity.

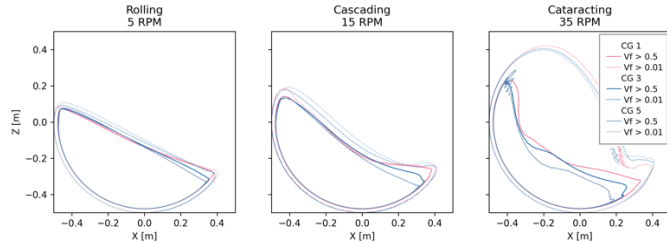


Figure 2. Volume fraction in the three regimes as CG ratio changes.

### 3.2. Mixing indices

Next, the mixing indices' consistency in different regimes are compared and properties are tested for different CG ratios.

Although we observe (no data shown here) small differences in the transient of the rolling and cascading regimes, the MIs stay mostly consistent and converge to the same steady-state value. However, there are greater differences in the cataracting regime, since the continuous fields and flow patterns are already different as the CG ratio changes.

Next, without including an exhaustive list, we would like to highlight a couple of our observations when comparing the different indices in the rolling regime. Fig. 3 shows two sets of mixing curves corresponding to two grid-based indices, the Lacey index (LI) and the mixing entropy (ME). We observe the mixing curves corresponding to the Lacey index are noisier compared to the ME. This is because the Lacey index is calculated from the particle fractions in the samples uniformly, whereas for ME, the contributions of the local entropies to the global entropy are weighted by the number of particles present in the samples. This weighting apparently helps to reduce the noise, especially at higher CG ratios.

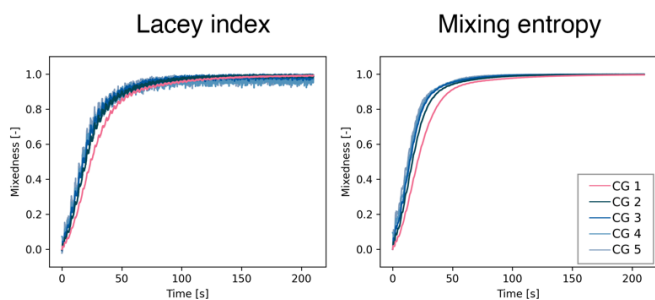


Figure 3. Lacey index and mixing entropy in rolling regime for different CG.

Fig. 4 shows two sets of mixing curves corresponding to the grid-based mixing entropy index. On the left it is evaluated with a fixed number of samples, on the right the number of samples is adjusted as the CG ratio changes to keep the number of particles per sample consistent. By comparing the two sets, we observe that with fixed number of samples the curves are different and converge to different values, but with adjusted sample numbers they stay similar and converge to the same value, although there are small differences in the transient as

discussed earlier. Therefore, adjusting the number of samples is necessary to achieve consistent mixing evaluation across CG.

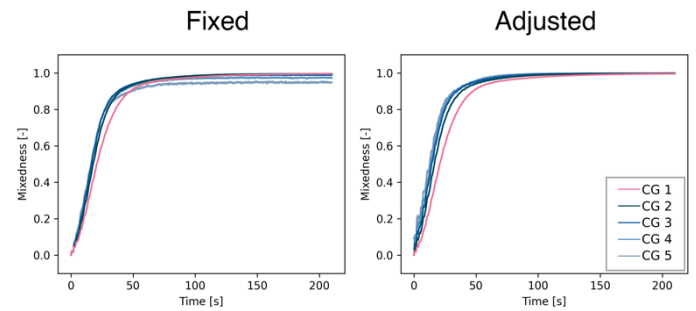


Figure 4. Mixing entropy in rolling regime, with fixed vs. adjusted number of samples for different CG.

## 4. Conclusion

In conclusion by comparing the continuous fields and flow patterns corresponding to different CG ratios in three regimes, we observed that they stay similar across the investigated CG ratios in rolling and cascading regimes, however, they differ in the most dynamic, cataracting regime. Therefore, we are planning further investigations with different upscaling rules.

As conclusion, each index has different advantages, disadvantages and properties. Down-weighting the contribution of samples containing fewer particles, helps to reduce the noise, especially at higher CG ratios. To allow consistent mixing evaluation, we recommend adjusting the number of samples taken according to the CG ratio, to keep the number of particles per sample similar across CG ratios.

Future work could involve other systems with more complex boundaries, or other flow regimes.

## Acknowledgement

This research is part of the project TUSAIL (Training in Upscaling Particle Systems: Advancing Industry across Length-scales, <https://tusail.eu>) and has received funding from the European Horizon2020 Framework Programme for research, technological development and demonstration under grant agreement ID 955661.

## References

- [1] P. A. Cundall and O. D. L. Strack, 'A discrete numerical model for granular assemblies', *Géotechnique*, 1979, doi: 10.1680/geot.1979.29.1.47
- [2] M. Poux, P. Fayolle, J. Bertrand, D. Bridoux, and J. Bousquet, 'Powder mixing: Some practical rules applied to agitated systems', *Powder Technology*, 1991, doi: 10.1016/0032-5910(91)80047-M.
- [3] Y. Wen, M. Liu, B. Liu, and Y. Shao, 'Comparative Study on the Characterization Method of Particle Mixing Index Using DEM Method', *Procedia Engineering*, 2015, doi: 10.1016/j.proeng.2015.01.299.
- [4] P. Bhalode and M. Ierapetritou, 'A review of existing mixing indices in solid-based continuous blending operations', *Powder Technology*, 2020, doi: 10.1016/j.powtec.2020.06.043.
- [5] R. Cai and Y. Zhao, 'An experimentally validated coarse-grain DEM study of monodisperse granular mixing', *Powder Technology*, 2020, doi: 10.1016/j.powtec.2019.10.023.
- [6] Y. Kosaku, Y. Tsunazawa, and C. Tokoro, 'Investigating the upper limit for applying the coarse grain model in a discrete element method examining mixing processes in a rolling drum', *Advanced Powder Technology*, 2021, doi: 10.1016/j.appt.2021.08.039.
- [7] A. V. Patil, J. Hofsteenge, J. M. Bujalski, and S. T. Johansen, 'DPM model segregation validation and scaling effect in a rotary drum', *Comp. Part. Mech.*, 2022, doi: 10.1007/s40571-021-00438-6.
- [8] C. Bierwisch, T. Kraft, H. Riedel, and M. Moseler, 'Three-dimensional discrete element models for the granular statics and dynamics of powders in cavity filling', *Journal of the Mechanics and Physics of Solids*, 2009
- [9] J. H. Kasper, V. Magnanimo, and A. Jarray, 'Dynamics of discrete wet granular avalanches in a rotary drum', *DEM8*
- [10] T. Weinhart, R. Hartkamp, A. R. Thornton, and S. Luding, 'Coarse-grained local and objective continuum description of three-dimensional granular flows down an inclined surface', *Physics of Fluids*, 2013, doi: 10.1063/1.4812809



# Mixed discrete–continuum modelling of dense granular flow

Akhil Mathews<sup>1</sup>, Hongyang Cheng<sup>2</sup>, Miguel Angel Celigueta<sup>3</sup>, Stefanos Papanicolopoulos<sup>1</sup>, and Jin Y. Ooi<sup>1</sup>

<sup>1</sup>University of Edinburgh; <sup>2</sup>University of Twente; <sup>3</sup>Altair EDEM

**Abstract—** This work presents a mixed discrete-continuum framework combining Discrete Element Methods (DEM) with Finite Element Methods (FEM) to model dense granular flows more efficiently. By coupling DEM with FEM, the approach balances computational efficiency and accuracy, ideal for large particle systems. A key feature is an overlapping zone where weighting functions ensure smooth load transfer and kinematic compatibility between the two domains. The study examines axial force transfer in cubic packing, assessing the impact of weighting functions and penalty parameters on stress and strain fields. The focus is to create the right hybrid-system-response compared to the ground truth (DEM) simulation. This hybrid model enhances the efficiency of large-scale industrial process simulations by significantly reducing computational time while maintaining high accuracy.

**Keywords:** DEM-FEM coupling; Hybrid modelling; Dense granular flows; Continuum-discrete; Computational efficiency

## 1. Introduction

Discrete Element Methods (DEM) are renowned for their precision in capturing the dynamics of particle systems, yet they demand substantial computational resources, particularly in simulations involving extensive particle counts. Dense granular flows can be characterized by zones of either stagnation or mass flow, which are readily approximated using continuum models, whereas regions of high shear flow necessitate the Lagrangian perspective offered by DEM to accurately capture the complex behaviour within these high shear regimes. Integrating continuum models with DEM represents a strategic approach to mitigating simulation time while preserving the detailed accuracy essential for comprehensive analysis especially as many particle systems in the real world involve large number of particles [1].

In this work, we present a mixed discrete-continuum framework for modelling dense granular flows using DEM and continuum mechanics through a DEM-FEM (Finite Element Method) coupling model [2,3]. This method significantly enhances computational efficiency without reducing accuracy, making it ideal for simulations involving numerous particles. The approach, depicted in Figure 1, features a DEM-FEM coupled simulation with an overlapping zone that integrates the continuum and DEM models using appropriate weighting functions. By penalizing the differences in displacements between the two domains, kinematic compatibility is maintained.

The research involved an in-depth analysis of the hybrid model response and comparing it with ground truth (DEM) simulation. The problem setup enforced the one-dimensional force transfer in the axial direction, facilitated by cubic packing of spherical particles within a rigid, frictionless container. The verification example with an exact solution allows the influence of the penalty parameter and the weighting function on the computed stresses and strains to be assessed with confidence.

This hybrid modelling technique promises to enhance the efficiency of large-scale industrial process predictions. Furthermore, we investigate discrepancies between ground truth DEM and the developed hybrid simulations, exploring effective strategies to reconcile these differences.

## 2. Methodology

To couple both DEM and FEM, the two domains are superimposed as shown in Fig. 1. The hybrid domain separating the DEM and FEM regions are modelled using a combined virtual work equation that weights the energy and mass distribution in the hybrid domain [1]; ensuring the total energy and mass does not exceed the ground truth model. A penalty parameter  $\epsilon$  is used to penalize the displacement difference between DEM and FEM in the hybrid zone. The virtual work of the hybrid model is equal to the weighted sum of the work done by the sub-models plus the work done by the penalty term, which can be expressed as  $\delta W = \delta W^{\text{FE}} + \delta W^{\text{DE}} + \delta W^{\text{C}}$ . To weight the virtual work done in the DEM model  $\delta W^{\text{DE}}$ , a smooth and continuous function  $w(\vec{x})$  of the particle position  $\vec{x} \in \Omega^{\text{H}}$  is used. This function increases monotonically from zero on  $\partial\Omega^{\text{FE}} \cap \Omega^{\text{H}}$  to one on  $\partial\Omega^{\text{DE}} \cap \Omega^{\text{H}}$ . The virtual work done in the FEM model  $\delta W^{\text{FE}}$  is weighted by the function  $1-w(\vec{x})$ , such that the coupling weights on the FEM and DEM sides sum to unity at any given location. The coupled governing equations are also adjusted by the corresponding coupling weights. In the equations shown,  $N_{\text{p}}$  is the total number of discrete particles. The short-hand notation  $w_{\alpha} = w(\vec{x}_{\alpha})$  and  $w_{\alpha\beta} = w(\vec{x}_{\alpha}\vec{x}_{\beta})$  is used for the weights at the particle positions and contact points.  $\delta \vec{x}_{\alpha}$  is a variation of the position of particle  $\alpha$ .  $\vec{b}^{\text{C}}$  is the FEM coupling force density (2) and  $\vec{f}^{\text{C}}_{\alpha}$  is the DEM coupling force [3].

$$\begin{aligned} \delta W = & \int_{\Omega^{\text{FE}}} (1-w) \left\{ \sigma : \delta \epsilon - \left( \vec{b} - \rho \frac{\partial^2 \vec{X}}{\partial t^2} \right) \cdot \delta \vec{X} \right\} dV \\ & + \int_{\Gamma^{\text{FE}}_{\vec{x}}} \vec{t} \cdot \delta \vec{X} dA + \int_{\Omega^{\text{FE}}} \vec{b}^{\text{C}} \cdot \delta \vec{X} dV \\ & + \sum_{\alpha=1}^{N_{\text{p}}} \left[ w_{\alpha} \left( m_{\alpha} \frac{d^2 \vec{x}_{\alpha}}{dt^2} - \vec{f}^{\text{b}}_{\alpha} \right) \cdot \delta \vec{x}_{\alpha} - \sum_{\beta}^{N_{\alpha}} w_{\alpha\beta} \vec{f}_{\alpha\beta} \cdot \delta \vec{x}_{\alpha} \right] \end{aligned} \quad (1)$$

$$\begin{aligned} & - \sum_{\alpha=1}^{N_{\text{p}}} \vec{f}^{\text{C}}_{\alpha} \cdot \delta \vec{x}_{\alpha}, \\ \vec{b}^{\text{C}} = & \epsilon (\vec{u}^{\text{DE}} - \vec{u}^{\text{FE}}), \end{aligned} \quad (2)$$

$$\vec{f}^{\text{C}}_{\alpha} = -\epsilon \sum_{i=1}^N \sum_{j=1}^N \Pi_{i\alpha} \int_{\Omega^{\text{C}}} \psi_i \psi_j dV (\vec{u}_j^{\text{DE}} - \vec{u}_j^{\text{FE}}). \quad (3)$$



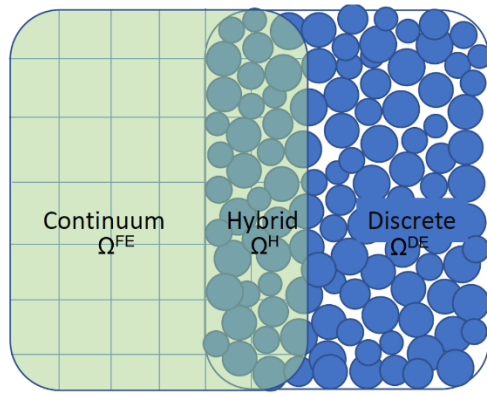


Figure 1. The schematic of the discrete continuum coupling domain.

### 3. Granular column setup

The verification test problem setup is as shown in Fig. 2. Modelling granular material using FEM involves calibrating the parameters used in the constitutive relations from the ground truth (DEM) simulations. For an isotropic linear elastic constitutive model there are 2 elastic constants that needs to be calibrated; which are Poisson's ratio and Young's modulus. In this verification test problem, the particles are mono-disperse, has no friction and the loading is purely uniaxial from the top, hence Poisson's ratio is assumed to be 0 in the continuum. The Young's modulus can be calculated by equating the equivalent stiffness of the particles and the continuum. Also, the density of the ground truth DEM particles needs to be coarse grained to match with the density of the FEM material specification.

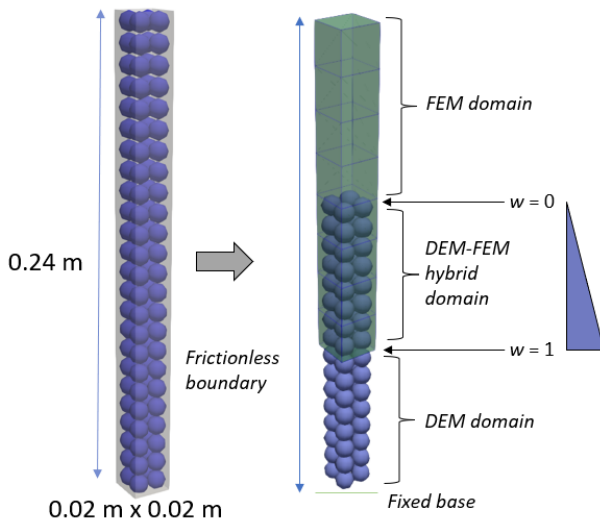


Figure 2. Showing ground truth simulation domain and the equivalent hybrid domain.

### 4. Results

The compressive stress and strain behaviour of the granular column was analysed following the application of a small displacement at the top. In the hybrid domain as shown in Fig. 3, stress computation was influenced by the weighting functions applied at each location. In the FEM region, the stresses were calculated by multiplying the stress values by the corresponding weights at the respective location. In the DEM region, stresses were determined based on the volume of the element containing the particles. The combined stress in the hybrid model was obtained by adding the DEM and FEM stresses. This combined stress closely matched the results from the ground truth DEM simulations.

The strain distribution in the hybrid model remained relatively constant across the domain, indicating consistency in the hybrid formulation. The penalty parameter ( $\epsilon$ ) significantly impacted the stress magnitude across the domain. A lower penalty value results in a more uniform stress profile, but under-predicts the overall stress magnitude i.e. lower than that of the ground truth DEM. Conversely, a higher penalty parameter led to a more non-uniform stress in the hybrid zone and an overshooting of the expected stress values. In this study, a penalty value of  $\epsilon = e^9$  provided the best agreement with the DEM ground truth stresses.

The effect of weighting on stress distribution was also explored. It was observed that the stress became increasingly non-uniform in the hybrid zone when the weighting was applied more abruptly. This behaviour also influenced strain distribution; abrupt changes in weights, for example from 1 to 0.5 resulted in non-uniform strains in the hybrid zone. A gradual weighting factor range between 0.01 and 0.99 was found to be a good approximation for maintaining consistency in stress and strain distribution within the domain.

Overall, the findings indicate that the choice of penalty parameter and weighting functions plays a critical role in determining the accuracy and uniformity of stress and strain profiles within the hybrid model.

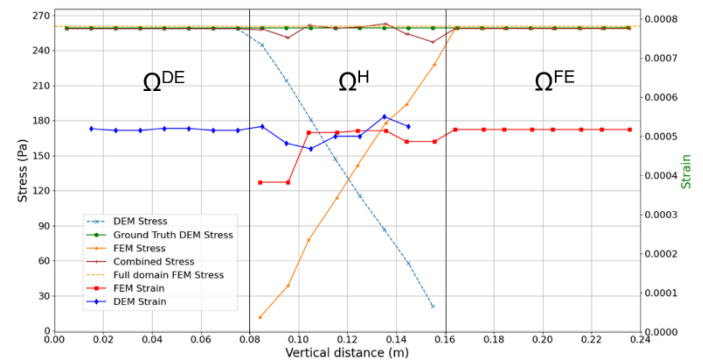


Figure 3. Shows the compressive stress and strain profile in the hybrid model. The x axis shows the vertical distance of the column starting from 0 m at the bottom. A penalty ( $\epsilon$ ) of  $e^9$  and weighting of 0.01 to 0.99 is used.

### Acknowledgement

This project has received funding from the European Union's Horizon 2020 research and innovation programme under the Marie Skłodowska-Curie grant agreement No 955661 (TU SAIL ITN, <https://tusail.eu/>).

### References

- [1] Hongyang Cheng, Anthony R Thornton, Stefan Luding, Andrew L Hazel, and Thomas Weinhart. Concurrent multi-scale modeling of granular materials: Role of coarse-graining in FEM-DEM coupling. *Computer Methods in Applied Mechanics and Engineering*, 403:115651, 2023.
- [2] Christian Wellmann and Peter Wriggers. A two-scale model of granular materials. *Computer Methods in Applied Mechanics and Engineering*, 205:46–58, 2012.
- [3] Chen, Peter Yichen, et al. "Hybrid discrete-continuum modeling of shear localization in granular media." *Journal of the Mechanics and Physics of Solids* 153 (2021): 104404.

# Coarse-grained DEM modelling of wet granulation drum process

R. Saghafian Larijani, V. Magnanimo, and S. Luding

University of Twente, Enschede, The Netherlands

**Abstract**— Discrete Element model (DEM) is a reliable tool for obtaining useful micro- and macro-scale data about particulate processes, including wet particle systems. However, it is computationally expensive when it comes to industrial scale systems with millions of particles. Coarse-graining (CG) is an upscaling approach in which groups of particles are represented by larger meso-particles, resulting in a significant improvement of DEM efficiency. It is important to consider appropriate scaling rules that account for the underlying physics of the system.

We compare two different scaling approaches for wet particle systems in a rotating drum namely Weber (We)-based and Bond (Bo)-based scaling. The results suggest that the We-based scaling can better reproduce the system's flow behaviour.

Using We-based scaling, we investigate the impact of coarse-graining on granulation, focusing particularly on the granule size distribution (GSD). Subsequently, we analyse and compare the granule size distributions across coarse-grained discrete element method (CG-DEM) simulations. The results suggest that the size distribution of the granules in the original particle system could be potentially predicted from the size distribution of an upscaled CG system.

**Keywords:** Coarse graining; Discrete Element Model (DEM); Wet particles; Granule size distribution (GSD)

## 1. Introduction

Wet granulation is an important process in various industries due to the enhancement of properties, including bulk flowability and particle strength [1]. In this process, liquid binder is added to the powder under shear, and the wet particles start to cluster into granules. Material and process parameters influence the micro-scale phenomena underlying wet granulation, and, in turn, the final characteristics of the granules. Experimental investigation of granulation across multiple scales is important though extremely challenging [2].

DEM [3] is widely used for the simulation of granular systems. However, high computational cost is a major drawback. To increase the efficiency of the simulations, it is possible to use coarse-grained (CG) particles which have  $n$ -times larger diameter than the original ones. This approach has a bifold effect on the computation, namely the number of particles reduces a lot, and the numerical time-step increases [4,5]. However, appropriate scaling rules should be considered in the CG model in order to reproduce the behaviour of the original particle systems accurately.

To upscale wet systems, Chan and Washino [6] proposed a quadratic scaling ( $n^2$ ) of the inter-particle particle forces in a vertical mixer and showed the validity of the CG-model for predicting the mixing behaviour. Four different scaling strategies for cohesive wet powders within a gas-solid fluidized bed were evaluated by Tausendschön et al. [7]. These strategies include dimensionless overlap-based, stress-based, and coefficient of restitution-based scaling (all resulting in  $n^2$  scaling of interparticle forces), as well as Bond number-based scaling, which leads to  $n^3$  scaling of interparticle forces, so that the Bond

number-based scaling results in an over-prediction of the cohesive force. Jarray et al. [8] validated the Weber-based scaling ( $n^2$ ) experimentally by using different size glass beads and tunable capillary forces.

To our knowledge, the effect of CG-DEM modelling on the granule size distribution has not been sufficiently investigated. In this study, firstly, scaling rules based on Weber and Bond numbers are compared. Then, using the appropriate Bo-based scaling, as resulting from the comparison, the applicability of the CG modelling for the prediction of granule sizes and their distribution is studied.

## 2. Modelling

YADE open-source DEM modelling framework [9] is used for the simulations in a drum granulator with 0.2 m diameter and 0.06 m length, with a periodic boundary in axial direction.

To compare the We- and Bo-based scaling rules, 360000 monodisperse particles with diameter 0.001 m are used as original (primary) particles. 48 lifters (baffles) of 0.001 m height are added to drum to avoid wall slip. To avoid ordering effects and to investigate the effect of CG on the size distribution of the formed granules, polydisperse spherical particles are used, with 80% of the particles having 0.001 m diameter ( $d$ ) and 20% having  $0.001 < d < 0.004$  m, and the geometry of the drum is varied in terms of the number and height of the baffles.

Furthermore, graph analysis is adopted to identify the granules, via the “Networkx” library in Python [10]. Following the study by Dong et al. [11], the particle contacts are filtered based on criteria related to the cohesive force and the angle between the velocity vectors of the colliding and contacting particles. Using a Breadth-First Search (BFS) algorithm for the filtered contacts, the granules are identified, and their volumes are reported.

## 3. Results

### 3.1. Comparing We and Bo-based scaling

Initially the scaling approaches based on constant Weber number (We) and constant Bond number (Bo) are compared. The former is given by the ratio between the inertial and capillary forces, as

$$\text{We} = \frac{\rho_p R v^2}{\gamma \cos\theta}, \quad (1)$$

where  $R$  is the particle radius,  $\rho_p$  is the particle density,  $v$  is the estimated velocity of the flowing particles,  $\gamma$  is the liquid surface tension, and  $\theta$  is the solid-liquid contact angle. On the other hand, the Bond number is the ratio between cohesion and gravity forces:

$$\text{Bo} = \frac{3\gamma \cos\theta}{2R^2 g \rho_p}. \quad (2)$$

Based on such non-dimensional numbers, interparticle contact and liquid bridge forces can be upscaled in the CG simulation to

maintain flow properties consistent with the original unscaled system [12], where  $We$  and  $Bo$  lead to the quadratic ( $n^2$ ) and cubic ( $n^3$ ) force scaling, respectively.

Figure 1 shows a comparison between the granular flow in the rotating drum for the original particles and two cases with particles upscaled to CG3, i.e., particle radius three times larger, based on  $We$  and  $Bo$  scaling. As shown, the bed flow behaviour does not show a good agreement when the  $Bo$ -based scaling is used. In fact, the  $n^3$  scaling of the inter-particle forces leads to overly large attractive forces and the formation of one big cluster in the drum. On the other hand,  $We$ -based scaling, properly reproduces the flow behaviour as well as the velocity profile of the particles (data not shown here, see [12]). Therefore,  $We$ -based upscaling is adopted in the following.

For a more detailed comparison of the rheological behaviour of the  $We$ -based CG and the original particle systems, involving several continuum fields, the reader is referred to [12].

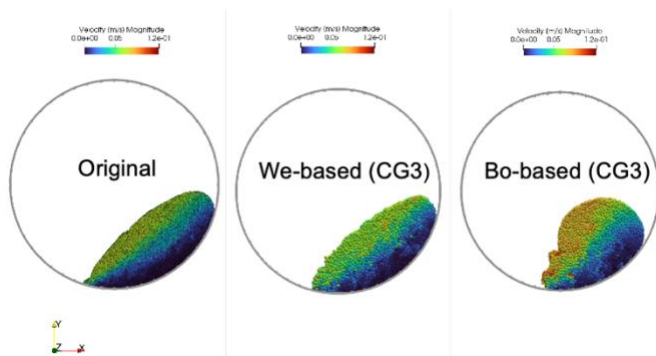


Figure 1. Comparing the  $We$  and  $Bo$ -based scaling in a rotating drum.

### 3.2. Effect of CG on the GSD

To investigate the effect of CG modelling on the size distribution of the granules, the Same Statistic Weight (SSW) approach is used for the poly-disperse system, in which the shape of the particle size distribution (PSD) of the CG particles remains identical to that of the original particles [13].

Figure 2 presents a snapshot of the CG1 (original particles) and  $We$ -based CG2, i.e., particles twice larger than the original ones and forces scaled with  $n^2$  in the drum granulator. As shown, the flow behaviours of the granulated system as well as the particle velocities (colour code) seem to be well captured in the CG2 system.

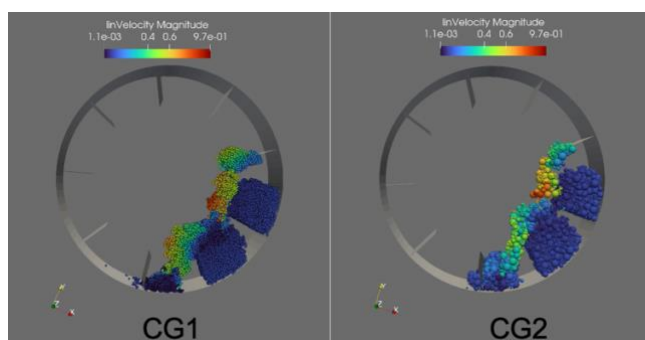


Figure 2. Snapshots of the drum granulator with CG1 and CG2 particles.

Using the granule identification approach [10], the GSD of the CG1 and CG2 systems are compared [12]. The results suggest that for the granules smaller than a limit of  $1.4 \times 10^{-7} \text{ m}^3$ , via scaling down the size of the formed granules in CG2 system by  $n^3$  times, the GSD of the original particles can be estimated (with an error  $< 15\%$ ). However, for granules larger than this limit, the size distribution of the CG2 granules does not

reproduce the size distribution of the CG1 granules appropriately (error  $> 30\%$ ), possibly due to an insufficient number of particles in the CG2 systems, and loss of information and poor statistics as a result.

## 4. Conclusion

We studied wet particles flow and granulation in a rotating drum using coarse grain DEM. Upscaling based on the  $We$  number corresponds to a quadratic scaling of the interparticle forces, and could reproduce the flow behaviour of the particles, whereas  $Bo$ -number based scaling could not. When using appropriate scaling rules for the physics in the system, CG-DEM is a good compromise between the accuracy and the computational efficiency of the DEM simulation.

Moreover, by using the appropriate  $We$ -based scaling, as preliminary result, the GSD of granulated particles under shear could be reproduced in the CG2 system for the granules smaller than a limit, above which statistics is too poor. The prediction of the full GSD could be possibly improved by assuring sufficient statistics, i.e., sufficient CG particles or ensembles, in the upscaled system, which is the subject of our future studies.

## Acknowledgement

This research is part of the project TUSAIL (Training in Upscaling Particle Systems: Advancing Industry across Length-scales, <https://tusail.eu>) and has received funding from the European Horizon2020 Framework Programme for research, technological development and demonstration under grant agreement ID 955661.

## References

- [1] P. Suresh, I. Sreedhar, R. Vaidhiswaran, and A. Venugopal, "A comprehensive review on process and engineering aspects of pharmaceutical wet granulation," 2017, *Elsevier B.V.* doi: 10.1016/j.cej.2017.07.091.
- [2] V. De Simone, D. Caccavo, G. Lamberti, M. d'Amore, and A. A. Barba, "Wet-granulation process: phenomenological analysis and process parameters optimization," *Powder Technol.*, vol. 340, pp. 411–419, Dec. 2018, doi: 10.1016/j.powtec.2018.09.053.
- [3] P. A. Cundall and D. L. Strack, "A discrete numerical model for granular assemblies," *Geotechnique*, vol. 29, no. 1, pp. 47–65, 1979.
- [4] M. Sakai and S. Koshizuka, "Large-scale discrete element modeling in pneumatic conveying," *Chem Eng Sci*, vol. 64, no. 3, pp. 533–539, Feb. 2009, doi: 10.1016/j.ces.2008.10.003.
- [5] S. Radl, C. Radeke, J. G. Khinast, and S. Sundaresan, "parcel-based approach for the simulation of gas-particle flows," 2011.
- [6] E. L. Chan and K. Washino, "Coarse grain model for DEM simulation of dense and dynamic particle flow with liquid bridge forces," *Chemical Engineering Research and Design*, vol. 132, pp. 1060–1069, Apr. 2018, doi: 10.1016/j.cherd.2017.12.033.
- [7] J. Tausendschön, J. Kolehmainen, S. Sundaresan, and S. Radl, "Coarse graining Euler-Lagrange simulations of cohesive particle fluidization," *Powder Technol.*, vol. 364, pp. 167–182, Mar. 2020, doi: 10.1016/j.powtec.2020.01.056.
- [8] A. Jarray, V. Magnanimo, M. Ramaioli, and S. Luding, "Scaling of wet granular flows in a rotating drum."
- [9] V. Šmilauer et al., "Yade documentation 3rd edition".
- [10] A. Hagberg and D. Conway, "Networkx: Network analysis with python.URL: <https://networkx.github.io/>."
- [11] M. Dong, Z. Wang, B. Marks, Y. Chen, and Y. Gan, "Partially saturated granular flow in a rotating drum: The role of cohesion," *Physics of Fluids*, vol. 35, no. 11, Nov. 2023, doi: 10.1063/5.0166241.
- [12] R. Saghaian Larijani, V. Magnanimo, and S. Luding, "A Coarse-Grained Discrete Element Model (CG-DEM) based on parameter scaling for dense wet granular system," *Powder Technol.*, to be resubmitted.
- [13] L. Lu, Y. Xu, T. Li, and S. Benyahia, "Assessment of different coarse graining strategies to simulate polydisperse gas-solids flow," *Chem Eng Sci*, vol. 179, pp. 53–63, Apr. 2018, doi: 10.1016/j.ces.2018.01.003.

# A comparison of regime-specific continuum models for granular flows

Retief Lubbe<sup>1,2</sup>, Hongyang Cheng<sup>1</sup>, Prashant Gupta<sup>2</sup>, Stefan Luding<sup>1</sup> and Vanessa Magnanimo<sup>1</sup>

<sup>1</sup> University of Twente, Enschede, The Netherlands

<sup>2</sup> Procter & Gamble Ltd, Newcastle, UK

**Abstract—** Continuum models are efficient mathematical tools used by scientists and practitioners for simulating granular materials under diverse loading conditions. However, material behaviour is determined by constitutive models that typically capture either fluid-like behaviour or solid-like behaviour only, often within limited pressure and strain rate ranges. In this study, three constitutive models, modified Cam-Clay, weakly compressible  $\mu(I)$ -rheology, and a Newtonian fluid are implemented in the Material Point Method (MPM). Their differences are compared in a non-homogeneous, static-dynamic boundary value problem, namely two-dimensional flat and inclined column collapse. The results show that the extreme case of Newtonian fluid cannot support the slope, as expected, while modified Cam-Clay and  $\mu(I)$ -rheology form qualitatively similar heaps, suggesting that unification is a viable option. Modified Cam-Clay captures larger density ranges, but has limited applicability in dynamic flows, while  $\mu(I)$ -rheology persistently flows when expected to stop.

**Keywords:** granular materials; constitutive laws; solid-fluid transition; material point method; column collapse

## 1. Introduction

Grains and powders are fascinating materials that display both solid-like and fluid-like behaviour [1, 2]. Their mechanical behaviour at slow strain rates relies on well-established models. Frameworks such as Critical State Soil Mechanics (CSSM) and Jenike flow theory form an integral part in the design processes of engineering systems (e.g., foundations or silos) [3, 4]. However, at low consolidation stresses and high shear rates, knowledge on the onset and development of flow is limited, especially during the transition from a solid-like to a fluid-like regime.

When considering computational cost, numerical descriptions that reproduce granular materials as continua, triumph over high fidelity particle-level solvers for large systems. However, continuum models are usually regime specific, and hamper the efforts of modelers to capture the full dynamics, states, and transitions, across solid-like and fluid-like regimes.

In this study, we explore the dynamics of three constitutive models: (a) modified Cam-Clay, a solid-like rate-independent model based on the CSSM framework [4], usually adopted to simulate soil; (b) weakly compressible  $\mu(I)$ -rheology, a fluid-like steady-state, rate-dependent model, that captures the steady-state flow behaviour of granular materials; (c) and Newtonian fluid, as simple reference model. These models are implemented into a Material Point Method (MPM) solver to capture the large deformation and material response in boundary value problems, i.e., a column collapse under flat and inclined configurations.

## 2. Models

### 2.1. Modified Cam-Clay

The modified Cam-Clay is a precursor to many elastoplastic CSSM models [3]. The yield surface is an ellipse:

$$F \equiv \frac{q^2}{M^2} - p(p_c - p) = 0, \quad (1)$$

where  $M$  is the slope of the critical state line (CSL) in the  $q - p$  space, with  $p = -\left(\frac{1}{\dim}\right) \text{trace}(\boldsymbol{\sigma})$ ,  $q = \sqrt{(3/2)\mathbf{s}:\mathbf{s}^T}$ ,  $\boldsymbol{\sigma}$  is the stress tensor and  $\mathbf{s} = \boldsymbol{\sigma} + p\mathbf{I}$  its deviatoric part. The pre-consolidation pressure  $p_c$  determines the size of the yield surface, and its evolution describes the plastic hardening until critical (steady) state is reached, corresponding to failure. The flow rule is associated, i.e., the yield surface is taken as the plastic potential, therefore the plastic strain increment tensor is defined by:

$$d\boldsymbol{\varepsilon}^p = \frac{\partial F}{\partial \boldsymbol{\sigma}} = d\Lambda \left[ \frac{3}{M^2} \mathbf{s} + (2p - p_c) \mathbf{I} \right], \quad (2)$$

where  $d\Lambda > 0$  is the plastic multiplier, and  $\mathbf{I}$  is the identity tensor. In the CSSM framework, all virgin material states start from the isotropic compression line (ICL) and fail on the CSL. Those are assumed to be parallel with slope  $\lambda$  in the  $\ln v - \ln p$  space [5], leading to the hardening rule:

$$dp_c = (\lambda - \kappa)^{-1} p_c d\varepsilon_v^p, \quad (3)$$

and the elastic law:

$$dp = \kappa^{-1} p d\varepsilon_v^e. \quad (4)$$

where  $d\varepsilon_v^e$  and  $d\varepsilon_v^p$  are the elastic and plastic volumetric strain increments, respectively. The parameter  $\kappa$  is slope of the overconsolidation line (OCL) and links with elastic bulk modulus as  $K(p) = \frac{dp}{d\varepsilon_v^e} = \frac{1}{\kappa} p$  via (4).

### 2.2. Newtonian fluid

The total stress tensor for fluid-like models is chosen as

$$\boldsymbol{\sigma} = -p\mathbf{I} + \eta \dot{\boldsymbol{\varepsilon}}_d, \quad (5)$$

where  $\eta$  is a scalar viscosity,  $\dot{\boldsymbol{\varepsilon}}_d$  is the deviatoric strain rate tensors and relates to the scalar shear strain  $\dot{\gamma} = \sqrt{(1/2)\dot{\boldsymbol{\varepsilon}}_d:\dot{\boldsymbol{\varepsilon}}_d^T}$ .

Fluid pressure for weakly compressible materials makes use of an equation of state (EOS):

$$p = K \left[ \left( \frac{\rho}{\rho_0} \right)^\alpha - 1 \right], \quad (6)$$

where  $\alpha$  is a compressibility parameter (for water  $\alpha = 7$ ),  $K$  is the bulk modulus,  $\rho$  and  $\rho_0$  are the initial and current bulk densities.

### 2.3. Weakly compressible $\mu(I)$ -rheology

In the case of granular flows,  $\eta$  can no longer be assumed to be constant, but rather dependent on the stress state and strain rate applied. The well-known  $\mu(I)$ -rheology [1, 6] is a model for uniform steady granular shear flows of perfectly rigid, frictionless particles. The dimensionless inertial number relates the pressure state of the flow, and shear strain rate, as

$$I = \frac{\dot{\gamma} d_0}{\sqrt{p/\rho_p}}, \quad (7)$$

where  $d_0$  and  $\rho_p$  are the particle diameter and density, respectively. The bulk friction in  $q - p$  space is the ratio  $\mu = q/\sqrt{3}p$ . The relation between bulk friction and inertial number is:

$$\mu(I) = \mu_0 + \frac{\mu_d - \mu_0}{\frac{I_0}{I} + 1}, \quad (8)$$



where  $I_0$  is a characteristic dimensionless inertial constant,  $\mu_0$  and  $\mu_d$  represents the zero and infinite strain rate limits, respectively. A method of determining the viscosity in (7), is by assuming the alignment condition (i.e., shear strain rate and deviatoric stress are co-axial and their eigenvalues carry equal ratios) and a partial regularization [6,7]:

$$\eta(I, p) = \frac{\mu_0 p}{\sqrt{\dot{\gamma}^2 + r^2}} + \frac{\mu_d - \mu_0 p}{\frac{I_0}{I} + 1} \dot{\gamma}, \quad \dot{\gamma} > 0 \quad (9)$$

where  $r = 0.0001$  is a parameter used to regularize the small  $\dot{\gamma}$  and  $I$  divergences. We solve pressure using (6) with  $\alpha=1$  (See Ref [8] for details).

### 3. Method

An Affine Particle in Cell (APIC) explicit MPM using cubic splines is employed. A frozen pre-release version of the (developing) code is openly made available to the public [9]. Two setups are studied. In the first case study, a granular column at a low stress state is allowed to collapse under gravity with the acceleration  $g = 9.8 \text{ m.s}^{-2}$ . Next, an identical setup, but the frame tilted to an  $35^\circ$  angle enforces more dynamic flows. In both cases, we assume plane strain conditions.

The initial column height and width are 0.4 and 0.2 m, respectively. A constant time step  $dt = 3 \times 10^{-6} \text{ s}$  and a cell size of  $h = 0.00625 \text{ m}$  with 4 material points per cell are used. The domain height and width are 0.56 and 1.2 m, respectively. The floor is set to no slip and walls to perfect slip boundary condition. The material is assigned a uniform initial density of  $1300 \text{ kg.m}^{-3}$ . The parameters of the three models in Section 2 are chosen arbitrarily for demonstration purposes as (a) modified Cam-Clay:  $M = 0.6614$ ,  $\lambda = 0.0186$ ,  $\kappa = 0.0010$ , and  $\nu = 0.3$ ; (b) weakly compressible  $\mu(I)$ -rheology:  $\mu_0 = 0.3819$ ,  $\mu_d = 0.5718$ ,  $I_0 = 0.279$ ,  $K = 26000 \text{ N.m}^{-2}$ ,  $d = 0.0053 \text{ m}$  and  $\rho_p = 2000 \text{ kg.m}^{-3}$ ; (c) Newtonian fluid with  $K=26000 \text{ N.m}^{-2}$  and  $\eta=0.002 \text{ Pa.s}$ .

### 4. Results

Fig. 1 shows a snapshot of the subsequent heaps after the collapse with the three models in Section 2. The modified Cam-Clay and  $\mu(I)$ -rheology are similar, with the latter showing a slightly longer runout distance, whereas the Newtonian model shows fluid-like behaviour, not supporting a finite slope. The  $\mu(I)$ -rheology predicts a smaller shear stress within the bulk, compared to the modified Cam-Clay. The simulation was stopped at 1.2 s. Modified Cam-Clay showed a (decreasing) kinetic energy of  $5.8 \times 10^{-5} \text{ J}$ , while  $\mu(I)$ -rheology continue to flow slowly, with a kinetic energy of  $2.2 \times 10^{-4} \text{ J}$ .

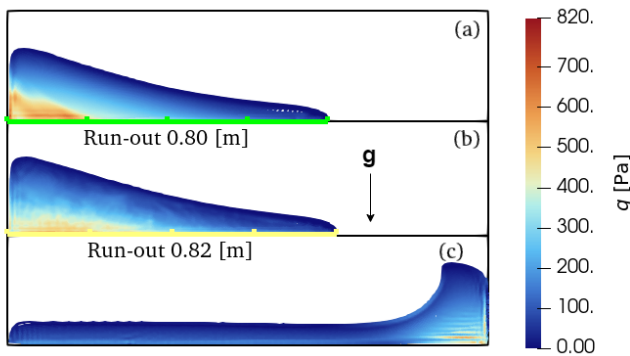


Figure 1. Flat column collapse of three models (a) modified Cam-Clay, (b) weakly compressible  $\mu(I)$ -rheology and (c) Newton fluid. Colour bar represents von-Mises shear stress. Green and yellow lines are rulers. Note, domain boxes are clipped for visibility purposes.

The simulations in Fig. 2 reveal that the modified Cam-Clay, predicts larger density peaks than the  $\mu(I)$ -rheology. However, the modified Cam-Clay (designed for finite confining stresses)

suffers from instabilities as the bulk density decreases and the pressure approaches zero, as indicated by some missing material points in Fig. 2 (a), that take undefined values. On the contrary, the  $\mu(I)$ -rheology flows and reaches the boundary. The Newtonian fluid flows much faster and further than the granular flow and reached the wall much earlier due to overall lower viscosity. The details and origins for these differences will be discussed in more details elsewhere [10].

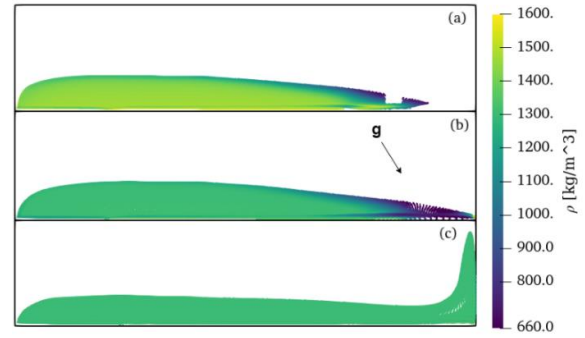


Figure 2. Inclined column collapse of three models (a) modified Cam-Clay, (b) weakly compressible  $\mu(I)$ -rheology and (c) Newton fluid. Domain boxes are clipped for visibility. The viewpoint is rotated at a  $35^\circ$  angle.

### 5. Conclusion

Overall, this study strengthens the idea that the modified Cam-Clay model and weakly compressible  $\mu(I)$ -rheology are suitable to reproduce granular flows, though in different pressure and strain regimes. Either model has problems in one or the other extreme case. Therefore, a multi-regime model could unify both models, capturing compressible, quasi-static deformations as well as high/low strain rate dynamics and low/large pressures. Interesting features observed from DEM simulations of granular flows with soft particles [2] could potentially be captured by a unified model.

### Acknowledgement

This research is part of the project TUSAIL (Training in Upscaling Particle Systems: Advancing Industry across Length-scales, <https://tusail.eu>) and has received funding from the European Horizon2020 Framework Programme for research, technological development and demonstration under grant agreement ID 955661.

### References

- [1] GDR MiDi, ‘On dense granular flows’, *The European Physical Journal E*, vol. 14, no. 4, pp. 341–365, 2004, doi: [10.1140/epje/i2003-10153-0](https://doi.org/10.1140/epje/i2003-10153-0).
- [2] A. Singh, V. Magnanimo, K. Saitoh, and S. Luding, ‘The role of gravity or pressure and contact stiffness in granular rheology’, *New Journal of Physics*, vol. 17, no. 4, p. 043028, 2015, doi: [10.1088/1367-2630/17/4/043028](https://doi.org/10.1088/1367-2630/17/4/043028).
- [3] K. H. Roscoe and J. B. Burland, ‘On the generalized stress-strain behaviour of wet clay’, *Engineering Plasticity*, pp. 535–609, 1968.
- [4] A. N. Schofield and P. Wroth, *Critical state soil mechanics*, vol. 310. McGraw-hill London, 1968.
- [5] I. F. Collins and P. A. Kelly, ‘A thermomechanical analysis of a family of soil models’, *Géotechnique*, vol. 52, no. 7, pp. 507–518, 2002, doi: [10.1680/geot.2002.52.7.507](https://doi.org/10.1680/geot.2002.52.7.507).
- [6] P. Jop, Y. Forterre, and O. Pouliquen, ‘A constitutive law for dense granular flows’, *Nature*, vol. 441, no. 7094, pp. 727–730, 2006, doi: [10.1038/nature04801](https://doi.org/10.1038/nature04801).
- [7] A. Franci and M. Cremonesi, ‘3D regularized  $\mu(I)$ -rheology for granular flows simulation’, *Journal of Computational Physics*, vol. 378, pp. 257–277, 2019, doi: <https://doi.org/10.1016/j.jcp.2018.11.011>.
- [8] A. M. Salehizadeh and A. R. Shafiei, ‘Modeling of granular column collapses with  $\mu(I)$  rheology using smoothed particle hydrodynamic method’, *Granular Matter*, vol. 21, no. 2, 32, 2019, doi: [10.1007/s10035-019-0886-6](https://doi.org/10.1007/s10035-019-0886-6).
- [9] Retiefasuarus, ‘GrainLearning/PymudokonMPM: pre-release-chops-2024’. Zenodo, Sep. 13, 2024, doi: [10.5281/zenodo.13756909](https://doi.org/10.5281/zenodo.13756909).
- [10] R. Lubbe, H. Cheng, S. Luding, V. Magnanimo, A multi-regime model for steady and transient granular flows, in preparation, 2024

# Effect of coarse-graining on simulated powder flow properties

Saeed Mahdavy<sup>1,2</sup>, Assem Zharbossyn<sup>1,2</sup>, Stefan Luding<sup>1</sup>, Vanessa Magnanimo<sup>1</sup>, Diego Barletta<sup>2</sup>, Massimo Poletto<sup>2</sup>, Luca Orefice<sup>3</sup>

<sup>1</sup> University of Twente, Netherlands

<sup>2</sup> University of Salerno, Italy

<sup>3</sup> MercuryLab, Enschede, Netherlands

**Abstract—** Among experimental devices, the Anton Paar Powder Rheometer is a tool for evaluating the bulk flow behavior of powder in dynamic conditions. This device measures the required torque for the rotation of the impeller inside the powder bed. The obtained experimental data can help to calibrate discrete element method (DEM) parameters. In order to speed up, larger, coarse-graining particles with proper scaling rules have to be applied. Some up-scaled simulations could produce a qualitatively similar trend to the experiment in one-tenth of the computing time. However, the applied coarse-graining scaling rules could not generate quantitatively the same results. In other words, the torque is not conserved by up-scaling stiffness alone, which to understand is ongoing work.

**Keywords:** DEM; Anton Paar Powder Rheometer; coarse-graining, bulk flow property;

## 1. Introduction

Powders are widely used in many industrial applications, such as pharmaceutical, chemical, food, cosmetic, and metallurgical. They are used in mixing, granulation, and reaction [1]. They consist of many small particles which interact with each other, and also with the surroundings. They behave differently under different conditions; moreover, they are considerably away from simple solids or fluids [2, 3].

The discrete element method (DEM) is a powerful tool for simulating granular materials. DEM can track each particle (microscale) and can predict the bulk property of a system (macroscale). Due to the high accuracy of DEM simulations, it uses lots of resources [4] to track each particle, and from a numerical experiment to identify the bulk properties of solids. As one way to overcome this bottleneck, the coarse grain method is introduced [5].

The coarse-grain discrete element method (CG-DEM) is a method to speed up DEM simulation. It utilizes an up-scaled collection of particles, as compared to the real, primary particles. Sakai and Koshizuka showed that a particular scaling rule for contact and drag force should be considered when the up-scaled particles are used [5]. Several studies confirmed that the DEM parameters should be changed when particle size is changed [1, 6, 7].

A precisely tuned set of input DEM parameters is required to simulate a practical condition for a given material. In order to have precise inputs, simulations need to be calibrated with experiments [8]. In this study, we use the Anton Paar Powder rheometer, and afterward, coarse-graining scaling rules are applied in the simulations.

## 2. Experimental procedure

### 2.1. Anton Paar Powder Rheometer

The Anton Paar Powder Rheometer is a device that operates in dynamic conditions. It consists of a concave grooved impeller and a cylindrical container. It measures the torque required for the rotation of the impeller within a bed of powder. In fact, the torque is the result of shear stress applied by the rotation of the impeller to the powder. In this study, the rotation speed of the

impeller was set to 600 rpm. Fig 2 shows the whole experimental setup.



Figure 1. Anton Paar Powder Rheometer setup [9].

### 2.2. Powder properties

High density polyethylene (HDPE) has been used as powder in the rheometer cell. This free-flowing powder has a 214.6  $\mu\text{m}$  median size. Before the experiment, the powder sample was dried in an oven. Subsequently, 43.6 g of the dried powder was poured into the cell.

## 3. DEM simulation

DEM is a tool that consists of a large number of discrete elements (particles). These particles can have arbitrary shapes. In DEM, each solid particle interacts with the surrounding medium (particle-particle, particle-fluid and particle-wall interactions). Based on the formulation of particle interactions, particles are assumed hard-sphere (event-driven) or soft-sphere (time-driven). In most granular flows, a particle may have contact with multiple other particles; therefore, we used the soft-sphere formulation. Newton's second law of motion describes the translational motion of each particle and, Euler's second law, its angular/rotational motion [4]:

$$m_i \frac{d\vec{v}_i}{dt} = m_i \frac{d^2\vec{x}_i}{dt^2} = \sum_{j \in CL_i} \vec{F}_{ij} + m_i \vec{g} \quad (1)$$

$$I_i \frac{d\vec{\omega}_i}{dt} = \sum_{j \in CL_i} (\vec{M}_{ij}^t + \vec{M}_{ij}^r) \quad (2)$$

where  $m_i$ ,  $I_i$ ,  $\vec{x}_i$ ,  $\vec{v}_i$  and  $\vec{\omega}_i$  are respectively mass, moment of inertia, displacement vector, velocity vector, and rotational speed vector of particle  $i$ . The sum  $\sum_{j \in CL_i} \vec{F}_{ij}$  involves the forces due to other particles  $j$  with particle  $i$ ,  $m_i \vec{g}$  is the gravity force as an external force, and the sum  $\sum_{j \in CL_i} (\vec{M}_{ij}^t + \vec{M}_{ij}^r)$  involves the tangential forces that generate torques, or rolling resistance torques, of other particles  $j$  with particle  $i$  [4].

The linear-viscoelastic force-displacement model was used to calculate the normal contact forces between particles, while also simple tangential forces and torques are used [10]. An open-source software, MercuryDPM, was used for the simulations, with the code implemented in modern C++.

### 3.1. Simulation condition

The cylindrical container is 50 mm in diameter and 100 mm in height. Particles are filled in the container to have the same mass as in the experiment. For the base case simulation, the impeller rotation speed was fixed at 600 rpm. Table 1 lists the parameters that were used in the DEM simulations. Upscaled particles with scale factor 5 (relative to the primary particles) were used in the base case simulation, which is considered as CG=1.

### 3.2. Coarse-graining

The coarse-graining scaling rules were used to adjust the force for the larger particles. In these cases, the coarse-graining factors were CG=1.6 and 2. The stiffness of the system has been scaled based on the coarse-graining factor:

$$k_{cg} = n k_{original} \quad (3)$$

where  $k_{original}$ ,  $n$  and  $k_{cg}$  are the normal stiffness of the base case, the coarse-graining scale factor, and the normal stiffness for the coarse-grained case. This is a preliminary set of simulations, without a detailed calibration carried out yet.

TABLE I. SIMULATION CONDITION FOR THE BASE CASE.

Parameter	Value	Unit
Normal stiffness	1000	N/m
Coefficient of restitution	0.8	-
Dynamic friction	0.55	-
Rolling friction	0.3	-
Particle density	950	kg/m <sup>3</sup>
Time step	$3.6 \times 10^{-6}$	s

## 4. Results and discussion

Fig. 2 shows the bulk response in the experiment and simulations, with the impeller torque plotted against time. The experimental result shows that the torque response of the powder reaches its peak at 20 s and decreases until reaching a steady state after 80 s. The simulations produce a similar trend in the result, they reach a peak and then decrease to a steady state level. While the experimental time scale is 100 s, the simulation needs only 10 s to produce similar results.

The base case simulation results (CG=1) closely match the experimental results. In contrast, the CG=1.6 and CG=2 produce a larger torque. An increase in coarse-graining scale also leads to higher fluctuations in the torque. The torque response of the coarse-grained cases (CG=1.6 and 2) could not generate the same results, even though the accepted stiffness scaling rule was applied, seemingly insufficient for the torque. This indicates that also other input parameters should be scaled, which is our ongoing research.

## 5. Conclusion

The bulk response of a non-cohesive HDPE powder was measured in the Anton Paar Powder Rheometer. The base case DEM simulation was performed to find reasonably matching DEM input parameters, and then scaling rules were applied for two cases (CG= 1.6 and 2). The DEM results produced a similar trend as the experiment but on a shorter time scale. The base

case DEM simulation torque agreed well with the experimental results, while applied coarse-grained rules could not generate the same results. To understand and correct this discrepancy is ongoing research, as well as calibrating other powder materials.

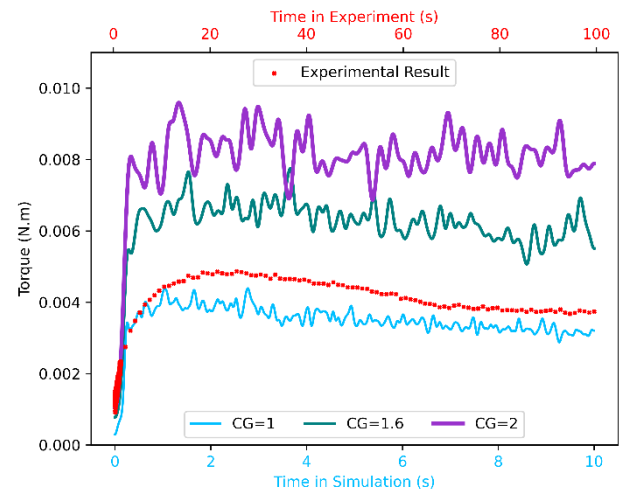


Figure 2. Bulk (torque) response in experiment and simulation.

## Acknowledgment

This research is part of the project TUSAIL (Training in Upscaling Particle Systems: Advancing Industry across Length-scales, <https://tusail.eu>), and has received funding from the European Horizon2020 Framework Programme for research, technological development, and demonstration under grant agreement ID 955661.

## References

- [1] B. Jadidi, M. Ebrahimi, F. Ein-Mozaffari, and A. Lohi, "A comprehensive review of the application of DEM in the investigation of batch solid mixers," *Rev. Chem. Eng.*, vol. 39, no. 5, pp. 729–764, Jul. 2023, doi: 10.1515/revce-2021-0049.
- [2] V. Francia, L. Ait Ali Yahia, R. Ocone, and A. Ozel, "From Quasi-static to Intermediate Regimes in Shear Cell Devices: Theory and Characterisation," *KONA Powder Part. J.*, vol. 38, no. 0, pp. 3–25, Jan. 2021, doi: 10.14356/kona.2021018.
- [3] W. Nan, M. Ghadiri, and Y. Wang, "Analysis of powder rheometry of FT4: Effect of air flow," *Chem. Eng. Sci.*, vol. 162, pp. 141–151, Apr. 2017, doi: 10.1016/j.ces.2017.01.002.
- [4] H. R. Norouzi, R. Zarghami, R. Sotudeh-Gharebagh, and N. Mostoufi, *Coupled CFD-DEM Modeling: Formulation, Implementation and Application to Multiphase Flows*, 1st ed. Wiley, 2016, doi: 10.1002/9781119005315.
- [5] M. Sakai and S. Koshizuka, "Large-scale discrete element modeling in pneumatic conveying," *Chem. Eng. Sci.*, vol. 64, no. 3, pp. 533–539, Feb. 2009, doi: 10.1016/j.ces.2008.10.003.
- [6] J. Tausendschön, J. Kolehmainen, S. Sundaresan, and S. Radl, "Coarse graining Euler-Lagrange simulations of cohesive particle fluidization," *Powder Technol.*, vol. 364, pp. 167–182, Mar. 2020, doi: 10.1016/j.powtec.2020.01.056.
- [7] C. J. Coetzee, "Particle upscaling: Calibration and validation of the discrete element method," *Powder Technol.*, vol. 344, pp. 487–503, Feb. 2019, doi: 10.1016/j.powtec.2018.12.022.
- [8] M. Ajmal, T. Roessler, C. Richter, and A. Katterfeld, "Calibration of cohesive DEM parameters under rapid flow conditions and low consolidation stresses," *Powder Technol.*, vol. 374, pp. 22–32, Sep. 2020, doi: 10.1016/j.powtec.2020.07.017.
- [9] H. Salehi, D. Sofia, D. Schütz, D. Barletta, and M. Poletto, "Experiments and simulation of torque in Anton Paar powder cell," *Part. Sci. Technol.*, vol. 36, no. 4, pp. 501–512, May 2018, doi: 10.1080/02726351.2017.1409850.
- [10] T. Weinhart et al., "Fast, flexible particle simulations—an introduction to MercuryDPM," *Comput. Phys. Commun.*, vol. 249, p. 107129, 2020.



# CFD-DEM-PBM Based Parametric Study on an Opposed Jet Mill

Jobin Raju<sup>1,2</sup>, Jan Henrik Finke,<sup>2</sup> Christoph Goniva<sup>1</sup> and Carsten Schilde<sup>2</sup>

<sup>1</sup> DCS Computing GmbH, Austria

<sup>2</sup> Technical University of Braunschweig, Germany

**Abstract—** In milling systems, accurate prediction of product output is crucial for process optimization and scale-up. Traditional empirical formulations for scale-up, reliant on geometric similarities, fails when faced with novel machine designs. To address this challenge, we propose a novel approach integrating Computational Fluid Dynamics-Discrete Element Method (CFD-DEM) simulations with Population Balance Models (PBM). This study aims to elucidate the transformation of particle-scale data into process-scale models, facilitating predictive insights into grinding rate and particle size distribution (PSD) evolution during milling operations. Our research employs CFD-DEM simulations to investigate the influence of various milling parameters on product output. Specifically, we analyse the effects of feed hold-up, suction pressure at the classifier, and grinding pressure on milling performance. By conducting a parametric study utilizing CFD-DEM-PBM integration, we seek to uncover key insights into the complex interplay between process parameters and product characteristics in opposed jet milling systems. This presentation will showcase our methodology for bridging simulation and operational time-scales, offering a robust alternative to traditional empirical models for scale-up. Through case studies and numerical analyses, we demonstrate the efficacy of our approach in predicting product output and optimizing milling processes.

**Keywords:** opposed jet mill; breakage; CFD-DEM; PBM;

## 1. Introduction

Process modeling of comminution devices have improved significantly due to the advances in simulation methods. CFD-DEM simulation provides valuable information on the collision dynamics in a mill. A Population Balance Model (PBM) portrays the evolution of a system. Combining both methods – CFD-DEM and PBM – would help to navigate larger time-scales to “look into” the future of the milling system under consideration. The present research focuses on developing a methodology to exploit CFD-DEM simulations to derive an expression for the grinding rate term in a Population Balance Equation (PBE) thereby describing the evolution of the system properties over larger time-scales.

## 2. Models and Complexity

### 2.1. First Principle Based Models

Computational Fluid Dynamics (CFD), Discrete Element Method (DEM), Finite Element Method (FEM) are examples of models based on first principles. These numerical methods are some of the most detailed ways to represent a real system. These models are expensive to solve and hence can only represent a system in the smallest time-scales (<1 second for an Opposed Jet Mill).

### 2.2. Multi-dimensional Models

Population Balance Model (PBM) and meso-scale models are examples of multi-scale models. Rather than resolving the individual system elements in its entirety, multi-scale model

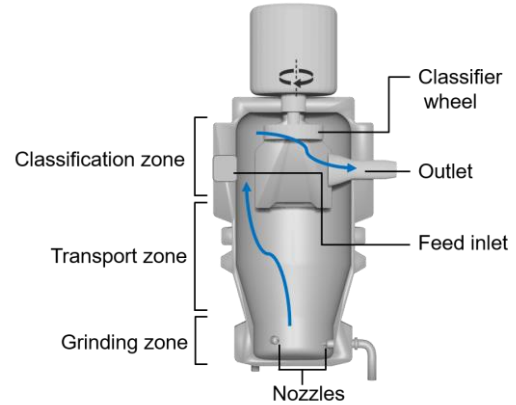


Figure 1. Section of a jet mill

solves the system evolution and spatial configurations as a whole. This would significantly reduce the computational cost of simulating the system and hence facilitates traversing through larger time-scales.

Using a fine blend of first-principles-based and multi-scale models, one can simulate complex systems with high accuracy, capturing detailed behaviours across actual operating time scales. Comminution devices are inherently complex to model. In an opposed jet mill, the flow is highly compressible and hence demands a very low time-step size for the CFD-DEM simulations. This limits the possibility to simulate the entire system for real operational durations. In the present study, a CFD-DEM based PBM method is introduced to simulate the jet mill system.

## 3. DEM-PBM Coupling

When operated in batch mode, the grinding rate in an opposed jet mill depends heavily on the instantaneous hold-up inside the mill. As the milling progresses, the effective holdup comprising of those particles from the coarse size class keeps decreasing thereby decreasing the grinding rate. Hence in batch mode, the grinding rate is a function of hold-up and time. We are interested in modelling the grinding rate,  $k$ , as a function of time –  $k(t)$  – as the first step in DEM-PBM coupling.

### 3.1. Collision Frequency and Grinding Rate

One can extract the collision frequency distribution from a (CFD-) DEM simulation. Capece et. al [1] describes how grinding rate is derived from DEM simulations for a ball mill.

$$k(t) \equiv k_1 = K_{const} f_{Mat} x_1 \sum_{l=1}^L f_{coll} (E_{m,l} - E_{m,min}) \quad (1)$$

In equation (1),  $f_{mat}$  and  $E_{m,min}$  are material parameters obtained from breakage calibration experiments,  $f_{coll}$  – collision frequency and  $x_1$  – particle size in coarse class-I.  $K_{const}$  is a grinding constant obtained from actual mill that is being modelled.

Another way to calculate the grinding rate is by plotting a modified collision distribution graph and using a breakage



function. A distribution of ‘number of particles’ corresponding to breakage probability or accumulated energy spectra would give us the number of particles in each energy/probability levels that has accumulated enough energy to initiate breakage. The number density in each energy/probability class combined with a breakage function would give the total mass fraction left from the particle size class under investigation.

### 3.2. Population Balance Equation

A PBE describes the evolution of a chosen system property. PBE in batch grinding and comminution systems often take the below form [2]:

$$\frac{dm_i(t)}{dt} = -k_i(t)m_i(t) + \sum_{j=1}^{i-1} b_{ij}k_j(t)m_j(t) \quad (2)$$

where  $b_{ij}$  is the breakage function and  $m_i$  is the mass fraction in size class  $i$ .  $k_i$  for different size classes are obtained from CFD-DEM simulations. Using appropriate modelling techniques, one can find an expression for  $k(t)$ .

## 4. CFD-DEM Simulation Setup

1-way CFD-DEM coupling is adopted to reduce computational cost. Once the CFD flow field reaches a steady-state, the velocity and pressure fields are averaged before coupling with DEM setup.

TABLE I. CFD-DEM CASE SETUP

Item	Description
CFD timestep	1e-8
DEM timestep	5e-8
Holdup	50k, 100k, 150k, 200k, 300k particles
Inlet BC	0.004 kg/m <sup>3</sup>
Outlet BC	0.8, 0.9, 1.0 Bar
Particle size, $x_1$	1200 $\mu$ m
Solver	cfdemSolverRhoPimple

The 1-way coupled CFD-DEM simulation reaches a pseudo-steady state where the collision frequency in different impact energy levels become constant or oscillate around a mean value. Collision data is extracted from an appropriate time window and analysed for grinding rate calculations.

## 5. Results

The effect of holdup on the collision dynamics and subsequently the grinding rate of the system is analysed below.

From the graph we observe that, the collision frequency increases as the holdup increases. But the rate of increase reduces as the holdup increases further. There is an optimum holdup corresponding to which the grinding rate is at the maximum.

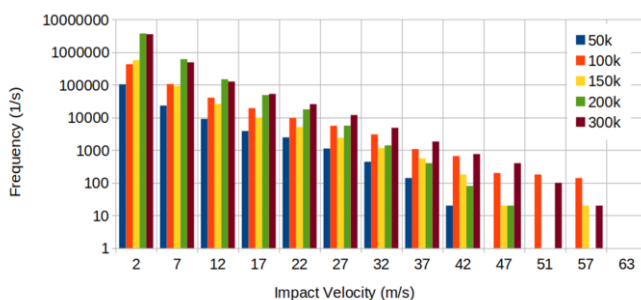


Figure 2. Collision frequency distribution for different holdups

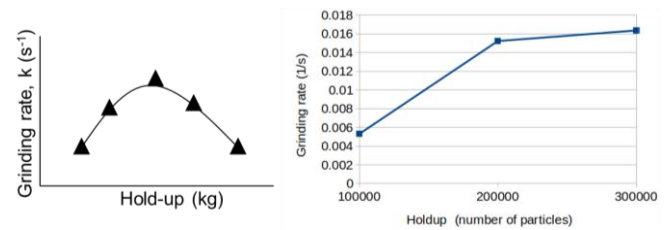


Figure 3. Grinding rate calculation: trend based on literature (left) and current case (right)

The grinding rate is directly proportional to the number of effective collisions. It is observed from literature that, when the holdup exceeds a critical level, the grinding rate drops significantly.

The magnitude of effective collisions can be increased by increasing the particle entrainment into the jet. The simulation results gives insights into how collision frequency cycles in the mill can be improved by suitable design modifications.

## 6. Conclusion

A method to model the grinding rate based on CFD-DEM-PBM coupling is explored in the current study. A CFD-DEM-PBM based model description provides insights based on the ‘machine function’ unlike empirical formulations. The method employed can be used as a metric to optimize mill designs for better efficiency and output quality. Analysis done on batch grinding case can serve as the basis for finding optimum mill settings for continuous mode of operation.

## Acknowledgement

The authors gratefully acknowledge the financial support from the Horizon 2020 program under the Marie Skłodowska-Curie Actions (MSCA) through the TUSAIL project.

## References

- [1] Capece, M., Bilgili, E., & Davé, R. (2014). Insight into first-order breakage kinetics using a particle-scale breakage rate constant. In *Chemical Engineering Science* (Vol. 117, pp. 318–330). Elsevier BV. <https://doi.org/10.1016/j.ces.2014.06.019>
- [2] Herbst, J. A., & Fuerstenau, D. W. (1980). Scale-up procedure for continuous grinding mill design using population balance models. In *International Journal of Mineral Processing* (Vol. 7, Issue 1, pp. 1–31). Elsevier BV. [https://doi.org/10.1016/0301-7516\(80\)90034-4](https://doi.org/10.1016/0301-7516(80)90034-4)

# Flowability assessment of weakly consolidated fine powders

Rahul Sharma<sup>1,2</sup>, Massimo Poletto<sup>1</sup>, Diego Barletta<sup>1</sup>, Stefanos Papanicopolous<sup>2</sup>, Stefan Pantaleev<sup>3</sup> and Jin Y. Ooi<sup>2</sup>

<sup>1</sup> University of Salerno, Salerno, Italy

<sup>2</sup> The University of Edinburgh, Edinburgh, United Kingdom

<sup>3</sup> Altair EDEM, Edinburgh, United Kingdom

**Abstract** — Flowability of powders is generally evaluated using the methodology proposed by Jenike, which is often referred to as the shear testing methodology. The shear testing methodology approaches the powder testing with a two-stage procedure; consolidation or pre-shear where a powder sample is sheared under a defined normal stress and attains the steady state when it shears at constant powder volume and shear stress; followed by a shear to failure where the powder's strength is measured by shearing the sample under a reduced normal stress. There are many handling scenarios in industry in which the powders might not be subjected to flow regimes leading to critical shearing states, such as in dosing, filling and small-scale silos/hoppers for storage and discharge. Where the internal shear of the powder is limited during powder flow in these situations, and the powder may not achieve steady-state deformation conditions, it is plausible that the Jenike method of flowability assessment may not apply. The present study attempts to characterise the flow properties of fine cohesive powders, considering the possibility of powders to be partially consolidated or at un-steady state conditions. The study utilized the Schulze Ring Shear Tester to characterize flowability of two cohesive powders at steady and partially consolidated states and the discrete element method (DEM) technique was used to model the particle interactions, a coarse-grained meso-scale DEM model was developed and calibrated using experimental data. The study shows that the flowability depends on the state of consolidation or the deformation state of the powder.

**Keywords:** Flowability; partial consolidation; Meso-scale DEM.

## 1. Introduction

The principles of shear testing, as first established by Jenike [1] and later elucidated by Schulze [2], approach powder flow testing with a two-stage procedure in which the first stage is used to critically consolidate the powder and the second stage to measure its shear strength under reduced normal stress states. Powder consolidation in the first measurement stage (pre-shear stage) is performed when the powder, sheared under a pre-shear normal stress, reaches a steady state (critical state) condition characterized by constant powder volume and shear stress values. After stopping the pre-shear, the powder strength is measured in the second stage (shear stage), in which the powder is sheared under a reduced normal stress. Shearing and travel distances in industrial silos and hoppers are of the order of the equipment size and ensure the attainment of steady state during flow. In shallow containers and other situations where the internal shear of a powder is limited during storage and flow, the powder may not achieve steady state conditions. Handling scenarios where the powder might not achieve the steady state deformation conditions may be classified as an un-steady state flow. The present study focuses on the systematic characterization of flow properties of fine cohesive powders, considering the possibility of partial consolidation.

## 2. Materials and methods

### 2.1. Experimental methodology

Magnesium Carbonate  $\text{MgCO}_3$  and Calcium Carbonate  $\text{CaCO}_3$  (ESKAL 500) were used for experiments. For testing the powder at the un-steady state, the powder is subjected to the same pre-shear normal stress as in the case of the steady state, as seen in Figure 1, but the pre-shearing of the sample is stopped before the sample reaches the steady state such that the shear stress in the un-steady state is a fraction of the shear stress obtained in the steady state. Afterwards, as in the standard procedure, the sample is sheared, applying a normal stress lower than the pre-shear normal stress. The peak shear stress is used to obtain a point of the yield locus. The whole yield locus is obtained by repeating the procedure by changing the normal stress applied in the shear phase.

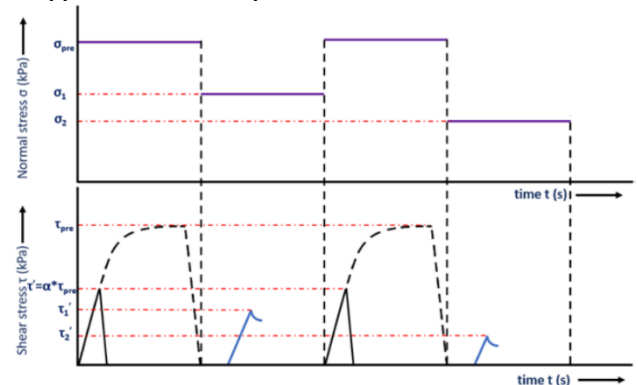


Figure 1. Shear test to obtain yield loci at under-consolidated states.

### 2.2. Modelling methodology

The discrete element method (DEM) simulations help to model granular flow problems at the particle scale, but it is computationally expensive to simulate industrial scale problems with the real particle size. A coarse-graining or meso-scale approach scales up the particle size to help reduce the number of particles in the system resulting in lower computation costs. The meso-scale cohesive DEM model of the shear testing was developed using the EEPA contact model [3] to model the powder with powder-geometry interactions modeled by Hertz-Mindlin model. Parametric sensitivity study of the various model parameters was done to ascertain critical parameters and their effect. A design of experiments (DOE) study of the identified sensitive parameters was carried out at two pre-shear normal loads and a multi-objective genetic algorithm was used to minimize the objective functions and to calibrate the DEM model. The objective functions were formulated as the error functions between the experimental and the modelling response. Responses such as the internal friction angle, yield locus and the flow function were compared to the experimental results to gauge the accuracy of the modelled system.

## 3. Results and discussions

The major principal stresses in the flow functions of ESKAL 500 measured with the Schulze ring shear tester were evaluated utilizing the Jenike methodology [1] and the coaxiality principle

[4]. The coaxiality principle considers the principal stress and the principal strain axis to be coincident and is used for calculating the principal stresses. The dashed curve labelled as Jenike in Figure 2 represents the steady-state flow function obtained from shear testing using Jenike methodology. The curve labelled SS is the steady state flow function derived from calculations based on the coaxiality principle, the flow functions at the partial consolidation states were also obtained using this principle. The flow function curves at the various states of consolidation show that the flowability of the powder when partially consolidated or deformed to an un-steady state is better than the case for the powder at a steady state. The flowability of the 75% un-steady state slotted in between the steady state and 50% un-steady state curve with the more significant difference seen when steady state and 50% un-steady state curves are compared. The shear strain evaluated for the various states of consolidation showed that the deformation required for the powder to be at steady (critical) and un-steady states (under consolidated) varied quite significantly. The deformation needed to achieve the steady state was five times larger than that required for achieving the 50% un-steady state (shear stress equal to 50% of the steady state). The deformation state of the powder impacts its flowability, with the powder subjected to a lower amount of deformation having a better flowability. The results show that the flowability of the powder depends on the deformation state of the powder necessitating the need for flowability characterization at the appropriate deformation state.

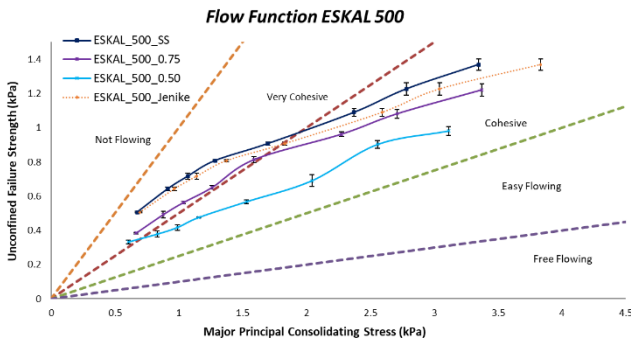


Figure 2. Flow function curves of ESKAL 500.

DEM parametric sensitivity study of particle-particle coefficient of static friction  $\mu_{s\ p-p}$ , particle-particle coefficient of rolling friction  $\mu_{r\ p-p}$ , plasticity ratio  $\lambda_p$ , contact adhesion energy  $\Delta\gamma$ , constant pull-off force  $f_0$ , particle-geometry coefficient of static friction  $\mu_{s\ p-g}$  and particle-geometry coefficient of rolling friction  $\mu_{r\ p-g}$  was carried out to ascertain the critical model parameters. The study helped determine the key parameters for calibration, which are  $\mu_{s\ p-p}$ ,  $\mu_{r\ p-p}$ ,  $\lambda_p$  and  $f_0$ . The calibration was initiated by exploring the design space by carrying out the shear cell simulations across two pre-shear normal loads. Modified Extensible Lattice Sequence (MELS) DOE [5,6] was used for this purpose as a full-factorial study was computationally expensive and may not be necessary. The DOE runs yielded the output responses w.r.t the input variables which were used in the objective functions for optimisation.

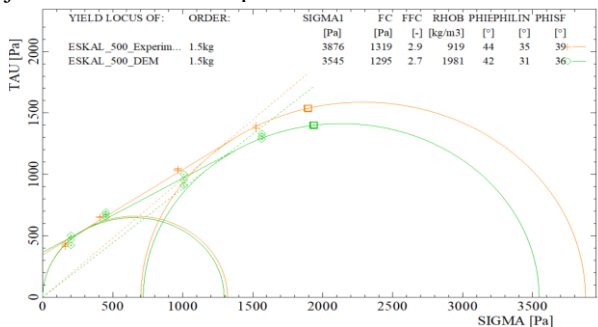


Figure 3. Experimental & DEM yield locus of ESKAL 500.

The Multi-Objective Genetic Algorithm (MOGA) [7] was run for the specified population size and generations, it converged to give the optimal Pareto front. MOGA was re-run to obtain the Pareto fronts, and the calibrated set of parameters were identified from these runs. The calibrated set of parameters were used to run the full shear test (four shear points) across four normal load levels. Flow function and yield locus outputs such as major principal consolidation stress  $\sigma_1$ , unconfined yield strength  $\sigma_c$  and internal friction angle were compared. The meso-scale DEM model was able to predict the yield locus and the powder flow function as seen in Figure 3 & Figure 4 respectively.

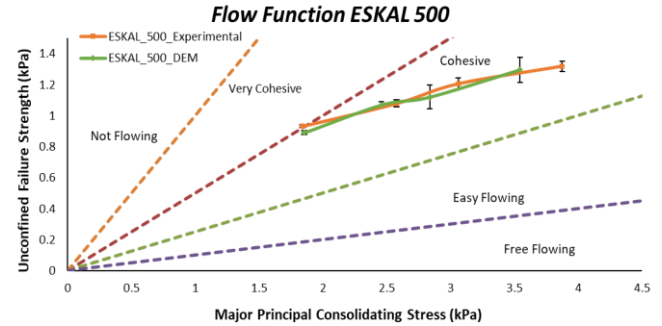


Figure 4. Experimental & DEM flow function curves of ESKAL 500.

## 4. Conclusion

In this study, a flowability characterization procedure was developed and tested for weakly compacted powders, such as powders might not be critically consolidated and instead be at an under-consolidated state during flow. The novel flowability characterization procedure was able to test the powder at un-steady state. Testing on the Schulze ring shear tester showed that the flowability depends on the deformation state of the powder, i.e., the shear strain or the amount of deformation the powder is subjected to has an impact on the flowability. A coarse-grained cohesive DEM model was developed and calibrated using the experimental data, a fractional DOE study was run to explore the parametric space & MOGA was used to minimize the values of the objective functions and to calibrate the model. The calibrated DEM model was able to predict and match the experimental powder flow behaviour.

## Acknowledgement

This study is part of a project associated with the TUSAIL (Training in Upscaling particle Systems: Advancing Industry across Length-scales) Training Programme. TUSAIL is funded from the European Union's Horizon 2020 research and innovation programme under the Marie Skłodowska-Curie grant agreement Number 955661. The authors would like to thank Dr. Carlos Labra for his support.

## References

- [1] Jenike, A.W., 1964. Storage and flow of solids. Bulletin No. 123, Utah State University.
- [2] Schulze, D., 2008. Powders and bulk solids. Behaviour, characterization, storage and flow. Springer, 22.
- [3] Thakur, S.C., Morrissey, J.P., Sun, J., Chen, J.F. and Ooi, J.Y., 2014. Micromechanical analysis of cohesive granular materials using the discrete element method with an adhesive elasto-plastic contact model. *Granular Matter*, 16, pp.383-400.
- [4] Hilden, J., Bowman, K., Morris, K., Wang, S., Sprockel, O. and Ennis, B., 2008. Note on the interpretation of powder shear test data. *Powder technology*, 182(3), pp.486-492.
- [5] Hickernell, F.J., Hong, H.S., L'Écuyer, P. and Lemieux, C., 2000. Extensible lattice sequences for quasi-Monte Carlo quadrature. *SIAM Journal on Scientific Computing*, 22(3), pp.1117-1138.
- [6] [https://2023.help.altair.com/2023/hwdesktop/hst/topics/design\\_exploratio n/method\\_modified\\_extensible\\_lattice\\_sequence\\_doe\\_r.htm](https://2023.help.altair.com/2023/hwdesktop/hst/topics/design_exploratio n/method_modified_extensible_lattice_sequence_doe_r.htm)
- [7] [https://2023.help.altair.com/2023/hwdesktop/hst/topics/design\\_exploratio n/method\\_multi\\_objective\\_genetirc\\_algorithm\\_r.htm](https://2023.help.altair.com/2023/hwdesktop/hst/topics/design_exploratio n/method_multi_objective_genetirc_algorithm_r.htm)

# An experimental and modelling investigation of solid state sintering using X-ray tomography and DEM- based elasto-plastic adhesive model

Afshin Taghizadeh<sup>1,2</sup>, Alexander Munnoch<sup>2</sup>, Aakash Varambhia<sup>3</sup>, Amer Syed<sup>1</sup>, Jin Y. Ooi<sup>1</sup>

<sup>1</sup>University of Edinburgh, Edinburgh, United Kingdom, <sup>2</sup>Johnson Matthey, Billingham, United Kingdom <sup>3</sup>Johnson Matthey, Reading, United Kingdom

## Abstract

Hydrogen production via processes such as steam reforming requires pelleted heterogeneous catalysts to strike a balance between catalyst strength and porosity in their final form, and this is achieved by two consecutive process steps: a High-Pressure Compaction (HPC) followed by Solid-state Sintering (SS). During the compaction stage, the powder is fed into a die and physically forced into a specific macro shape called a 'green compact'. Subsequently, in the sintering stage, the 'green compact' is heated, typically with a holding time, to a temperature near but below the melting point. Neighbouring particles in contact within the 'green compact' bond through Ostwald ripening, modifying the final microstructure of the compact. Thus, controlling the shrinkage and microstructural evolution during SS is crucial to the dimensional accuracy and properties of final products.

The purpose of this study was to develop an improved understanding of the densification and the pore structure evolution during the two-stage process. The compaction behaviour was investigated using both experiment and simulation using the Discrete Element Method (DEM). Then, the microstructural evolution during sintering was investigated using tomographic X-ray microscopy (XRM) of the 'green compact' and the sintered pellets.

DEM typically models particles to be whole rigid spheres whereas real particles such as the, spray dried  $\alpha$ -alumina pelleting feed used in this study have been found to have porosity within each particle that significantly affected the particle compaction behaviour under high pressure loading. An intra-particle porosity term is proposed to account for the reducing porosity during HPC. The model calibration and the validation of the simulation results were based on the experimental measurements performed at various compaction pressures. Firstly, the fundamental collisional, frictional, and cohesion characteristics of the model are calibrated using a single compaction pressure result. The calibrated model was then used to predict the compaction responses for a wide range of compaction pressures in the experiments. The results show that using the proposed contact model with the intra-porosity term can provide a good prediction of the compression profiles across a wide range of relative densities. This provides useful insights on the compressibility properties of the  $\alpha$ -alumina powder.

The tomographic XRM dataset was obtained on a ZEISS XradiaTM 620 Versa microscope operated at 50 kV acceleration voltage with a voxel size of 0.73  $\mu\text{m}$  with 30 s dwell time. Data acquisition in the XRM was carried out by taking multiple 2D transmission images of an object in different orientations. Once the acquisition was complete, the data was reconstructed using the inbuilt automatic tomography reconstruction algorithms within the ZEISS Scout-and-Scan software. The 'green compact' and a sintered product, created under 70 MPa compaction pressure and 1400°C and 6 hr dwell time, respectively, were used in this analysis for comparative purposes. The XRM result was analysed using the GeoDict and Dragonfly software. The results indicated pore enlargement following the sintering process. Notably, there was a substantial increase in the proportion of pores exceeding 4  $\mu\text{m}$  in diameter, with a rise of up to 12 percent – consistent with Ostwald ripening. Therefore, both the overall level of porosity and the distribution of pore sizes experienced substantial changes during the sintering process. These observed alterations in pore structure offer valuable insights into the complex microstructural evolution that takes place during the sintering process and crucially how it related to strength evolution of the pelleted material.



## 5 ABSTRACTS

## A review of triboelectrification and electrostatic charge measurement techniques - promises and challenges

Tariq Hussain<sup>1</sup>, Tong Deng<sup>2</sup>, John Pillai<sup>1</sup>, Waseem Kaialy<sup>3</sup>, Muhammad Ghori<sup>4</sup>, Mike Bradley<sup>2</sup>

<sup>1</sup>Military Technological College, Muscat, Oman, <sup>2</sup>University of Greenwich, Kent, United Kingdom <sup>3</sup>University of Wolverhampton, Wolverhampton, United Kingdom, <sup>4</sup>University of Huddersfield, Huddersfield, United Kingdom

### Abstract

Electrostatic charging usually takes place due to triboelectrification. Tribocharging is a popular phenomenon in bulk solid material handling that arises from particle-particle and particle-wall collisions. Electrostatics could be a serious problem in industrial handling applications. This work reviews the literature related to the field of electrostatic behaviour in powder technology. The fundamentals, generation mechanisms, and measurement methods for electrostatic charge have also been revised.

Many charge characterisation methods demonstrate a similar approach in measurement principles but differ in data collection or data processing analysis. Those charge characterisation methods still suffer from several limitations relating to the measurement of charge distribution, the difficulty in providing accurate charge measurements for fine cohesive particulates, and the inability to characterize bipolar charging. Additionally, different measurement principles were employed along with similar instrument designs. A range of charge measurement methodologies exists for measuring the net-charge, the sum total of all positive and negative charges of the powder sample collected, such as the Faraday pail method. The problem with this approach is that it doesn't present a clear picture considering, for instance, if the positively charged particles and the negatively charged particles are distributed equally, then the total charge will be close to 0 which makes the tribocharging phenomenon more complex to understand as well as hiding what is going on. Hence, the measurement of the net-charge-to-mass ratio of the powder, where the processes were known to cause bipolar charging due to the differences in the work functions, is not an accurate indicator for correlating the true charge-to-mass ratio. The purpose of this review article is to briefly summarize the current state of charge sensing, both net and bipolar, and to discuss their advantages and disadvantages.

# Hard Modeling of Raman spectra for coating endpoint detection in a titanium dioxide-free pharmaceutical coating process

René Brands, Jens Bartsch, Markus Thommes

TU Dortmund University, Dortmund, Germany

## Abstract

The pharmaceutical industry is shifting from  $\text{TiO}_2$  containing coatings to alternatives due to its carcinogenic potential. However, Raman spectroscopy is frequently utilized to monitor the coating endpoint based on peak integration models of the  $\text{TiO}_2$  peaks. Accordingly, this shift towards  $\text{TiO}_2$  free alternatives has increased the need for alternative methods to analyze the spectra since more frequent overlap of peaks is observed. In this context, Hard Modeling (HM) is a promising method. HM is a mechanistic model that combines high robustness with relatively low calibration effort [1]. In this study, the suitability of HM for a  $\text{TiO}_2$  free coating in a pharmaceutical semi-continuous coater was evaluated.

Experiments were conducted in a semi-continuous coater (KOCO 25, L.B. Bohle Maschinen & Verfahren, Germany) using a  $\text{TiO}_2$  free coating suspension (15 wt% aqueous, Aquarius prime TF pink, Ashland, USA). As an alternative pigment, calcium carbonate ( $\text{CaCO}_3$ ) is utilized here. Raman spectra were obtained in-line using a Raman spectrophotometer (Process Guardian, Tornado Spectral Systems, USA) combined with a non-contact probe (Hudson 785, Tornado Spectral Systems, USA). All spectra were preprocessed (PEAXACT, S-PACT, Germany) with a baseline correction and a peak normalization in the selected spectral range. The characteristic Raman peak of  $\text{CaCO}_3$  can be observed as a shoulder on the core signal at  $1087\text{ cm}^{-1}$ , which increases linearly with the amount of  $\text{CaCO}_3$  during the coating process (Fig. 1, left). The spectral structure of the tablet core is modeled by a sum of 3 peak functions of pseudo-Voigt type. The  $\text{CaCO}_3$  in the coating material is modeled by an extra peak function, which represents the signal contribution from the coating and serves for quantification (Fig. 1, right).

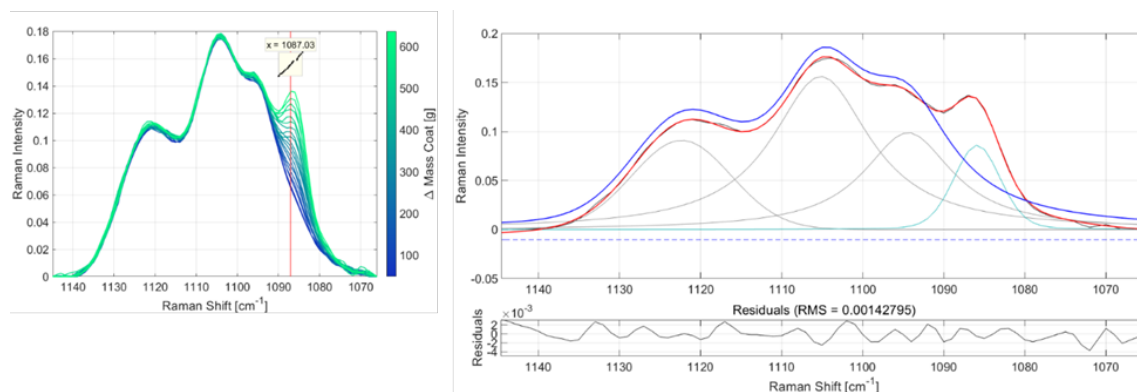


Figure 1: Spectral range from  $1065$  to  $1145\text{ cm}^{-1}$  exemplarily shown for one batch with correlation Raman intensity and mass of coating material at  $1087\text{ cm}^{-1}$  (left) and coated tablet spectrum (black) with hard model (red) including peak functions (right).

Overall, the calibration model quality is sufficient indicated exemplarily by a coefficient of determination of 0.99. In addition, the cross-validation of the two training batches resulted in a RMSECV of 5.46%. Finally, the prediction of the test batch was successful, indicated by an RMSEP of 2.77%. This makes hard modeling a promising alternative for coating processes without containing  $\text{TiO}_2$ .

[1] A. Echtermeyer, C. Marks, A. Mitsos, J. Viell, Inline Raman Spectroscopy and Indirect Hard Modeling for Concentration Monitoring of Dissociated Acid Species, Appl Spectrosc 75 (2021) 506–519.

## Effect of Relative Humidity and Temperature on Particle Adhesion Using MSET

Vivek Garg, Tong Deng, Michael Bradley

*University of Greenwich, Chatham, United Kingdom*

### Abstract

Understanding the dynamics of particle adhesion is crucial in powder handling systems. This study focuses on examining the influence of relative humidity (RH) and temperature on particle adhesion using a Mechanical Surface Energy Tester (MSET). The experimental setup allows for precise control of RH and temperature conditions, enabling systematic investigation of their effects on particle adhesion and powder flowability.

The investigation was undertaken using seven pharmaceutical powders varying in particle size distribution, shape distribution, and different particle density. Through a series of experiments, different combinations of RH and temperature were applied to the dispersed samples/ surfaces, and the corresponding adhesion forces were measured using the MSET. The results reveal intricate dependencies of particle adhesion on RH and temperature, highlighting the complex interplay between surface properties, environmental conditions, and adhesion forces.

At lower RH levels, adhesion forces tend to increase due to reduced moisture content, leading to stronger intermolecular interactions between particles and surfaces resulting in more cohesion. Conversely, higher RH levels promote the formation of moisture layers, potentially weakening particle adhesion by lubricating the interface resulting in the free-flowing nature of the materials. Moreover, temperature variations influence the viscoelastic properties of the contacting materials, further modulating adhesion behaviour.

This study contributes to a deeper understanding of the mechanisms underlying particle adhesion in varying environmental conditions. The insights gained can inform the development of strategies for controlling and mitigating particle adhesion in diverse applications, such as manufacturing processes, air quality management, and surface engineering. Additionally, the utilization of MSET offers a robust experimental platform for investigating adhesion phenomena under controlled conditions and predicting the flowability of the powder using a small quantity of the material.

**Keywords :** Powder Adhesion; Pharmaceutical powders; Powder Flowability; Environment conditions



## Particulate emission control in port operations

Velan Balan

SCORPIO ENGINEERING GROUP, BANGALORE, India

### Abstract

90 percent of world trade is by shipping. In 2021, 11 billion tonnes of cargo including oil and gas was moved across oceans of which 70% comprised of major and minor dry bulk. Most of these products produce dust when being grab-unloaded from ships and barges. With increasingly stringent environmental pollution norms, the containment of such dust to acceptable levels becomes a major responsibility of ports and port operators. Techniques of dust control were often improvisations of the operators with no formal technology bias leaving a gap between clean and dirty ports. Attempts to bridge the gap and connect technology with port operations were inadequate because of a lack of knowledge of available technologies for scientific and effective dust containment systems.

This paper presents basics of technology based equipment and systems that dry bulk ports could use to have a clean environment around ship unloading operations. Methods of dust filtration and control in both mechanical and pneumatic ship unloading systems, containment in port storage and reclaim, dust emission measurement methods etc to ensure clean port operations are some of the aspects covered.

The presentation will look at products like grain, rock phosphate, clinker, fertilizer, gypsum, fine aggregate, chemicals, agriproducts, cement, flyash, alumina, agriproducts and other dry bulk from 20mm to submicron particle sizes.

Dry bulk ports predominantly use hoppers for grab unloaded material and pneumatic or mechanical ship unloaders when the product is unsuitable for grabbing. Primary sources of particulate emission (PM10) are at the interfaces of such equipment with the product and its collection and discharge. Wind currents also play a significant role in the dispersion of fugitive dust in some of these equipments. A technical and scientific approach to the design of dust control measures in these equipments will be reviewed. The degree of dust emission that is not often known to the scientific community at large is illustrated below.



Delegates will learn of available technologies from a scientific point of view covering basic principles of containment that would guarantee stringent PM10 emission standards .

# Dynamic granular flow in a continuous blender: GPU-based DEM simulation and Positron Emission Particle Tracking (PEPT) experimental validation

Jiawei Hu, Chuan-yu Wu

University of Surrey, Guildford, United Kingdom

## Abstract

The Positron Emission Particle Tracking (PEPT) technique and the Discrete Element Method (DEM) are widely utilised to investigate the intricate behaviours of powder flow within continuous blenders.

In this study, the Discrete Element Method (DEM) and Positron Emission Particle Tracking (PEPT) techniques were employed for the first time in a comparative analysis of powder flow behaviours in continuous blenders, focusing on residence time distribution (RTD), velocity magnitude distribution, radial movement, and dispersion coefficients across various blade configurations. As shown in Figure 1, the full-scale of continuous blender is modelled by the GPU-based Blaze-DEM code, which is developed by Govender et al. [1]. During experiments, the continuous blender was positioned between two PEPT cameras. Once the radioactive tracer passes through the PEPT camera zone, the back-to-back gamma rays from the radioactive tracer would be detected and its position can be determined [2].

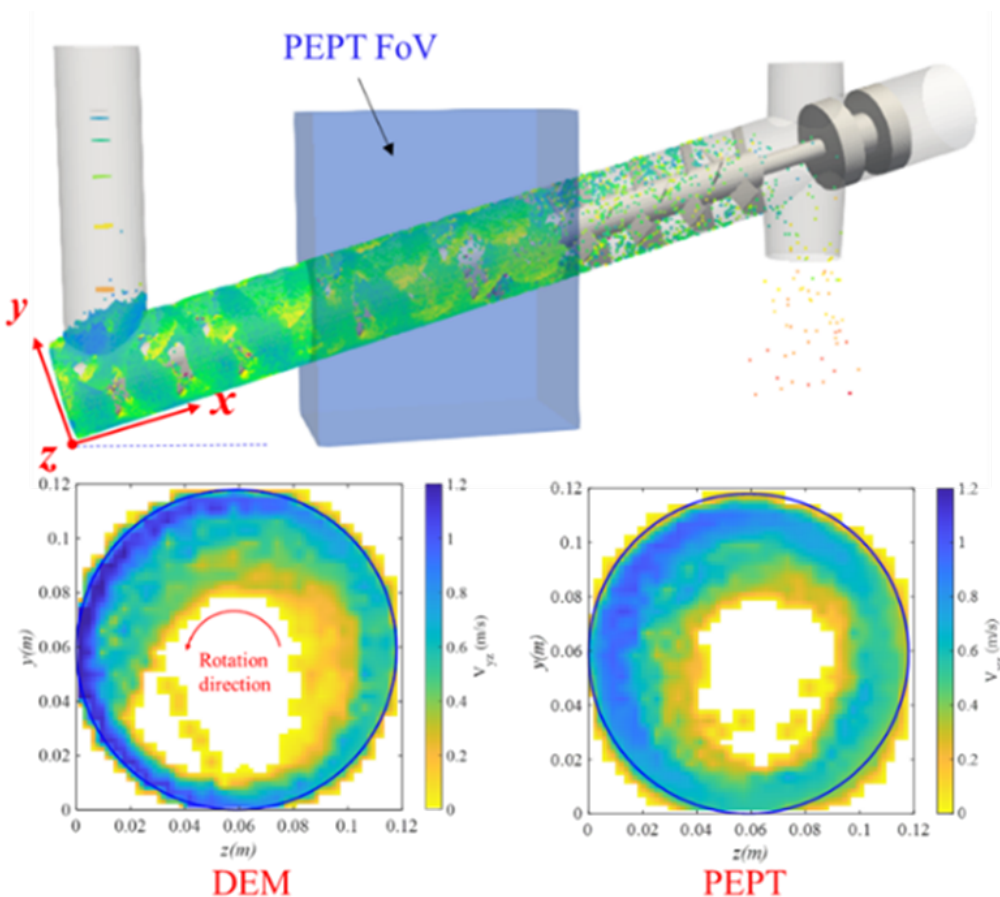


Figure 1 - Schematic diagram of relative position of PEPT cameras and the continuous blender, and asymmetrical patterns in radial velocity distributions across the blender's cross-section observed from both DEM and PEPT.

Results reveal nearly identical RTDs and average radial dispersion coefficients between DEM and PEPT. Both methods yield consistent trends in average velocity magnitude distributions and similar asymmetrical patterns in radial velocity distributions across the blender's cross-section. Notably, a decrease in mixing elements leads to reduced mean residence times and increased average axial dispersion coefficients, as observed through both DEM simulations and PEPT measurements.

In conclusion, DEM simulations predict powder flow behaviours comparable to the PEPT measurements across various aspects.

## Flowability and processability of reactive particles

Alex Munnoch

*Johnson Matthey, Billingham, United Kingdom*

### Abstract

Flowability and the implications of that flowability on processing equipment design, selection or operation is an area of rigorous characterisation and evaluation. However, the nature and extent to which the physical properties of particles can change through reaction with their processing environment is a topic that straddles particle engineering and surface chemistry. This interdisciplinary nature can mean factors affecting primary, secondary or storage properties of reactive particles can be challenging to understand and resolve. Resolution of these challenges is critical to industrial production of functional or reactive materials.

This presentation will cover the highly varied nature of changes that can occur with reactive particles and how that can impact particle processability, with case studies taken mainly from Johnson Matthey internal projects. These will include:

- ('pH-dependent impurity effects on aggregation') The agglomeration and wettability of alumina in aqueous stirred tanks
- ('simple' adhesive forces with water-hydroxyl physical chemistry) Flowability and wall adhesion challenges with metal-impregnated and rotary calcined zeolite. When shear cells and operational observations don't tally-up.
- ('dissolution-recrystallisation in the presence of atmospheric water') The caking of alkali/alkaline hydroxides.
- ('transitional 'sticky' phase') —Transient sticky chars during organic burnoffs/catalyst regeneration.
- ('oxidation/pyrophoric') PGMs reacting —touching on sub-ambient reactivity, process safety, changing carbon surface chemistry and density, adhesion, inert gas blanketing and concept and effects of passivation.



Pictures of the same zeolite under different operating conditions (left) —dominant wall adhesion and (right) —minimal wall adhesion

## Ensuring reliable feed of shredded biomass to a pyrolysis system

Christian Wurzer<sup>1</sup>, Eddie McGee<sup>2</sup>

<sup>1</sup>UK Biochar Research Centre (UKBRC), Edinburgh, United Kingdom, <sup>2</sup>Ajax Equipment Limited, Bolton, United Kingdom

### Abstract

*Sustainable - Negative Emissions Technology - extreme shape bulk solids - hopper design - screw feeders*

The UK Biochar Research Centre (UKBRC) based at the University of Edinburgh's School of Geosciences, investigates how biochar can be used in resource management, soil improvement and energy production. Biochar is a specially designed charcoal which contains extremely stable carbon, and sustainable production of biochar can be a significant, viable Negative Emissions Technology for mitigating human-induced climate change. It is produced by pyrolysis of biomass feedstocks such as miscanthus grass, wood residues, sewage sludge, coconut shells or leather waste etc. See figure 1.

The original feed system used had limited ability to provide suitable feed to the pyrolysis process especially when awkward flow materials were being used. This paper reports on the development of a new screw feeder and hopper to provide improved feed capability and reliability.

Most shredded wastes and biomasses exhibit varied and awkward flow behaviours which present significant challenges for discharging from hoppers and providing stable, consistent feed. The pyrolysis process works best if a consistent and adjustable feed rate can be assured as unstable conditions can cause process upset, even downstream equipment failure. Whilst understanding the flow behaviour of fine, cohesive powders is well established, the techniques used to predict hopper and feeder design are not fully translatable to larger, extreme shaped bulk solids such as those in figure 1 so the task is challenging. Using a range of test techniques in combination with an understanding of flow and the material's interaction with equipment, a new design was developed. Using larger hopper outlets with better approach geometry can help avoid stable arches, rat holes and the stable structures that interlocking and 'bird nesting' shredded biomass and wastes tend to form when confined. Reliable and regulated mass flow demands that the feeder employed extracts from the full area of the hopper outlet; if this is not achieved then flow reliability from the hopper can be adversely affected. Consideration in type and design of the feeder to serve such outlets is an essential element in achieving proper feed control. This required suitable interfacing and matching the needs of feed rate with constructional and geometrical aspects of both feeder and hopper to best accommodate the materials' properties.

The performance of the new hopper and screw feeder system with various materials will be reported.



Figure 1: Some of the bulk solids handled in the feed system at UKBRC Edinburgh



# Computationally efficient boundary representation for the particle-scale simulation of filtration

Damla Serper<sup>1</sup>, Kevin J. Hanley<sup>2</sup>, Pekka A. Oinas<sup>1</sup>

<sup>1</sup>Aalto University, School of Chemical Engineering, Department of Chemical and Metallurgical Engineering, Helsinki, Finland, <sup>2</sup>The University of Edinburgh, School of Engineering, Institute for Infrastructure and Environment, Edinburgh, United Kingdom

## Abstract

Filtration is a commonly applied separation method in industry. When solids are separated from a liquid, the liquid (filtrate) is forced through a filter medium due to the effect of rotation, a pressure difference or a density difference, while the solids are retained on the filter medium as a porous layer (cake). Cake formation in filtration is a multi-scale phenomenon. The micro-scale behavior of the granular material affects the macro-scale cake formed, although the relationship between these scales is poorly understood. Discrete element method (DEM) is a particle-scale simulation tool which is capable of providing information that is hard to obtain experimentally, such as details of the process of cake formation in complicated processes such as centrifugal filtration. It is commonly used in conjunction with computational fluid dynamics (CFD) to simulate multi-phase flow systems.

Unfortunately, modelling cake formation with DEM presents computational challenges. A major challenge is the computationally efficient representation of a highly porous boundary. Conventionally these boundaries could be represented by a mesh, but at significant computational cost, adding to the challenge of simulating systems which often contain very large numbers of particles. In this work, a novel boundary representation method has been developed to overcome this for the process of centrifugal filtration. The mesh geometry is replaced with a solid cylinder within the selected DEM platform, LIGGGHTS. When a particle comes into contact with a region on the cylinder that has been designated as a pore, the contact force between the particle and the wall is disabled, allowing the particle to pass through. A maximum of five potential contact points are checked per particle so that particles larger than the pores in the filter medium are always retained and cannot egress from the filter. The required code modifications have been implemented in LIGGGHTS.

The conventional and novel boundary representation methods were compared on a supercomputer for the example application of centrifugal filtration. The computation time was reduced up to 40% by adopting the novel boundary representation method while the particle retention was similar to the mesh-boundary cases. This time reduction, while maintaining similar levels of particle retention, could make DEM a more feasible option for investigating filtration processes in the future.

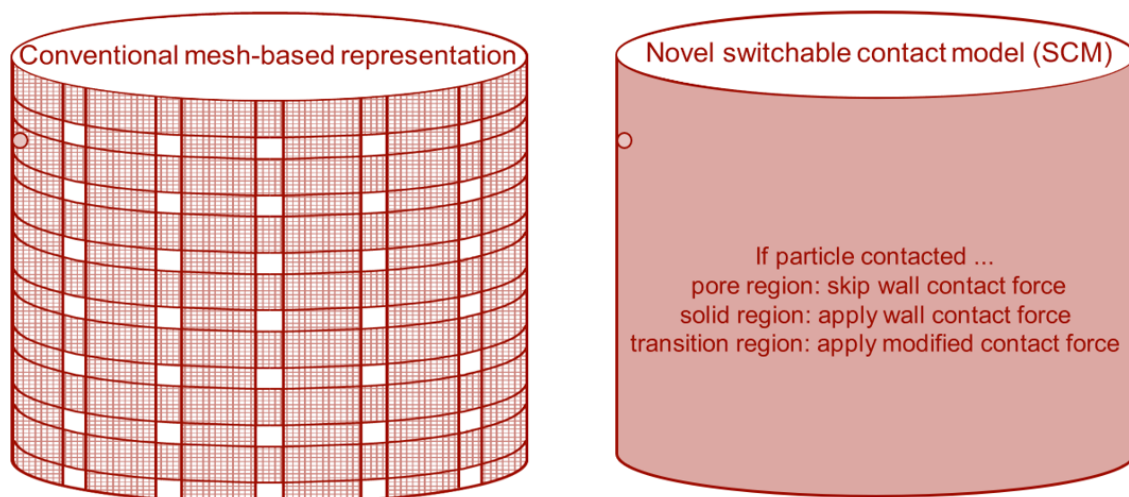


Fig 1. Illustration of mesh-based and novel mesh-free (SCM) boundary representations

## The role of machine learning for intelligent digital twins of fluidized beds

Robert Kräuter<sup>1</sup>, Xiye Zhou<sup>1</sup>, Sven Schiffner<sup>2</sup>, Swantje Pietsch-Braune<sup>1</sup>, Mirko Peglow<sup>3</sup>, Przemyslaw Komarnicki<sup>2</sup>, Stefan Heinrich<sup>1</sup>

<sup>1</sup>Hamburg University of Technology (TUHH), Institute of Solids Process Engineering and Particle Technology, Hamburg, Germany, <sup>2</sup>Fraunhofer Institute for Factory Operation and Automation IFF, Magdeburg, Germany, <sup>3</sup>Pergande Group, Weißandt-Gölzau, Germany

### Abstract

Digital twins are a promising strategy to address the many optimization challenges in the industrial application of fluidized beds, such as the improvement of product quality, energy efficiency and production yield. However, the development of digital twins is a resource-intensive and slow process as it requires large data sets, high domain expertise and reliable methods for the cyber-physical fusion [1]. In this contribution, we discuss the importance of machine learning (ML) to accelerate the development of digital twins, specifically for batch processes in fluidized beds. We have identified three main applications for ML methods within the investigated fluidized bed processes: Soft sensing, process forecasting and multivariable control.

Soft sensing describes the derivation of desired process data from other available measurements [2]. In fluidized beds, soft sensing is particularly useful for a non-invasive inline estimation of the particle water content and the particle size distribution. We demonstrate, how ML-based soft sensors outperform traditional models such as mass-balances.

Accurate process forecasting is essential for any model-predictive control setup, but fluidized bed processes exhibit highly non-linear dynamics, which makes them inherently difficult to predict. We show, how recurrent neural networks can be used in fluidized beds either to generate entirely data-driven forecasts or to predict time-dependent coefficients within flowsheet simulations.

Multivariable control in fluidization processes is used to achieve desired particle properties as fast as possible and within safe operating constraints. We show how Bayesian optimization and reinforcement learning can optimize fluidized bed control parameters under such given constraints.

We report the performance of the proposed ML application in lab-scale fluidized bed experiments of a drying and a spray granulation process. In addition, the applicability of the proposed ML applications in an industrial setting with respect to model interpretability, robustness against concept drift and computational cost is discussed.

[1] F. Tao, H. Zhang, A. Liu, and A. Y. C. Nee, Digital Twin in Industry: State-of-the-Art, *IEEE Trans. Ind. Inform.*, 15 (2019) 2405—2415.

[2] P. Kadlec, B. Gabrys, and S. Strandt, Data-driven Soft Sensors in the process industry, *Comput. Chem. Eng.*, 33 (2009) 795—814.

## The Behaviour of Rotating Intruders in Dense Granular Beds

Robin H Burton<sup>1</sup>, Aidan Brown<sup>1</sup>, John Royer<sup>1</sup>, Lorenzo Conti<sup>2</sup>

<sup>1</sup>The University of Edinburgh, Edinburgh, United Kingdom, <sup>2</sup>Crover Ltd, Edinburgh, United Kingdom

### Abstract

We investigate, via simulation and experiment, the forces felt by a cylindrical intruder pushed vertically into a dense granular bed. When the intruder rotates about its axis perpendicular to gravity it experiences a reduction in the vertical force resisting penetration. To begin to understand how this arises we study the force curve as a function of depth and analyse the flow fields around the intruder, showing that flow field disruption is key to this force reduction.

Unlike movement through liquids or air, our understanding of locomotion in granular media is still quite limited [1]. As well as being of scientific interest, identifying the key factors that aid rotation driven granular locomotion will help our industrial partner Crover to enhance the performance of their granular drone [2].

1. A. E. Hosoi and D. I. Goldman, 'Beneath Our Feet: Strategies for Locomotion in Granular Media', *Annu. Rev. Fluid Mech.*, vol. 47, no. 1, pp. 431-453, Jan. 2015, doi: (<https://doi.org/10.1146/annurev-fluid-010313-141324>).

2. Crover - Grain Storage Management. Accessed: Mar. 19, 2024. [Online]. Available: (<https://www.crover.tech/>)

## Scaling of battery slurry mixing processes using CFD

Selasi Dogbe<sup>1</sup>, Ellie Gibson<sup>1</sup>, William Poizer<sup>1,2</sup>, Scott Gorman<sup>1</sup>, Tommy Coyle<sup>1</sup>, Keri Goodwin<sup>1</sup>

<sup>1</sup>Centre of Process Innovation, Sedgefield, United Kingdom, <sup>2</sup>University of Sheffield, Sheffield, United Kingdom

### Abstract

Battery slurry mixing is an important step in the manufacture of battery cells, with the slurry mixing conditions affecting the final battery cell performance. Slurry mixing can be achieved using different types of mixing mechanisms and the mixers used can vary at different scales with mixers optimised for small volumes favoured at lab scale due to the high cost of battery materials. An example of this would be a dual asymmetric centrifugal (DAC) mixer. These mixers are not typically suitable for use at larger industrial scales where their use becomes less efficient, and high intensity mixers are used instead. However, due to the different mixing mechanisms involved in these mixer types, developing formulations in the lab for use in an industrial scale process can prove difficult.

The work explores the suitability of using Computational Fluid Dynamics (CFD) to simulate the mixing behaviour of different mixing mechanisms at two different scales and establishing the scale up/down rules between the mixers. The models will be presented alongside experimentally produced slurry mixes and their resultant electrochemical performance. This computational approach has the potential to save significant active materials costs when optimising slurry mixing processes for cell manufacturing lines.



# Thermo-mechanical characterization of polymer powders via powder-pocket DMA and shear cell measurements

Thomas Troescher<sup>1</sup>, Helena Weingrill<sup>2</sup>, Denis Schütz<sup>2</sup>

<sup>1</sup>Montanuniversitaet Leoben, Leoben, Austria, <sup>2</sup>Anton Paar, Graz, Austria

## Abstract

Polymers change their morphology in dependence of the temperature. Several measuring techniques are available for identifying the accompanying transition temperatures. These comprise differential scanning calorimetry (DSC), dynamic mechanical analysis (DMA) and thermo-mechanical analysis (TMA) and are i.a. used for detecting the glass transition temperature (T<sub>g</sub>) and crystalline transitions. They differ in their detection technique (changes in heat capacity vs. mechanical characteristics vs. volume) and consequently also in their sensitivity. However, the particulate character of powders often implies measuring difficulties with these techniques as they are rather designed for bulk specimen. The study therefore investigated the suitability and sensitivity of a special powder pocket for conducting DMA measurements on particulate specimen as well as of shear cell tests at elevated temperatures for the detection of T<sub>g</sub> and crystalline transitions of polymer powders. Both methods enabled direct measurement of the powder without any additional preparations which could possibly change the polymer's morphology.

For this purpose, the T<sub>g</sub> (and crystalline transitions if applicable) of three different polymer powders (polyvinylchloride (PVC), polytetrafluoroethylene (PTFE) and thermoplastic polyurethane (TPE-U)) were first determined via powder pocket DMA and then compared to reference measurements of conventional DMA with bulk specimens and DSC. The emphasis was put on optimizing specimen preparation (powder pocket material, sample volume, sample distribution and pre-compression) and evaluation. Due to differences in the thermal conductivity, the outer material of the powder pocket showed the largest impact on the measurement results, whereas the evaluation via the loss factor  $\tan(\delta)$  proved to be the best fitting property function. The sensitivity of powder pocket DMA aligned with the sensitivity of the DSC.

Shear cell tests were conducted at up to six temperatures based on the expected number of transitions. Based on a round-robin test from Berry et al<sup>1</sup>, an evaluation method for free-flowing powders was applied for constructing the yield locus. Characteristic values of the yield locus analysis were then investigated in terms of their sensitivity for detecting the transitions. For all three tested polymers, the angle of linearized yield locus  $\phi_{lin}$  and the angle of internal friction  $\phi_{ef}$  turned out to be most suitable for T<sub>g</sub> detection. Furthermore, it was possible to determine the crystalline transition of PTFE close to ambient temperature by evaluating the major principle stress  $\theta_1$  and the unconfined yield strength  $\theta_c$ .

<sup>1</sup> Berry RJ, et al. Proceedings of the Institution of Mechanical Engineers, Part E: Journal of Process Mechanical Engineering. 2015;229:215-230

## Comparing open-source DEM frameworks for simulations of common bulk processes

Thomas Weinhart<sup>1</sup>, Damien Andre<sup>2</sup>, Vasileios Angelidakis<sup>3,4</sup>, Robert Caulk<sup>5</sup>, Miguel Celigueta<sup>6</sup>, Bruno Chareyre<sup>7</sup>, Jeff Dietiker<sup>8,9</sup>, Jeremie Girardot<sup>10</sup>, Nicolin Govender<sup>11</sup>, Cedric Hubert<sup>12,13</sup>, Rafal Kobylka<sup>14</sup>, Augusto Moura<sup>15</sup>, Vasył Skorych<sup>16</sup>, Dion Wetherley<sup>17</sup>

<sup>1</sup>University of Twente, Enschede, Netherlands, <sup>2</sup>University of Limoges, Limoges, France, <sup>3</sup>Friedrich-Alexander-Universität Erlangen-Nürnberg, Erlangen, Germany, <sup>4</sup>Newcastle University, Newcastle, United Kingdom, <sup>5</sup>Univ. Grenoble Alpes, Grenoble, France, <sup>6</sup>CIMNE, Barcelona, Spain, <sup>7</sup>Univ. Grenoble Alpes, Grenoble, France, <sup>8</sup>National Energy Technology Laboratory, Pittsburgh, USA, <sup>9</sup>Leidos Research Support Team, Pittsburgh, USA, <sup>10</sup>Arts et Metiers Institute of Technology, Talence, France, <sup>11</sup>Research Center Pharmaceutical Engineering, Graz, Austria, <sup>12</sup>Univ. Polytechnique Hauts-de-France, Valenciennes, France, <sup>13</sup>INSA Hauts-de-France, Valenciennes, France, <sup>14</sup>Polish Academy of Sciences, Lublin, Poland, <sup>15</sup>DCS Computing, Linz, Austria, <sup>16</sup>Hamburg University of Technology, Hamburg, Germany, <sup>17</sup>The University of Queensland, St. Lucia, Australia

### Abstract

Multiple software frameworks based on the Discrete Element Method are available for simulating granular materials. All of them employ the same principles of explicit time integration, with each time step consisting of three main steps: contact detection, calculation of interactions, and integration of the equations of motion. However, there exist significant algorithmic differences, such as the choice of contact models, particle and wall shapes, and data analysis methods. Further differences can be observed in the practical implementation, including data structures, architecture, parallelization and domain decomposition techniques, user interaction, and the documentation of resources.

This study [1] compares, verifies, and benchmarks nine widely-used software frameworks. Only open-source packages were considered, as these are freely available and their underlying algorithms can be reviewed, edited, and tested. The benchmark consists of three common bulk processes: silo emptying, drum mixing, and particle impact (see figure 1). To keep it simple and comparable, only standard features were used, such as spherical particles and the Hertz-Mindlin model for dry contacts. Scripts for running the benchmarks in each software are provided as a dataset.



Figure 1: The three common bulk processes, used as benchmarks. Silo emptying (left), drum mixing (centre), and particle impact (right).

### References:

[1] M. Dosta et al , Comparing open-source DEM frameworks for simulations of common bulk processes, Computer Physics Communications 296 (2024), 109066, <https://doi.org/10.1016/j.cpc.2023.109066>.

# Development of a Hybrid Model for battery electrode production with a physics-inspired data-driven approach

Somayeh Hosseinihashemi, Christoph Thon, Carsten Schilde

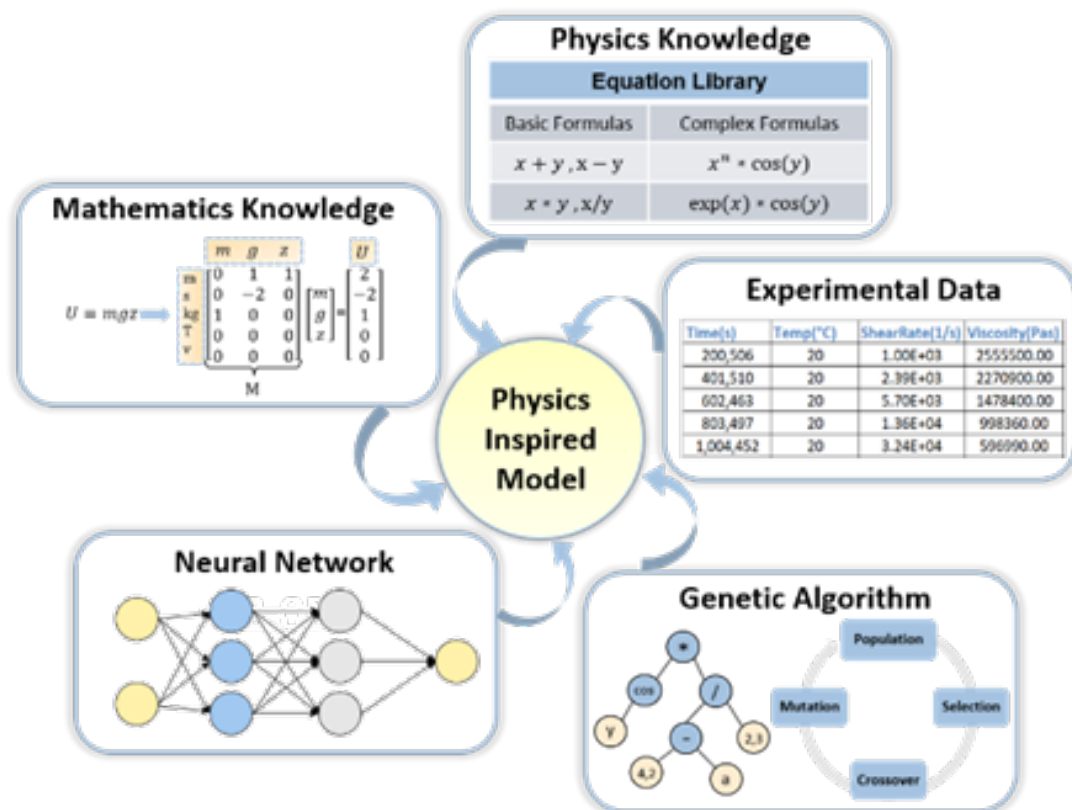
Technische Universität Braunschweig, Braunschweig, Germany

## Abstract

Process development in the industry is primarily based on trial and error and often involves expensive and time-consuming experiments. Typically, simulation analyses are used to build a process model. However, the simulations cannot always consider the manufacturing process's limitations in their modeling. Therefore, the process parameters determined by such a model remain almost theoretical. Alternatively, artificial intelligence methods can be beneficial. The expression of the relationship between physical quantities is widely used in many fields. However, these relationships are quite complex for many systems, making it difficult for conventional methods to determine the correct model. This work uses a hybrid modeling technique, incorporating physics-based knowledge and data-driven techniques. The goal of this approach is to combine the accuracy and physical insight provided by physics-based knowledge with the flexibility and scalability of data-driven models.

To achieve this goal, we combine a deep neural network with a genetic algorithm to determine the existing physical relationships between the data and then estimate the final model for the system. Figure 1 shows the general overview of our modeling technique. More precisely, we set out to determine the symbolic expression for an unknown function  $f$  using a genetic algorithm. To do this, we created a table of data consisting of rows in the form  $x_1, \dots, x_n, y$ , where  $y = f(x_1, \dots, x_n)$ . We first attempted to simplify the data by analyzing it and identifying dimensionless parameters. Next, we utilized a neural network to search for any underlying physical properties within the data. Finally, we employed the genetic algorithm to generate various symbolic functions, selecting the most accurate one as the final expression. The resulting function was then applied as a white-box model to predict the behavior of our system.

This hybrid model allows for a more comprehensive and accurate prediction of the performance of the battery electrode and thus can be used to optimize the production process and improve the performance of the battery.



# Contact Electrification of Rough Particles in Particle-Laden Flows

Simon Jantač<sup>1</sup>, Holger Grosshans<sup>1,2</sup>

<sup>1</sup>Physikalisch-Technische Bundesanstalt (PTB), Braunschweig, Germany, <sup>2</sup>Otto von Guericke University of Magdeburg, Magdeburg, Germany

## Abstract

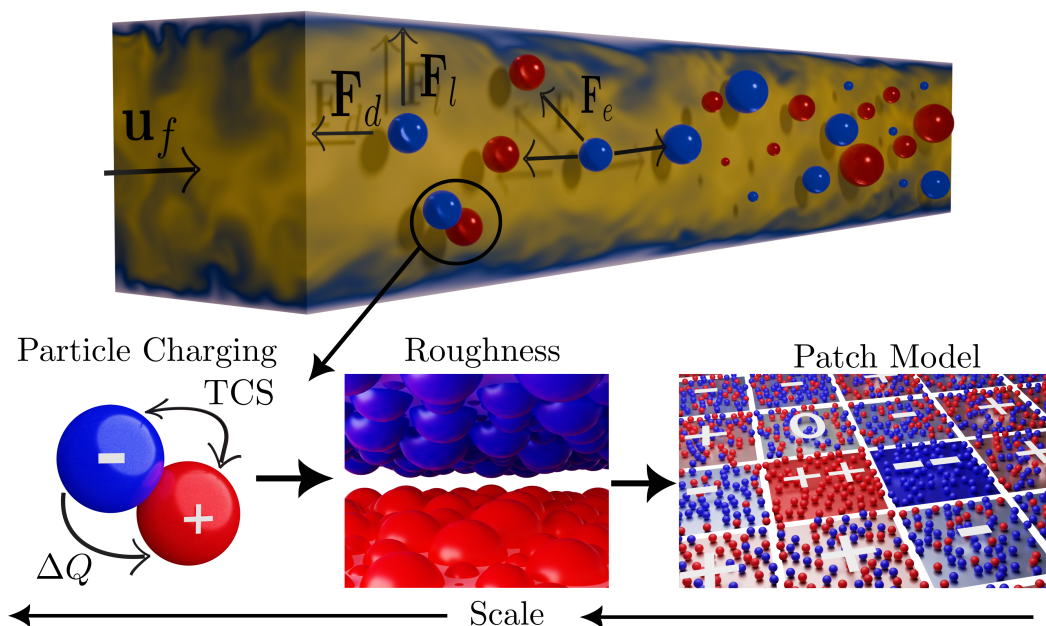
The accumulation of electric charge on particles resulting from contact electrification challenges the handling and pneumatic conveying of powders. Specifically, pneumatically conveyed powders exhibit high charge levels, leading to hazards when storing the powder in silos, where cone discharges can ignite flammable gases or gas-solid mixtures. Moreover, charged particles adhere to container walls, impeding efficient heat transfer. In pharmaceutical industries, precise dosing of charged powders is difficult because they tend to agglomerate and segregate. The mentioned problems underscore the importance of accurately predicting particle charging dynamics within powder handling systems.

Until now, no simulation tool can precisely predict contact electrification in particle-laden flows. The difficulty stems from interacting and competing mechanisms significantly affecting the charging dynamics. For instance, suspended particles collide among themselves and the system walls, separating charge that gradually builds up on the particles. This charge accumulation profoundly affects particle movement within the flow, thereby modifying collisions and subsequent charge accumulation dynamics. Those competing mechanisms are often studied isolated despite being interconnected, limiting the accuracy of simulations.

This study presents a new simulation framework that integrates the complex interactions between particles, flow dynamics, electric fields, and charge accumulation. Our simulations couple a Discrete Element Method to a Computational Fluid Dynamics (DEM-CFD) approach, resolving the flow field through Direct Numerical Simulations (DNS). Contact electrification is described by the donor-acceptor model, allowing for charge transfer between particles of similar materials and between particles and conveyor walls of different materials. Furthermore, we incorporate the influence of the particles' surface roughness on the charge transfer.

To investigate particle charging during pneumatic conveying, we simulate a turbulent channel flow with dispersed particles. These simulations predict the charge distribution in polydisperse powders and the effect of mass loading and wall lining on charge dynamics.

By adopting this approach, we uncovered that turbulence suppresses charging. That means our simulation tool enables finding operating conditions under which particles charge less, and thus, the powder is handled safer and more sustainably.





# DEM analysis of compression process of cohesive elastoplastic powder

Shuji Ohsaki<sup>1</sup>, Takeru Yano<sup>1,2</sup>, Hideya Nakamura<sup>1</sup>, Satoru Watano<sup>1</sup>

<sup>1</sup>Osaka Metropolitan University, Sakai, Japan, <sup>2</sup>Kyushu University, Hakata, Japan

## Abstract

Purpose.

All-solid-state batteries are composed completely of powder, which are expected to the next generation batteries. They are manufactured by compressing powder materials, and understanding the compaction process must be important. Although powder properties affect the compact structure, these effects remain unclear. In this study, we used the discrete element method to investigate the effects of particle cohesiveness and plasticity on the compression of bimodal powders.

Methods.

The DEM is a numerical method for powder motion that considers the motion of each element based on Newton's second law. The Edinburgh elastoplastic adhesion model, which considers particle cohesiveness and plastic deformation, was applied as the contact model. The particle plasticity  $\lambda_p$  was varied from 0 to 0.7. The macroscopic and microscopic properties of the powder compression were investigated.

Results.

In contrast to that for the elastic model, the void fraction at  $V_f = 0.5$  was smaller than that at  $V_f = 0.3$  for the high plastic condition ( $\lambda_p = 0.7$ ). In addition, as the number of fine particles increased, the largest contact type changed in the order of coarse-coarse, coarse-fine, and fine-fine. The plasticity of the particles enhanced the effects of fine particle addition.

Conclusions.

This study demonstrated that the plasticity of the particles affected both the macroscopic and microscopic powder properties. It is important to determine the optimal addition ratio of fine particles based on the plastic deformability of the material [1].

Reference.

[1] Takeru Yano, Shuji Ohsaki, Hideya Nakamura, Satoru Watano, "Compression properties of bimodal powders with different plasticities in the elastoplastic powder compression process: A numerical analysis", *Advanced Powder Technology*, **34**, 1042445 (2023)

## Leveraging a DEM Solids Database for Material Bulk Calibration: Analysis of the Database

Thomas Forgber<sup>1</sup>, Giulia Tranquillini<sup>1</sup>, Paul Kieckhefen<sup>2</sup>, Lukas Kropfing<sup>2</sup>, Philipp Grohn<sup>3</sup>, Johannes G. Khinast<sup>1,4</sup>

<sup>1</sup>RCPE GMBH, Graz, Austria, <sup>2</sup>BASF SE, Ludwigshafen, Germany, <sup>3</sup>Bayer AG, Leverkusen, Germany, <sup>4</sup>Graz University of Technology, Graz, Austria

### Abstract

In material science and engineering, accurate calibration of granular bulk material properties is crucial for process optimization and product quality assurance. Discrete Element Method (DEM) simulations offer valuable insights into the behavior of granular materials. Yet, tuning model parameters to accurately represent the material of interest remains time-intensive.

In this study, we present an analysis of a large numerical solids database used for calibrating DEM model parameters. Focused on commonly used bulk characterization tests such as shear testing, dynamic angle of repose, and powder compressibility, the database facilitates rapid exploration of various bulk properties. By leveraging advanced statistical techniques including Support Vector Regression (SVR), decision trees (XGBoost), and Artificial Neural Networks (ANNs), we establish correlations between DEM parameters and experimental measurements. We highlight the advantages of the Luding contact model over others. Specifically, adjusting the plasticity depth allows us to match bulk behavior, particularly in scenarios involving a wide range of shear and confining stresses.

Our research supports the calibration process across diverse material types, with a focus on pharmaceutical and chemical powders. Sensitivity analyses aid in identifying critical factors influencing bulk behavior. Ultimately, our investigation enables faster parameter calibration and provides insights into the uncertainty introduced by missing characterization data, thus advancing the understanding and optimization of processes involving powders.

# Enhancing Recycling Efficiency of Residual Refractory Materials: Experimental Methods and Fine Particle Classification Techniques

Kristin Søliland<sup>1</sup>, Franz Otto von Hafenbrädl<sup>1</sup>, Akhilesh Kumar Srivastava<sup>1</sup>, Chandana Ratnayake<sup>1,2</sup>

<sup>1</sup>SINTEF AS, Porsgrunn, Norway, <sup>2</sup>University of Southeastern Norway, Porsgrunn, Norway

## Abstract

Refractory linings, essential for high-temperature industrial furnaces and vessels such as cement rotary kilns and steel casting ladles, consist of various tailored refractory product types. Upon reaching the end of their service life, these linings turn into waste with diverse chemical compositions when they are mixed up during the breakout procedure. Recycling of these material presents significant challenges due to the formation of fine powders originating from the removal procedures, consequently these material volumes often need to be landfilled. Particles, particularly those smaller than 5 mm, may also pose health risks to workers and affect environmental quality.

A comprehensive understanding of fine particle behaviour and sorting methods is still lacking, restricting the advancement of efficient handling, sorting, and processing technologies. This limitation obstructs the application of circular economy principles by hindering the utilization of reclaimed materials for reuse as secondary raw materials.

To tackle these challenges, the present study, as a part of 'ReSoURCE' (Refractory Sorting Using Revolutionizing Classification Equipment) project funded by EU Horizon program, explores experimental methods to minimize dust generation and develop direct sorting techniques for maximizing material recovery for recycling. Air-assisted classification techniques, such as crossflow air classifiers and multi-chamber fluidized bed classifiers (Figure 1), show promising results by leveraging differences in particle size and density. The presentation will outline the methodologies used, experimental findings, and future directions towards achieving effective recycling of residual refractory materials, thereby contributing to sustainable resource management in industrial settings.

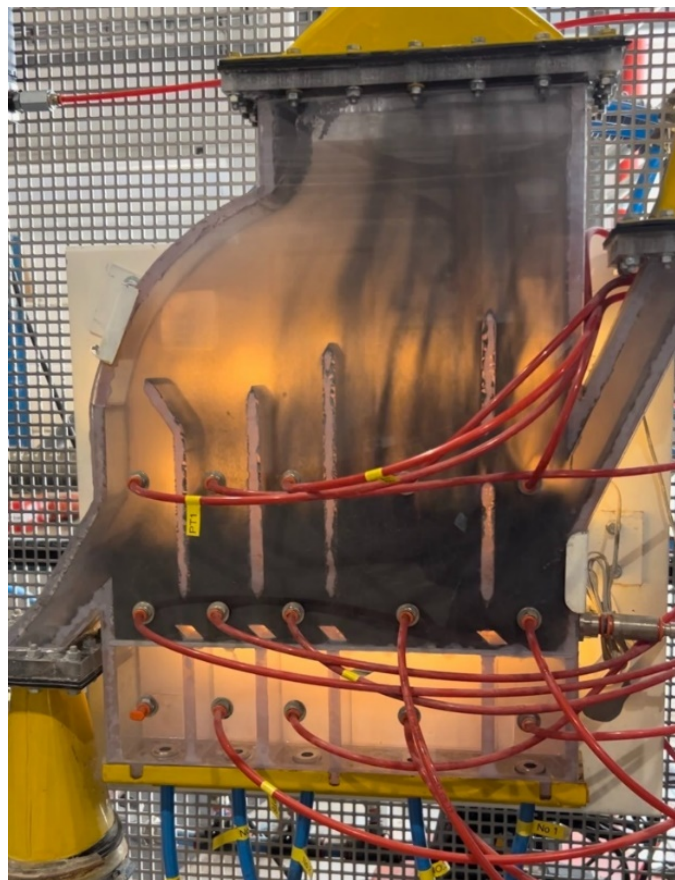


Figure1: Multi-chamber fluidised bed classifier

# Modeling of Agglomeration Processes in Multi-Component Suspensions: Challenges and Data-Driven Solutions

Frank Rhein, Haoran Ji

Particle Dynamics in Heterogeneous Systems, Karlsruhe Institute of Technology, Karlsruhe, Germany

## Abstract

Agglomeration is a unit operation in mechanical process engineering and thus relevant for almost all processes in particle technology. Targeted or selective agglomeration in multi-component suspensions finds wide applications. A current example is the microstructure in lithium-ion batteries, which is adjusted by hetero-agglomeration and significantly influences the resulting product properties. Only limited analytical tools exist to determine relevant properties, such as the material-specific agglomerate composition. This motivates the search for predictive computational methods that provide insight into the micro-processes taking place and thus access to process information that cannot be measured.

Generally, population balance equations (PBE) are used for this purpose, which allow a calculation of macroscopic agglomeration processes. A reliable determination of the agglomeration and breakage rates, the so-called *kernels*, is essential. Especially in multi-component suspensions this is challenging and hardly described so far, since all interactions between all occurring components have to be considered and their description is further complicated by locally heterogeneous surface properties. Another challenge in modeling real systems is the availability of reliable and comprehensive material data. In the field of agglomeration, in particular pH-dependent surface potentials, Hamaker constants, but also fundamental correlations for the hydrophobic interaction are not available or are subject to errors. Including breakage further complicates the models. This totality of uncertainties prevents a purely predictive modeling.

This presentation provides a broad overview of the challenges laid out above. Solution strategies and valuable kernel-models are presented that enable simplification of the system while maintaining physical accuracy. Data-driven models from the field of machine learning are presented can help to incorporate material data into mechanistic PBE models. The resulting hybrid model (HM) combines the advantages and mitigates the disadvantages of purely data-driven and physics-based approaches (Rhein et al., 2023). Application examples and perspectives on future developments are given.

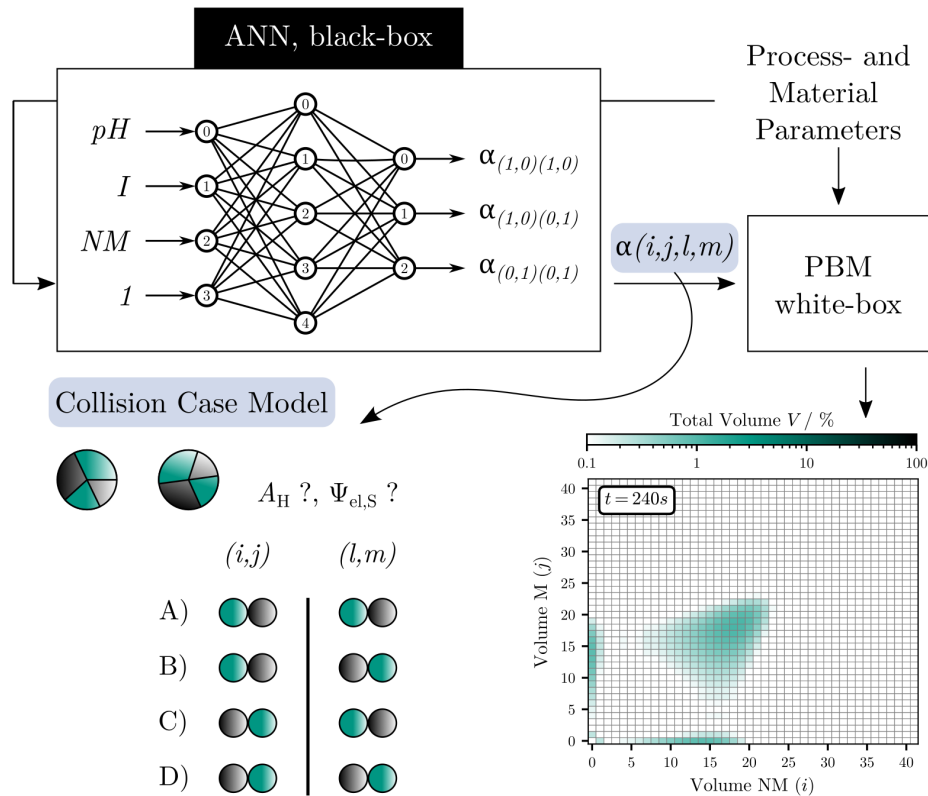


**Fig. 1 :** Scheme of a serial hybrid model consisting of an ANN and PBE for the calculation of 2D agglomerate distributions. The collision case model is used for reducing the number of required kernel parameters.



## Industrial-Scale Bin Blending: Insights from DEM Simulations of Realistic Pharmaceutical Powders

Fatemeh Mostafaei<sup>1</sup>, Benedict Benque<sup>1</sup>, Dalibor Jajcevic<sup>1</sup>, Doshi Pankaj<sup>2</sup>, Matthew Santangel<sup>3</sup>, Rolf Larsen<sup>3</sup>, Hong-Guann Lee<sup>3</sup>, Diogo GomesLopes<sup>4</sup>, Mario Schaefer<sup>4</sup>, Johannes Khinast<sup>5</sup>

<sup>1</sup>Research Center Pharmaceutical Engineering, Graz, Austria, <sup>2</sup>Worldwide Research and Development, Pfizer Products India Pvt Ltd, Mumbai, India, <sup>3</sup>Worldwide Research and Development, Pfizer Inc, Groton, USA, <sup>4</sup>Catalent Pharma Solutions, Schorndorf, Germany, <sup>5</sup>Institute for Process and Particle Technology, TU Graz, Graz, Austria

### Abstract

Bin blending is a commonly employed unit operation in oral dosage form manufacturing that is essential in achieving a consistent blend from individual powder components. While its implementation is straightforward, attaining the desired blend uniformity presents challenges such as the time required for blending and the potential for segregation of components. Selecting an appropriate blender and operational conditions becomes crucial, considering material characteristics, batch size, sensitivity to attrition, and other factors.

Numerous studies have delved into mixing behavior in various types of lab-scale blenders. It is generally observed that the fill level and loading pattern significantly influence blending behavior and that differences in particle size, density, or cohesivity between materials increase the risk of segregation. Segregation patterns under different geometries and operational conditions have been documented in the literature, mostly focusing on lab-scale processes involving components with markedly different properties. The risk of segregation in pharmaceutical powders, i.e., powders that have similar properties, at an industrial scale remains unexplored.

Discrete Element Method (DEM) simulations offer a valuable tool for understanding industrial-scale blending processes, aiding in process design, troubleshooting, and risk assessment. Nevertheless, DEM simulation of industrial-scale blending poses computational challenges related to particle number, shape, and size distribution. Correctly capturing the bulk powder behavior with a reasonable computational effort necessitates simplification of the model and calibration of DEM parameters.

This study addresses the blending performance of realistic pharmaceutical powders in an industrial-scale bin blending process through DEM simulations using XPS. Specifically, the investigation focuses on blending two granular materials in commercial-scale (200, 600, and 1400L) cone blenders. DEM parameters were calibrated using experimental small-scale powder characterization data. The predicted blend uniformity for different batch sizes in various blenders was then assessed to guide operating condition selection. For cone blenders, the study explores the influence of fill level, presence of baffles, alternating the rotation direction, filling order, and bin size on blend quality. Model results were compared to experimentally determined blend uniformities for validation.

The simulations correctly predict prolonged blending times at higher fill levels. The simulations also show that angled baffles in the lid enhance mixing along the rotation axis but also increase the risk of axial segregation. This enhanced segregation risk can be mitigated by periodically changing the rotation direction, showcasing how DEM simulations can be used to find the delicate balance required in optimizing industrial-scale bin blending processes.

# DEM Modeling of direct shear test using periodic boundary: Sample size, boundary conditions, and computation efficiency

Anas Almudahka<sup>1,2</sup>, Mohammad Salehian<sup>2</sup>, Stefan Pantaleev<sup>3</sup>, John Robertson<sup>2</sup>, Daniel Markl<sup>2</sup>

<sup>1</sup>Department of Pharmaceutics, Kuwait University, Kuwait City, Kuwait, <sup>2</sup>Centre for Continuous Manufacturing and Advanced Crystallisation (CMAC), Strathclyde Institute of Pharmacy and Biomedical Sciences (SIPBS), University of Strathclyde, Glasgow, United Kingdom, <sup>3</sup>Altair Engineering, Edinburgh, United Kingdom

## Abstract

Quality by Design (QbD) is an integral part of the development of new drug products in the pharmaceutical industry. The quality target product profile (QTPP) is achieved through an excellent understanding of the product's critical quality attributes (CQAs) and its link to critical process parameters (CPPs) and critical material attributes (CMAs). The industry is undergoing a notable transition towards embracing modelling techniques in their QbD efforts to enhance product quality and reduce material waste during development and manufacturing.

One such modelling technique used in the pharmaceutical industry is discrete element modelling (DEM) that allows for a detailed mechanistic understanding of material behaviour in the process. However, calibration of DEM parameters is a significant challenge that arises when employing such mechanistic models. This work aims to standardise the DEM calibration process while employing a mix of different concepts to allow for more rapid and precise calibration of any pharmaceutical powder. Shear cell is one of the tools that is used in the industry to characterise material flowability and, consequently, its behaviour in different manufacturing scenarios. Previous works explored shear behaviour in DEM but their is lack of detailed exploration of critical parameters that affect the results. This works dives into different critical parameters that affect result's accuracy such as how to save precious computaional time, sample size needed to accurately capture a yield locus, and how to properly shear a material.

This study demonstrated the use of a cubic miniature digital shear cell (designed in Autodesk Inventor Professional 2024) in a DEM simulator (v2023.1, Altair® EDEM™ ©) to efficiently and accurately calibrate DEM parameters. This approach mimics the key characteristics of an experimental shear cell while ensuring computational efficiency for parameter optimisation. Major consolidating stress (MPS), unconfined yield strength (UYS), angle of internal friction (AIF), and effective angle of internal friction (eAIF) from DEM and experimental data (Brookfield PFT, Ametek) are used as calibration targets to capture the yield locus.

The DEM shear cell delivers precise calibration parameters for simulating experimental shear cell outputs. The use of inertial scaling among other techniques accelerated the simulations significantly allowing rapid and extensive exploration of the design space to develop a predictive model. The techniques and parameters explored in this work allowed understanding of several questions not addressed in the literature and enables accurate shear cell simulation and reduced computational cost.

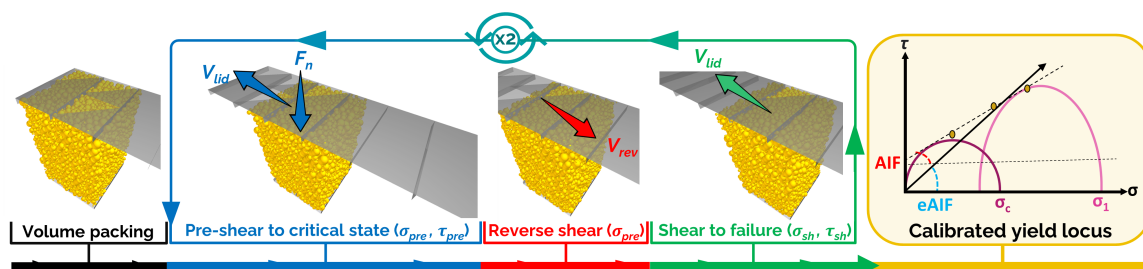


Figure 1: Overview of a pharmaceutical material flowability characterisation in DEM

## The second decade of DEM at BASF

Paul Kieckhefen, Dominik Weis, Rouven Weiler

*BASF SE, Ludwigshafen, Germany*

### Abstract

The use of Computational-Fluid-Dynamics (CFD) has become increasingly prevalent in industries that deal with fluid-dominated processes. It has become a standard tool in the automotive industry and is now gaining traction in other sectors. On the other hand, the application of Discrete-Element-Methods (DEM) for simulating processes dominated by solids was introduced to the chemical industry in the early 2000s and has recently reached an appreciable level of maturity and track record.

This presentation will discuss the evolution of DEM in addressing the challenges faced in the chemical industry. Specifically, it will focus on advancements made in the last decade, including successful problem-solving, ongoing research at BASF, and challenges to be addressed in its second decade of application to industrial issues. Both standalone DEM simulations and coupled CFD-DEM simulations in industrial practice will be explored.

# Calibrating the Bonded-Particle Model for coated tablets in order to investigate the occurrence of chipping defects during coating processes

Tobias Nolte

*Merck Healthcare KGaA, Darmstadt, Germany, Technische Universität Berlin, Berlin, Germany*

## Abstract

In the development phase, various coating processes and formulations can be tested using smaller lab-scale coaters. However, transferring the process to production-scale coaters comes along with a risk of higher mechanical stress. Coating processes that worked well in the lab-scale settings may unexpectedly result in defects such as fractures or more superficial edge chipping during production as a result of mechanical stress. Even though tablet fracture is certainly more critical, these superficial chipping defects, usually with no impact on efficacy or safety, are much more frequent and thus represent a bigger economic impact as they lead to sorting of the batch with many rejections. Therefore, an enhanced strategy is required to accurately predict and mitigate these issues during scale-up.

Given the difficulty of experimentally determining the forces exerted on tablets within a coater, Discrete Element Method in combination with Bonded-Particle Method (DEM-BPM) simulations offer a promising approach. Calibrating the DEM-BPM to reliably predict chipping for coated tablets is challenging and has not been previously accomplished. In my research showcase, I will present the developed calibration strategy for DEM-BPM, which will later be used to predict the defect probability of coated tablets during coating processes. The essential parameters that require calibration for the DEM-BPM simulations include:

- Static friction coefficient: Primarily determined by the angle of repose of the tablets.
- Rolling friction coefficient: Adjusted through a rotating drum and the dynamic angle of repose formed.
- Coefficient of restitution: Experimental determination for irregular bodies is comprehensive as they rarely rebound perfectly upwards, making the evaluation of the restitution coefficient quite intricate. However, securing the tablets in a pendulum apparatus allowed for an assessment as the tablet is constrained to move only in two dimensions due to the fixation.
- Bond strength within the BPM: The tablets are not completely shattered but rather experience localized detachment of portions of the coating. For that, a force is required that stresses the adhesion of the coat only within a specific area of the tablet. This was achieved by using an adhesive on a specified area, which is being pulled perpendicularly upwards, and recording the force required to detach the coating.

Future work will be required to further validate the calibrated DEM-BPM and to use it to better understand defect genesis in dependence of the forces involved during large-scale production.



## Optimisation of Overland Conveyor Systems using Large Diameter Idler Rolls

Peter W Robinson<sup>1</sup>, Tiago Cousseau<sup>1</sup>, Jayne O'Shea<sup>2</sup>, Yusuf Badat<sup>2</sup>, Michael Carr<sup>1</sup>, Craig Wheeler<sup>1</sup>, Jason Willis<sup>1</sup>

<sup>1</sup>The University of Newcastle, Newcastle, Australia, <sup>2</sup>TUNRA Bulk Solids, Newcastle, Australia

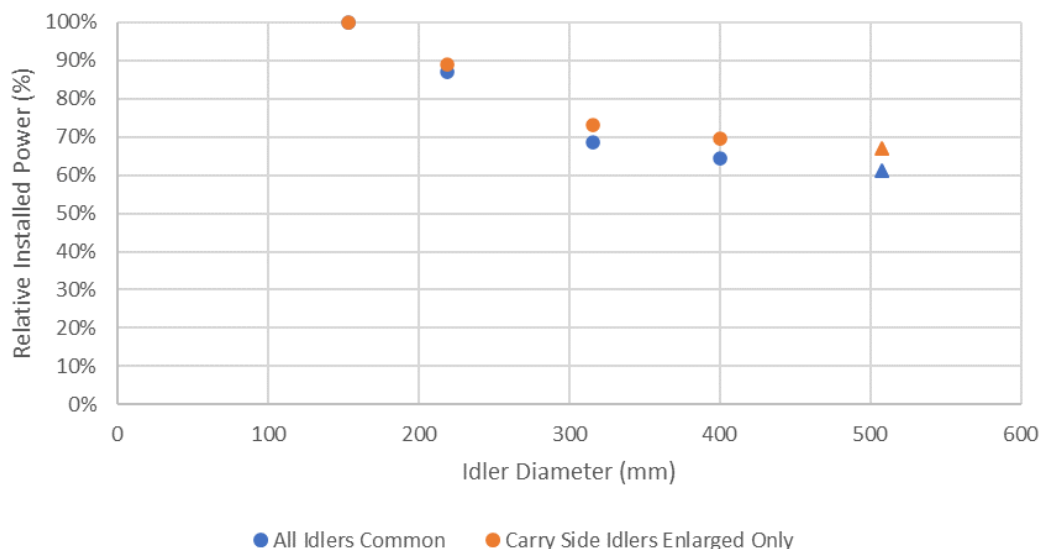
### Abstract

Belt conveying systems are a highly effective solution for transporting large quantities of bulk materials over long distances. In comparison to trucks and rail transport, overland conveyors are continuous and cost-effective, with the ability to transport in excess of 10,000 tonnes per hour. Their primary limitation lies in the use of a rubber belt running over rigid idler rolls, giving rise to Indentation Rolling Resistance (IRR). Indentation rolling resistance arises due to the viscoelastic contact between the conveyor belt and an idler roll. As a belt travels over an idler, an asymmetric pressure distribution is formed within the belt bottom cover that opposes the direction of movement, resulting in a drag force to the system. For conventional systems, this resistance can account for up to 60% of the total drive power.

Idler diameter is known to have a considerable influence on the indentation rolling resistance of belt conveying systems, by reducing the indentation and contact stress. But how big is too big? As handling equipment becomes more developed and readily available on-site to aid in conveying component installation, larger idler diameters are becoming a more viable option to install on long conveying systems due to their energy-saving potential. This research measures the indentation rolling resistance of idlers, on a scale considerably larger than anything previously attempted, with idler roll diameters of 152.4 mm, 219 mm, 316 mm and 400 mm. These results were further extrapolated to 500mm, using industry-accepted models.

The second consideration relating to large-diameter rollers lies in the performance of the bearings, and the requirement to use a larger bearing with a higher load rating. Rim Drag describes the frictional losses within a bearing, primarily due to grease or lubricants within the bearing and seals and can account for up to 5% of the total drive power. Experimental testing of bearings suited for larger idlers determined a reduction in rim drag of between 58% and 79%, due to the increase in idler diameter relative to bearing diameter.

Lastly, to fully quantify the benefits of larger idler rolls for overland conveying, a case study is presented. This study determines the drive power required for a 10km system when using a range of idler diameters. In comparison to a baseline exhibiting 153mm idlers, a potential energy reduction of between 30-39% can be achieved through the appropriate selection of idlers with a diameter between 400 and 500mm.



# Characterizing sulfur/porous-carbon composite particles prepared from the hot-melt kneading process for all-solid state batteries

Motoshi Iwao, Hideya Nakamura, Shuji Ohsaki, Satoru Watano

Osaka Metropolitan University, Sakai, Japan

## Abstract

All-solid-state lithium sulfur batteries (ASSLSBs) have attracted much attention owing to their high safety and high energy density. When fabricating cathode of ASSLSBs, it is necessary to composite sulfur (cathode active material) with porous carbon (electron conductor) and solid electrolyte (lithium-ion conductor) due to electron and lithium-ion insulating nature of sulfur. As a productive compositing process of sulfur and porous carbon, we proposed to use a hot-melt kneading process [1]. In the hot-melt kneading process, heat and shear force are applied to particles, resulting in that sulfur with lower melting temperature (120 °C) was melted and melted sulfur was kneaded with porous carbon. We have demonstrated that composite particles prepared from the hot-melt kneading process improved electrochemical performance [1]. In the composite particles, sulfur can exist inside and/or outside the pore of porous carbon. This sulfur-existing region can be a key structural parameter to determine the battery performance. However, a key parameter to control the sulfur-existing region in the composite particles was unclear. Furthermore, correlation between the sulfur-existing region and electrochemical performance of ASSLSBs was also unclear. Thus, in this study, we examined to clarify the aforementioned unclear key parameter and structural-performance correlation.

By changing the weight ratio of sulfur to porous carbon, two types of composite particles were prepared; those with almost whole sulfur existing inside the pore and those with a part of sulfur existing outside the pore. Therefore, we clarified that the weight ratio of sulfur to porous carbon is the key parameter to control sulfur-existing region in the composite particles. Moreover, with an increasing amount of sulfur existing outside the pore of porous carbon, particle size of composite particles increased due to agglomeration of porous carbon by melted sulfur existing outside the pore. The two types of composite particles showed different electrochemical properties. The composite particles with almost all sulfur existing inside the pore exhibited higher initial capacity, whereas the composite particles with a part of sulfur existing outside the pore exhibited higher cycling stability.

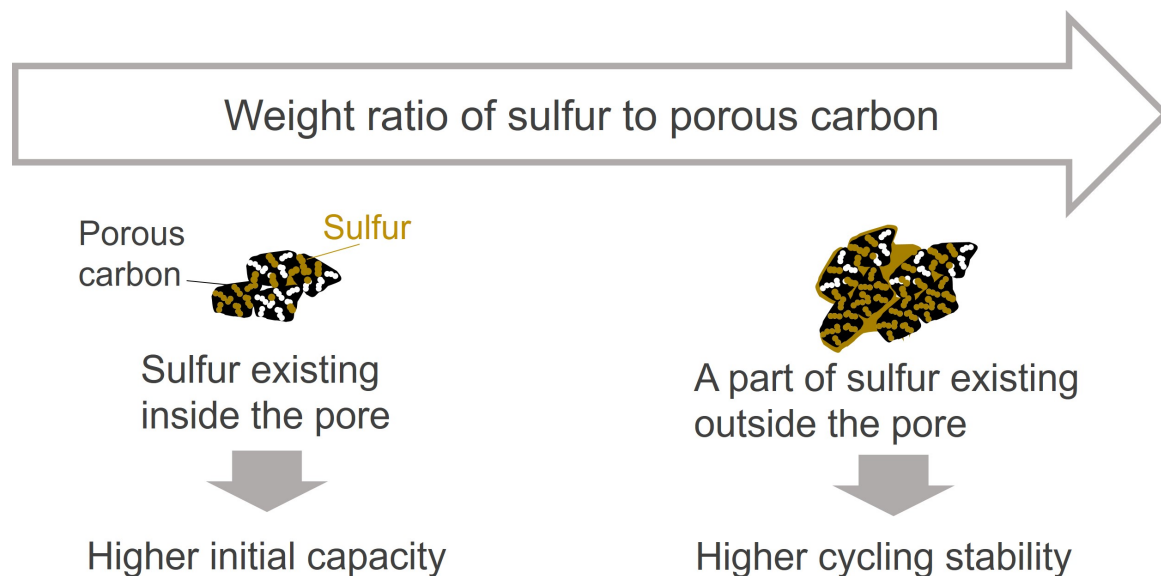


Figure. Summary of this study

**Reference** [1] Iwao, M. et al., Advanced Energy and Sustainability Research , (2023), 2200206

# Influence of surface modifications on bulk solids properties of powders for concrete 3D-printing

Niklas Meier, Harald Zetzener, Arno Kwade

*TU Braunschweig - iPAT, Brunswick, Germany*

## Abstract

Concrete is the most widely used building material in the world. At its simplest, it consists of aggregate, the hydraulic binder cement and water. Over the last few decades, concrete formulas have been further developed so that ever higher strengths are possible, for instance due to additives. However, the formation is still done by simple and often hand-build formwork. As these forms can hardly be structurally optimised, more material is used than necessary and architectural freedom is limited. In order to be able to produce complex and customised concrete components cost-effectively, various additive manufacturing processes are currently being investigated, such as concrete 3D printing using selective cement activation (SCA). This additive manufacturing process is a so-called particle bed process in which a mixture consisting of sand and cement is first applied in layers (particle bed). The cement is then activated by selectively jetting water onto the relevant areas so that it sets locally. This binds the particles and the designed component is created layer by layer. However, there are still some challenges with this process, e.g. the achievable strengths are still too low for structural use.

One reason for the comparatively low strength of components printed with SCA is the low part density of around  $1.7 \text{ g/cm}^3$ . This can be improved by increasing the packing density in the powder bed, in order to produce stronger components. One way of increasing the packing density is to modify particle surfaces in order to achieve customised bulk material properties. This has been successfully carried out in this study, by modifying the particles with nanoparticulate coatings or liquid additives in different amounts. Thereby, the tapped density of the material could be increased by more than 8 % for both types of surface modification. This lead to an increase in compressive strength by more than 30 %. However, it was observed, that only the nanoparticulate coatings lead to an increased flowability, while the liquid additives have no significant effect. In this submission, the influence of the different mechanisms of surface functionalisations on various bulk solid characteristics (e.g. bulk and tap density, flowability  $FF_C$ , dynamic angle of repose) is compared and discussed in detail.

## Introduction to the ON-DEM COST Action

**Daniel Barreto**

*School of Computing, Engineering and the Built Environment. Edinburgh Napier University, Edinburgh, United Kingdom*

### Abstract

The ON-DEM COST Action (CA22132: Open Network on DEM Simulations) started in October 2023 and will continue until October 2027. This COST Action was created with the aim of unifying knowledge and people across wide/diverse DEM communities. The Action will assess and extend what can be achieved with DEM by disseminating new developments, promoting best practice, providing simulation examples, validation experiments, common tools for data analysis, as well as training of young researchers and involving other interested parties.

The ON-DEM COST Action has five themes: (i) tackling real (large) industrial and engineering problems; (ii) using physics to account for complex phenomena more realistically; (iii) big data and visualization tools for better and quicker DEM analysis of results; (iv) normalisation and best practice; (v) enhancing commercial utilisation of DEM codes. Each of these themes is aligned to a different Working Group, addressing major current challenges related to DEM simulation. Further details of ON-DEM and instructions on how to join the network can be found at

This talk from the Action Chair will introduce the ON-DEM Cost Action, summarise progress to date and the next steps. This will lead into a set of five talks selected for their particular relevance to the activities of ON-DEM.



# Development of a model for die filling under suction for different scales and setups of rotary tablet presses

Lars Wagner<sup>1,2</sup>, Ann Kathrin Schomberg<sup>1,2</sup>, Arno Kwade<sup>1,2</sup>, Jan Henrik Finke<sup>1,2</sup>

<sup>1</sup>Technische Universität Braunschweig, Institute for Particle Technology, Braunschweig, Germany, <sup>2</sup>Technische Universität Braunschweig, Center of Pharmaceutical Engineering (PVZ), Braunschweig, Germany

## Abstract

Tablets are the most commonly used dosage form. The filling process is considered to be a critical step in tablet production as it influences critical quality attributes and is not yet fully understood. The commonly used filling mechanism is suction filling, where the lower punch is pulled down below the powder bed inside the feed frame. To ease future work on rotary presses, the aim is to develop a first model to describe suction filling behavior on rotary presses, with particular focus on the transferability to different scales. The prediction of the tablet weight by the new developed model should be only based on material and process parameters. In addition, the model's applicability from rotary presses with one paddle wheel to rotary presses with two paddle wheels is investigated. To ensure the broad applicability of the developed model, different materials with varying flow properties and permeabilities were used.

In order to predict tablet weight, the main goal was to model the powder volume flows into the dies. Throughout the modeling process, different correlations were found between the powder volume flow and process parameters such as the turret and paddle wheel speed and the material parameters already mentioned. Modeling is particularly advantageous if it is carried out on the basis of relatively simple experiments and still allows more complex conditions to be predicted. For this reason, the model development is based on experiments on one-paddle feed frames (on X 3 and XL 400 from KORSCH AG). The transferability to two-paddle feed frames as well as to a larger scale (XT 600 from KORSCH AG) is proved by means of parity plots, where the critical paddle wheel speeds for complete die filling is compared (see Figure 1).

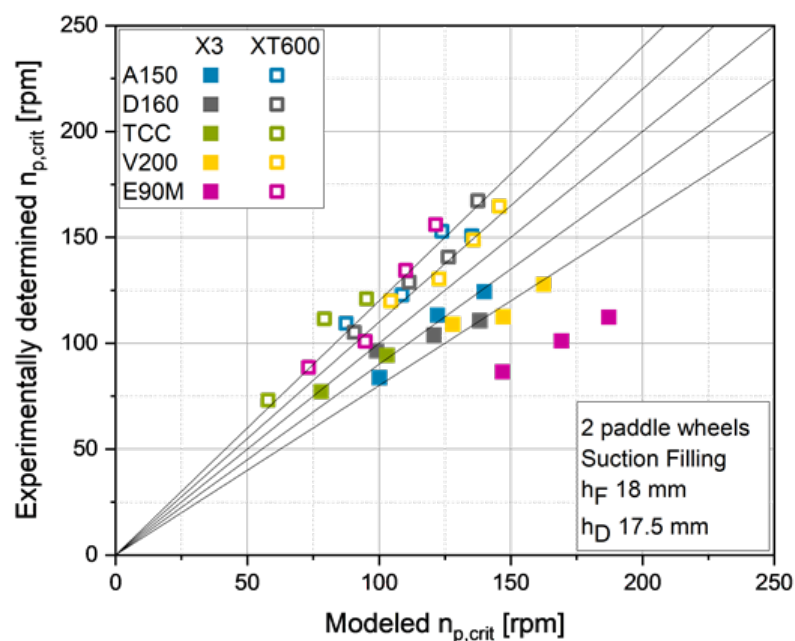


Figure 1: Parity plot to show the transferability to two-paddle setups

When applying the model to the X3 and the XT600 with two-paddle setup without further adaption, an acceptable applicability can be identified, but with a slight tendency to overestimate or underestimate the critical paddle speed. This is particular beneficial for the XT600, as two scale-up challenges are considered: the larger machine scale and the higher number of paddle wheels. However, the model still is under further improvement because some aspects are still not taken into account, such as the influence of the direction of rotation or the geometry of the feed frame and paddle wheel.

## Dry What? Dry Water: Bulk Properties and Mechanical Stability

Leigh D. Hamilton, Harald Zetzener, Arno Kwade

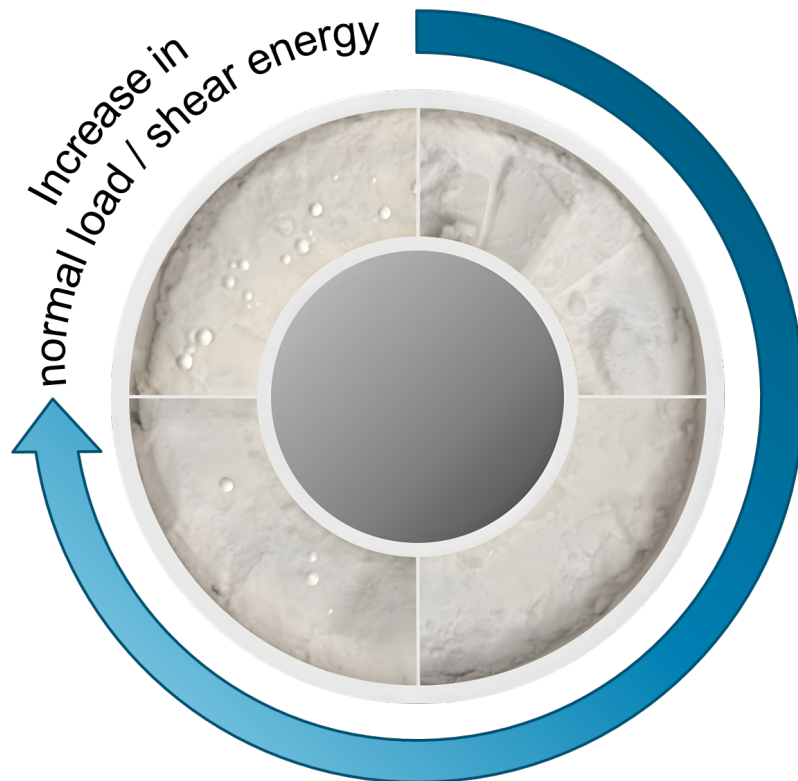
TU Braunschweig - iPAT, Brunswick, Germany

### Abstract

The ongoing climate change requires innovative approaches to solving problems thereof. Issues such as storing greenhouse gas emissions or extinguishing fires are thereby becoming more relevant. One lesser-known material that has the potential to be used in both cases is dry water. Dry water first appeared in 1964 when a patent was filed with the title "Predominantly aqueous compositions in a fluffy powdery form approximating powdered solids". Decades later, dry water found its first industrial application as a carrier material for creams and powders. Since then, the high specific surface area of dry water has led to further fields of application, such as extinguishing fires, carbon as well as methane sequestration, and implementing it as a reaction catalyst. In general, dry water consists of microscale water droplets surrounded by stabilising hydrophobic silica nanoparticles, which renders it an encapsulated form of water. Even though dry water can contain up to 98 wt.% water, it appears as a powder with initially cohesive bulk behaviour. The cohesive properties can be overcome by slight agitation, resulting in a free-flowing powder. However, mechanical or thermal stress can disrupt the structure of the stabilising nanoparticles, subsequently leading to capsule disintegration.

In this study, the bulk properties of the water-in-air dispersion are analysed in more detail to make predictions about the transportability, storability and stability of the encapsulated water. Firstly, dry water was produced in an Eirich intensive mixer with different parameter settings and the process was described using a stress intensity and stress number. The bulk properties of the samples were then analysed at various consolidation stresses in a ring shear tester as well as in a rotating cylinder (dynamic angle of repose).

Initial results showed an influence of the process properties on the resulting product and its unconventional bulk material properties. For example, higher intensities resulting from the stirrer tip speed produced finer dry water particles, which became more cohesive. However, excessive intensities led to coagulation or instability of the capsules, which in turn are identifiable in the ring shear tester. Furthermore, higher stress conditions in the ring shear tester altered the bulk material or the capsule condition, thus releasing water in the shear plane (see *figure 1*). Consequently, conclusions can be drawn about the mechanical stability of the sensitive capsules whilst providing interrelations between disperse properties and material handling.



# Decoding Attractive Interactions in Granular Materials through Vibration-Induced Densification

Maria G Cares, Veronique Falk

Université de Lorraine, CNRS, LRGP, Nancy, France

## Abstract

Within the intricate realm of granular materials, the behavior of grain assemblies introduces complexities marked by nonlinear and inelastic phenomena that seamlessly bridge the microscopic grain scale to the macroscopic scale of flow. Understanding the mechanics of granular materials faces a crucial challenge in establishing connections between microscopic grain properties and macroscopic flow properties. This study investigates the densification of granular materials, a phenomenon relevant across various technological domains in powder processing and manufacturing. Specifically, we explore the vibrational conditions leading to the compaction and decompaction of industrial granular materials subjected to vertical vibration utilizing a particle damper (Figure 1.a), across over a dozen industrial powder samples as varied as plaster, wheat flour, and pharmaceutical excipients. The experiments involve controlling the vibration wave by adjusting parameters such as frequency, amplitude, and time between oscillations while measuring and recording the acceleration and force signals. The height of the powder bed is determined through image analysis from a high-speed camera, enabling the assessment of the dynamics of both compactness and the Hausner ratio for numerous experimental conditions.

Our findings reveal a significant correlation between the energy required to decompact the powder bed and the cohesive forces between grains. This correlation facilitates the determination of a dimensionless number offering insights into flow indexes such as the flow factor,  $\phi$ , and the Hausner ratio, HR (Figure 1.b). Studying elastic properties through damping experiments reveals the limitations of HR and classifications for softer or more elastic particles prone to deformation during densification. This experimental approach seems to provide a straightforward method to unveil the intricate relationship between local particle interactions and the overarching mechanical behavior of granular materials contributing to advancements in understanding and predicting powder flow behavior.

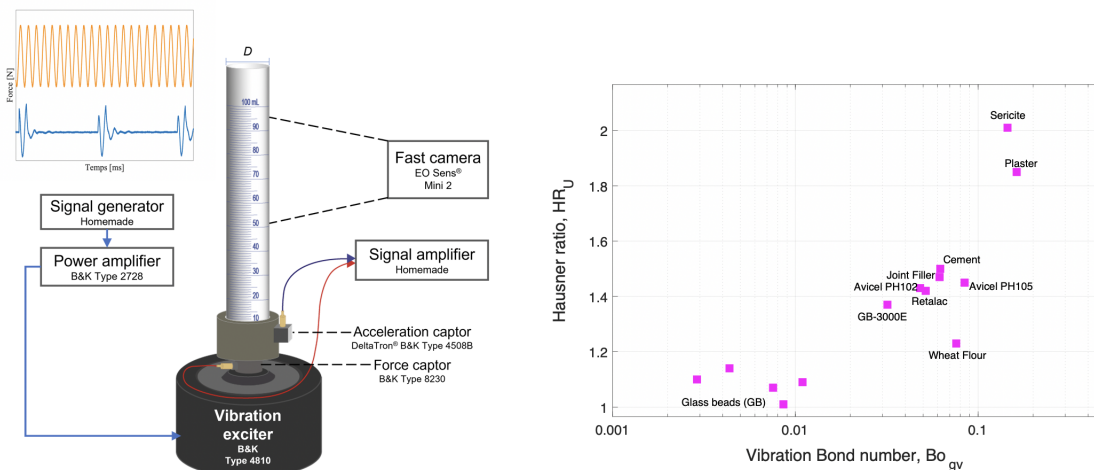


Figure 1. (a) Experimental setup of the particle damper. (b) The relationship between the vibration Bond number, determined from the force required to decompact the powder bed, and the Ultimate Hausner ratio ( $HR_U$ ) measured at the densest state.

## Dead zones aren't dead: state of the art and a model concept for eccentric discharge

Merle Schröder, Harald Zetzener, Arno Kwade

*TU Braunschweig - iPAT, Brunswick, Germany*

### Abstract

Although, the development of silo construction began in the 19th century with the work of Janssen and following extensive research in the last century, many questions regarding flow in silos remain unanswered. Oversizing or, in the case of incorrect design, silo damage must be avoided, i.e. preventing dead zones is thereby one of the key factors. Dead zones may arise from shallow or rough hopper slopes and in addition, the choice of shaft diameter is crucial for the hindrance of dead zones. Since dead zones often cannot be avoided from a process engineering point of view due to changes of the stored bulk solid in an existing silo, it is even more important to understand their development, the effects they have on the bulk solids (e.g. deviation from initial stresses in the silo), and the resulting loads on the silo wall. This presentation will begin by providing an overview of the current state of research in order to demonstrate the importance of research regarding dead zones.

In the second part of the presentation, a new research approach will be presented which investigates the load effects caused by dead zones on the silo wall that occur during eccentric discharge. Generally, eccentric openings lead to asymmetrical load effects, thereby requiring special attention. In the current load approach for the design of eccentric discharge (DIN EN 1991-4), several assumptions are necessary. As a means of contributing to a sturdy and sustainable silo design without oversizing or silo damage, fundamental research is important. An engineering model for load effects during eccentric discharge has already been developed at the TU Braunschweig. Systematic experimental and numerical investigations of various bulk solids characterise the flow behaviour and gain insights into the position and extent of the flow channel for various eccentricities and slendernesses. Both small-scale experiments as well as experiments using a silo with a height of several metres will be carried out. Initial results show that the flow channel in the silo can be modelled successfully on a small scale. It was also confirmed that the position and size of the outlet opening influence the expansion of the flow channel while the dependence of the load distribution remains to be investigated. Nevertheless, the initial results showed that further investigations are worthwhile for the silo design assumptions described in DIN EN 1991-4 for eccentric discharge outlets to ensure more reliable and safer processes.



## Pneumatic conveying of irregular solids: experimental study and CFD-DEM simulation at pilot scale

Manuela L Quezada Henry<sup>1</sup>, Elias Daouk<sup>1</sup>, Mikel Leturia<sup>1</sup>, Jelena Macak<sup>2</sup>, Mathieu Morin<sup>2</sup>, Fabrice Bonny<sup>3</sup>, Antoine Flament<sup>3</sup>, Thierry Destoop<sup>4</sup>, Khashayar Saleh<sup>1</sup>

<sup>1</sup>Université de Technologie de Compiègne, Compiègne, France, <sup>2</sup>IFP Energies Nouvelles, Solaize, France, <sup>3</sup>NEU-JKF Process, La Chapelle d'Armentières, France, <sup>4</sup>Thierry Destoop Consulting, Bondues, France

### Abstract

Pneumatic conveying of biomass and solid waste has a key role in recovery processes, which are of fundamental importance in the current context of environmental crisis. However, these solids can be quite challenging to transport as they are highly heterogeneous in terms of physical properties (size, shape, etc.) and behavioral properties (permeability, flowability, etc.), and can vastly differ in their origins. Different problems can be encountered when conveying these “irregular” solids, sometimes affecting performance and even leading to stoppages, which in consequence compromises the potential of recovery processes. While pneumatic conveying is well controlled for “regular” solids (pellets, granules, etc.), further research is needed to predict the behaviour and improve the handling of biomass and solid waste. To this end, it is necessary to reach a better understanding of the link between the physical properties of these materials and their hydrodynamic behaviour during pneumatic transport.

The main goal of the present work was to develop a reliable and efficient numerical model for the simulation and optimization of pneumatic conveying of biomass and waste solids. For this purpose, different particulate solids were studied both experimentally and numerically, starting with regular reference materials and then progressing to more complex irregular materials (rubber granules, straw, shredded plastic, etc.).

Experimental studies were carried out in a pilot-scale pneumatic conveying line. The solids were transported under different operating conditions and loadings, in order to study the effect of gas and solids flow rates on the hydrodynamics of the system. The gas velocity and the pressure drop in the different sections (horizontal, vertical, bends) of the pipeline were measured and the state diagrams corresponding to the different solid flow rates were plotted. A high-speed camera combined with PIV (Particle Image Velocimetry) technique were used to assess the particle velocity profile. Then, a series of numerical simulations were performed using a CFD-DEM (Computational Fluid Dynamics-Discrete Element Method) approach, in order to reproduce conveying experiments. Solids were initially modeled as spherical particles and different drag models were tested and then adapted to account for the non-sphericity of the actual irregular solids. The validity of the simulation results was evaluated by comparison with the experimental data, in particular the pressure drop in the different sections, the phase diagram and the particle velocity profiles.

# A novel experimental setup to study powder spreading with a wide range of process conditions

Bruno Nicola Dose, Sina Zinatlou Ajabshir, Diego Barletta, Massimo Poletto

*Department of Industrial Engineering, University of Salerno, Salerno, Italy*

## Abstract

The ease of powder spreading for the Powder Bed Fusion (PBF) process differs from flowability [1,2]. Therefore, spreadability has to be tested using specifically designed setups and procedures. Some experiments revealed poor spreadability performances of purposely designed powders at temperatures in the windows of process applications [3,4]. The source of discrepancy with these results may rely on the method adopted to feed the powder to the system and on the spreader geometry. In this project, a spreading apparatus was built to investigate different powders' spreadability at different temperatures and powder feeding and spreading conditions. This equipment has interchangeable steel plates bearing square-shaped engravings to simulate the region where the powder bed is built. Two different spreading devices can be used: a blade or a roller. Horizontal motion actuators allow moving the spreading device forward at a speed similar to those in real PBF systems. A different high-precision actuator ensures accurate vertical positioning of the spreading tool to accurately define the gap between the spreading device and the working plate. The heating system is made of radiative elements mounted on the wall of a removable insulated cover and a conduction heating pad below the steel plate. The heated cover and the heating pad have two separate control systems to control the working plate's temperature and the fed particles separately. The setup will allow spreadability procedures for single- and multi-layer experiments. At the end of the spreading experiment, a high-resolution camera is used to acquire highly resolved images of the powder bed taken with grazing light. Image analysis of the pictures is used to evaluate the homogeneity of the bed. Assuming shadows are related to powder roughness, the procedure allows for evaluating surface homogeneity.

## References

- [1] M. Lupo, S.Z. Ajabshir, D. Sofia, D. Barletta, M. Poletto, *Powder Technol* 419 (2023) 118346.
- [2] M. Mehrabi, J. Gardy, F.A. Talebi, A. Farshchi, A. Hassanpour, A.E. Bayly, *Powder Technol* 413 (2023) 117997.
- [3] M. Rüther, S.H. Klippstein, S. Ponusamy, T. Rüther, H.-J. Schmid, *Powder Technol* 422 (2023) 118460.
- [4] S. Zinatlou Ajabshir, D. Sofia, C. Hare, D. Barletta, M. Poletto, *Advanced Powder Technology* 35 (2024) 104412.

# DEM modelling of the effect of particle shapes on packing behaviours and their resistances to plate penetrations

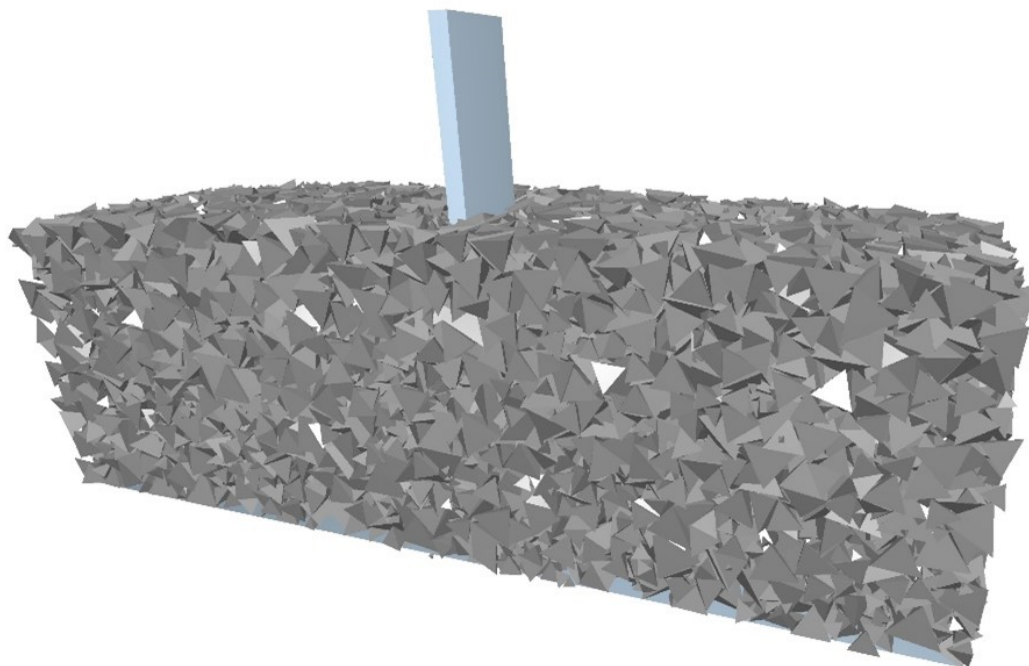
Hao Shi, Gert-Jan van Selm, Jovana Jovanova, Dingena Schott

Delft University of Technology, Delft, Netherlands

## Abstract

In most industrial applications, coarse materials like gravel, minerals and rocks are found with non-spherical shapes. Coarse materials with non-spherical shapes show a different flow behaviour compared to materials with more spherical shapes, such as glass beads, sand and iron pellets. To model coarse materials, Discrete Element Method (DEM) is a popular method as it can capture the discrete nature of particle interactions. DEM simulations are computationally expensive, spherical discs (2D) or particles (3D) are often preferred when selecting the shape of particles. However, using these idealised shapes creates limitations in capturing the geometrical effect, such as interlocking between particles, which is one of the critical characteristics of coarse materials. It is thus preferable to model the coarse granular materials using more realistic, non-spherical shapes, like clumps (multi-spheres) or polyhedrons[1]. Furthermore, in geotechnical, mining, and bulk handling applications, investigating and modelling penetration tests are crucial to capture realistic interactions between the particle bed and geometries.

In the current study, we will shed light on the following aspects: i) the eligibility of both spherical and non-spherical DEM models capturing the interlocking behaviour in coarse granular media; ii) the approach to generate homogeneous packings with various particle sizes, shapes and inter-particle frictions; iii) the dominating parameters on packing resistance during the penetration process. A plate penetration test is used to compare idealised shapes like spheres & tetrahedrons and more realistic shapes like multi-spheres & polyhedrals. In general, coarse granular materials show non-cohesive bulk behaviour, hence the Hertz-Mindlin contact model is used. Additionally, the ratio of nominal particle diameter ( $d_{50}$ ) over the width of the plate ( $w$ ) is close to 1, which makes the findings relevant to industrial applications. It is found that spheres can only represent the particle shapes to a limited extent and modelling non-spherical shapes is needed to go beyond this limit. Packings with non-spherical particle shapes result in higher penetration resistance, whereas the packing itself is mainly influenced by the particle shapes. Including different particle sizes in one packing increases both the penetration resistance and packing density, and inter-particle frictions have a similar effect on the penetration resistance. This study provides deeper insights to support modelling realistic interactions between coarse granular materials and geometry.



[1] C. J. Coetzee, 'Review: Calibration of the discrete element method', *Powder Technology*, vol. 310, pp. 104–142, Apr. 2017, doi: 10.1016/j.powtec.2017.01.015.

## Estimate of solids rate in air-impeded silo discharge with a novel calculation procedure

Salvatore La Manna, Diego Barletta, Massimo Poletto

*University of Salerno, Fisciano (SA), Italy*

### Abstract

During the discharge of fine powders from a hopper, an experimentally observed negative pressure gradient often emerges close to the outlet. This reduction in pressure counteracts the natural gravitational motion of particles, resulting in a discharge flow rate lower than the expected value. In this study, this phenomenon is addressed by defining a systematic sequence of steps and equations to estimate the solids discharge rate more accurately in air-impeded silos.

Specifically, the analysis focuses on cylindrical bins followed by conical hoppers; the effect of hopper diameter on the discharge rate of different materials was evaluated. The experimental results and procedure outputs were compared to verify algorithm reliability.

The procedure involves the following key steps: first, material properties such as bulk density, effective internal friction angle, etc., were collected and expressed as functions of stress state; next, the unit was discretized to trace stress and pressure profiles along its length. Using well-known equations by Janssen and Walters, stress distribution within the unit is predicted, and a recent equation proposed in the literature to estimate the pressure gradient is applied. Material properties are updated incrementally to refine stress and pressure profiles.

Finally, starting from the Brown and Richards equation for discharge rate estimation, the pressure gradient is accounted for by introducing a reduction in gravitational acceleration. As proposed in the existing literature, the discharge rate can be linked to the region where the pressure gradient reaches a zero value. By combining information regarding the material stress state near the outlet with the observed pressure gradient trend, we achieved a more accurate estimation of the discharge flow rate than conventional methods. This approach underscores the significance of developing a predictive model for pressure profile trends and assessing the efficacy of the proposed approach.



# Characterizing the mixing quality of nanoscale hetero-aggregates by TEM-EDX image analysis

Simon Buchheiser<sup>1</sup>, Hermann Nirschl<sup>2</sup>, Frank Rhein<sup>1</sup>

<sup>1</sup>Particle Dynamics in Heterogeneous Systems, MVM, Karlsruhe Institute of Technology, Karlsruhe, Germany, <sup>2</sup>Institute of Mechanical Process Engineering and Mechanics (MVM), Karlsruhe Institute of Technology, Karlsruhe, Germany

## Abstract

The urgent need for a reduction in the use of fossil fuels has led to an increasing importance of electrical storage in the form of lithium ion batteries. Carbon black is added therein to improve the conductivity by ensuring electrical pathways through binder polymers and active material. Therefore, high dispersion on nanoscale levels is necessary. However, during dry mixing cluster formation and aggregate breakage of carbon black may lead to decreased conductivity. In order to ease the manufacturing of batteries other methods for stabilization are investigated.

The presented approach is the hetero-aggregation of a nanoparticulate silica on-to the aggregate structure of carbon black in spray flames. By achieving sintering bridges of the two distinct materials on the primary particle level the aggregate stability can be improved. In order to produce a high amount of hetero-contacts it is necessary to reach high dispersity during the mixing of both nanoparticles. However, the quantification and assessment of the mixing quality of the hetero-aggregates is still a major challenge.

Therefore, a multi-scale approach for the characterization of hetero-aggregates has been applied. The approach includes a combination of small angle X-ray scattering (SAXS), analytical disc centrifugation (ADC) and transmission electron microscopy (TEM) to grant a comprehensive understanding of multiple particle properties by uniting primary particle properties, the fractal dimensions and aggregate properties. By considering both, the primary particle properties and their influence on the overarching aggregate structure, a fundamental understanding of hetero-aggregation is achieved. This information aids in the determination of the mixing quality within the hetero-aggregates by extensive image analysis of TEM-Images.

The presentation will cover results of the multiscale structural characterization of hetero-aggregates consisting of carbon black and silica. Therein, the key influences of the experimental conditions on the aggregate structure are determined. Afterwards, a methodology to assess the mixing quality by analyzing TEM-EDX images is presented. The basic workflow is depicted in fig. 1. In this context, the presentation covers how classic mixing theory needs to be adapted to be suitable for image analysis of nanoparticles. Furthermore, a metric which allows the comparison of hetero-aggregates of different composition and scale will be presented.

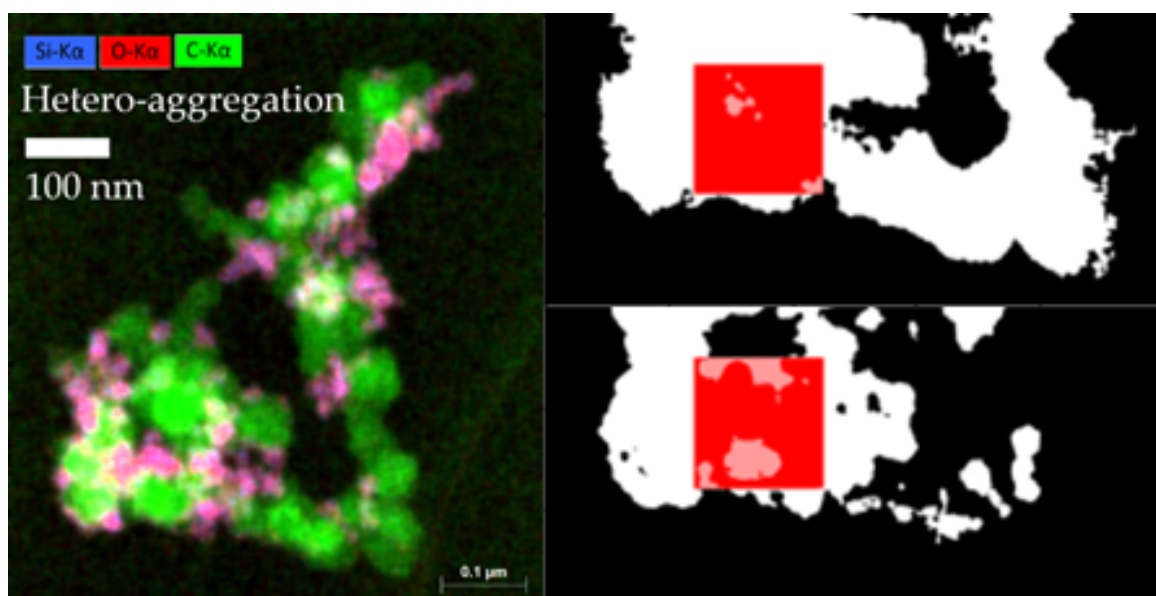


Figure 1: Workflow of the methodology. The TEM EDX scans of carbon and silicium are digitized and the composition of randomized samples is analyzed and compared to the bulk.

# Numerical and Experimental Investigation of Sodium Borohydride as Circular Fuel for Marine Vessels

Marcel C van Benten, Johan T Padding, Dingena L Schott

Delft University of Technology, Delft, Netherlands

## Abstract

The maritime sector accounts for approximately 3% of the global emissions and to limit these emissions, a transition towards alternative fuels is ongoing. In this work, a novel circular bunkering process for marine vessels is considered, such that a renewable fuel economy for the maritime industry can be realised. The proposed bunkering process is shown in Figure and uses sodium borohydride ( $\text{NaBH}_4$ ) as the fuel, due to its favourable gravimetric and volumetric energy density compared to other alternatives  $\text{NaBH}_4$  is fed into a reactor during vessel operation, where it reacts with water to form hydrogen and sodium metaborate ( $\text{NaBO}_2$ ). While the hydrogen can be used in e.g. fuel cells to power the ship, the  $\text{NaBO}_2$ , also referred to as spent fuel, has to be stored for the remainder of the voyage. Both  $\text{NaBH}_4$  and  $\text{NaBO}_2$  are bulk solids with a particle size distribution ranging from a hundred micrometres to several millimetres.

To this moment,  $\text{NaBH}_4$  has predominantly been used in the chemical industry as a reducing agent and consequently, the mechanical characteristics and the effects of operational conditions such as humidity, temperature, and stress on the behaviour of the material are virtually unknown. However, this knowledge is essential to be able to design the required storage and handling equipment to realise the aforementioned circular bunkering process. Therefore, this work focuses on acquiring the relevant data using experiments. While most experiments show that  $\text{NaBH}_4$  is initially free-flowing, particular combinations of operational conditions show a significant change in the materials flow characteristics, some results showing very cohesive material or even non-flowing characteristics. Using the acquired experimental data, the Discrete Element Method (DEM) will be used to calibrate, verify, and validate material models, such that the flow characteristics of this novel fuel can be captured numerically. These models can then be used to conceptualise the bunkering process in a virtual environment. Finally, an outlook on how to use the gained insights to develop and design the storage and handling equipment for the proposed circular bunkering process is presented.

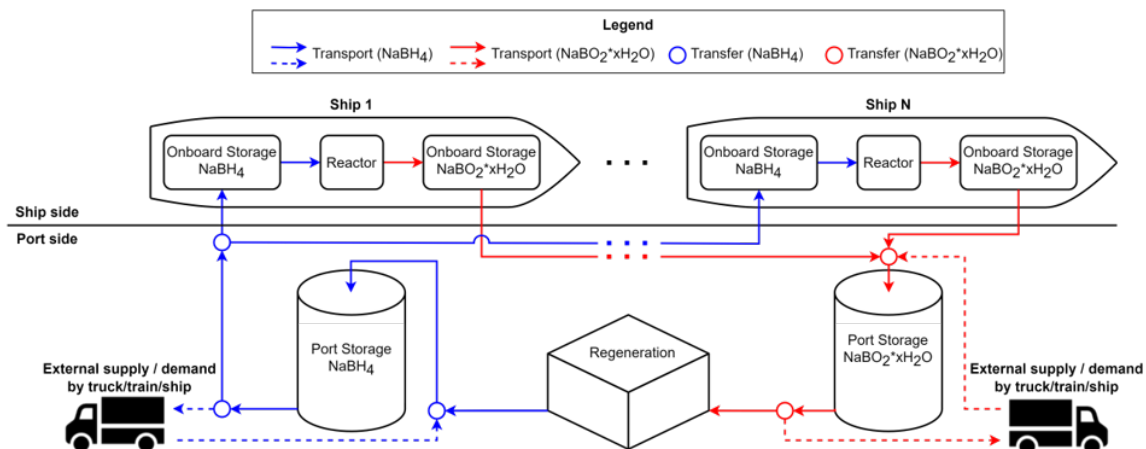


Figure 1: Circular bunkering process for marine vessels using  $\text{NaBH}_4$

## References

- [1]: M.C. van Benten, J.T. Padding, and D.L. Schott. "Towards Hydrogen-Fuelled Marine Vessels using Solid Hydrogen Carriers". In: The 14th International Conference on Bulk Materials Storage, Handling and Transportation. Wollongong, Australia, July 2023
- [2]: Kaiqiang Zhang et al. "Recent Advances in the Nanocatalyst-Assisted  $\text{NaBH}_4$  Reduction of Ni-troaromatics in Water". DOI: 10.1021/acsomega.8b03051

## Taking One-Way Coupled CFD-DEM to the Next Level

Christoph Goniva, Marcel Kwakkel, Martin Niemann, Christoph Kloss

*DCS Computing GmbH, Linz, Austria*

### Abstract

The Discrete Element Method (DEM) and its combination with Computational Fluid Dynamics (CFD-DEM) represent fundamental tools in the realm of particle process optimization and design. Their versatility transcends various industrial and environmental applications, catering to a wide array of needs. In recent times, the democratization of computational resources has facilitated the execution of larger-scale simulations. However, it is noteworthy that the computational demands associated with fully coupled CFD-DEM simulations persist as a substantial challenge, particularly in contrast to the computational efficiency of pure DEM simulations. Efficient simulation workflows are of paramount importance, particularly in endeavors related to equipment design and optimization, where time is often a critical factor. In certain contexts, shorter simulation runtimes may outweigh potential compromises in accuracy. In order to better understand that trade-off, the authors present different application cases, where fully coupled CFD-DEM simulation are compared to pure DEM simulations which account for the presence of a fluid phase. It is shown that recent developments drastically extend the applicability of one-way coupled CFD-DEM simulations. Depending on the application the fluid is considered as (i) a static single phase field, (ii) a transient single phase field and (iii) a static multiphase field or (iiii) an artificially scaled flow field. The application cases considered in this work span environmental flow, agricultural machinery and battery technology. By comparing gain in accuracy to gain in computational cost, some guidance in the applicability of highly efficient one-way coupled CFD-DEM simulations is given.

## **Make measurable that which is not: How to deal with terrible samples in powder flow measurements**

**Denis Schütz, Natali Unterberger, Helena Weingrill**

*Anton Paar GmBh, Graz, Austria*

### **Abstract**

Both pre-shear/shear cells as well as stirrer-based measurements have become ubiquitous in recent decades and have more or less become standardized across industries and fields.

This does not however mean that they are easy to use on anything besides cooperative samples. While what constitutes a cooperative sample is different from method to method problems with unusual powders with unusual properties persist.

While the basis of powder mechanics in the silo case or storage is well understood, a shear cell will be hard pressed to produce the necessary values to apply them even with relatively common cases such as fibers, powders with unusually high air retention, fast time consolidation, partially fibrous samples or even with something as common as infant formula.

This talk will take the form as a series of industrial case studies with both a defined industrial problem and solutions that may take the form on measurement schemes and adaptations to the classical measurement modes in order to generate both process insight as well as usable data for process monitoring and quality control.

To make it less depressing the talk will conclude with an application of these measurement modes to a more cooperative sample made uncooperative by sintering it inside a shear cell during measurement.



# Production and powder properties of nanoparticle coated metal particles for additive manufacturing

Arne Lüddecke, Harald Zetzener, Arno Kwade

*Institute for Particle Technology, Technische Universität Braunschweig, Braunschweig, Germany*

## Abstract

The additive manufacturing (AM) of metals is primarily used in lightweight construction and prototyping in various branches of industry. These include the automotive, aircraft and medical industries. A frequently used process in the additive manufacturing of metals is the powder bed fusion process using a laser beam (PBF-LB/M). This process involves the application of a powder bed onto a build platform, followed by selective melting using a laser beam. In this way, the final component is built layer by layer. Currently, productivity is being increased through higher laser intensities or the use of multiple lasers. However, this is accompanied by an increase in investment and operating costs. The approach of this work is to improve the efficiency of the process on the powder side by modifying the metal particle surface with nanoparticles. Previously published results show increased absorption values of the laser beam, better flow properties, improved component properties and faster build-up rates for silicon carbide nanoparticles applied in the fluidized bed. [1, 2]

This paper will mainly focus on the production method of the modified metal powders and their influence on the resulting bulk material properties. For this purpose, an overview of possible coating processes is given and wet coating and dry coating are compared. Stainless steel (1.4404) powder, which is already established in PBF LB/M, is used as a model material. This powder is coated with nanoparticles (silicon carbide, SiC) or graphene platelets. Surface phenomena such as agglomeration and distribution of the nanoparticles on the surface are discussed, utilizing scanning electron microscope measurements, energy dispersive X-ray spectroscopy (EDX) and measurement of the specific surface area. A main topic is thereby the influence of added surface roughness on the flowability (Ringshear tester, rotating drum). Furthermore, the influence of the coatings on the laser light absorptivity of the powders and the microstructure of additively manufactured sample bodies is shown.

To make use of the benefits of the coated powders, they need to be durable enough for transport and conditioning, i.e. sieving. Therefore, we investigate the adhesive strength of the nanoparticles on the metal surface by vibration.

[1] A. Lüddecke et al. 2021, Materials & Design, vol. 202, DOI:10.1016/j.matdes.2021.109536.

[2] O. Pannitz et al. 2021, Materials & Design, vol. 201, DOI:10.1016/j.matdes.2021.109530.

# Investigating the effect of temperature on powder spreading behaviour in powder bed fusion additive manufacturing process by Discrete Element Method

Sina Zinatlou Ajabshir<sup>1,2</sup>, Colin Hare<sup>2</sup>, Daniele Sofia<sup>1</sup>, Diego Barletta<sup>1</sup>, Massimo Poletto<sup>1</sup>

<sup>1</sup>University of Salerno, Fisciano (SA), Italy, <sup>2</sup>Newcastle University, Newcastle upon Tyne, United Kingdom

## Abstract

In this study, a Discrete Element Method (DEM)-based model was developed to simulate the powder spreading process in Powder bed Fusion (PBF) for Polyamide 6 (PA6) powder, which considered the spreading speed (3 mm/s and 30 mm/s) and temperature (25°C and 110°C) as parameters affecting the final spreading powder layer quality. The particle horizontal and vertical velocities were analysed in regions near the spreading blade, where at the lower spreading speed, particle velocities are far less compared to the higher spreading speed. The lower particle velocities lead to gently settling down and rearranging particles during spreading on the bed, allowing a uniform powder layer to form. Increasing the spreading speed led to an increase in shear stress and inertia number. At higher temperatures, shear stresses also rise while the inertia number is slightly reduced due to the greater cohesion between particles. The generated powder layer by the DEM model was analysed using the wavelet analysis technique and compared to experiments. The spreadability index of experiments can be estimated with less than 5% error using DEM simulations, though in an approximately consistent manner that captures the experimental trends of spreading speed and temperature. The packing fraction of simulated powder layers was investigated in the spreading direction. The DEM simulations show that packing fraction decreases as temperature or spreading speed are increased, with its variation across the bed increasing for higher spreading speeds. Increasing the spreading speed leads to greater motion and inertia number of particles and, consequently, it intensifies the particle ejection and results in many unfilled areas in the spread powder layer. Increasing temperature leads to an increase in cohesivity between particles, resulting in aggregates forming on the spread powder layer.

## Modelling of Parameters of Resonant Acoustic Mixer

Hazal Sezer<sup>1,2</sup>, Christopher Windows-Yule<sup>1</sup>

<sup>1</sup>University of Birmingham, Birmingham, United Kingdom, <sup>2</sup>AWE, Reading, United Kingdom

### Abstract

In order to form shaped components, multi-material blended components are mixed in planetary mixers, cast to blocks/blanks, and then undergo subtractive machining. Blending composites like syntactics and resin-based systems conventionally occurs through extended mixing in rotary drums or traditional blade-based mixers. After the blending process, the mixture is poured, molded into blocks, and subjected to subtractive machining. These procedures are time-intensive, generate waste, and pose potential hazards, especially when dealing with materials sensitive to energy.

To address these challenges, this study will explore Resonant Acoustic Mixing (RAM), an innovative technology for blending powder/powder, powder/fluid, and fluid/fluid mixtures. The method also carries the unique advantage of being able to directly mix materials into the final net (or near-net) component shape without the need for additional processing, thereby minimizing or eliminating material waste, reducing time, and mitigating potential hazards.

RAM is currently undergoing testing with AWE, and so far it has demonstrated excellent results. However, the modeling of this mixing technique is in its early stages and needs optimization. Numerous factors, including mixing parameters (intensity, time, pressure, temperature), material properties (particle size, shape, pre-blending, order of addition), and tooling characteristics (shape, composition, mixing headspace), influence the efficiency of RAM. If these parameters are modeled, it can significantly enhance the optimization of the mixing process. Modeling these variables can enhance our understanding of RAM's capabilities, shedding light on both its limitations and advantages..

In the present part of the project, we are focussing on the two most fundamental variable parameters in RAM mixing – the fill height of the vessel and the strength with which it is vibrated. In order to test how the fill level and the vibrational acceleration to which it is exposed affect mixing efficiency, we have run some experiments imaging a simple, model material within a RAM mixer using positron emission particle tracking (PEPT) as an initial set of experiments. During these experiments we have changed the fill level of the vessel and acceleration of the mixing using a simple, full-factorial DoE so as to gain fundamental insight into the influence of these key parameters on flow within the system.

## From solid to powder- Multilevel approach of coffee bean and powder characterization

Natali Unterberger, Denis Schütz, Helena Weingrill, Henrique Brasil

*Anton Paar GmbH, Graz, Austria*

### Abstract

Every day, an estimated 2.2 billion cups of coffee are being consumed, making coffee one of the most popular drinks and most traded goods globally.<sup>(1)</sup> Coffee is not only traded in large quantities, it also comes in a wide range of varieties, qualities and states. These include different coffee bean types, roasting degrees as well as grinding grades.<sup>(2)</sup> In order to ensure large harvest numbers and at the same time control final product quality and flavor, new technologies can be used to characterize all product stages – starting from the green coffee bean up to the final coffee powder.

This study focuses on the course of the coffee bean from the initial raw product to the finished coffee and shows various state-of-the-art technologies for product analysis and characterization. The talk will present various measurement methods for analyzing quality-determining factors of the coffee bean and the powder, with a particular focus on solid density and porosity, particle size and shape, as well as the permeability of the powder. In addition to the characterization of the raw material, the contribution includes the analysis of two different roast levels, namely medium and dark roast, as well as the investigation of fine/espresso grind to coarse/filter coffee grind for both roast levels. In addition, the geometric and bulk densities over these processing steps will be given special attention.

In summary, our results outline the possibilities of solid matter and powder characterization beyond conventional powder rheology and particle characterization. The combination of the presented methods enables a complete material characterization that can be applied to a wide range of applications additionally to the one covered in this work.



# Development of a Process Control Strategy for Continuous Aqueous Two-Phase Flotation (ATPF)

Kim Carina Lohfink, Frank Rhein, Hermann Nirschl

Karlsruhe Institute of Technology (KIT), Karlsruhe, Germany

## Abstract

Aqueous Two-Phase Flotation (ATPF) is a novel separation technique for the isolation of industrial enzymes such as phospholipase from crude complex biosuspensions. It combines several process steps of a typical downstream process into a single unit operation while yielding high purities and concentrations. The continuous operation mode of ATPF allows high throughput while maintaining a high separation efficiency. In order to design an autonomous ATPF process that is stable against feed fluctuations, the development of a suitable control strategy is essential.

Figure 1 shows the setup of a laboratory ATPF plant with the flotation tank in the center. The basis for ATPF is an aqueous two-phase system (ATPS). When the phase-forming components (e.g. a polymer and a salt) are present above critical concentrations, the system separates into a high-density bottom phase (light green) and a low-density top phase (light blue). The biosuspension containing the enzymes to be separated is added to the bottom phase. Three gassing units introduce gas bubbles through porous media at the bottom of the flotation tank. The enzymes accumulate with their hydrophobic areas on the bubble surfaces and are thus selectively transported into the collecting top phase.

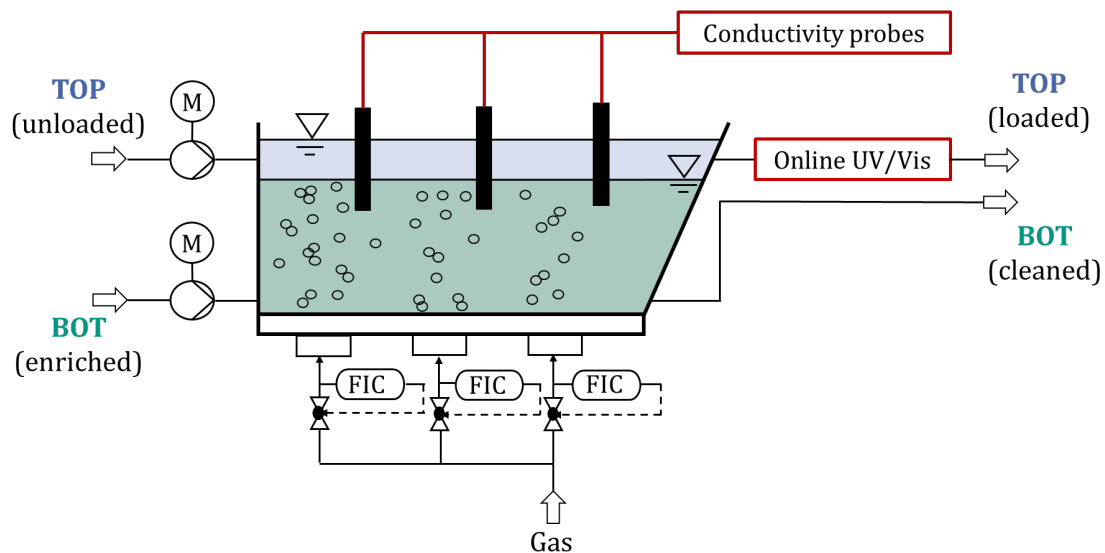


**Figure 1:** Scheme of the setup of a laboratory plant for continuous ATPF with integrated online measurement technology.

Online measurement technology is integrated into the plant in order to monitor various process parameters. A spatially resolved determination of the phase mixing caused by rising bubbles is realized with three electrical conductivity probes (see figure 1). This takes advantage of the significantly different salt concentrations of the two phases. Since the electrical conductivity probes are located slightly below the phase boundary in the salt-rich bottom phase, high phase mixing causes the top phase to displace the salt ions in the bottom phase near the electrical conductivity probes, resulting in a lower measured electrical conductivity. Online UV/Vis spectroscopy is used to measure the enzyme concentration at the top phase outlet to determine the separation efficiency. ATPF experiments with varying process parameters are performed to characterize the process behavior. The experimental results allow the identification and validation of a process model as the basis for the development of a suitable control strategy. The autonomous ATPF process is able to respond to feed fluctuations in real time and ensures a consistently high separation efficiency.

# Influence of viscous liquid bridges on wet particle dynamics in DEM simulations

Kimiaki Washino<sup>1</sup>, Ei L. Chan<sup>1</sup>, Shunta Tsukuma<sup>2</sup>, Yuma Hirose<sup>2</sup>, Sota Otsuka<sup>2</sup>, Taiki Tsunajima<sup>1</sup>, Takuya Tsuji<sup>1</sup>, Toshitsugu Tanaka<sup>1</sup>, Koichiro Ogata<sup>2</sup>

<sup>1</sup>Osaka University, Suita, Japan, <sup>2</sup>National Institute of Technology, Oita College, Oita, Japan

## Abstract

In many particulate processes in industry, liquid is often added to particles for various reasons. Typical examples include wet granulation and particle coating where relatively small amount of liquid is added and dispersed in particles. In such processes, particles may be bonded together by a pendular liquid bridge, i.e., a single bridge formed between a pair of particles. Liquid bridge forces can be classified into capillary and viscous forces; the former is caused by the surface tension and the latter is due to the liquid viscosity and relative motion of particles.

Discrete Element Method (DEM) is a powerful and versatile method for simulating the flow of granular materials. One of the major advantages of DEM over continuum models is that complex inter-particle forces can be directly considered. Many researchers have incorporated pendular liquid bridge forces into DEM to predict the behaviour of wet particles. However, most of such simulations consider water bridges where the capillary force is much more dominant than the viscous force; the existence of the viscous forces does not have visible impact on the flow, or in an extreme case, they are completely ignored.

Relatively recently, the authors proposed new viscous force models (for both normal and tangential directions) which are more accurate than the existing ones. In this work, these models are implemented in DEM to simulate real-life wet particles with sugar solution in the FT4 powder rheometer. Several input parameters for both dry contact and liquid bridge forces are determined by calibration. These parameters are then used for other simulations with different operating conditions, and the results are compared with experiments. It is demonstrated that the simulation effectively replicates the complex behaviour of dry and wet particles in the experiments (Fig. 1).

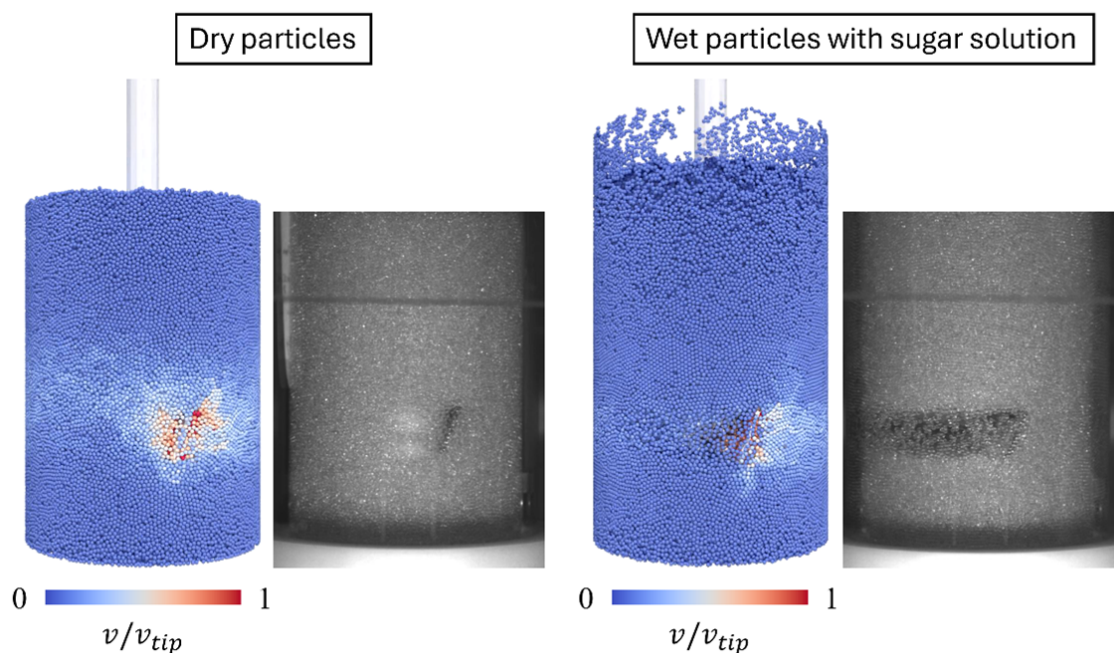


Fig. 1 Dynamics of dry and wet particles obtained from DEM simulation and experiment.

## Particle interactions in the submicrometer range - A combined colloidal probe AFM and capillary rise approach

Nane Kuehn, Finn Frankenberg, Arno Kwade, Carsten Schilde

*Institut für Partikeltechnik, Technische Universität Braunschweig, Braunschweig, Germany*

### Abstract

Heteroagglomerates can be important in many industrial applications, such as in the field of energy conversion and storage, due to their potential to create tailor-made particle products with integrated functions. Heteroagglomeration by gas phase processes is one method of combining existing particle properties, especially of submicron particle systems, to create new functions. However, understanding the complex interactions between process parameters, particle properties and interactions requires significant measurement effort. This is necessary for a fundamental understanding of agglomeration process mechanisms and to exploit new properties of heteroagglomerates. The adhesive forces involved play a central role in this process.

The research approach employed in this study involves a combination of experimental and simulative methods to systematically analyse the influences on the adhesive forces. Experimental investigations were conducted using model particles of silicon dioxide and polystyrene. Colloidal probe atomic force microscopy (cp-AFM) was used to measure the adhesive forces for different contact combinations of the model particles. Spray-dried aggregates were applied to the cantilever and the substrates were coated using the dip-coating method. In order to identify any surface changes, AFM was also used to measure the topography before and after the cp-AFM measurements, as plastic deformation may occur as a result of numerous contacts. The capillary rise method was used to measure the surface energy and to determine the Hamaker constants of the aggregates. It is important to note that the results of the two experimental methods are not directly comparable. Therefore, a discrete element method simulation is used as a link. The simulation setup includes specific surface topographies and has been parameterised based on the results of the capillary rise method. It is used to conduct virtual AFM measurements, which are then compared and validated with experimental results. The validated simulation has the potential to independently investigate the acting forces and thus perform fundamental analyses of the agglomeration behaviour.

The aim of the research is to systematically analyse potential factors that may influence adhesion, including surface roughness, plastic deformation, moisture and surfactant residues. Furthermore, this approach is expected to reduce the measurement effort required to determine adhesion forces by combining capillary rise, roughness measurement and simulations as an alternative to cp-AFM.

## Dynamics of model cohesive granular materials in a rotating drum

Antonio Pol<sup>1</sup>, Riccardo Artoni<sup>2</sup>, Patrick Richard<sup>2</sup>

<sup>1</sup>INRAE, Montpellier, France, <sup>2</sup>Université Gustave Eiffel, Bouguenais, France

### Abstract

In this contribution, we present our recent experimental studies on the dynamic behavior of a cohesive granular material in a rotating drum configuration. We use a cohesive model material consisting of glass beads with a polyborosiloxane (PBS) coating. As described by Gans et al. (Phys Rev E 101 (3), 032904, 2020), the coating can be prepared by mixing glass beads, PDMS and an aqueous solution of boric acid in a heated mixer. The coating gives the grains a cohesive behavior, and the apparent cohesion between the grains can be tuned by adjusting the amount of PBS. First of all, we show that the introduction of cohesion between grains enriches the phenomenology of the medium, notably revealing a variety of flow regimes, ranging from intermittent avalanches to continuous flows, with a surface that can be flat, concave or convex. We discuss the combined effect of the level of cohesion and the geometry of the drum (radius, length) on the flow regime, focusing our attention on the morphology of the free surface of the medium and the avalanches. The effect of the rotation speed of the drum is also studied. Finally, we discuss a scaling law for the shape of the surface of the medium, taking into account the properties of the granular material, the geometry of the drum and its rotation speed.



## Cohesion of ice powders at very low temperatures

Benoit Jabaud<sup>1</sup>, Erwan Le Menn<sup>1</sup>, Patrick Richard<sup>2</sup>, Gabriel Tobie<sup>1</sup>, Riccardo Artoni<sup>2</sup>

<sup>1</sup>Laboratoire de Planétologie et Géosciences (LPG), UMR-CNRS 6112,, Nantes, France, <sup>2</sup>MAST-GPEM, Université Gustave Eiffel,, Bouguenais, France

### Abstract

Numerous planetary surfaces in the solar system are covered by granular ices resulting from various processes, such as cryo-volcanism, condensation/sublimation, meteorite bombardment or atmospheric transport. These materials present a particle size distribution  $\sim 10\text{-}100\mu\text{m}$ , with properties unique to each body depending on their mode of formation and the surface environment, including characteristic solar radiation or microprojectile bombardment. Anticipating the properties of the icy surfaces is important for both better understanding the evolution of surface morphologies and minimizing the technical issues that future missions may face when landing, sampling, drilling and analyzing. This study aims at characterizing the mechanical behavior of micrometric ice powders as a function of temperature. In order to do so, we developed a liquid-nitrogen cooled rotating drum to perform dynamical measurements and quantify the cohesion based on bed slope statistics (Lumay et al., 2012) on a wide range of temperatures ( $\sim 80\text{-}250\text{K}$ ). We use different systems to produce ice powders, by freezing a water spray in a liquid nitrogen bath. Different grain populations are produced by varying the parameters of the setup ; the size distributions are characterized with the help of a digital microscope equipped by a cryostat. Tests are also performed on reference powders (glass microbeads, limestone powder), and on mixtures of ice and glass beads. A simple mechanical analysis is employed to isolate the effect of temperature from that of particle size, yielding an estimate for the surface energy. Our results (Jabaud et al 2024) show an increase of the cohesion of ice with the temperature, which is surprising in comparison with reference powders, but in agreement with previous studies dealing with more limited temperature ranges (Musiolik & Wurm, 2019). We discuss the possible microscopic origin of such a behavior and its implications for planetary science and technology.

### References:

- Jabaud, B., Artoni, R., Tobie, G., Le Menn, E., & Richard, P. 2024. Cohesive properties of ice powders analogous to fresh plume deposits on Enceladus and Europa. *Icarus*, 409, 115859.
- Lumay, G., Boschini, F., Traina, K., Bontempi, S., Remy, J.-C., Cloots, R., & Vandewalle, N. 2012. Measuring the flowing properties of powders and grains. *Powder Technology*, 224(jul), 19-27.
- Musiolik, G., & Wurm, G. 2019. Contacts of Water Ice in Protoplanetary Disks - Laboratory Experiments. *The Astrophysical Journal*, 873, 58

## Relation between the powder layer quality and the GranuDrum Dynamic Cohesive Index for polymeric powders at SLS process temperatures

Marco Lupo<sup>1</sup>, Daniele Sofia<sup>2,3</sup>, Sina Zinatlou Ajabshir<sup>2</sup>, Diego Barletta<sup>2</sup>, Massimo Poletto<sup>2</sup>, Aurélien Neveu<sup>1</sup>

<sup>1</sup>Granutools, Awans, Belgium, <sup>2</sup>Department of Industrial Engineering, University of Salerno, Salerno, Italy, <sup>3</sup>Department of Computer Engineering, Modeling, Electronics and Systems, University of Calabria, Rende (CS), Italy

### Abstract

Selective Laser Sintering (SLS) is an additive manufacturing process, characterized by the creation of 3D objects, obtained by alternating a powder distribution step with a spreading tool to get a thin layer and the sintering of the particles with a laser beam. To get acceptable 3D objects, the powder layers must be uniform, smooth, and with low porosity. The characteristics of the layers depend on the powder spreadability, which is the capacity of a powder to be spread across a plate. The spreadability depends on the characteristics of the powder, e.g. particle size and shape, interparticle forces, and process conditions like blade speed and process temperature. Therefore, it is important to assess the powder spreadability in the same process conditions to properly predict the quality of the powder layers.

Two different approaches have been used to investigate the quality of the layer generated in the spreading process by a moving blade: a set-up from the University of Salerno (UNISA) and the GranuDrum (Granutools, Belgium). The UNISA set-up and the GranuDrum can work up to temperatures of about 150-200 °C, conditions similar to those occurring in a typical SLS machine. The UNISA setup mimics the distribution step of the SLS process, creating a layer of controlled thickness. Macroscopic pictures of the obtained layers are taken to do a qualitative analysis of the powder layer quality. In the GranuDrum, the cylindrical cell containing the powder rotates at different angular velocities. Snapshots of the powder are taken for each angular velocity and the air/powder interface is detected from each snapshot. For each velocity, the Dynamic Cohesive Index (DCI) is measured from the interface fluctuations, that depend on the cohesive forces acting between the particles. Tests with the GranuDrum have been performed at rotating speeds consistent with the scrolling velocities of the blade of the UNISA set-up to reproduce consistent shear conditions. Different polymeric powders have been tested at temperatures between the ambient and 140°C: two kinds of polyamide 6, thermoplastic polyurethane, and polypropylene powders. A good correlation has been found between the cohesiveness of the powder, evaluated by the Dynamic Cohesive Index metric, and the quality of the powder layer in the UNISA setup.

# DEM Simulation of the Fundamental Response of Multi-disperse Granular Materials to Applied Vibration

Peter Watson<sup>1</sup>, Marcello Lappa<sup>1</sup>, Sebastien Vincent Bonnieu<sup>2</sup>, Ali Anwar<sup>1</sup>

<sup>1</sup>University of Strathclyde, Glasgow, United Kingdom, <sup>2</sup>European Space Agency, Noordwijk, Netherlands

## Abstract

Following the growing interest in returning to the moon to further explore and ultimately inhabit it, widespread consensus exists that novel ways should be identified to most efficiently make use of the abundantly available in-situ resources, i.e. the so-called “lunar regolith” that makes up the lunar surface. This study focuses on how mechanical stimuli in the form of vibrations can be used to facilitate this goal by forcing granular materials to behave like fluids, thereby making their transportation and distribution simpler. The problem is addressed in the framework of Discrete Element Method (DEM) numerical simulations.

Granular materials made up of particles of varying sizes and shapes are considered in the attempt to elucidate the material dynamics under the effect of vibrations in realistic situations for which the assumption of constant-diameter spherical particles is no longer valid. Building on previous literature regarding pattern formation in monodisperse granular materials, situations of increasing complexity are considered, i.e. binary and ternary particle distributions. To assess the role played by the particle size distribution, the DEM simulations are conducted for a fixed mass of the material. The differences in the generated patterns are evaluated quantitatively in terms of wavelength and amplitude and qualitatively by focusing on purely topological and convective cell morphological aspects. Additional insights are obtained through the analysis of statistical data accounting for the collisions of the particles during one vibration cycle and the related power dissipated due to inelastic effects or shear.

It is shown that an increase in complexity due to the presence of particles with different sizes generally leads to symmetry breaking effects and disordered patterns similar to those experimentally obtained by shaking lunar regolith simulants; however, specific cases also exist where a multi-disperse granular material can lead to ordered waveforms with heretofore unseen properties.

## Understanding the effect of permeability on tablet manufacturing

Roozbeh Valadian<sup>1</sup>, Marco Lupo<sup>1</sup>, Michela Beretta<sup>2</sup>, Geoffroy Lumay<sup>3</sup>, Aurélien Neveu<sup>1</sup>, Filip Francqui<sup>1</sup>

<sup>1</sup>Granutools, Awans, Belgium, <sup>2</sup>Research Center Pharmaceutical Engineering GmbH, Graz, Austria, <sup>3</sup>GRASP, University of Liège, Liège, Belgium

### Abstract

Tablet manufacturing is a widely used pharmaceutical process as tablets are the most common oral solid dosage form. However, this process presents challenges as it involves many steps, which must be controlled to guarantee that the tablet meets the quality and safety standards. Among these steps, die-filling can be crucial. Depending on the powder permeability, defined as the capacity of a material to transmit air through its bulk, and the process conditions, e.g. tableting and paddle speed, the powder reaches a certain packing fraction in the die. The packing fraction quantifies the densification of the powder. The final permeability in the die depends on the packing fraction reached and is expected to affect the final properties of the tablet. Therefore, it is important to measure the permeability at the same packing conditions as the process.

For permeability measurements, the GranuPack instrument (Granutools, Belgium) equipped with the permeability cell was used. The GranuPack is a high-resolution tapped density analyzer. It allows the application of the desired number of taps to obtain similar packing fractions as during densification in the die. The permeability cell allows measuring the permeability in correspondence with these packing fraction values. In this study, three different powder mixtures composed of an excipient (SuperTab<sup>®</sup> 11SD, SuperTab<sup>®</sup> 30GR, and SuperTab<sup>®</sup> 21AN, DFE Pharma, Germany) and a lubricant (Magnesium stearate, Peter Greven, Germany) were tested. To relate the permeability to the tablet properties, tablets composed of the aforementioned powders were produced with the STYLCAM200R compaction simulator (Medelpharm, France). During tablet production, the filling height and the main compression force were fixed, while six different paddle speeds (10, 20, 30, 40, 50, 60 %) and three tableting speeds (10, 25, 40 tab/min) were used. Critical tablet properties were measured for each combination of paddle and tableting speeds.

Comparative analysis was conducted between the tablet properties and permeability. The latter was described by permeability values at various packing fractions and two parameters describing the impact of densification on permeability: the permeability ratio and the rate of variation of permeability. The new insights gathered from this approach give a better understanding of the material properties and allow the development of improved formulations for better processability.



# Effect of particle properties on stable/unstable flow on powder discharge and pneumatic conveying using fluidization

Koichiro Ogata<sup>1</sup>, Kazuki Tokumaru<sup>1</sup>, Daiki So<sup>1</sup>, Sora Kanokogi<sup>1</sup>, Naoyuki Kato<sup>1</sup>, Terutoshi Kai<sup>1</sup>, Yusuke Kujirasaki<sup>2</sup>, Takashi Ikeda<sup>2</sup>, Kenji Yamamoto<sup>2</sup>, Katsuhiko Yokohama<sup>2</sup>

<sup>1</sup>National Institute of Technology, Oita College, Oita, Japan, <sup>2</sup>Mitsubishi Heavy Industries, Ltd., Nagasaki, Japan

## Abstract

Fluidization technology is widely used in many powder-handling processes, such as feeding, transportation, mixing and drying. Fluidization has the advantage of continuously processing many particulate materials and feeding and transporting the powder in a simple operation using fluidized air. On the other hand, poor fluidization and unstable flow in the equipment may occur due to powder properties such as flowability and cohesiveness. Therefore, it is essential to clarify the effect of particle properties on stable and unstable flow in fluidized bed operation.

We fabricated a pressurized fluidization transport equipment that discharges and transports powder by supplying air to the top and bottom of the powder bed in a powder discharge hopper. The test particles were glass beads of  $56\mu\text{m}$  and  $2500\text{kg/m}^3$ , formed glass beads of  $63\mu\text{m}$  and  $1400\text{kg/m}^3$ , and pulverized coal of  $55\mu\text{m}$  and  $1400\text{kg/m}^3$ ; these belong to the Geldart A particle. Regarding the experimental conditions, the air velocities at the top and bottom of the powder bed were varied based on the minimum fluidization velocity for each particle. As a result, glass beads have high flowability and floodability properties, which are measured by the powder tester (PT-X), while formed glass beads and pulverized coal have low flowability. Also, shear cell and wall friction tests of the powder rheometer (FT4) confirmed that glass beads have low cohesion, internal friction, and wall friction angles.

Figure 1(a) shows times histories of the transported mass of glass beads and the pressures under the conditions of  $u_t/u_{mf}=1$  and  $u_b/u_{mf}=4$ , where  $M_p$  is the mass of the receiving vessel,  $p_t$  is the pressure at the top of the powder bed,  $p_b$  is the bottom pressure,  $\Delta p_L$  is the differential pressure in the horizontal pipe, and  $t$  is the elapsed time. The figure shows stable transport characteristics, such as an almost constant gradient of the transported mass and the differential pressure inside the horizontal pipeline, were obtained. The mass-flow regime appeared in the hopper, as shown in Figure 1 (b-1). Figures 1 (b-2) and (b-3) indicated that the fluidized bed and the horizontal pipeline obtained satisfactory fluidization states and a dense phase powder flow mode.

On the other hand, unstable flow, such as funnel flow and channelling, was observed in the hopper and fluidized bed for foam glass beads and pulverized coal with low flowability. The results suggest that pressure and powder behaviour have a reasonable correlation.

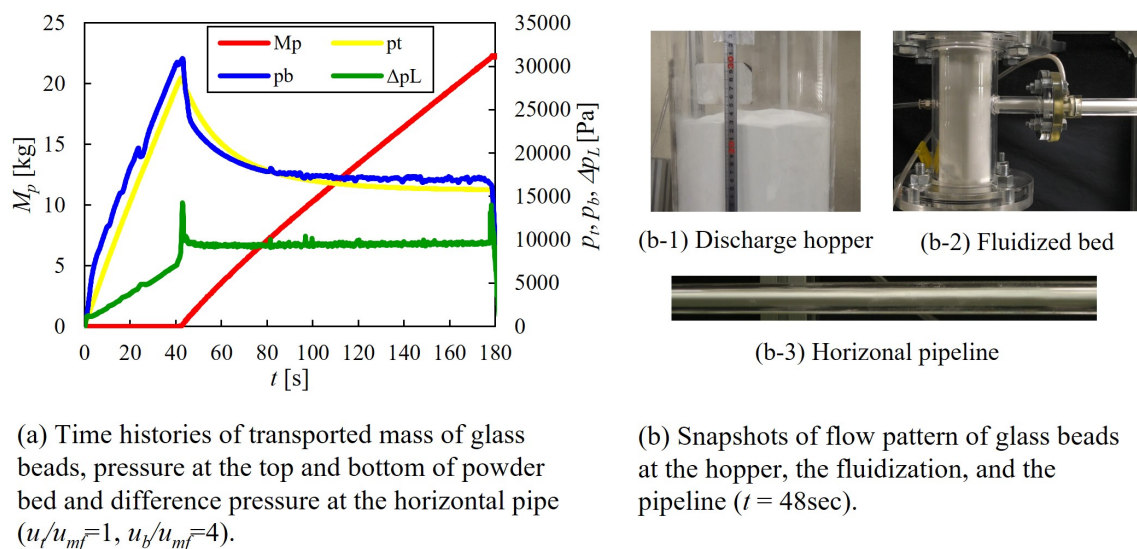


Fig.1 Powder discharge and conveying characteristics using fluidization

# Influence of the implementation method of liquid bridge force model on DEM simulation results of wet powder behavior

Tomotaka Otsu, Hideya Nakamura, Shuji Ohsaki, Satoru Watano

Osaka Metropolitan University, Sakai, Japan

## Abstract

Wet powders are widely used in various fields. Thus, there is a great need for simulation technology that can accurately calculate the wet powder behavior. The discrete element method (DEM), which solves the equations of motion of individual particles to obtain the behavior of the entire powder, has proven to be able to accurately calculate the dry powder behavior. In contrast, accuracy of DEM simulation of wet powder behavior is still insufficient, nevertheless theory and model for the inter-particle liquid bridge force have been well studied. This is due to the following reasons. First, in the DEM simulation, how to define the necessary input variables (namely the liquid bridge characteristic quantities such as bridge formation distance, liquid bridge volume, and minimum bridge distance) have not been determined. Second, it is not clear how to implement liquid bridge force model, and various calculation methods has been applied.

We here focused on the two kinds of calculation methods for wet powders: one is a method for calculating the bridge formation distance, and the other is a method for calculating the liquid bridge force during particle overlapping. In this study, DEM simulations were performed using a total of four calculation methods by combining the two kinds of methods for calculating the bridge formation distance and the method for calculating the liquid bridge force during particle overlapping. By comparing with each result in rotating drum and cylinder lift, we investigated the influence of the implementation method of liquid bridge force model on the simulation results of wet powder behavior. The results show that for static cylinder lifts, both calculation methods have little effect. On the other hand, in rotating drum, the simulation results differed significantly depending on the calculation method of bridge formation distance, especially at high liquid volumes. However, the calculation method of the liquid bridge force during particle overlapping had little influence on the results. These results suggest that liquid bridge forces during non-contact are more important in the behavior of wet powders in dynamic systems than the small difference in adhesion forces during particle overlapping.

	LFC-JKR	LFC-H-LB	SC-JKR	SC-H-LB
Liquid bridge force during particle overlapping	JKR	Hertz-Mindlin + Capillary force	JKR	Hertz-Mindlin + Capillary force
Bridge formation distance	Liquid film contact	Liquid film contact	Solid contact	Solid contact

## Extreme electrostatic charge peaks in powder processing

Holger Grosshans<sup>1,2</sup>, Wenchao Xu<sup>1</sup>, Simon Jantač<sup>1</sup>, Gizem Özler<sup>1</sup>, Christoph Wilms<sup>1</sup>

<sup>1</sup>Physikalisch-Technische Bundesanstalt, Braunschweig, Germany, <sup>2</sup>University Magdeburg, Magdeburg, Germany

### Abstract

Powders acquire a high electrostatic charge during transport and processing. Consequently, in the aftermath of dust explosions, electrostatic discharge is often suspected to be the ignition source. However, definite proof is usually lacking since the rise of electrostatic charge cannot be seen or smelled, and the explosion destroys valuable evidence. Moreover, conventional methods to measure the bulk charge of powder flows, such as the Faraday pail, provide only the aggregate charge for the entire particle ensemble. Our simulations show that, depending on the flow conditions, contacts between particles lead to bipolar charging. Bipolar charged powder remains overall neutral; thus, a Faraday pail detects no danger, even though individual particles are highly charged. To address this gap, we have developed a measurement technology to resolve the powder charge spatially. The first measurements have revealed a critical discovery: a localized charge peak near the inner wall of the conveying duct is 76 times higher than the average charge that would be measured using the Faraday pail. This finding underscores the possibility of extremely high local charges that can serve as ignition sources, even though they remain undetected by conventional measurement systems. Our new technology offers a solution by spatially resolving the charge distribution within powder flows, unmasking hidden ignition sources, and preventing catastrophic incidents in the industry.

## Optimizing Continuous Pharmaceutical Blending through Advanced AI / ML Techniques.

Owen Jones-Salkey<sup>1,2</sup>, Christopher Windows-Yule<sup>2</sup>, Andrew Ingram<sup>2</sup>, Lois Stahler<sup>1</sup>, Andrei Nicusan<sup>2</sup>, Sean Clifford<sup>1</sup>, Luis Martin de Juan<sup>3</sup>, Gavin K. Reynolds<sup>1</sup>

<sup>1</sup>AstraZeneca, Macclesfield, United Kingdom, <sup>2</sup>University of Birmingham, Birmingham, United Kingdom, <sup>3</sup>AstraZeneca, Gothenburg, Sweden

### Abstract

Continuous Oral Solid Dosage (OSD) Manufacturing presents a unique opportunity for the pharmaceutical industry to enhance production efficiency, reduce waste, and support environmental sustainability. However, the transition to this new modality requires extensive development and validation to meet stringent regulatory standards. Traditional experimental planning approaches are time-consuming and costly, which poses a significant challenge to the swift introduction of new medicines to market to help patients.

One of the greatest challenges in the process development of Continuous Direct Compression (CDC) is the variability in bulk powder characteristics across different projects. This variability makes it difficult to streamline process development, especially in the blending stage where achieving optimal blend homogeneity and content uniformity is critical but can only be achieved through extensive empirical and analytical experimentation. To address this challenge, Artificial Intelligence/Machine Learning (AI/ML) models were developed to optimize blending conditions based on the unique powder characteristics of the formulation. Three AI/ML models were developed and compared on the basis of accuracy and variable explainability. The Artificial Neural Network model demonstrated superior predictive power showcasing an  $r^2$  of 0.97. This (ANN) model has been successfully deployed to AstraZeneca's intranet, facilitating the real-time prediction through interactive sliders and value entry boxes. The implementation of this tool is expected to reduce development experimentation by up to 70%, yielding substantial savings of approximately £100k and 21.5 tonnes of CO<sub>2</sub>e per drug project.

The deployment of this model through the intranet democratizes access to advanced predictive analytics, enabling immediate, informed decision-making and strategic planning across various stages of pharmaceutical development. This revolutionizes experimental planning, drastically reducing the time and resources needed for drug development projects. Furthermore, it enhances regulatory submissions by providing empirical evidence of process understanding and sensitivities. As a development/operational risk management tool, it pre-emptively identifies potential process challenges, facilitating smoother project progression and reducing the likelihood of failure. This research demonstrates the practical application of AI/ML in enhancing pharmaceutical manufacturing and highlights the transformative potential of these technologies in expediting drug development, ensuring product quality, safety and compliance, whilst effectively managing development risks. The deployment of this model through the intranet fosters a collaborative, efficient, and data-driven culture in pharmaceutical manufacturing, signalling a new benchmark for innovation and excellence within the industry.



**Abstract Figure:** The Artificial Neural Network (ANN) model can be employed, via. interactive web application, to forecast the operational landscape of a newly formulated drug.



# Computational analysis of the tribocharging and electrostatic behaviour of polarisable particles in fluidised beds

Giordano Maria, Francesca O. Alfano, Giovanni Iozzi, Francesco P Di Maio, Alberto Di Renzo

University of Calabria, Department of Computer Engineering, Modelling, Electronics and Systems Engineering, Rende, Italy

## Abstract

Gas-solid fluidisation is a widely utilized process in the chemical industry because of the high mass and heat transfer coefficients due to the effective fluid-particle interactions. However, in dealing with dielectric particles, the incidental transfer of electrostatic charge (tribocharging) during particle collisions poses significant challenges. Electrostatic charges tend to accumulate and can lead to particle agglomeration and defluidisation. In turn, for example with exothermically reacting polymer particles, the particles tend to melt and then form layers adhering on the fluidisation column inner walls. This “sheeting” phenomenon can cause costly reactors shut-down, because at a certain size the sheets dislodge and block the distributor plate [1,2]. Despite the ongoing efforts, the underlying mechanisms of such severe issues are not fully understood. Certain aspects appear counterintuitive and are still debated. For example, particles with same charge polarity are intuitively expected to repel. Yet, the electrical interaction between surfaces can cause charge polarisation, producing an attractive force contribution. As a result, under certain conditions, the global force between particles charged with the same polarity becomes attractive. This behaviour may prevail in dielectric material and be responsible, at least in part, for similar particles sticking to the column walls in industrial fluidised bed units. Another important contribution originates from the electric fields of the charged particles and walls. With its ability to track contacts in detail, CFD-DEM has been recently coupled to tribocharging models to study electric charge build up in fluidised beds. However, existing DEM models with electrostatic interactions fail to capture the full spectrum of complex particle behaviours, like forces and charge exchange between polarised particles.

In this study, a new model for tribocharging and electrostatic interactions in DEM is presented, in which interactions including both net and polarisation-induced charges are accounted for [3], as well as the role of the electric field generated by the charged particles and walls. The required formalism is introduced, and the assumptions discussed. After tests on pairs of interacting particles, applications to small-scale fluidised systems are illustrated and discussed, showing the role of each contribution in the observed fluidisation behaviour.

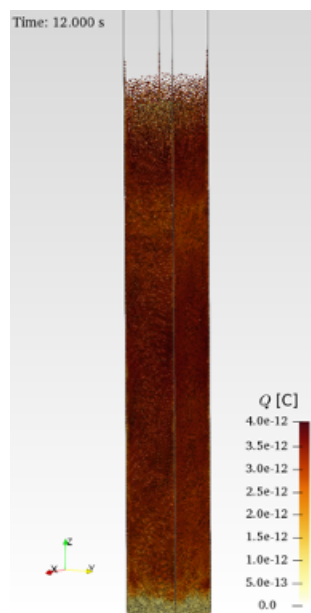


Figure 1. DEM simulation results showing charged particles adhering to the wall of a small-scale fluidised bed.

## References

- [1] P. Mehrani, et al., *Journal of electrostatics* , 87 (2017) 64-78.
- [2] A. Giffin and P. Mehrani, *Journal of electrostatics* , 68 (2010) 492-502.
- [3] E.B. Lindgren et al. *Physical Chemistry Chemical Physics* , 18(8), (2018) 5883-5895.

# Simulation of the moisture and temperature dynamics in electromagnetic field assisted drying of particles in fluidised beds

Francesca O. Alfano, Alberto Di Renzo, Rossella Girimonte, Daniele Sofia, Francesco P. Di Maio

University of Calabria, Department of Computer Engineering, Modelling, Electronics and Systems Engineering, Rende, Italy

## Abstract

Transfer processes in gas-solid fluidised beds are highly effective and homogeneous due to the improved inter-phase exchange and solids mixing compared to packed beds, which in turn improve performance and process control. Conventional fluidised bed drying operations benefit from high heat and mass transfer, in which the fluidising agent is a hot and dry air stream. However, such processes are highly energy intensive, mostly due to the air thermal pre-treatment, which is often carried out burning fossil-derived fuels. A recent alternative is the use of alternating electromagnetic (EM) field, like radiofrequency (RF) or microwaves (MW), applied directly on the fluidised particle bed. The two key advantages are: (i) sustainability, associated with the direct use of electric energy, and (ii) theoretical cost savings, as energy consumption is focussed on the targeted material, i.e. water. These electromagnetic fields are known to cause quick water molecule heating while transparently passing through many other materials, leading to efficient energy utilisation. Current applications are mainly in the food, textile and pharmaceutical industry. In general, the technology is not fully mature and widespread, as there are strict requirements on, among others, component materials and field shielding. Different sources of the EM field, for example micro- or radiofrequency waves, possess different characteristics and requirements. In addition, the real cost savings must be fully demonstrated at scales relevant to the industrial reference sector.

To help address some of these uncertainties, CFD-DEM simulations can be extended from traditional hydrodynamics to include transfer processes and EM field. Also, consideration of wet particles requires taking inter-particle cohesive forces into account. In this work, a CFD-DEM model including moisture-dependent cohesive forces and the volumetric heating effect originating by the two EM field sources (RF and MW) is presented and discussed. Then, the results of a simulated batch fluidized bed dryer (Figure 1), in which the particles are subjected to simple air flow, RF and MW fields are presented and compared. Investigated variables include moisture and temperature dynamics.

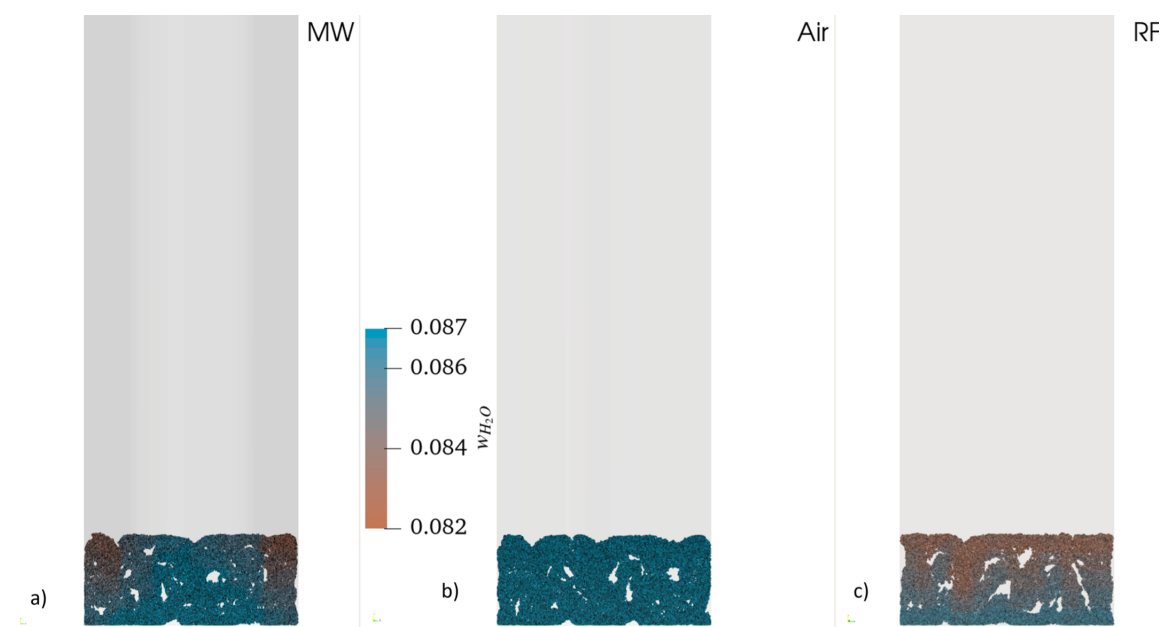


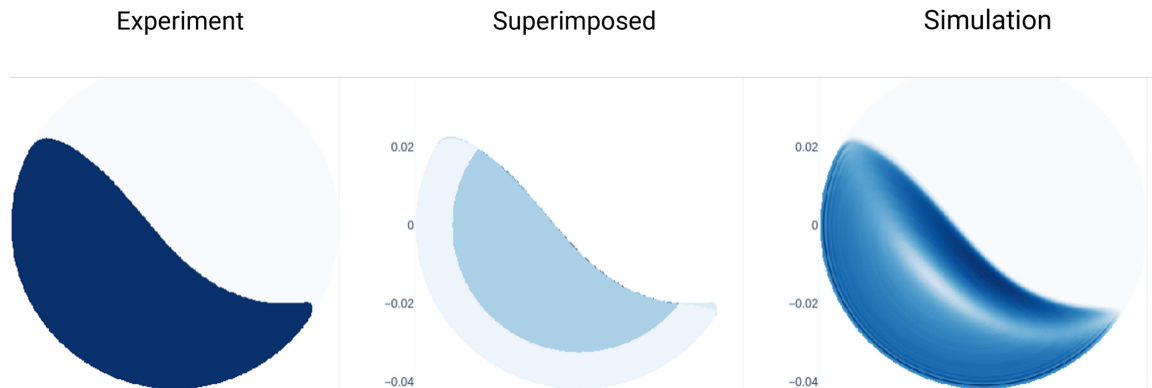
Figure 1. DEM simulation results showing fluidised particles subjected to different drying processes: a) using microwaves; b) conventional air; c) radiofrequency.

## Toward a Best Practice for DEM Calibration: Learnings from 5 years working with industrial DEM users

Kit Windows-Yule, Leonard Nicusan, Dominik Werner, Ben Jenkins

*University of Birmingham, Birmingham, United Kingdom*

### Abstract



Numerical methods such as the discrete element method (DEM), computational fluid dynamics (CFD), coupled CFD-DEM, and multiphase particle-in-cell (MP-PIC) simulations provide potentially powerful tools for the investigation and optimisation of diverse food processing systems, from coffee roasters to mills for producing cocoa liquor. However, without rigorous calibration and validation, their outputs may be inaccurate, or even entirely unphysical. The process of calibration can, however, prove highly time- and labour-intensive, and both calibration and validation are sorely lacking a clearly-defined "Best Practice".

In this talk, we introduce novel methods for both the calibration and validation of numerical simulations based on the results of a 5-year project funded by the Industrial Fine Particle Research Institute. In the project, we worked with a dozen industrial partners who use DEM in their processes, conducting detailed interviews to learn about their calibration methods, before testing the validity of these methods against detailed experimental ground-truth data produced using Positron Emission Particle Tracking. The results of these tests were used to determine the effectiveness of different calibration tools and methodologies, with the ultimate goal of determining what works well – and, equally importantly, what doesn't – ultimately distilling our findings down into a Best Practice for industrial DEM calibration.

In this talk, we briefly outline key findings from the project, and present novel, open-source tools developed during the project which can be used freely by the DEM community to support and expedite calibration and validation activities.

## Reaching below the Surface: Breaking the Boundaries of Granular Locomotion

Lorenzo Conti

*Crover, Edinburgh, United Kingdom*

### Abstract

The human pursuit to explore new horizons has brought us to be able to build machines that can reach the seas and the skies, but we have somewhat forgotten to get past what is under our feet: solid granular surfaces.

The first part of the talk will provide a summary of previous attempts to move through granular materials, followed by a presentation of the story and science behind the first feasible method for multi-directional fully-buried locomotion in dense granular systems.

The second part of the presentation will cover recent developments in the use of new and known granular concepts in designing remotely controlled and autonomous robots capable of navigating through static granular beds, along with learnings and open challenges in the area.

The talk will conclude with a discussion of some of the industrial use cases that self-propelled granular robots are helping to address and the potential that advancements in granular locomotion can unlock.



# Enhancing Concentrated Solar Power Plant Efficiency: A Comparative Study of Flowability and Heat Transfer Properties of Non-Spherical and Spherical Bauxite Particles

Aidana Boribayeva, Boris Golman

*Nazarbayev University, Astana, Kazakhstan*

## Abstract

A novel approach to energy generation, characterized by extended operational cycles, minimal waste, and recyclability, stems from concentrated solar power (CSP) technology. The efficacy of CSP systems relies on the interplay between the flow dynamics of granular materials and heat transfer efficiency. Bauxite emerges as a promising medium for thermal energy storage due to its cost-effectiveness and global abundance.

This abstract outlines a comparative investigation centered on the flow dynamics and heat transfer characteristics of bauxite particles, distinguishing between non-spherical and spherical morphologies, in moving bed heat exchangers for CSP systems. The research methodology entails comprehensive experimentation, including granular flow tests such as static and dynamic angles of repose, Carr index, Hausner ratio, and Jenike's shear test. Additionally, detailed shape analysis is conducted on non-spherical bauxite particles to elucidate shape irregularities.

Key flowability parameters such as angle of repose, flow function, internal friction angle, and cohesive indices are investigated to evaluate particle-particle interactions and packing dynamics. Despite the decreased flowability attributed to irregular shapes and surface cohesiveness of non-spherical particles, their flow behavior remains competitive compared to the expected performance of spherical particles.

Our experimental setup features a custom-designed tubular moving bed heat exchanger (MBHE), enabling the examination of flow characteristics and dynamics of both spherical and non-spherical particles within tubes. This facilitates a detailed examination of heat transfer phenomena at the granular level, providing essential data for validating computational investigations of heat exchange processes.

Computational simulations complement experimental efforts, allowing thorough examination of heat transfer and flow properties inside the MBHE. Parameters such as heat transfer coefficient, effective thermal conductivity, pressure drop, velocity profiles, and flow field distributions provide deeper insights into the interplay between particle morphology, flow dynamics, and heat transfer mechanisms.

Insights from this comparative study are instrumental in optimizing the design and operation of CSP systems, with the goal of enhancing energy conversion and storage performance. This research contributes to the field of powder technology by providing a comprehensive analysis of how particle morphology influences flowability and heat transfer properties. The findings not only advance understanding of granular materials but also offer valuable insights for the development of efficient and sustainable concentrated solar power technologies.

This research was supported by the research grant 20122022CRP1612 from Nazarbayev University.

## Surrogate and transformer models for particulate process modelling

Christoph Thon, Carsten Schilde

*Technische Universität Braunschweig - Institute for particle technology (iPAT), Braunschweig, Germany*

### Abstract

Artificial Intelligence (AI) is currently undergoing a revolution in capabilities and adoption rates in academia and throughout industries. A rough distinction in the field separates narrow AI, specializing in only one dedicated field/ task vs. the high goal of general AI or AGI, capable of performing across a broad spectrum of cognitive (and physical) tasks on or above human levels. In recent years very advanced narrow AIs were published such as AlphaFold (protein folding) or GNoME (material science) from Google, acting as highly accurate and quick surrogate models, demonstrating the ability to accelerate progress by orders of magnitude, achieving equivalents of up to 800 years of progress. At the same time generative AI, specifically transformer and large language models (LLMs) and to an extent diffusion models, represent a new kind of general purpose AIs which many AI researchers deem as examples of early or emergent AGI. In this contribution the impact on the field of particle technology and particulate processing will be covered, covering general trends as well as own research.

Regarding narrow AI, among others, a quick to apply DEM surrogate model will be shown, see figure 1. Other than in previous works [1] the AI does not emulate a particular simulation but dynamically emulates DEM simulation itself. The simulation domain is discretized into a grid of neighbouring cells in which a neural network periodically predicts particle motion, contacts and other properties such as forces over time followed by grid updates. High accuracies could be reached for different use cases such as particle bed compression or free particle flow in a stirred tank.

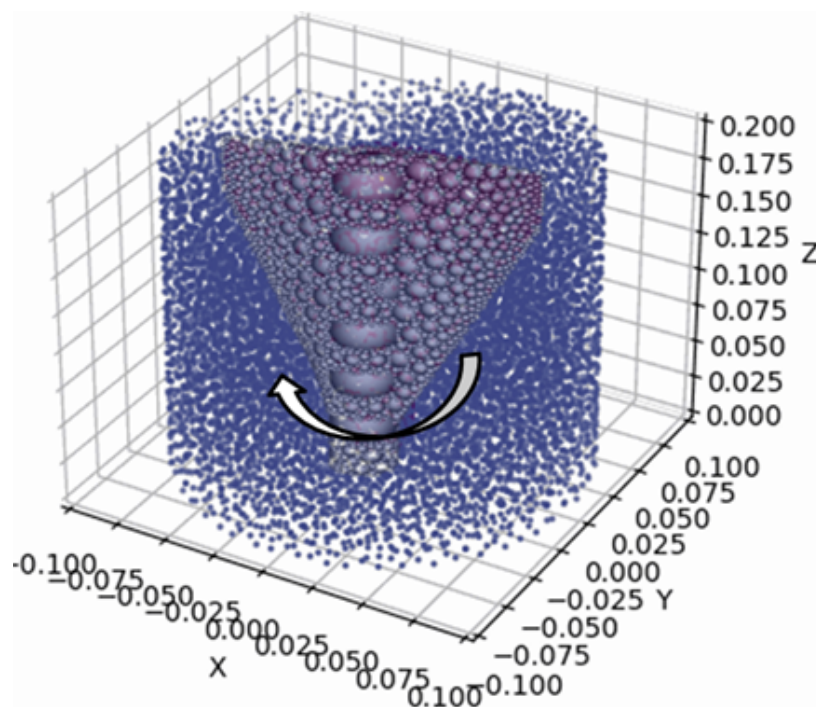


Figure1: Depiction of a surrogate DEM model for a stirred tank with particles

In regards to generative AI a transformer/ LLM based case study for the use as an autonomous agent will be shown, investigating the ability for autonomous simulation handling (testing capabilities without prior fine-tuning or specialization) across the spectrum of related tasks. Furthermore, ways of customization will be demonstrated such as the use of external repositories or fine-tuning to specialize open source models to act as domain expert in process engineering.

### References

- [1] C. Thon, M. Röhl, S. Hosseinihashemi, A. Kwade, C. Schilde, Artificial Intelligence and Evolutionary Approaches in Particle Technology, KONA Powder and Particle Journal advpub (2023) 2024011. <https://doi.org/10.14356/kona.2024011>.

# Characterization of the Heat Sealing Process Based on the Heat-Seal Strength of Pharmaceutical Blister Packages

Anna Márton<sup>1,2</sup>, Roman Heumann<sup>2</sup>, Werner Hoheisel<sup>3</sup>, Matthias Markus<sup>3</sup>, Jens Bartsch<sup>1</sup>, Markus Thommes<sup>1</sup>

<sup>1</sup>Technical University Dortmund, Dortmund, Germany, <sup>2</sup>Invite GmbH, Cologne, Germany, <sup>3</sup>Bayer AG, Leverkusen, Germany

## Abstract

The packaging of goods in the pharmaceutical and food industry is facing a revolutionary paradigm shift regarding the applied packaging materials with respect to the overall megatrend “sustainability”. Hereby, one of the main objectives is reducing waste. Correctly chosen process parameters based on process understanding can ensure the product quality thus preventing production of refuse. Considering pharmaceutical packaging, about 80% of the solid dosage forms are packed in blisters [1]. Here, the major motivation is the ability to protect each tablet from environmental influences, such as the humidity of air or contaminations.

The essential quality attribute of the blister packages filled with tablets is the tightness, which has to be tested according to the United States Pharmacopeia. The industry prefers the blue dye ingress test, however applying other methods could be also possible, for instance vacuum decay or tracer gas detection. Furthermore, the package seal strength test or peel test characterizing the strength of the bond of two sealed surfaces can describe quite sensitively the quality of the packages [2]. This quantitative method is sufficient for examining the influence of the relevant process parameters (sealing temperature, sealing pressure and production speed) on the packaging quality. Therefore, the aim of this study was to explore the influence of the important parameters of the heat sealing process using a Design-of-Experiment approach. The experimental results showed that the heat-seal strength significantly ( $\alpha=0.05$ ) increases with the heat-seal temperature and the heat-seal pressure linearly, however the sealing temperature has a quadratic effect as well (Figure 1). In an additional experiment the influence of the production speed was also examined, where higher heat-seal strength results were obtained when using slower production speeds i.e. longer dwell times.

In summary, the influence of the heat sealing process parameters on the heat-seal strength of pharmaceutical blister packages was examined in this study. As a result of the Design-of-Experiment concept a statistical model was developed which could help determining the sufficient process parameters more easily. Furthermore, the heat-seal strength test can be used as an on-line testing method for process monitoring. In future, the establishment of a physical model is planned as well.

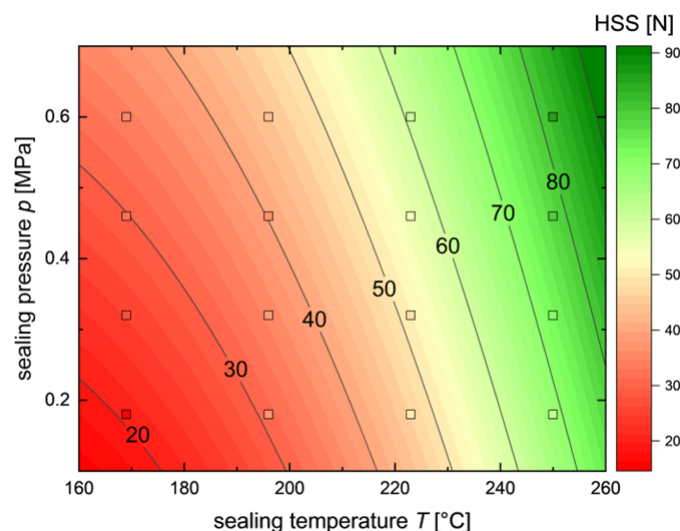


Figure 1: The sealing pressure is shown over the sealing temperature, while the colour code indicates the heat-seal strength. Measurement points are marked with squares and coloured based on measurement results.

[1] Pilchik, R. Pharmaceutical Blister Packaging, Rationale and Materials, PharmTech., 68-77 (2000).

[2] USP, 1207.

# Microdosing: Small-scale powder handling to create 3D property gradients

Lisa Windisch, Jil Mann, Carsten Schilde

TU Braunschweig, Braunschweig, Germany

## Abstract

As new areas of application continue to emerge, the importance of acquiring know-how about conveying and dosing of bulk solids does not diminish. This includes everything from large to very small quantities. However, the state of research on the ladder remains very scarce. So-called microdosing allows high-precision deposition of tiny amounts of powder down to the  $\mu\text{g}$  range. Microdosing is relevant, for instance, for locally adjusting the properties of components in powder-based processes, or in the pharmaceutical industry for precisely dosing minute amounts of expensive and potent active substances. It can also minimize material consumption and make processes more sustainable.

The aim of this study is to provide an insight into particle-level dosing mechanisms and the design freedom they offer for multi-material components. For this, a piezo-based dosing system has been developed that can reproducibly deposit small amounts of powder down to  $50\text{ }\mu\text{g}$ . The setup is used to discuss the relationships between powder properties and dosing results. In combination with an XYZ positioning stage, test specimens with three-dimensional property gradients have been produced. Carbon black as an electrically conductive component and aluminum oxide as a ceramic electrically insulating component were embedded in an epoxy resin matrix. The powders were prepared from suspensions with different compositions and particle mass contents. Material specific properties such as electrical conductivity and deformation behavior of the hot-pressed samples were then determined and compared.

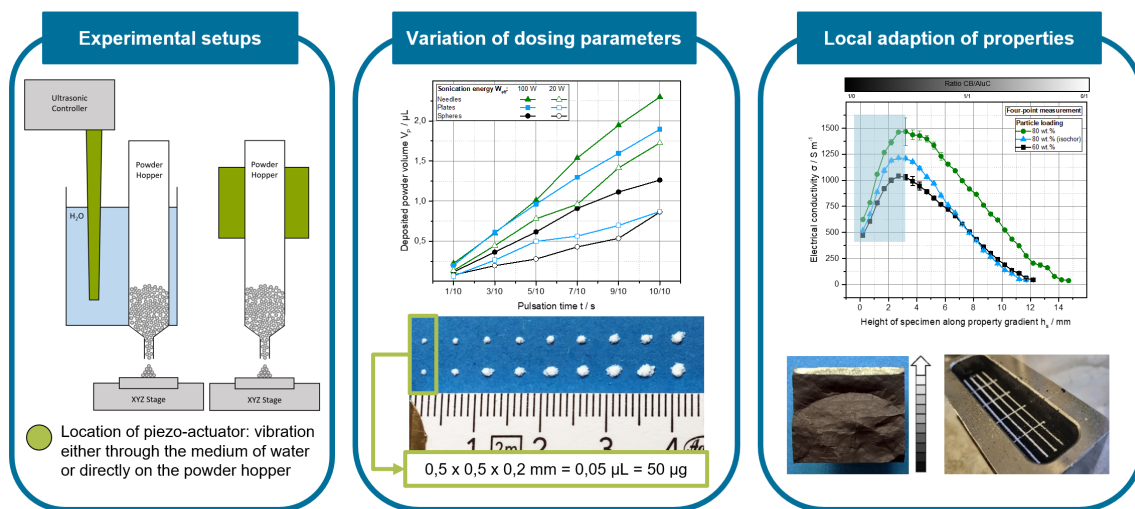


Figure 1: Insights from the experimental setup to the properties of three-dimensionally graded samples.



## Effect of particle size, shape and density differences on binary mixture segregation during blast furnace charging

Raïsa Roeplal<sup>1</sup>, Yusong Pang<sup>1</sup>, Jan van der Stel<sup>2</sup>, Allert Adema<sup>2</sup>, Dingena Schott<sup>1</sup>

<sup>1</sup>TU Delft, Delft, Netherlands, <sup>2</sup>TATA Steel Europe, Velsen-Noord, Netherlands

### Abstract

A blast furnace is a counter-current reactor which produces liquid iron through a series of chemical reactions occurring between ascending hot reduction gas, which is injected through nozzles at the bottom of the furnace, and a descending packed bed consisting of different raw materials (the “burden”) which are charged at the furnace top. Bed permeability is a crucial factor in furnace efficiency which depends on the burden distribution which is achieved through charging.

It is well known that segregation is likely to occur during charging since the material mixture contains particles differing simultaneously in size, shape and density. However, predicting how the burden will be distributed is particularly difficult due to the combined effect of these differences. The Discrete Element Method has been used extensively to gain understanding of the prevalent segregation mechanisms during charging and the resulting burden distribution. So far, researchers have focused mostly on investigating size segregation while the effect of density difference has hardly been studied, and the effect of particle shape has not yet been considered systematically. A few works modelled mixtures of particles differing in both size and density, however, fundamental understanding of how size and density differences contribute to the final burden distribution is still lacking.

In this work, we systematically investigate the effects of size, shape and density differences on mixture segregation using Response Surface Methodology. We first identify the importance of these material properties separately and subsequently investigate combined effects on burden distribution. The novelty of this work is that, for the first time, we investigate the importance of all these material properties as well as their interactions on mixture segregation. These findings provide insight on how segregation can be mitigated when charging different kinds of mixtures to the furnace.

# A world of pure imagination? Understanding the dynamics of Vertical Stirred Mills within chocolate processing

Daniel Rhymer, Andy Ingram, Kit Windows-Yule

University of Birmingham, Birmingham, United Kingdom

## Abstract

While it would be nice to imagine a Willy Wonka world where perfectly smooth chocolate is produced by waterfall, the reality is very different. Cocoa liquor is a particle-laden slurry, and these particles need to be reduced in size to create the smooth texture and desired mouthfeel needed for tasty chocolate. A vertical stirred mill is often used to achieve this, as they have greater specific energy transfer and a smaller physical footprint than other grinding techniques [1], but there is still little understanding about its exact dynamics on an industrial scale. This is a problem not just within chocolate, but industry as a whole, as grinding is the most commonly used step in manufacturing. Up to 4% of global electricity consumption goes into reducing the size of materials [2].

Simulation has opened a new world of possibility to explore the detail of vertical mills and the talk presents a validated simulation using the Discrete Element Method (DEM) technique and experimental data from particle tracking data. The model is trained and optimised using machine learning and while there are limitations in trying to align complex multiphase systems, a good level of agreement with the experimental results can be reached (Figure 1). The model can also reproduce the dynamics of unseen trials to the same level of accuracy as the initial training set, further validating the optimal conditions and means the model can be used with confidence beyond the experimental trials. This truly unlocks a world of pure imagination in better understanding and optimising the process, improving efficiency and tackling the climate crisis.

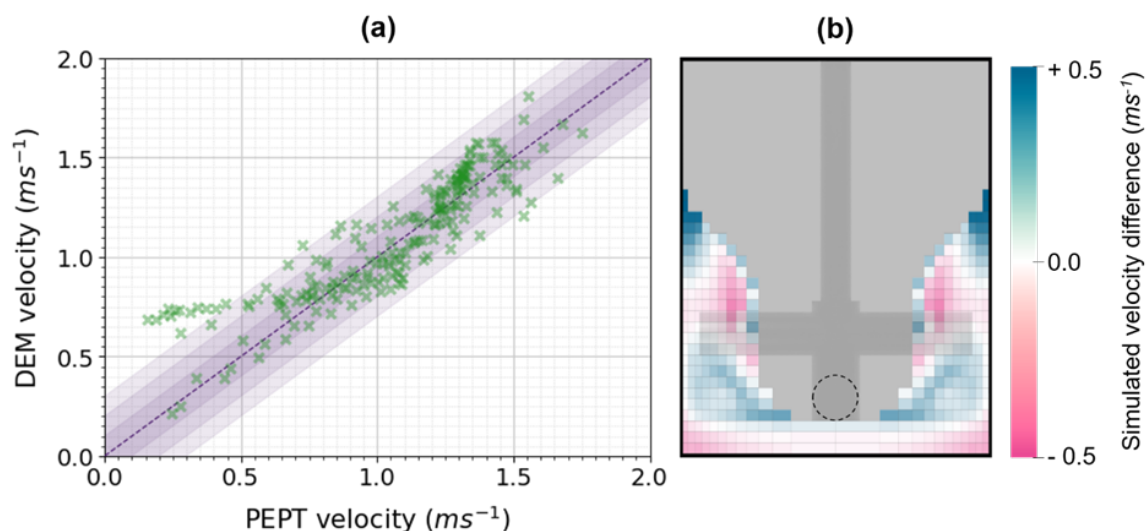


Figure 1. The results of the best performing simulation within the trial conditions from Figure 1. (a) Velocity parity plot for each cell with purple banding an indicator of the difference (b) Mapped velocity difference from the perspective of the simulation.

## References

- [1] A. Jankovic (2003) Min Eng. 16(4): pp. 337-345.
- [2] J. Jeswiet and A. Szekeres (2016) Procedia CIRP. 48: pp.140-145.

## Transient particulate flow statistics: between static and dynamic

Stefan Luding

University of Twente, Enschede, Netherlands

### Abstract

How do soft granular materials (or dense amorphous systems) respond to externally applied deformations at different rates – from fast to slow to very slow – and for different system sizes? This long-standing question was intensively studied for shear deformation modes, but only more recently also for isotropic deformations, like compression-decompression cycles [1,2]. For moderate strain rates, in the solid-like state, above jamming [3,4,5], the system appears to evolve more or less smoothly in time/strain, whereas for slow enough deformations, the material flips intermittently between the elastic, reversible base-state and plastic, dynamic “events”. Only during the latter events the micro-structure changes, it re-arranges, irreversibly. The reversible base state involves both affine and non-affine deformations, while the events are purely non-affine. Besides their phenomenology and statistical properties, in particular, the system size- and rate-dependence [6] of the events is studied, providing reference data, to be compared in future to experiments on model materials like hydrogel particles using modern techniques. Finally, perspectives and consequences for real materials in applications are addressed.

### References:

- [1] K. Taghizadeh, S. Luding, R. Basak, L. Kondic, *Understanding slow compression of frictional granular particles under slow compression by network analysis*, Soft Matter (submitted 2023)
- [2] S. Luding, K. Taghizadeh, C. Cheng, L. Kondic, *Understanding slow compression and decompression of frictionless soft granular matter by network analysis*, Soft Matter 18, 1868 (2022)
- [3] S. Luding, *Granular matter: so much for the jamming point*, Nature Physics 12, 531-532, 2016
- [4] N. Kumar, S. Luding, *Memory of jamming – multiscale models for soft and granular matter*, Granular Matter 18, 58, 2016
- [5] S. Luding, Y. Jiang, and M. Liu, *Un-jamming due to energetic instability: statics to dynamics*, Granular Matter 23, 80, 2021
- [6] S. Luding, *How does static granular matter re-arrange for different isotropic strain rate?*, in Powders & Grains 2021 – EPJ Web of Conferences (2021), Vol. 249, p. 10001
- [7] S. Luding, *Elastic-plastic intermittent re-arrangements of frictionless, soft granular matter under very slow isotropic deformations*, Frontiers Physics 11, 1211394, 2024

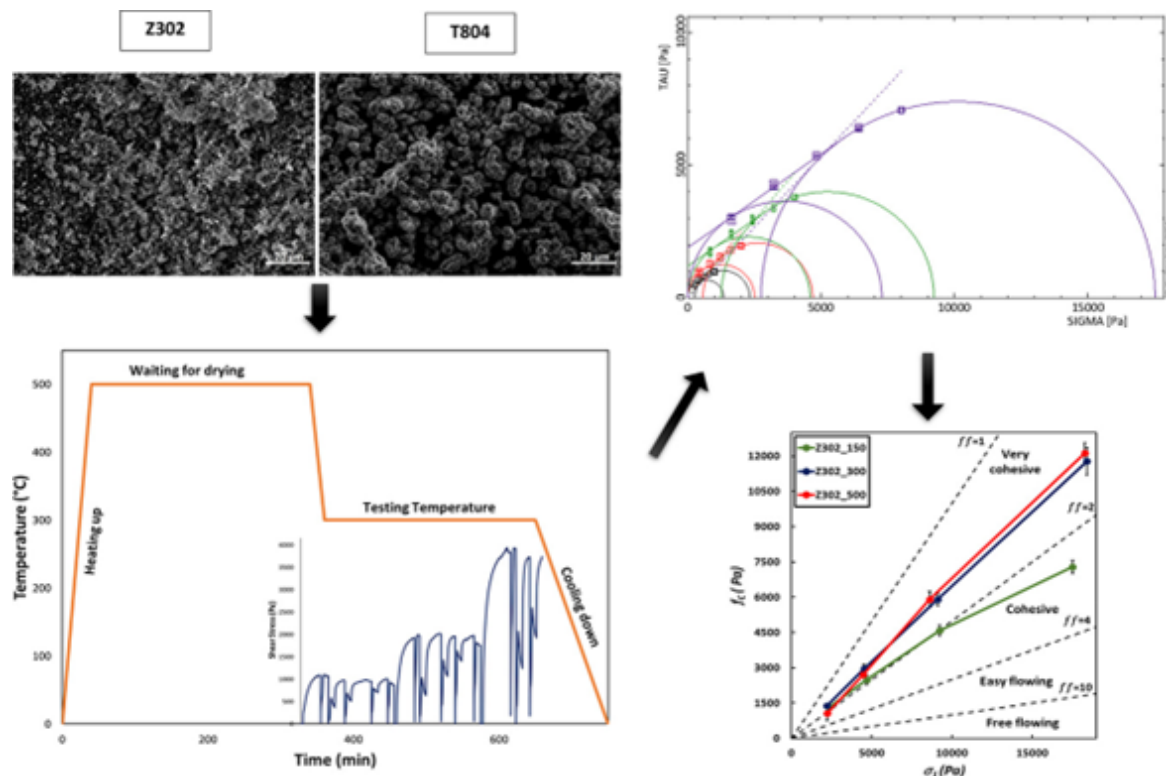
# The Effect of High Process Temperature on the Flow Behaviour of Zeolite Powders

Diego Barletta<sup>1</sup>, Sina Zinatlou Ajabshir<sup>1</sup>, Canan Gucuyener<sup>2</sup>, Vincenzino Vivacqua<sup>2</sup>, Darren Gobby<sup>2</sup>, Hugh Stitt<sup>2</sup>, Massimo Poletto<sup>1</sup>

<sup>1</sup>University of Salerno, Fisciano (SA), Italy, <sup>2</sup>Johnson Matthey Technology Centre, Billingham, United Kingdom

## Abstract

Zeolite powders are used in various applications, and their flow behaviour can be affected by processing conditions. Temperature is a crucial process condition that changes during manufacturing and can alter particle properties, affecting powder flow properties. Therefore, it is necessary to test the powder flow properties under the process conditions. Therefore, it is necessary to test the powder flow properties under the process conditions. The flow properties of two types of zeolite powders, Z302 and T804, were evaluated at temperatures of 150, 300, and 500 °C under normal consolidation stresses ranging from 1 to 8 KPa using an Anton Paar shear cell. The two materials exhibited distinct flowability behaviours, even at the lowest temperature tested. At 500°C, the temperature has a more significant effect on the T804 zeolite than on the Z302 zeolite. The flow function of T804 zeolite falls into the cohesive range. In contrast, the flow function of Z302 zeolite changes only for large values of consolidation stresses, falling entirely within the very cohesive range. To explain the disparate behaviour of the two materials under changing temperature and consolidation stress, we developed a theoretical framework that considers the differing particle size distributions of the powders. The analysis supports the effectiveness of the general approach, which involves estimating the average material fabric to provide averaged estimates of contact forces. This approach can explain the different behaviours of temperature and consolidation changes shown by powders. Additionally, a new analysis of flowability is introduced, which calculates a structural length to account for different powder bulk densities.





# Modelling the Breakage Behaviour of Irregular Particles with Varied Contact Curvature and Area

Bin Zhang, Sadegh Nadimi

Newcastle University, Newcastle upon Tyne, United Kingdom

## Abstract

Particle breakage plays a crucial role in understanding the mechanical properties and revealing failure mechanisms in granular materials. In recent years, significant attention has been devoted to modelling particle breakage through the Discrete Element Method (DEM), typically assuming spherical particles. However, in natural granular materials, the irregular shapes of particles present challenges for numerical modelling, as the contact topologies are complex [1].

This study addresses the impact of contact topology on material fragmentation using a numerical approach. It extends the micro finite element method proposed in [1] by incorporating cohesive interface elements to enhance its capability to simulate particle breakage [2]. By adjusting the radius of the rigid ball at the loading ends, various contact curvatures can be replicated. The model's validity is assessed through comparison with X-ray computed tomography observations and experimental data. The simulation results in terms of load-strain curves, fracture patterns, and contact areas, are recorded and analysed.

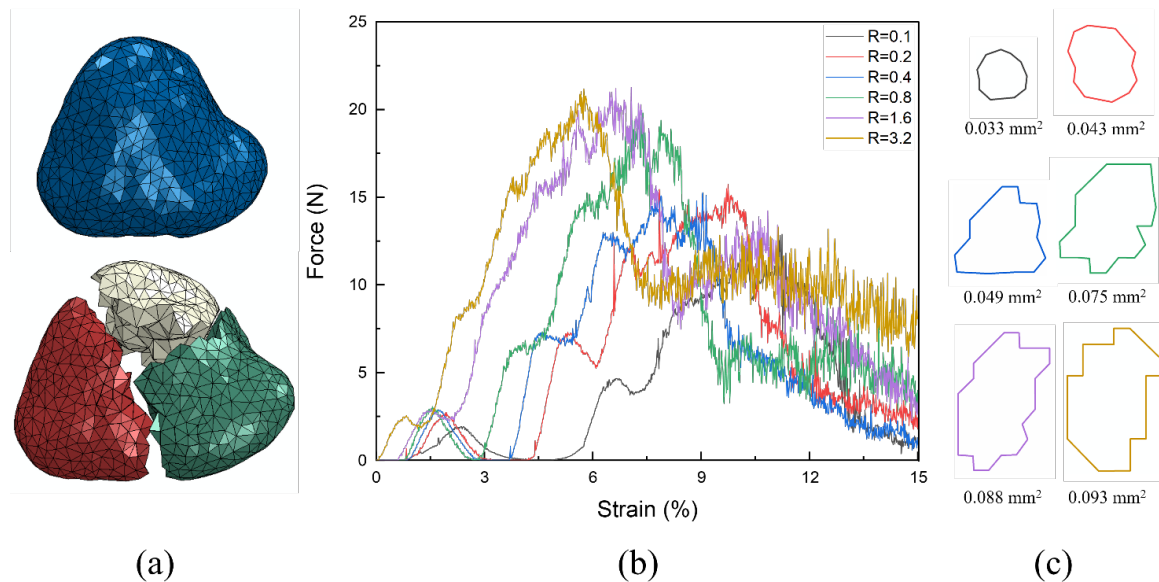


Figure 1 . (a) Particle prior to (top) and post (bottom) breakage, (b) load-strain curves using different rigid balls and (c) colour coded contact area at peak force prior to breakage.

## References

- [1] Nadimi, S., & Fonseca, J. (2018). A micro finite-element model for soil behaviour. *Géotechnique* , **68** (4), 290-302.
- [2] Zhang, B., Nadimi, S., Eissa, A., & Rouainia, M. (2023). Modelling fracturing process using cohesive interface elements: theoretical verification and experimental validation. *Construction and Building Materials* , **365** , 130132.

# Parallel Discrete Element Method Software for Heterogeneous Shared- and Distributed-Memory Architectures

Arnas Kačeniauskas, Ruslan Pacevič, Oleg Bystrov, Rimantas Kačianauskas

*Vilnius Gediminas Technical University, Vilnius, Lithuania*

## Abstract

The low cost and diversity of heterogeneous resources available through cloud providers encourage moving time-consuming parallel computations, such as discrete element method (DEM) [1] applications, to clouds. However, heterogeneous architectures of virtual cloud resources can cause severe degradation of parallel performance because of the irregular partitions for heterogeneous resources, limitations of memory bandwidth, communication overhead and increased load imbalance. The parallel DEM software [2] was developed by using OpenCL for shared-memory multi-core architectures and MPI for distributed-memory architectures. The presented resource-aware partitioning algorithm for heterogeneous architectures is distinguished by repartitioning condition defined by the skinning technique and granular flow physics. The DEM model for granular flows of the non-cohesive frictional visco-elastic spherical particles is implemented in the parallel software. The novel research on the parallel software performance was conducted in co-located Docker containers.

Six cases of heterogeneous resources, including NVIDIA® Tesla™ P100 GPU and co-located containers, were considered in the performed research. The speedup of parallel computations up to 6.0 was measured on 8 heterogeneous containers. In three considered cases of heterogeneous cloud resources, the load imbalance varied from 11% to 81%. In the case the container equipped by GPU, the load imbalance of computations without weighting varied from 18.0% to 20.3%, while the decrease of the execution time up to 36.1% of the execution time obtained without weighting was observed. The highest improvement in performance equal to 48.7% of the execution time obtained without weights was achieved by using the resource-aware repartitioning in the case of the highest load imbalance. Memory stress tests caused heterogeneity of non-isolated containers, which reduced the performance of memory bandwidth-bound DEM computations on the co-located cloud resources. The decrease in the total execution time achieved by applying resource-aware repartitioning varied from 6.7% to 20.1% of the total execution time obtained without using weights, which depended on load imbalance. The resource-aware repartitioning decreased the computation time on co-located containers when the synthetic stress was applied on one co-located container longer than 30% of the whole simulation time.

**ACKNOWLEDGEMENT:** The research was performed in the frame of the COST action CA22132 - Open Network on DEM Simulations (ON-DEM).

## REFERENCES

1. P.A. Cundall, O.D.L. Strack, A discrete numerical model for granular assemblies, *Géotechnique*, Vol. 29, pp. 47-65, 1979.
2. O. Bystrov, R. Pacevič, A. Kačeniauskas, Cost- and performance-aware resource selection for parallel software on heterogeneous cloud, *Concurr Comput Pract Exp*, Vol. 36, Iss. 10, e7877, 2024.

# The effect of particle size distribution on the behaviour of assemblies of spheres under generalised stress condition - A comparison of results between two different open-source DEM codes.

Daniel Barreto

*Edinburgh Napier University, Edinburgh, United Kingdom*

## Abstract

The use of spheres as an idealisation of more realistic particle shapes is ubiquitous amongst researchers using Discrete Element Method simulations. The simulation of drained triaxial compression on assemblies with uniform particle size distributions is also very common as a means to reduce the computational cost of DEM simulations despite well recognised effects of fine(r) and coarse(r) particles on the behaviour of granular material on things such as instability, strength, deformation and permeability, amongst others. Despite the significant knowledge that DEM simulations have provided to understand soil behaviour under these "standard" (triaxial) stress conditions, there are significant gaps on the effect of well-graded and gap-graded spherical assemblies under more generalised stress conditions.

Furthermore, there are comprehensive efforts to validate benchmark DEM simulations. Examples of these include a round robin test carried out by the Japanese Geotechnical Society in relation to the simulation of angle of repose experiments, and the benchmarking exercise involving silo emptying, drum mixing and particle impact across nine open-source DEM codes carried out by Dosta et al (2024). Despite the widespread use of triaxial simulations in geotechnical research there is no comparable exercise with respect to it.

A large comparative exercise has been performed using two open-source codes by the author. Simulations included uniform, well-graded and gap-graded specimens of spheres with particle sizes ranging between 0.0625 and 4 mm diameter. In addition to this, a wide range of initial densities, stress levels and drained general stress paths beyond drained triaxial compression. In some cases, different hardware architectures were also used to assess performance issues. For comparison purposes and added simplicity, in addition to spheres a Hertz-Mindlin model for dry contacts was used.

This study presents some of the typical findings of this study. From a mechanical perspective, the results highlight the significance of particle size distributions on granular material behaviour, the need (or not) to simulate the full range of (real) particle sizes in a DEM simulations as well as some interesting results involving the need to also adequately choose the hardware to perform a given DEM simulation.

## References

M. Dosta, D. Andre, V. Angelidakis, R.A. Caulk, M.A. Celigueta, B. Chareyre, J.-F. Dietiker, J. Girardot, N. Govender, C. Hubert, R. Kobyłka, A.F. Moura, V. Skorych, D.K. Weatherley, T. Weinhart. Comparing open-source DEM frameworks for simulations of common bulk processes, *Computer Physics Communications*, Volume 296, 2024, 109066, .

# On the role of numerical calibration in setting up real-time recurrence CFD (rCFD) simulations of single- and multiphase flows

Stefan Pirker, Thomas Lichtenegger, Daniel Queteschiner

*Johannes Kepler University, Linz, Austria*

## Abstract

rCFD has been shown to speed up pseudo-periodic flows like fluidized beds by three to four orders of magnitude. While early success stories just focused on the bright side of rCFD by emphasizing on its fascinating computational efficiency, this methodology still suffers from a series of potential pitfalls.

To start with, the existing version of rCFD exhibits significant propagation errors in nearly stagnant flow regions. In order to overcome this problem, an automated numerical calibration procedure for cell-to-cell shifts is introduced, which is based on a novel discretization scheme for the Lagrangian propagator of fluid flow. In a first lid-driven cavity test case, we prove that this new version of rCFD reduces propagation errors significantly. Finally, this new method is applied to secondary gas injection in a fluidized bed.

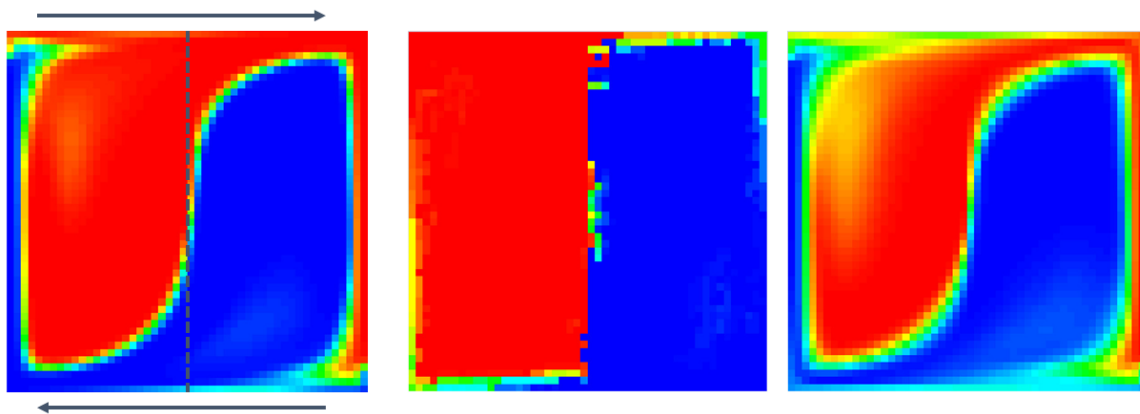


Figure 1: Lid driven cavity test case: (left) full CFD, (middle) uncalibrated and (right) numerically calibrated rCFD

Next, we discuss the case of non-passive propagation of temperature. Obviously, resulting gradients in the temperature field give rise to buoyancy driven natural flow, thus changing the original flow field. Consequently, any isothermal flow database will be violated. Based on a lab-scale demonstrator experiment, we show that in this case multiple databases are needed and we further discuss ways of how to establish and execute them.

Since multiple databases are prone to excess data requirements, we finally propose a grid coarsening concept for rCFD for the purpose of data reduction. This coarsened rCFD can be regarded as a spatially filtered representation of a high-resolution Lagrangian propagator. Based on a metallurgical process, we show the functionality of this data-reduction methodology.

While all of these potential pitfalls of rCFD still exist, we introduced conceptual counter-measures. We believe that these under-the-hood improvements will lead to an extended applicability of rCFD in the realm of process modelling.



## Modelling hydrodynamic lubrication using DEM

Richard Wood<sup>1</sup>, Ben D Goddard<sup>2</sup>

<sup>1</sup>Altair Engineering, Edinburgh, United Kingdom, <sup>2</sup>University of Edinburgh, Edinburgh, United Kingdom

### Abstract

There are many well-established simulation methods for systems consisting of either dry granular media (e.g., with DEM) or complex fluids (e.g., with CFD, SPH, or DDFT). However, for systems which contain both granular media and fluids there is currently no single framework that can completely capture the complex interactions between the two phases in industrially-relevant systems.

Some methods exist in various ‘limiting’ cases. One example being relatively sparse, insoluble granular particles suspended in a fluid where drag and buoyancy forces can be captured through a coupled DEM-CFD simulation. In contrast, other applications, such as dense particle systems that dissolve in a fluid require the modelling of chemical reactions, which may in turn affect the local fluid viscosity; a ‘standard’ DEM-CFD coupling is not capable of capturing these complex interactions.

We will present a model for one aspect of suspensions that is not present in standard DEM: short-range hydrodynamic interactions. Our approach uses principles from lubrication theory to capture these forces which arise due to the squeezing and shearing effects caused by neighbouring particles and wall boundaries. A key advantage of our approach is that one does not need to explicitly resolve either particle boundary layers or the interstitial fluid momentum equations, both of which are computationally expensive.

Our work is based on the approaches developed by O’Neil & Stewartson (1967), Cheal & Ness (2018), and Goddard et al. (2020), which we have unified into a single DEM contact model; this has been implemented into the commercial software Altair EDEM. As a first application, we describe the motion of a dense suspension of particles in a slow-moving, viscous fluid. A key assumption is that the material is fully saturated. This is quite different to the commonly used ‘liquid bridge’ models which also aim to capture the effects of fluids solely in a DEM framework by considering each pair of contacting elements as having their own ‘bridge’.

The model is still in its infancy in terms of commercial applications but has already been used to great effect in the battery sector. It is anticipated that the model will also be of use in the pharmaceutical industry and applications involving cement or concrete. In lieu of these commercially-sensitive applications, we will present some hypothetical example simulations.

# Revolutionizing the generation and reconstruction of particle models using advanced AI-driven computational techniques

Kostas Giannis, Christoph Thon, Jiqian Guo, Carsten Schilde

TU Braunschweig, Braunschweig, Germany

## Abstract

Traditional approaches to 3D model reconstruction of powders and particles, such as X-ray computed tomography (XRCT), require long experimental times and duplication of effort for different objects. In contrast, dynamic image analysis is time efficient, e.g. QicPic and Camsizer, which obtain a limited number of particle images. To provide an efficient alternative for particle reconstruction, this research introduces an AI-driven method that combines dynamic image analysis, generative adversarial networks (GANs), and diffusion models. This integrated approach aims to effectively reconstruct complex 3D particle models and 3D XRCT structures. In addition, a variational autoencoder (VAE) has been integrated to improve control over particle shape.

Trained on 3D models generated by our GAN, the VAE enables smooth, continuous changes in particle shape through manipulation in latent space. Our novel GAN architecture is tailored to generate realistic 3D particle models using only these 2D images, bypassing the need for actual 3D data. The generator creates models from Gaussian noise, which are then projected into three orthogonal views. These projections, together with real images from experiments, are evaluated by the discriminator, allowing the generation of numerous models that replicate experimental features. We also propose a conditional GAN variant that constructs 3D models from a single 2D input image and predicts particle shapes with high fidelity to the provided shapes, even when these contain complex, unseen patterns. This model was trained using only 2D images obtained through dynamic image analysis, eliminating the need for 3D ground truth data. In addition, a variational autoencoder (VAE) was integrated to improve control over particle shape. Trained on 3D models generated by our GAN, the VAE enables smooth, continuous changes in particle shape through manipulation in latent space.

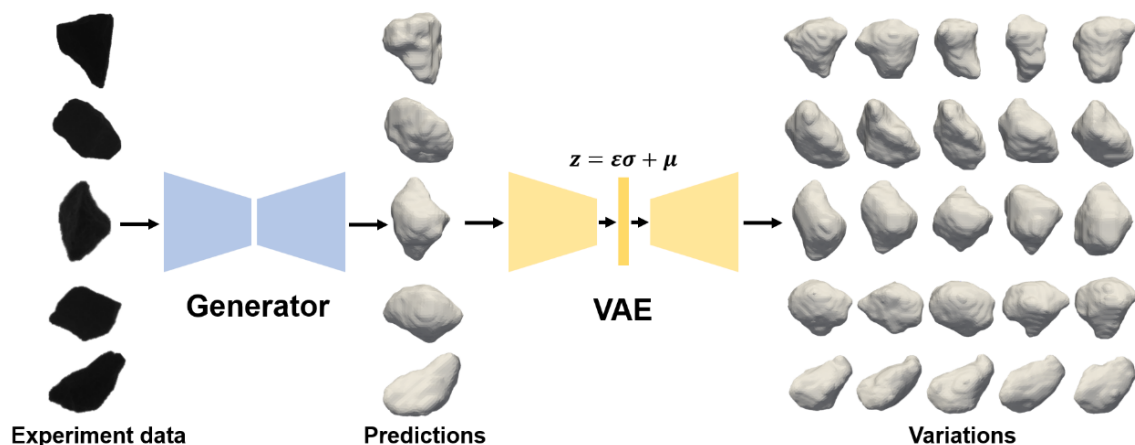


Fig. 1. Flowchart of the 3D modelling process: 1) Acquisition of 2D images through dynamic image analysis; 2) Prediction of 3D particle structures using Generative Adversarial Networks (GAN); 3) Refinement of 3D particle models through Variational Autoencoder (VAE) adjustments.

These advancements significantly accelerate the particle model reconstruction process and broaden the scope for practical applications, particularly in discrete element method (DEM) simulations. The enhanced model accuracy and customizable particle dimensions provided by our methods improve the realism and variability of simulation scenarios. This is crucial for more accurately predicting the behavior of granular materials, powders, and complex particulate systems under various conditions.

# Overcoming Crushing Challenges: DEM-MBD Simulation for Jaw Crusher Optimization

Andrew Hobbs<sup>1</sup>, Marina Sousani<sup>2</sup>

<sup>1</sup>Astec Industries, Chattanooga, USA, <sup>2</sup>Astec Industries, Patras, Greece

## Abstract

Aggregate crushing is an essential step in the process of producing the raw materials needed in infrastructure and construction. Some crusher designs such as jaw crushers have existed for over one hundred years. Effective crushing equipment design must balance product throughput, energy consumption, and wear. Simulation offers the potential to better understand and optimize these long-standing designs to produce a more robust and efficient jaw crusher. In this study we use discrete element method (DEM) coupled to multi-body dynamics (MBD) to investigate the effect of the moving jaw kinematics on crushing performance and energy input. Using a modified version of the Tavares breakage model (Tavares and King, 2002; Tavares, 2009) to ensure repeatability, the kinematics of the moving jaw were parameterized to create and solve a design of experiment (DOE) using DEM. The results were analyzed to identify an optimum configuration. A similar DOE of DEM coupled to MBD was performed to more accurately calculate the reaction forces and torques on critical components of the crusher. While both the DEM-only and coupled DEM-MBD produced similar predictions for particle throughput, the coupled DEM-MBD results were found to provide a more holistic view of the impact of different configurations on machine components with respect energy consumption and wear (Figure 1). The inclusion of the MBD coupling provided information on operational bearing loads that were not available from the DEM-only simulations helping inform a more robust and reliable crusher design.

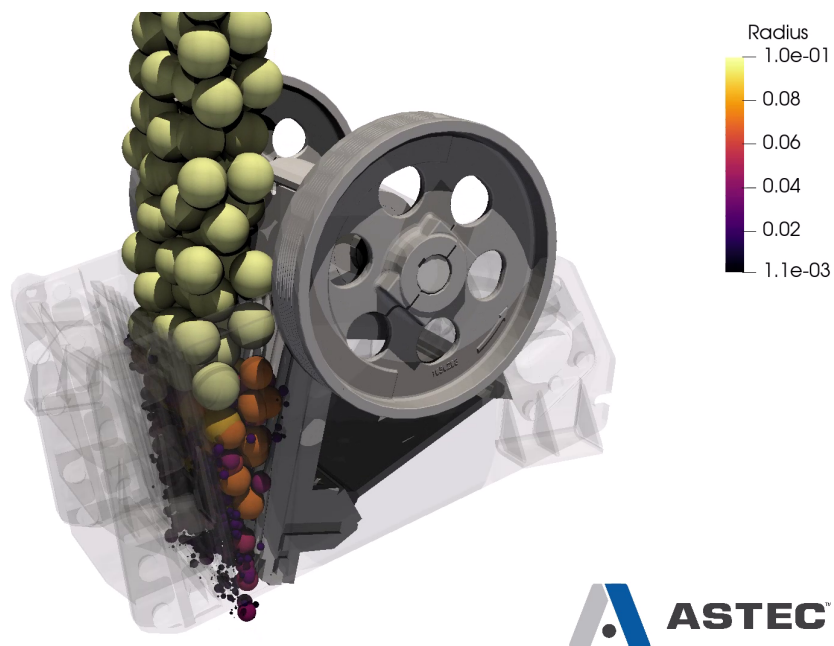


Figure 1. DEM results of jaw crusher showing particles colored by radius

## References:

- Tavares L.M. and King R.P. (2002) *Modeling of particle fracture by repeated impacts using continuum damage mechanics*. Powder Technology **123** (2): p. 138-146.
- Tavares L.M. (2009) *Analysis of particle fracture by repeated stressing as damage accumulation*. Powder Technology **190** (3): p. 327-339.

## Powder characterisation and analysing flow behaviour of metal powders during the dosing process in a 3D printing system

Mozhdeh Mehrabi<sup>1</sup>, Marie E Baxter<sup>2</sup>, Syed F Islam<sup>2</sup>, Gavin J Baxter<sup>3</sup>, Ali Hassanpour<sup>1</sup>, Andrew Bayly<sup>1</sup>

<sup>1</sup>University of Leeds, Leeds, United Kingdom, <sup>2</sup>Advanced Manufacturing Research Centre (AMRC), Sheffield, United Kingdom, <sup>3</sup>University of Sheffield, Sheffield, United Kingdom

### Abstract

Reliable quantification of bulk behaviour of powders in high value additive manufacturing process is essential. The selection of appropriate metal powders and maintaining powder consistency throughout the entire process, from dosing in front of the blade to spreading, significantly impacts the final component. In some 3D printing systems, the dosing process remains somewhat enigmatic, often relying on the operator to assess optimum dosing percentage through trial and error. Hence it is essential to define and establish a feasible dosing metric by investigating the combined effects of powder characteristics and process parameters, such as opening percentage, and opening speed of the doser, on the dosing behaviour of powders.

In this research two batches of Ti6Al4V powders (virgin and recycled) have been fully characterised and their dosing behaviour has been investigated using the gravity-fed dosing setup of a 3D printing system. The aim of this research is to understand how powders are positioned in front of the spreader and to develop a metric for quantifying the amount of dosed powder based on different process conditions for different powder types. This can lead to deeper understanding of the dosing process in the 3D printing system and offers insights into predicting the optimal dosing settings for each powder batch based on its unique physical properties.



# One dimensionless number to rule the dimensionless performance characteristics of a cyclone

Dzmitry Misiulia, Sergiy Antonyuk

*University of Kaiserslautern-Landau (RPTU), Kaiserslautern, Germany*

## Abstract

Due to simplicity, reliability, relatively low manufacturing costs, and the ability to work under high pressures and temperatures, cyclone separators have been widely used in various applications and in a wide range of sizes, from less than 1 cm up to several meters in diameter. The main cyclone performance characteristics are the pressure drop, the cut-size, and the slope of the separation curve. Several studies demonstrate that the dimensionless cut-size is a function of the Reynolds number but this conflicts with some popular theories for cyclones, which assume that the dimensionless cut-size is constant.

The main objective of this work was to investigate the cyclones at different operating conditions and flow regimes, covering the operation regime of small-scale and large-scale (industrial) cyclones and reveal the dependence of the dimensionless cyclone performance characteristics (Euler number, Stokes number and separation slope) on the operation conditions characterised by another dimensionless parameter, the Reynolds number. This was realised with the Computational Fluid Dynamics simulations, which were validated based on the experimental data.

For accurate prediction of the swirling flow in a cyclone, the Large Eddy Simulation with a dynamic Smagorinsky-Lilly subgrid-scale model was applied. The dispersed phase was modelled by tracking particles through the flow. Five different sizes of the high-efficiency Stairmand cyclone were investigated at inlet velocities from 0.5 up to 25 m/s and at various temperatures (from 20 to 500C) and pressures (from 0.5 to 4 bar), thus the outlet Reynolds numbers covered the range of 84 to 252875.

It was found, that the Reynolds number is the key parameter that rules all dimensionless performance parameters of the cyclone. Regardless of cyclone diameter, flow rate, and operating temperature and pressure, all dimensionless cyclone performance characteristics are ruled by solely the Reynolds number. Based on the flow field and cyclone performance characteristics four critical Reynolds numbers were determined which correspond to the transition from the laminar to transition regime, from transition to the turbulent regime, and two for transitions between three turbulent sub-regimens.

The results of this study showed, that when one knows the performance parameters of a cyclone at some Reynolds numbers, varying the operating conditions but keeping the same Reynolds numbers one can predict the expected performance characteristics of the cyclone. This could be very useful for researchers and engineers who deal with modelling and application of cyclones.

# Utilizing Machine Learning for Efficient Parameter Inference of Granular Material Simulations

Luisa Orozco<sup>1</sup>, Aron Jansen<sup>1</sup>, Retief Lubbe<sup>2</sup>, Hongyang Cheng<sup>2</sup>

<sup>1</sup>The Netherlands eScience Center, Amsterdam, Netherlands, <sup>2</sup>University of Twente, Enschede, Netherlands

## Abstract

Numerical models are essential for predicting the history- and regime-dependent behavior of granular materials in various industries, including civil engineering and particle technology. These models often rely on parameters that cannot be directly measured. GrainLearning, a Bayesian Calibration tool introduced by Cheng et al. (2019), addresses these challenges by probabilistically estimating model parameters constrained by real-world data, thus enhancing the simulations with uncertainties to serve as digital twins for real-world processes. This method contrasts with the traditional trial-and-error approach and leverages reduced-order modeling techniques like artificial neural networks. GrainLearning not only refines parameter estimation through Sequential Monte Carlo filtering and variational Gaussian mixtures but also significantly reduces computational demands by substituting model evaluations with surrogate models like recurrent neural networks. This approach has shown promising results in various granular material applications, using particle- and continuum-based numerical methods.

[1] H. Cheng, T. Shuku, K. Thoeni, P. Tempone, S. Luding, V. Magnanimo. An iterative Bayesian filtering framework for fast and automated calibration of DEM models. *Comput. Methods Appl. Mech. Eng.*, 350 (2019), pp. 268-294

# Journey to the CFD-DEM model of a cold plasma-assisted fluidized bed powder coating process

Pedro Martin Salvador<sup>1</sup>, Rik H. Verschueren<sup>2</sup>, Thomas De Beer<sup>1</sup>, Ashish Kumar<sup>1</sup>

<sup>1</sup>Gent University, Gent, Belgium, <sup>2</sup>PartiX NV, Leuven, Belgium

## Abstract

Cold plasma coating technology for surface functionalization of pharmaceutical powder particles is a novel approach to introduce new characteristics such as controlled release layers, improved powder flow properties, stability coatings, and binding of active components to the surface. This is typically achieved in a fluidized bed reactor, where a jet containing the chemical precursor and the plasma afterglow is introduced through a nozzle while extra fluidization gas is injected from the bottom plate. However, the process requires proper mixing of the particles and precursor inside the plasma active zone to ensure a homogeneous coating of all particles. Therefore, such coating processes are challenging to optimize, given the complex phenomena involved in fluidization, plasma species reactions, and surface reactions.

In this contribution, the system is modelled using the coupled Computational Fluid Dynamics-Discrete Element Method (CFD-DEM) approach. It is implemented within an open-source environment (CFDEM<sup>®</sup> coupling, Gonia et al. 2012) and incorporates all relevant interactions –particle-particle/wall, and particle-fluid. The rate of coating is modelled as mass transfer from the bulk of the fluid to the particle surface, which allows the coating amount to be tracked by the individual particle mass.

We share our journey to develop, calibrate, and validate the CFD-DEM model for this novel application in particle coating. First, the contact model parameters are calibrated using experimental tests composed of powder rheometry and a rotating drum. Then, this calibration and the application of the interfacial force models are validated from spouting tests. Second, the coating implementation is validated from fluorescence measurements of plasma-coated particles at different operating conditions. Finally, a design-of-simulation approach is used to study the effect of the operating conditions of the plasma reactor, with the metrics chosen as response being the average coating amount and its coefficient of variation. The results are not linear - for example, the fluidization flow has a positive influence on the quality until good mixing is achieved. After that, it has a negative impact on the coating amount due to a dilution effect.

# Optimising the rheology of dense granular suspensions using DEM modelling and machine learning

Stefan Pantaleev

*Altair Engineering Ltd., Edinburgh, United Kingdom*

## Abstract

Achieving optimal dense suspension rheology is key to meeting product quality requirements in a wide range of industries, but the traditional optimization approach, which is heavily reliant on physical trial-and-error, is prohibitively time consuming and expensive. Virtual optimisation can lead to significant time and costs savings in this context.

This work demonstrates an efficient virtual optimisation methodology that combines Discrete Element Method (DEM) simulation and machine learning to rapidly identify the optimal particle properties for a target suspension viscosity. The effect of the liquid phase of the dense granular suspension is obtained by combining a short-range hydro-dynamic force model with a fluid drag model.

The optimization methodology consists of parametrizing the particle size distribution, morphology, volume fraction and surface frictional properties, automatically generating and running DEM simulations of dense granular suspensions subjected to simple shear for a well distributed quasi-random sample of the parameter space, and training a Reduced Order Model (ROM) on the resulting synthetic data using machine learning. A multi-objective genetic algorithm is then utilized to rapidly estimate the globally optimal parameter set from the ROM. This results in several orders of magnitude reduction in computational expense relative to the equivalent purely simulation-based approach and makes the virtual optimisation of dense suspension rheology from particle properties practical. The advantages and limitations of the proposed methodology are further discussed in the talk.



## **Timestep in DEM Modelling: Critical Component or Minor Detail?**

**Hao Shi, Raïsa Roeplal, Marcel van Benten, Ahmed Hadi, Wouter Schuitemaker, Santiago Garrido Nuñez, Sabine van Epen, GertJan van Selm, Dingena Schott**

*TU Delft | Mechanical Engineering | Dept Maritime and Transport Technology | Section Machine Interactions, Delft, Netherlands*

### **Abstract**

The discrete element method (DEM), created by Cundall and Strack, typically employs various versions of the central difference numerical integration scheme. However, similar to other explicit schemes, its stability relies on the timestep size. DEM users can follow guidelines for establishing a timestep from literature or the software documentation but eventually decide themselves. One common reason to increase the timestep is to reduce the computational time. Although the current developments of hardware and software enable shorter computational times, the complexity of the modelled systems in terms of number and shape of particles increases at the same time, requiring similar or even higher computational costs.

Overall, the role of timestep in DEM simulations is to find a balance between accuracy, stability, and computational efficiency, ensuring that the simulation produces meaningful results within acceptable computational costs. The drive to speed up simulations is understandable from a practical viewpoint. However, the way a stable simulation is ensured throughout all development stages (model setup, calibration, verification & validation) while delivering accurate and reliable predictions of real systems is not always clear.

This work aims to address the importance of the timestep by, first, analysing published DEM work in established journals. Keeping in mind the FAIR principle, the stability of simulations and the role of the timestep herein, we analysed tens of papers that used DEM for different applications. We considered applications ranging from models of simple calibration tests to large full-scale industrial processes. Second, we present diverse examples from our research group, including penetration and blast furnace charging simulations, to underscore the importance of timestep selection. These results will be used to develop a framework as a guideline for researchers and engineers to ensure reliable and accurate DEM simulations.

# Effect of aspect ratio of ellipsoidal particles on mixing in vibrated packed bed using discrete element method

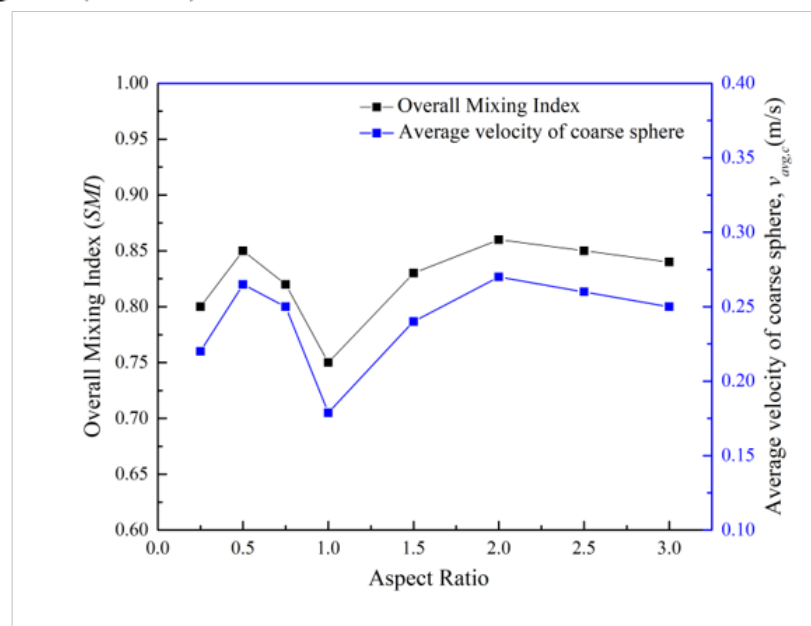
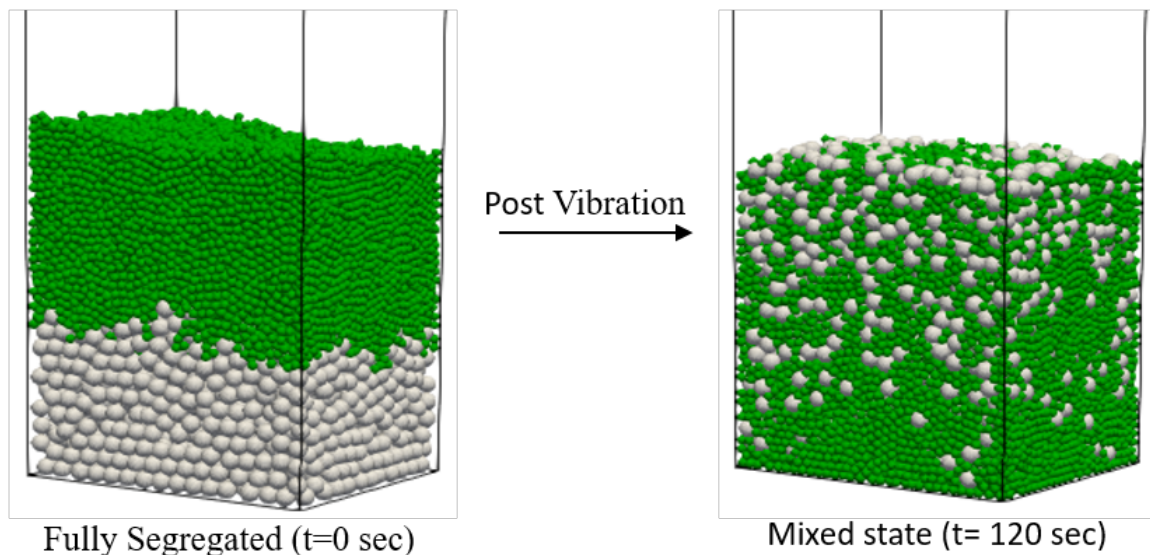
Salma Khatoon, Anshu Anand

Indian Institute of Technology Roorkee, Roorkee, India

## Abstract

The uniform mixing of particles is crucial in many industrial applications. In industries, most granular materials are nonspherical, with ellipsoids being a common deviation from the sphere. The study employs the DEM model to investigate the mixing of a binary mixture in a vibrated packed bed with fixed amplitude and frequency. The study explores the behavior of the binary mixture of coarse and fine particles, with one particle being ellipsoid of aspect ratios (0.25–3.0) and the other being a sphere. The subdomain mixing index quantifies the mixing. The mixing of binary mixtures is determined by the aspect ratio of coarse and fine particles. The mixing efficiency is indicated by the average velocity of reference spherical particles, reflecting the convection strength within the bed. The results show higher average velocity in an ellipsoidal-sphere mixture than in a sphere-sphere mixture. The DEM results are validated with an identical experimental system.

## Particle shape-induced segregation in vibrating packed bed



# A DEM bonding contact model for curved, heterogeneous fibers with bending and torsion

Miguel Angel Celigueta<sup>1</sup>, Eric Veikle<sup>2</sup>

<sup>1</sup>Altair Engineering, Barcelona, Spain, <sup>2</sup>Altair Engineering, Lititz, PA, USA

## Abstract

The Discrete Element Method (DEM) has been used to model fibers in diverse areas. Initially, the fibers were discretized with spheres, which were bonded by a set of forces and torques to prevent separation, sliding and relative rotation. However, increasingly complex models were being published, aiming at modeling the physical response with more accuracy, consuming less computational resources, bonding more types of particles like non-spherical and widening fields of application of such models.

The contact model presented in this work tries to fill one gap in the existing literature: simulate curved fibers of heterogeneous radius making emphasis on the difference between shear and axial forces and bending and torsion moments.

The novel idea of this contact model is to use spherocylinders and two springs (instead of one) for each force and torque considered in the bond, thus respecting the orientation of the particles in contact. The stiffness of each spring can be computed from the physical properties, the cross section, and the length of the fiber [1]. The relative displacement at the contact point is computed from the relative displacement and rotation of both particles, and the relative angle is computed from the relative rotation of both particles, both using the Total Lagrangian approach. The decomposition of the angle into bending and torsion must be done in a univocal way, avoiding non-univocal decompositions like the Euler angles. This model uses the bi-normal vector to decompose the total relative angle into one bending angle around the bi-normal vector and one torsion angle. Because of the heterogeneity of the particles and the different nature of shear and axial stiffness (or bending and torsional stiffness), this model accepts that the stiffness of the springs at both sides of the bond are different, so the bond itself needs to be re-located and re-oriented at every time step to ensure that the forces and torques generated by the springs at both sides are equal.

The present work also shows the possibilities of the model when it comes to non-linear response once the elastic bound is reached: plasticity, buckling and breakage.

[1] Effeindzourou, A., Chareyre, B., Thoeni, K., Giacomini, A., & Kneib, F. (2016). Modelling of deformable structures in the general framework of the discrete element method. *Geotextiles and Geomembranes*, 44 (2), 143-156.

# DEM simulation of the compaction behaviour of compressible powders with a new elastic-plastic contact model

Sergiy Antonyuk, Fabian Krull

University of Kaiserslautern-Landau, Kaiserslautern, Germany

## Abstract

In many processes the powders are subjected to high mechanical stresses, for example during compaction in a tablet press or in a extruder to produce pharmaceutical products. The high stresses can lead to the significant plastic deformations and increase the adhesion of particles in contacts resulting in high strength of the products. The powder compaction behavior can be simulated with the Discrete Element Method. However, a good prediction of real compressibility mechanisms with the simulation can be achieved only by experimentally validated contact models that describe the adhesion and deformation behavior of particles in the studied process. For low stresses, particles can be assumed to be mostly elastic, whereby elastic force and cohesion modeling are more forgiving and has already been accomplished in the past. Many materials, however, deform dominant plastically. Therefore, in this contribution we developed and validated a new contact model (Fig. 1 left), which describes different contact behavior: adhesion, viscoelastic, elastic-plastic and cyclic hardening [1].

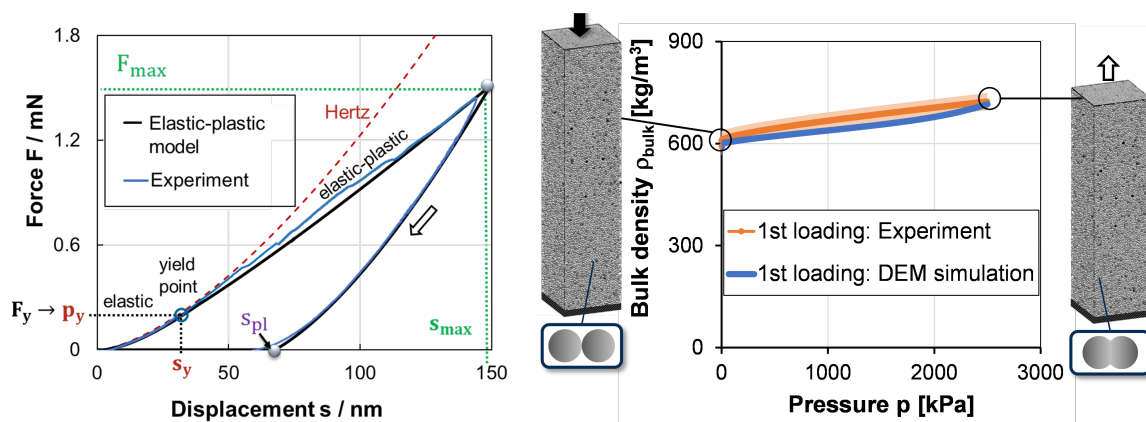


Fig.1: The loading-unloading curve obtained by single particle nanoindentation and described by the developed elastic-plastic contact model (left) and the compression curve of the powder measured in compression test and simulated with DEM (right)

The model only contains the measurable material parameters and no fitting is required. By analytically solving the model, we found an equation for the plastic particle deformation remaining after unloading. With this parameter the unloading and further loading-unloading cycles can be calculated more accurately. Also, the plastically deformed contact area can be predicted to calculate the adhesive forces in the contact. An algorithm was developed that takes into account the history of plastic deformation in each contact.

The model is implemented in the open-source software LIGGGHTS<sup>®</sup> for Discrete Element Method (DEM) simulations. For the validation of the model and simulation, a lactose powder was investigated. The properties of single particles were measured by nanoindentation, impact and shear tests. The cyclic compaction tests of the powder at different normal pressures were performed in a compression die in experiments and simulations (Fig. 1 right). The comparison of the experiment with simulations showed that the new model can accurately predict the deformation and forces occurred during the compaction as well as the compressibility of the bulk material.

## Reference

[1] R. Hesse, P. Lösch, S. Antonyuk: CFD-DEM analysis of internal packing structure and pressure characteristics in compressible filter cakes using a novel elastic-plastic contact model, *Advanced Powder Technology* 34 (2023) 104062. <https://doi.org/10.1016/j.appt.2023.104062>



## Towards an Understanding of Tablet Bonding Fundamentals

Zoe Chu<sup>1,2</sup>, Christopher Windows-Yule<sup>1</sup>, Ian Gabbott<sup>2</sup>, Gavin Reynolds<sup>2</sup>, Rachael Shinebaum<sup>2</sup>, Andrew Ingram<sup>1</sup>

<sup>1</sup>University of Birmingham, Birmingham, United Kingdom, <sup>2</sup>AstraZeneca, Macclesfield, United Kingdom

### Abstract

A tablet consists of the drug, the active pharmaceutical ingredients (API), and the other components, excipients. The tensile strength of a tablet is one of the most important outcome parameters of compression as it will need to withstand coating, packing, and shipping stresses but also not affect the dissolution time. Currently, there is a lack of understanding of why excipients improve the bulk powder properties and the bonding mechanisms of the powder during compression. This makes tablet formulation development an inefficient trial-and-error process that is needed for every new API. Therefore, there is a need to understand the fundamentals of the bonding mechanisms of the powder during compaction. In literature, surface energy of powders contributes a significant amount towards the tensile strength (1) as hydrophobic powders, which have a lower surface energy (2), are seen to disrupt the tablet strength significantly (3). This was seen in author's previous study where the more hydrophobic (measured by sessile drop method surface energy calculations) the powders, the lower the surface energy.

For that previous experiment, measuring the surface energy of all the powders is important for analysing the tensile strength data and to confirm the hypothesis that the surface energy really has an impact on tablet tensile strength. However, there are many different ways to measure surface energy and all of them from literature seem to have their obstacles. The 'industry standard way' to measure surface energy is deemed as inverse gas chromatography (IGC). When comparing results from the IGC to the sessile drop contact angle test, these presented very contrasting results and had different surface energy descending order. Therefore, a comparison study has been completed where the sessile drop method, IGC, dynamic vapor sorption, and kinetic adhesion test have all been compared. This study aims to highlight these limitations and address the gaps in getting an accurate surface energy measurement of powders.

1. Sun CC. 4 Role of Surface Free Energy in Powder Behavior and Tablet Strength. In: Adhesion in Pharmaceutical, Biomedical and Dental Fields. 2017. p. 75–88.
2. Sunkara D, Capece M. Influence of Material Properties on the Effectiveness of Glidants Used to Improve the Flowability of Cohesive Pharmaceutical Powders. AAPS PharmSciTech. 2018;19(4):1920–30.
3. Zuurman K, Maarschalk KVDV, Bolhuis GK. Effect of magnesium stearate on bonding and porosity expansion of tablets produced from materials with different consolidation properties. 1999;179:107–15.

## Characterisation of the breakage behaviour of multi-component systems

Simon Bahn Müller, Arno Kwade, Carsten Schilde

TU Braunschweig - Institut für Partikeltechnik, Braunschweig, Germany

### Abstract

Slags, which are by-products of metallurgical processes, are complex multi-component systems composed of a variety of mineral constituents and metal residues. This composition makes slags a potentially valuable resource for recycling and reuse. Due to their heterogeneous structure and the different chemical properties of their constituents, they pose a particular challenge for the recovery of valuable materials.

Understanding the physical and chemical properties of slags is crucial to developing efficient methods for their separation and reuse. This is where the research project funded by the Deutsche Forschungsgemeinschaft (DFG) priority programme SPP2315 EnAM sets out to help. The aim of this project is to analyse the breakage behaviour of slags through detailed investigations, thereby improving the possibilities for recycling and reuse.

In the study, slag samples are pre-crushed and classified into five particle size classes ranging from 250  $\mu\text{m}$  to 25  $\mu\text{m}$ . The investigations focus on the particle size distribution and the specific energy required to break the slag particles using a two-roller breakage-tester with adjustable gap width. Over 225 million particles from 75 samples per slag type are analysed in three experimental iterations to systematically investigate the crushing behaviour of different slag types.

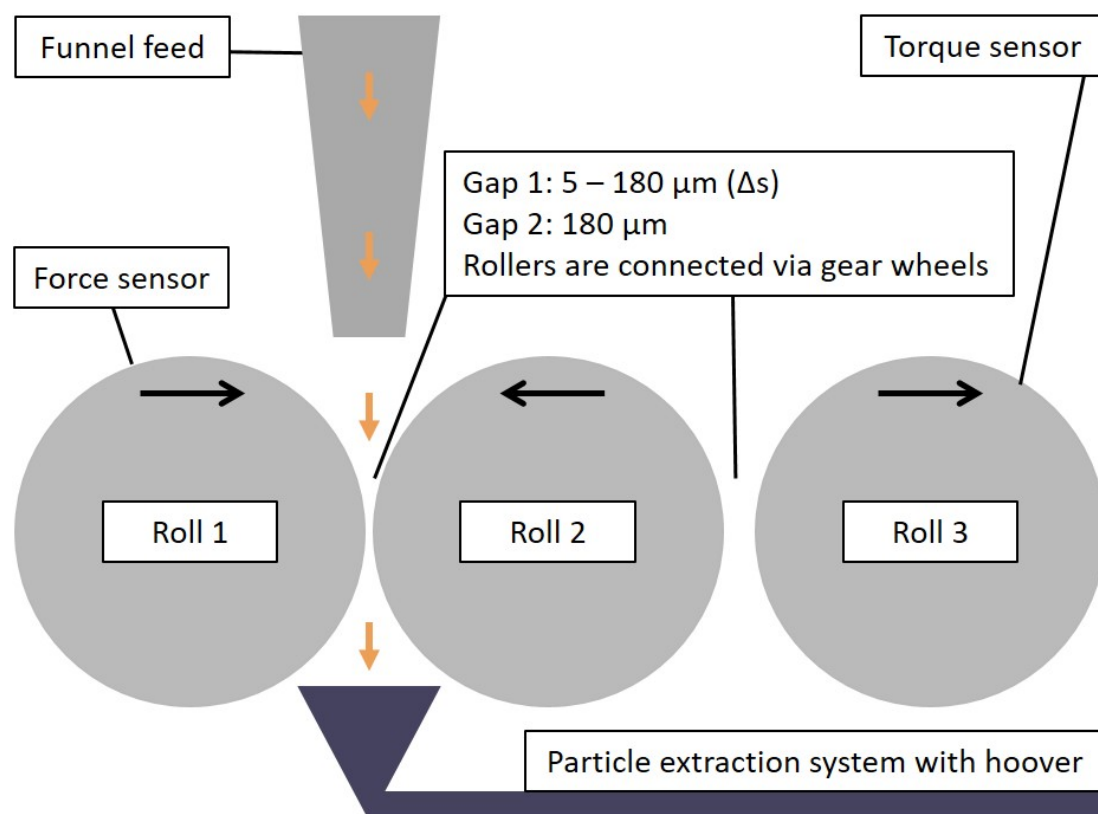


Fig. 1: Schematic construction of the two-roller breakage tester

Another focus is the study of four artificially produced lithium aluminate slags, which differ in composition and crystal structure due to different cooling rates during production. These differences will allow the structural influence on fracture properties to be investigated.

The results of the project will provide fundamental insights into the mechanisms of breakage and structural changes in the slags due to comminution. Supported by advanced SEM/EDX technology, they will provide valuable information for the development of semi-mechanistic models to predict breakage behaviour and contribute significantly to the development of effective recovery strategies. This will enhance the understanding of slag as a valuable resource and support the principles of circular economy in the industrial sector.

## Process design in planetary roller melt granulation

Tom Lang, Markus Thommes, Jens Bartsch

TU Dortmund University, Dortmund, Germany

### Abstract

Granulation is a standard unit operation to modify the particle size for improved material handling and dosing properties in powder processing. Hereby, the focus of research endeavors in recent years was twofold. First, on continuous operation in order to reduce quality fluctuations by processing in a dynamic steady state. Second, on melt granulation as a method for handling moisture sensitive materials, which spares the resource water and an energy intensive subsequent drying step.

In this context, planetary roller melt granulation has been introduced recently as a promising, new alternative [1] due to the unique process concept (Figure 1) enhancing the potential for temperature control. In addition, the machine fill level determined via residence time measurements [2] was identified as linking element to the transport and energy input mechanisms. Also, correlations of direct process parameters (feed rate, rotation speed) to indirect measures (residence time, fill level) and quality attributes (particle size) have been demonstrated.

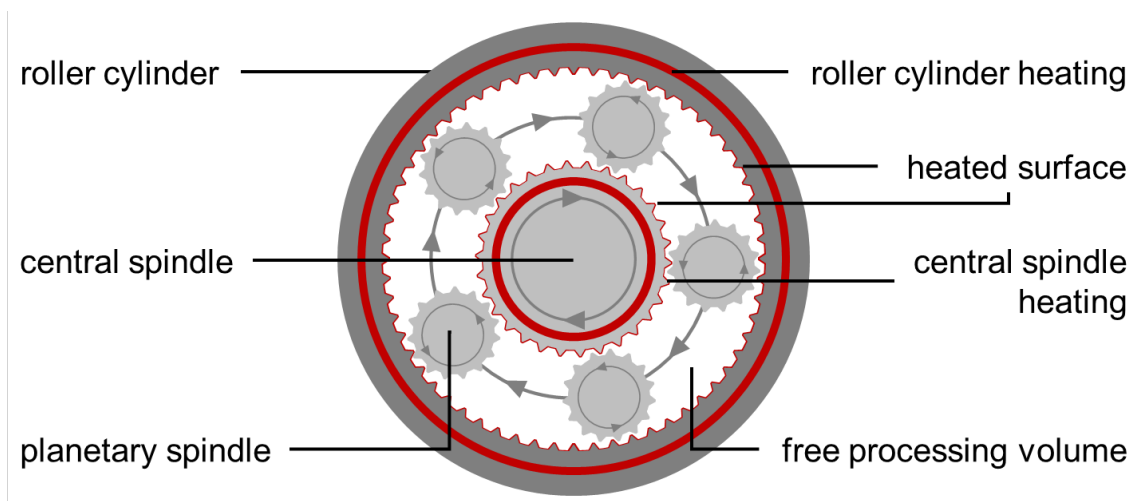


Figure 1: Radial processing cross-section of planetary roller granulator including mechanical parts (roller cylinder, central spindle and planetary spindles), the two independent heating systems as well as free processing volume in comparison to heated surface. Adapted from [01].

In this study, the previous investigations are expanded by the module configuration as one central objective of the process design. This includes the number of planetary spindles within the processing section as well as the type of these. The corresponding results cover hereby the normalization of the data with respect to the module configuration, e.g. by considering the free processing volume varied by the applied spindle number [3]. Moreover, the effect of the configuration on the product quality is discussed. Finally, the shift function of the particle size distribution as a new, objective indicator is introduced for the evaluation of the performance.

[1] D. Nesges, T.M. Lang, T. Birr, M. Thommes, J. Bartsch, Planetary roller melt granulation (PRMG) - A new continuous method for powder processing, *Powder Technol.* 427 (2023).

[2] T.M. Lang, A. Bramböck, M. Thommes, J. Bartsch, Material Transport Characteristics in Planetary Roller Melt Granulation, *Pharmaceutics*, 15 (2023).

[3] T. Lang, J. Bartsch, Impact of the spindle number on the material transport and mixing during planetary roller melt granulation, *Particuology*, 91 (2024) 260-267.

## **A multi-scale study of the dissolution process of wet soybean meal based on the three-phase Euler model**

**Yefeng Yang, Yin Wang**

*Dalian University of Technology, Dalian, China*

### **Abstract**

In the field of grain and oil processing, assessing the efficiency of the dissolution process of wet soybean meal requires a comprehensive understanding of the process by which liquid hexane on the soybean meal evaporates into gaseous hexane at different temperatures. This process is determined by solid-gas-liquid interactions, involving heat transfer and phase change. The key to investigating the influence of temperature and particle flow characteristics on the dissolution efficiency is a combination of the Euler - Euler model and the Volume of Fluid (VOF) method to capture the evolution of the liquid and gaseous hexane, respectively. At the same time, by introducing a local thermal non-equilibrium model to establish a convective heat transfer relationship between hexane and the solid phase, an enhanced three-phase Euler model considering heat transfer is established in our in-house solver. The accuracy of this novel model is validated by comparing the results with the experimental data. Subsequently, the influence of the plate spacing and initial temperature on the flowability of soybean meal particles and the efficiency of hexane desorption is unveiled in terms of liquid hexane concentration distribution, flow field characteristics, and particle motion state. This coupling of macro- and micro-scale insights into the dissolution process of wet soybean meal will contribute significantly to various fields, particularly providing optimization methods for chemical engineering and grain and oil machinery development.



## Assessing dry powder coating in a pilot-scale ribbon mixer

Francisco Kisuka<sup>1</sup>, Colin Hare<sup>1</sup>, Mingzhe Yu<sup>2</sup>, Alex Munnoch<sup>2</sup>

<sup>1</sup>Newcastle University, Newcastle, United Kingdom, <sup>2</sup>Johnson Matthey, Billingham, United Kingdom

### Abstract

Dry powder coating is a process used to manipulate the surface properties of solids, e.g., to provide protection or control dissolution rates of tablets, or to improve the flowability of poorly flowing powders. Our previous work demonstrated a regime map for dry powder coating in a small-scale agitated mixer (FT4 Rheometer), which informs the energy input required to achieve a given surface area coverage for known material properties. In this work we analyse to what extent this map can be applied to a pilot scale (12l) ribbon mixer. The mixtures of guest (alumina) and host (zeolite) go through sample division to obtain representative samples for analysis. Flowability analysis (FT4 dynamic test and shear cell) shows the sample division is effective, and that an optimum mixing time exists after which flow performance worsens. Mixing speed is shown to have a limited effect, with increasing speed causing a slight improvement in terms of flow function coefficient, and a slight worsening in terms of basic flow energy. Several approaches are taken to determine surface area coverage, including SEM (+EDX), colorimetry and iso-electric point determination. The regime map correctly predicts coating improving with energy input, however, does not capture the reduction occurring due to over-mixing.

Further research should look to determine the mechanisms for reduction in flowability at extended times (e.g., guest detachment, particle breakage), and aim to predict the optimum mixing time required, to minimise energy input and maximise product performance.

## Exploration of segregation in large size ratio two-sized vibrated systems using DEM

Aaron Wiggin<sup>1,2</sup>, Christopher R. K. Windows-Yule<sup>1</sup>, Thomas Abadie<sup>1</sup>, Phil D. D. Monks<sup>2</sup>, Shirley Fong<sup>2</sup>

<sup>1</sup>University of Birmingham, Birmingham, United Kingdom, <sup>2</sup>AWE, Reading, United Kingdom

### Abstract

Segregation in granular systems can cause changes in system behaviour and reduce the quality of products in industrial applications where product homogeneity is sought after. Despite this, research into the causes and potential preventative measures of segregation is still ongoing, owed in part to both the complexity and breadth of the research area. The use of numerical methods such as discrete element method (DEM) in investigating and preventing the segregation of granular systems has great potential, due to their ability to investigate systems across wide parameter spaces whilst avoiding the significant cost and time expenses typically associated with such investigations.

This talk will explore ongoing work into the factors influencing particle segregation within a vibrated binary system consisting of two different sized particles with a large size ratio (1:15), conducted as part of an industry-sponsored project. As part of the project, a quasi-two-dimensional (Q2D) system was simulated using DEM and used to investigate the effects of the initial system packing prior to vibration and the size ratio of the particles on the segregation in the system. The results of these investigations contribute towards a greater understanding of particle segregation within vibrated granular systems, particularly in those containing large particle size ratios.

This talk will outline the key findings from the study and showcase the potential of numerical methods such as DEM in understanding and preventing segregation within granular systems.

© UK Ministry of Defence Crown Owned Copyright 2024/AWE

# Quasistatic response in DEM versus size, boundary conditions, and other numerical parameters.

Théo Dumas, Bruno Chareyre, Antoine Naillon

Univ. Grenoble Alpes, Grenoble, France

## Abstract

Some of the most common simulation with the discrete element method (DEM) is the so-called triaxial test simulation, which is used to evaluate bulk properties of granular materials in quasistatic deformation. This simulation mimics the conditions of a laboratory experiment more or less closely depending on the method to control boundary conditions: commonly periodicity, rigid walls, or a membrane model. Evaluating a quasistatic response needs very slow deformation, and an accurate evaluation of bulk properties requires large amounts of particles, unfortunately both constraints lead to large computational efforts.

We propose a systematic analysis of triaxial simulations to quantify variability and bias of the results in various conditions. The study includes the three classical boundary conditions (figure below). The parameters analyzed include the number of particles in the simulation, the strain rate and a numerical damping parameter (Cundall's non-viscous damping). The simulated materials are either cohesive-frictional or simply frictional.

The results confirm expectations on some aspects. Namely, periodic boundary conditions give the fastest convergence to a unique response when the number of particles grow. They also reveal less well known features that all DEM users should be aware of. It is found, for instance, that 1/ the most efficient setting in most (not all) cases is to not introduce any numerical damping, and 2/ the bias associated to excessive strain-rates cannot be uniquely linked to the inertial number despite two decades of claim in that sense.

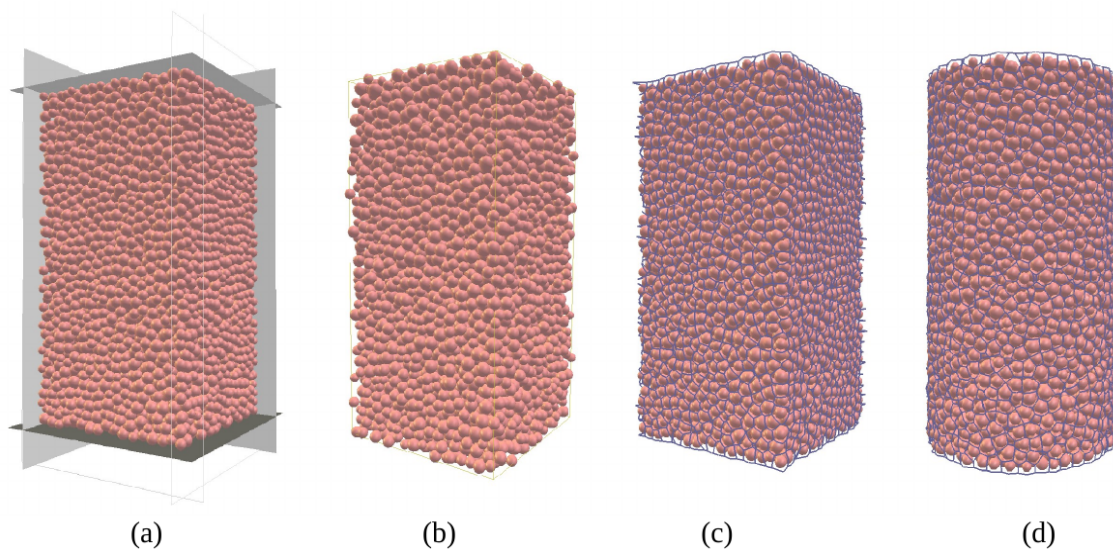


**Figure 1.** Various ways to impose stress on boundaries: (a) rigid walls, (b) periodicity, (c,d) membrane model with two different specimen shapes.

# Micromechanical Differences Between Spherical and Ellipsoidal Representations of Sand Particles in Direct Shear Testing

Javier E Necochea<sup>1,2</sup>, Esteban Sáez<sup>2</sup>, Kevin J Hanley<sup>1</sup>

<sup>1</sup>University of Edinburgh, Edinburgh, United Kingdom, <sup>2</sup>Pontificia Universidad Católica de Chile, Santiago, Chile

## Abstract

The representation of real-world particles in Discrete Element Method (DEM) is a common challenge in research. Commonly, many simplifications are made to represent particulate systems in DEM. Different methods have been developed to include shape effects in DEM, for example, rolling friction, aspherical particle representations, such as ellipsoids or polyhedra, and particle ensembles. In this study, the micromechanical differences between spheres with rolling friction and ellipsoids were investigated using simulations of direct shear tests. The material used corresponded to a poorly graduated sand, composed of grains retained between the 1.18 and 2.00 mm sieves. Ellipsoidal templates were generated from an image analysis of the grains, while the spherical templates were defined as equivalent volume particles from the ellipsoidal templates. Three sets of direct shear tests were carried at Pontificia Universidad Católica de Chile, at vertical confining pressures of 50, 100 and 200 kPa. The tested cuboidal samples had dimensions of 20x60x60 mm, and each contained approximately 16,000 grains. Subsequently, direct shear tests were recreated with the open-source code LIGGGHTS 3.7. Rigid walls were used as boundary conditions. While both shape approaches are a simplification of the real sand particles, both methods were able to match the bulk behaviour obtained in the laboratory experiments. At a micromechanical level, the inclusion of rolling friction affects the interparticle interactions in the system, as more restrictions on the degrees of freedom are imposed. The average coordination number was lower while the average contact forces were higher for the sphere-based samples. More marked differences were seen in the cumulative rotations of the spherical particles, which were one order of magnitude higher compared to those of the ellipsoidal particles. This is evidenced by Figure 1, where the accumulated particle rotations at the end of each simulation are presented [1]. Although ellipsoids allow a better representation of the micromechanical behaviour, the computational cost is increased fivefold compared to spheres with rolling friction.

[1] Necochea, J. E., Sáez, E., & Hanley, K. J. (2024). Effect of sand particle shape on micromechanical modeling in direct shear testing. *Computers and Geotechnics*, 169.

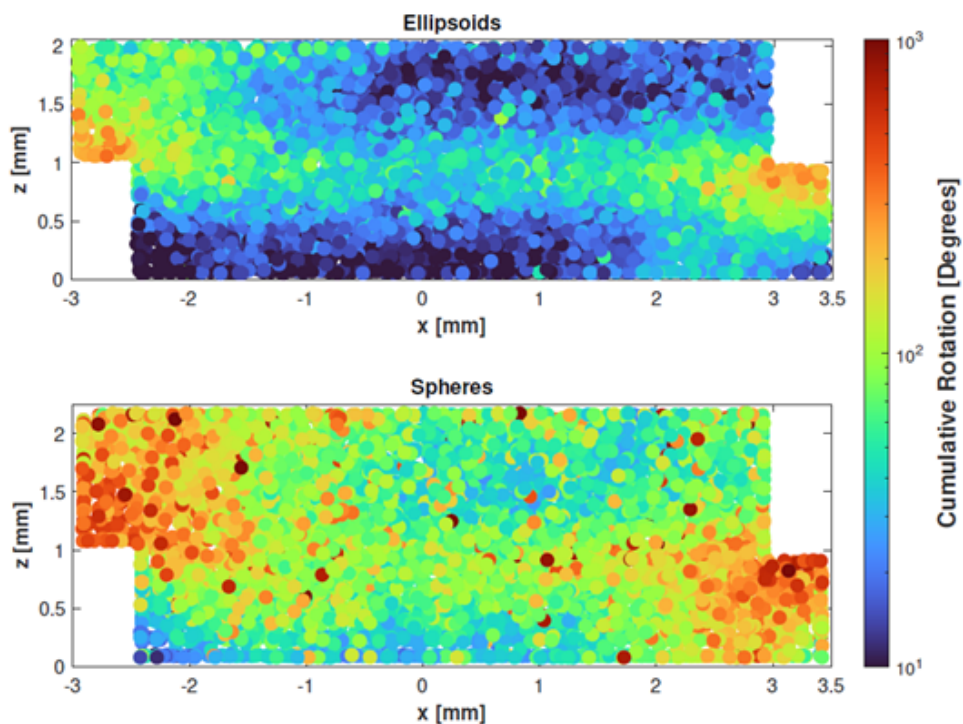


Figure 1: Cumulative particle rotations at a horizontal displacement of 5 mm for ellipsoids (top) and spheres (bottom) under 50 kPa of vertical confining pressure [1].



# Simulating the Abrasion of Arbitrarily Shaped Particles in DEM

Haydn Rogan<sup>1</sup>, Kevin Hanley<sup>1</sup>, Rosario Capozza<sup>1</sup>, Kevin Stratford<sup>2</sup>

<sup>1</sup>The University of Edinburgh, Edinburgh, United Kingdom, <sup>2</sup>EPCC, Edinburgh, United Kingdom

## Abstract

The discrete element method (DEM) models granular systems by resolving Newton's equations of motion for individual particles. [1] The shape of these particles - often reduced to simple spheres in DEM - is a crucial factor affecting their resultant bulk dynamics. [2] With 70% of industrial feedstocks comprising non-spherical particles, shape represents an often neglected but key control parameter in numerous industries from oil and gas to pharmaceuticals. [3] Previous efforts have introduced non-spherical particles into DEM. [4] However, these implementations often fall short by considering the particles' shape as immutable. In reality, particle shape may change through a variety of attrition mechanisms. [5] Most pertinent to this research is the gradual removal of material from their surface through the process of abrasion. By modifying the existing LAMMPS rigid-body implementation [6], a comprehensive novel wear model, initially developed for flat surfaces [7], is expanded to simulate the abrasion of arbitrarily shaped dynamic particles. These abradable particles are represented as hollow shells of discrete spheres collated into a series of triangular facets. Following an impact exceeding a material yield criterion, surface spheres are displaced inwards along their normals. The result is a reduction in volume and a permanent change in particle shape. Following any abrasion, the particles' inertia is recomputed and used to resolve future rigid-body dynamics. [8] In this way, particle-level changes in shape are communicated up to the bulk dynamics of the system which in turn informs all subsequent abrasion. Thus, the cyclic process connecting bulk dynamics to particle shape in DEM has been closed. Additionally, a novel localised re-meshing scheme has been implemented to counteract the well-documented contact model errors introduced by multi-sphere clumps. [9] Initial tests exhibit particle shape evolution in agreement with a variety of abrasion scenarios in existing literature. [5,10] Moving forward, the methodology will be employed to explore abrasion in large-scale engineering systems. The conclusions drawn aim to inform future design and operation heuristics to reduce losses and increase production yields.

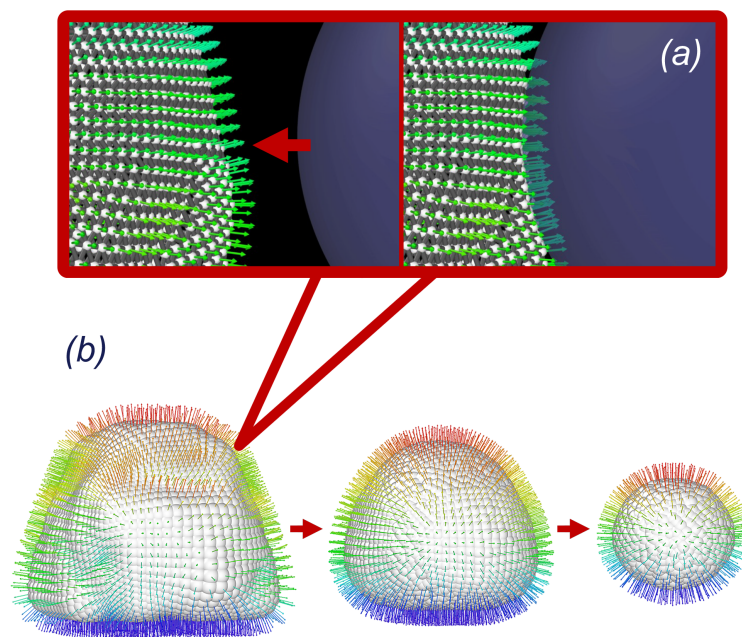


Figure 1: (a) An impactor displaces surface spheres along their normals to alter the particle shape. (b) Simulated abrasion, following repeated isotropic impacts, exhibits characteristic rounding as the particle's volume reduces. Surface normals are coloured by their vertical alignment.

[1] C. W. Hong, "Computer-Aided Process Design for Forming of Pore-Gradient Membranes," in *Functionally Graded Materials* 1996, pp. 29–34, Amsterdam: Elsevier Science B.V., Jan. 1997.

[2] P. W. Cleary and M. L. Sawley, "DEM modelling of industrial granular flows: 3D case studies and the effect of particle shape on hopper discharge," *Applied Mathematical Modelling*, vol. 26, pp. 89–111, Feb. 2002.

[3] W. Zhong et al., "DEM/CFD-DEM Modelling of Non spherical Particulate Systems: Theoretical Developments and Applications," *Powder Technology*, vol. 302, pp. 108–152, Nov. 2016.

- [4] G. Lu et al., “Discrete element models for non-spherical particle systems: From theoretical developments to applications,” *Chemical Engineering Science*, vol. 127, pp. 425–465, May 2015.
- [5] T. Novák-Szabó et al., “Universal characteristics of particle shape evolution by bed-load chipping,” *Science Advances*, vol. 4, p. 4946, Mar. 2018.
- [6] A. P. Thompson et al., “LAMMPS - a flexible simulation tool for particle-based materials modeling at the atomic, meso, and continuum scales,” *Computer Physics Communications*, vol. 271, p. 108171, Feb. 2022.
- [7] R. Capozza and K. J. Hanley, “A comprehensive model of plastic wear based on the discrete element method,” *Powder Technology*, vol. 410, p. 117864, Sept. 2022.
- [8] F. Tonon, “Explicit Exact Formulas for the 3-D Tetrahedron Inertia Tensor in Terms of its Vertex Coordinates,” *Journal of Mathematics and Statistics*, vol. 1, 2004.
- [9] N. Berry, Y. Zhang, and S. Haeri, “Contact models for the multi-sphere discrete element method,” *Powder Technology*, vol. 416, p. 118209, Feb. 2023.
- [10] F. J. Bloore, “The shape of pebbles,” *Mathematical Geology*, vol. 9, pp. 113–122, Apr. 1977.

## Author Index

- Abadie, Thomas, 278  
Ablitzer, Carine, 88  
Achiaga, Beatriz, 157  
Adema, Allert, 253  
Agbonkhese, Edward, 131  
Ajabshir, Sina Zinatlou, 41, 222, 230, 238, 256  
Alfano, Francesca O., 245, 246  
Alhaddad, Yani, 92  
Almudahka, Anas, 210  
Alshahed, Osamh Sabri, 31  
Anand, Anshu, 270  
Andre, Damien, 202  
Angelidakis, Vasileios, 202  
Antonyuk, Sergiy, 133, 147, 153, 265, 272  
Anwar, Ali, 239  
Ardekani, Mohammad M, 90  
Arianer, Lina Cayla, 88  
Armour-Chelu, David, 31  
Artoni, Riccardo, 236, 237  
  
Badat, Yusuf, 213  
Bahnmüller, Simon, 274  
Balan, Velan, 193  
Balasooriya, Dasun, 59  
Balasubramanian, Prabu, 57  
Barletta, Diego, 17, 41, 131, 182, 186, 222, 224, 230, 238, 256  
Barreto, Daniel, 216, 259  
Bartsch, Jens, 191, 251, 275  
Bauer, Albert, 61  
Baxter, Gavin J, 264  
Baxter, Marie E, 264  
Bayly, Andrew, 264  
Beer, Thomas De, 139, 267  
Beitz, Steffen, 145  
Bell, Timothy A, 25  
Bengston, Eric, 81  
Benque, Benedict, 209  
Beretta, Michela, 240  
Bisschop, Jan-Willem, 71  
Blanc, Nicolas, 37  
Blanco, David, 149  
Bonnieu, Sebastien Vincent, 239  
Bonny, Fabrice, 221  
Boots, Mitch, 137  
Boribayeva, Aidana, 249  
Bozon, Annabel, 79  
  
Bradley, Michael S. A., 27, 29, 31, 33, 69, 73, 125, 129, 141, 159, 190, 192  
Bradney, David, 115  
Bradney, Lauren, 135  
Brands, René, 191  
Brandt, Viktor, 49  
Brasil, Henrique, 232  
Bright, Elis I, 163  
Brown, Aidan, 199  
Brutsch, Linda, 77  
Buchheiser, Simon, 225  
Burton, Robin H, 199  
Bystrov, Oleg, 258  
  
Capozza, Rosario, 281  
Cares, Maria G, 219  
Carr, Michael J., 59, 213  
Carson, John, 4, 81  
Caulk, Robert, 202  
Celigueta, Miguel Angel, 176, 202, 271  
Chakraborty, Shruti, 85  
Chalup, Stephan, 59  
Chan, Ei L., 234  
Chareyre, Bruno, 202, 279  
Cheng, Hongyang, 176, 180, 266  
Chew, Jia Wei, 15  
Chu, Zoe, 273  
Cleary, Paul W., 59  
Clifford, Sean, 244  
Cocco, Ray, 15  
Conti, Lorenzo, 199, 248  
Cousseau, Tiago, 213  
Cowell, Andrew, 57  
Coyle, Tommy, 200  
Cromvik, Christoffer, 67  
  
D'Angelo, Christophe, 37  
Daouk, Elias, 88, 221  
Deng, Tong, 27, 29, 190, 192  
Destoop, Thierry, 221  
Dewulf, Luc, 79  
Di Maio, Francesco P., 245, 246  
Di Renzo, Alberto, 245, 246  
Dietiker, Jeff, 202  
Diviš, Jan, 103, 151  
Dogbe, Selasi, 200  
DONOHOE, Elif ERGUN, 135  
Dose, Bruno Nicola, 222  
  
Dumas, Théo, 279  
Durán-Olivencia, Francisco J., 123  
  
Ellis, Dean, 59  
Ellis, Richard, 129  
Emerson, Joe, 35  
Epen, Sabine van, 269  
Erken, Oguzhan, 166  
Esgandari, Behrad, 168  
  
Falk, Veronique, 219  
Finke, Jan Henrik, 170, 184, 217  
Flament, Antoine, 221  
Fominykh, A., 51, 75  
Fong, Shirley, 278  
Forgber, Thomas, 206  
Fraccarollo, Luigi, 157  
Francqui, Filip, 240  
Frankenberg, Finn, 235  
Franqui, Filip, 39  
Füvesi, Balázs, 65, 174  
  
Gabbott, Ian, 273  
Garcia-Trinanes, Pablo, 145  
Garg, Vivek, 27, 29, 159, 192  
Ghori, Muhammad, 190  
Giannis, Kostas, 262  
Gibson, Ellie, 200  
Girardot, Jeremie, 202  
Girimonte, Rossella, 246  
Gobby, Darren, 256  
Goddard, Ben D, 261  
Golman, Boris, 249  
GomesLopes, Diogo, 209  
Goniva, Christoph, 65, 105, 174, 184, 227  
Goodwin, Keri, 200  
Gorman, Scott, 200  
Govender, Nicolin, 101, 202  
Grabe, Jürgen, 105  
Grabowski, Janna, 49  
Grasser, Daniel, 107, 115  
Greener, Simon, 166  
Griffiths, Alison L, 85, 90  
Grohn, Philipp, 206  
Grosshans, Holger, 204, 243  
Gucuyener, Canan, 256  
Guo, Jiqian, 262  
Gupta, Prashant, 166, 180  
Gurung, Virat, 95  
Gómez, Luz N Naranjo, 139

- Hadi, Ahmed, 63, 269  
 Haeri, Sina, 143  
 Hafenbrädl, Franz Otto von, 207  
 Hamilton, Leigh D., 218  
 Hamilton, Vincent, 117  
 Hancock, Ian K., 141  
 Hanley, Kevin J., 43, 166, 197, 280, 281  
 Harada, Shusaku, 53  
 Hare, Colin, 230, 277  
 Harshe, Yogesh M., 170  
 Hashemloo, Z., 51  
 Hassanpour, Ali, 264  
 Hausmann, Michael Karlheinz, 79  
 Heinrich, Dennis, 105  
 Heinrich, Stefan, 198  
 Hendrickson, Willie, 8  
 Henry, Manuela L Quezada, 221  
 Heumann, Roman, 251  
 Hirose, Yuma, 234  
 Hlostá, Jakub, 103, 151  
 Hobbs, Andrew, 263  
 Hoffmann, Niklas, 111  
 Hoheisel, Werner, 251  
 Holmes, Corin, 81  
 Horabik, Józef, 101  
 Hosseinihashemi, Somayeh, 203  
 Hu, Jiawei, 194  
 Hubert, Cedric, 202  
 Hussain, Tariq, 190  
 Hussaini, Zaki, 141  
 Ikeda, Takashi, 241  
 Ilic, Dusan, 95  
 Ingram, Andrew, 244, 254, 273  
 Iozzi, Giovanni, 245  
 Islam, Syed F, 264  
 Iwao, Motoshi, 214  
 Jabaud, Benoit, 237  
 Jackson, Carl, 35  
 Jajcevic, Dalibor, 209  
 Jamshidian, Farid Jalili, 121  
 Jansen, Aron, 266  
 Jantač, Simon, 204, 243  
 Jauhar, Tahir Abbas, 59  
 Jenkins, Ben, 39, 247  
 Ji, Haoran, 208  
 Jones, Mark, 137  
 Jones-Salkey, Owen, 244  
 Jonge, Wessel de, 63  
 Jovanova, Jovana, 223  
 Juppo, Anne Mari, 149  
 Jurtz, Nico, 49  
 Kahrizsangi, Hamid Salehi, 129  
 Kai, Terutoshi, 241  
 Kaialy, Waseem, 190  
 Kalman, Haim, 45, 47, 127  
 Kanokogi, Sora, 241  
 Karalasingam, Anushanth, 143  
 Karatza, Zeynep, 155  
 Karunanayake, Yashodh, 77  
 Katayama, Tomoki, 53  
 Kato, Naoyuki, 241  
 Katterfeld, Andre, 109, 111  
 Kaur, Baldeep, 31, 73, 125, 129, 141  
 Kačeniauskas, Arnas, 258  
 Kačianauskas, Rimantas, 258  
 Kharaghani, A., 51  
 Khatoon, Salma, 270  
 Khinast, Johannes G., 206, 209  
 Kieckhefen, Paul, 206, 211  
 Kisuka, Francisco, 277  
 Kloss, Christoph, 65, 105, 227  
 Kobyłka, Rafał, 101, 202  
 Komarnicki, Przemyslaw, 198  
 Konno, Haruhi, 53  
 Krasovitev, B., 51, 75  
 Kraume, Matthias, 49  
 Kropfinger, Lukas, 206  
 Kruggel-Emden, Harald, 16, 49, 61  
 Krull, Fabian, 133, 147, 272  
 Kräuter, Robert, 198  
 Kuehn, Nane, 235  
 Kujirasaki, Yusuke, 241  
 Kumar, Ashish, 139, 267  
 Kwade, Arno, 2, 170, 215, 217, 218, 220, 229, 235, 274  
 Kwakkel, Marcel, 65, 227  
 Labra, Carlos, 19, 186  
 Lang, Tom, 275  
 Lappa, Marcello, 239  
 Larijani, Roxana Saghaian, 178  
 Larsen, Rolf, 209  
 Laurent, Olivier, 37  
 Lavrinec, Aleksej, 95, 117  
 Lee, Hong-Guann, 209  
 Leturia, Mikel, 88, 221  
 Levy, A., 51, 75  
 Li, Xuqian, 119  
 Lichtenegger, Thomas, 260  
 Liedekerke, Paul Van, 139  
 Lier, André, 147  
 Liu, Jiayuan, 43  
 Lohfink, Kim Carina, 233  
 Lotz, Christoph, 111  
 Lubbe, Retief, 180, 266  
 Luding, Stefan, 172, 174, 178, 180, 182, 255  
 Lumay, Geoffroy, 39, 240  
 Lupo, Marco, 17, 238, 240  
 López, Alejandro, 157  
 Lüddecke, Arne, 229  
 Macak, Jelena, 221  
 Magnanimo, Vanessa, 19, 172, 174, 178, 180, 182  
 Mahdavy, Saeed, 182  
 Mallick, S.S., 83  
 Mann, Jil, 252  
 Manna, Salvatore La, 41, 131, 224  
 Maria, Giordano, 245  
 Markl, Daniel, 210  
 Markus, Matthias, 251  
 Martin de Juan, Luis, 11, 244  
 Martín-Alfonso, Manuel A., 123  
 Mathews, Akhil, 176  
 McGee, Eddie, 131, 196  
 McGlinchey, Don, 57, 131  
 Mehos, Greg J, 21  
 Mehrabi, Mozhddeh, 264  
 Meier, Niklas, 215  
 Menn, Erwan Le, 237  
 Meunier, Vincent, 77  
 Misiulia, Dzmitry, 265  
 Monks, Phil D. D., 278  
 Moreno, Helena, 123  
 Morin, Mathieu, 221  
 Morrissey, John P, 13, 163  
 Mostafaei, Fatemeh, 209  
 Moura, Augusto F., 65, 202  
 Mudiyansele, Chehan L K Y Yapa, 69  
 Munnoch, Alexander, 188, 195, 277  
 Márton, Anna, 251  
 Nadimi, Sadegh, 257



- Naillon, Antoine, 279  
 Nakamura, Hideya, 14, 205, 214, 242  
 Naugler, Kurt LG, 81  
 Necochea, Javier E, 280  
 Neveu, Aurélien, 39, 238, 240  
 Nečas, Jan, 103, 151  
 Nicusan, Andrei Leonard, 39, 244, 247  
 Niederreiter, Gerhard, 79  
 Niemann, Martin, 105, 227  
 Nikolaus, Kai, 153  
 Nirschl, Hermann, 225, 233  
 Nolte, Tobias, 212  
 Nuñez, Santiago Garrido, 269
- O'Shea, Jayne, 213  
 Ogata, Koichiro, 53, 234, 241  
 Ohsaki, Shuji, 205, 214, 242  
 Oinas, Pekka A., 197  
 Ooi, Jin Y., 155, 163, 166, 176, 186, 188  
 Orefice, Luca, 71, 182  
 Orozco, Luisa, 266  
 Orozovic, Ognjen, 117  
 Otsu, Tomotaka, 242  
 Otsuka, Sota, 234  
 Oudshoorn, Tijmen, 161  
 Overmeyer, Ludger, 111  
 Özler, Gizem, 243  
 O'Sullivan, Catherine, 6
- Pacevič, Ruslan, 258  
 Padding, Johan T, 226  
 Pang, Yusong, 63, 253  
 Pankaj, Doshi, 209  
 Pantaleev, Stefan, 210, 268  
 Papanicolopulos, Stefanos-Aldo, 172, 176, 186  
 Pedrolli, Lorenzo, 157  
 Peglow, Mirko, 198  
 Pfeufer, Rike, 97  
 Pietsch-Braune, Swantje, 198  
 Pillai, John, 190  
 Pirker, Stefan, 168, 260  
 Poddar, Rachit, 83  
 Poizer, William, 200  
 Pokorná, Kamila, 103, 151  
 Pol, Antonio, 236
- Poletto, Massimo, 17, 41, 182, 186, 222, 224, 230, 238, 256  
 Pontiga, Francisco, 123  
 Portnikov, Dmitry, 45, 47  
 Pour, Y. David, 51, 75  
 Premarathna, Chanaka Prasad, 129  
 Pusch, Matthias, 111
- Queteschner, Daniel, 168, 260  
 Quist, Johannes, 67  
 Qyteti, Klidi, 41
- Raju, Jobin, 184  
 Ramírez-Gómez, Álvaro, 92  
 Ratnayake, Chandana, 207  
 Ratzabi, Arnon, 127  
 Raupert, Marvin, 111  
 Redka, Yevhen, 109  
 Reid, Shaun, 115, 137  
 Rem, Peter, 161  
 Reynolds, Gavin K., 244, 273  
 Rhein, Frank, 208, 225, 233  
 Rhymer, Daniel, 254  
 Richard, Patrick, 236, 237  
 Rioual, Francois, 99  
 Robertson, John, 210  
 Robinson, Peter W, 213  
 Robisson, Anne-Charlotte, 37, 88  
 Roeplal, Raïsa, 253, 269  
 Rogan, Haydn, 281  
 Royer, John, 199  
 Rozbroj, Jiří, 103, 151
- Sadhukhan, Jhuma, 121  
 Saleh, Khashayar, 88, 221  
 Salehian, Mohammad, 210  
 Salman, Agba D., 77, 79, 119  
 Salvador, Pedro Martin, 267  
 Santangel, Matthew, 209  
 Sarnavi, Hamed Johnny, 33  
 Schaefer, Mario, 209  
 Scherer, Viktor, 41  
 Schiffner, Sven, 198  
 Schilde, Carsten, 170, 184, 203, 235, 250, 252, 262, 274  
 Schneider, Hans, 97, 145
- Schneiderbauer, Simon, 168  
 Schomberg, Ann Kathrin, 217  
 Schott, Dingena L., 63, 223, 226, 253, 269  
 Schröder, Merle, 220  
 Schuitemaker, Wouter, 269  
 Schwandtke, Rolf, 109  
 Schütz, Denis, 201, 228, 232  
 Serper, Damla, 197  
 Seville, Jonathan, 39  
 Sezer, Hazal, 231  
 Sharma, Atul, 69, 73, 141  
 Sharma, Rahul, 186  
 Shi, Hao, 223, 269  
 Shinebaum, Rachael, 273  
 Sinnwell, Yannik, 153  
 Skorych, Vasyl, 202  
 Smith, Rachel, 9  
 So, Daiki, 241  
 Sofia, Daniele, 230, 238, 246  
 Soria-Hoyo, Carlos, 123  
 Sousa, Lucas Massaro, 27  
 Sousani, Marina, 263  
 Srivastava, Akhilesh Kumar, 207  
 Stahler, Lois, 244  
 Stel, Jan van der, 253  
 Stitt, Hugh, 35, 256  
 Stratford, Kevin, 281  
 Syed, Amer, 188  
 Sáez, Esteban, 280  
 Søliland, Kristin, 207
- Taghizadeh, Afshin, 188  
 Tanaka, Toshitsugu, 234  
 Tanneru, Yeswanth Sai, 170  
 Thomas, Amalia L, 55  
 Thommes, Markus, 191, 251, 275  
 Thon, Christoph, 203, 250, 262  
 Thornton, Anthony Richard, 71  
 Tobie, Gabriel, 237  
 Tokumaru, Kazuki, 241  
 Tranquillini, Giulia, 206  
 Trepnau, Dietrich, 109  
 Troescher, Thomas, 201  
 Tsaoulidis, Dimitrios, 121  
 Tsotsas, E., 51  
 Tsuji, Takuya, 234  
 Tsukuma, Shunta, 234  
 Tsunajima, Taiki, 234

- Ullrich, Anita, [67](#)  
Unterberger, Natali, [228](#),  
[232](#)
- Valadian, Roozbeh, [240](#)  
Valverde, José M., [123](#)  
van Benten, Marcel C., [226](#),  
[269](#)  
van Selm, Gert-Jan, [223](#),  
[269](#)  
Varambhia, Aakash, [188](#)  
Veikle, Eric, [271](#)  
Verschueren, Rik H., [267](#)  
Viciconte, Giovanni, [105](#)  
Vivacqua, Vincenzino, [256](#)  
Vivakanantha, Ashwanth,  
[90](#)  
Vriend, Nathalie, [18](#)
- Wagner, Lars, [217](#)  
Wang, Yin, [276](#)  
Wang, Zheng, [113](#)  
Washino, Kimiaki, [234](#)  
Watanabe, Masahiko, [155](#)
- Watano, Satoru, [205](#), [214](#),  
[242](#)  
Watson, Peter, [239](#)  
Weiler, Rouven, [211](#)  
Weingrill, Helena, [201](#), [228](#),  
[232](#)  
Weinhart, Thomas, [71](#),  
[202](#)  
Weis, Dominik, [211](#)  
Werner, Dominik, [247](#)  
Wetherley, Dion, [202](#)  
Wheeler, Craig A., [59](#), [213](#)  
Wiggin, Aaron, [278](#)  
Williams, Charles, [85](#), [90](#)  
Williams, Kenneth, [19](#), [95](#),  
[135](#)  
Willis, Jason, [213](#)  
Wilms, Christoph, [243](#)  
Wilms, Harald, [23](#)  
Windisch, Lisa, [252](#)  
Windows-Yule, Christopher R. K.,  
[39](#), [231](#), [244](#), [247](#), [254](#),  
[273](#), [278](#)  
Winkelmann, Max, [172](#)
- Wiącek, Joanna, [101](#)  
Wood, Richard, [261](#)  
Wu, Chuan-Yu, [121](#), [194](#)  
Wu, Yongli, [161](#)  
Wurzer, Christian, [196](#)
- Xu, Wenchao, [243](#)
- Yamamoto, Kenji, [241](#)  
Yang, Yefeng, [276](#)  
Yano, Takeru, [205](#)  
Yokohama, Katsuhiko,  
[241](#)  
Yu, Mingzhe, [277](#)
- Zegzulka, Jiří, [103](#), [151](#)  
Zetzener, Harald, [215](#), [218](#), [220](#),  
[229](#)  
Zhang, Bin, [257](#)  
Zharbossyn, Assem, [182](#)  
Zhou, Xiye, [198](#)  
Zigan, Stefan, [145](#)  
Zinatlou, Sina, [17](#)  
Ziskind, Gennady, [127](#)  
Žurovec, David, [103](#), [151](#)

